Modal Testing

Modal Testing

A Practitioner's Guide

Peter Avitabile
University of Massachusetts Lowell, USA

This Work is a co-publication between The Society for Experimental Mechanics and John Wiley & Sons Ltd

WILEY

SEM

Registered Offices
John Wiley & Sons, Inc., 111 River Street, Hoboken, NJ 07030, USA
John Wiley & Sons Ltd, The Atrium, Southern Gate, Chichester, West Sussex, PO19 8SQ, UK

Editorial Office
The Atrium, Southern Gate, Chichester, West Sussex, PO19 8SQ, UK

For details of our global editorial offices, customer services, and more information about Wiley products visit us at www.wiley.com.

Wiley also publishes its books in a variety of electronic formats and by print-on-demand. Some content that appears in standard print versions of this book may not be available in other formats.

Library of Congress Cataloging-in-Publication data applied for

ISBN Hardback: 9781119222897

Cover design by Wiley
Cover images: (Background) © Gerard Hermand/Gettyimages; (Inset image) Courtesy of the author

Set in 10/12pt WarnockPro by SPi Global, Chennai, India

10 9 8 7 6 5 4 3 2 1

To my wife and family and those who have crossed my path in writing this book…
my life has been expanded and enhanced through my interactions with you.

Contents

Preface *xv*
About the Companion Website *xix*

Part I Overview of Experimental Modal Analysis using the Frequency Response Method *1*

1 Introduction to Experimental Modal Analysis: A Simple Non-mathematical Presentation *3*
1.1 Could you Explain Modal Analysis to Me? *6*
1.2 Just what are these Measurements called FRFs? *10*
1.2.1 Why is Only One Row or Column of the FRF Matrix Needed? *13*
1.3 What's the Difference between a Shaker Test and an Impact Test? *17*
1.3.1 What Measurements do we Actually make to Compute the FRF? *18*
1.4 What's the Most Important Thing to Think about when Impact Testing? *21*
1.5 What's the Most Important Thing to Think about when Shaker Testing? *22*
1.6 Tell me More About Windows; They Seem Pretty Important! *24*
1.7 So how do we get Mode Shapes from the Plate FRFs? *25*
1.8 Modal Data and Operating Data *29*
1.8.1 What is Operating Data? *29*
1.8.2 So what Good is Modal Data? *33*
1.8.3 So Should I Collect Modal Data or Operating Data? *34*
1.9 Closing Remarks *36*

2 General Theory of Experimental Modal Analysis *37*
2.1 Introduction *37*
2.2 Basic Modal Analysis Theory – SDOF *38*
2.2.1 Single Degree of Freedom System Equation *38*
2.2.2 Single Degree of Freedom System Response due to Harmonic Excitation *40*
2.2.3 Damping Estimation for Single Degree of Freedom System *42*
2.2.4 Response Assessment with Varying Damping *43*
2.2.5 Laplace Domain Approach for Single Degree of Freedom System *46*
2.2.6 System Transfer Function *47*
2.2.7 Different Forms of the Transfer Function *48*
2.2.8 Residue of the SDOF System *49*
2.2.9 Frequency Response Function for a Single Degree of Freedom System *49*
2.2.10 Transfer Function/Frequency Response Function/S-plane for a Single Degree of Freedom System *51*

2.2.11 Frequency Response Function Regions for a Single Degree of Freedom System *51*
2.2.12 Different Forms of the Frequency Response Function *53*
2.2.13 Complex Frequency Response Function *53*
2.3 Basic Modal Analysis Theory – MDOF *56*
2.3.1 Multiple Degree of Freedom System Equations *57*
2.3.2 Laplace Domain for Multiple Degree of Freedom System *66*
2.3.3 The Frequency Response Function *68*
2.3.4 Mode Shapes from Frequency Response Equations *68*
2.3.5 Point-to-Point Frequency Response Function *71*
2.3.6 Response of Multiple Degree of Freedom System to Harmonic Excitations *72*
2.3.7 Example: Cantilever Beam Model with Three Measured DOFs *75*
2.3.8 Summary of Time, Frequency, and Modal Domains *83*
2.3.9 Response due to Forced Excitation using Mode Superposition *87*
2.4 Summary *89*

3 General Signal Processing and Measurements Related to Experimental Modal Analysis *93*
3.1 Introduction *93*
3.2 Time and Frequency Domain *93*
3.3 Some General Information Regarding Data Acquisition *96*
3.4 Digitization of Time Signals *97*
3.5 Quantization *97*
3.5.1 ADC Underload *98*
3.5.2 ADC Overload *100*
3.6 AC Coupling *100*
3.7 Sampling Theory *101*
3.8 Aliasing *103*
3.9 What is the Fourier Transform? *105*
3.9.1 Fourier Transform and Discrete Fourier Transform *107*
3.9.2 FFT: Periodic Signal *108*
3.9.3 FFT: Non-periodic Signal *108*
3.10 Leakage and Minimization of Leakage *109*
3.10.1 Minimization of Leakage *111*
3.11 Windows and Leakage *111*
3.11.1 Rectangular Window *112*
3.11.2 Hanning Window *116*
3.11.3 Flat Top Window *116*
3.11.4 Comparison of Windows with Worst Leakage Distortion Possible *116*
3.11.5 Comparison of Rectangular, Hanning and Flat Top Window *119*
3.11.6 Force Window *119*
3.11.7 Exponential Window *119*
3.11.8 Convolution of the Window in the Frequency Domain *119*
3.12 Frequency Response Function Formulation *119*
3.13 Typical Measurements *123*
3.13.1 Time Signal and Auto-power Functions *123*
3.13.2 Typical Measurement: Cross Power Function *124*
3.13.3 Typical Measurement: Frequency Response Function *124*
3.13.4 Typical Measurement: Coherence Function *124*
3.14 Time and Frequency Relationship Definition *126*
3.15 Input–Output Model with Noise *127*

3.15.1 H_1 Formulation: Output Noise Only *127*
3.15.2 H_2 Formulation: Output Noise Only *128*
3.15.3 H_1 Formulation: Input Noise Only *128*
3.15.4 H_2 Formulation: Input Noise Only *128*
3.16 Summary *129*

4 Excitation Techniques *131*
4.1 Introduction *131*
4.2 Impact Excitation Technique *132*
4.2.1 Impact Hammer *132*
4.2.2 Hammer Impact Tip Selection *136*
4.2.3 Useful Frequency Range for Impact Excitation *137*
4.2.4 Force Window for Impact Excitation *137*
4.2.5 Pre-trigger Delay *137*
4.2.6 Double Impact *140*
4.2.7 Response due to Impact *140*
4.2.8 Roving Hammer vs Stationary Hammer and Reciprocity *143*
4.2.9 Impact Testing: an Example Set of Measurements *147*
4.3 Shaker Excitation *159*
4.3.1 Modal Shaker Setup *161*
4.3.2 Historical Development of Shaker Excitation Techniques *162*
4.3.3 Swept Sine Excitation *163*
4.3.4 Pure Random Excitation *163*
4.3.5 Pure Random Excitation with Windows Applied *165*
4.3.6 Pure Random Excitation with Overlap Processing *165*
4.3.7 Pseudo-random Excitation *167*
4.3.8 Periodic Random Excitation *167*
4.3.9 Burst Random Excitation *168*
4.3.10 Sine Chirp Excitation *170*
4.3.11 Digital Stepped Sine Excitation *170*
4.4 Comparison of Different Excitations for a Weldment Structure *172*
4.4.1 Random Excitation with No Window *172*
4.4.2 Random Excitation with Hanning Window *173*
4.4.3 Burst Random Excitation with No Window *173*
4.4.4 Sine Chirp Excitation with No Window *174*
4.4.5 Comparison of Random, Burst Random and Sine Chirp *175*
4.4.6 Comparison of Random and Burst Random at Resonant Peaks *175*
4.4.7 Linearity Check Using Sine Chirp *175*
4.5 Multiple-input, Multiple-output Measurement *175*
4.5.1 Multiple Input vs Single Input Testing *177*
4.5.2 Multiple Input vs Single Input for a Weldment Structure *181*
4.5.3 Multiple Input vs Single Input Testing *181*
4.5.4 Comparison of Multiple Input and Single Input for Weldment Structure *182*
4.5.5 MIMO Measurements on a Multi-component Structure *182*
4.6 Summary *187*

5 Modal Parameter Estimation Techniques *189*
5.1 Introduction *189*
5.2 Experimental Modal Analysis *190*
5.2.1 Least Squares Approximation of Data *190*

5.2.2 Classification of Modal Parameter Estimation Techniques *193*
5.3 Extraction of Modal Parameters *198*
5.3.1 Peak Picking Technique *198*
5.3.2 Circle Fitting – Kennedy and Pancu *199*
5.3.3 SDOF Polynomial *200*
5.3.4 Residual Effects of Out of Band Modes *200*
5.3.5 MDOF Polynomial *201*
5.3.6 Least Squares Complex Exponential *201*
5.3.7 Advanced Forms of Time and Frequency Domain Estimators *203*
5.3.8 General Time Domain Techniques *203*
5.3.9 General Frequency Domain Techniques *203*
5.3.10 General Consideration for Time vs Frequency Representation *204*
5.3.11 Additional Remarks on Modal Parameter Estimation *204*
5.3.12 Two Step Process for Modal Parameter Estimation *205*
5.4 Mode Identification Tools *206*
5.4.1 Summation Function *206*
5.4.2 Mode Indicator Function *206*
5.4.3 Complex Mode Indicator Function *207*
5.4.4 Stability Diagram *208*
5.4.5 PolyMAX *210*
5.5 Modal Model Validation Tools *212*
5.5.1 Synthesis of Frequency Response Functions using Extracted Parameters *212*
5.5.2 Modal Assurance Criterion *213*
5.5.3 Mode Participation Factors *215*
5.5.4 Mode Overcomplexity *215*
5.5.5 Mean Phase Co-linearity and Mean Phase Deviation *216*
5.6 Operating Modal Analysis *216*
5.7 Summary *219*

Part II Practical Considerations for Experimental Modal Testing *221*

6 Test Setup Considerations *223*
6.1 Test Plan? *224*
6.2 How Many Modes Required? *225*
6.3 Frequency Range of Interest? *228*
6.4 Transducer Possibilities? *232*
6.5 Test Configurations? *232*
6.6 How Many Measurement Points Needed? *235*
6.7 Excitation Techniques *238*
6.8 Miscellaneous Items to Consider *238*
6.9 Summary *245*

7 Impact Testing Considerations *247*
7.1 Hammer Impact Location *247*
7.2 Hammer Tip and Frequency Range *248*
7.3 Hammers for Different Size Structures *249*
7.4 How Does Impact Skew and Deviation of Input Point Affect the Measurement? *256*
7.4.1 Skewed Impact Force *256*
7.4.2 Inconsistent Impact Force Location *256*

7.5 Impact Hammer Frequency Bandwidth *256*
7.6 Accelerometer ICP Considerations for Low Frequency Measurements *264*
7.7 Considerations for Reciprocity Measurements *264*
7.8 Roving Hammer vs Roving Accelerometer *267*
7.9 Picking a Good Reference Location *268*
7.10 Multiple Impact Difficulties and Considerations *268*
7.10.1 Academic Structure *269*
7.10.2 Large Wind Turbine Blade *271*
7.11 What is "Filter Ring" during an Impact Measurement? *274*
7.12 Test Bandwidth Much Wider than Desired Frequency Range *275*
7.13 Why Does the Structure Response Need to Come to Zero at the End of the Sample Time? *279*
7.14 Measurements with no Overload but Transducers are Saturated *282*
7.14.1 Case 1: Sensitive Accelerometer with Exponential Window *282*
7.14.2 Case 2: Sensitive Accelerometer with No Window *283*
7.14.3 Case 3: Less Sensitive Accelerometer with No Window *283*
7.15 How much Roll Off in the Input Hammer Force Spectrum is Acceptable? *286*
7.16 Can the Hammer be Switched in the Middle of a Test to Avoid Double Impacts? *289*
7.17 Closing Remarks *292*

8 Shaker Testing Considerations *293*
8.1 General Hardware Related Issues *293*
8.1.1 General Information about Shakers and Amplifiers *293*
8.1.2 What is the Difference between the Constant Current and Constant Voltage Settings on the Shaker Amplifier? *294*
8.1.3 Some Shakers have a Trunnion: Is it Really Needed and Why Do You Have It? *294*
8.1.4 Where is the Best Location to Place a Shaker for a Modal Test? *295*
8.1.5 How Should the Shaker be Constrained when Testing? *296*
8.1.6 What's the Best Way to Support a Shaker for Lateral Vibration When it is Hung? *296*
8.1.7 What are the Most Common Practical Failures with Shaker Setup? *297*
8.1.8 What is the Correct Level of Shaker Excitation for Modal Testing? *297*
8.1.9 How many Shakers should I use in my Modal Test? *297*
8.1.10 Shaker and Stinger Alignment Issues *297*
8.1.11 When should the Shaker be Attached to the Structure? *298*
8.1.12 Should I Disconnect the Stingers while not Testing? *298*
8.1.13 Force Gage or Impedance Head must be Mounted on Structure Side of Stinger? *300*
8.1.14 What's an Impedance Head? Why use it? Where does it go? *301*
8.2 Stinger Related Issues *302*
8.2.1 Why should Stingers be used? *302*
8.2.2 Can a Poorly Designed Shaker/Stinger Setup Produce Incorrect Results? *303*
8.2.3 Stingers and their Effect on Measured Frequency Response Functions *306*
8.2.3.1 Stinger Location *307*
8.2.3.2 Stinger Alignment *307*
8.2.3.3 Stinger Length *308*
8.2.3.4 Stinger Type *310*
8.2.3.5 Sleeved Stingers *310*
8.2.3.6 How do Piano Wire Stingers Work? How are they Pretensioned?? *314*

8.3 Shaker Related Issues *314*
8.3.1 Is MIMO needed for Structures with Directional Modes? *314*
8.3.2 Shaker Force Levels and SISO vs MIMO Considerations *316*
8.3.2.1 High Shaker Force Levels *316*
8.3.2.2 High Shaker Force Levels *318*
8.3.2.3 Effects of FRF Measurements in the Modal Parameter Estimation Process *320*
8.4 Concluding Remarks *325*

9 Insight into Modal Parameter Estimation *327*
9.1 Introductory Remarks *327*
9.2 Mode Indicator Tools Help Identify Modes *328*
9.3 SDOF vs MDOF for a Simple System *330*
9.4 Local vs Global: MACL Frame *332*
9.5 Repeated Root: Composite Spar *334*
9.6 Wind Turbine Blade: Same Geometry but Very Different Modes *335*
9.7 Stability Diagram Demystified *337*
9.8 Curvefitting Demystified *340*
9.9 Curvefitting Different Bands for the Poles and Residues *343*
9.10 Synthesizing the FRF from Parameters from Several Bands Stitched Together *344*
9.11 A Large Multiple Reference Modal Test Parameter Estimation *346*
9.11.1 Case 1: Use of All Measured FRFs *346*
9.11.2 Case 2: Use of Selected Sets of Measured FRFs *350*
9.11.3 Case 3: Use of PolyMAX *352*
9.12 Operating Modal Analysis *357*
9.13 Concluding Remarks *363*

10 General Considerations *365*
10.1 An Experimental Modal Test: a Thought Process Divulged *369*
10.2 FFT Analyzer Setup *377*
10.2.1 General FFT Analyzer Setup *377*
10.2.2 Setup for Impact Testing *378*
10.2.3 Setup for Shaker Testing *379*
10.3 Log Sheets *379*
10.4 Practical Considerations: Checklists *379*
10.4.1 Checklist for Analyzer Setup *380*
10.4.2 Checklist for Impact Testing *382*
10.4.3 Checklist for Shaker Testing *384*
10.4.4 Checklist for Measurement Adequacy *386*
10.4.5 Checklist for Miscellaneous *388*
10.5 Summary *391*
Appendix: Logbook Forms *392*

11 Tips, Tricks, and Other Stuff *395*
11.1 Modal Testing Primer *396*
11.1.1 Impact Setup *396*
11.1.2 Shaker Setup *397*
11.1.3 Drive Point Measurements *398*
11.1.4 Reciprocity *398*
11.1.5 Inappropriate Reference Location *399*
11.1.6 Multiple-input, Multiple-output Testing *399*

11.1.7 Multiple Reference Testing *400*
11.2 Impact Hammer and Impulsive Excitation *400*
11.2.1 The Right Hammer for the Test *400*
11.2.2 Hammer – Get the Swing of it *401*
11.2.3 Hammer Tripod *401*
11.2.4 Hammer tip selection *401*
11.2.5 No Hammer: Improvise *402*
11.2.6 Pete's Hammer Test Impact Ritual *402*
11.3 Accelerometer Issues *403*
11.3.1 Mass Loading *403*
11.3.2 Mass Loading Effects from Tri-axial Accelerometers *404*
11.3.3 Accelerometer Sensitivity Selection *407*
11.3.4 Tri-axial Accelerometers *408*
11.4 Curvefitting Considerations *411*
11.4.1 Should all Measurements be used when Curvefitting *412*
11.5 Blue Frame with Three Plate Subsystem *414*
11.6 Miscellaneous Issues *422*
11.6.1 Modal Test Axis Labels *422*
11.6.2 Testing Does Not Need to Start at point 1 *423*
11.6.3 Test to a Wider Frequency Range *423*
11.6.4 U_i times U_j; the key to many questions *423*
11.7 Summary *425*

A Linear Algebra: Basic Operations Needed for Modal Analysis Operations *427*
A.1 Define a Matrix *427*
A.2 Define a Column Vector *427*
A.3 Define a Row Vector *428*
A.4 Define a Diagonal Matrix *428*
A.5 Define Matrix Addition *428*
A.6 Define Matrix Scalar Multiply *428*
A.7 Define Matrix Multiply *429*
A.8 Matrix Multiplication Rules *429*
A.9 Transpose of a Matrix *430*
A.10 Transposition Rules *430*
A.11 Symmetric Matrix Rules *430*
A.12 Define a Matrix Inverse *431*
A.13 Matrix Inverse Properties *431*
A.14 Define an Eigenvalue Problem *431*
A.15 Generalized Inverse *431*
A.16 Singular Value Decomposition *432*

B Example Using Two Degree of Freedom System: Eigenproblem *433*

C Pole, Residue, and FRF Problem for 2-DOF System *437*

D Example using Three Degree of Freedom System *443*

E DYNSYS Website Materials *451*
E.1 Technical Materials Developed *451*
E.1.1 Theoretical Aspects of First and Second Order Systems *452*

E.1.2 First Order Systems: Modeling Step with ODE and Block Diagram *452*
E.1.3 Second Order Systems: Modeling Step, Impulse, IC with ODE and Block Diagram *452*
E.1.4 Mathematical Modeling Considerations *452*
E.1.5 Simulink and MATLAB Primer Materials *453*
E.1.6 Miscellaneous Materials *453*
E.2 DYNSYS.UML.EDU Website *453*

F Basic Modal Analysis Information *463*
F.1 SDOF Definitions *463*
F.1.1 Damping Estimates *463*
F.1.2 System Transfer Function *464*
F.1.3 Different Forms of the System Transfer Function *464*
F.1.4 Frequency Response Function *465*
F.2 MDOF Definitions *466*

Part III Collection of Sets of Modal Data Collected for Processing *467*

G Repeated Root Frame: Boundary Condition Effects *469*
G.1 Corner Supports Set #1 *470*
G.2 Midlength Supports Set #2 *474*
G.3 Modal Correlation between Set #1 and Set #2 *474*

H Radarsat Satellite Testing *479*
H.1 Data Reduction Set 1: Reference BUS:109:Z, BUS:118:Z, PMS:217:X and PMS:1211:Y *479*
H.2 Data Reduction Set 2: Reference PMS:217:X and PMS:1211:Y *479*

I Demo Airplane Testing *487*
I.1 Impact Testing *487*
I.2 SIMO Testing with Skewed Shaker *487*
I.3 MIMO Testing with Two Vertical Modal Shakers *493*

J Whirlpool Dryer Cabinet Modal Testing *497*

K GM MTU Automobile Round Robin Modal Testing *501*

L UML Composite Spar Modal Testing *505*

M UML BUH Modal Testing *509*

N Nomenclature *515*

Index *519*

Preface

This is a book about experimental modal analysis. Yes…there are other text books on this subject but this one is different. Other books have deep theoretical developments that researchers and PhDs all relish but do not get to the core of what is needed, from a practical standpoint, to provide practitioners with the critical information needed to perform the day to day modal test and develop a model from measured data.

This book is really written for the novice, manager, engineer and technician; the novice that may come in any shape or form.

- the newbie to modal testing and needs basics to get started
- the engineer that has not been involved in experimental dynamic testing
- the research/graduate student who has a need to make measurements and no one to guide them
- the engineer in a small company that gets tasked to perform modal tests
- the engineer promoted to fill the shoes of a well-seasoned modal test engineer who moves to management or retires
- the manager who needs to understand basics to properly secure funding to support important projects
- the engineer that needs to write test plans, conduct tests and extract useful information from data acquired
- the technician who needs to acquire data that is useful for development of a model
- for all to understand what each needs to do in order to be able to provide a model that can be used to evaluate systems, understand dynamic characteristics and solve complicated structural dynamic problems

While this book is not written to impress those well versed in modal analysis, many of the theoretical oriented folks will find very useful practical information regarding modal tests if they have never actually worked in a lab environment and have only developed theoretical approaches to solve these problems. But this text is also good for the graduate students who have research that has a need for experimental structural dynamic models to be developed but the PhD candidate is not focused on experimental modal analysis directly and his advisor is not familiar either – but there is a need for the PhD student to make meaningful measurements but not get bogged down with the intricate details of experimental modal analysis.

This book is also useful as a textbook for an undergraduate course to introduce very basic concepts necessary to perform an experimental modal test – possibly as a laboratory related class or as an addition to a vibrations class or for a graduate class on structural dynamics. This book definitely has sufficient material to be used as a first introduction to experimental modal analysis as an upper level undergraduate class or beginning graduate level class.

This book is meant to focus on the practical aspects of experimental modal analysis. Only limited theory is presented in the text in order to illustrate or expound upon certain methodologies of experimental modal testing that have their roots in the underlying theory. In many cases, the theory (or final equation of a long derivation) is just presented; this text is not about developing the details of the theory but rather applying the theory to solve real problems. There are an abundance of good textbooks in the area of vibrations but very few contain even a small piece of the content of this book. There are some textbooks on experimental modal analysis but most concentrate on the theoretical side of modal analysis assuming the implementation of a real test is easy and straightforward.

Back in the late 1990s, the Society for Experimental Mechanics had a series in Experimental Techniques magazine entitled "Modal Space – Back to Basics" – that series published for 17 continuous years. The series addressed very simple problems commonly encountered by experimental modal analysis testers. The articles were never more than 2 pages and had a variety of experimental modal analysis topics addressed. But the material was scattered from one article to the next and they were just intended to be "snip-its" of information that resulted from years and years of teaching industry modal seminars, teaching in-house modal seminars and many, many emails received over 20 or more years working in this area. This book is about pulling all that information together and providing a more complete treatment of that material.

So this text is laid out in two parts – the first part is more of the traditional theory related to analytical and experimental modal analysis whereas the second part is about the practical issues related to experimental modal tests followed by appendices with additional useful information. Chapter 1 is a very simple overview of the entire experimental modal test to set the stage for the entire text; this is extremely useful to the new folks starting into modal analysis. Chapter 2 through 5 have some of the cornerstones of basic information. Chapter 2 has all the pertinent theory summarized related to single degree of freedom systems to multiple degree of freedom systems with equations presented in the physical domain, modal domain, Laplace domain and the frequency domain. Chapter 3 presents a good summary of all the pertinent digital signal processing techniques that are needed for the acquisition of measured data; sampling issues to frequency data to noise are all addressed here. Chapter 4 presents the most common excitation techniques used for modal testing today – impact and shaker excitation. Chapter 5 contains some of the rudimentary information necessary for modal parameter estimation. Chapter 6 through 9 have a more practical side of the material. Chapter 6 is related to the issues related to setting up a test from start to finish. Chapter 7 has many examples related to impact testing which is the most widely used excitation technique for traditional experimental modal tests. Chapter 8 further discusses shaker excitation techniques and issues related to running these types of tests as well as multiple input multiple output testing. Chapter 9 provides some very practical insights into the reduction of the data collected using different modal parameter estimation approaches. Chapter 10 and 11 have a variety of different issues related to modal testing that are difficult to place in one of the previous chapters because they span more than one topic or were just not appropriate for a particular chapter. There are several appendices that have some very simple analytical models that help to show the math in action. A few more appendices have a scattering of broad information that may be useful to the modal test engineer. And a few final chapters have some data sets that have been used for modal parameter estimation with results for the user to try to decompose with their own software used in their lab; the data sets are available in universal file format on the book webpage so that they can be downloaded and processed and compared to the users results.

Finally, there are the thanks to so many that have crossed paths during my time spent in this modal community. I started working in the mid-seventies and early on came across John O'Callahan and G. Dudley Shepard up at then the University of Lowell (the former Lowell Tech).

John, analytical and Dudley, experimental – they were a pair that started modal at the University of Massachusetts Lowell in the Modal Analysis and Controls Laboratory. I worked with John in many different ways – as a consultant, a mentor and advisor, and as a colleague. His analytical roots were strong and deep and I learned much from him. From the late 80's to the end of the century, there were many experimental modal analysis seminars that were taught with Chuck Van Karsen; these seminars were often referred to as the Chuck and Pete show. Many commented how the material taught was so complementary to each other and that the lectures should always be arranged the same way because they were so well orchestrated; the reality was that we would pick straws at the start of each and every seminar and we never taught the same sections of the seminar each time – so much for complementary material. I hope that Chuck learned as much from me as I learned from him – those years teaching seminars reinforces the need for this book. Phillip Cornwell at Rose Hulman is one of the best teachers that I have run across in my years as an educator in this field. Phil has provided very useful comments in the development of this book.

Over the many years at the University of Massachusetts Lowell in the former Modal Analysis and Controls Laboratory and the current Structural Dynamics and Acoustic Systems Laboratory, I have been blessed with a wide number of excellent students in my research lab and their research efforts. All of them have made significant contributions to the research performed. While it is impossible to name all of them, they certainly know their contributions scattered throughout this book. But there are several that need special mention due to extra support and effort that is far beyond over and above. PawanPingle has been very helpful in looking at this book and giving a different perspective on things to address. Louis Thibault and Tim Marinone were always available to support some of the special items that were requested to illustrate a point or two. Sergio Obando had many test runs of which data is used in this book. Julie Harvie also provided useful feedback for the book as well as had many tests performed that help to highlight many issues that are addressed in this book. And Patrick Logan, Tina Dardeno and Dagny Joffre all were contributors, in many ways, especially at this time as this writing of this book came together. All of these folks have all made decades of work worthwhile. The words stated here are short and brief, but my gratitude for my interaction with all of them cannot be described easily by me in simple words. They are all part of my modal family. They all were willing to meet the sometimes crazy requests that I asked them to do.

One in particular was the day we decided to perform a modal impact test with a different approach on a very large complicated structure. The student with the 3 foot sledge hammer was up in the cherry picker to provide excitation to this large structure that was being tested. Single impact methodology provided very noisy measurements with a low frequency bandwidth and long time record. I decided to try something different. Speaking into my walkie talkie I said "*Listen carefully. Over.*" Then I continued with "*I want you to impact the structure with many randomly spaced impacts for 20 seconds of the 30 second time of the measurement. Keep the measurements sporadic as you impact the same point on the structure. Over.*" There was a very long delay of 5 to 10 seconds before the student responded with this clear and concerned response " *WHAT? Can you repeat that? Over*". Of course I repeated it but said it a little more slowly to make sure the words were heard correctly. The student down at the data acquisition system with me was just as shocked as the student up in the cherry picker with the impact hammer. The student next to me running the data acquisition system simply said this "*OMG. You have told us to never perform an impact test with a double hit and now you want us to perform a test with multiple impacts! Have you become a monster – I can't believe my ears*". Of course once everything was assessed and evaluated, this multiple impact test really is nothing more than what we do when we perform a burst random shaker test – just with an impact hammer excitation. This book has many examples where the urban legends of modal testing

are put to test and data collected to show that some of these long standing rules of testing may not really be correct. This book is about understanding the basics and trying to think beyond the rules that have been stated as tried and true. This book is about understanding the basic underlying concepts and providing insight so that modal tests are performed properly, with the best measurements possible, and with an understanding of the basics about extracting valid modal parameters.

It turns out that I still learn things every day that were not necessarily apparent to me. Detective work is a basic skill needed when acquiring measurements – to look at each piece of the puzzle and try to understand its effect on measurements and extraction of modal parameters and trying to do that with in the scope of the basic theory of modal analysis. This is not always easy. Hopefully, this book helps to provide some of the basic fundamental information in regards to modal testing and extraction of modal parameters. Every test is different and all the answers may not be contained in this book but the concepts and ideas will certainly help you run better experimental modal tests.

And one last thing

to all modal testers…
past, present and future…
question assumptions!

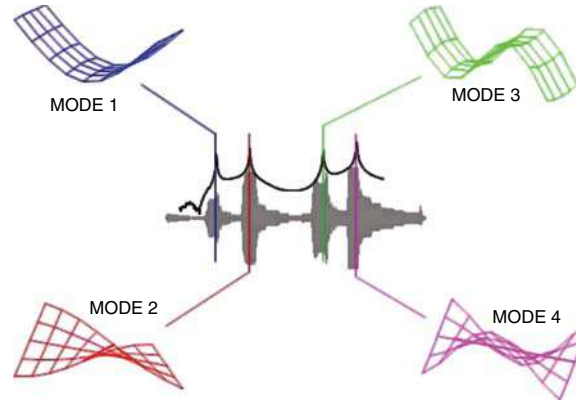

About the Companion Website

Don't forget to visit the companion website for this book:
www.wiley.com/go/avitabile/modal-testing

There you will find valuable material designed to enhance your learning, including:

- Modal Space articles – Back to Basics by Society for Experimental Mechanics
- Modal Book appendix databases
- DYNSYS web site materials

Part I

Overview of Experimental Modal Analysis using the Frequency Response Method

1

Introduction to Experimental Modal Analysis: A Simple Non-mathematical Presentation

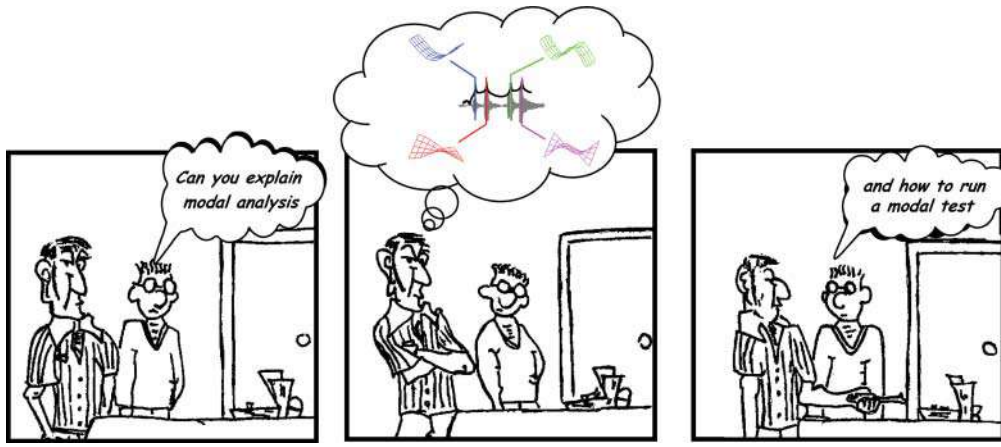

All structures and systems have operating conditions that cause them to respond due to these excitations. The loadings are generally not just static. Just about any structure is exposed to both static and dynamic loads, and it is the dynamic loads that are of concern to a structural dynamics or vibrations engineer. These excitations cause responses that may not be acceptable for the intended operation of the structure. When this is the case, the engineer must determine what if, anything, can be done to minimize or eliminate the undesirable response in the structure. Sometimes this can be very difficult if the cause of the unwanted response is unknown.

Now structural dynamics is the study of the response of a system to applied loads. These loads can cause responses at different frequencies depending on the dynamic characteristics of the structure. These dynamic characteristics are the frequency, damping and mode shapes. Each of the modes of the structure may contribute in varying degrees to the response of the system and it is sometimes very difficult to understand how the structure responds from the total response of all the modes of the system. So looking at the complete picture may not provide an insight as to how to fix a particular problem. This is where modal analysis comes in.

Modal analysis is the study of the dynamic character of a system that is defined independently from the loads applied to the system and the response of the system. Each of the modes of a system has a certain frequency, with a particular damping, and, most importantly, the characteristic deformation that the structure will undergo given an excitation at its natural frequency. This deformation is related to the mode shape characteristic for the particular mode. Modal analysis, by itself, can only identify the characteristics and not the actual physical deformations. The actual response and physical deformation can only be identified if loads are known

Modal Testing: A Practitioner's Guide, First Edition. Peter Avitabile.

Companion Website: www.wiley.com/go/avitabile/modal-testing

and applied to the structure. This is sometimes confusing to many people, but let's put it in perspective with a simpler case.

Let's consider a cantilever beam. Now the beam can be described in terms of its characteristics. These might be the length, width, weight, density, Young's modulus, cross-sectional area, and moment of inertia. But given these characteristics, the deformation of the beam cannot be identified, nor can it be determined if the beam is going to fail in a particular application. This can only be done if the load is known: loads must be identified to determine the deformation, stress, or strain. But once loads are identified, and then the displacement, stress and strain can be determined. But even at this point, the usefulness of the beam for a particular application cannot be determined until the design specification is identified. This specification will identify the relevant design criteria (such as allowable deflection, allowable stress, and allowable strain) and then an engineering judgment can be made as to the suitability of the cantilever beam for the intended use.

Well, modal analysis falls into this same situation. The frequency, damping, and mode shapes are just characteristics of a structure. But whether or not these are good or bad cannot be stated until the intended application is identified, loads identified, and design specification identified. So modal analysis, by itself, is not sufficient to decide if a structure is acceptable or not; the loads and design specification must be identified. (But it is important to point out that in solving many vibration problems, there is sometimes very little understood about the actual loading and often there is no relevant specification available; this is the reality of real-world engineering.)

However, understanding the modal characteristics of a structure can be very useful when performing a structural dynamic analysis. Depending on how the structural dynamic analysis is performed, the underlying modal characteristics may be used for the determination of the response, which helps in gaining an understanding of which modes, how many modes, and to what degree the modes all contribute to the response of the system. Suffice it to say that modal analysis is a very important part of gaining an understanding of a structural dynamic system.

Figure 1.1 shows a computer cabinet, which has responses to a variety of inputs: disk drive inputs, fan inputs and of course any external inputs that "excite" the system. The response comprises the response to all of these individual excitations. The structural dynamics analysis is the study of how the computer cabinet responds to all of these inputs. The time input force shown may be a combination of rotating inputs as well as random inputs. The output time response is due to all those inputs. But the inputs and output responses are not easy to interpret in the time

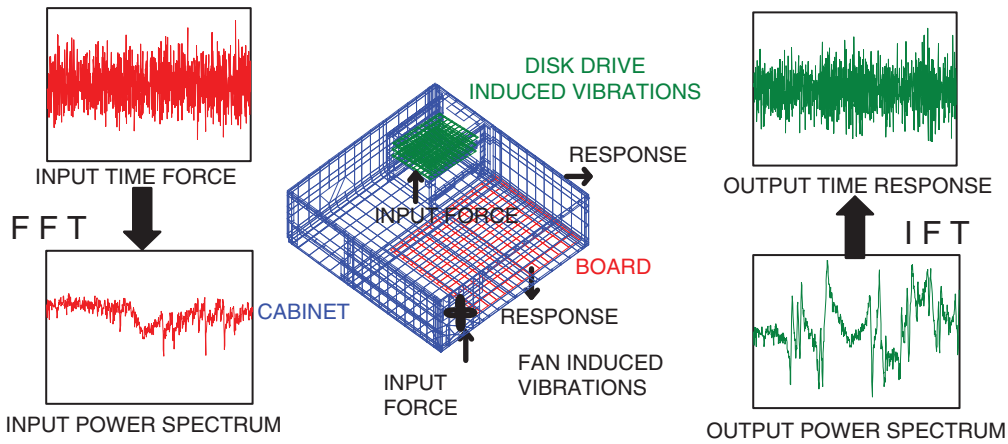

Figure 1.1 Structural dynamics vs modal analysis.

domain. But once they have been transformed to the frequency domain, there is a better picture of the energy distribution in the input force as well as the output response. Clearly, there are some frequencies that seem to have larger responses in the output frequency spectrum. Now if an experimental modal test was performed, those high frequency response peaks are likely associated with the modes of the system. So having modal information helps the designer to understand how the structure might respond to various frequency excitations – be it a discrete or a broadband response.

Now that the input–output scenario has been shown and described, it is useful to discuss a slightly simpler structure that is subject to some input excitation. Figure 1.2 shows a simple plate structure that has a random input excitation. And the output time response is also random in nature. From the time domain signal, there are no hints as to how or why the structure responds in the way it does. However, if the input is transformed to the frequency domain then there is a much clearer picture of the input force excitation. In the frequency domain, the modes of the system (the natural frequencies, damping, and mode shapes) act just like bandpass filters. Each mode "knows" exactly how to amplify and attenuate the input excitation on a frequency basis. And each mode has a separate effect on the input, but all the responses from each filter (each mode) are added together to determine the overall response. This combined response gives hints about where the response is high and generally corresponds to where the modes of the system lie. But in this output response spectrum, all of the modes are not equally excited because the input force spectrum does not have equal energy at all frequencies. So the response is strongly affected by the variation of the input force spectrum. But overall, the modes of the system can be seen as very important indicators as to where the response may be large (if there is significant input at that frequency). So a signal flow diagram provides a very good insight into why the modes of the system are critical pieces of information that need to be clearly understood.

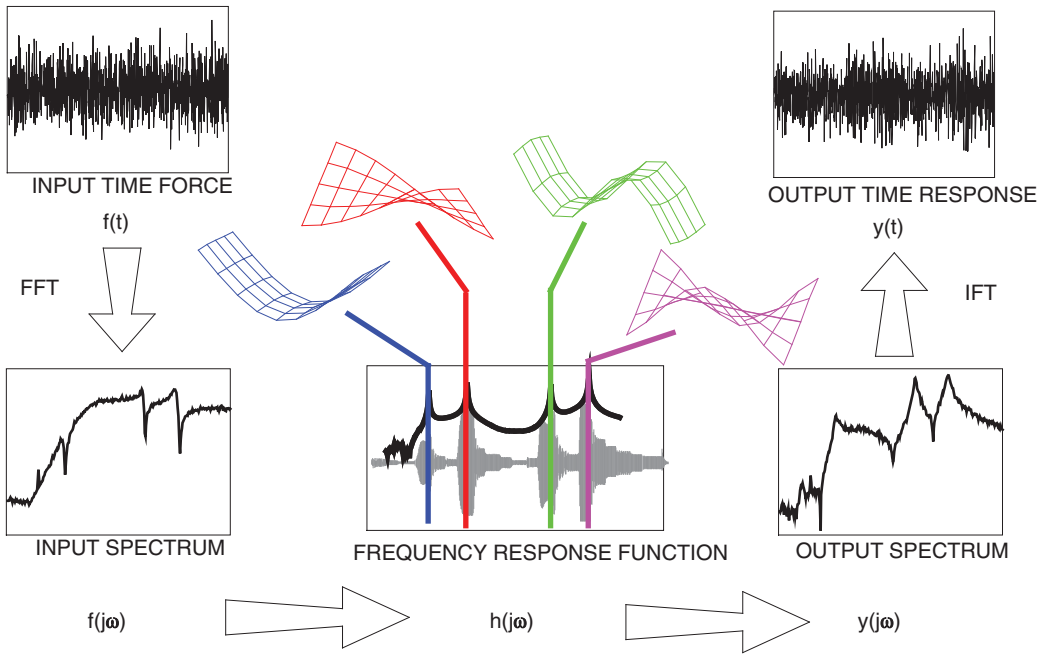

Figure 1.2 Signal flow diagram showing modal filtering of input resulting in output.

So now let's move on to the subject at hand, namely modal analysis. This seems to be an important part of the puzzle: frequencies and mode shapes appear to be central to understanding any structural dynamic problem.

Often times, people ask simple questions regarding modal analysis and how to run a modal test. Mostly, it is impossible to describe the process simply and some of the basic underlying theory needs to be addressed in order to fully explain some of the concepts involved. However, sometimes the theory is just a little too much to handle, although some of the concepts can be described without a rigorous mathematical treatment. This chapter will attempt to explain some concepts about how structures vibrate and to introduce aspects of modal analysis that are used to solve structural dynamic problems. The intent is to simply explain how structures vibrate from a non-mathematical perspective. This chapter serves to introduce some very basic material, which is then expanded on in later chapters.

With that being said, let's start with the first question that is usually asked in regards to experimental modal analysis.

1.1 Could you Explain Modal Analysis to Me?

In a nutshell, we could say that modal analysis is a process whereby we describe a structure in terms of its natural characteristics or "dynamic properties", namely the frequency, damping, and mode shapes. Well that's a mouthful so let's explain what it means. Without getting too technical, modal analysis can be very simply introduced in terms of the modes of vibration of a simple plate. This explanation is usually useful for engineers who are new to vibrations and modal analysis. While the structure of a plate is very simple compared to more complicated everyday structures that are evaluated, it can be used to explain the basic underlying theory and concepts very easily.

Let's consider a freely supported flat plate, as shown in Figure 1.3. Let's apply a constant force to one corner of the plate. We usually think of a force in a static sense, with the force causing some static deformation of the plate. But here the force applied varies in a sinusoidal fashion. Let's consider a fixed frequency of oscillation of the constant force: we will change the rate of oscillation but the peak force will always be the same value. We will measure the response of the plate due to the excitation with an accelerometer attached to one corner of the plate.

Now if we measure the response on the plate we will notice that the amplitude changes as we change the rate of oscillation of the input force (see Figure 1.4). There will be increases as well as decreases in amplitude at different points as we sweep up from low frequency to high frequency over time. This seems very odd: we are applying a constant force to the system yet the amplitude varies depending on the rate of oscillation of the input force. But this is exactly what happens; the response amplifies as we apply a force with a rate of oscillation that gets closer and closer to the natural frequency (or resonant frequency) of the system and reaches a maximum when the rate of oscillation is at the resonant frequency of the system. When you think about it, that's pretty amazing because we are applying the same peak force all the time; only the rate of oscillation is changed.

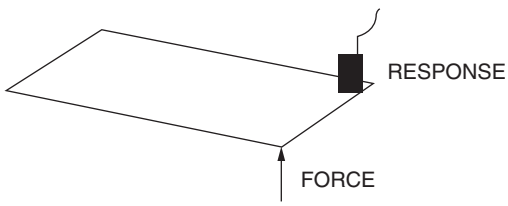

Figure 1.3 Simple plate excitation–response model.

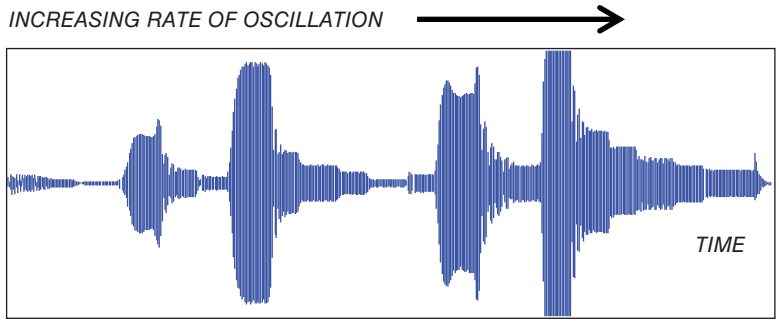

Figure 1.4 Simple plate response due to sinusoidal sweep excitation.

Figure 1.5 Simple plate frequency response function.

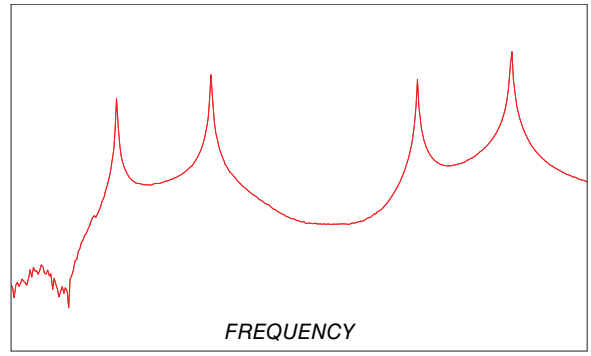

The accelerometer time response data in Figure 1.4 provides very useful information. But if we take the time data and transform it to the frequency domain using the fast Fourier transform (FFT) then we can compute something called the frequency response function (Figure 1.5). Now there are some very interesting aspects to note in this graph. We see that there are four peaks in this function, which occur at the resonant frequencies of the system, and we notice that they occur at the frequencies at which the time response was observed to have its maximum response corresponding to the rate of oscillation of the input excitation.

Now if we overlay the time trace and the frequency trace, what we will notice is that the frequencies at which the time trace reaches its maximum values correspond to the frequencies at which the peaks in the frequency response function reach their maxima (Figure 1.6). So you can see that we can use either the time trace to determine the frequencies at which maximum amplitude increases occur or the frequency response function to determine where these natural frequencies occur. Clearly the frequency response function is easier to evaluate. And it is important to note that while the sine sweep is very easy to evaluate, a random time signal would not be easy to interpret at all. And it is this frequency response that is widely used in measurements describing responses of structural systems.

Now most people are amazed at how the structure has these natural characteristics. Well, what's more amazing is that the deformation patterns at these natural frequencies also take on a variety of different shapes depending on which frequency is used for the excitation force. Identifying and understanding these patterns (or what are called *mode shapes*) is critically important when designing a structure or solving a dynamic response problem. But with only one measurement location, the actual deformation pattern cannot be identified.

Now let's see what happens to the deformation pattern of the plate structure at each one of these natural frequencies. Let's evenly distribute 45 accelerometers on the plate and measure

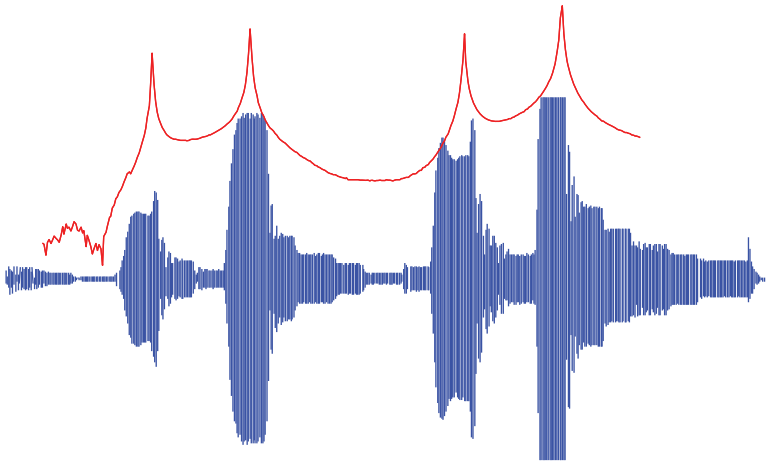

Figure 1.6 Overlay of time and frequency response functions for the simple plate structure.

the response of the plate at different excitation frequencies. If we were to dwell at each one of the four natural frequencies, we would see the deformation patterns that exist in the structure shown in Figure 1.7. The structure will have a very specific deformation pattern depending on the resonant frequency at which we dwell while we measure the response. The figure shows the deformation patterns that will result when the excitation coincides with one of the natural frequencies of the system. We see that when we dwell at the first natural frequency, there is a first *bending* deformation pattern (mode 1, blue). When we dwell at the second natural frequency, there is a first *twisting* deformation pattern (mode 2, red). At the third and fourth natural frequencies, the second bending and second twisting deformation patterns are seen (mode 3, green and mode 4, magenta, respectively). These deformation patterns are referred to

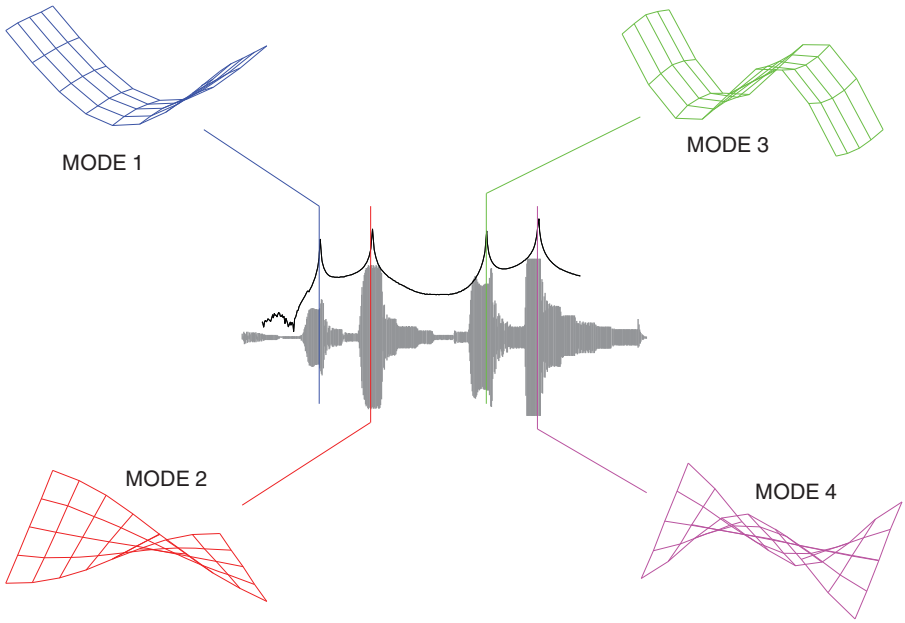

Figure 1.7 Simple plate sine dwell response.

as the *mode shapes* of the structure, although it should be noted that from a pure mathematical standpoint this is not strictly true. However, for the simple discussion here and from a practical standpoint, these deformation patterns are very close to the mode shapes.

Natural frequencies and mode shapes occur in all structures: the mass and stiffness of the structure determines where these natural frequencies and mode shapes will exist. As a design engineer, you need to identify these frequencies and know how they might affect the response of my structure when a force is applied. Understanding the mode shape and how the structure will vibrate when excited helps the design engineer to design better structures. And these frequencies and mode shapes are also critical for test engineers trying to troubleshoot operational problems.

Now there is much more to it all but this is just a very simple explanation of modal analysis. But in order to try to put it into a simpler context, there are two analogies that I commonly use to help people understand what is really needed; see Box 1.1.

Box 1.1 Analogy to help explain modal analysis

Example 1: We all know that there are many, many ingredients that are needed for a multitude of different recipes that we might find in a cookbook. But each recipe might only use a very small subset of ingredients that are needed for each recipe in the cookbook. And each of the identified ingredients is only added in certain proportions for each recipe. Well the frequencies and mode shapes for a structure behave in a very similar manner. If there is a certain loading condition on a structure, then there may be only a particular set of modes that "participate" in the response of the structure. Some modes may participate much more than other modes depending on the particular loading applied to the structure. And under a completely different loading condition, different modes may participate for that particular circumstance. And for the two loading conditions, there may be some common modes that are needed for both loading conditions but all the same modes may not be excited for each of the loading scenarios. Plus there will be differences in the modes that participate especially when the excitation has either low frequency content or high frequency content. So the structure will have many modes that describe its response and there are certain sets of modes that are necessary for the description of the response for each of the different loading scenarios. This is analogous to the cookbook which has many recipes but each recipe has a different set of ingredients for the individual recipes.

Example 2: We know that we may have a large 100-piece orchestra that is needed to play a variety of different scores. Each of the scores requires a different set of instruments that will participate at different times during the score with different intensities. And some scores do not necessarily use all of the instruments in the orchestra for each score. So each individual instrument will participate to a different degree for each of the particular scores to be played. And each instrument has a useful frequency band that will be heard from each instrument. Again these instruments are very much like all of the modes that make up the dynamic characteristic of a structure; each mode has a particular frequency slice and will participate to varying degrees and intensities depending on the particular loading that is applied. One additional item to note is that when we listen to a well-tuned orchestra, the music will be very good and easy to listen to. But all it takes is one member of the orchestra to play out of tune and then the entire score may not sound very good at all. If we just look at the orchestra as a whole unit, it may be very difficult to identify what is wrong and how to fix it. But if we look at each one of the members of the orchestra separately then it is easier to identify where the problem may be and then easy to correct. Well it turns out that structural response is very similar. If the response is acceptable then there is no need to look at all the contributors. But if the structural response is poor then it is very hard to determine how to fix the problem unless we can determine what each mode is and how it contributes. This is where modal analysis has its greatest strength and contribution to design. The structure can be evaluated in terms of its frequencies and mode shapes to identify how each mode behaves and how it contributes to the overall response of the system.

In essence, modal analysis is the study of the natural characteristics of structures. Understanding both the natural frequencies and mode shapes helps in designing a structural system for noise and vibration applications. We use modal analysis in the design of many types of structures, including automotive structures, aircraft structures, spacecraft, computers, tennis rackets, golf clubs…the list goes on and on. There is more detail in later chapters.

Now in the discussion above, we have introduced this measurement called a frequency response function, but exactly what is a frequency response function or what we commonly call an FRF?

1.2 Just what are these Measurements called FRFs?

In Section 1.1, we introduced the frequency response function, but exactly what *is* this? The frequency response function (FRF) is very simply the ratio of the output response of a structure due to an applied force. We measure both the applied force and the response of the structure due to the applied force simultaneously. (The response can be measured as a displacement, a velocity or an acceleration.) Now the measured time data is transformed from the time domain to the frequency domain using an FFT algorithm, which can be found in any signal processing analyzer and in many computer software packages. Due to this transformation, the functions end up being complex valued numbers; the functions contain real and imaginary components, or magnitude and phase components to describe the function. So let's take a look at what some of the functions might look like and try to determine how modal data can be extracted from these measured functions.

Let's first evaluate a simple beam with only three measurement locations and three mode shapes (Figure 1.8). There are three possible places forces can be applied, and three possible places where the response can be measured. For this example, we will have as many modes as degrees of freedom (DOFs), but in a typical application we have many more measurements than modes. For this example, there is a total of nine possible complex valued frequency response functions. The frequency response functions are usually described with subscripts to denote the input and output locations: as $h_{out,in}$ (or in normal matrix notation $h_{row,column}$).

Figure 1.8b–e shows the magnitude, phase, real, and imaginary parts of the frequency response function matrix. Note that a complex number is made up of a real and imaginary part that can be easily converted to a magnitude and phase; because the frequency response is a complex number, we can look at any and all of the parts that can describe the frequency response function. More detail on this subject is left for subsequent chapters. Now let's take a look at each of the measurements.

First let's drive the beam with a force from an impact at the tip of the beam at point 3 and measure the response of the beam at the same location at point 3 shown in Figure 1.9a. This measurement is denoted as h_{33}. This is a special measurement, which is referred to as a drive point measurement. Some important characteristics of a drive point measurement are:

- all resonances (peaks) are separated by anti-resonances
- the phase loses 180° as we pass over a resonance and gains 180° as we pass over an anti-resonance
- the peaks in the imaginary part of the frequency response function must all be in the same direction.

We can then move the impact force to point 2 while continuing to measure the response at point 3, and then move the impact force to point 1, still measuring the response at point 3. This gives two more measurements (Figure 1.9b). Notice that all measurements are made

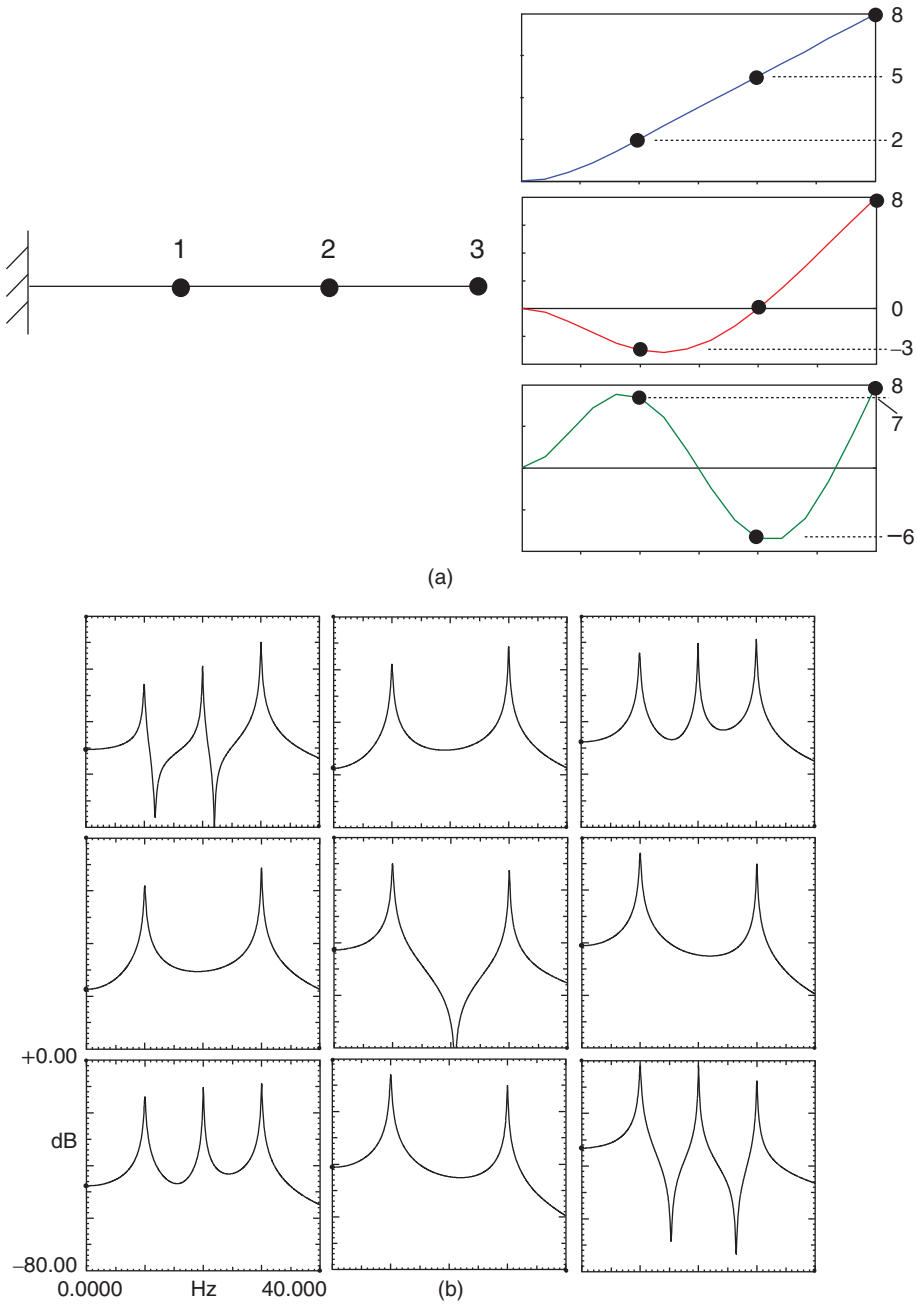

Figure 1.8 3 DOF beam: (a) model for input–output frequency response function matrix and (b) magnitude, (c) phase, (d) real, and (e) imaginary portions of the frequency response matrix.

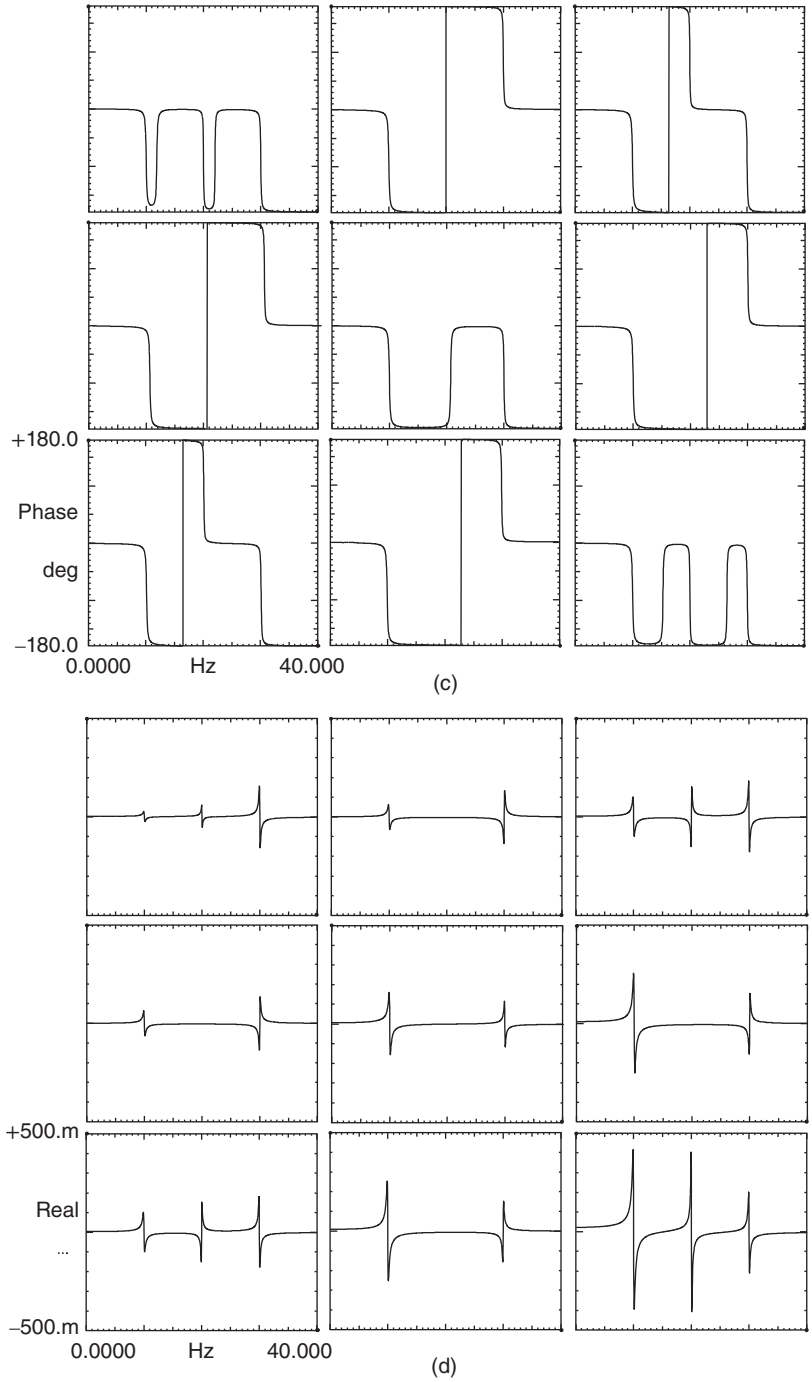

Figure 1.8 (*Continued*)

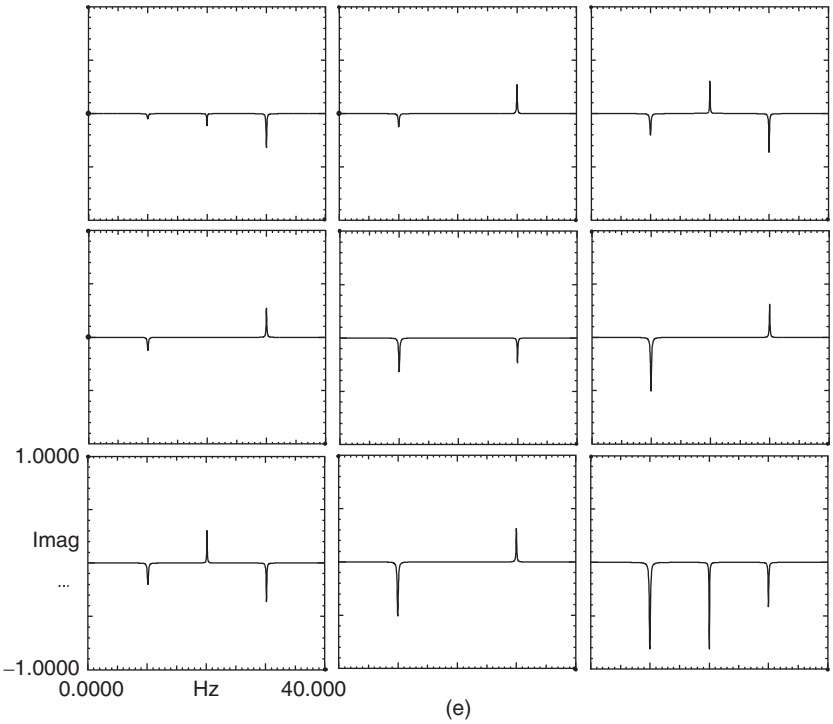

Figure 1.8 (*Continued*)

relative to point 3 and this is commonly called a "reference". Of course, it would be possible to also collect some or all of the remaining input–output combinations. So now we have some idea about the measurements that we *could* possibly acquire. However, in this case, we have taken measurements for just one row of the frequency response function matrix, which is the last row of the matrix of possible terms. It is important to note that the frequency response function matrix is symmetric. This is because the mass, damping, and stiffness matrices that describe the system are symmetric. We can therefore see that $h_{ij} = h_{ji}$; this characteristic is called "reciprocity". It means that we don't need to measure all the terms of the frequency response function matrix; many can be determined using the reciprocity characteristic.

One question that always seems to arise is whether or not it is necessary to measure all of the possible input–output combinations and why it is possible to obtain mode shapes from only one row or column of the frequency response function matrix.

1.2.1 Why is Only One Row or Column of the FRF Matrix Needed?

It is very important for us to understand how we arrive at mode shapes from the measurements in the frequency response function matrix. Without getting mathematical just yet, let's discuss this; the math will come later in the theoretical development of the equations.

Let's just take a look at the third row of the frequency response function matrix and concentrate on the first mode (in blue). Examining the peak amplitude of the imaginary part of the frequency response function for each FRF, the first mode shape for mode 1 is as shown in Figure 1.10a. It therefore seems fairly straightforward to extract the mode shape from measured data. A quick approach is just to measure the peak amplitude of the frequency response

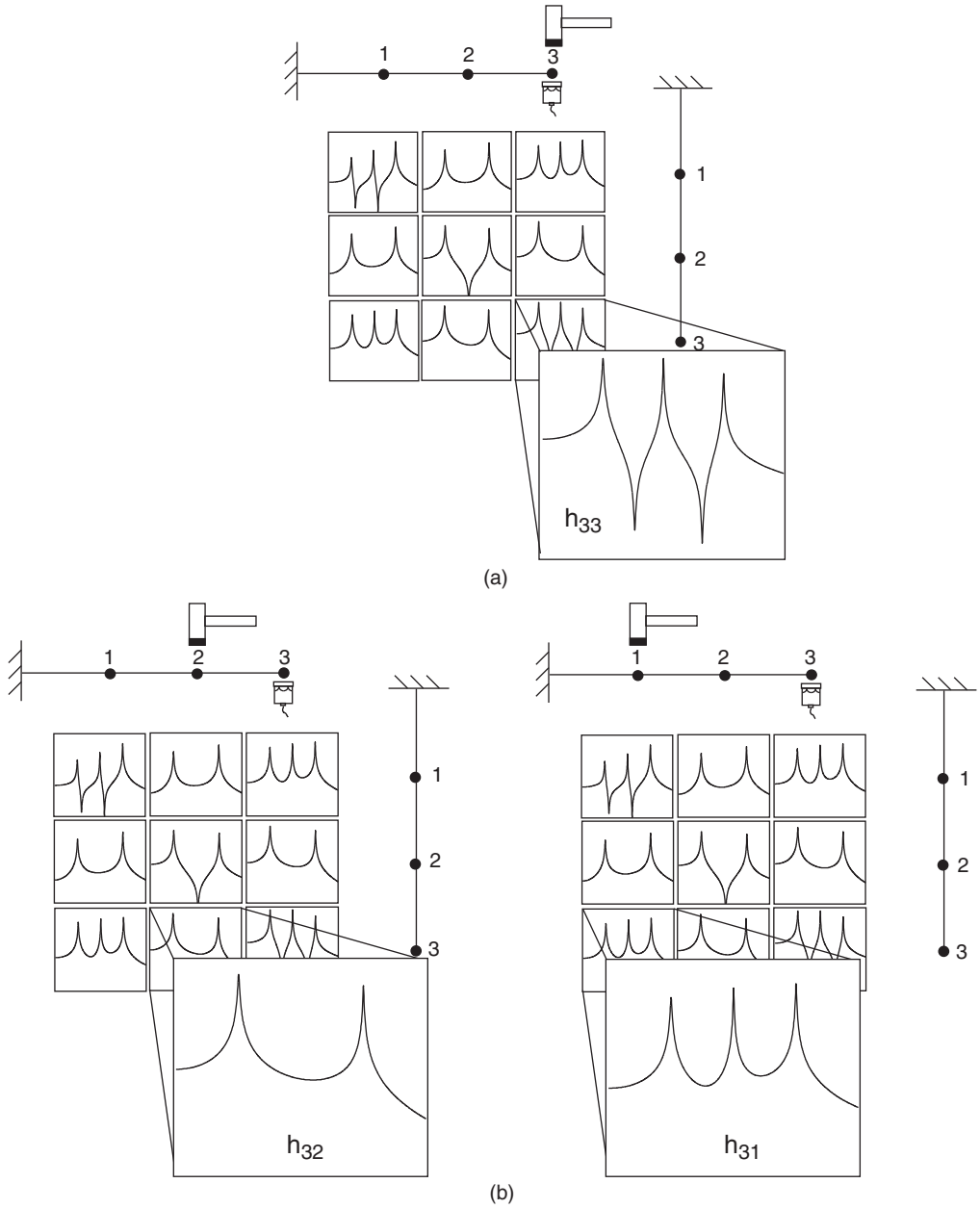

Figure 1.9 3DOF beam: (a) drive point FRF (magnitude) for reference 3; (b) cross FRFs (magnitude) for Reference 3.

function for a number of different measurement points. Clearly, the first bending deformation pattern for the first mode (in blue) is seen from these amplitudes at each of the three points.

So the measurement in Figure 1.10a was taken with the accelerometer stationary at point 3 as we impacted all three points. But if we had the accelerometer positioned at point 2 then we would collect the data in row two of the matrix as we impacted each of the points. Now look at the second row of the frequency response function matrix and concentrate on the first

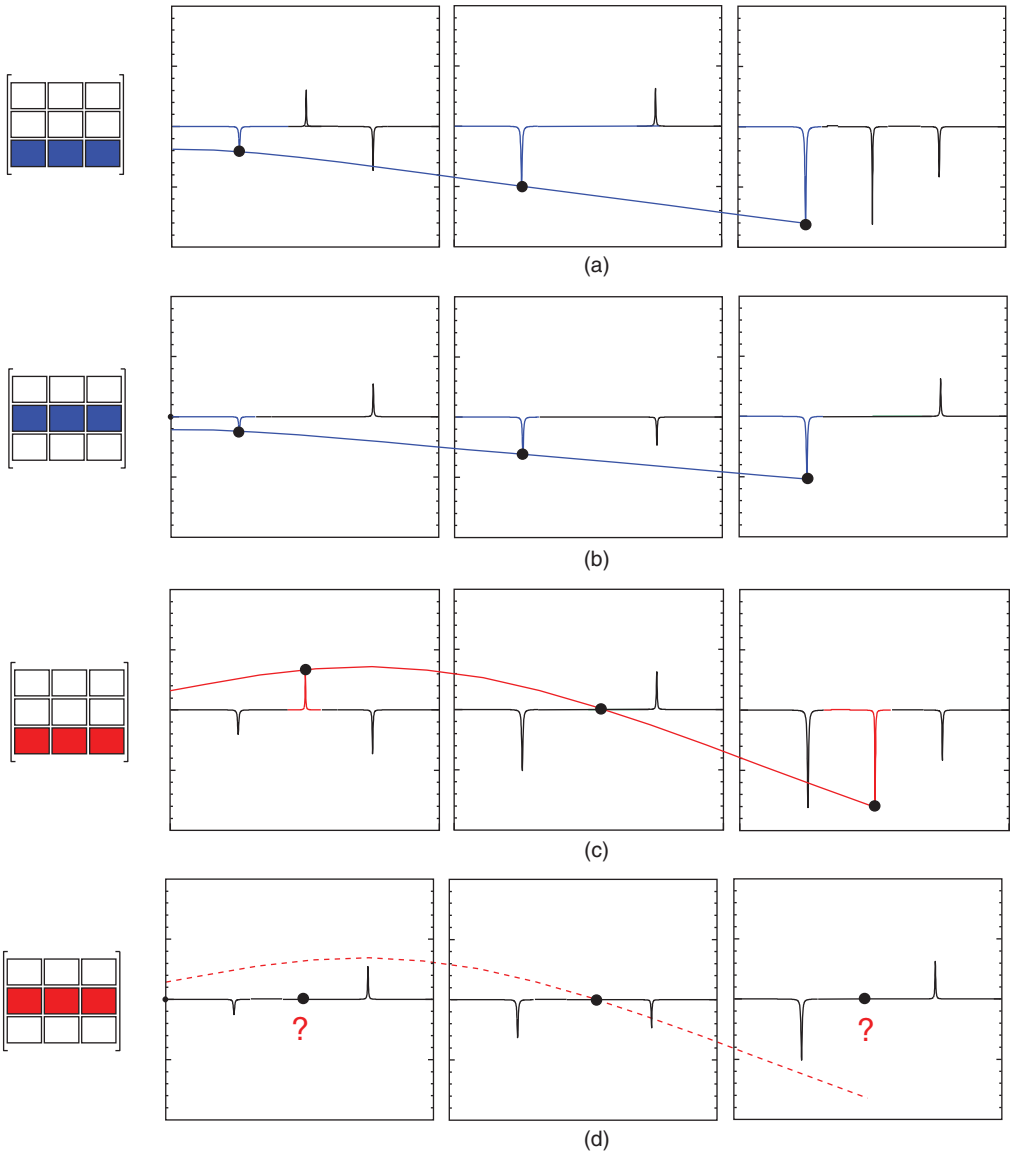

Figure 1.10 3DOF beam: (a) Mode 1 from third row of frequency response matrix; (b) Mode 1 from second row of frequency response matrix; (c) Mode 2 from third row of frequency response matrix; (d) Mode 2 from second row of frequency response matrix.

mode (Figure 1.10b). The first mode shape of mode 1 (in blue) can easily be seen in the peak amplitudes of the imaginary part of the frequency response function; mode 1 can be seen from this row also. Again, the deformation pattern for the first mode (in blue) is clearly seen from these amplitudes at each of the three points. But one important thing to note is that all of the amplitudes are lower from the second row when compared to the third row of the frequency response function matrix.

We could also look at the first row of the frequency response function matrix and see the same shape. This is a very simple pictorial representation of what the theory indicates. We can use

any row to describe the mode shape of the system. So it is very obvious that the measurements contain information pertaining to the mode shapes of the system.

Let's now take a look at the third row again and concentrate on mode 2, in red, (Figure 1.10c). Again if I look at the peak amplitude of the imaginary part of the frequency response function, I can easily see the second bending mode shape for mode 2 (in red) in the peak amplitudes of the imaginary part. Clearly, the deformation pattern for the second mode (in red) is seen from these amplitudes at each of the three points.

Now if I look at the second row of the frequency response function matrix (as we did for mode 1) and concentrate on the second mode, I will be a little surprised because there is no amplitude for the second mode shown in Figure 10d. I wasn't expecting this but if we look at the mode shape for the second mode then we can quickly see that this is a node point for mode 2. The reference point is located at the node of the mode and the peak amplitude of the imaginary part of the frequency response function is zero. The second mode cannot be observed from this reference location on the beam (this is actually expected).

So this reveals a very important aspect of modal analysis and the experimental measurements we collect during a modal test. The reference point cannot be located at the node of a mode, otherwise that mode will not be seen in the frequency response function measurements and the mode cannot be obtained. Later, in our theoretical analysis, this will be very clear.

Now we have only used three measurement points to describe the modes for this simple beam. If we add more input–output measurement locations then the mode shapes can be seen more clearly. Figure 1.11 shows 15 measured frequency response functions and the three measurement points used in the discussion above are highlighted. This figure shows the 15 frequency response functions in a waterfall style plot. Using this type of plot, it is much easier to see that the mode shapes can be determined by looking at the peaks of the imaginary part of the frequency response function. The theory involved is explained in other chapters. In the figure, mode 1 is in blue, mode 2 in red, and mode 3 in green; this color scheme will be used throughout this book.

Now the measurements that we have discussed thus far have been obtained from an impact testing consideration. What if the measured frequency response functions come from a shaker test?

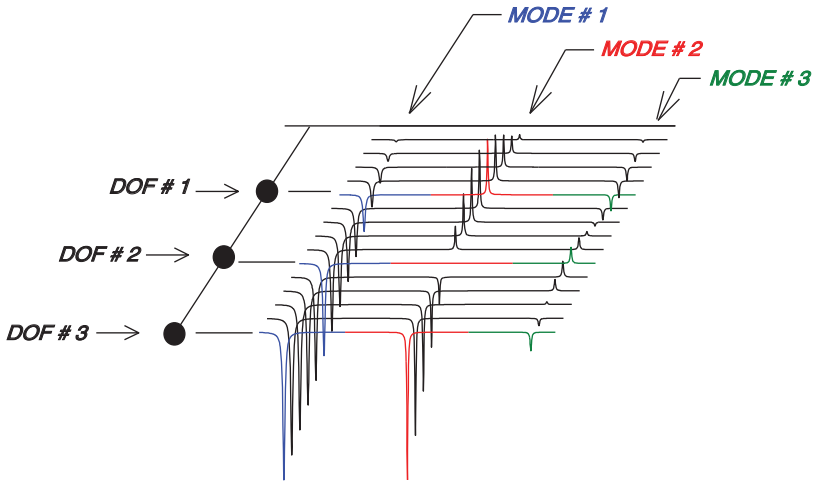

Figure 1.11 Waterfall plot of 3DOF beam frequency response functions.

1.3 What's the Difference between a Shaker Test and an Impact Test?

From a theoretical standpoint, it doesn't matter whether the measured frequency response functions come from a shaker test or an impact test. Figures 1.12a and b show the measurements that are obtained from an impact test and a shaker test of the 3DOF beam. A roving

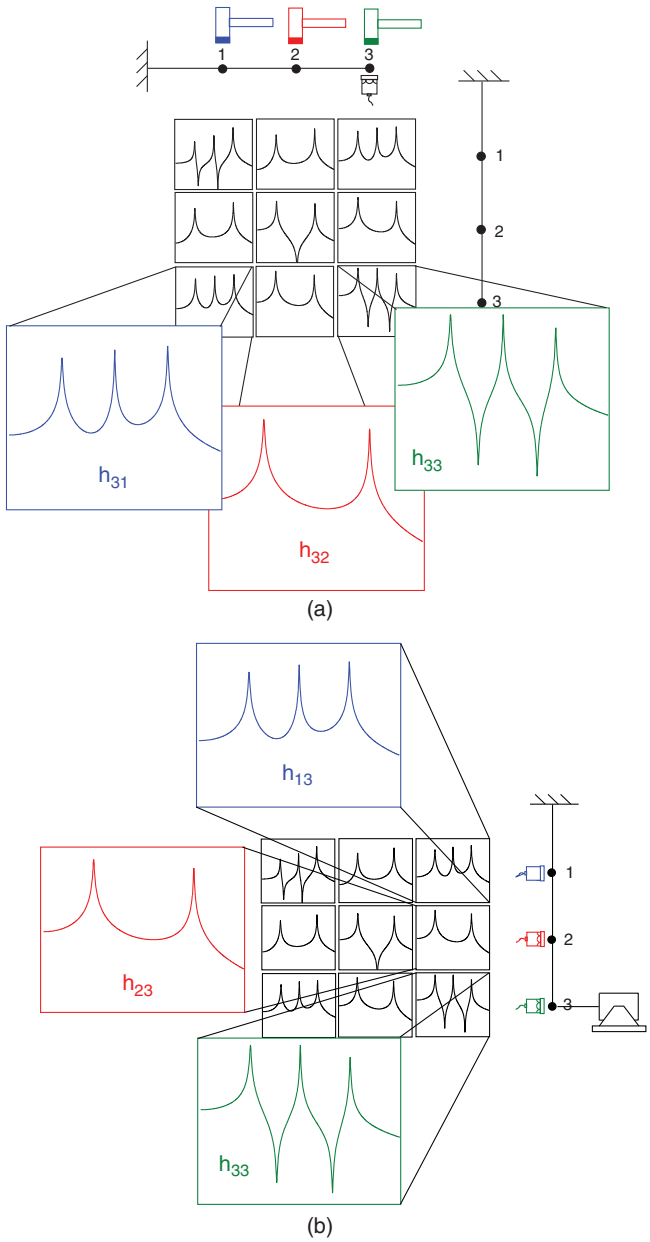

Figure 1.12 Test scenarios for frequency response matrix for the 3DOF beam. (a) roving impact hammer test, (b) shaker test.

impact hammer test generally results in completing one of the *rows* of the frequency response function matrix, whereas the shaker test generally results in measuring one of the *columns* of the frequency response function matrix. Because the matrices describing the system are square symmetric, the reciprocity characteristic is true. It is very important to note that the stationary accelerometer reference will be related to a row of the frequency response matrix whereas a stationary force reference will be related to a column of the frequency response matrix. For the case shown in Figure 1.12, the third row is exactly the same as the third column, for instance.

Theoretically, there is no difference between a shaker test and an impact test. If pure forces can be applied to a structure without any interaction between the applied force and the structure and the response is measured with a massless transducer that has no effect on the structure, then this is true. But what if it is not the case?

Well let's think about performing the test from a practical standpoint. The point is that shakers and response transducers generally do have an effect on the structure during the modal test. The main point to remember is that the structure under test is not just the structure for which you would like to obtain modal data; it is the structure plus everything involved in the acquisition of the data: the structure suspension, the mass of the mounted transducers, the potential stiffening effects of the shaker/stinger arrangement, and so on. So while theory tells us that there shouldn't be any difference between the impact test results and the shaker test results, often there will be differences due to the practical aspects of collecting data; later in the text there will be examples to illustrate this.

The most obvious difference will occur as a result of the roving of accelerometers during a shaker test. The weight of the accelerometer may be extremely small relative to the total weight of the whole structure, but its weight may be quite large relative to the effective weight of different parts of the structure, particularly in multi-channel systems where many accelerometers are moved around the structure in order to acquire all the measurements. This can be a problem, especially on lightweight structures. One way to correct for this problem is to mount all of the accelerometers on the structure even though only a few are used at a time. Another way is to add dummy accelerometer masses at locations that are not being measured; this will minimize the roving mass effect.

Another difference is due to shaker/stinger effects. The modes of the structure may be affected by the mass and stiffness effects of the shaker attachment, which may exist even if efforts are made to minimize them. The purpose of the stinger is to uncouple the effects of the shaker from the structure. However, on many structures, the effects of the shaker attachment may be significant. Because an impact test does not suffer from these problems, different results may be obtained. So while theory says that there is no difference between a shaker test and an impact test, there are some very basic practical aspects that may cause some differences. The subsequent chapters have more detail and depth on this.

1.3.1 What Measurements do we Actually make to Compute the FRF?

The most important measurement that is needed for experimental modal analysis is the frequency response function. Very simply stated, this is the ratio of the output response to the input excitation force. This measurement is typically acquired using a dedicated instrument such as an FFT analyzer or a data acquisition system with software that performs the FFT.

Let's briefly discuss some of the basic steps that occur in the acquisition of data to obtain the frequency response function. First, there are analog signals that are obtained from the measuring devices. These analog signals must be filtered to ensure that there is no aliasing of higher

frequencies into the analysis frequency range. This is usually done through the use of a set of analog filters on the front end of the analyzer. These are called anti-aliasing filters. Their function is to remove any high frequency signals that may exist in the signal. Good, high-quality phase-matched anti-aliasing filters contribute to the higher costs of FFT analyzers compared to the much cheaper analog-to-digital converters (ADCs).

The next step is to digitize the analog signal to form a digital representation of the actual signal. This is done by the analog to digital converter that is called the ADC. Typically, this digitization process will use 12, 16 or 24 bit converters; the more bits available, the better the resolution in the digitized signal. Some of the major concerns lie in the sampling and quantization errors that could potentially creep into the digitized approximation. The sampling rate controls the resolution in the time and frequency representation of the signals. Quantization is associated with the accuracy of the magnitude of the captured signal. Both sampling and quantization can cause errors in the measured data but are not nearly as significant and devastating as the worst of all the signal processing errors, namely leakage.

Leakage occurs in the transformation of time data to the frequency domain using the FFT. The FFT process requires that the sampled data consist of a complete representation of the data for all time or that it contain a periodic repetition of the measured data. When this is satisfied, then the FFT produces a true representation of the data in the frequency domain. However, when this is not the case, then leakage will cause a serious distortion of the data in the frequency domain. In order to minimize the distortion due to leakage, weighting functions called "windows" are used to make the sampled data better satisfy the periodicity requirement of the FFT. While the use of windows greatly reduces the leakage effect, it cannot be completely removed. There are many windows that can be used for general signal processing, but there are only a few that are commonly used for experimental modal testing. These windows are discussed in more depth in the signal processing chapter.

Once the data has been sampled, the FFT is computed, so as to form linear spectra of the input excitation and output responses. Typically, averaging is performed on power spectra obtained from the linear spectra. The main averaged spectra computed are the input power spectrum, the output power spectrum and the cross spectrum between the output and input signals. These functions are averaged and used to compute two important functions that are used for modal data acquisition: the frequency response function and the coherence. The coherence function is used as a data quality assessment tool, by determining how much of the output signal is related to the measured input signal. The frequency response function contains information regarding the system frequency and damping and a collection of frequency response functions contains information regarding the mode shape of the system at the measured locations. This is the most important measurement in experimental modal analysis. An overview of these steps is shown in Figure 1.13, which shows the steps in the measurement process from an input to a system to the resulting output from the system. These are the acquisition of the signal, filtering to prevent aliasing, digitization of the signal, windowing (if needed), the FFT to form linear spectra, followed by the averaging of power spectra and the computation of the frequency response function and coherence.

Of course, there are many important aspects to measurement acquisition – averaging techniques to reduce noise and so on – that are discussed more in the signal processing chapters. Any good reference on digital signal processing will also provide assistance in this area. Now the input excitation needs to be discussed next. There are two commonly used types of excitation for experimental modal analysis: impact excitation and shaker excitation.

Now let's consider some of the testing considerations when performing an impact test.

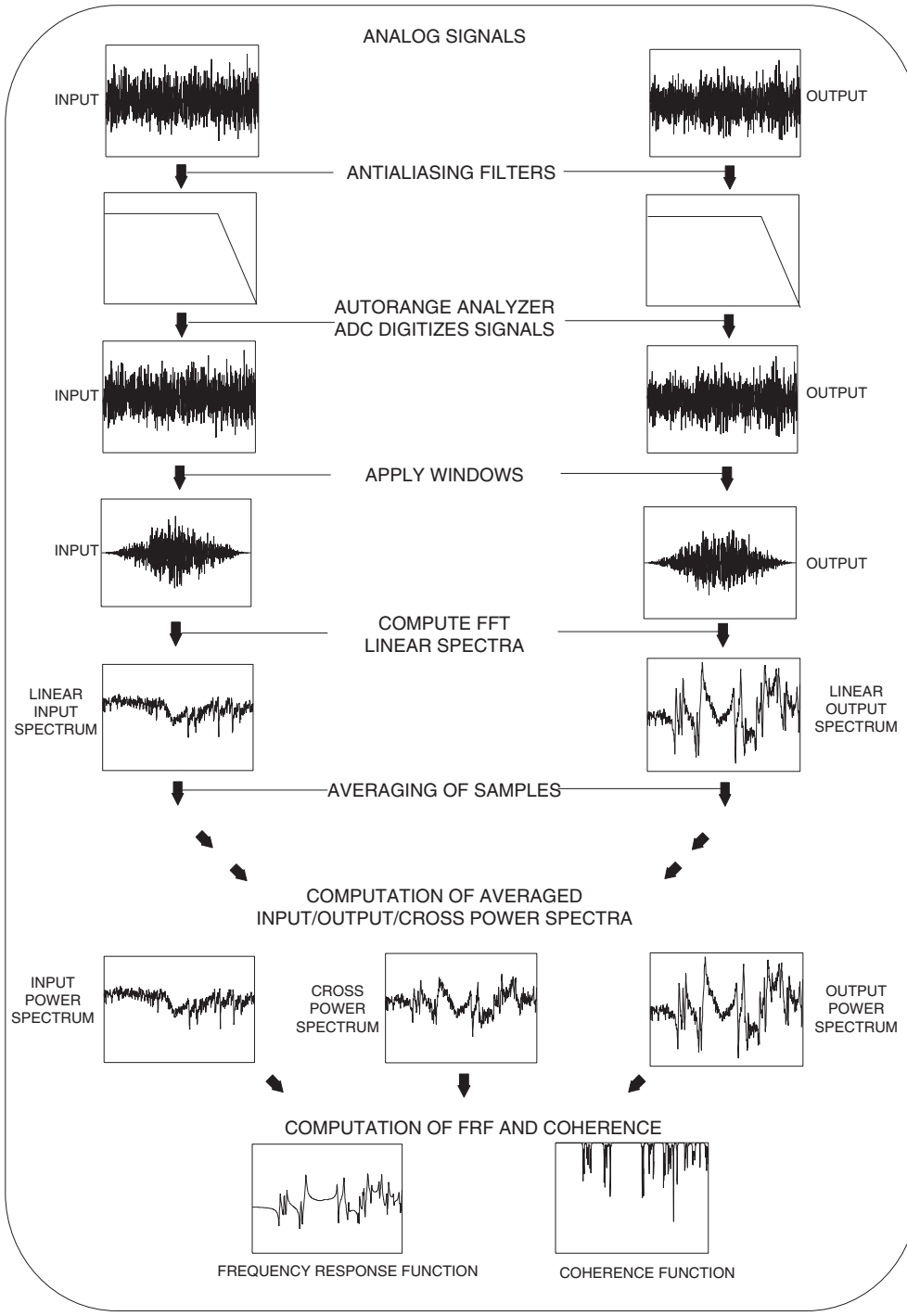

Figure 1.13 Anatomy of an FFT analyzer for typical experimental modal test measurements.

1.4 What's the Most Important Thing to Think about when Impact Testing?

There are many important considerations when performing impact testing. Only two of the most critical items will be mentioned here; a detailed explanation of all the aspects of impact testing is presented in the impact chapter and the applications of impact testing are described throughout this book.

First, the selection of the hammer tip can have a significant effect on the measurement acquired. The input excitation frequency range is controlled mainly by the hardness of the tip selected. The harder the tip, the wider the frequency range that is excited by the excitation force; the softer the tip, the narrower the frequency range excited. This is a general statement, but there can be exceptions to this rule and these are discussed in detail later. But basically, the tip needs to be selected such that all the modes of interest are excited by the impact force over the frequency range to be considered. If too soft a tip is selected, then not all the modes will be adequately excited, preventing a good measurement from being obtained (Figure 1.14a). The input power spectrum does not excite all of the frequency range, as evidenced by the roll off of the power spectrum; the coherence is also seen to deteriorate, as well as the frequency response function over the second half of the frequency range. However, this measurement may not be a problem if we are only interested in the first half of the frequency spectrum shown. Typically, we strive to have a fairly good and relatively flat input excitation forcing function, as seen in Figure 1.14b. The frequency response function is measured much better, as evidenced by the much improved coherence function. When performing impact testing,

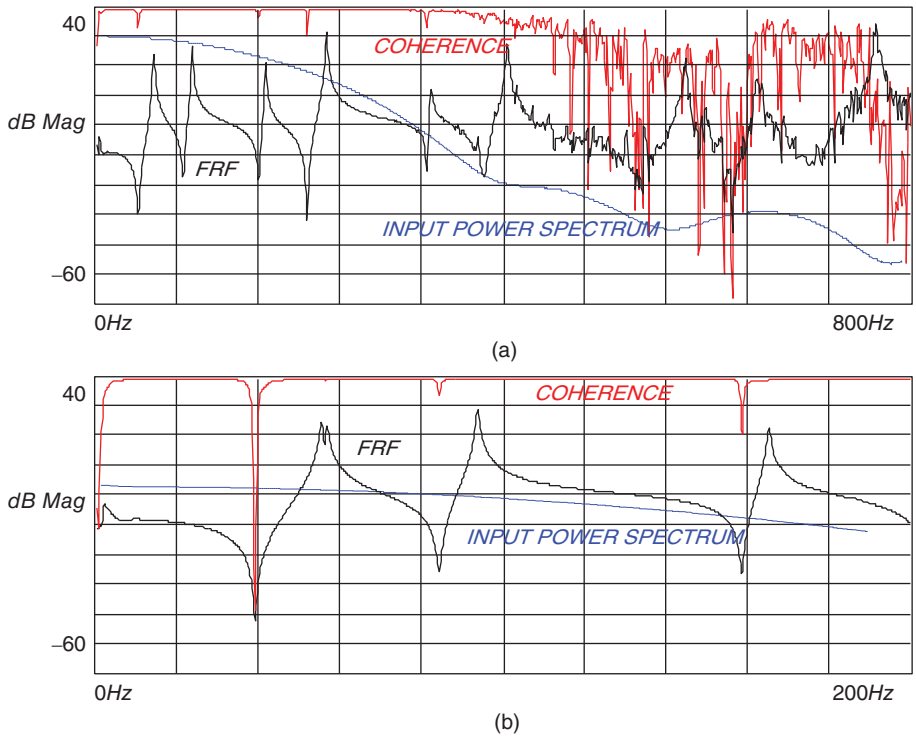

Figure 1.14 Hammer tip choice: (a) hammer tip insufficient to excite all modes; (b) hammer tip adequate to excite all modes.

care must be taken to select a suitable tip, so that all the modes are excited well and a good frequency response measurement is obtained. It typically requires a few iterations in order to achieve acceptable results for a particular measurement scenario.

The second most important aspect of impact testing is the use of a window for the response transducer. Generally, for lightly damped structures, the response to the impact excitation will not die down to zero by the end of the sample interval. When this is the case, the transformed data will suffer significantly from a digital signal processing effect referred to as leakage.

To minimize leakage, a weighting function referred to as a window is applied to the measured data. This window is used to force the data to better satisfy the periodicity requirements of the FFT process, thereby minimizing the distortion effects of leakage. For impact excitation, the most common window used on the response transducer measurement is the exponentially decaying window. The implementation of this window to minimize leakage is shown in Figure 1.15. The exponential window is one way to minimize leakage, but there are also others, as discussed in the impact excitation chapter and the applications sections.

Windows themselves cause some distortion of the data and should be avoided whenever possible. For impact measurements, two alternative ways to always consider are the selection of a narrower bandwidth for measurements and to increase the number of spectral lines of resolution. Both of these signal processing parameters have the effect of increasing the amount of time required to acquire a measurement. These will both tend to reduce the need for the use of an exponential window and should always be considered to reduce the effects of leakage. Impact testing is covered extensively in the chapter on impact testing and applications.

Now let's consider some of the testing considerations when performing a shaker test.

1.5 What's the Most Important Thing to Think about when Shaker Testing?

As with impact testing, there are many important considerations when performing shaker testing, but the most important is the use of excitation signals that minimize the need for windows or eliminate the need for windows altogether. There are many other important considerations, however, a detailed explanation of these is contained in the chapter on shaker testing.

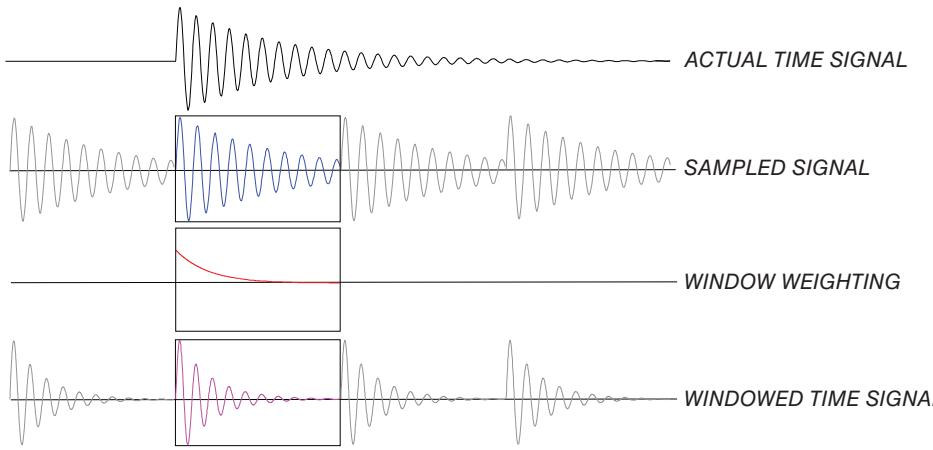

Figure 1.15 Exponentially decaying window to minimize leakage effects.

One of the more common excitation techniques used today is random excitation. This is due to its ease of implementation, but because of the nature of this excitation signal, leakage is a critical concern and a Hanning window is commonly employed. However, the leakage effect when random excitation is used is serious and causes distortion of the measured frequency response function even when windows are used. A typical random excitation signal with a Hanning window is shown in Figure 1.16. As seen in the figure, the Hanning window weighting function helps to make the sampled signal appear to better satisfy the periodicity requirement of the FFT process, thereby minimizing the potential distortion effects of leakage. While this reduces the distortion of the frequency response function due to leakage, the window will never totally remove these effects; the measurements will still contain some distortion effects due to leakage.

Two very common excitation signals are known as burst random and sine chirp. Both have the special characteristic that they do not require windows to be applied to the data because the signals are inherently leakage free in almost all testing situations. They are relatively simple to employ and are found on most signal analyzers available today. The two signals are shown schematically in Figures 1.17 and 1.18.

In the case of burst random excitation, the periodicity requirement of the FFT process is satisfied because the entire transient excitation and response are captured in one sample interval of the FFT. For the sine chirp excitation, the repetition of the signal over the sample interval satisfies the periodicity requirement. While other excitation signals also exist, these are the most common ones in use in modal testing today. Much more detail on shaker testing and excitation signals is discussed in the chapter related to shaker testing and applications. So now we have a better idea how to make some measurements.

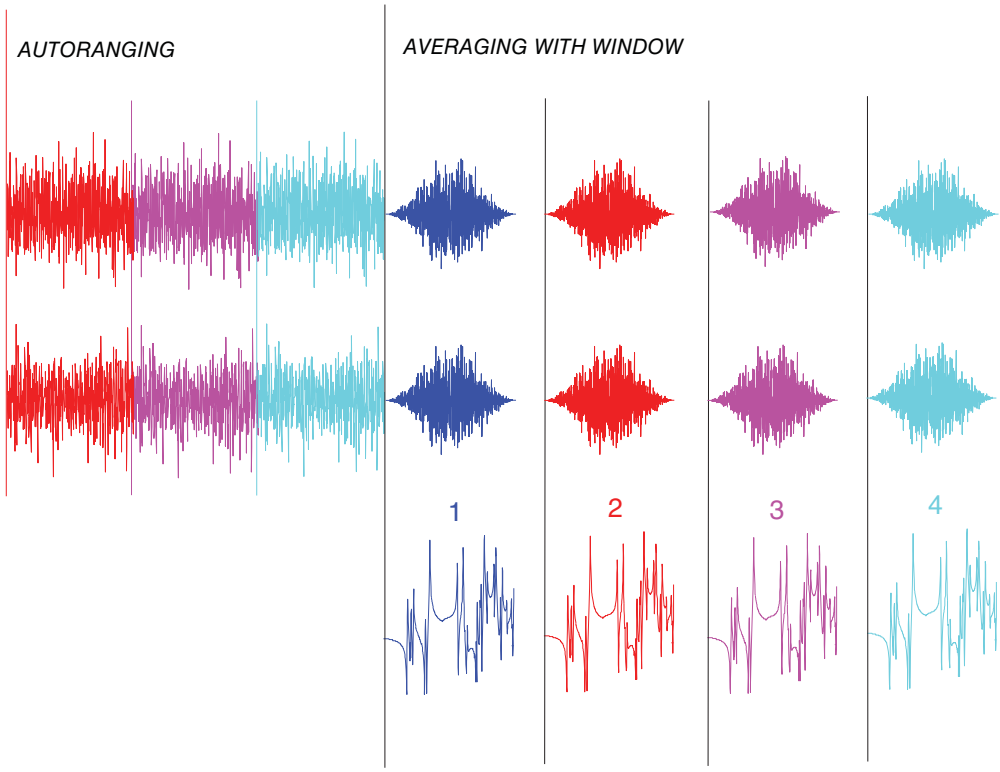

Figure 1.16 Shaker testing: random excitation with Hanning window.

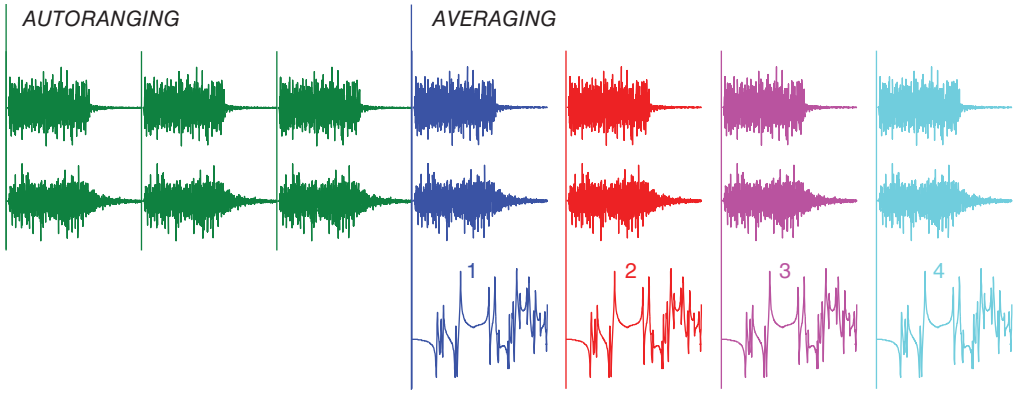

Figure 1.17 Burst random excitation without a window.

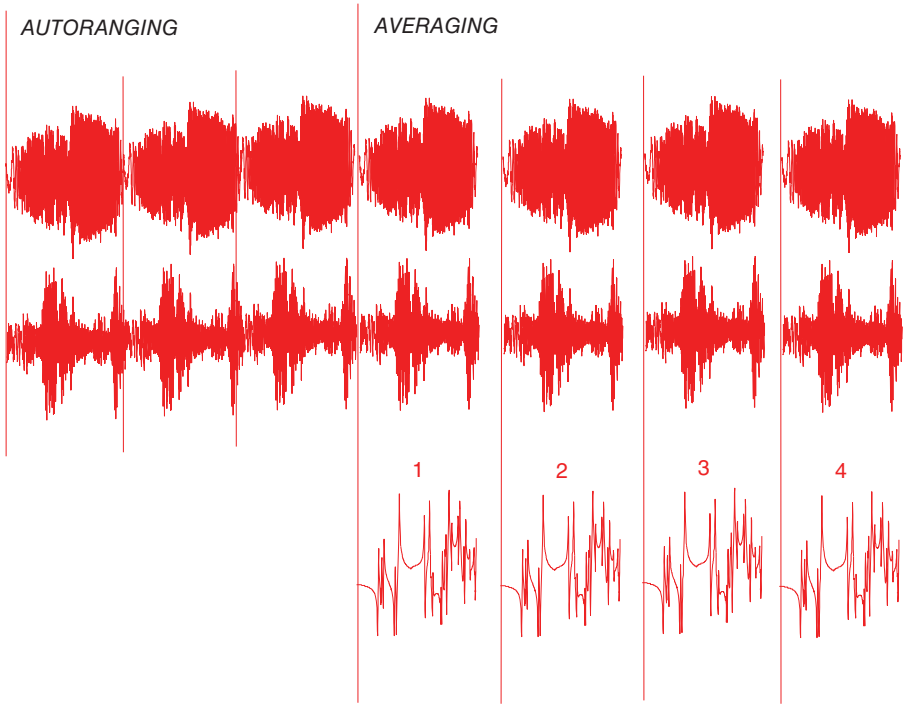

Figure 1.18 Sine chirp excitation without a window.

1.6 Tell me More About Windows; They Seem Pretty Important!

Windows are, in many measurement situations, a necessary evil. While it would be preferable to use no windows at all, the alternative of leakage is definitely not acceptable either. As discussed above, there are a variety of excitation methods that can be used to provide leakage free measurements and which do not require the use of any window. However, there are many times, especially when performing field testing and collecting operating data, where the use of windows is necessary.

So what are the most common windows used? Basically, the most common windows used today are the uniform, Hanning, flat top and force/exponential windows. Rather than detail all these, let's just simply state when each is used for experimental modal testing. More discussion on windows is contained in the signal processing and measurements chapters.

The uniform window (which is also referred to as the rectangular window, boxcar or no window) is a unity-gain weighting function that is applied to all the digitized data points in one sample or record of data. It is applied to data where the entire signal is captured in one sample or record of data or when the data is guaranteed to satisfy the periodicity requirement of the FFT process. This window can be used for impact testing where the input and response signals are totally observed in one sample of collected data. This window is also used when performing shaker excitation tests with, for example, burst random, sine chirp, pseudo-random, or digital stepped sine excitation signals, all of which generally satisfy the periodicity requirement of the FFT process.

The Hanning window is a cosine shaped weighting function (that is, bell-shaped) that forces the beginning and end of the sample interval to be heavily weighted to zero. It is useful for signals that generally do not satisfy the periodicity requirement of the FFT process. Random excitations and general field signals usually fall into this category and therefore require the use of a window such as the Hanning window.

The flat top window is most useful for sinusoidal signals that do not satisfy the periodicity requirement of the FFT process. Most often this window is used for calibration purposes or when there is a constant speed excitation.

The force and exponential windows are typically used when using impact excitation. The force window is a unity-gain window that acts over a portion of the sample interval in which the impulsive excitation occurs. The exponential window is used when the response signal does not die out within the sample interval. The exponential window is applied to force the response to better satisfy the periodicity requirement of the FFT process.

Each of the windows has an effect on the frequency representation of the data. In general, the windows will cause a degradation in the accuracy of the peak amplitude of the function and will suggest more damping than really exists. While these errors are not totally desirable, they are far more acceptable than the significant distortion that results from leakage. The chapter on signal processing and measurement definition has much more in depth material related to this.

1.7 So how do we get Mode Shapes from the Plate FRFs?

So now that we have discussed various aspects of acquiring measurements, let's take several measurements on the plate structure discussed at the start of this chapter. Let there be six measurement locations on the plate. Now there are six possible places where forces can be applied to the plate and six possible places where we can measure the responses. This means that there are a total of 36 possible input–output measurements that could be taken. The frequency response function describes how the force applied to the plate causes the plate to respond. If we apply a force to point 1 and measured the response at point 6, then the transfer relation between 1 and 6 describes how the system behaves for this measurement (Figure 1.19).

Now if we were to take six measurements on the plate, then we could go through the same simple peak picking process as we did for the beam in Section 1.2. If we evaluate the first mode and look at the imaginary part of the frequency response function and evaluate the peaks for mode 1 (in blue), as shown in Figure 1.20, then we would see that points 1 and 2 both have −1 amplitude, as do points 5 and 6, but points 3 and 4 have an equal +1 amplitude. From these six points it can be seen that this is really a first bending mode of the plate. Of course, all 45

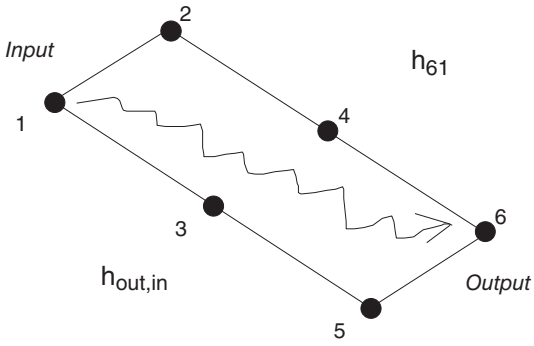

Figure 1.19 Input–output measurement locations.

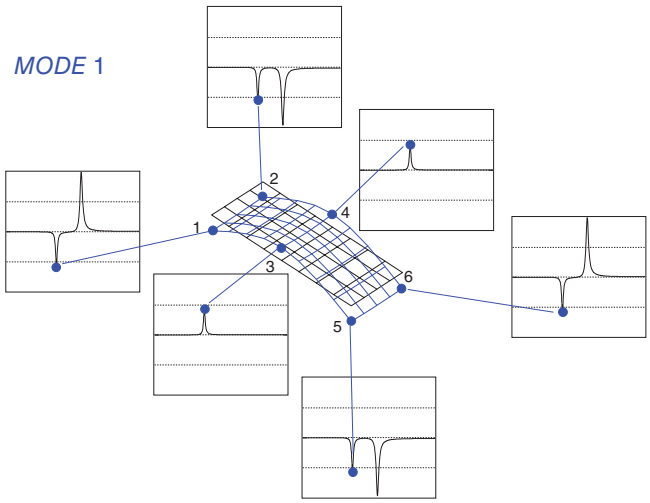

Figure 1.20 Plate mode shapes for Mode 1: peak pick of FRF.

points are shown in this figure, revealing the resulting mode shape for mode 1; showing all the measurements would be cumbersome and would clutter the figure, rendering it useless. But clearly the trend of the measurements would map out the first bending mode of the plate (in blue).

If we then move on to the second mode in red (Figure 1.21), we could also look at the peak amplitude of the imaginary part of the frequency response function. Point 1 is shown to have +2 units of amplitude, and point 2 has −2 units of amplitude. At the other end of the plate, point 5 has −2 units of amplitude and point 6 has +2 units of amplitude. This suggests that this is a torsional mode of the plate, which is confirmed when all 45 points are shown. However, it is very important to note that points 3 and 4 have no amplitude, which implies that these are node points, as indicated by the mode shape.

While the peak pick technique is adequate for very simple structures, mathematical algorithms are typically used to estimate the modal characteristics from measured data. The modal parameter estimation phase, which is often referred to as curvefitting, is implemented using computer software to simplify the extraction process. The basic parameters that are extracted from the measurements are the frequency, damping, and mode shapes, known collectively as the dynamic characteristics. The measured frequency response function is broken down into many single DOF (SDOF) systems, as shown in Figure 1.22. The upper portion of the figure shows the magnitude of a typical frequency response function and the lower portion shows

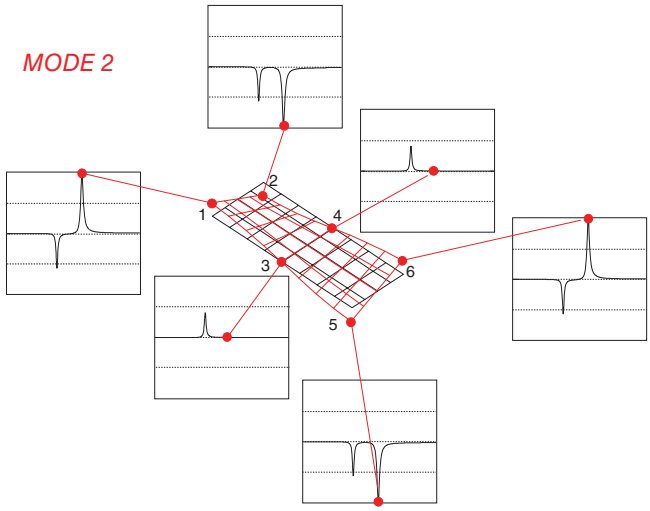

Figure 1.21 Plate mode shapes for Mode 2: peak pick of FRF.

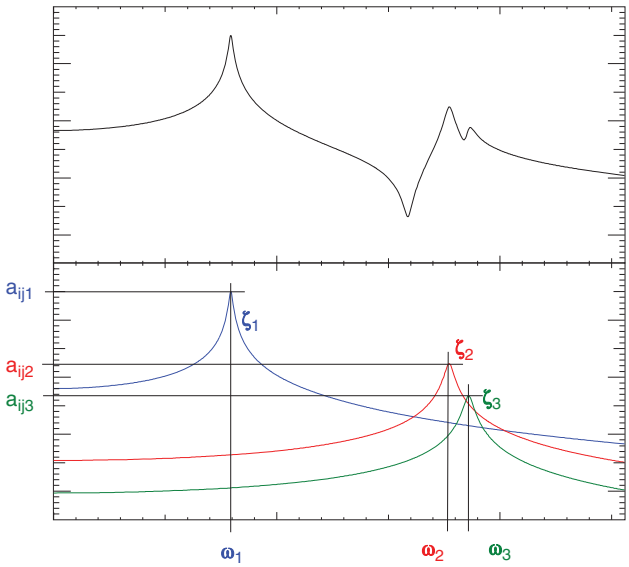

Figure 1.22 Breakdown of a frequency response function.

the magnitude of the frequency response function of each of the individual single degree of freedom (SDOF) systems that form the frequency response function in the upper plot. In fact, the modal parameter estimation process is intended to decompose the measured frequency response function into the basic fundamental or primary parts that make up the measurement. These are the frequency, damping, and mode shape for the structure. The main job for the structural test engineer is to acquire measurements that characterize the overall combined response and to convert or decompose all the data acquired into the primary information that is embedded in it.

These curvefitting techniques use a variety of different methods to extract data. Some techniques employ time domain data while others use frequency domain data. The most

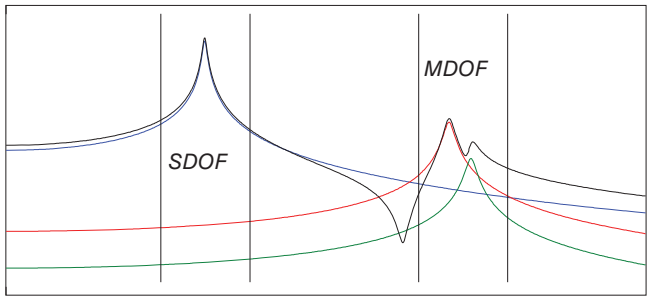

Figure 1.23 Curvefitting different bands using different methods.

common methods employ multiple mode analytical models but at times very simple single mode methods will produce reasonably good results, as shown in Figure 1.23. Again, it is very clear that the individual modes form the entire frequency response function measurement. All of the estimation algorithms attempt to break down measured data into the principal components that make up the measured data, namely the frequency, damping, and mode shapes.

The key inputs that the analyst must specify are the band over which data is extracted, the number of modes contained in the data, and the inclusion of residual compensation terms for the estimation algorithm. This is schematically shown in Figure 1.24. While the measurement to obtain the frequency response functions is a critical and sometimes a time consuming process, the extraction of modal parameters can also be tedious, especially when good measurements are not acquired. Generally, frequency response function data is fit over bands of the frequency range, in which several modes may be grouped. The identification of how many modes are

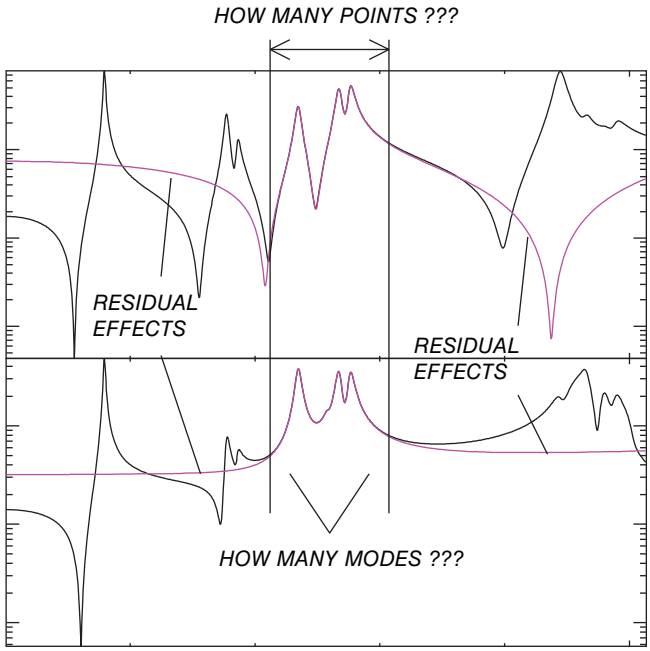

Figure 1.24 Curvefitting a typical FRF.

present in the band can be difficult in some situations, especially when the modes are extremely close together in frequency. Certain tools exist to help with this mode number determination.

Much more needs to be said concerning the estimation of modal parameters from measured data, the tools available for deciphering data, and the validation of the extracted model. A detailed explanation is contained in the chapter related to modal parameter estimation.

1.8 Modal Data and Operating Data

All structures respond to externally applied forces. But often the forces are not known or cannot be measured easily. We could still measure the response of a structural system even though the forces may not be measured. So the next question that is often asked concerns operating data.

1.8.1 What is Operating Data?

We first need to recognize that the system responds to the forces that are applied to the system (whether or not they can be measured). Assume that we know what the forces are. While the forces are actually applied in the time domain, there are some important mathematical advantages to describing the forces and response in the frequency domain. For a structure that is exposed to an arbitrary input excitation, the response can be computed using the frequency response function multiplied by the input forcing function. This is very simply shown in Figure 1.25. The excitation shown is a random excitation that excites all frequencies. The most important thing to note is that the frequency response function acts as a filter on the input force that results in some output response. The excitation shown causes all the modes to be activated and therefore the response is, in general, the linear superposition of all the modes that are activated by the input excitation.

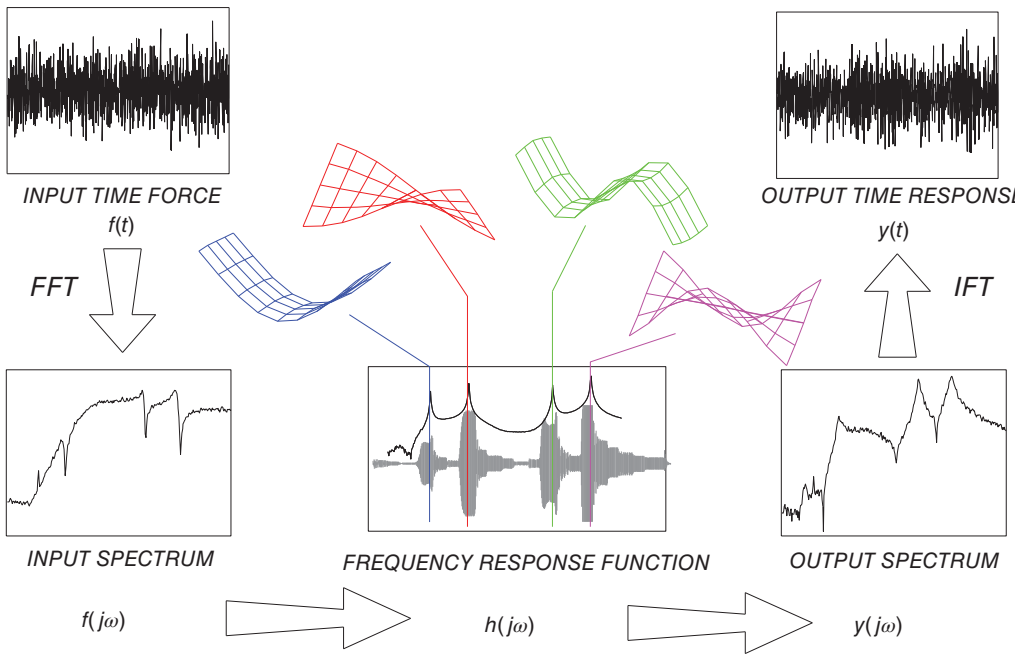

Figure 1.25 Schematic overview of the input–output structural response problem.

The excitation shown is a random excitation and the response is also random in nature, as seen in the time data in Figure 1.25. However, looking at this time data, it is very hard to determine what is dominating the response. Now if the response level was acceptable then there really wouldn't be a need to further evaluate the response. But if the response was unacceptable, then it would be very advantageous to look at what frequency or frequencies were causing the objectionable response. So by taking the FFT of the input and response signals, there is a much clearer picture as to what mode or modes may be causing the objectionable response. And looking at the output power spectrum, there are two peaks that seem to be much more dominant in the overall response. The actual deformation pattern would also be of interest, in order to understand what is happening.

Now what would happen if the excitation did not contain all frequencies but rather only excited one particular frequency (which is common in the case of constant rotating speeds, for instance)? In this case, it is very beneficial to understand the deformation pattern due to the forced response.

To illustrate this, let's use the simple plate again. Let's assume that there is some operating condition that exists for the system; a fixed frequency operating imbalance will be considered to be the excitation. It seems reasonable to use the same set of accelerometers that were on the plate to measure the response of the system. If we acquire data, we may see something that looks like the deformation pattern shown in Figure 1.26. Looking at this deformation, it is not very clear why the structure responds this way or what to do to change the response. Why does the plate behave in such a complicated fashion? It doesn't appear to be anything like any of the mode shapes that we measured before.

In order to understand this, let's take the plate and apply a simple sinusoidal input at one corner of the plate. For the example here, we are only going to consider the response of the plate assuming that only two modes are activated by the input. Of course there are more modes, but let's keep it simple to start with. The key to determining the response is the frequency response function between the input and output locations. Also, we need to remember that when we collect operating data, we don't measure the input force on the system and we don't measure the system frequency response function; we only measure the response of the system.

First let's excite the system with a sinusoidal signal that is very close to the first natural frequency of the plate structure. The response of the system for one frequency response function is shown in Figure 1.27. So even though we excite the system at only one frequency, we know that the frequency response function is the filter that determines how the structure will respond. We can see that the frequency response function is made up of a contribution from both mode

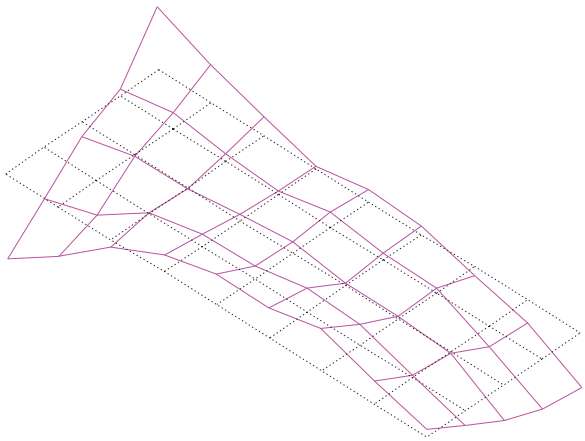

Figure 1.26 Measured operating displacements.

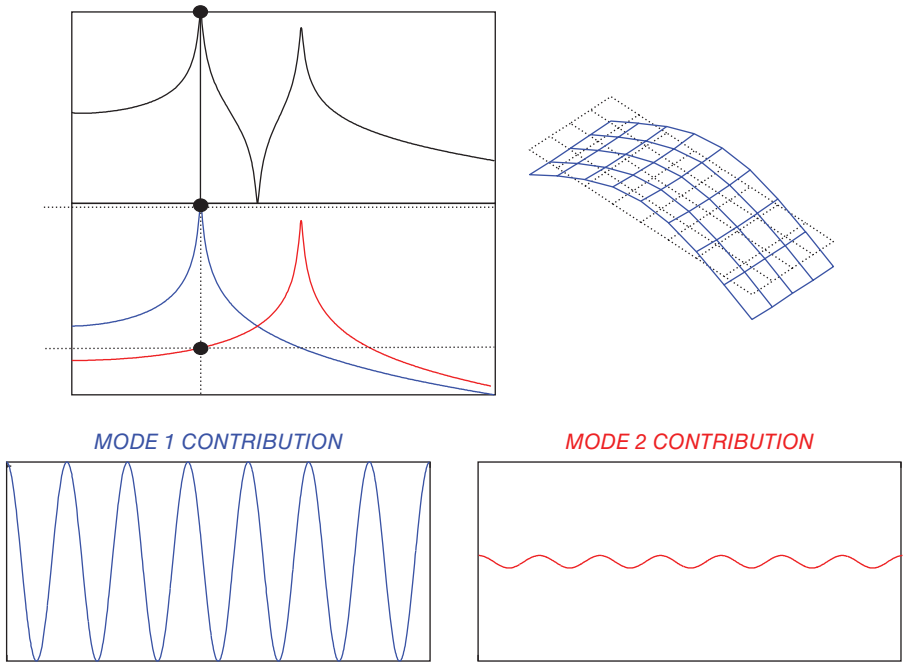

Figure 1.27 Excitation close to mode 1.

1 and mode 2. We can also see that the majority of the response, whether it is in the time or frequency domain, is dominated by mode 1. Now if we were to measure the response only at that one frequency and measure the response at many points on the structure, then the operating deflection pattern would look very much like mode 1, with a small contribution due to mode 2. Remember that with operating data, we never measure the input force or the frequency response function – we only measure the output response; the deformations that are measured are the *actual response* of the structure due to the input excitation, whatever it may be.

When we measure frequency response functions and estimate the modal parameters, we actually determine the contribution to the total frequency response function solely due to the effects of mode 1mode 1 acting alone (as shown in blue), and mode 2 acting alone (as shown in red), and so on for all the other modes of the system. Notice that with operating data, we only look at the response of the structure at one particular frequency – which is the linear combination of all the modes that contribute to the total response of the system. We can now see that the operating deflection pattern will look very much like the first mode shape if the excitation primarily excites mode 1.

Now let's excite the system very close to the second natural frequency. Figure 1.28 shows the same information as just discussed for mode 1. But now we see that we primarily excite the second mode of the system. Again, we must realize that the response looks like mode 2, but there is a small contribution from mode 1.

But what happens when we excite the system away from a resonant frequency. Let's excite the system at a frequency midway between mode 1 and mode 2. Here we see the real difference between modal data and operating data. Figure 1.29 shows the deformation shape of the structure.

At first glance, it appears that the deformation doesn't look like anything that we recognize, as displayed in the upper right corner of Figure 1.29. But if we look at the deformation pattern

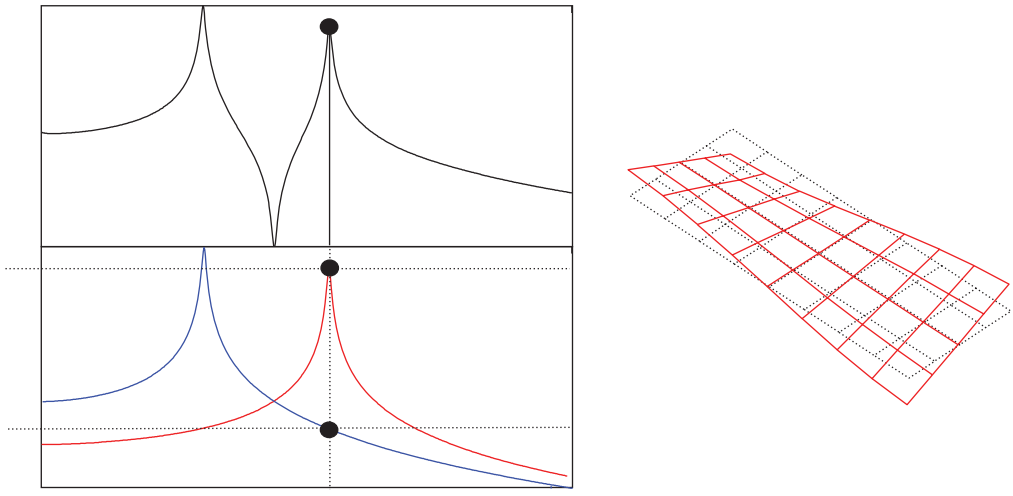

Figure 1.28 Excitation close to mode 2.

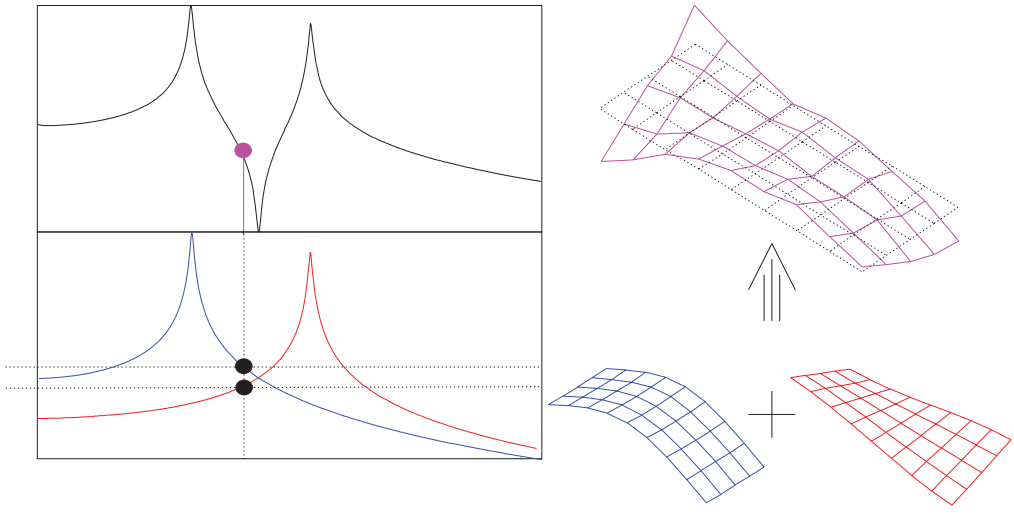

Figure 1.29 Excitation somewhere between mode 1 and mode 2.

long enough, we can actually see a little bit of the first bending and a little bit of first torsion patterns in the deformation. So the operating data is primarily a combination of the first and second mode shapes. (Yes, there will actually be other modes, but primarily modes 1 and 2 are the major participants in the response of the system.)

Now, we have discussed all of this by understanding the frequency response function contribution on a mode-by-mode basis. When we actually collect operating data, however, we don't collect frequency response functions but rather we collect output spectrums, from which it will not be very clear why the operating data looked like the mode shapes. Figure 1.30 shows an output spectrum measured at one location on the plate structure. Now the input applied to the structure is much broader in frequency, and many modes are excited. However, by understanding how each of the modes contributes to the operating data, it is much easier to see how each one contributes to the total response of the system.

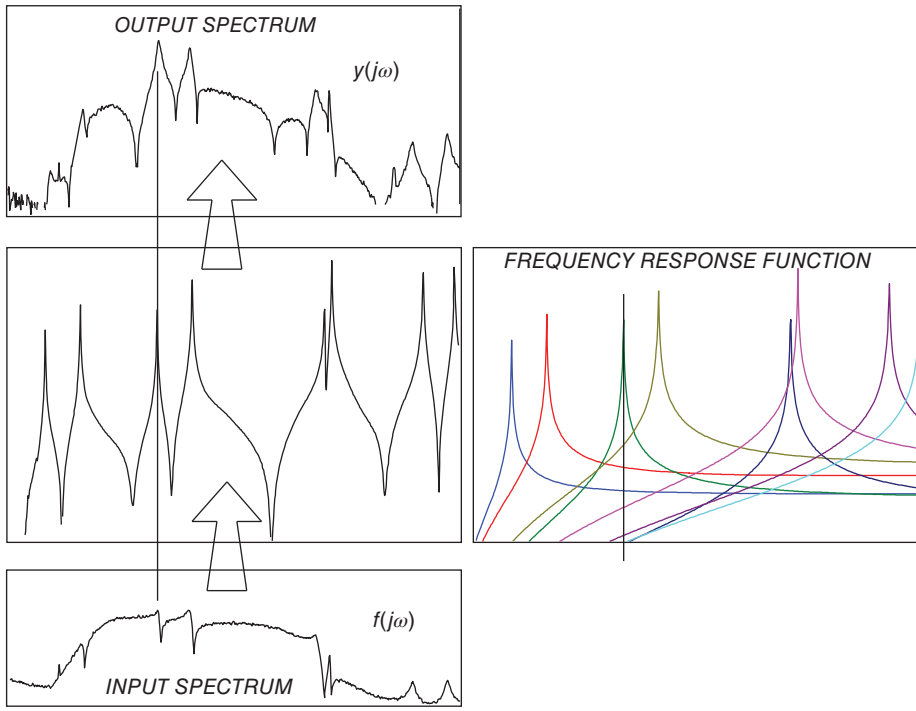

Figure 1.30 Broadband plate excitation.

So there is a big difference between operating deflections and mode shapes. We can now see that the modes shapes are summed together in some linear fashion to form the operating deflection patterns. However, typically we are interested in the total deformation or response of the system. Why even bother to collect modal data? It seems like a lot of work to acquire measurements and extract data.

1.8.2 So what Good is Modal Data?

Modal data is extremely useful in the design of almost any structure; the understanding and visualization of mode shapes is invaluable in the design process, helping to identify areas of weakness in the design. The development of a modal model is useful for simulation and design studies. One of these studies is called *structural dynamic modification* (SDM). This is a mathematical process that uses modal data (frequency, damping, and mode shapes) to determine the effects of changes in the system characteristics due to physical structural changes. These calculations can be performed without having to *physically* modify the actual structure until a suitable set of design changes is achieved. A schematic of the process is shown in Figure 1.31. There is much more that could be discussed concerning structural dynamic modification but is beyond the scope of this book.

In addition to structural dynamic modification studies, other simulations can be performed, for example force response simulations to predict system responses to applied forces. And another very important aspect of modal testing is the correlation and correction of an analytical model, such as a finite element model. These are a few of the more important aspects of the use of a modal model, which are schematically shown in Figure 1.32.

And one of the final questions that are often asked is which test is best to perform – a modal test or an operating test.

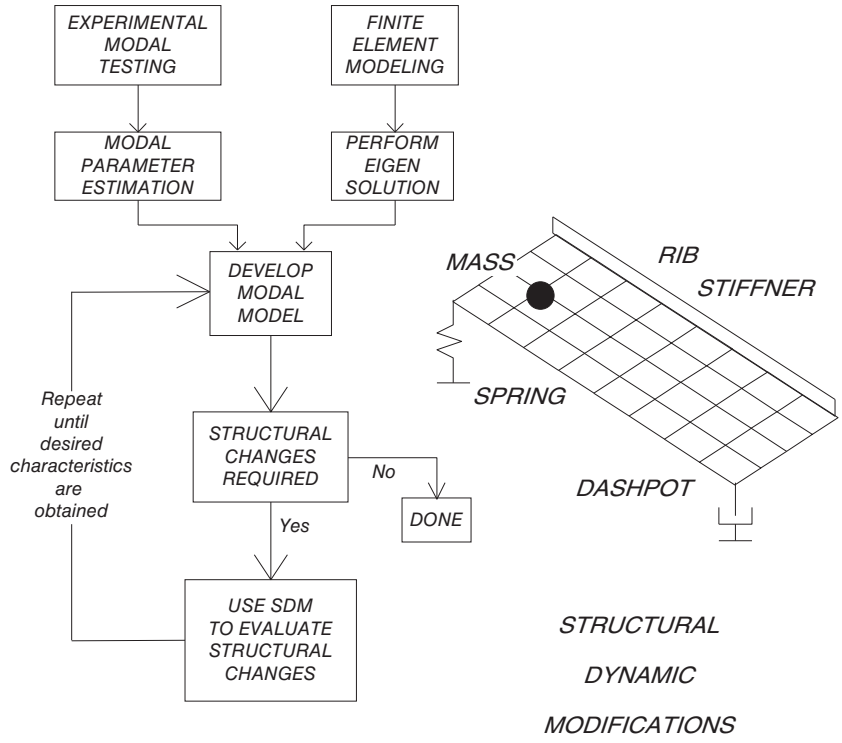

Figure 1.31 Schematic of the SDM process.

1.8.3 So Should I Collect Modal Data or Operating Data?

One of the other questions that is often asked is whether it is better to perform a modal test or an operating test. With tight schedules and budgets, it is debatable whether it is necessary to collect both modal data and operating data. This is always difficult to answer but it is always better to have both whenever possible. If only one of the two is available, then some engineering decisions may have to be made without full knowledge of the system characteristics. To summarize, let's point out the differences between each of the datasets.

Modal data requires that the force is measured, in order to determine the frequency response function and resulting modal parameters. Only modal data will give the true principal characteristics of the system. In addition, structural dynamic modifications and forced responses can only be studied using modal data (operating data cannot be used for these types of studies); Figure 1.33 shows this idea schematically. Moreover, correlation with a finite element model is best performed using modal data, but of course it needs to be clearly stated that modal data alone does not identify whether a structure is adequate for an intended service or application because modal data is independent of the forces on the system.

Operating data, on the other hand, is an actual depiction of how the structure behaves in service, as shown in Figure 1.34. This is extremely useful information, but the operating shapes are often confusing and do not necessarily provide clear guidance as to how to solve or correct an operating problem (and structural dynamic modification and response tools cannot be utilized on operating data).

The best situation is when both operating and modal data are used in conjunction to solve structural dynamic problems.

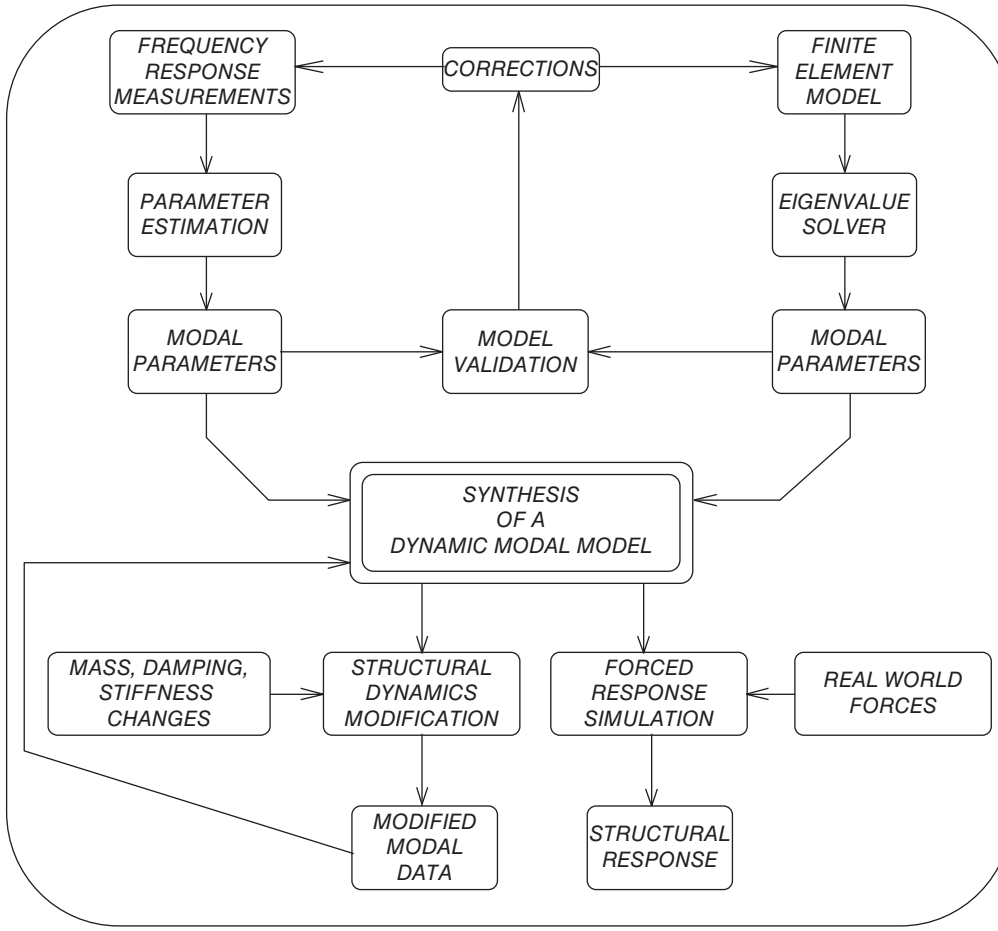

Figure 1.32 Overall dynamic modeling process.

Figure 1.33 Modal model characteristics.

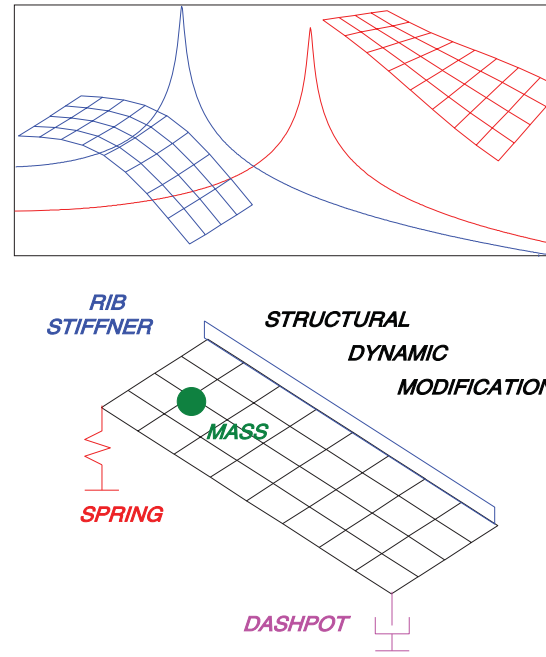

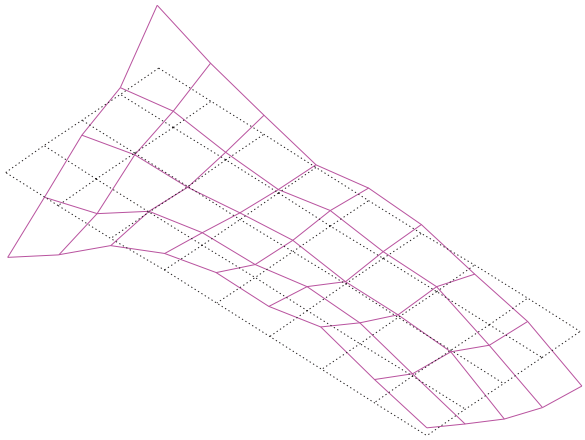

Figure 1.34 Operating data characteristics.

1.9 Closing Remarks

Simple approaches have been used to describe structural vibration and the use of some of the available tools for the solution of structural dynamic problems. This was all achieved without the use of any detailed mathematics. However, in order to better understand the details of the data presented here, a theoretical treatment of this material is necessary. The next chapter provides some of the basic theoretical material upon which experimental modal analysis is based. This is then followed by chapters on signal processing, measurement definitions, excitation techniques and parameter estimation concepts. The remainder of the book then addresses some very practical aspects of experimental modal analysis and gives many hints and tips as to how to perform a modal test to acquire good frequency response functions and then extract the modal parameters.

2

General Theory of Experimental Modal Analysis

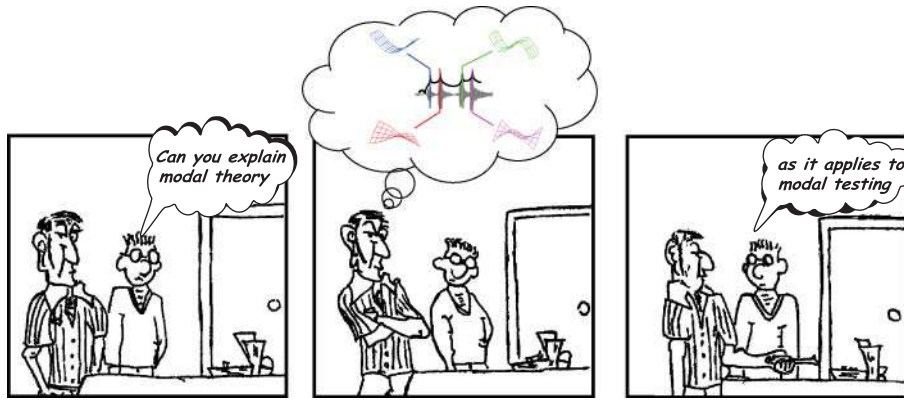

2.1 Introduction

Today, several techniques exist to assist in the development of models for dynamic applications. Finite element models and experimental modal models are two such techniques.

For many years, finite element modeling (FEM) has been used for the characterization of dynamic systems. The FEM process has been very successful in the early stages of the development of prototypes and allows for the optimization of specific design parameters. Thus, before hardware is manufactured, the majority of design characteristics can be assessed and tuned to some degree. These dynamic FEMs are generally developed to assess the response of structures with respect to design specifications and measured input forces. The analytical model can be easily modified to achieve the appropriate or desired response prior to committing to actual hardware. Once a design has been developed, prototypes are fabricated for testing purposes to verify that the desired characteristics have been obtained. Depending on the severity of the dynamic application, the FEM may need to be verified using test data and adjusted accordingly.

Experimental modal analysis (EMA) techniques have become very popular in recent decades due to the affordability of modal test systems and the ease of use of their associated software packages. An experimental modal test will give frequency, damping, and modal vector information for the structure. Experimental modal testing has been a growing field since the 1980s. A number of significant developments have taken place over that time, and these have greatly enhanced the overall data acquisition and data reduction processes. The main developments have been the introduction of multiple-input, multiple-output data acquisition and data reduction schemes and the expansion of modal parameter estimation approaches to include

Modal Testing: A Practitioner's Guide, First Edition. Peter Avitabile.

Companion Website: www.wiley.com/go/avitabile/modal-testing

traditional experimental modal analysis as well as operating modal analysis approaches. This has allowed for better test data from which to acquire parameters, and has also allowed for more accurate modal models to be developed. In addition, a number of computational tools have been added to help test engineers better decipher and interpret frequency response data.

The purpose of this chapter is to overview the basic theory related to modal analysis, and more specifically experimental modal analysis. This chapter will not attempt to develop and derive all the equations related to this subject. Rather, the introduction of the equations important to modal testing will be shown and will be explained, allowing the reader to understand the implications for conducting a test. Some derivations will be provided where these are critical for explaining important concepts. For further theoretical background, the reader is referred to any good vibration textbook and to several detailed theoretical texts on modal analysis; references are provided for some of the more theoretical textbooks related to this material. Additional information on all types of issues related to modal analysis can be obtained from the "Proceedings of the International Modal Analysis Conferences" (IMAC), which have been held annually since the early 1980s.

A review of the pertinent equations for single and multiple degree of freedom systems for the development of the theory of experimental modal analysis is outlined in this chapter. More detailed theory can be found in the reference material.

2.2 Basic Modal Analysis Theory – SDOF

A review of the pertinent equations for single degree of freedom systems for the development of the theory of experimental modal analysis is outlined in this section. More detailed theory can be found in the reference material.

2.2.1 Single Degree of Freedom System Equation

Equations of motion are generated with the assumption that the mass of the system is modeled as a lumped mass, the spring stiffness is proportional to displacement on a linear basis, and the damper is proportional to velocity on a linear basis. This is the most basic model and will be used as the starting point for the theory outlined here. Only linear assumptions for the development of these equations are considered.

The equations will be described first from a classical approach and then from the Laplace domain approach. Figure 2.1 shows a single degree of freedom (SDOF) system, where m is the lumped mass, c is the viscous damping, k is the linear stiffness with x(t) describing the displacement due to the applied force f(t).

With these assumptions, a force balance can be performed to derive the second order differential equation with constant coefficients for the equation of motion as

$$m\frac{d^2x}{dt^2} + c\frac{dx}{dt} + kx = f(t) \qquad \text{or} \qquad m\ddot{x} + c\dot{x} + kx = f(t) \tag{2.1}$$

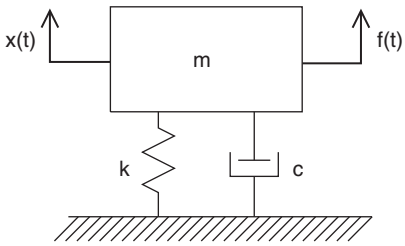

Figure 2.1 SDOF model.

Assuming a solution of an exponential form for the homogeneous solution, then Eq. (2.1) can be written as

$$(ms^2 + cs + k)Xe^{st} = 0$$

Because the exponential term cannot be zero, if x = 0 then a trivial solution exists; only the term in parentheses can be zero. This is commonly called the *characteristic equation* and can then be written as

$$ms^2 + cs + k = 0 \tag{2.2}$$

The *roots* or *poles* of this characteristic equation are given by

$$p_{1,2} = -\frac{c}{2m} \pm \sqrt{\left(\frac{c}{2m}\right)^2 + \frac{k}{m}} \tag{2.3}$$

Now this equation can be evaluated for three distinct cases. One solution exists for systems with damping less than that of critical damping, one solution exists for systems with damping equal to critical damping and one solution exists for systems with damping greater than that of critical damping. While all the solutions are important, only the case with damping less than critical is considered because this is an important solution for the structural dynamic engineer and for experimental modal testing.

The roots can be expressed (for the case of damping less than critical) simply as

$$p_{1,2} = -\zeta\omega_n \pm \sqrt{(\zeta\omega_n)^2 - \omega_n{}^2} = -\sigma \pm j\omega_d \tag{2.4}$$

where

$\sigma = \zeta\omega_n$	damping factor
$\omega_n = \sqrt{\frac{k}{m}}$	natural frequency
$\zeta = \frac{c}{c_c}$	percentage of critical damping
$c_c = 2m\omega_n$	critical damping
$\omega_d = \omega_n\sqrt{1-\zeta^2}$	damped natural frequency

These definitions are used by most structural dynamic and vibration engineers. Several points need to be noted here. First, the damped natural frequency is approximately equal to the natural frequency for small values of damping (less than 10%). Second, the natural frequency of the system increases/decreases as the stiffness increases/decreases. Third, the natural frequency increases/decreases and the mass decreases/increases. Notice that the natural frequency is independent of the damping in the system – only the damped natural frequency changes as the damping changes. It is also important to notice that the roots of this equation are expressed as a complex number with real and imaginary parts to describe the pole. These roots occur in complex conjugate pairs with the real part of the root associated with the damping of the pole and the imaginary part of the root associated with the frequency of the pole. Also, the real part of the root will be negative for underdamped systems so the minus sign is redundant, but it is often shown this way in the literature, which sometimes causes confusion.

An illustration that is often used is the S-plane plot (Figure 2.2), which is a plot of the location of the root in terms of its real (damping) and imaginary (frequency) parts. As the damping increases with constant mass and stiffness, the pole moves to the left of the $j\omega$ axis and the value of the damped natural frequency decreases. As the damping increases, the pole maps out a circular path in the S-plane. As the damping approaches the critical level, the root and its

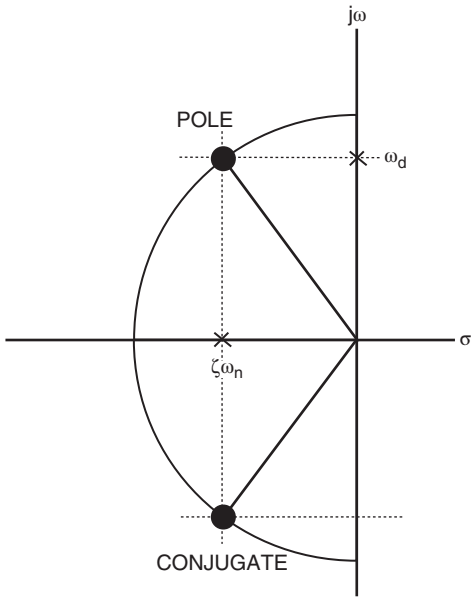

Figure 2.2 S-plane nomenclature.

conjugate approach the σ-axis. The length of the vector from the origin to the pole (radius of a circle) is the natural frequency.

Now another item to discuss is how the poles move in the S-plane when the damping is varied from an undamped system, to an underdamped system, to a critically damped system and then finally to an overdamped system; the responses are also shown due to an impulsive excitation. Figure 2.3 shows this progression and each step is described next. For the undamped case, the poles are located on the $j\omega$ axis and occur as complex conjugate pairs $\pm j\omega_n$. If the time response and frequency response were plotted for this undamped case, then the time response would be sinusoidal, with no damping in the response; the frequency response would be just one frequency line in the spectrum. However, the reality is that we will never have a case where there is no damping so this illustration is only shown for completeness. Now if the damping ζ is 0.1 of critical damping, the pole at $-\sigma \pm j\omega_d$ will move to the left from the $j\omega$ axis and the damped natural frequency will be slightly less than the natural frequency; this is shown in blue in Figure 2.3. Notice that the time response is shown to be a lightly damped sinusoidal decaying response and the frequency response is seen to be slightly wider, indicating that the damping is increased. As the damping ζ is increased from of 0.1, to 0.3 and then 0.7 of critical damping, the pole moves further back, away from the $j\omega$ axis; the time response and frequency response are seen to be more damped in these plots. Now as the damping is increased from no damping to critical damping, the poles are seen to move in a circular arc until they meet at the damping axis, where the damping is critical and there are two real repeated roots. As the damping is increased further, to the overdamped case, the two poles split and remain real, with one pole moving towards infinity as the damping is increased beyond critical and the other real root moving towards zero.

2.2.2 Single Degree of Freedom System Response due to Harmonic Excitation

An important case to consider is the forced response due to harmonic excitation. Without laboring through all the mathematics to develop this equation, the response of a single degree of freedom system due to a harmonic input can be written in terms of displacement and phase

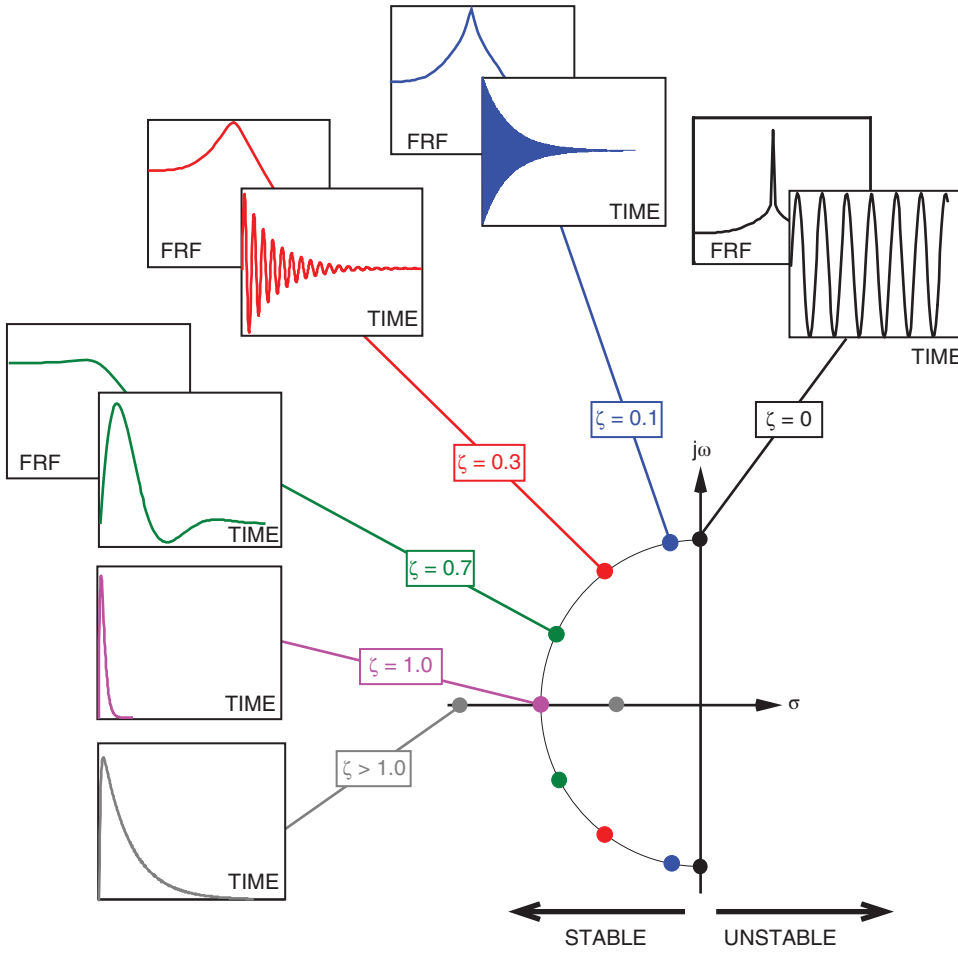

Figure 2.3 Pole migration through the S-plane for a SDOF system with increasing damping (time and frequency plots are not to scale and are for illustration purposes only).

(with force preceeding the displacement) as

$$x = F_0/\sqrt{(k - m\omega^2)^2 + (c\omega)^2} \qquad \varphi = \tan^{-1}\left(\frac{c\omega}{k - m\omega^2}\right) \tag{2.5}$$

Using the definitions above for a single degree of freedom system, and letting β be the ratio of driving frequency of the excitation to the natural frequency of the single degree of freedom system – as is often done in all vibrations textbooks – the response can be written in normalized form as

$$\frac{x}{\delta_{st}} = \frac{1}{\sqrt{(1 - \beta^2)^2 + (2\zeta\beta)^2}} \qquad \varphi = \tan^{-1}\left(\frac{2\zeta\beta}{1 - \beta^2}\right) \tag{2.6}$$

In this form, the function can be plotted in dimensionless form in terms of the dynamic displacement relative to the static displacement, with the driving frequency represented in terms of a percentage of the natural frequency of the single degree of freedom system. Figure 2.4 shows the dynamic amplification and phase for the single degree of freedom system. From these equations, it can be seen that for a lightly damped system, the peak amplitude occurs

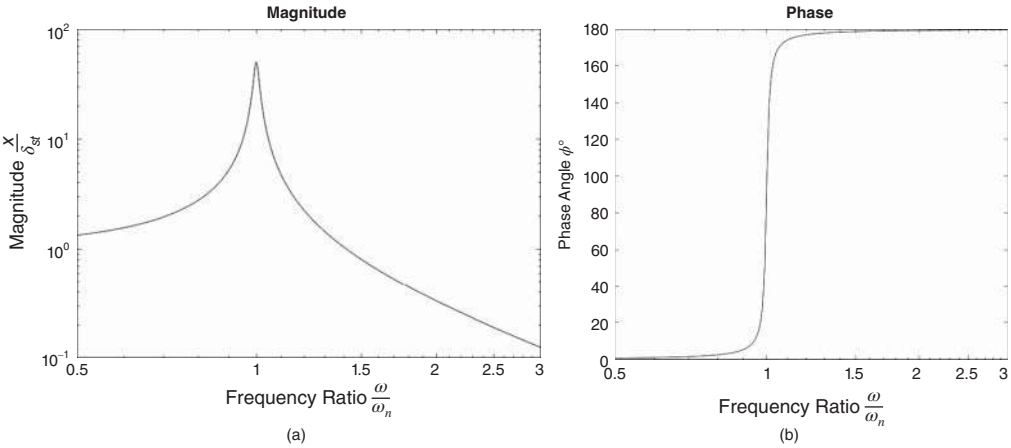

Figure 2.4 The dynamic amplification and phase for an SDOF system: (a) dynamic amplification; (b) phase.

at the damped natural frequency (which is approximately the natural frequency) and that there is a lag of 90° between the force and response at resonance.

2.2.3 Damping Estimation for Single Degree of Freedom System

The damping of the system often needs to be measured. The damping can be computed by several different techniques. Two popular ones are the half power method and the log decrement method.

In the half power method (Figure 2.5), the damping is related to the frequency divided by the difference of the frequencies obtained at the "half power" points. This value is often referred to as the "Q" of the system, or the *amplification factor*.

$$Q = \frac{1}{2\zeta} = \frac{\omega_n}{\omega_2 - \omega_1} \tag{2.7}$$

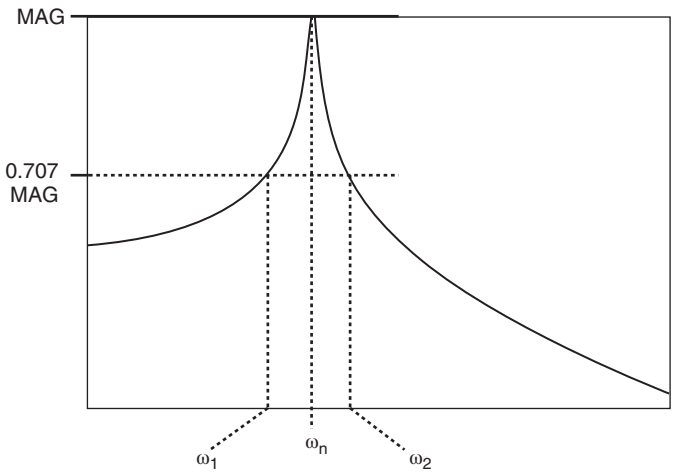

Figure 2.5 Magnitude plot depicting the half power method.

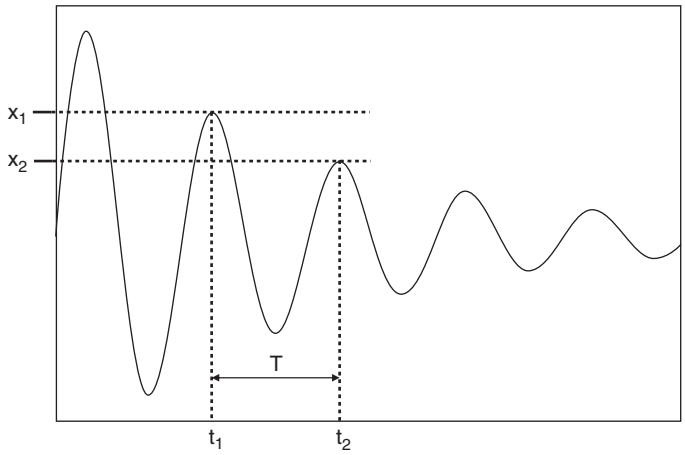

Figure 2.6 Time response depicting the log decrement method.

For instance, a system with a damping of 1% of critical damping has a Q of 50. While analytically this is an approach that seems viable for damping estimation, in practice there is not enough frequency resolution in a typical measurement for it to be accurate.

In the log decrement method (Figure 2.6), a decay in amplitude over one or several cycles of the system is used to determine the damping.

$$\delta = \ln \frac{x_1}{x_2} \approx 2\pi\zeta \tag{2.8}$$

The log decrement method is a very good technique to estimate the damping; the problem is that it is very rare that the response will be that of only one mode, so from a practical standpoint it is not viable.

These two approaches are presented more from a historical perspective and because they are frequently referenced in the literature. The best way to approximate the damping for a set of modes is to use the modal parameter estimation tools and modal data to obtain mode shapes. These tools are mathematical algorithms that process the data in a least squares fashion to find the best fit for the parameters of interest; in this case, damping. This technique is covered later in this book.

It must be noted that the damping is the only mechanism to minimize the response at resonance. And it is equally important to point out that the inertial forces (the product of mass and acceleration) are counterbalanced (equal and opposite) by the elastic forces (the product of stiffness and displacement) in the system.

2.2.4 Response Assessment with Varying Damping

Up to this point, the damping has been evaluated as a fixed parameter. But the damping will vary depending on the system under consideration. A very common plot often seen is the assessment of different values of damping applied on the SDOF system. As the damping is varied for the single degree of freedom system, a set of magnitudes and phases can be plotted for comparison. This is shown in Figure 2.7 for the magnitude and phase.

From these plots, it can be seen that as the damping is increased, the response of the system decreases. In fact, at resonance, the inertial forces of the system are counterbalanced by the elastic forces in the system. This implies that the only mechanism to counterbalance the

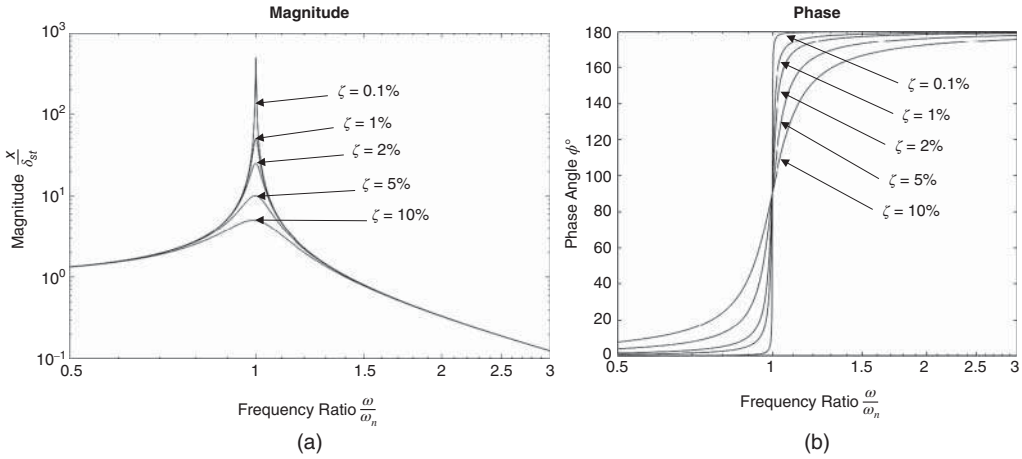

Figure 2.7 SDOF FRF effects of different damping values.

applied force is the damping in the system. Notice that as the damping increases, the response amplitude changes more gradually, and over a wider frequency range. Also notice that the phase lag occurs more gradually, and over a wider frequency range. These two effects will always be seen in a measured frequency response function.

Another explanation of resonance is through the use of the force vector parallelogram. This is a very useful way to explain some of the regions related to resonance. Figure 2.8 shows this force balance concept. Before the pieces of Figure 2.8 are discussed, let's consider a simple static case where F = K x. Here we have a force vector, which is balanced by a Kx vector; in other words they are equal to each other. Now as damping is added along with mass, there are extra pieces of this force balance that need to be considered; there will be four vectors that need to be balanced by the equation of motion. Remember that the velocity is 90° from the displacement and the acceleration is 90° from the velocity (which means that the acceleration is 180° from the displacement). So there will be three non-static conditions to be discussed:

- the excitation frequency is much below the resonant frequency (but not 0 Hz, which is actually the static case)
- the excitation frequency is at the resonant frequency
- the excitation frequency is much higher than the resonant frequency.

There is a force applied and then there are three additional forces related to the elastic force, the damping force, and the mass inertia force. Now the force precedes the elastic force related to displacement; or we could say the response of the system lags behind the applied force. There is a damping force, but that is 90° from the elastic force, because the velocity and displacement have a 90° phase difference. There is also an inertial force, but that is 180° out of phase with the elastic force and 90° out of phase with the damping force, because the acceleration is 180° out of phase with the displacement. Now the displacement, velocity, and acceleration have scale factors related to the elastic force (Kx), the damping force ($c\omega x$) and inertial force ($m\omega^2 x$). All these forces must be added in a vector sense to complete the force diagram. Note in this example that the damping was specified to be much higher than the damping that might actually be seen in practice, in order to provide plots to show the effects of each case.

Now let's consider the three cases: one where the sinusoidal excitation is much less than the natural frequency (top plot), one where is at the natural frequency (middle plot) and one where

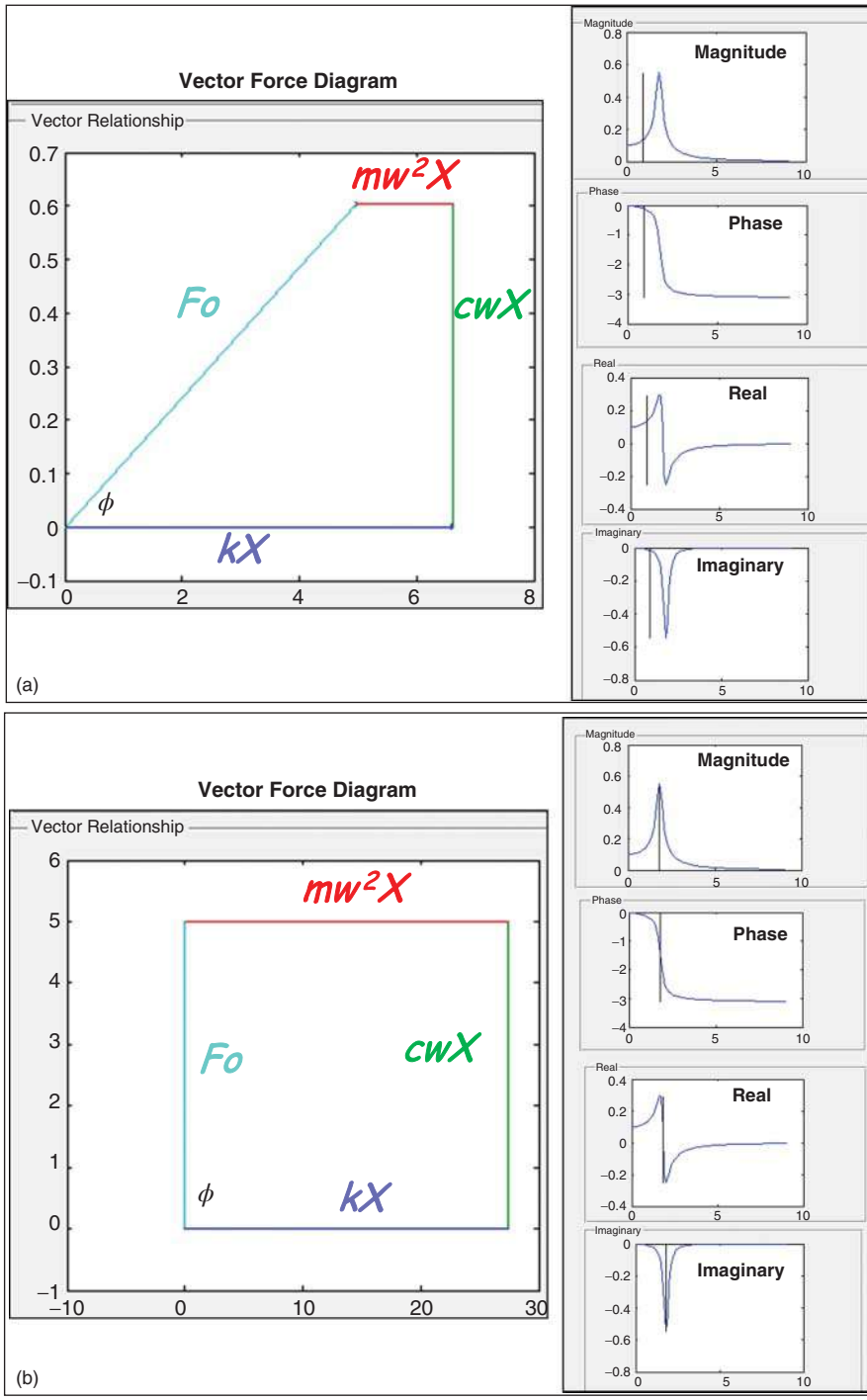

Figure 2.8 SDOF FRF force balance. Sinusoidal excitation is (a) much less than natural frequency; (b) at natural frequency; (c) higher than natural frequency.

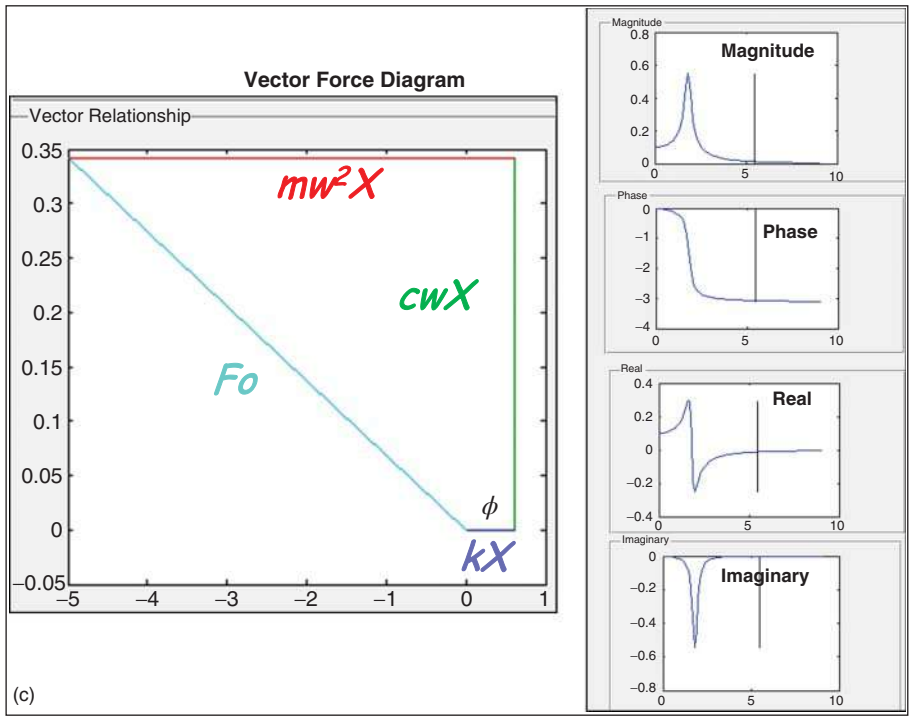

Figure 2.8 (*Continued*)

it is much higher than the natural frequency (bottom plot). If the sinusoidal excitation is much less than the natural frequency (Figure 2.8a), the system will be appear static. The left-hand plot shows that the force is mainly counterbalanced by the elastic force (as in the case of a static load) but that there is a small contribution from the damping and inertial forces. As the excitation frequency increases the inertial and damping forces will increase. When the excitation is at the natural frequency (Figure 2.8b), the elastic force and inertial force are equal and that the only force counterbalancing the applied force is the damping force. Also note that the vectors are all at 90° from each other, that the inertia forces and elastic forces are equal and opposite to each other, and that the only vector opposing the force is the damping, which controls the response at resonance. As the excitation frequency is increased again (Figure 2.8c), the force is mainly counterbalanced by the inertial force but there is a small contribution from the elastic force and the damping force.

This vector formulation helps to reveal the dominant forces at different excitations relative to the natural frequency of the SDOF system. In all of the plots, the force diagram is shown along with the frequency response function for magnitude, phase, real and imaginary parts of the function, with an indicator to show where the excitation frequency is with respect to the resonant frequency.

2.2.5 Laplace Domain Approach for Single Degree of Freedom System

Now let's write the equations of motion for the single degree of freedom system using a Laplace domain approach. Starting from the equation of motion:

$$m\ddot{x} + c\dot{x} + kx = f(t) \tag{2.9}$$

the Laplace transform for acceleration, velocity, displacement and force is

$$\mathcal{L}(\ddot{x}) = s^2 x(s) - s x_0 - \dot{x}_0$$
$$\mathcal{L}(\dot{x}) = s x(s) - x_0$$
$$\mathcal{L}(x) = x(s)$$
$$\mathcal{L}(f(t)) = f(s)$$

where the 0 subscript denotes initial conditions. Taking a Laplace transform, the substituting and rearranging terms, the equation of motion becomes

$$\underbrace{(ms^2 + cs + k)\, x(s)}_{\text{Characteristic equation}} = \underbrace{f(s)}_{\text{Applied force}} + \underbrace{(ms + c)x_0}_{\text{Initial displacement}} + \underbrace{m\dot{x}_0}_{\text{Initial velocity}} \tag{2.10}$$

Assuming initial conditions (velocity and displacement) are zero, this equation can be written as

$$(ms^2 + cs + k)\ x(s) = f(s) \tag{2.11}$$

If we let $b(s) = (ms^2 + cs + k)$ then the more commonly written form of the system equation is obtained:

$$b(s)x(s) = f(s) \tag{2.12}$$

Solving for the displacement variable gives

$$x(s) = b^{-1}(s)f(s) \tag{2.13}$$

This can be written as

$$x(s) = h(s)f(s) \tag{2.14}$$

where h(s), the *system transfer function*, is given by

$$h(s) = \frac{1}{ms^2 + cs + k} \tag{2.15}$$

From the system equation, if we solve the homogeneous solution (that is, $f(s) = 0$), then $b(s)$ $x(s) = 0$ and because $x(s) = 0$ is a trivial solution then $b(s) = 0$ is the only possible solution. Again, the solution to this equation for a system with less than critical damping results in

$$p_{1,2} = -\zeta\omega_n \pm \sqrt{(\zeta\omega_n)^2 - \omega_n{}^2} = -\sigma \pm j\omega_d \tag{2.16}$$

For the underdamped case evaluated, the roots of the characteristic equation are complex valued.

2.2.6 System Transfer Function

The system transfer function is a complex valued function (Figure 2.9). Because the system transfer function is a function of two variables, a plot of this function produces a surface plot, with σ and $j\omega$ axes, above the S-plane. Typically this plot can be viewed in several different forms: magnitude portion, phase portion, imaginary portion, or real portion of the transfer function surface as shown in Figure 2.9. If the system transfer function is evaluated at the root or pole, then the function is undefined.

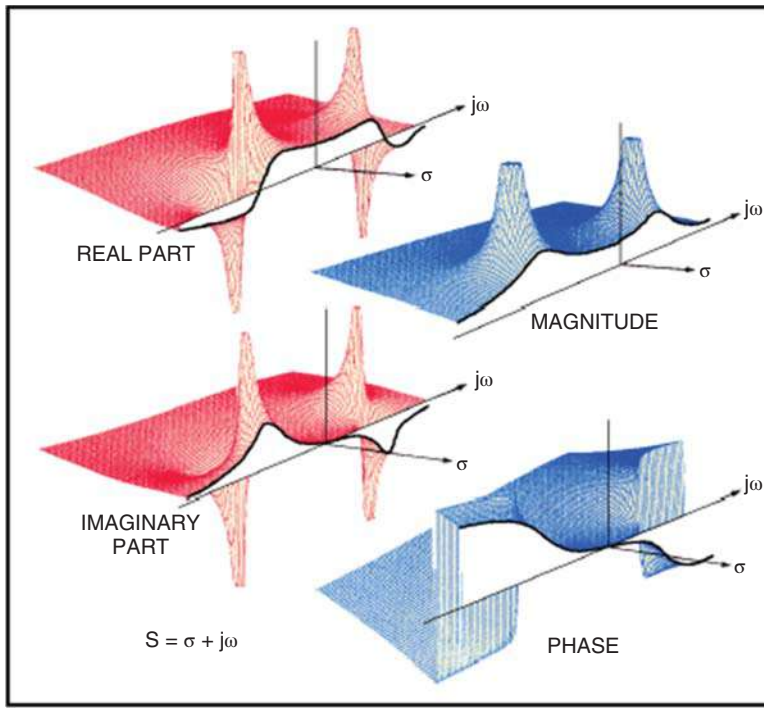

Figure 2.9 System transfer function for a single degree of freedom system. *Source:* Image courtesy Vibrant Technology, Inc.

2.2.7 Different Forms of the Transfer Function

The system transfer function can be expressed in several forms. One has been presented already, with the expression in *polynomial* form. Another form is the factored form of the polynomial, which is referred to as the *pole-zero* form; the poles are seen in the denominator and the zeros are seen in the numerator in factored form. The most popular form for experimental modal analysis is the *partial fraction* form where the expression is clearly seen to contain the contribution from the pole and its complex conjugate. If an impulse is applied to the system and an inverse Laplace transform is made, then the impulse response (commonly referred to as the *complex exponential* form) is obtained. It is very important to note that in each of the equations the same information is displayed, only in different forms. There is no inherent difference in any of these representations of the single degree of freedom system.

Polynomial form	$h(s) = \dfrac{1}{ms^2 + cs + k}$
Pole-zero form	$h(s) = \dfrac{1/m}{(s - p_1)(s - p_1^*)}$
Partial fraction form	$h(s) = \dfrac{a_1}{(s - p_1)} + \dfrac{a_1^*}{(s - p_1^*)}$
Complex exponential form	$h(t) = \dfrac{1}{m\omega_d} e^{-\zeta\omega t} \sin\omega_d t$

2.2.8 Residue of the SDOF System

As stated in Section 2.2.5, the system transfer function is not defined when it is evaluated at one of the roots of the system. In order to evaluate this function at one of its roots using the partial fraction form, a mathematical tool called the residue theorem is used. The resulting value is referred to as the residue of the SDOF system, and is obtained when the system transfer function is evaluated at one of its roots using the residue theorem and is shown to be

$$a_1 = h(s)(s - p_1)\big|_{s \to p_1} = \frac{1}{2\,jm\omega_d} \tag{2.17}$$

In a similar fashion, the complex conjugate pole residue is shown to be

$$a_1^* = -\frac{1}{2\,jm\omega_d} \tag{2.18}$$

In some of the literature, residues are denoted as r. In regards to the notation presented herein

$$r_1 = 2\,j\,a_1 \text{ and } r_1^* = 2\,j\,a_1^*$$

It is very important to note that the system transfer function (as well as the frequency response function in the next section) can be obtained from just two parameters: the pole and the residue. From these two parameters, we can construct the frequency response function over *all frequencies* as well as the transfer function surface for all values of σ and $j\omega$.

2.2.9 Frequency Response Function for a Single Degree of Freedom System

The frequency response function is the transfer function evaluated along $s = j\omega$ and is

$$h(j\omega) = h(s)\big|_{s=j\omega} = \frac{a_1}{(j\omega - p_1)} + \frac{a_1^*}{(j\omega - p_1^*)} \tag{2.19}$$

The frequency response function is nothing more than a slice taken out of the system transfer function surface. It is very important to remember that the system transfer function is a complex valued function, and that the frequency response function is a complex function. Some common forms of the frequency response function are the Bode plot (magnitude and phase), the coincident and quadrature plot (real and imaginary) and the Nyquist or Argand plot (real vs. imaginary). Figure 2.10a shows all three of these plots together to illustrate the relationship between these different forms.

The Bode diagram is the most common form of the frequency response plot. It displays the magnitude and phase together in one plot. Notice that the magnitude is a peak at resonance and that the phase angle is 90°; there is a loss of a total of 180° as the resonant frequency is crossed.

The coincident-quadrature diagram is another very common form of frequency response plot. The magnitude and phase are converted into the real (coincident) and imaginary (quadrature) parts and the plot is often referred to as the co-quad plot. Notice that the real part of the frequency response function is zero and the imaginary is a peak at resonance.

The Nyquist or Argand diagram is a plot of the real and imaginary parts of the frequency response function. Notice that the shape looks like a circle when the data is plotted in this fashion.

Now looking closer around the resonant frequency of the system, there are several things to note in Figure 2.10b. The plot shows the Nyquist and co-quad plots. Looking at the half power points for the imaginary part of the frequency response function, the half power points occur at half of the peak amplitude of the imaginary part. This amplitude in the imaginary occurs at the

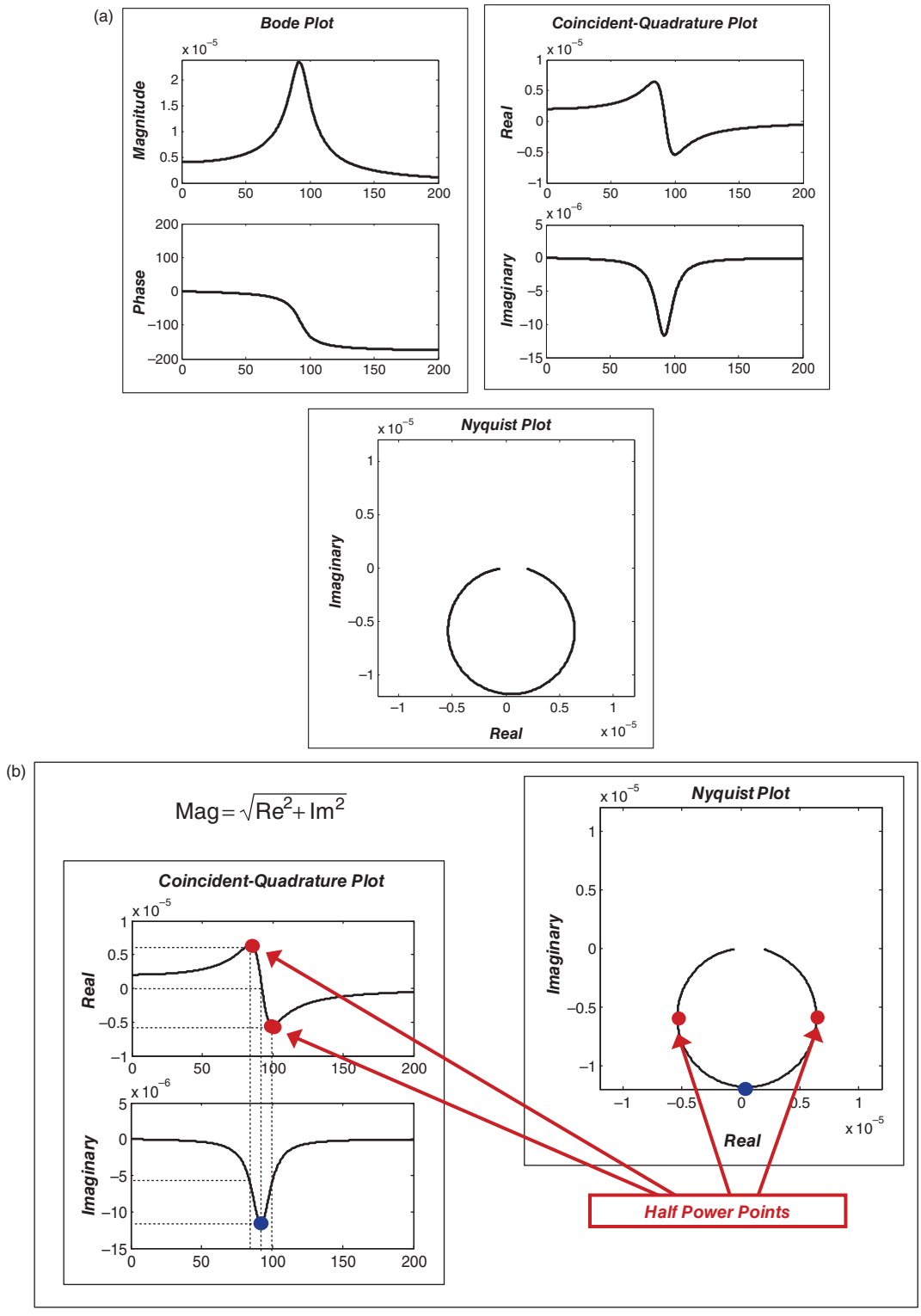

Figure 2.10 Illustration plots of the acceleration frequency response function: (a) Bode, co-quad and Nyquist plots; (b) half power points for the co-quad and Nyquist plots.

peaks in the real part of the frequency response function which is exactly the same amplitude of the half power of the imaginary part. Viewing these same points on the Nyquist plot, the peak of the imaginary part is directly opposite (0, 0), with no real part value. The half power points occur at points that are 90° away from the peak in the imaginary part.

2.2.10 Transfer Function/Frequency Response Function/S-plane for a Single Degree of Freedom System

The slice of the system transfer function ($s = j\omega$) can be projected away from the surface and is commonly called the *frequency response function*. If we project the location of the poles down onto the system transfer function, the S-plane can be viewed. This is shown in the Figure 2.11. This figure is included to show the inter-relationship between the system transfer function, the frequency response function and the S-plane. Both the positive and negative portions of the frequency response function are shown, but typically only the positive part of the frequency axis is shown. However, the conjugate portion does exist.

2.2.11 Frequency Response Function Regions for a Single Degree of Freedom System

The frequency response function is made up of different regions, as shown in Figure 2.12. At frequencies much less than that of resonance, the response of the system is dominated by the stiffness of the system. At frequencies much greater than that of resonance, the response of the system is dominated by the mass inertia of the system. At frequencies close to resonance, the response of the system is controlled by the amount of damping in the system; at resonance, the inertial forces are counterbalanced by the elastic forces of the system such that the only way to counterbalance the applied forces to the system is through the damping forces in the system. Typically, regions of the frequency response function will be described in terms of

- the stiffness controlled portion of the frequency response, which is less than that of the resonant frequency
- the damping controlled portion of the frequency response, which is in the region of the resonant frequency

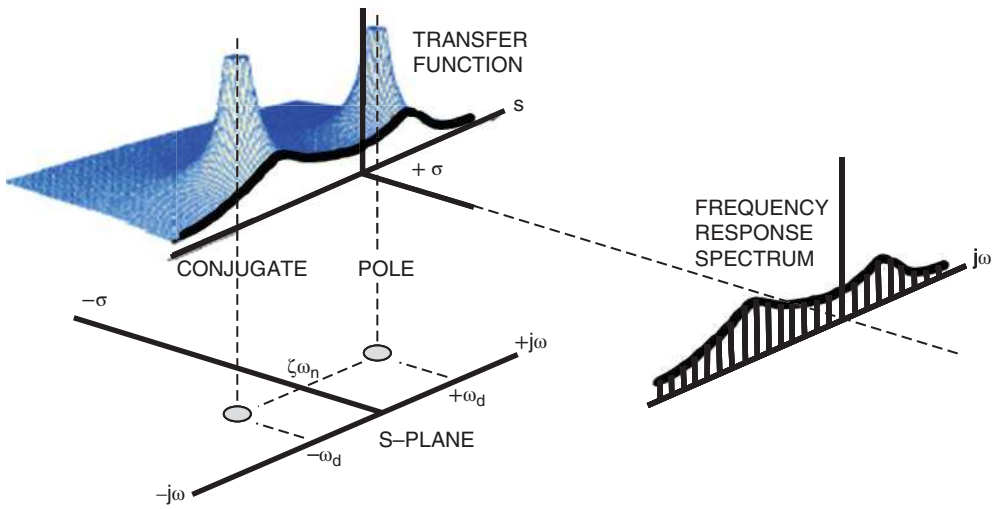

Figure 2.11 Laplace transform, S-plane and frequency response function projections.

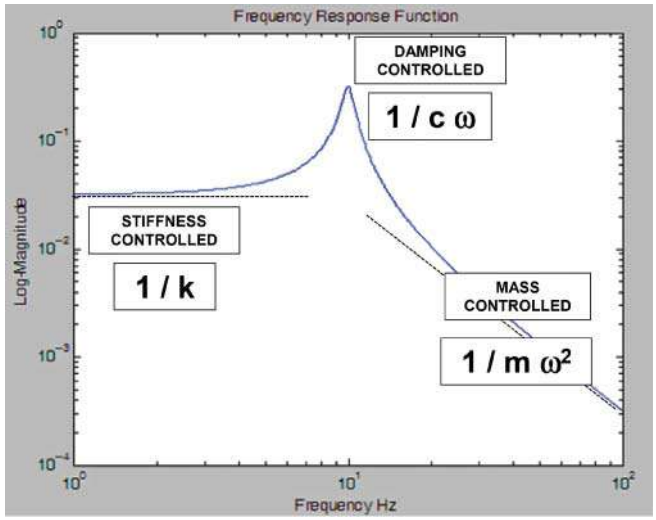

Figure 2.12 Stiffness, damping and mass controlled portions of the magnitude of the FRF.

- the mass controlled portion of the frequency response, which is greater than that of the resonant frequency.

Up to this point, the frequency response function has only been discussed in terms of the displacement relative to the input force, which is referred to as the *dynamic compliance*. The frequency response function could also be measured in terms of the velocity relative to the force, which is referred to as the *mobility*. And the frequency response function could also be measured in terms of the acceleration relative to the force, which is referred to as the *inertance*. In addition, the inverses of these relations can also be measured for displacement, velocity, and acceleration and these are referred to as the dynamic stiffness, impedance, and dynamic mass, respectively. The magnitude portion of the frequency response function is shown in Figure 2.13. There are several very important items to note in this plot.

The plot on the left is the displacement divided by force (D/F). In order to obtain the center-plot, of velocity divided by force (V/F), all that is necessary is to multiply the D/F function by $j\omega$. And then to obtain the right hand plot, for acceleration divided by force (A/F), all that is necessary is to multiply the V/F function by $j\omega$. And from that, it is clear that the relationship between

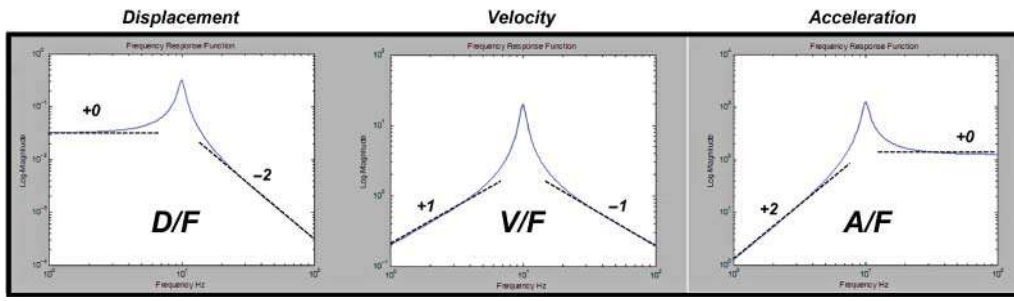

Figure 2.13 Forms of the FRF and slopes of stiffness and mass controlled regions: (left) D/F; (center) V/F; (right) A/F.

acceleration and displacement is (A/F) = $-\omega^2$ (D/F); that is, the acceleration and displacement are 180° out of phase and scaled by ω^2.

The other important observation is the relationship between the slopes of the stiffness controlled and the mass controlled regions. In the D/F frequency response function, the slope of the stiffness controlled region has a zero slope and the mass controlled region has a −2 slope. The V/F (when compared to the D/F) has a +1 slope and a −1 slope in the stiffness controlled and mass controlled regions, respectively; the A/F has a +2 slope and a zero slope in these same regions, respectively. At times this is very useful when looking at measured frequency response function data that may not have been labeled properly or if there was some mix up in transfer of data between systems.

In order to have a complete description of each of the frequency response function types (D/F, V/F, A/F) and all forms of the frequency response function, the real, imaginary, magnitude, phase and Nyquist plots are shown in Figure 2.14–2.16 for D/F, V/F, and A/F, respectively. To display all of this information as accurately as possible, the negative frequency should also be plotted for completeness; the conjugate information is not normally shown on most commercial FFT analyzers, but it is important to point out that mathematically it is needed for completeness. This is shown in Figure 2.17 with the plot shown above and the results of the GUI provided from the book webpage.

Now there is one more thing to discuss for the SDOF system in order to pull all of this information together. Figure 2.18 shows the system transfer function h(s) with all of the complex pieces. Only the magnitude is highlighted in the middle of the figure, with the equation of the system transfer function shown. The frequency response function is the system transfer function evaluated along the $j\omega$ axis with the equation shown at the bottom of the figure. To the far right of the figure, the magnitude of the frequency response function is shown, along with the frequency spacing along the x-axis. At this point, it is very clear that the frequency response function is a part of the system transfer function and that the frequency response function measured can easily be seen. Later, this sampled discrete set of data will be used to extract the constants that are used to define this function, namely the pole and residue. And it will be the extraction of these parameters that will be the focus of the modal parameter estimation process. This process will be discussed more later in the book.

2.2.12 Different Forms of the Frequency Response Function

Earlier the system transfer function was presented in polynomial, pole-zero and partial fraction forms. For completeness, the frequency response function can be presented in these forms too. Again, it is very important to note that in each of the equations the *same information* is displayed in all of the different forms. There is no difference in any of these representations of the single degree of freedom system.

Polynomial form:
$$h(j\omega) = \frac{1}{m(j\omega)^2 + c(j\omega) + k}$$

Pole-zero form:
$$h(j\omega) = \frac{1/m}{(j\omega - p_1)(j\omega - p_1^*)}$$

Partial fraction form:
$$h(j\omega) = \frac{a_1}{(j\omega - p_1)} + \frac{a_1^*}{(j\omega - p_1^*)}$$

2.2.13 Complex Frequency Response Function

At times, the frequency response function will be referred to as the complex frequency response function. The frequency response function is always a complex value and this extra terminology

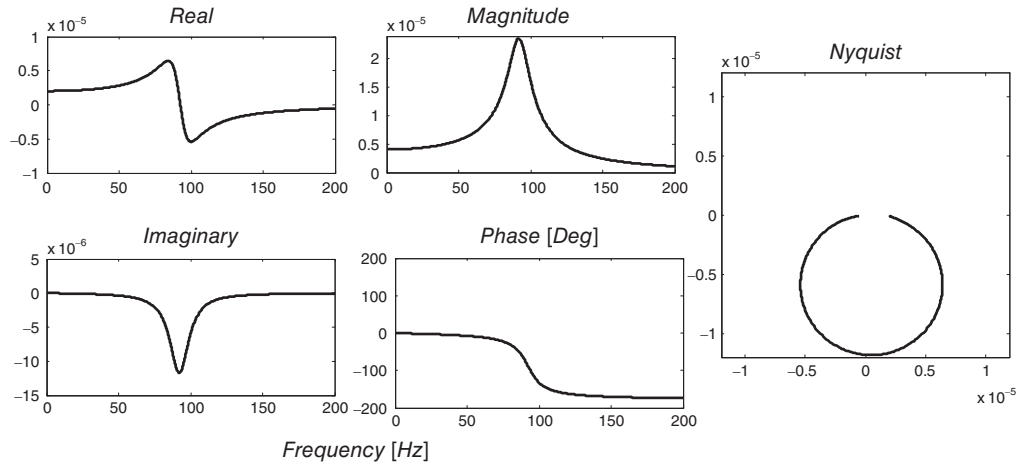

Figure 2.14 D/F FRF with real, imaginary, magnitude, phase and Nyquist forms of the FRF.

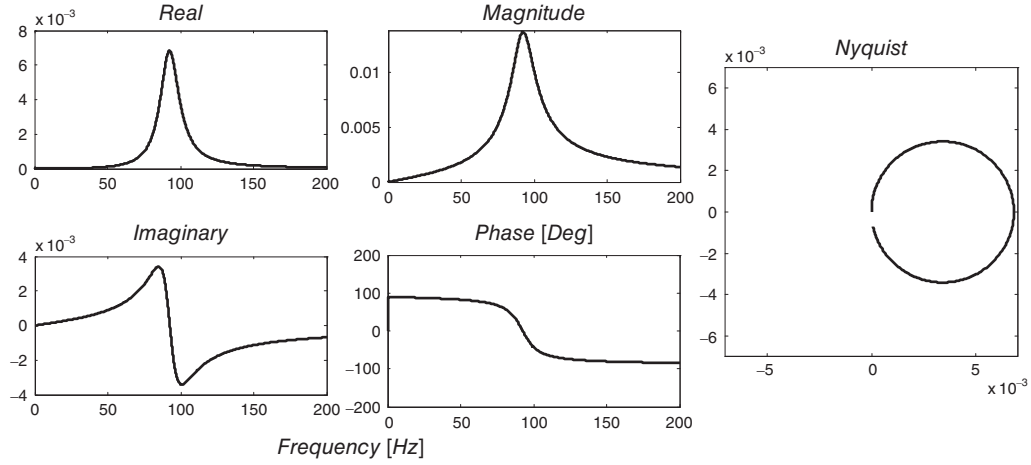

Figure 2.15 V/F FRF with real, imaginary, magnitude, phase and Nyquist forms of the FRF.

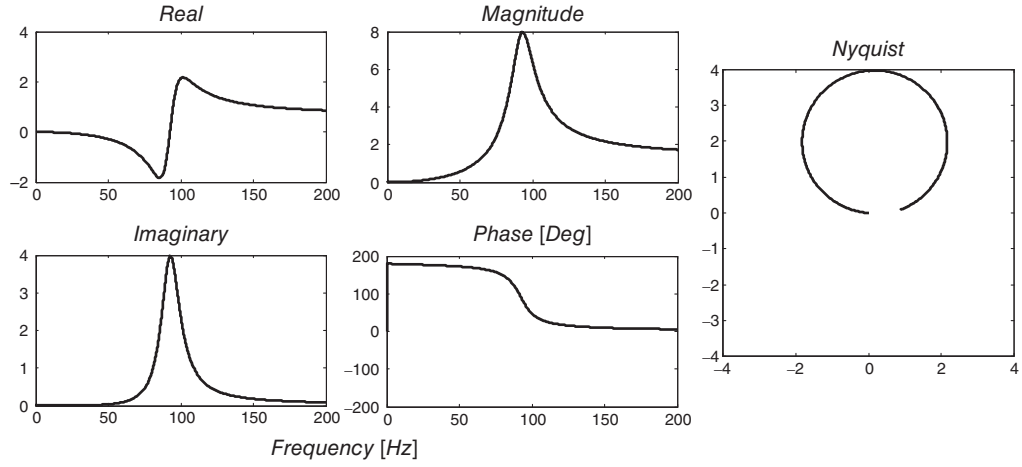

Figure 2.16 A/F FRF with real, imaginary, magnitude, phase and Nyquist forms of the FRF.

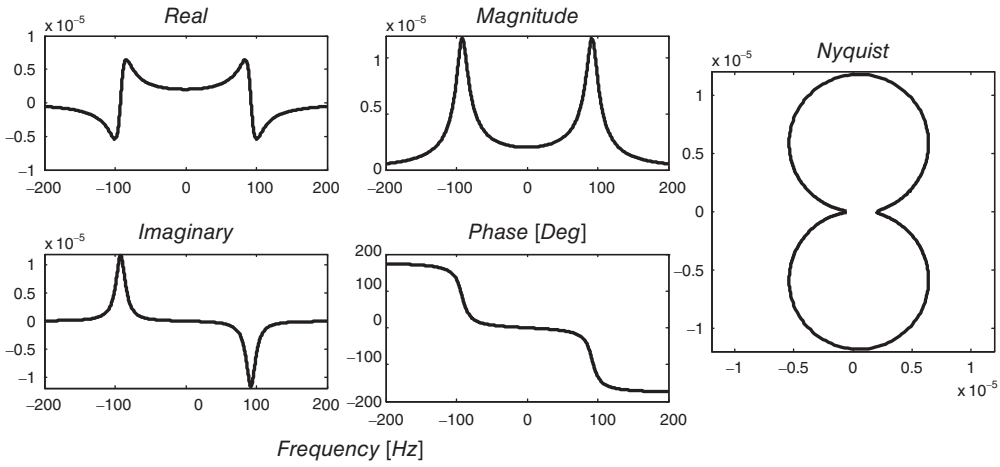

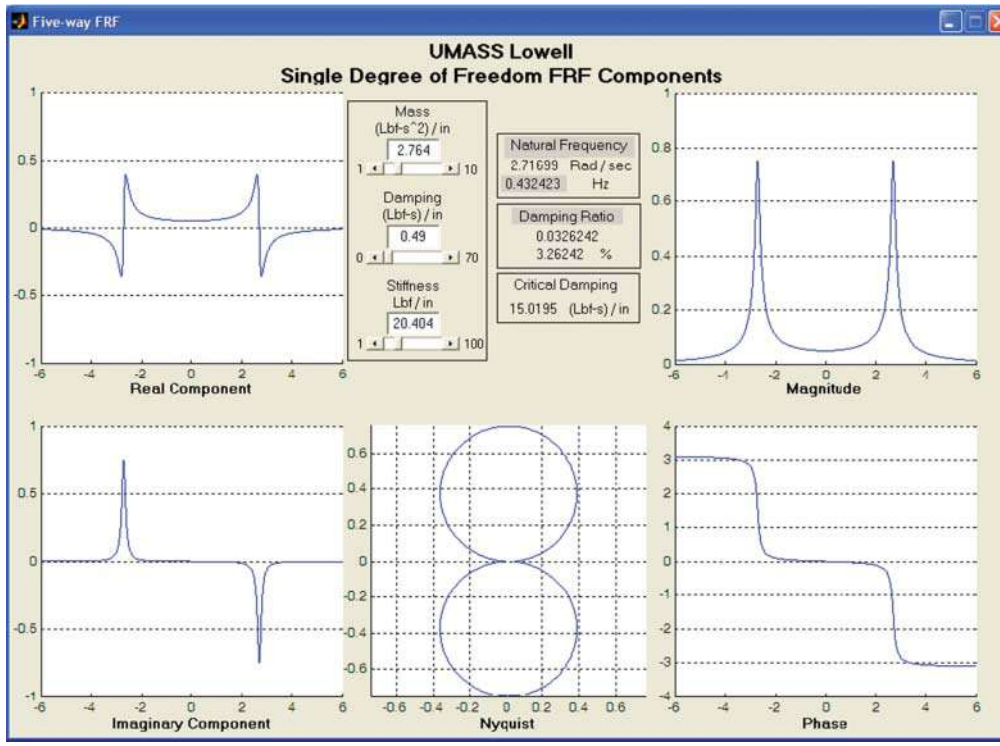

Figure 2.17 Complete D/F FRF with pole and conjugate pole.

is sometimes confusing. But just to be complete, the complex FRF is sometimes written as

$$h(j\omega) = \frac{1-\left(\frac{\omega}{\omega_n}\right)^2}{\left(1-\left(\frac{\omega}{\omega_n}\right)^2\right)^2+\left(2\zeta\left(\frac{\omega}{\omega_n}\right)\right)^2} - j\,\frac{2\zeta\left(\frac{\omega}{\omega_n}\right)}{\left(1-\left(\frac{\omega}{\omega_n}\right)^2\right)^2+\left(2\zeta\left(\frac{\omega}{\omega_n}\right)\right)^2} \tag{2.20}$$

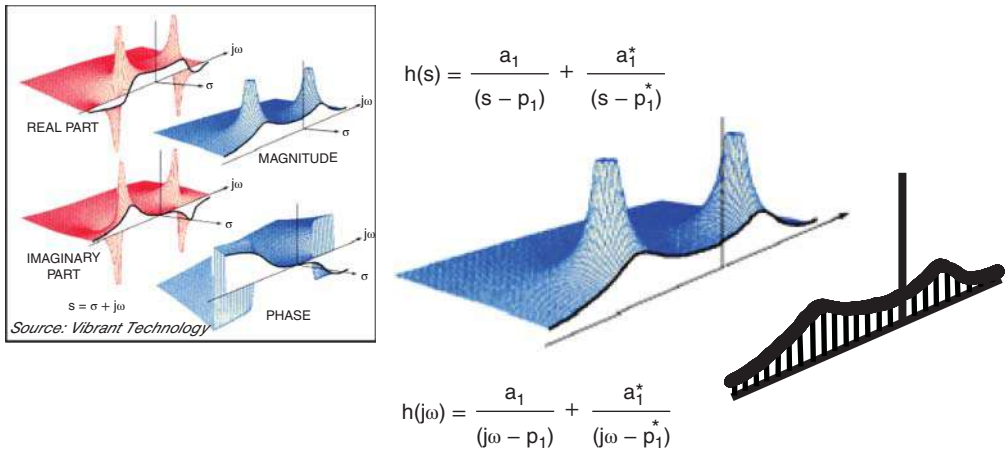

Figure 2.18 Relationship of transfer function, h(s) and frequency response function, h(jω). *Source:* Image courtesy Vibrant Technology, Inc.

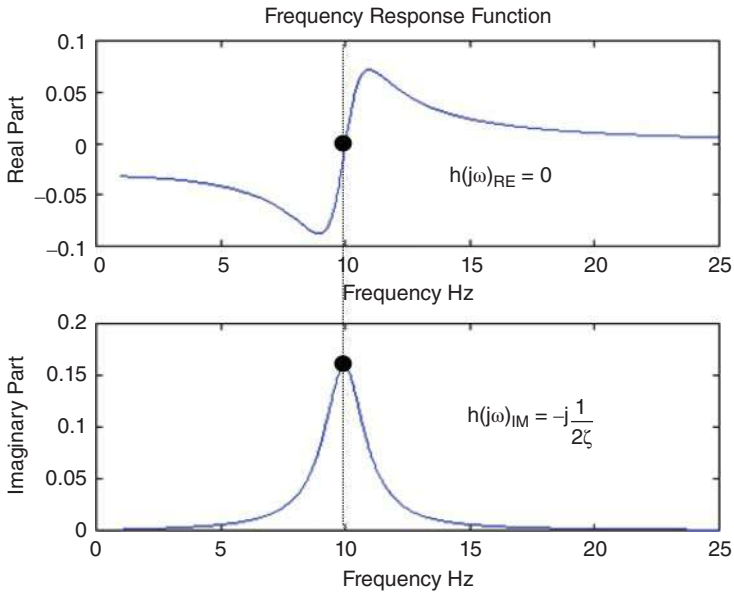

Figure 2.19 Complex frequency response function evaluated at resonance.

In this notation, the function is broken up into the real and imaginary parts. This reveals some important characteristics of the equation. Figure 2.19 shows the value of the complex FRF at resonance. In this way, it is very clear that the real part of the frequency response function is zero at resonance and the imaginary part is a peak at resonance.

2.3 Basic Modal Analysis Theory – MDOF

A review of the pertinent equations for multiple degree of freedom systems for the development of the theory of experimental modal analysis is outlined in this section. More detailed theory can be found in the reference material.

2.3.1 Multiple Degree of Freedom System Equations

Next a multiple degree of freedom system is considered. As was assumed for the single degree of freedom system, the equation of motion can be written as shown below with the following assumptions:

- the mass is modeled as a lumped mass
- the spring stiffness is proportional to displacement on a linear basis
- the dashpot is proportional to velocity on a linear basis.

In addition, it is important to note that the system is linear and time invariant. The system can be described by a second order differential equation with constant coefficients.

First, let's consider a simple two degree of freedom system. Again, a force balance can be performed for each of the two masses of the system resulting in two equations and two unknowns. For details on developing these equations, refer to any vibration textbook. Figure 2.20 shows a schematic of the two degree of freedom system on the left and the free body diagram for the two degree of freedom system on the right.

Newton's second law is used to write the equations of motion as:

$$\begin{aligned} m_1\ddot{x}_1 &= f_1(t) - c_1\dot{x}_1 + c_2(\dot{x}_2 - \dot{x}_1) - k_1x_1 + k_2(x_2 - x_1) \\ m_2\ddot{x}_2 &= f_2(t) - c_2(\dot{x}_2 - \dot{x}_1) - k_2(x_2 - x_1) \end{aligned} \tag{2.21}$$

These can be rearranged, and then collecting terms gives

$$\begin{aligned} m_1\ddot{x}_1 + (c_1 + c_2)\dot{x}_1 - c_2\dot{x}_2 + (k_1 + k_2)x_1 - k_2x_2 &= f_1(t) \\ m_2\ddot{x}_2 - c_2\dot{x}_1 + c_2\dot{x}_2 - k_2x_1 + k_2x_2 &= f_2(t) \end{aligned} \tag{2.22}$$

Notice that the first equation has terms that involve the displacement and velocity of mass 2, as well as the terms involving the displacement, velocity and acceleration of mass 1. Likewise, the second equation involves terms for mass 1 and mass 2. In other words, these equations have terms that are interrelated or coupled.

For simplicity, these equations can also be cast in the form of a matrix of masses times a vector of accelerations, plus a matrix of dashpots times a vector of velocities, plus a matrix of

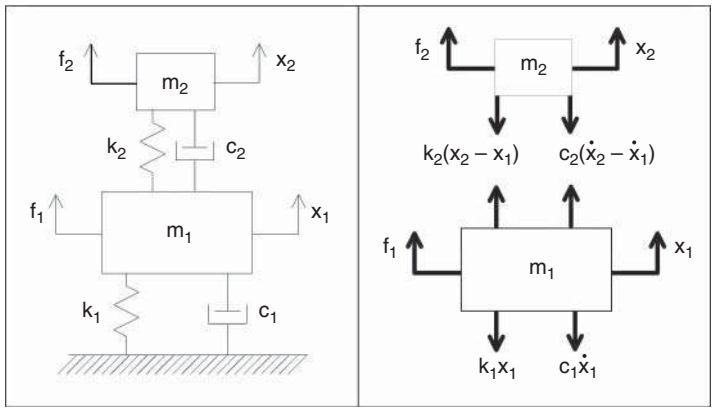

Figure 2.20 2DOF system: (left) schematic; (right) free body diagram.

stiffnesses times a vector of displacements, which is equal to a vector of applied forces.

$$\begin{bmatrix} m_1 & \\ & m_2 \end{bmatrix} \begin{Bmatrix} \ddot{x}_1 \\ \ddot{x}_2 \end{Bmatrix} + \begin{bmatrix} (c_1 + c_2) & -c_2 \\ -c_2 & c_2 \end{bmatrix} \begin{Bmatrix} \dot{x}_1 \\ \dot{x}_2 \end{Bmatrix} + \begin{bmatrix} (k_1 + k_2) & -k_2 \\ -k_2 & k_2 \end{bmatrix} \begin{Bmatrix} x_1 \\ x_2 \end{Bmatrix} = \begin{Bmatrix} f_1(t) \\ f_2(t) \end{Bmatrix} \tag{2.23}$$

Notice that the damping and stiffness matrices have off-diagonal terms. These are the terms that describe the coupling between mass 1 and mass 2. The size of these matrices is directly related to the number of degrees of freedom of the multiple degree of freedom system. Therefore, the matrices are all square and it is important to note that they are all symmetric.

While the equations are useful for the 2DOF system, the more general case of a multiple DOF system will be addressed now. In order to understand some of the matrix manipulations, a brief review of matrix and vector operations is set out in an appendix to this text. Figure 2.21 shows a more general nDOF model. It is important to note that while it seems small, the approach taken here is also applicable to any large, finite element model, as shown in Figure 2.22b.

Now let's extend beyond two degrees of freedom and write the equation of motion for a general "n" multiple degree of freedom system in matrix form:

$$[M]\{\ddot{x}\} + [C]\{\dot{x}\} + [K]\{x\} = \{F(t)\} \tag{2.24}$$

where [M] is the mass matrix (n,n), [C] is the damping matrix (n,n), [K] is the stiffness matrix (n,n), {F} is the forcing vector (n,1) and {x} is the vector (n,1) of displacements, velocities and accelerations as noted. These equations are coupled as before.

It would be very convenient if these matrices could somehow be cast in an uncoupled form for easier processing; the eigensolution helps to achieve this simpler solution. The eigensolution is obtained using only the mass and stiffness matrices, along with an assumption that the damping matrix is zero or proportional to either the mass and/or stiffness matrix.

$$[[K] - \lambda[M]]\ \{x\} = 0 \tag{2.25}$$

At this point, a conceptual explanation of the eigensolution is very helpful in understanding how the frequencies are obtained and what mode shape results at each of these frequencies. The first thing to say is that the eigensolution actually gets us both the frequencies and mode

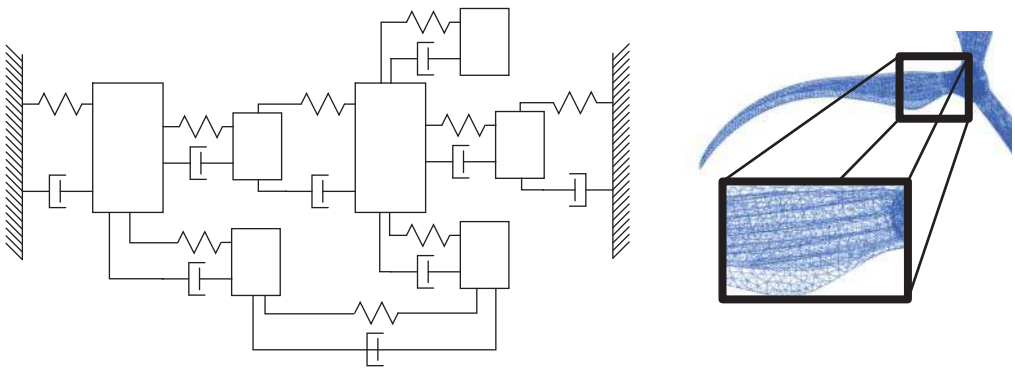

Figure 2.21 A general "n" multiple degree of freedom system: (a) a simple lumped mass model; (b) a more detailed finite element model.

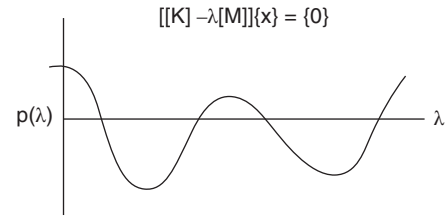

Figure 2.22 Graphical representation of roots of determinant.

shapes. The mathematical process of the eigensolution can be performed a number of different ways, and these can be categorized into direct and indirect techniques. For smaller matrices, the direct techniques decompose the set of equations to get all of the eigenvalues and eigenvectors. Techniques such as the Jacobi, Givens and Householder approaches are common direct methods. However, when the matrices get larger, as is the case for the large finite models that are developed today, then an indirect technique is used. Here, only a few of the lower order modes are obtained. Examples include the subspace iteration, simultaneous vector iteration and Lanczos approaches. A good numerical methods text will have the details of the eigensolution and all of the methods that can be used.

But let's explain what is going on conceptually, which makes it easier to understand the results of the eigensolution process. The first thing to note is that the eigenvalues can be found from the determinant of the matrix, as schematically shown in Figure 2.22. That determinant will really be nothing more than a high order polynomial the roots of which are the eigenvalues. Numerically, those can be obtained from any root solving algorithm such as Secant method or the Newton–Rapson method, among several well known approaches.

This gives us the frequencies of the set of equations and the next step is to determine the mode shapes. The first eigenvalue, $\lambda = \omega_1{}^2$, is substituted into the eigensolution equation, which is then solved for the $\{x_1\}$ vector because [M], [K], and $\omega_1{}^2$ are known. The solution for that vector is straightforward using a decomposition scheme, such as the Crout–Doolittle, Cholesky, or LDL decomposition, among others.

The $\{x_1\}$ vector is actually the mode shape $\{u_1\}$ for the particular frequency that was used to solve the set of equations. Figure 2.23 shows this schematically for the first free–free mode for

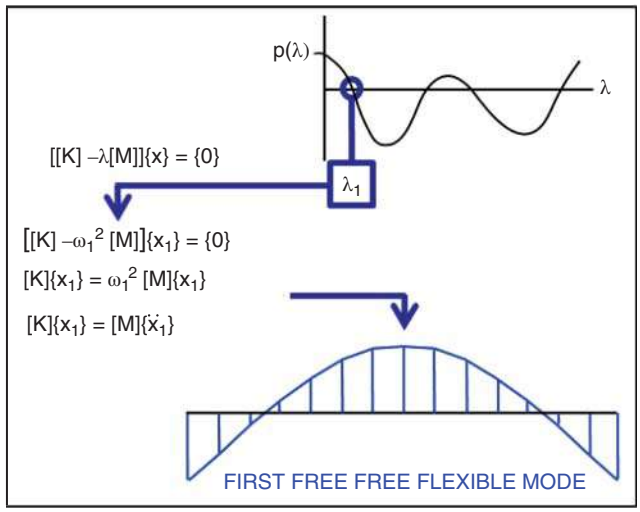

Figure 2.23 Schematic for eigensolution for mode 1.

a simple beam; note that blue is used to identify this as the first mode of the system. And follow through with the equation in Figure 2.23, notice that the elastic forces are equal to the inertial forces in the way they are written. One could also say the beam is in dynamic equilibrium at that frequency, which is $\omega_1{}^2$. Looking at the system from an energy perspective, it can be seen that there are nodes about which the system oscillates and where there are equal positive and negative parts of the shape to maintain the equilibrium.

Of course the same thing can be done for the second frequency. Take the second eigenvalue, $\lambda = \omega_2{}^2$, and substitute it into the eigensolution equation, then solve for the $\{x_2\}$ vector knowing [M], [K], and $\omega_2{}^2$. The $\{x_2\}$ vector is actually the mode shape $\{u_2\}$ for the second frequency. Figure 2.24 shows this schematically for the second free–free mode for a simple beam; note that red is now used to identify this as the second mode of the system. Again let's follow through with the equation in Figure 2.24 in red, the elastic forces are equal to the inertial forces in the way they are written. The beam is in dynamic equilibrium, but now at a frequency of $\omega_2{}^2$. And just as seen with mode 1, the node points locations about which the system oscillates and where there are equal positive and negative parts of the shape to maintain the equilibrium.

This process can be continued for all the modes of interest. Of course, explaining it this way may not be the way the different algorithms actually decompose the matrices and obtain the final answer. But this explanation will probably give a much better overall idea how the frequencies and mode shapes emerge from the system set of equations.

It is important to realize that the eigensolution is used to obtain what is called the *eigenpair*: the frequency and the vector associated with the eigenequation. This is in fact the mode shape. Moreover, the mode shapes are linearly independent and they are orthogonal with respect to the mass and stiffness matrices. This is a by-product of the eigensolution. This is a very important fact that is often used when checking finite element models with measured experimental data. An orthogonality check, often called a pseudo-orthogonality check, is performed to compare the measured experimental vectors with those obtained from the eigensolution.

Now these eigenvectors or mode shapes have a very unique property: they are orthogonal to the mass and stiffness matrices and linearly independent from each other. In order to show this, the eigensolution can be written in general form as

$$[K][U] = [M][U][\Omega^2] \tag{2.26}$$

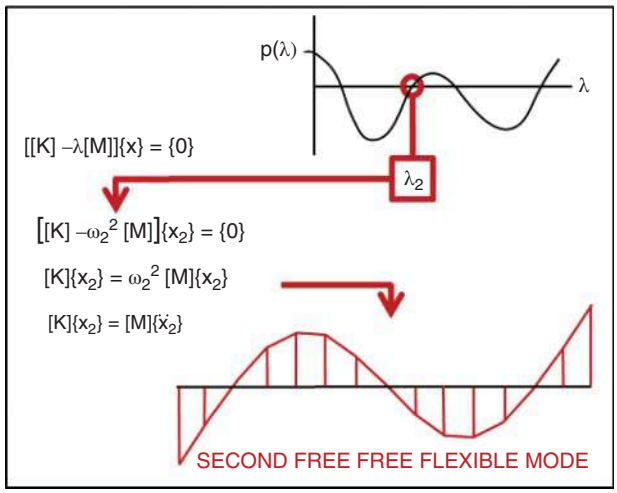

Figure 2.24 Schematic for eigensolution for mode 2.

Now writing the ith vector, the eigen problem becomes

$$[K]\{u_i\} = \lambda_i[M]\{u_i\} \tag{2.27}$$

which can then be multiplied by the jth eigenvector to give

$$\{u_j\}^T[K]\{u_i\} = \lambda_i\{u_j\}^T[M]\{u_i\} \tag{2.28}$$

And then do the same steps as above for the jth eigenvector to give another equation as

$$\{u_i\}^T[K]\{u_j\} = \lambda_j\{u_i\}^T[M]\{u_j\} \tag{2.29}$$

Subtracting these two equations results in

$$(\lambda_i - \lambda_j)\{u_i\}^T[M]\{u_j\} = 0$$

and because the two eigenvalues for i and j are different, the solution must be for $i \neq j$ to be

$$\{u_i\}^T[M]\{u_j\} = 0 \qquad i \neq j \tag{2.30}$$

which is the proof for the orthogonality of the eigenvectors. However, when $i = j$, then the values are not zero and this results in the two terms: the modal mass and modal stiffness for the ith mode. These are given by

$$\left.\begin{aligned}\{u_i\}^T[M]\{u_i\} &= \overline{m}_{ii}\\ \{u_i\}^T[K]\{u_i\} &= \overline{k}_{ii}\end{aligned}\right\} \quad i = j \tag{2.31}$$

So that the orthogonality condition can be stated as

$$\{u_i\}^T[M]\{u_j\} = \begin{cases}\overline{m}_{ii} & \text{when } i = j\\ 0 & \text{when } i \neq j\end{cases} \qquad \{u_i\}^T[K]\{u_j\} = \begin{cases}\overline{k}_{ii} & \text{when } i = j\\ 0 & \text{when } i \neq j\end{cases} \tag{2.32}$$

Therefore, the eigensolution provides a set of eigenpairs: frequencies (eigenvalues) and mode shapes (eigenvectors). For convenience, the *modal matrix* is constructed by arranging the eigenvalues in diagonal form and the eigenvectors in column fashion.

$$\begin{bmatrix}\backslash & & \\ & \Omega^2 & \\ & & \backslash\end{bmatrix} = \begin{bmatrix}\omega_1^2 & & \\ & \omega_2^2 & \\ & & \backslash\end{bmatrix} \text{ and } [U] = \begin{bmatrix}\{u_1\} & \{u_2\} & \cdots\end{bmatrix} \tag{2.33}$$

Some new coordinate system is desirable, wherein the equations describing the system can be written in a simpler form in which the coupling is eliminated. The modal transformation equation helps to do this. This modal matrix [U] will be used to uncouple the physical set of equations. The modal transformation that transforms *physical space* to *modal space* is shown as

$$\{x\} = [U]\ \{p\} = \begin{bmatrix}\{u_1\} & \{u_2\} & \cdots\end{bmatrix}\begin{Bmatrix}p_1\\ p_2\\ \vdots\end{Bmatrix} \tag{2.34}$$

where {p} is the new modal space variable. The modal matrix can be as large as (n,n) but in general will only be of size (n,m). While there are n possible modal vectors that can be obtained, generally only m modes are extracted because this is all that is typically necessary to solve most structural dynamic problems; the number of modes m is generally far fewer than the number of measurement points n. If we now substitute this modal transformation expression into the

equation of motion and premultiply the equation by the transpose of the projection operator to put the equations into normal form, this gives

$$[U]^T[M][U]\{\ddot{p}\} + [U]^T[C][U]\{\dot{p}\} + [U]^T[K][U]\{p\} = [U]^T\{F\} \tag{2.35}$$

Now let's multiply out some terms from this. Looking at the first term, associated with the mass and acceleration, the result is

$$[U]^T[M][U] = \begin{bmatrix} (\{u_1\}^T[M]\{u_1\}) & (\{u_1\}^T[M]\{u_2\}) & (\{u_1\}^T[M]\{u_3\}) & \cdots \\ (\{u_2\}^T[M]\{u_1\}) & (\{u_2\}^T[M]\{u_2\}) & (\{u_2\}^T[M]\{u_3\}) & \cdots \\ (\{u_3\}^T[M]\{u_1\}) & (\{u_3\}^T[M]\{u2\}) & (\{u_3\}^T[M]\{u_3\}) & \cdots \\ \vdots & \vdots & \vdots & \ddots \end{bmatrix} \tag{2.36}$$

But recall the orthogonality condition:

$$\{u_i\}^T[M]\{u_j\} = 0 \qquad i \neq j \tag{2.37}$$

Then all of the terms of the matrix can be rewritten as

$$[U]^T[M][U] = \begin{bmatrix} (\{u_1\}^T[M]\{u_1\}) & 0 & 0 & \cdots \\ 0 & (\{u_2\}^T[M]\{u_2\}) & 0 & \cdots \\ 0 & 0 & (\{u_3\}^T[M]\{u_3\}) & \cdots \\ \vdots & \vdots & \vdots & \ddots \end{bmatrix} \tag{2.38}$$

Doing this for all three terms of the transformed equation results in three matrices: the modal mass, modal damping (with the assumption of proportional damping), and modal stiffness matrices:

Modal mass

$$[U]^T[M][U] = \begin{bmatrix} \overline{m}_{11} & 0 & 0 & \cdots \\ 0 & \overline{m}_{22} & 0 & \cdots \\ 0 & 0 & \overline{m}_{33} & \cdots \\ \vdots & \vdots & \vdots & \ddots \end{bmatrix} \tag{2.39}$$

Modal damping

$$[U]^T[C][U] = \begin{bmatrix} \overline{c}_{11} & 0 & 0 & \cdots \\ 0 & \overline{c}_{22} & 0 & \cdots \\ 0 & 0 & \overline{c}_{33} & \cdots \\ \vdots & \vdots & \vdots & \ddots \end{bmatrix} \tag{2.40}$$

Modal stiffness

$$[U]^T[K][U] = \begin{bmatrix} \overline{k}_{11} & 0 & 0 & \cdots \\ 0 & \overline{k}_{22} & 0 & \cdots \\ 0 & 0 & \overline{k}_{33} & \cdots \\ \vdots & \vdots & \vdots & \ddots \end{bmatrix} \tag{2.41}$$

So due to the orthogonality condition, this transformation *uncouples* the highly coupled set of equations in physical space into a set of uncoupled single DOF systems in modal space as

$$\begin{bmatrix} \overline{m}_1 & & \\ & \overline{m}_2 & \\ & & \ddots \end{bmatrix} \begin{Bmatrix} \ddot{p}_1 \\ \ddot{p}_2 \\ \vdots \end{Bmatrix} + \begin{bmatrix} \overline{c}_1 & & \\ & \overline{c}_2 & \\ & & \ddots \end{bmatrix} \begin{Bmatrix} \dot{p}_1 \\ \dot{p}_2 \\ \vdots \end{Bmatrix} + \begin{bmatrix} \overline{k}_1 & & \\ & \overline{k}_2 & \\ & & \ddots \end{bmatrix} \begin{Bmatrix} p_1 \\ p_2 \\ \vdots \end{Bmatrix} = \begin{Bmatrix} \{u_1\}^T & \{F\} \\ \{u_2\}^T & \{F\} \\ \vdots & \end{Bmatrix} \tag{2.42}$$

with diagonal matrices for modal mass (m,m), modal damping (m,m) (with assumed proportional damping in the model), and modal stiffness (m,m). It is very important to note that the size of these matrices is (m,m) and not (n,n). And the transformation also takes the applied force and projects it to each of the individual single degree of freedom systems as a modal force for each.

Now these diagonalized equations can be written as

$$\begin{bmatrix} \backslash & & \\ & \overline{M} & \\ & & \backslash \end{bmatrix}\{\ddot{p}\} + \begin{bmatrix} \backslash & & \\ & \overline{C} & \\ & & \backslash \end{bmatrix}\{\dot{p}\} + \begin{bmatrix} \backslash & & \\ & \overline{K} & \\ & & \backslash \end{bmatrix}\{p\} = [U]^T\{F\} \tag{2.43}$$

These diagonal equations drastically reduce the complication of the problem especially if the necessary number of *modal DOFs* needed to characterize the problem is much smaller than the number of *physical DOFs* ($m \ll n$). In essence, the complicated set of coupled DOFs has been reduced to a simpler system, described by a set of single degree of freedom systems that are related to the multiple degree of freedom system through the modal transformation equation. Figure 2.25 schematically shows the decomposition of the coupled physical equations into a set of equivalent single degree of freedom systems, one for each mode of the system, that are linearly independent of each other and orthogonal with respect to the mass and stiffness matrices. This is very important (or actually rather clever) because it means that any complicated system, including, say, a million degree of freedom finite element model can be reduced to an equivalent set of single degree of freedom systems, which are very simple to solve.

Looking at any one equation from this diagonal set of matrices, the resulting equation is the single degree of freedom equation written in general for the i mode as

$$\overline{m}_i\ddot{p}_i + \overline{c}_i\dot{p}_i + \overline{k}_i p_i = \overline{f}_i \tag{2.44}$$

Of course it is very important to note that this is really just a simple single degree of freedom system but it is one of the simplest equations to solve for any forces applied to the system. So the response of each single degree of freedom to the equivalent force can be used to determine the response of each mode. And each mode has a contribution to the total response of the system. But each response is only a single transient time response over all time due to the individual mode contribution. This individual mode response needs to be projected back to the physical set of degrees of freedom using the same equation used to uncouple all the equations in the first

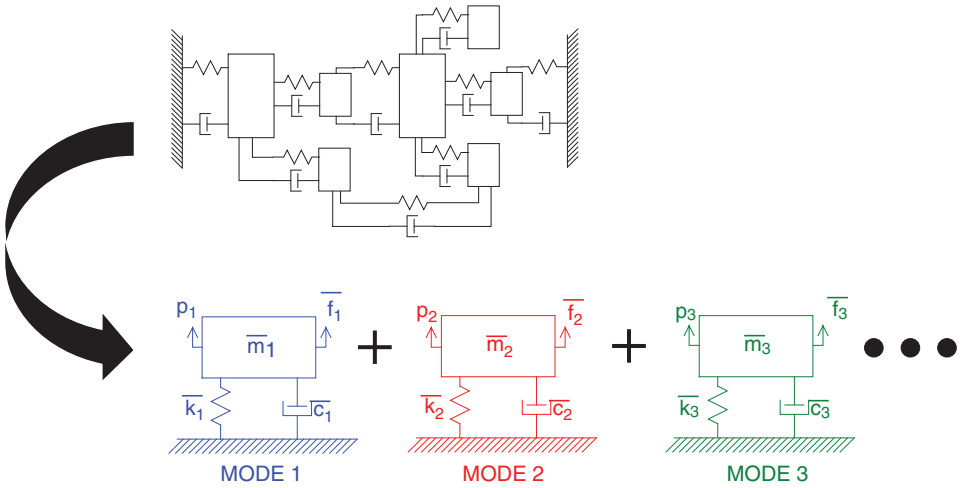

Figure 2.25 Modal transformation converting coupled MDOF system into SDOF modal systems.

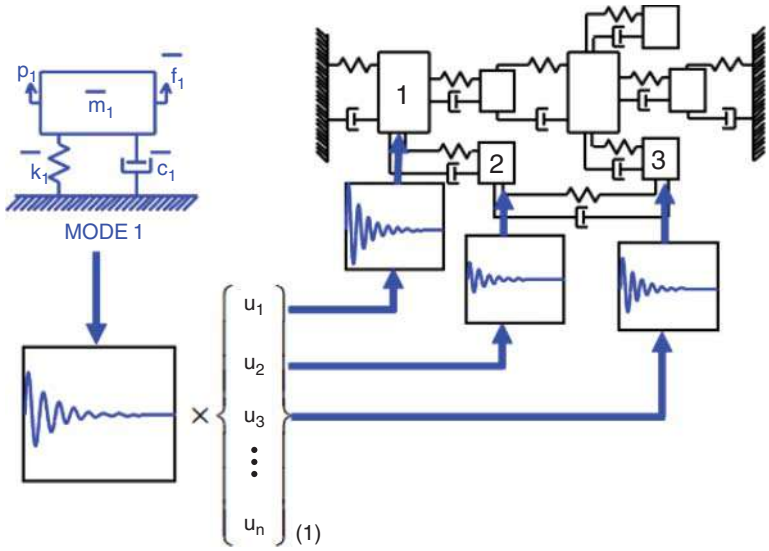

Figure 2.26 Mode 1 modal response projected to all physical DOFs for mode 1 contribution.

place. So the individual response for mode 1, for instance, is given by

$$\begin{Bmatrix} x_1 \\ x_2 \\ x_3 \\ \vdots \\ x_n \end{Bmatrix}_1 = \begin{Bmatrix} u_1 \\ u_2 \\ u_3 \\ \vdots \\ u_n \end{Bmatrix}_1 p_1 \tag{2.45}$$

The distribution of response from the modal degree of freedom for mode 1 is expanded back to all the physical degrees of freedom in physical space with the first mode shape to identify the contribution of mode 1 for the total response of the system, as seen in Figure 2.26.

The individual response for mode 2, for instance, is given by

$$\begin{Bmatrix} x_1 \\ x_2 \\ x_3 \\ \vdots \\ x_n \end{Bmatrix}_2 = \begin{Bmatrix} u_1 \\ u_2 \\ u_3 \\ \vdots \\ u_n \end{Bmatrix}_2 p_2 \tag{2.46}$$

Again, the distribution of response from the modal degree of freedom for mode 2 is expanded back to all the physical degrees of freedom in physical space with the second mode shape to identify the contribution of mode 2 for the total response of the system, as seen in Figure 2.27.

The total response of the system can then be expressed as the summation of each of the modes that contributes to the total response of the system:

$$\begin{Bmatrix} x_1 \\ x_2 \\ x_3 \\ \vdots \\ x_n \end{Bmatrix} = \begin{Bmatrix} u_1 \\ u_2 \\ u_3 \\ \vdots \\ u_n \end{Bmatrix}_1 p_1 + \begin{Bmatrix} u_1 \\ u_2 \\ u_3 \\ \vdots \\ u_n \end{Bmatrix}_2 p_2 + \begin{Bmatrix} u_1 \\ u_2 \\ u_3 \\ \vdots \\ u_n \end{Bmatrix}_3 p_3 + \cdots \tag{2.47}$$

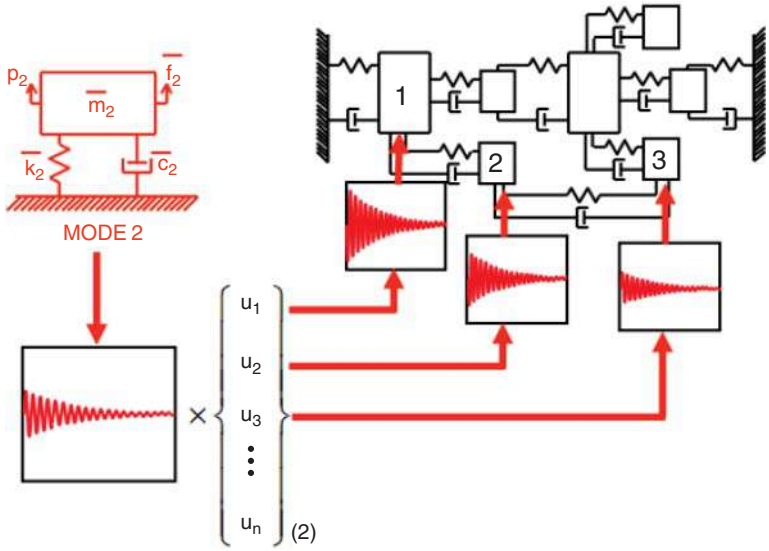

Figure 2.27 Mode 2 modal response projected to all physical DOFs for mode 2 contribution.

In modal space, each mode describes the contribution to the physical response for that particular mode. Because the modes are linearly independent to each other and orthogonal with respect to the system mass and stiffness matrices, the contribution to the physical system can be made up from linear combinations of each individual mode uncoupled from every other mode. The entire process of the physical equations projected to modal space to compute the response of each single degree of freedom system and the projection of the modal response of each mode back to physical space is conceptually shown in Figure 2.28.

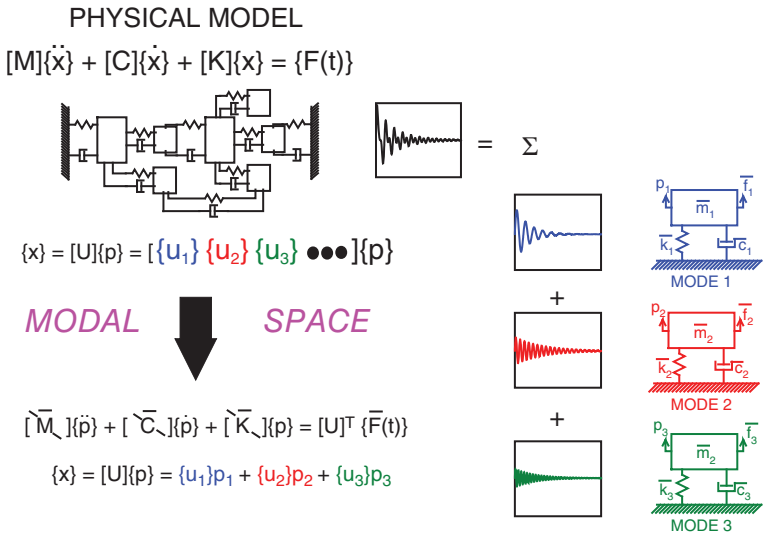

Figure 2.28 Schematic of the transformation of the physical/coupled MDOF system into equivalent SDOF systems.

2.3.2 Laplace Domain for Multiple Degree of Freedom System

A transformation similar to the Laplace evaluation performed for the single degree of freedom system can be performed for the multiple degree of freedom system. The original equation of motion in physical space can be transformed into the Laplace domain using the Laplace transform and is given as

$$\underbrace{\left[[M]s^2 + [C]s + [K]\right]}_{\text{Characteristic equation}} \{X(s)\} = \underbrace{\{F(s)\}}_{\text{Applied force}} + \underbrace{[[M]s + C]\{x_0\}}_{\text{Initial displacement}} + \underbrace{[M]\{\dot{x}_0\}}_{\text{Initial velocity}} \tag{2.48}$$

where s is the Laplace variable. The main advantage of this formulation is that the equation has the characteristic equation, the applied force, and the initial conditions all in one equation. If the initial conditions are assumed to be zero, as is typically done, then

$$\left[[M]s^2 + [C]s + [K]\right] \{X(s)\} = \{F(s)\} \tag{2.49}$$

The homogeneous equation can be written as

$$\left[[M]s^2 + [C]s + [K]\right] \{x(s)\} = 0 \quad \Rightarrow \quad [B(s)]\{x(s)\} = 0 \tag{2.50}$$

where [B(s)] is referred to as the *system matrix*. Note that because the mass, damping, and stiffness matrices are square symmetric, the system matrix [B(s)] is also square symmetric.

The solution of the homogeneous equation yields 2n solutions where n is the number of equations. If the damping is less than critical damping then the solution to this equation contains roots that are referred to as the *poles* of the system and occur in complex conjugate pairs given by

$$\det\left[[M]s^2 + [C]s + [K]\right] = 0 \quad \Rightarrow \quad p_k = -\sigma_k \pm j\omega_{dk} \tag{2.51}$$

This complex valued function has a portion of the pole (real part) that is the percentage of critical damping, ζ, times the undamped natural frequency of the system, ω_n, and a portion of the pole (imaginary part) that is the damped natural frequency, ω_d. Notice that the poles occur in complex conjugate pairs.

Returning to the system equation and rearranging terms to obtain a ratio of response to input gives

$$[B(s)]\{x(s)\} = \{F(s)\} \quad \Rightarrow \quad [B(s)]^{-1} = \frac{\{x(s)\}}{\{F(s)\}} \tag{2.52}$$

The inverse of the system matrix [B(s)] gives the *system transfer matrix*:

$$[B(s)]^{-1} = [H(s)] = \frac{\text{Adj}[B(s)]}{\det[B(s)]} = \frac{[A(s)]}{\det[B(s)]} \tag{2.53}$$

which is the adjoint of the system matrix divided by the determinant of the system matrix. Expanding this out would reveal:

$$\begin{bmatrix} h_{11}(s) & h_{12}(s) & h_{13}(s) & \cdots \\ h_{21}(s) & h_{22}(s) & h_{23}(s) & \cdots \\ h_{31}(s) & h_{32}(s) & h_{33}(s) & \cdots \\ \vdots & \vdots & \vdots & \ddots \end{bmatrix} = \frac{\begin{bmatrix} a_{11}(s) & a_{12}(s) & a_{13}(s) & \cdots \\ a_{21}(s) & a_{22}(s) & a_{23}(s) & \cdots \\ a_{31}(s) & a_{32}(s) & a_{33}(s) & \cdots \\ \vdots & \vdots & \vdots & \ddots \end{bmatrix}}{\det[B(s)]} \tag{2.54}$$

The system transfer function is a complex valued surface. The numerator of this equation is [A(s)], which is referred to as the *residue matrix*; the denominator of this equation is det [B(s)], which is a scalar quantity and is called the *characteristic equation*. The denominator yields the

poles of the system and it is interesting to note that the poles are constant and do not depend on which term of the residue matrix is evaluated. This is why the poles are referred to as "global properties" of the system.

Now in order to evaluate some interesting items in the system transfer matrix, let's write

$$[B(s)][B(s)]^{-1} = [I] \tag{2.55}$$

and substitute the system transfer function into the equation. Rearranging terms gives,

$$[B(s)][A(s)] = \det[B(s)][I] \tag{2.56}$$

This equation has two very important components that that are the basic underlying items of interest for experimental modal analysis:

$[A(s)]$	Residue matrix	→	Mode shapes
$\det [B(s)]$	Characteristic equation	→	Poles

The determinant of the characteristic equation results in a high order polynomial, which can be solved to find the roots or poles of the system. The residue matrix needs further manipulation to reveal some important aspects of the matrix, then resulting in the mode shapes of the system; the symmetry in the matrix is also important for the extraction of mode shapes as well as definition of the reciprocity principle. When the system transfer function is evaluated at a pole of the system, the solution can be written as

$$[B(p_k)][A(p_k)] = 0 \tag{2.57}$$

which can be broken up into column format as

$$[B(p_k)]\left[\{a_1(p_k)\}\ \{a_2(p_k)\}\ \cdots\right] = [\{0\}\ \{0\}\ \cdots] \tag{2.58}$$

Now each column of the residue matix can be written as a separate equation as

$$\begin{aligned}
&[B(p_k)]\{a_1(p_k)\} = \{0\}\\
&[B(p_k)]\{a_2(p_k)\} = \{0\}\\
&[B(p_k)]\{a_3(P_k)\} = \{0\}\\
&\quad\vdots
\end{aligned} \tag{2.59}$$

Notice that every column of Eq. (2.59) is a solution to Eq. (2.57). Also, due to symmetry, every row of the matrix is also a solution to this equation. Therefore, every row and column is a solution to this equation when the system transfer function is evaluated at a pole of the system. This means that in order to evaluate the modal vector, any one of the rows or columns may be used to estimate the system vector characteristics. This will be illustrated shortly.

As was done for the single degree of freedom system, the system transfer function can be written in *partial fraction form* as

$$[H(s)] = \sum_{k=1}^{m} \frac{[A_k]}{(s - p_k)} + \frac{[A_k^*]}{(s - p_k^*)} \tag{2.60}$$

or in *pole-zero form* (or in polynomial form by expanding out the factors) as

$$[H(s)] = \prod_{k=1}^{m} \left[\frac{(s - z_k)(s - z_k^*)}{(s - p_k)(s - p_k^*)}\right] \tag{2.61}$$

Alternatively, by taking the inverse Laplace transform, the *impulse response function* in the time domain is given by

$$[h(t)] = \left[\sum_{k=1}^{m} \frac{1}{m_k \omega_{dk}} e^{-\sigma_k t} \sin \omega_{dk} t\right] \tag{2.62}$$

Now looking at a particular term of the matrix, the system transfer function can be written in *partial fraction form* as

$$h_{ij}(s) = \sum_{k=1}^{m} \frac{a_{ijk}(s)}{(s - p_k)} + \frac{a_{ijk}(s)^*}{(s - p_k^*)} \tag{2.63}$$

or in *polynomial form* as

$$h_{ij}(s) = \frac{a_{ij}(s)}{\det[B(s)]} = \frac{s^{2n-1} + b_1 s^{2n-2} + b_2 s^{2n-3} + \cdots}{s^{2n} + a_1 s^{2n-1} + a_2 s^{2n-2} + \cdots} \tag{2.64}$$

or as the *impulse response as*

$$h_{ij}(t) = \sum_{k=1}^{m} \frac{1}{m_k \omega_{dk}} e^{-\sigma_k t} \sin \omega_{dk} t \tag{2.65}$$

2.3.3 The Frequency Response Function

The *frequency response function* is the system transfer function evaluated at $s = j\omega$. Letting $s = j\omega$ (which effectively takes a slice out of the transfer function surface), then the frequency response function is given by

$$[H(s)]_{s=j\omega} = [H(j\omega)] = \sum_{k=1}^{m} \frac{[A_k]}{(j\omega - p_k)} + \frac{[A_k^*]}{(j\omega - p_k^*)} \tag{2.66}$$

An individual ij term is given by

$$h_{ij}(s)_{s=j\omega} = h_{ij}(j\omega) = \sum_{k=1}^{m} \frac{a_{ijk}}{(j\omega - p_k)} + \frac{a_{ijk}{}^*}{(j\omega - p_k^*)} \tag{2.67}$$

Notice that the frequency response function is made up of a collection of single degree of freedom systems summed over all of the modes of the system. The frequency response function is the same one shown previously for the single degree of freedom system, but now there is a contribution to the total frequency response function due to each mode. A typical acceleration frequency response function is shown in Figure 2.29 to illustrate the sum of many modes over a broad frequency range; note that only the magnitude of the frequency response function is shown for brevity. The equation is also shown in the figure 2.29 with the summed frequency response function in part (a) and the individual contributions of each mode in part (b).

And to pull all the pieces together, the system transfer function and the complex frequency response function are shown in Figure 2.30. The figure shows the equation with the magnitude of the transfer function, along with the frequency response functions for the real, imaginary, magnitude and phase parts of the frequency response function for a system with 3 modes.

2.3.4 Mode Shapes from Frequency Response Equations

The solution to the system equation can be obtained using any row or any column of B(s); when the system transfer function is evaluated at a pole of the system, a corresponding shape vector is obtained. Now let's look at this a little further using some advanced techniques. Using singular valued decomposition techniques, when [H(s)] is evaluated at a pole, it can be shown that [H(s)] is singular and of rank = 1 and can be decomposed as

$$[H(s)]_{s=p_k} = \{u_k\} \frac{q_k}{s - p_k} \{u_k\}^T \tag{2.68}$$

$$[H(s)]_{s=j\omega} = [H(j\omega)] = \sum_{k=1}^{m} \frac{[A_k]}{(j\omega - p_k)} + \frac{[A_k^*]}{(j\omega - p_k^*)}$$

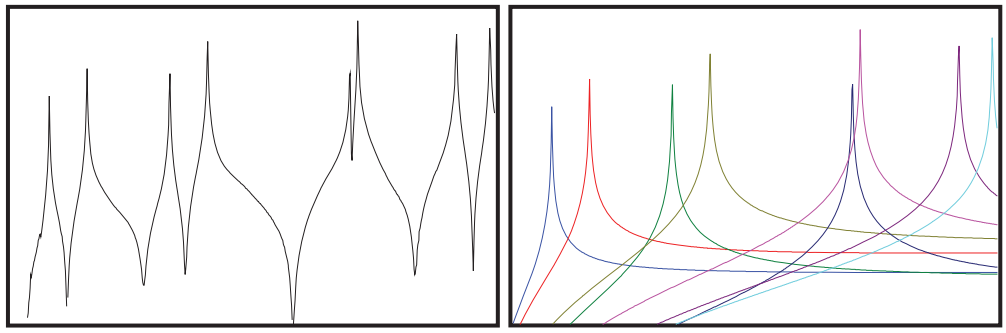

Figure 2.29 FRF for Multiple DOF system: (a) summed FRF; (b) individual mode contributions.

Notice that from this, a relationship between the residue matrix and the mode shapes of the system can be written as

$$[A(s)]_k = q_k \{u_k\} \{u_k\}^T \tag{2.69}$$

where q is a scaling constant and will be discussed shortly.

Looking at the adjoint matrix and expanding out some of the terms of this equation for the kth mode of the system reveals

$$\begin{bmatrix} a_{11k} & a_{12k} & a_{13k} & \cdots \\ a_{21k} & a_{22k} & a_{23k} & \cdots \\ a_{31k} & a_{32k} & a_{33k} & \cdots \\ \vdots & \vdots & \vdots & \ddots \end{bmatrix} = q_k \begin{bmatrix} u_{1k}u_{1k} & u_{1k}u_{2k} & u_{1k}u_{3k} & \cdots \\ u_{2k}u_{1k} & u_{2k}u_{2k} & u_{2k}u_{3k} & \cdots \\ u_{3k}u_{1k} & u_{3k}u_{2k} & u_{3k}u_{3k} & \cdots \\ \vdots & \vdots & \vdots & \ddots \end{bmatrix} \tag{2.70}$$

It is very important to note that the residues are directly related to the system mode shapes. For illustration purposes, expanding out some of these terms is useful. Let us regroup some of these terms in the form of column vectors.

$$\left[\begin{Bmatrix} a_{11k} \\ a_{21k} \\ a_{31k} \\ \vdots \end{Bmatrix} \begin{Bmatrix} a_{12k} \\ a_{22k} \\ a_{32k} \\ \vdots \end{Bmatrix} \begin{Bmatrix} a_{13k} \\ a_{23k} \\ a_{33k} \\ \vdots \end{Bmatrix} \cdots \right] = \left[q_k u_{1k} \begin{Bmatrix} u_{1k} \\ u_{2k} \\ u_{3k} \\ \vdots \end{Bmatrix} \quad q_k u_{2k} \begin{Bmatrix} u_{1k} \\ u_{2k} \\ u_{3k} \\ \vdots \end{Bmatrix} \quad q_k u_{3k} \begin{Bmatrix} u_{1k} \\ u_{2k} \\ u_{3k} \\ \vdots \end{Bmatrix} \quad \cdots \right] \tag{2.71}$$

The first column of this matrix contains an estimate of the kth mode of the system scaled by q_k and u_{1k}

$$\begin{Bmatrix} a_{11k} \\ a_{21k} \\ a_{31k} \\ \vdots \end{Bmatrix} = q_k u_{1k} \begin{Bmatrix} u_{1k} \\ u_{2k} \\ u_{3k} \\ \vdots \end{Bmatrix} \tag{2.72}$$

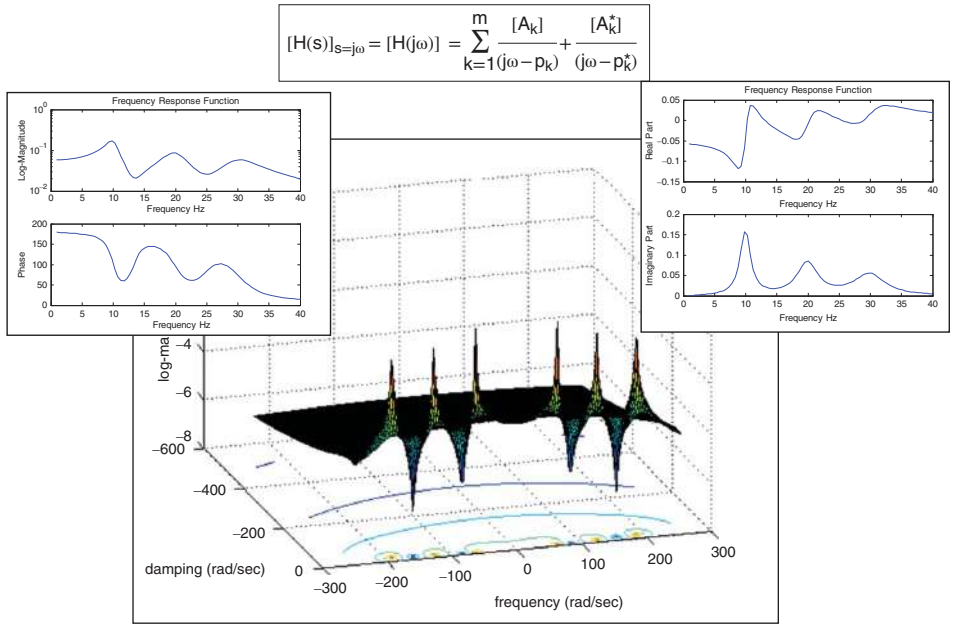

Figure 2.30 Transfer function and FRF for 3DOF system: (left) phase and magnitude; (right) real and imaginary; (main image) system transfer function.

The second column of this matrix contains an estimate of the kth mode of the system scaled by q_k and u_{2k}

$$\begin{Bmatrix} a_{12k} \\ a_{22k} \\ a_{32k} \\ \vdots \end{Bmatrix} = q_k u_{2k} \begin{Bmatrix} u_{1k} \\ u_{2k} \\ u_{3k} \\ \vdots \end{Bmatrix} \tag{2.73}$$

The third column contains an estimate of the kth mode of the system scaled by q_k and u_{3k}

$$\begin{Bmatrix} a_{13k} \\ a_{23k} \\ a_{33k} \\ \vdots \end{Bmatrix} = q_k u_{3k} \begin{Bmatrix} u_{1k} \\ u_{2k} \\ u_{3k} \\ \vdots \end{Bmatrix} \tag{2.74}$$

Now let us regroup some of these terms in the form of row vectors.

$$\begin{bmatrix} \{a_{11k} & a_{12k} & a_{13k} & \cdots\} \\ \{a_{21k} & a_{22k} & a_{23k} & \cdots\} \\ \{a_{31k} & a_{32k} & a_{33k} & \cdots\} \\ & \vdots & & \end{bmatrix} = \begin{bmatrix} q_k u_{1k}\{u_{1k} & u_{2k} & u_{3k} & \cdots\} \\ q_k u_{2k}\{u_{1k} & u_{2k} & u_{3k} & \cdots\} \\ q_k u_{3k}\{u_{1k} & u_{2k} & u_{3k} & \cdots\} \\ & \vdots & & \end{bmatrix} \tag{2.75}$$

It is clear that the first row of this matrix contains an estimate of the kth mode of the system scaled by q_k and u_{1k}

$$\{a_{11k} \quad a_{12k} \quad a_{13k} \quad \cdots\} = q_k u_{1k} \{u_{1k} \quad u_{2k} \quad u_{3k} \quad \cdots\} \tag{2.76}$$

the second row contains an estimate of the kth mode of the system scaled by q_k and u_{2k}

$$\{a_{21k} \quad a_{22k} \quad a_{23k} \quad \cdots\} = q_k u_{2k} \{u_{1k} \quad u_{2k} \quad u_{3k} \quad \cdots\} \tag{2.77}$$

and the third row contains an estimate of the kth mode of the system scaled by q_k and u_{3k}

$$\{a_{31k} \quad a_{32k} \quad a_{33k} \quad \cdots\} = q_k u_{3k} \{u_{1k} \quad u_{2k} \quad u_{3k} \quad \cdots\} \tag{2.78}$$

For unit modal mass scaling, the scaling constant can be shown to be

$$q_k = \frac{1}{2\, j\omega_k} \tag{2.79}$$

From the above equations, it can be seen that the frequency response function can be obtained from the eigenvalues and eigenvectors of the system. If this frequency response function could be measured, then the parameters of interest (frequency, damping, and mode shape) can be extracted from measured data.

2.3.5 Point-to-Point Frequency Response Function

The point-to-point frequency response function will be evaluated next. Let's consider the response at point i due to an input at point j in the system. Evaluating the system transfer function at $s = j\omega$ for a particular ij (input–output) location, gives

$$h(s)_{ij}\big|_{s=j\omega} = h_{ij}(j\omega) = \sum_{k=1}^{m} \frac{a_{ijk}}{(j\omega - p_k)} + \frac{a^*_{ijk}}{(j\omega - p^*_k)} \tag{2.80}$$

It is very important to note that this is the same as written earlier for the single degree of freedom system, except that now the effects of all the modes are summed together. This is shown in Figure 2.31 (considering only two modes of the system) to illustrate the summation.

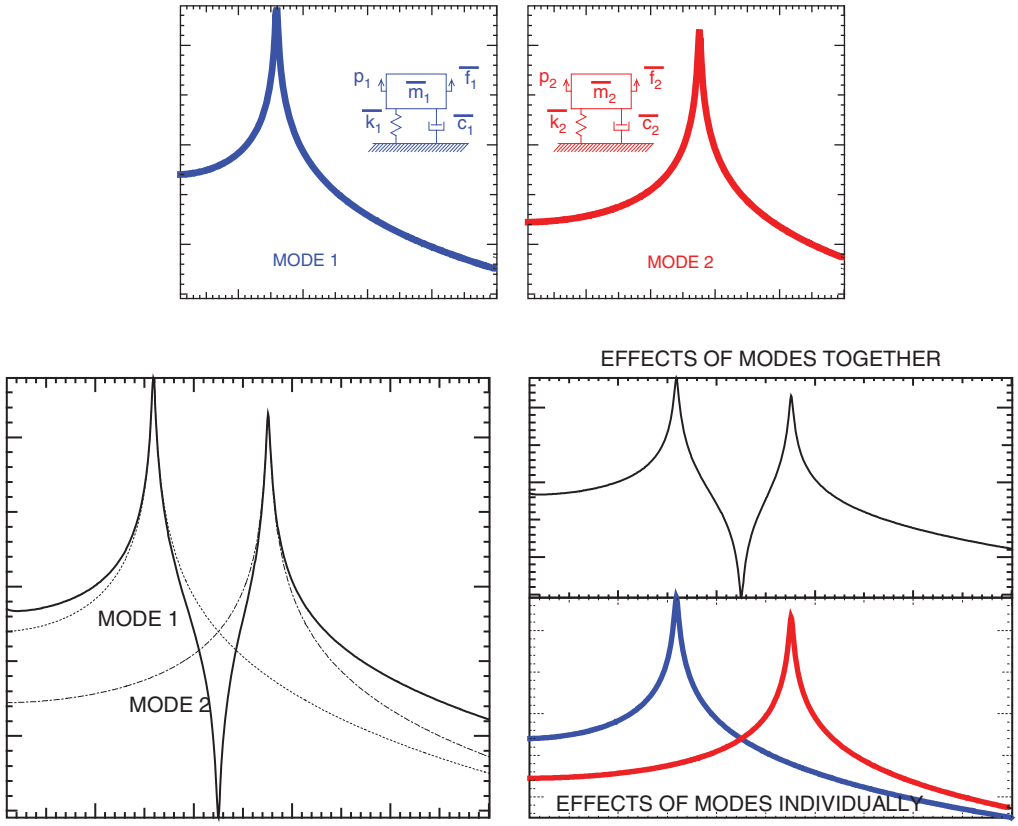

Figure 2.31 FRF composition of SDOF FRFs summed together.

This is further shown in Figures 2.32–2.34 for the D/F, V/F, and A/F frequency response functions plotted in real, imaginary, magnitude, phase and Nyquist plots. In each plot, the complete frequency response function is shown in black in the upper plot and the contributions of each individual mode are shown in the lower plot, with mode 1 in blue and mode 2 in red.

In addition, recall that $a_{ijk} = u_{ik}\, u_{jk;}$ the point-to-point frequency response function can therefore be written as

$$h(s)_{ij}\big|_{s=j\omega} = h_{ij}(j\omega) = \sum_{k=1}^{m} \frac{q_k u_{ik} u_{jk}}{(j\omega - p_k)} + \frac{q_k^* u_{ik}^* u_{jk}^*}{(j\omega - p_k^*)} \tag{2.81}$$

From this equation, the point-to-point frequency response function is made up a set of single degree of freedom oscillators and the amplitude of each is controlled by the filtering effect of the input excitation location (based on the value of the mode shape at the j DOF) and the filtering effect of the output response location (based on the value of the mode shape at the i DOF).

2.3.6 Response of Multiple Degree of Freedom System to Harmonic Excitations

Previously, the single degree of freedom system response to sinusoidal excitations was considered. Now let's look at the same sinusoidal excitation for a multiple degree of freedom system.

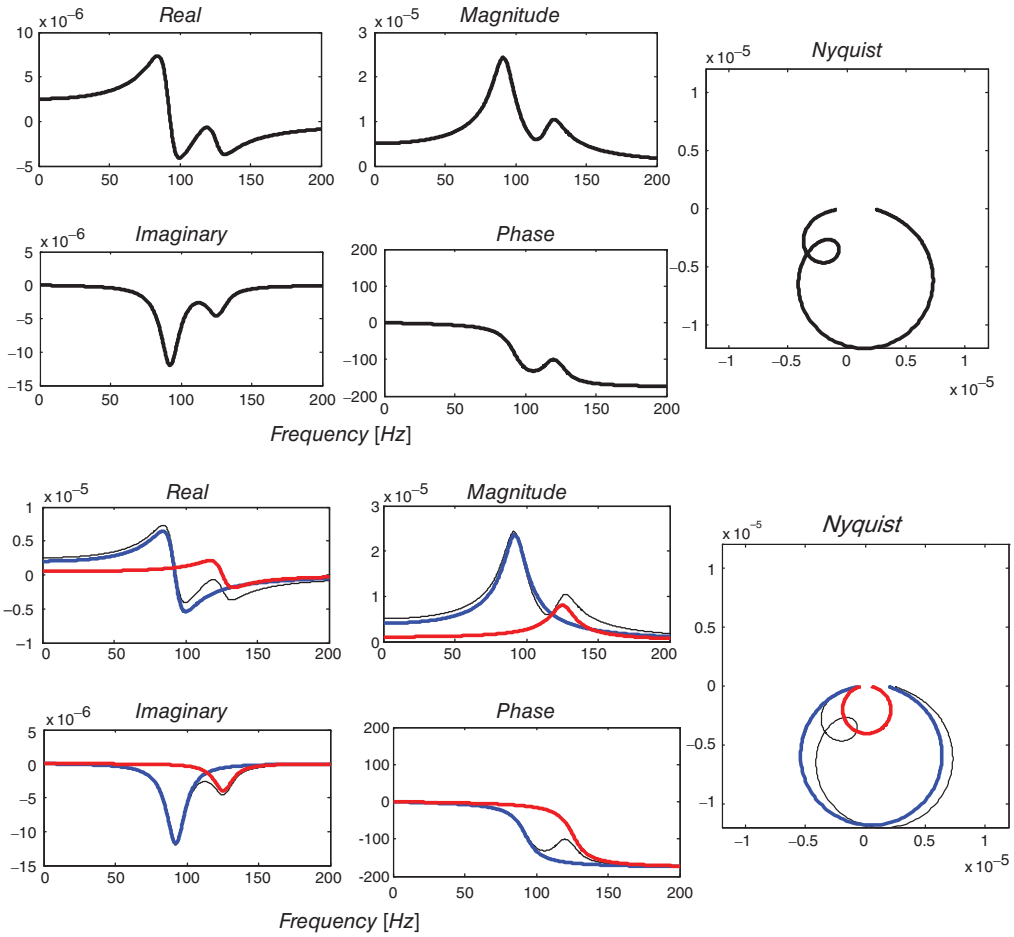

Figure 2.32 D/F FRF with real, imaginary, magnitude, phase and Nyquist forms of the FRF.

The response of a multiple degree of freedom system due to a sinusoidal excitation is the sum of the responses of each of the single degree of freedom systems that make up the multiple degree of freedom system. In order to illustrate the effects of contributions from each of the modes, several different excitation frequencies for a simple 2DOF system are considered.

First let's consider a sinusoidal input where the excitation frequency is lower than both of the natural frequencies for the two modes of the system. The response is mainly made up of the response of the first mode, which is larger than the response from the second mode, as shown in Figure 2.35. The upper plot shows the contribution of each of the frequency response functions for each mode to the total frequency response function. The lower portion of this plot shows the corresponding time domain responses.

In Figure 2.36, the excitation frequency is close to the natural frequency of the first mode and the majority of the response is due to the first mode although there is a small contribution due to the second mode. The upper plot shows the contribution of each of the frequency response functions for each mode to the total frequency response function. The lower portion of this

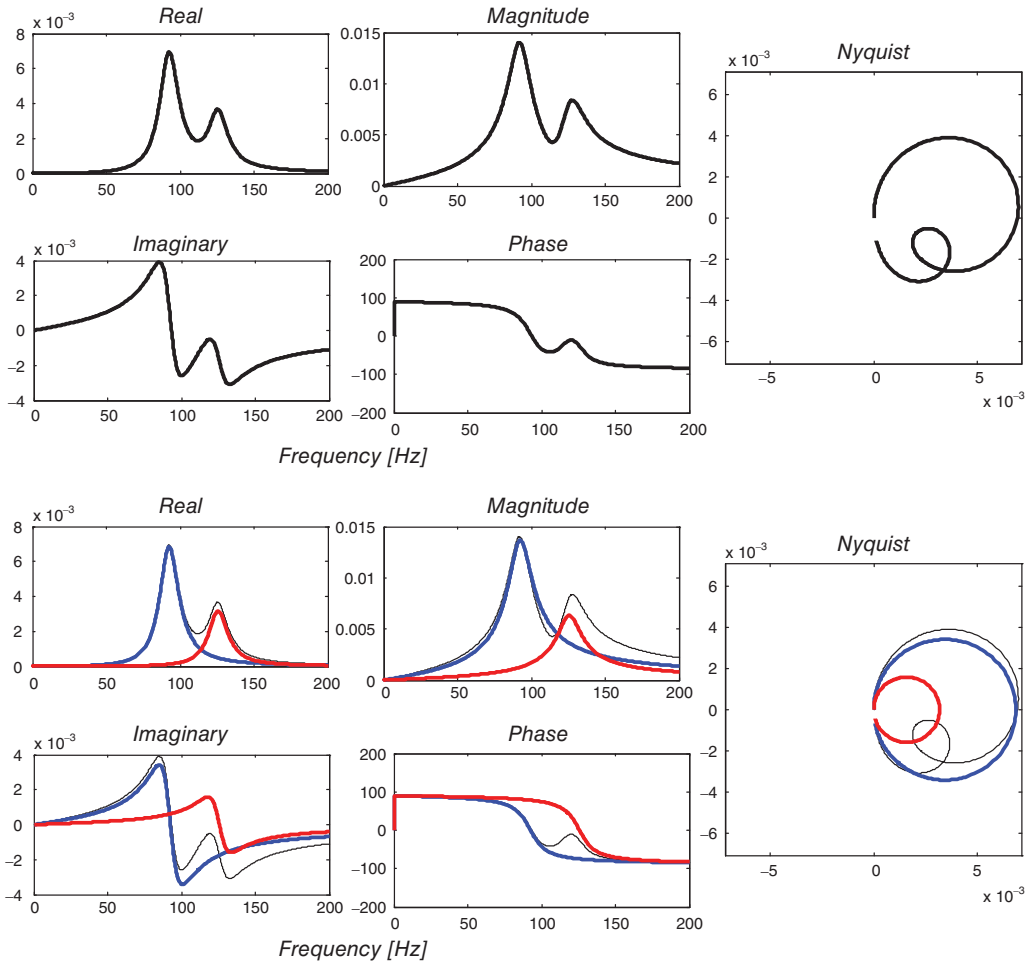

Figure 2.33 V/F FRF with real, imaginary, magnitude, phase and Nyquist forms of the FRF.

plot shows the corresponding time domain response due to mode 1 in the left plot and mode 2 in the right plot.

In Figure 2.37, the excitation frequency is between that of the two modes but is fairly close to the natural frequency of the second mode. The majority of the response is due to the second mode of the system while there is some response from the first mode. Again the upper plot shows the contribution of each of the frequency response functions for each mode to the total frequency response function; the lower portion shows the corresponding time domain responses.

From these plots, the advantage that is gained through the modal transformation of the system becomes much more apparent. It is much easier to understand the response of the system if it can be broken down into the modes that contribute to the response. For example, the frequency response function can be expanded for three modes, as shown in Figure 2.38. The frequency response equation is shown, along with the contribution of each mode: mode 1 in

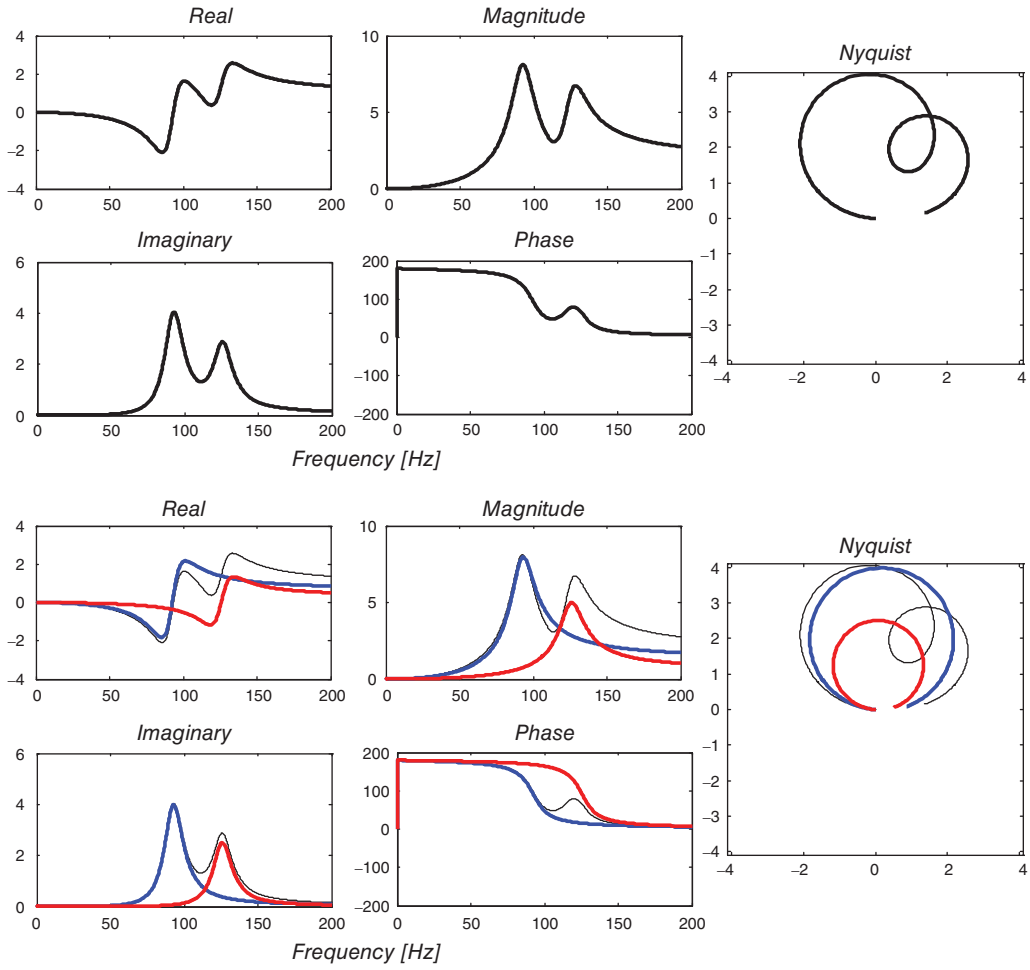

Figure 2.34 A/F FRF with real, imaginary, magnitude, phase and nyquist forms of the FRF.

blue, mode 2 in red, and mode 3 in green. The two equations are written in terms of residues and in terms of mode shapes to emphasize the importance of the mode shapes to the amplitude of the frequency response function.

2.3.7 Example: Cantilever Beam Model with Three Measured DOFs

As an example, a cantilever beam is used to develop the frequency response matrix for three measurement points for the first three modes of a cantilever beam (the values for the mode shape for each of the modes is shown in Figure 2.39).

To measure three locations along the length of the beam, we know that we could make nine total frequency response function measurements for this beam: there would be a total of three possible input forcing locations and three possible output locations to measure the response of the system. Figure 2.40 shows the 3×3 frequency response function matrix that would result. Notice that there are four sets of frequency response function matrices: magnitude, phase, real,

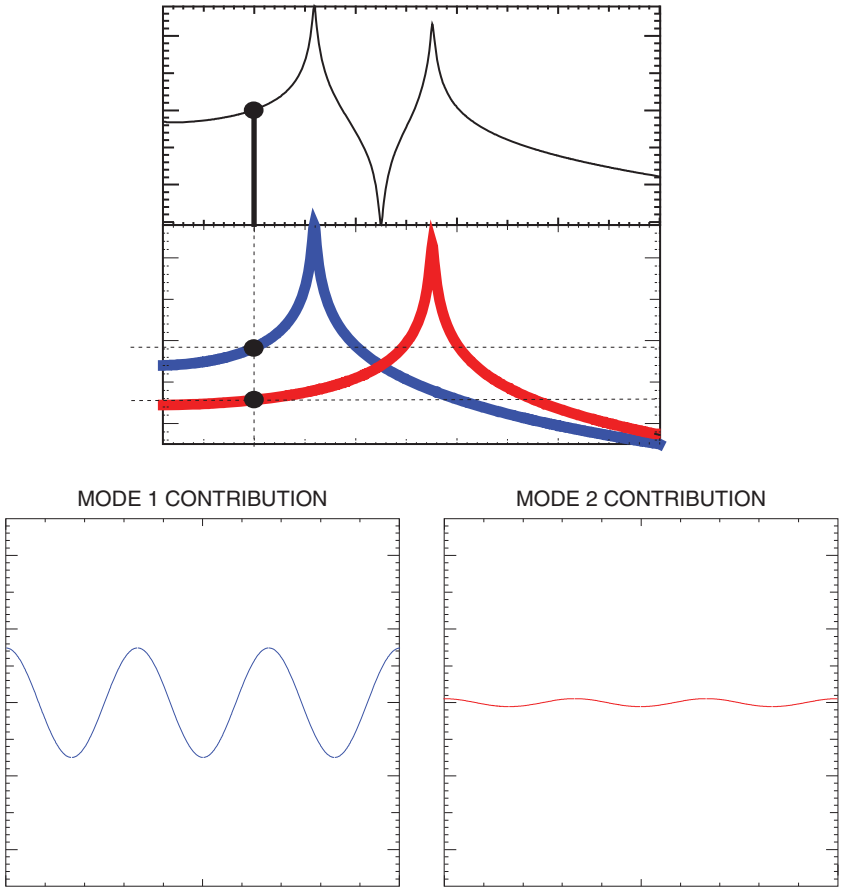

Figure 2.35 Sinusoidal excitation lower than natural frequency: (top) contribution of each of the FRFs; (bottom) time domain responses.

and imaginary. This shows us all the measurements that could possibly be made on this beam with three measurement locations. Now let's take a look at measuring each individual location, first in an impact test and then in a shaker test.

Now let us describe the measurements that could be made for this beam and let us describe a typical set of measurements that could be acquired. Let's assume that a force is applied at the tip of the beam at point 3; this is called the *reference location*. If we were to measure the response of the beam also at point 3, then we would measure h_{33}, the tip driving point frequency response function for the beam. This is shown in Figure 2.41. The driving point measurement is a special measurement where the input force and response of the system are measured at the same location.

The drive point measurement at the tip of the beam can be viewed as a summation of all the modes or as the contribution due to each mode. As seen in the four plots in Figure 2.42, the upper plot contains the summation due to all the modes and the lower plot shows the contribution due to each mode. For the first three modes of the beam, the frequency response function

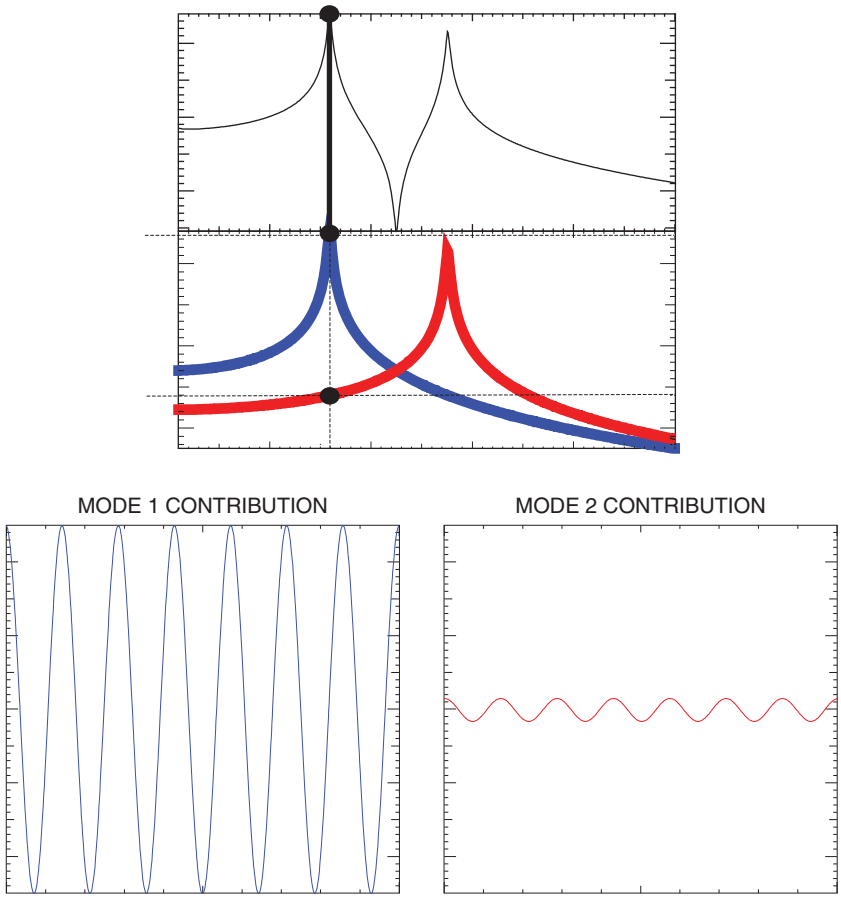

Figure 2.36 Sinusoidal excitation at mode 1 natural frequency: (top) contribution of each of the FRFs; (bottom) time domain responses.

is made up of the sum of each of the single degree of freedom oscillators describing each mode of the beam. For reference, recall that the frequency response function equation can be written as either residues or mode shapes.

Now let's excite the beam at point 2 and measure the response at point 3. This would correspond to h_{32} in Figure 2.43.

Now let's excite the beam at point 1 and measure the response at point 3. This would correspond to h_{31} in Figure 2.44.

Due to the manner in which these measurements were acquired, one row of the frequency response function matrix, namely the last row, was acquired. Note that the response location was the same for all three measurements, which implies that this is the reference location and determines which row of the frequency response function matrix was acquired. If the reference transducer is located at point 3, then this is the reference point and then the third row of the frequency response function matrix would be measured, as shown in Figure 2.45.

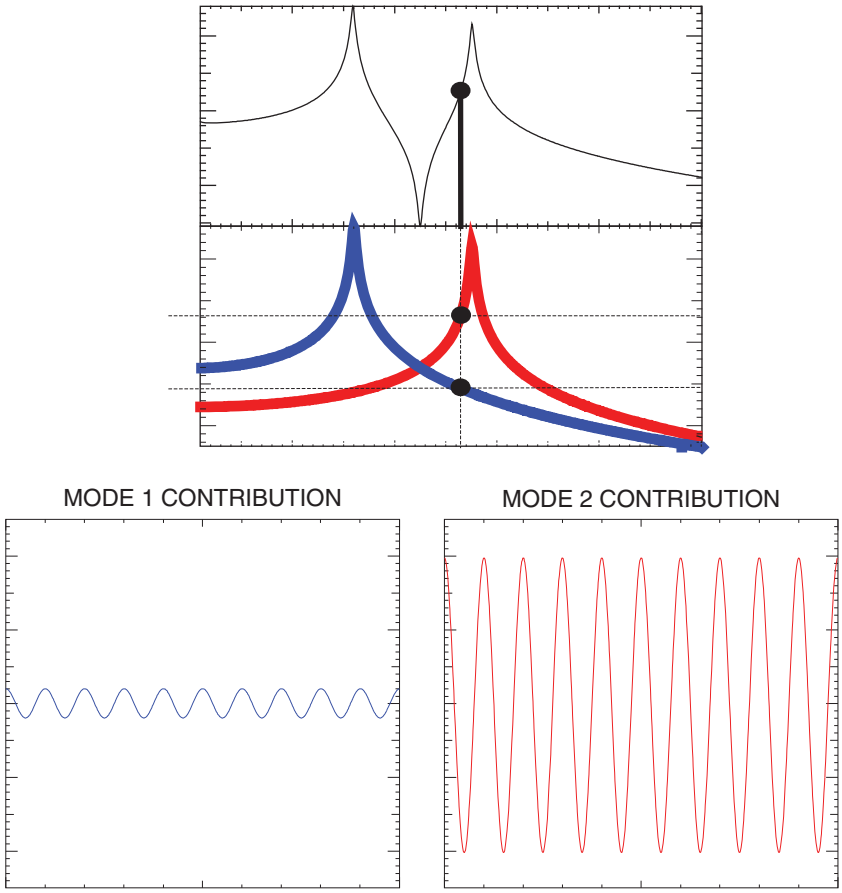

Figure 2.37 Sinusoidal excitation between mode 1 and 2 natural frequency: (top) contribution of each of the FRFs; (bottom) time domain responses.

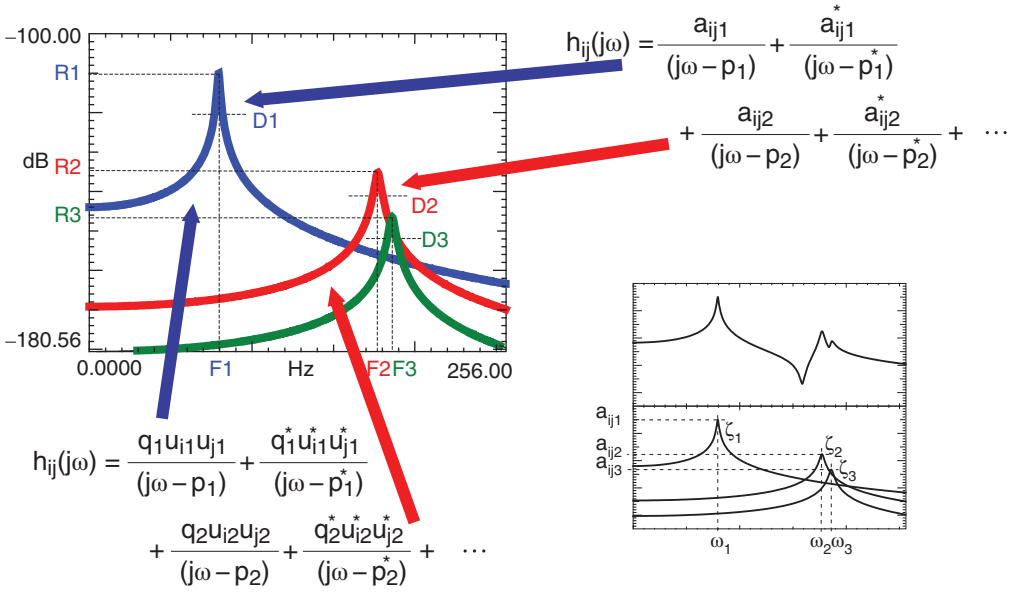

Figure 2.38 FRF broken down by mode, showing FRF both in residue equation form and shape equation form.

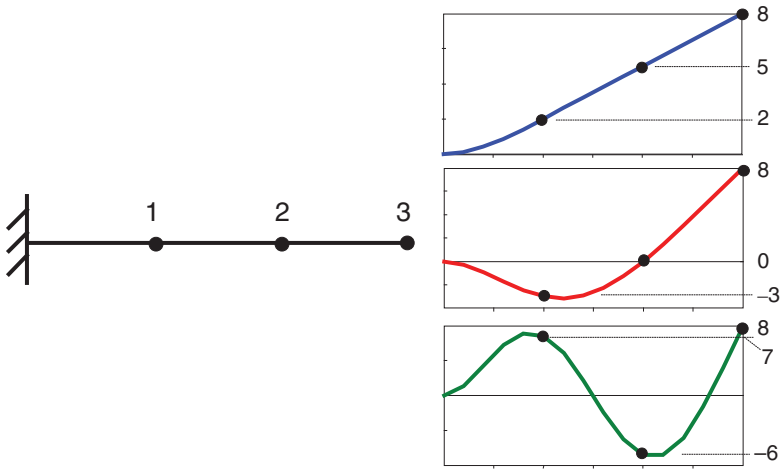

Figure 2.39 3DOF cantilever beam with first three mode shapes.

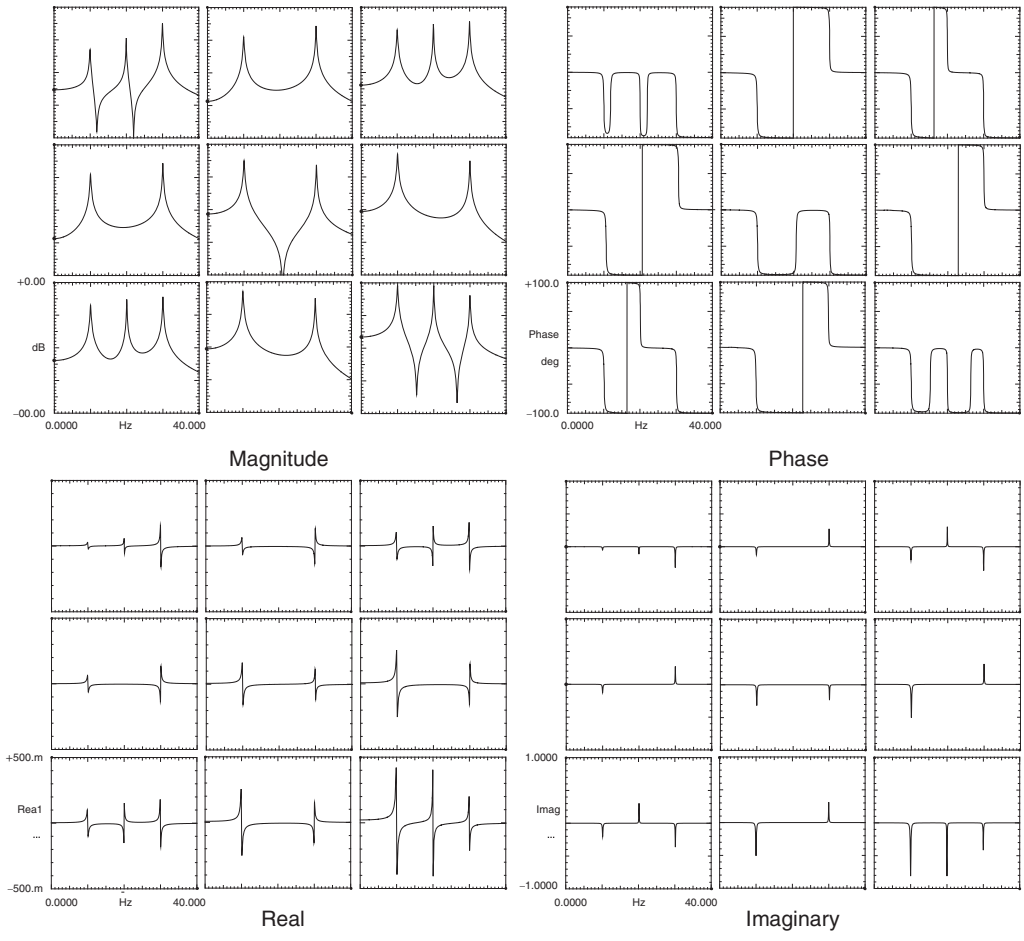

Figure 2.40 3DOF cantilever beam FRF matrix: magnitude, phase, real, imaginary parts of the FRF.

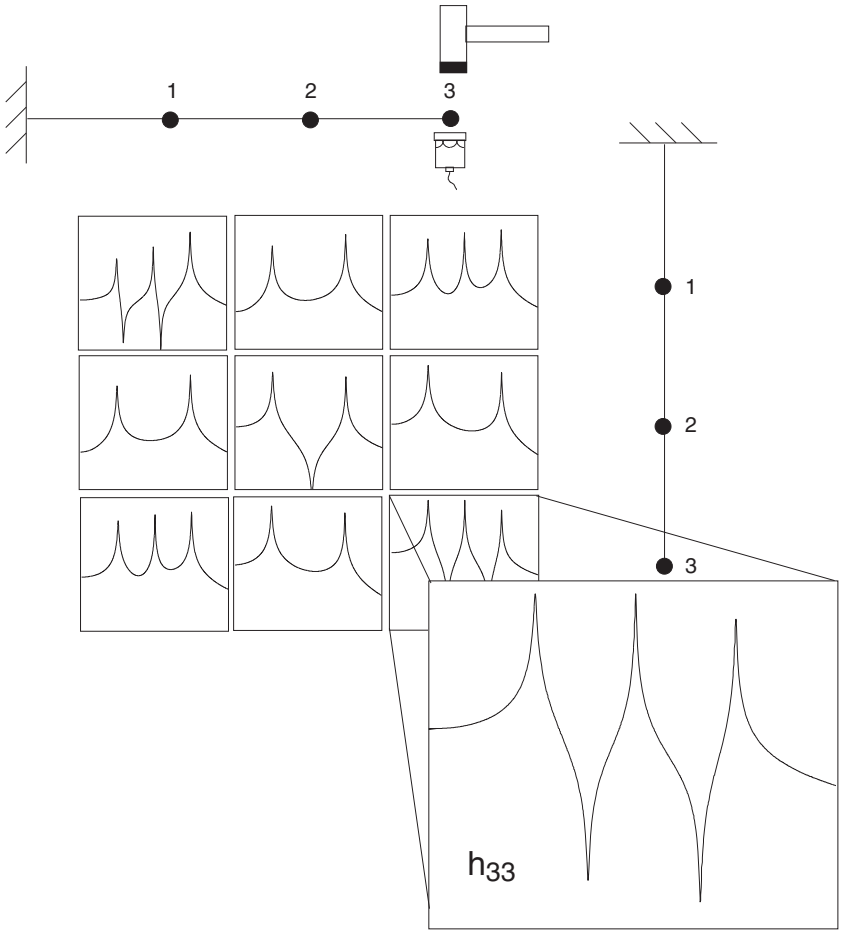

Figure 2.41 3DOF cantilever beam FRF matrix, highlighting h_{33}.

If the reference accelerometer was located at point 1 (or 2) and all the points were excited with this reference location, then the first row (or second row) of the frequency response function matrix would be acquired. This is a typical test setup configuration used for impact testing. Typically in impact testing, the response transducer is stationary and the system is excited with an impact hammer at all the measurement locations. Thus for this type of test, a row of the frequency response function matrix is acquired.

Now if the input force was stationary (as in shaker excitation), then columns of the frequency response function matrix would be acquired; the column extracted would depend on where the input excitation was placed. A typical measurement of a column of the frequency response function matrix is shown in Figure 2.46 for three measurement locations with the stationary force shaker at reference point 3.

So now that the 3DOF system frequency response matrix has been written, the pieces of the contribution of each mode can be seen in Figure 2.47. In this figure, the frequency response function for any "ij" input–output location can be easily seen. Figure 2.48 shows the same information but in summation form. Note that only the magnitude portion of the complex frequency response measurement is shown for illustration.

$$h_{ij}(j\omega) = \frac{a_{ij1}}{(j\omega - p_1)} + \frac{a^*_{ij1}}{(j\omega - p^*_1)} + \frac{a_{ij2}}{(j\omega - p_2)} + \frac{a^*_{ij2}}{(j\omega - p^*_2)} + \frac{a_{ij3}}{(j\omega - p_3)} + \frac{a^*_{ij3}}{(j\omega - p^*_3)}$$

$$h_{ij}(j\omega) = \frac{q_1 u_{i1} u_{j1}}{(j\omega - p_1)} + \frac{q_1 u_{i1} u^*_{j1}}{(j\omega - p^*_1)} + \frac{q_2 u_{i2} u_{j2}}{(j\omega - p_2)} + \frac{q_2 u_{i2} u^*_{j2}}{(j\omega - p^*_2)} + \frac{q_3 u_{i3} u_{j3}}{(j\omega - p_3)} + \frac{q_3 u_{i3} u^*_{j3}}{(j\omega - p^*_3)}$$

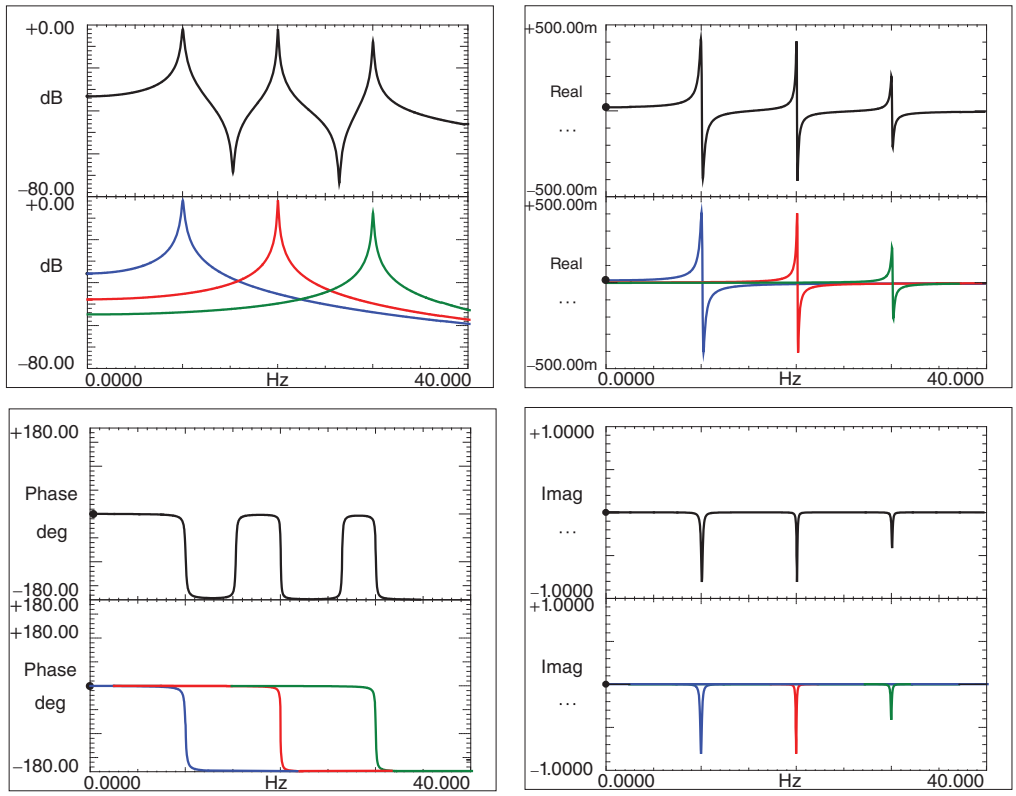

Figure 2.42 3DOF FRF showing drive point measurement; complete FRF and contribution by mode.

Now let's recall that the residue matrix for this beam can be written for the kth mode as

$$\begin{bmatrix} a_{11k} & a_{12k} & a_{13k} & \cdots \\ a_{21k} & a_{22k} & a_{23k} & \cdots \\ a_{31k} & a_{32k} & a_{33k} & \cdots \\ \vdots & \vdots & \vdots & \ddots \end{bmatrix} = q_k \begin{bmatrix} u_{1k}u_{1k} & u_{1k}u_{2k} & u_{1k}u_{3k} & \cdots \\ u_{2k}u_{1k} & u_{2k}u_{2k} & u_{2k}u_{3k} & \cdots \\ u_{3k}u_{1k} & u_{3k}u_{2k} & u_{3k}u_{3k} & \cdots \\ \vdots & \vdots & \vdots & \ddots \end{bmatrix} \tag{2.82}$$

Now noting that the scaling constant q and value of the mode shape at the tip of the beam are just constants, the first mode for this equation becomes

$$\begin{Bmatrix} a_{13k} \\ a_{23k} \\ a_{33k} \end{Bmatrix} = q_k u_{3k} \begin{Bmatrix} u_{1k} \\ u_{2k} \\ u_{3k} \end{Bmatrix} \tag{2.83}$$

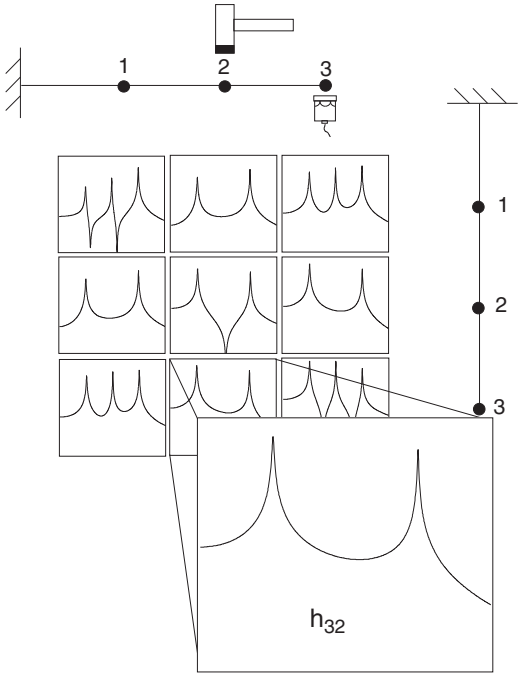

Figure 2.43 3DOF cantilever beam FRF matrix, highlighting h_{32}.

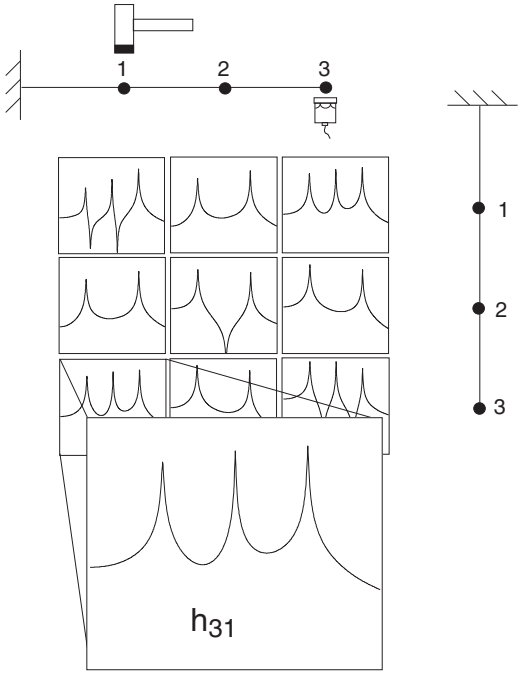

Figure 2.44 3DOF cantilever beam FRF matrix, highlighting h_{31}.

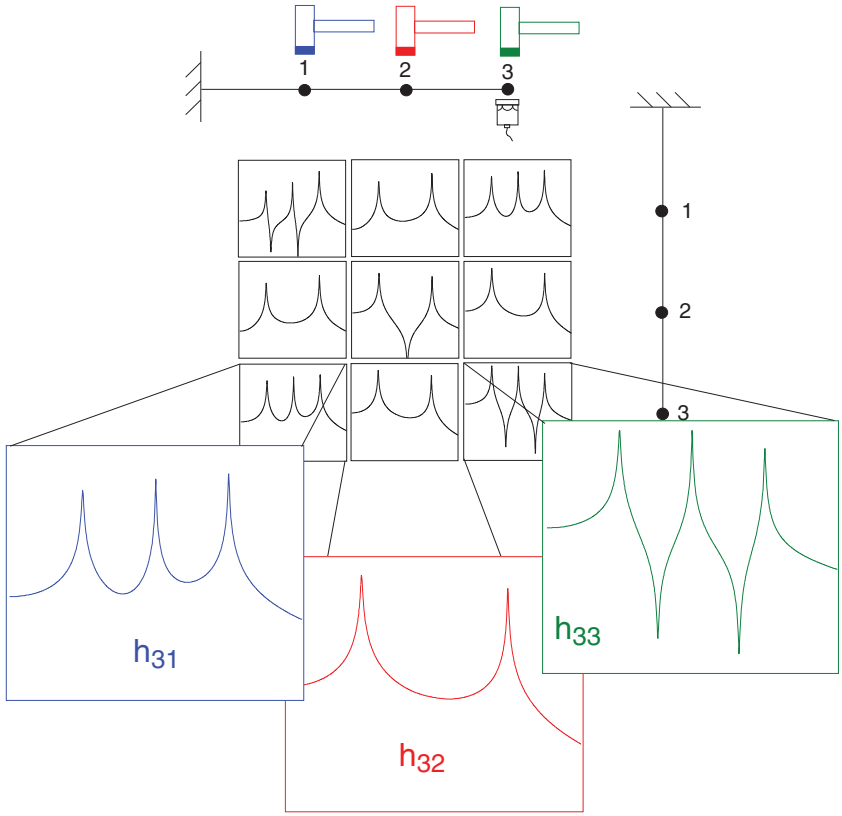

Figure 2.45 Roving impact test with stationary reference accelerometer at point 3.

Then looking at the first mode of the system with DOF 3 as a reference:

$$\begin{Bmatrix} a_{131} \\ a_{231} \\ a_{331} \end{Bmatrix} = q_1 u_{31} \begin{Bmatrix} u_{11} \\ u_{21} \\ u_{31} \end{Bmatrix} \qquad \begin{Bmatrix} a_{131} \\ a_{231} \\ a_{331} \end{Bmatrix} = q_1(8) \begin{Bmatrix} 2 \\ 5 \\ 8 \end{Bmatrix} \tag{2.84}$$

Now looking at the third column of the frequency response function matrix for the first mode, the amplitude of the frequency response function is directly related to the mode shape as seen in Figure 2.49. The amplitudes can be read directly from these plots; these numbers are for illustration only. This could also be done for modes 2 and 3.

So the 3 × 3 matrix of measurements describes all the possible measurements. Any one of the rows or columns can be used to extract information pertaining to the frequency and mode shape for the beam. The cantilever beam is shown with a waterfall plot of the imaginary part of the frequency response plot using the tip of the beam as a reference. The mode shape can be clearly seen from the measurements shown in Figure 2.50.

2.3.8 Summary of Time, Frequency, and Modal Domains

As a further illustration of the response of the system, Figure 2.51 overviews the whole time–frequency–modal relationship. A system can be described as a physical system or in terms of an analytical representation. If we consider the response of the system to some

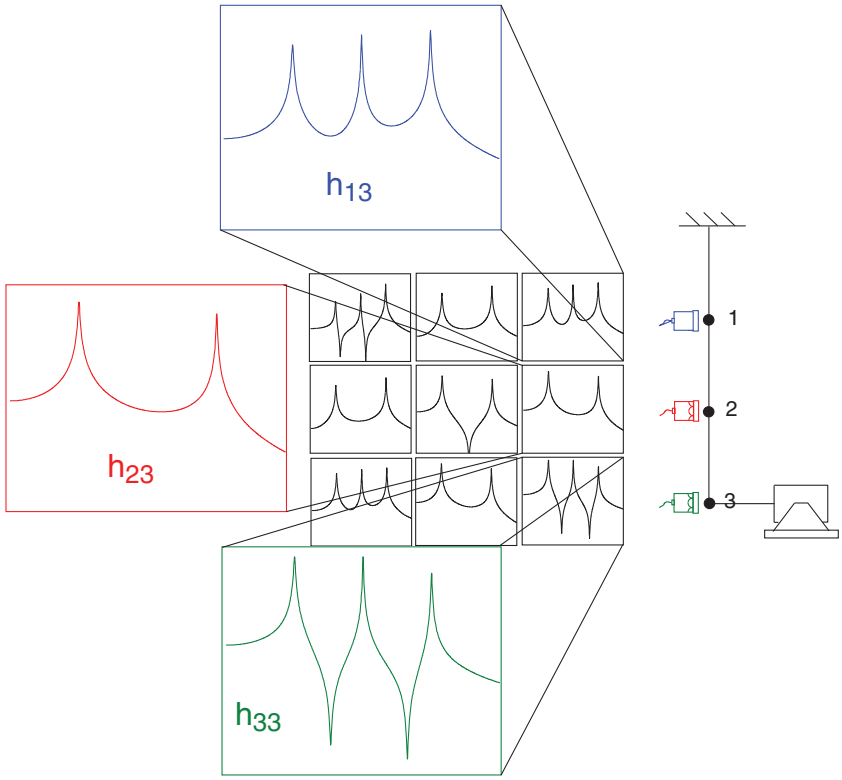

Figure 2.46 Roving accelerometer test with stationary reference shaker force at point 3.

$$h_{ij}(j\omega) = \frac{a_{ij1}}{(j\omega - p_1)} + \frac{a^*_{ij1}}{(j\omega - p^*_1)} + \frac{a_{ij2}}{(j\omega - p_2)} + \frac{a^*_{ij2}}{(j\omega - p^*_2)} + \frac{a_{ij3}}{(j\omega - p_3)} + \frac{a^*_{ij3}}{(j\omega - p^*_3)}$$

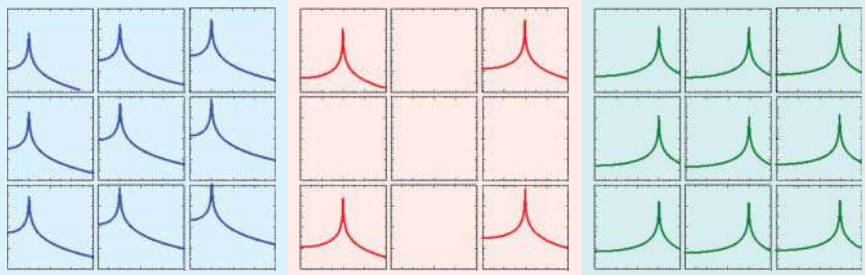

$$h_{ij}(j\omega) = \frac{q_1 u_{i1} u_{j1}}{(j\omega - p_1)} + \frac{q_1 u^*_{i1} u^*_{j1}}{(j\omega - p^*_1)} + \frac{q_2 u_{i2} u_{j2}}{(j\omega - p_2)} + \frac{q_2 u^*_{i2} u^*_{j2}}{(j\omega - p^*_2)} + \frac{q_3 u_{i3} u_{j3}}{(j\omega - p_3)} + \frac{q_3 u^*_{i3} u^*_{j3}}{(j\omega - p^*_3)}$$

Figure 2.47 FRF matrix (magnitude) with each mode contribution shown individually.

$$h_{ij}(j\omega) = \sum_{k=1}^{m}\left(\frac{a_{ijk}}{(j\omega - p_k)} + \frac{a^{*}_{ijk}}{(j\omega - p^{*}_k)}\right)$$

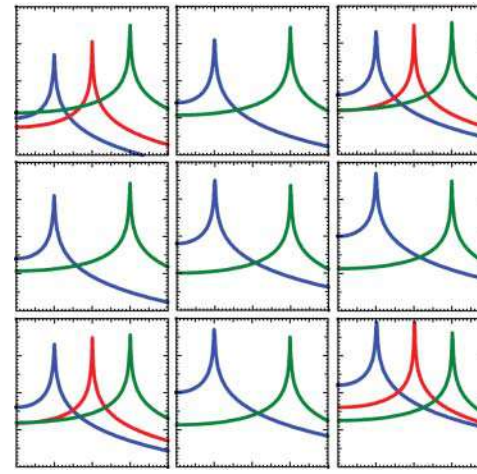

$$h_{ij}(j\omega) = \sum_{k=1}^{m}\left(\frac{q_k u_{ik} u_{jk}}{(j\omega - p_k)} + \frac{q_k u_{ik} u^{*}_{jk}}{(j\omega - p^{*}_k)}\right)$$

Figure 2.48 FRF matrix (magnitude) with all modes combined.

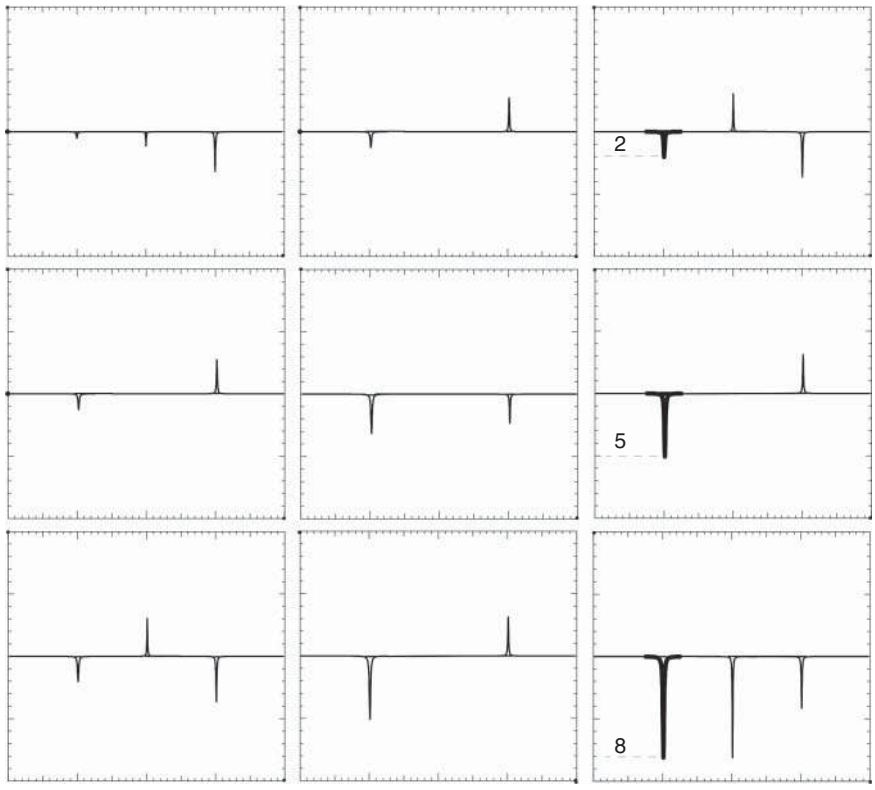

Figure 2.49 3DOF FRF matrix: third column highlighting mode 1 shape.

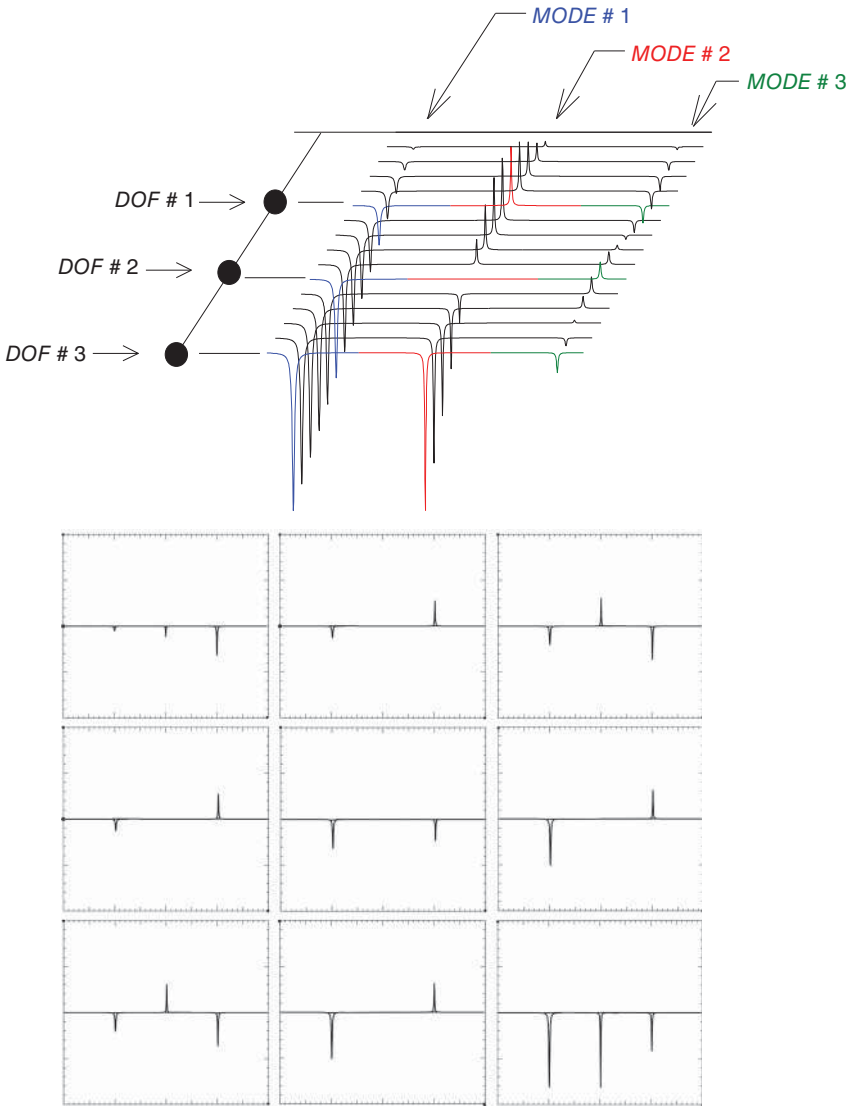

Figure 2.50 Waterfall plot illustrating mode shapes for 3x3 FRF matrix.

excitation, such as an impact, then we see that we can measure the response in either the time domain or the frequency domain. If we look at the time domain response at the tip of the beam, we see that the total response is made up of the sum of a set of damped exponentially decaying sine waves due to mode 1, mode 2, and mode 3. In the frequency domain, we see that the total frequency response function is nothing more than the sum of all the single degree of freedom modal oscillators that are activated by the input excitation. We can also see that we can easily convert the response of each single degree of freedom system from the time to the frequency domain and from the frequency to the time domain. We can also see that the physical model can be described in terms of its modes: mode 1, mode 2, and mode 3. If we

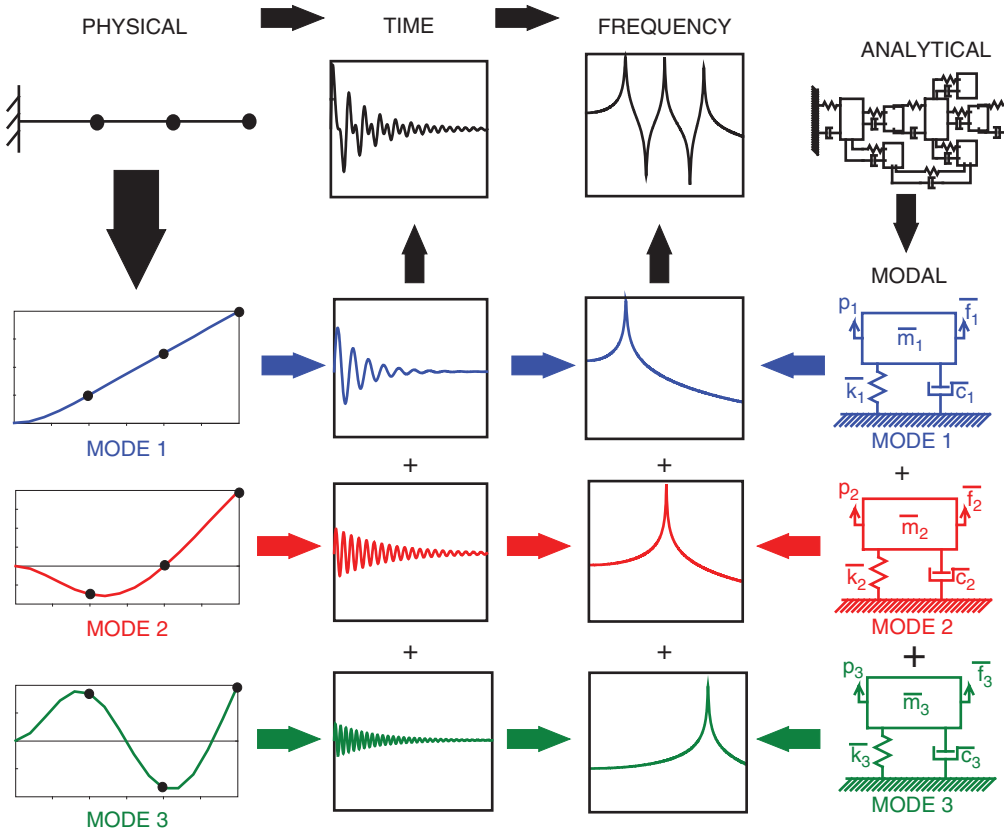

Figure 2.51 Physical, time impulse, FRF and SDOF model for each mode.

were to make an analytical model of the system, we could decompose the coupled model in physical space into a set of single degree of freedom modal oscillators in modal space. Notice how all the time–frequency–modal information is all interrelated.

2.3.9 Response due to Forced Excitation using Mode Superposition

Now that all the pieces of the theory have been laid out, an example of how structural response is computed will help to illustrate the entire process. Let's consider a simple excitation, such as an impulsive pulse applied to a small wind turbine blade, that is modeled as a very simple cantilever beam, an approximation that allows us to illustrate the response computation using the mode superposition approach. Figure 2.52 shows the cantilever beam model, with an impulsive force applied towards the root of the wind turbine blade and the response at the tip of the beam.

Once the finite element beam model has been developed, an eigensolution can be performed to find all the modes for the system; for this illustration of the mode superposition, just three modes are used. Of course the modal space single degree of freedom equation which was written earlier as

$$\overline{m}_i\ddot{p}_i + \overline{c}_i\dot{p}_i + \overline{k}_i p_i = \overline{f}_i \tag{2.85}$$

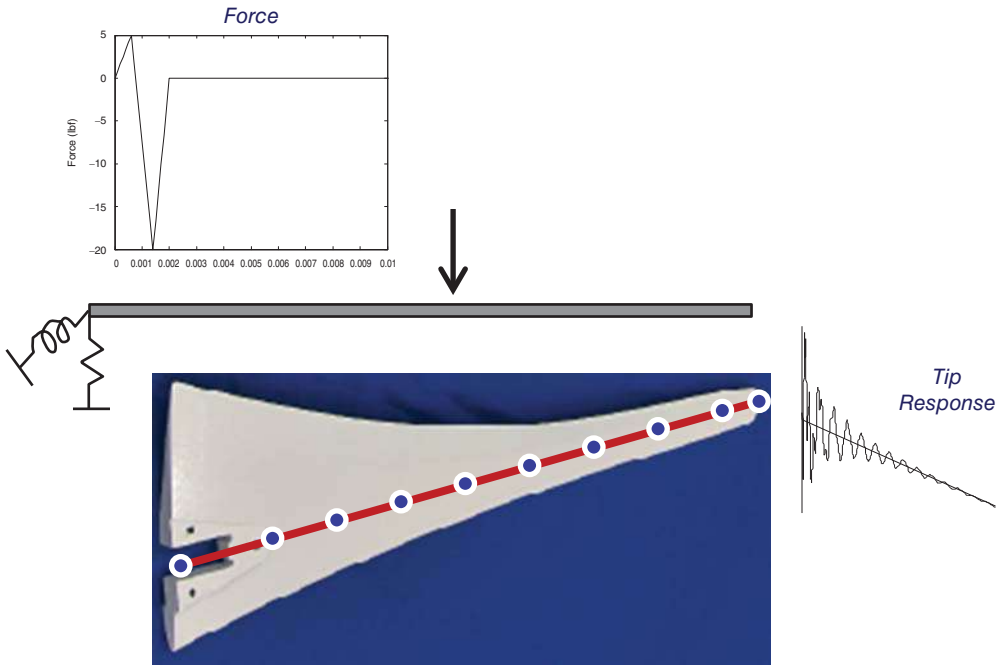

Figure 2.52 Simple cantilever beam impulse and response schematic for small wind turbine blade.

will be used for the single degree of freedom response calculations for the contribution for each of the modes. Considering mode 1 of the system, we can use the modal transformation to get the modal mass, modal damping, and modal stiffness (shown in blue) along with the modal force applied to the modal approximation. Once the response has been computed over all time, the modal response is projected back to the physical degrees of freedom using the mode shape to spatially distribute the response to all physical degrees of freedom. The contribution that mode 1 makes to the total physical response is shown in Figure 2.53.

The same process is performed for mode 2 and mode 3 and the total physical response is shown in Figure 2.53b and c, respectively.

Now the entire system response can be illustrated as shown in Figure 2.54. The physical equations from the finite element model are shown at the upper right, along with the transformed equations in modal space, with the modal mass, modal damping, modal stiffness, and modal force; these basic single degree of freedom equations are used to compute the response of each mode. The response of each of the three separate modes are seen as the major contributors to the total response. The response of each mode is then added to obtain the physical response, shown on the left in the figure. One additional point is that the tip response of the blade is shown at the bottom of the figure, with the combined response of all the modes along with the individual responses for each mode. This is shown with the impulse response broken down for the individual mode contributions. This figure summarizes the entire process for the time response computation, and is available on the book webpage as a GIF animation.

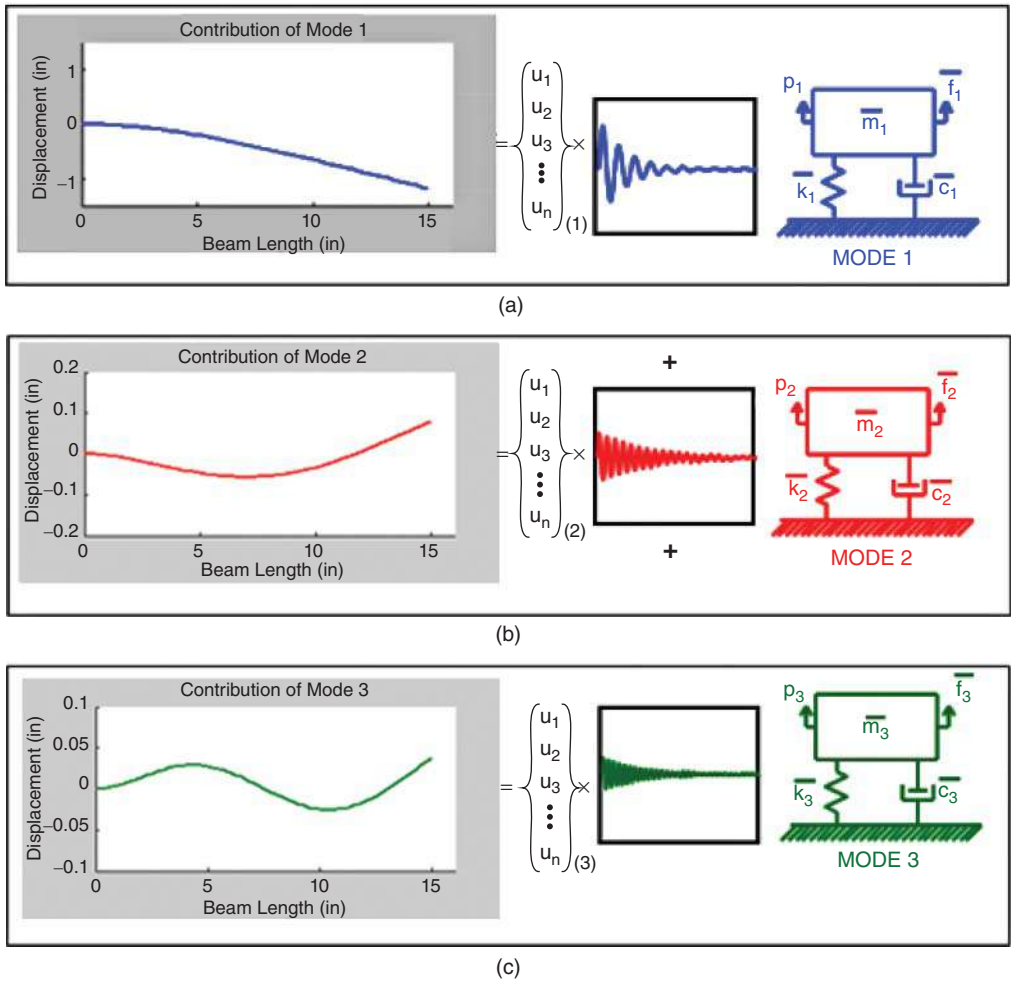

Figure 2.53 Illustration of modal responses projected to physical space: (a) mode 1; (b) mode 2; (c) mode 3.

2.4 Summary

Figure 2.55 summarizes the whole experimental modal analysis process. Let's describe some of the pieces of this schematic to re-emphasize some of the material already covered.

The finite element model is generated based on assumptions of the mass and stiffness distributions in the system. The large number of highly coupled equations are decomposed, using an eigensolution technique, to extract the system frequencies and mode shapes. These same equations can be cast in the Laplace domain to formulate the system transfer function. The key to modal analysis lies in the fact that the system transfer function is the adjoint of the system matrix divided by the determinant of the system matrix, which is directly related to the residues (mode shapes) and the poles (frequencies). So the Laplace domain is nothing more than another form of the system representing the same thing as the finite element model.

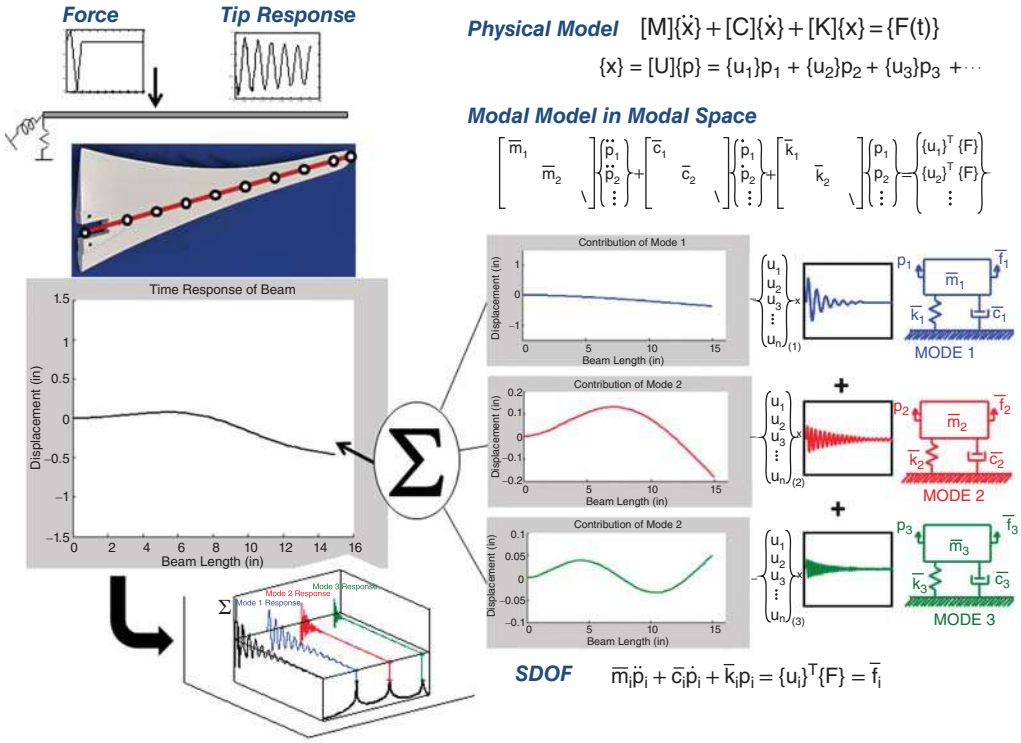

Figure 2.54 Overview of the entire physical, modal response and expansion to finite element model space. (animation is available on the book webpage).

Now a frequency response function can be synthesized for any input–output location and in fact could generate the whole frequency response matrix. Because the frequency response function is made up from the poles and residues (frequencies and mode shapes), it seems reasonable that poles and residues can be extracted from the frequency response function is referred to as "modal parameter estimation" or, in common terms, "curvefitting". Now rather than developing frequency response functions from assumptions of the mass, damping, and stiffness distributions in the Laplace domain, let's consider measuring input–output characteristics.

If the input force used to excite the system is measured and the response of the system due to the time input excitation is also measured, then this time data can be transformed to the frequency domain and a ratio of output to input can be used to compute the frequency response function. Once this frequency response function and a series of frequency response functions are acquired, then the parameters of interest can be extracted from the data. This sounds very simple but there are a few significant items that need to be understood and addressed. These are digital signal processing techniques, excitation considerations, and modal parameter estimation techniques, all of which are discussed in the following chapters.

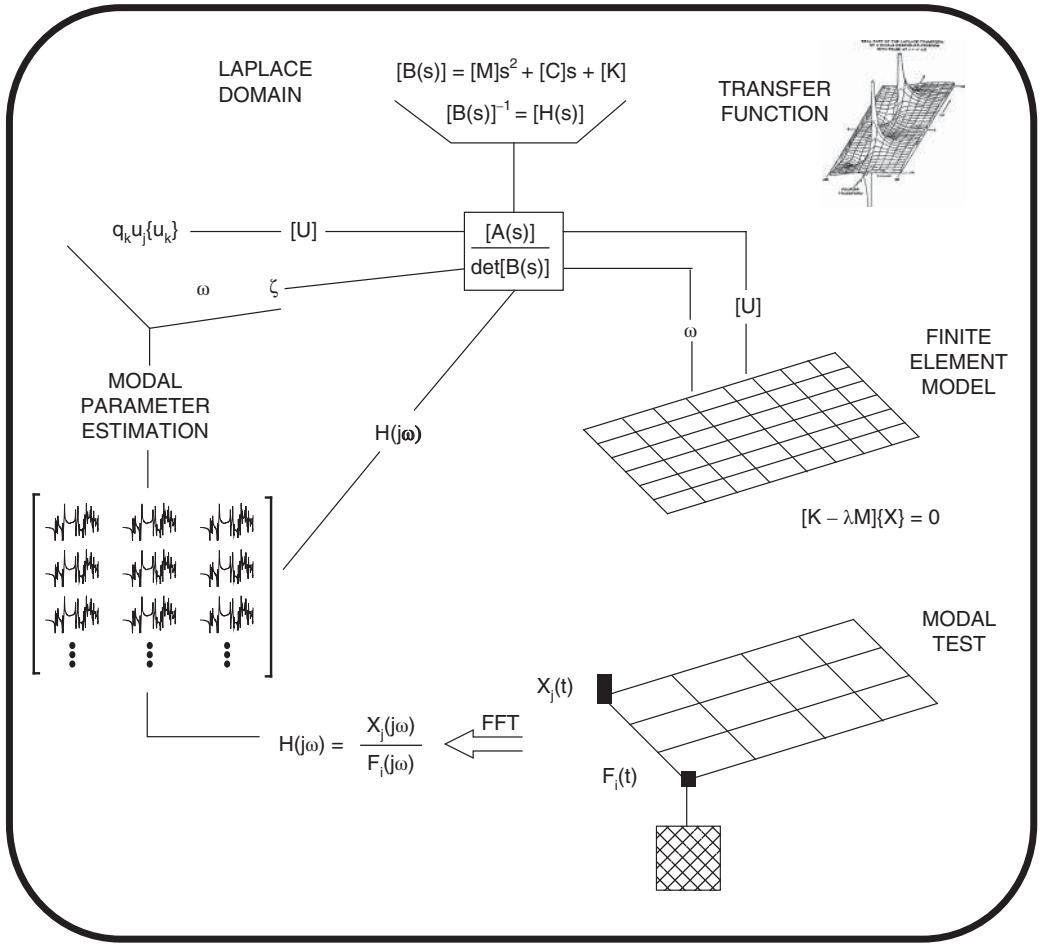

Figure 2.55 Overview of analytical and experimental modal analysis.

3

General Signal Processing and Measurements Related to Experimental Modal Analysis

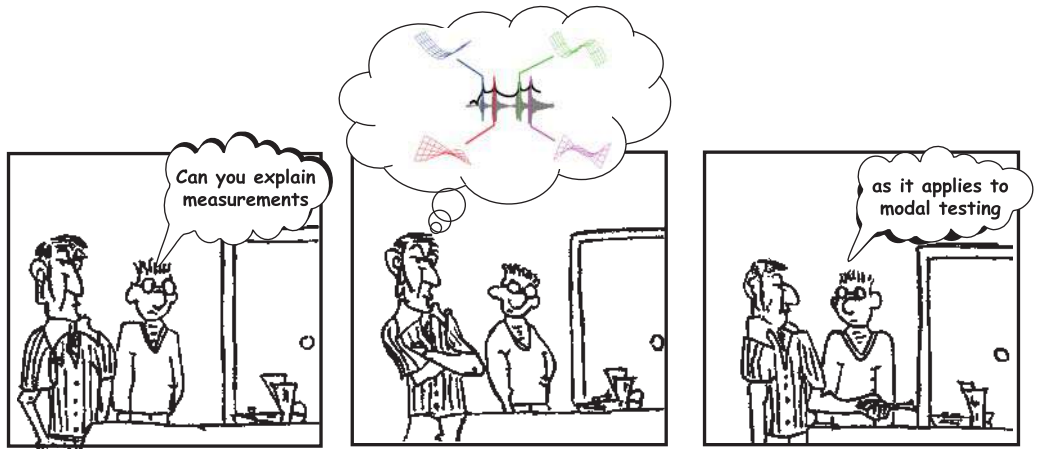

3.1 Introduction

Upon reviewing the modal theory, it is evident that from the mass, damping, and stiffness matrices, that the system transfer relationships can be determined and that the point-to-point frequency response function has embedded in it the parameters of interest, namely the frequency, damping, and residue or mode shape for all of the modes of the system. If the frequency response function can be measured, then mathematical procedures can be employed to extract this information from measured functions. In order to obtain these frequency response functions from an experimental standpoint, several issues relating to digital signal processing must be addressed.

3.2 Time and Frequency Domain

Often time domain signals are very difficult to understand. By transforming from the time domain to the frequency domain, a complicated signal can often be more easily understood. For instance, Figure 3.1 shows the summation of four sine waves at different amplitudes and phases, which can be extremely difficult to interpret in the time domain. However, in the frequency domain, it is much clearer as to which frequencies have which amplitudes and phases. A Fourier series is an example of a transformation that allows a complex time representation

Modal Testing: A Practitioner's Guide, First Edition. Peter Avitabile.

Companion Website: www.wiley.com/go/avitabile/modal-testing

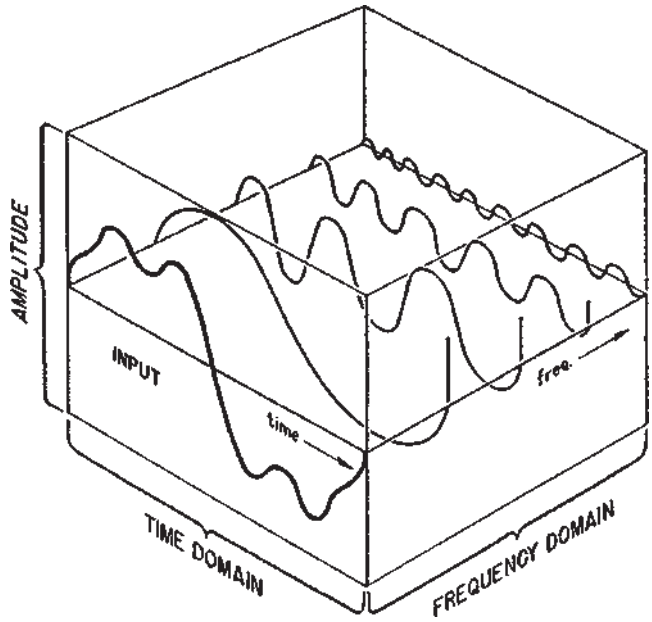

Figure 3.1 Time/frequency representations for a sinusoidal signal.

to be characterized as a series of sine waves at different frequencies with different amplitude and phase.

The advent of the digital computer brought the ability to digitally acquire data and then perform Fourier transforms of time data, allowing it to be represented in an equivalent form in the frequency or Fourier domain. Until the introduction of the *Fast Fourier Transform* (FFT) algorithm by Cooley and Tukey, the analysis of time domain signals was limited to very special critical needs. With the efficient FFT algorithm, it became possible to analyze time signals on a

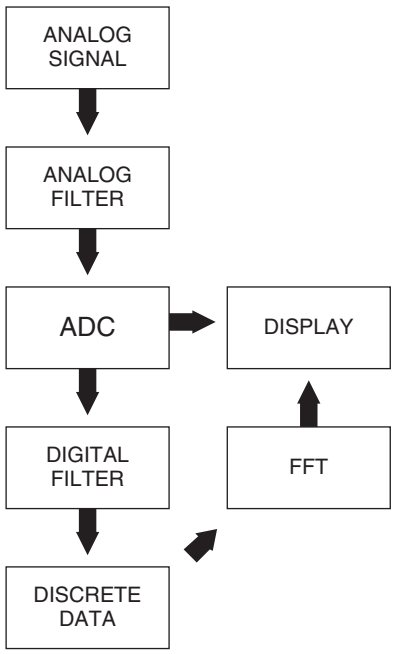

Figure 3.2 Basic configuration of an FFT analyzer.

routine basis. However, the digitization and capturing of time domain signals presents aspects that must be carefully handled, otherwise distortion of the time signals will result, thereby producing erroneous results.

So to start the discussion, the basic configuration of an FFT analyzer is depicted in Figure 3.2. While there may be variations from one analyzer manufacturer to another, this basic schematic is a good depiction of a generic FFT analyzer.

An analog signal is measured from a transducer and it is first input into a low pass filter which is an anti-aliasing filter. The signal is then digitized in the analog to digital converter (ADC) before it is digitally filtered to provide the discrete data that are needed for the particular frequency range and parameters chosen by the test engineer. The data is then used in the FFT, after which the spectral measurement can be viewed.

Now the overall measurement process using the FFT can be best seen in Figure 3.3; this is the same as Fig. 1.13 but with additional annotation discussed here. This basically shows the

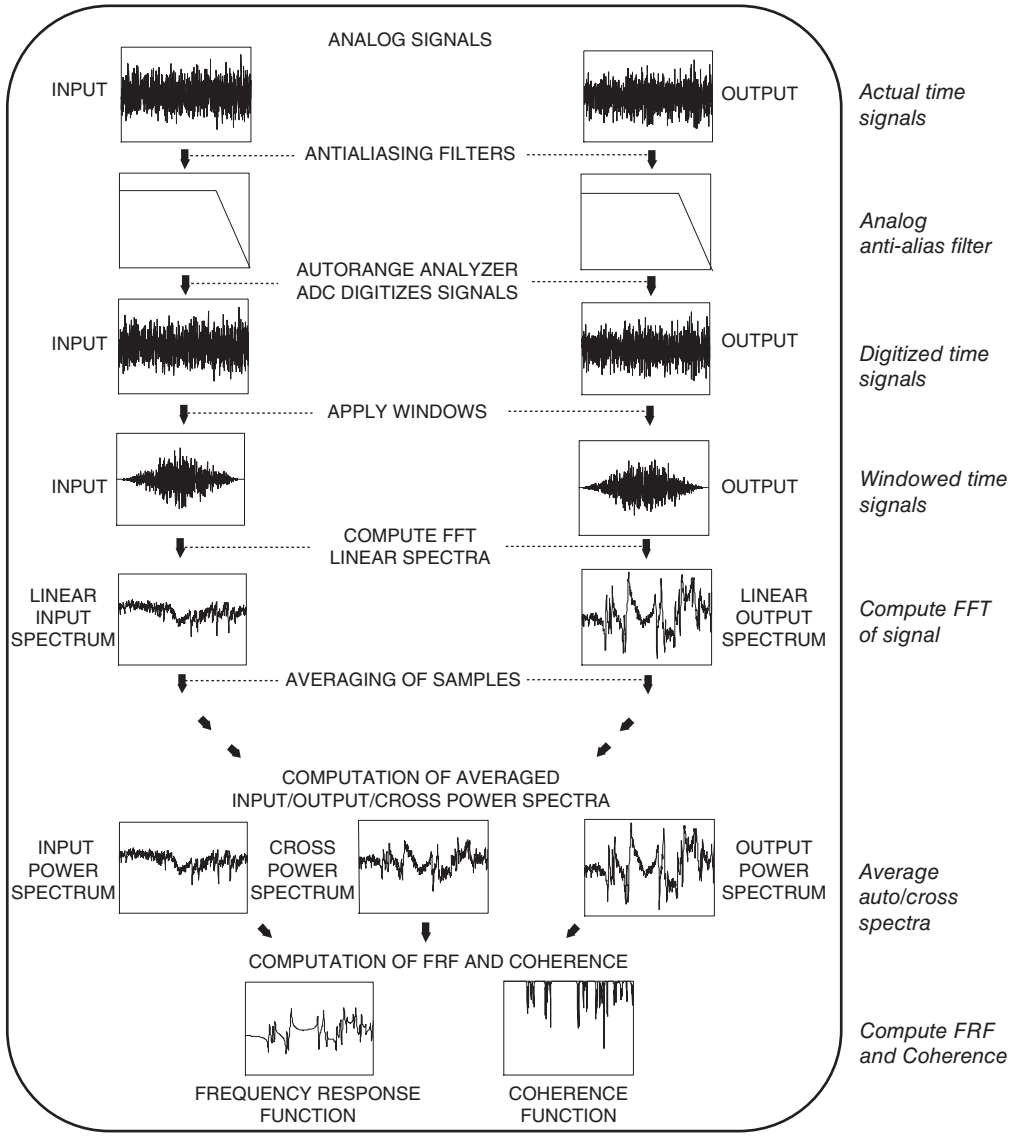

Figure 3.3 Anatomy of the FFT measurement process.

overall anatomy of the FFT processing involved in the measurement process. The actual time signals are captured and passed through a low pass filter, which serves as an anti-aliasing filter. The signals are then digitized. Before the signal is passed to the FFT, there may be a need to apply weighting functions (commonly called *windows*) to better condition the data if it does not satisfy the periodicity requirements of the FFT process. This prevents the serious signal processing problem called leakage. Once the FFT is computed for one sample, then the process is continued to obtain an averaged set of auto-power spectrums and cross power spectrums. From this procedure, the frequency response function and coherence are computed.

3.3 Some General Information Regarding Data Acquisition

Before some of the specific topics related to experimental modal testing are discussed, some general items are considered first. Data acquisition systems can be either multiplexed or simultaneous sample and hold (which is generally what is used for most data acquisitions for experimental modal testing today). A multiplexed system uses one ADC, shared among all the channels of measurements made; this type of acquisition is acceptable for low frequency occurrence of events and where small phase lag between channels is not of concern. However, for most data acquisition systems for experimental modal analysis, there are multiple ADC cards for each channel to be measured, and all channels are sampled simultaneously. This allows for acquisition to be performed without any phase distortion across channels. Systems generally are arranged in four channel groupings so that systems with four channels and eight channels are very commonly used in smaller experimental modal test systems. But from there the number of channels varies, with common sizes of up to 64 channels and up to 128 channels; larger systems with 256 channels and more are less common, but can be found in some larger companies requiring simultaneous sampling of many channels.

Depending on the number of bits in the analog to digital converter (ADC), digitization of the analog signal may cause some distortion of the actual signal. Typically today, most FFT analyzers and data acquisition systems have 16 bits, 24 bits or even 32 bits. This relates to the finite voltage that can be measured. Generally, the number of possible discrete voltage steps is

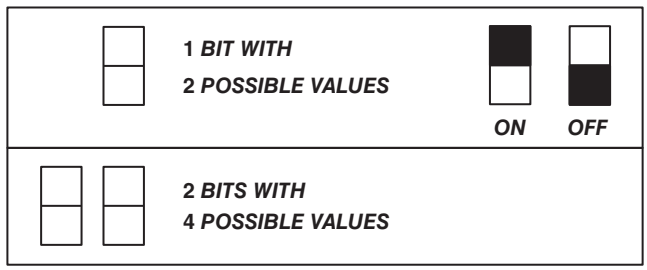

A 4 bit ADC has 2^4 or 16 possible values

A 6 bit ADC has 2^6 or 64 possible values

A 12 bit ADC has 2^{12} or 4096 possible values

$4\,\text{bit} = 0000 = 2^3 + 2^2 + 2^1 + 2^0 = 16$ levels

$12\,\text{bit} = 000000000000 = 2^{11} + 2^{10} + \cdots + 2^1 + 2^0 = 4096$ levels

Figure 3.4 Schematic showing ADC bits, possible levels, dynamic range.

2^n; that is 2 raised to the number of "n" bits for the ADC. Each bit can have two states; they are either "on" or "off". So a 1 bit system has only two possible values whereas a 2 bit system has four possible values. And a 3 bit system has eight possible values. Figure 3.4 shows a simple schematic of this.

3.4 Digitization of Time Signals

With analog sampling devices, only the performance of the analog instrumentation was of concern. With the use of digital signal processing (DSP) techniques, additional consideration must be given to the analog to digital conversion (ADC) process. The analog signal must be digitized and several additional items become important in order to minimize distortion of the original signal. These are *quantization*, *sampling*, *aliasing* and *leakage*.

Two important parameters of digital signal processing used in converting an analog signal into a digital signal are *sampling* and *quantization*. Sampling refers to the timing at which the analog signal is sampled to form a digital signal. If a signal is not sampled at a fast enough sample rate, then higher frequency signals can alias themselves into the frequency analysis band as lower frequencies, which will distort the analysis being performed. In order to prevent aliasing, most signal analyzers offer anti-aliasing filters to prevent this from occurring. Quantization refers to the accuracy with which the amplitude of an analog signal is digitized. If sufficient resolution is not available, the signal will be distorted. A digitized signal obtained from an analog measurement is shown in Figure 3.5.

3.5 Quantization

Now there is always concern that there is adequate amplitude resolution to properly present the signal measured. As more bits of resolution are used, the measured signal will be measured more accurately, but there will always be some error due to the fact that the data is sampled

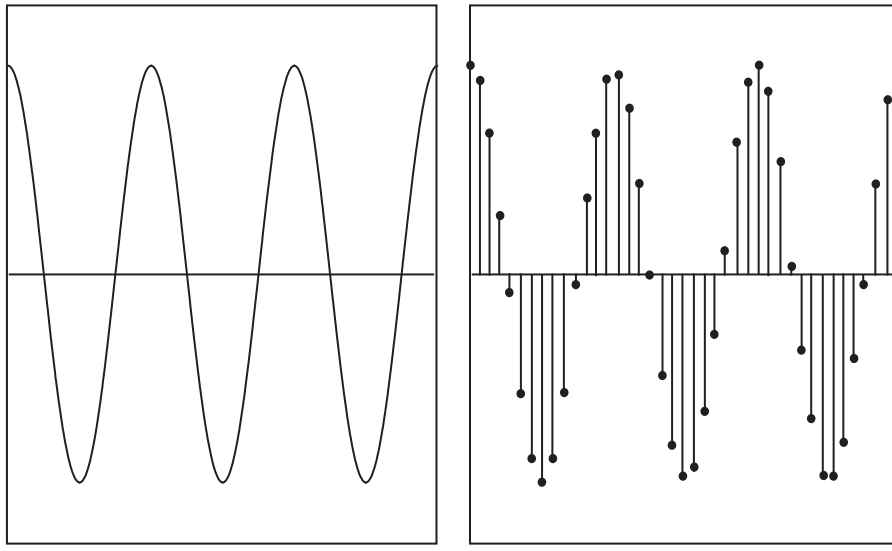

Figure 3.5 Analog signal digitized to obtain digital representation: (a) analog signal; (b) digital representation.

digitally and there are discrete voltage steps that are used to digitally describe the signal. A very good example is digital pictures, which today everyone takes with their digital cameras. The resolution can be set to different values, such as 1 megapixel, 3 megapixels, or up to 10 or 20 megapixels. With higher resolutions, there is a finer and finer definition to the picture; but if you zoom in far enough you will always get down to the discrete values that make up the picture and sub-pixel resolution is not possible. Of course, a very high resolution means that the overall picture size stored in memory is much larger for larger resolutions. The same is true for our measured signals. If too coarse a resolution is used, then there will be a lack of resolution, but the file size will be much smaller in terms of storage. If a very high resolution is specified, then the signal will be captured with finer resolution, but the file size will be much bigger in terms of storage. So, at times there are trade-off considerations, especially when streaming a large number of channels with very high resolution, where the throughput file size needs to be considered.

Figure 3.6 shows a comparison of a 4 bit and 6 bit ADC used to measure the same sine wave. This shows the differences that may result in the amplitude of the signal measured. The circled areas in the figure clearly show the difference in the amplitude that is recorded with the two different resolutions.

3.5.1 ADC Underload

Optimization of the ADC through autoranging minimizes some of the problems with underloading, but the signals with low amplitude generally still suffer from quantization error because

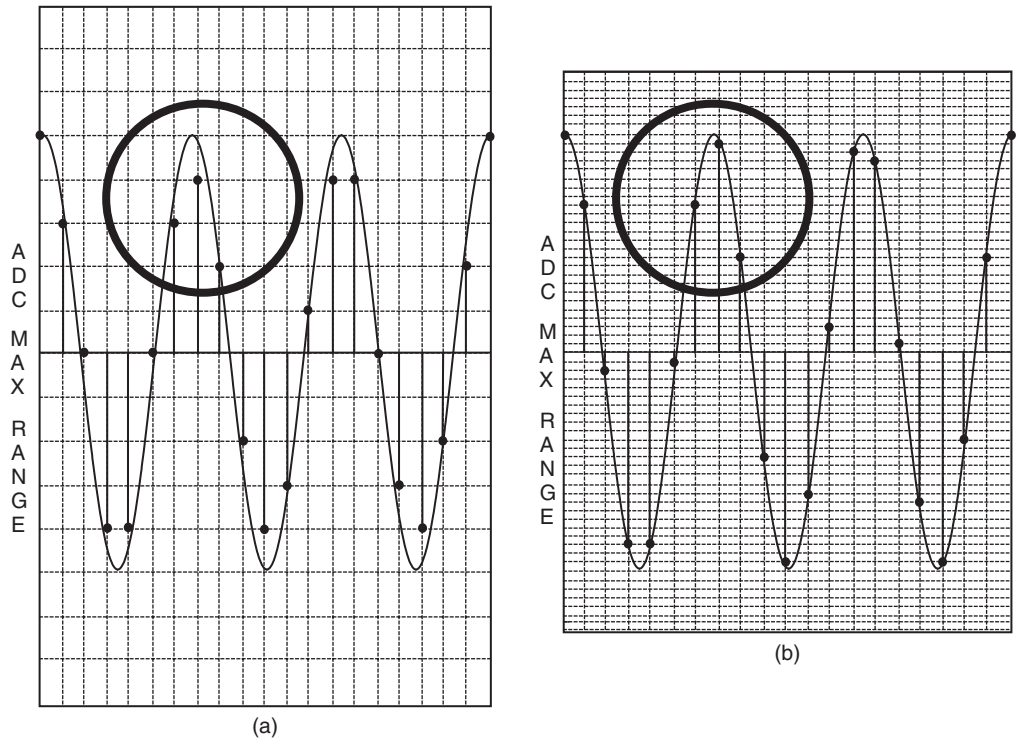

Figure 3.6 Amplitude distortion when capturing a pure sine wave with (a) 4 bit ADC; (b) 6 bit ADC.

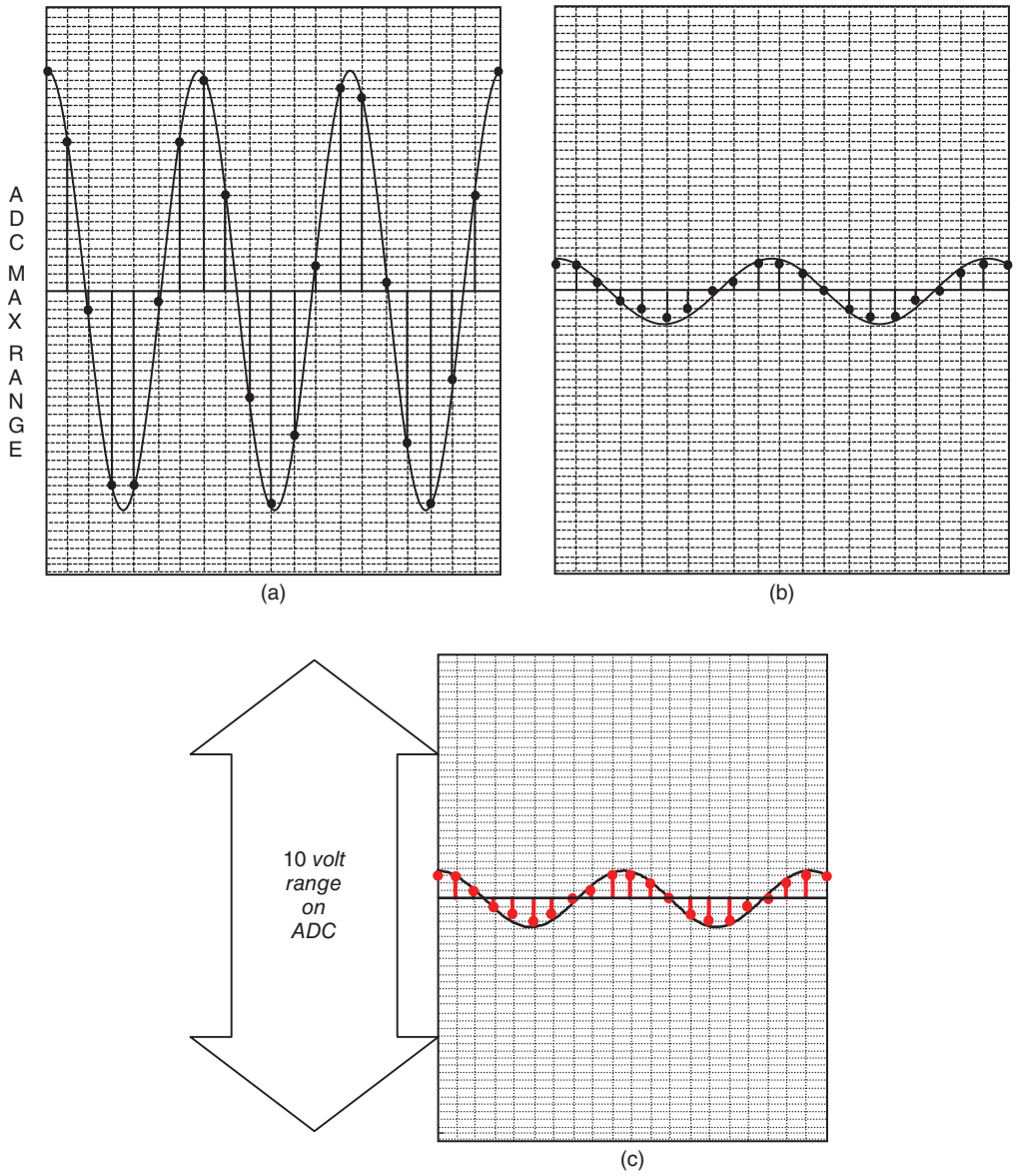

Figure 3.7 Signal distortion due to fixed resolution for (a) large amplitude and (b) small amplitude sine waves at two different frequencies. (c) Poor use of ADC range with a small amplitude sine signal.

the ADC level is set based on the largest signal amplitude and is not necessarily optimized for all of the components of the signal. Figure 3.7a shows the distortion due to two sine waves at different frequencies with different amplitudes measured with the same resolution. The smaller amplitude signal is not characterized as well. The figure on the right in Figure 3.7a shows the amplitude is not captured well because the voltage range is set by the larger amplitude sine wave

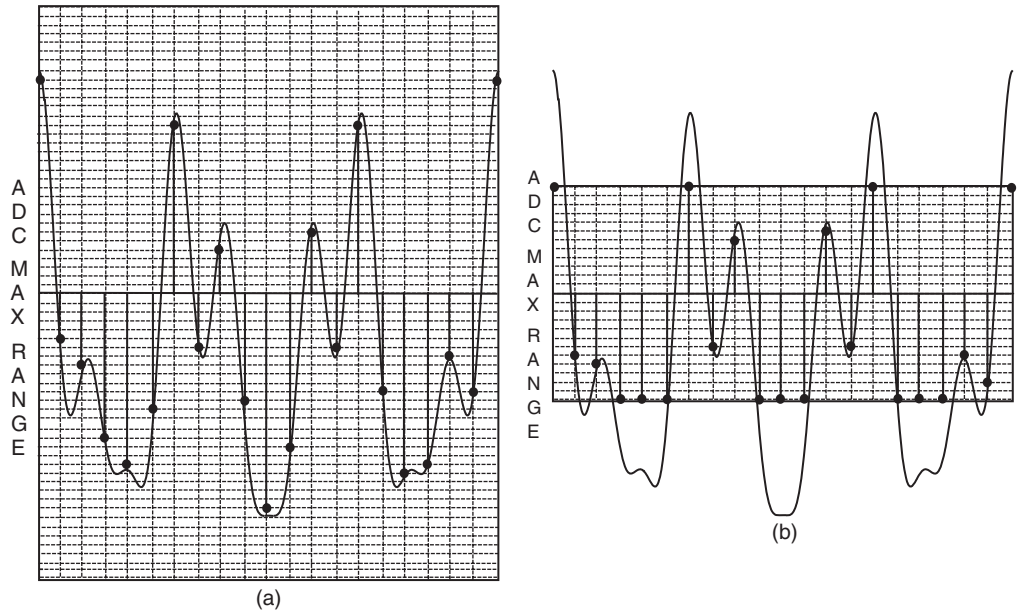

Figure 3.8 Signal distortion due to overloading of the ADC: (a) proper voltage range setting; (b) inappropriate setting and overload.

shown in the Figure on the left in Figure 3.7a. Figure 3.7b further shows the poor use of the total dynamic range of the smaller amplitude signal.

3.5.2 ADC Overload

Overload of the ADC can occur if the ADC levels are not properly set. Figure 3.8 shows the same signal with two different voltage ranges: one that is appropriate on the left and one that overloads and clips the signal to be measured on the right. This clipping can cause a severe distortion of the measured signal due to clipping of the measured signal. In both underload and overload, the distortion of the signal is seen in an incorrect amplitude in the frequency domain as well as the presence of other frequency components that result from the distortion of the amplitude in the time domain. The distortion is most pronounced in the severe overload clipping situation, but can also be observed in the underload situation as well.

3.6 AC Coupling

Often there may be a significant DC portion of the signal, with the AC signal superimposed on top of the DC signal. This is shown in Figure 3.9, illustrating how the DC signal may dominate the overall signal to be measured. A very large voltage range is therefore required to measure the large DC component, which may not really be of interest. The DC signal dominates the dynamic range and may not actually be of interest in the dynamic measurements involving

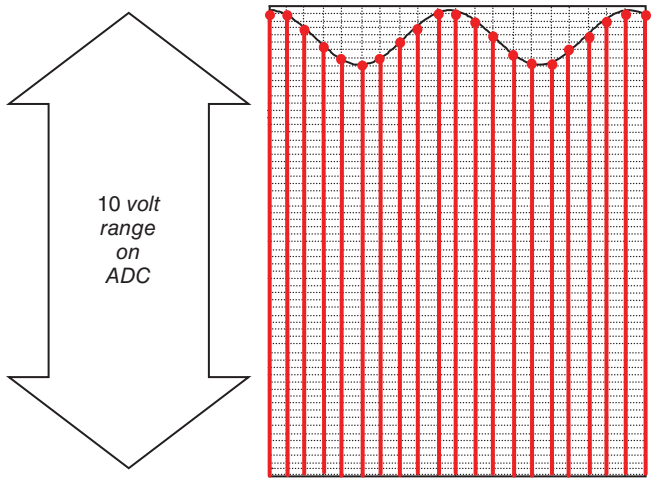

Figure 3.9 Signal showing need for AC coupling to remove large dominating DC signal.

higher frequencies. Often the DC signal may be effectively removed from the desired AC portion of the signal using AC coupling; this essentially adds a high pass filter to the signal to remove the unwanted DC portion of the signal. This is routinely done in many dynamic measurements but it is necessary to point out that sometimes the DC signal is actually needed for some of the processing and modeling performed, so AC coupling, while often used, must be used with regard to the actual data needed. If the DC portion of the signal is needed, then DC coupling must be selected for the ADC. And it is very important to state right now that the ICP signal conditioners built into many data acquisition systems inherently have a high pass filter integrated into their amplifiers and therefore will always filter away the low DC components of the measured signal.

3.7 Sampling Theory

In order to extract valid frequency information, digitization of the analog signal must occur at a certain rate. Shannon's sampling theorem states

$$f_s > 2\, f_{max}$$

That is, the sampling rate must be greater than twice the desired frequency to be measured. For a time record of T seconds, from Rayleigh's criteria, the lowest frequency component measurable is

$$\Delta f = 1/T$$

With these two properties above, the sampling parameters can be summarized as

$$f_{max} = 1/2\, \Delta t \quad \text{or} \quad \Delta t = 1/2\, f_{max}$$

This is shown in Figure 3.10.

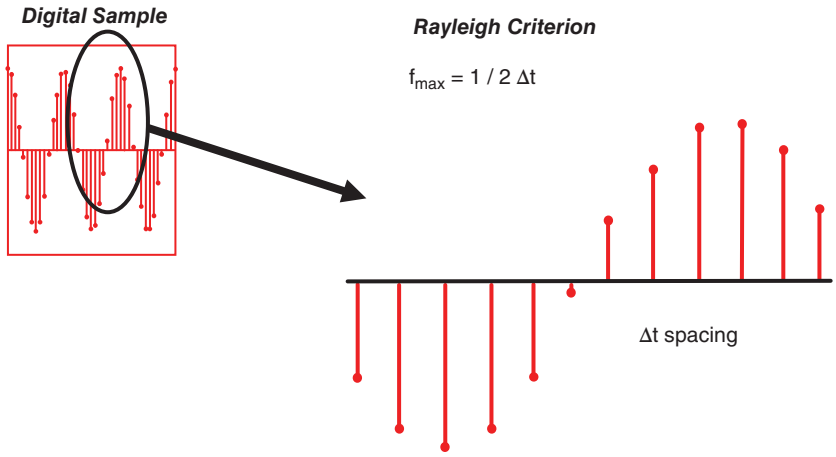

Figure 3.10 Time step sampling of a sine wave.

Box 3.1 Typical time-frequency nomenclature

With respect to the number of sample increments per period N

$$T = N \Delta t$$

$$BW = N \Delta f/2$$

Where

Δt	sample interval; time resolution
N	number of data points
T	sample record length
f_{max}	highest desired frequency – BW
fs	sampling frequency
Δf	frequency resolution

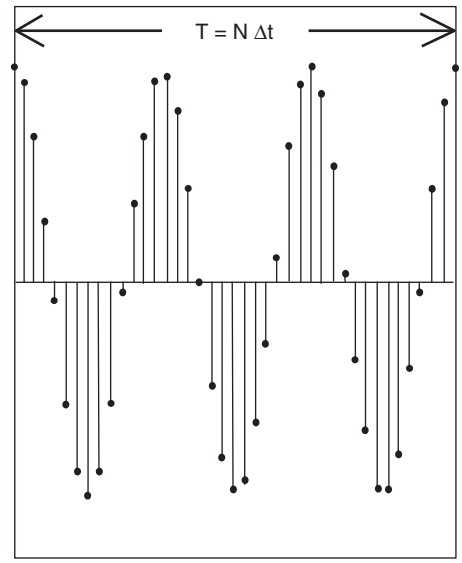

These sampling parameters result in several rules regarding the relationship between the time spacing, frequency resolution, number of samples, and bandwidth that are all interrelated. These rules are shown in Figure 3.11, along with an example to show the relationships. This chart is very useful when acquiring time streamed data for later processing, because it helps ensure that appropriate data is collected to achieve the desired spectral parameters; users can post it near the data acquisition system for quick reference when running any tests.

In regards to any data that is collected, it is very critical to point out that the test engineer really needs to have some idea as to what data and sampling rate is most appropriate. Figure 3.12 shows the results from sampled data (in red) where the time resolution was not carefully thought out. Notice that the actual signal (in blue) shows that there is some higher

PICK	THEN	AND
Δt	$f_{max} = 1 / (2\ \Delta t)$	$T = N\ \Delta t$
f_{max}	$\Delta t = 1 / (2\ fmax)$	$\Delta f = 1/(N\ \Delta t)$
Δf	$T = 1 / \Delta f$	$\Delta t = T / N$
T	$\Delta f = 1 / T$	$f_{max} = N\ \Delta f / 2$

Example

$\Delta f = 5$ Hz and $N = 1024$

Then

$T = 1 / \Delta f = 1 / 5$ Hz $= 0.2$ sec

$f_s = N\ \Delta f = (1024)\ (5\ Hz) = 5120$ Hz

$f_{max} = f_s = (5120\ Hz) / 2 = 2560$ Hz

Figure 3.11 Relationship of time resolution, frequency resolution, number of samples and bandwidth.

frequency information. This is entirely missed due to sampling at too low a rate to capture all the hidden dynamic response.

One often confusing point is that there is an inverse relationship between the time and frequency domains. Generally, what is long in one domain is short in the other domain. Figure 3.13 shows this effect graphically (along with some simple parameters to show their actual numerical values). In the upper portion of the figure (blue), there are 16 time lines and 8 corresponding frequency spectral lines; there are half as many frequency spectral lines because the real time signal, with 16 time values, has to be represented with complex numbers, with 8 sine waves and 8 cosine waves characterizing the signal in the frequency domain. Now if you look at the middle of the figure (red), the same 16 time lines are spaced closer, with half the time step. This will result in 8 complex sines and cosines, spaced twice as far apart from when compared to the upper trace in blue; the bandwidth is twice as wide when the time step is halved. The last time signal in the lower portion of the figure (green) shows that in order to keep the original bandwidth (blue), there are half as many time lines spaced as in the original time step (blue) to create the same original bandwidth (blue) but with the frequency spacing of the red trace. The numerical example with each of these three scenarios is helpful in understanding this commonly confusing issue.

3.8 Aliasing

There is one additional issue in regards to sampling that must be discussed. *Aliasing* occurs when sampling occurs at less than twice the desired frequency. Most of us have seen aliasing in many rotating systems. Possibly, if you have used a timing light to set the timing in your car, you have used a strobe that samples at a much lower rate than the rotating frequency of the car engine. Or maybe you have witnessed a car driving by at a changing speed; at first the wheels seem to be moving forward but then as the car slows down they appear to change direction. Another example is looking at the blades on a helicopter, which may appear to move clockwise and then counterclockwise.

In any event, if frequency components larger than one half the sampling frequency occur in the analog time history, then both amplitude and frequency errors will result. In order to prevent aliasing, typically a low pass filter is used to seriously attenuate the higher frequencies that are not of interest. But remember that the test engineer needs to understand what frequencies are of interest, otherwise filtering may actually remove important characteristics of the

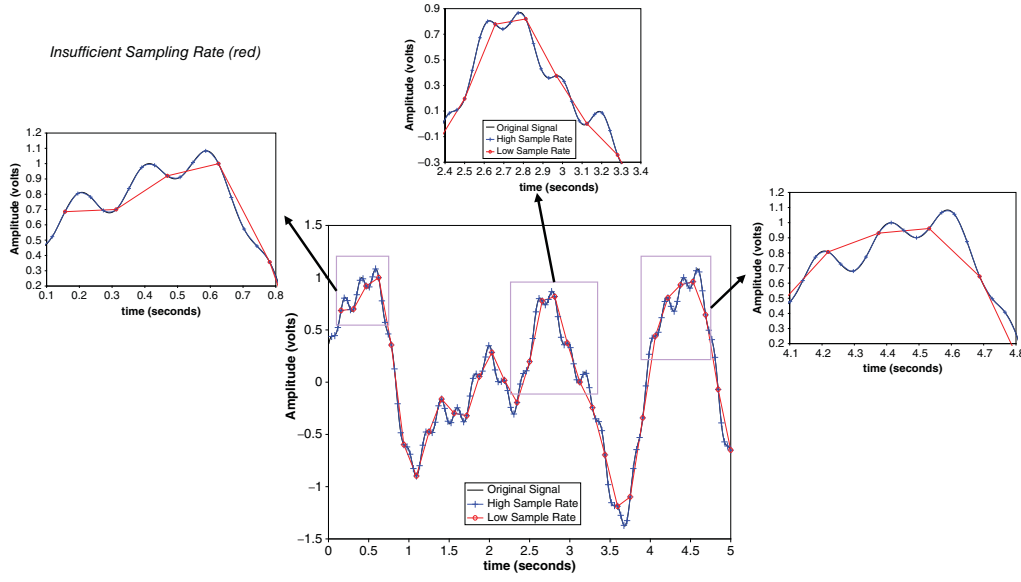

Figure 3.12 Illustration of distortion of data (red) when inappropriate sampling rates are specified. *Source*: Image courtesy Jim De Clerck.

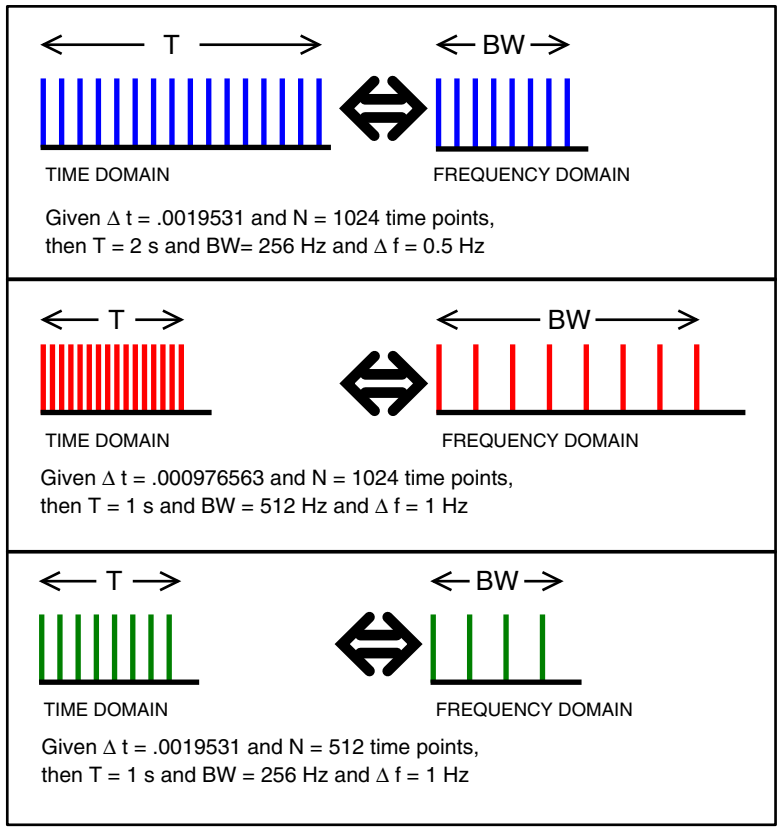

Figure 3.13 Graphical representation of the time frequency relationships.

dynamic signal. Typically, the front end (ADC) has low pass filters to prevent aliasing. These are often referred to as anti-aliasing filters.

Aliasing is also sometimes referred to as "wrap around" error because the undesired high frequency components *fold* or *wrap around* into the desired lower frequency range. Figure 3.14 shows the "aliased" signal (in red) that is observed from the actual signal (in blue) when sampling has not been performed at faster than twice the desired frequency to be measured; the figure also schematically shows the wrap around error effect.

Most good FFT analyzers have anti-aliasing filters that protect against aliasing. These filters typically have a roll off and are not ideal. Usually only 80% of the anti-aliasing filter range is used to provide additional protection against aliasing. This is why most FFT analyzers only provide spectral resolution of 400, 800, 1600… lines of resolution. Some analyzers allow the use of all of the available spectral lines of resolution of 512, 1024, 2048… but the user must be cautioned that the last 20% of the frequency block may not have sufficient alias protection and these frequencies should therefore be used with care.

3.9 What is the Fourier Transform?

Let's try to understand the FFT from a conceptual standpoint to try to avoid all the intricate mathematical details; there are many excellent books on signal processing that go into

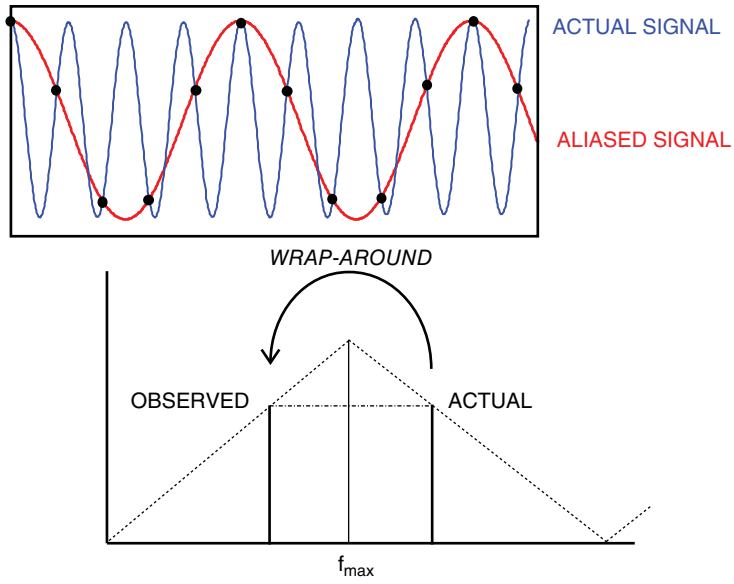

Figure 3.14 Schematic showing aliasing and the wrap around error.

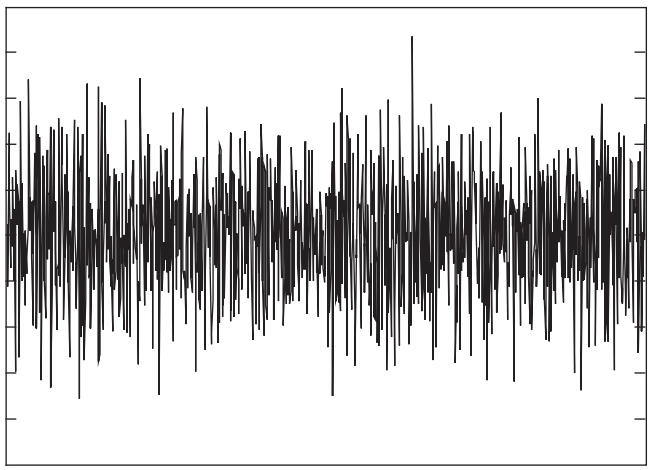

Figure 3.15 A general random signal.

excruciating detail on all of this material if needed. An arbitrary signal may be very difficult to interpret. For instance, the random time signal in Figure 3.15 has certain characteristics, but they are very difficult to determine from the time representation of the signal; specific time and amplitude axes are omitted because they really don't affect the comments regarding this signal.

Any signal can always be broken up into a series of sine waves, with different amplitudes and different frequencies. This is what Fourier said and is the basis of the famous Fourier series. By breaking up the complicated signal into its parts, certain characteristics can be seen much more clearly. For instance, one can determine

- frequency content of the signal
- particular frequencies that are more predominant
- amplitude on a frequency basis

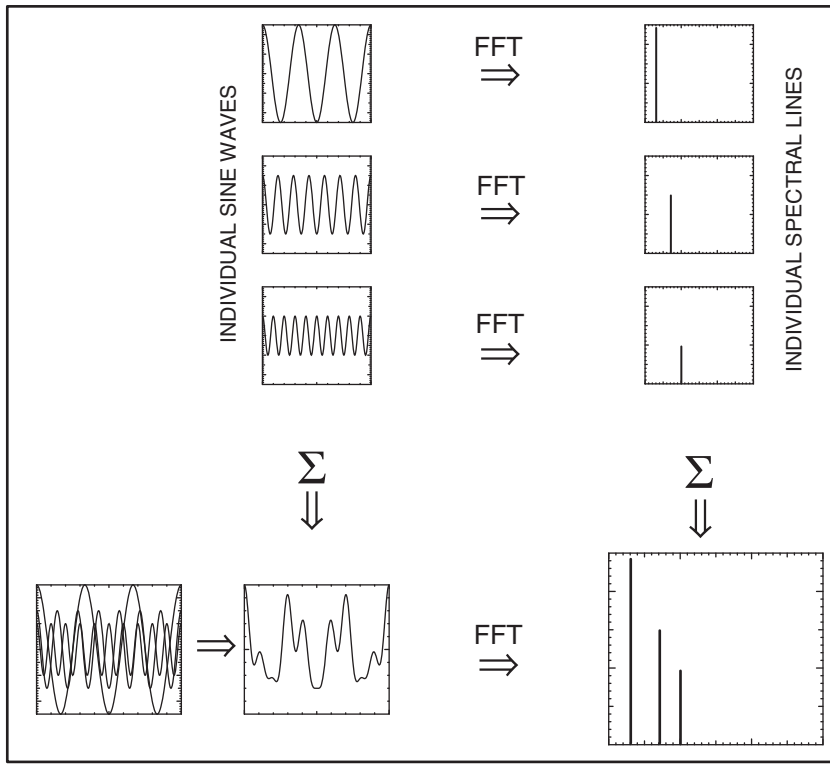

Figure 3.16 Several simple sine waves with corresponding frequency representations.

The fast Fourier transform (FFT) is the Fourier series written in discretized form with some extra restrictions.

But to get the concepts across, consider some simple sine waves at different frequencies (Figure 3.16). The upper portion of the figure shows three separate sine waves as a time signal and as a frequency representation for each sine wave as a single spectral line. The lower portion shows the summation of the three sine waves, which is a much more complicated signal in the time domain but much easier to understand in the frequency domain.

Considering the summation of the three sine waves in Figure 3.16, the information is more clearly understood in the frequency domain than in the time domain. So now let's discuss the Fourier transform.

3.9.1 Fourier Transform and Discrete Fourier Transform

The discrete Fourier transform algorithm is the basis for the formulation of the frequency signal representation in most FFT analyzers available today. Because this transform is written as a continuous integral for all time, there must be some consideration given to the fact that sampled time data is recorded only for short time periods. Provided that the time signal is represented with an integer number of sinusoids in the frequency domain or provided that the signal is totally observed in one sample record, then there is no distortion of the signal in the transformation process. If this is not true, then significant distortion of the signal may result. This distortion is referred to as *leakage* and is by far the most serious of the signal processing errors that can occur. Leakage can be minimized through the use of special excitation techniques or

through the use of time weighting functions referred to as *windows*. First, let's summarize the Fourier transform equations; they will be presented but not formally derived.

For the Fourier transform, the transformation from time to frequency and back is given by

Forward transform

$$S_x(f) = \int_{-\infty}^{+\infty} x(t)\ e^{-j2\pi ft} dt$$

Inverse transform

$$x(t) = \int_{-\infty}^{+\infty} S_x(f)\ e^{j2\pi ft} df$$

For the discrete Fourier transform, although the actual time signal is continuous, the signal is discretized and the transformation at discrete points is

$$S_x(m\Delta f) = \int_{-\infty}^{+\infty} x(t)\ e^{-j2\pi m\Delta ft} dt$$

This integral is evaluated as

$$S_x(m\Delta f) \approx \Delta t \sum_{n=-\infty}^{+\infty} x(n\Delta t)\ e^{-j2\pi\, m\Delta f\, n\Delta t}$$

However, if only a finite sample is available (which is generally the case), then the transformation becomes

$$S_x(m\Delta f) \approx \Delta t \sum_{n=0}^{N-1} x(n\Delta t)\ e^{-j2\pi\, m\Delta f\, n\Delta t}$$

3.9.2 FFT: Periodic Signal

When the transformation is made from the time to the frequency domain, the mathematical representation of the Fourier series is exact, provided that the signal is known from minus infinity to plus infinity. However, because only one sample that is T seconds long is acquired, the entire signal is not captured. Provided that the measured signal is periodic in the sample interval, then the FFT of the sampled signal produces the correct frequency representation of the observed signal. Figure 3.17 shows the actual time signal along with the sample of length T. If an integer number of cycles of the signal is obtained, then the original signal can be recreated from the sample, as shown in the lower time trace. The FFT of this signal correctly results in one spectral line in the time domain. Note that time or amplitude scales are not shown; this is just a schematic to show the process.

3.9.3 FFT: Non-periodic Signal

When the transformation is made from the time to the frequency domain, the mathematical representation of the Fourier series is exact, provided that we know the signal from minus infinity to plus infinity. However, because only one sample that is T seconds long is acquired, the entire signal is not obtained. If the signal is not periodic in the sample interval (does not contain N integer cycles of the signal), then errors will result in the FFT process. Figure 3.18 shows the actual time signal along with the sample of data of length T. If the signal is recreated, there is a discontinuity in the lower time trace, indicating that an integer number of cycles of the sine wave were not captured in T seconds of data. If an FFT of this sample of data of length T is taken, then the expected single spectral line is not obtained due to this distortion of the time signal caused by our sampling process.

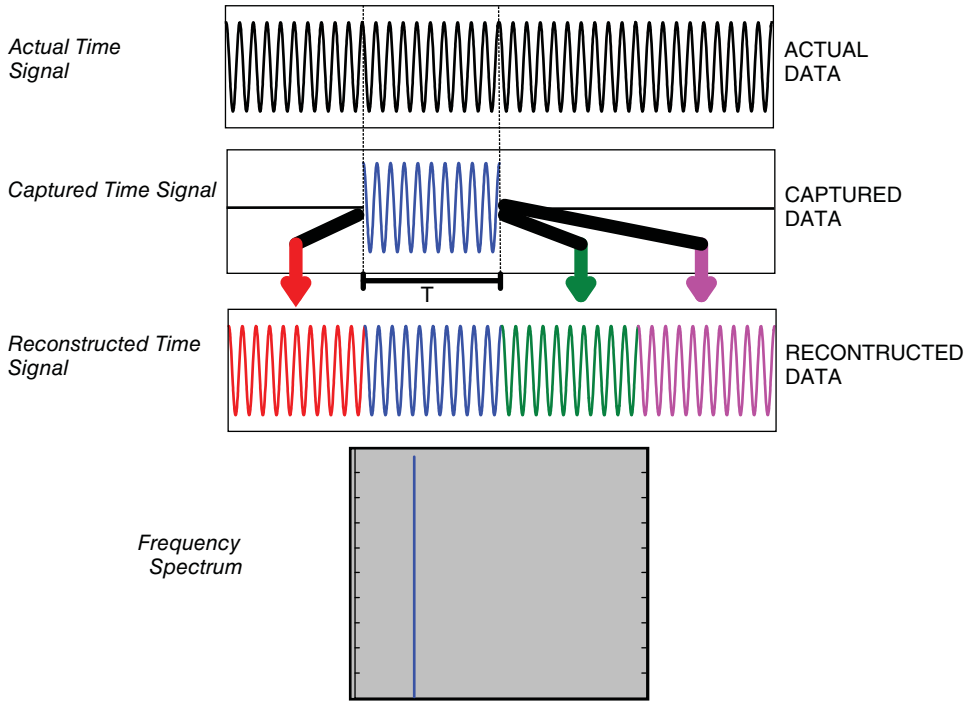

Figure 3.17 Actual time signal, sampled and reconstructed along with the resulting frequency spectrum from the FFT for properly sampled data.

3.10 Leakage and Minimization of Leakage

When the measured signal is not periodic in the sample interval, incorrect estimates of the amplitude and frequency occur. This error is referred to as *leakage*. Basically, the actual energy distribution is smeared across the frequency spectrum and energy *leaks* from a particular Δf into adjacent ones. The time signal appears to be distorted from one time sample to the next, as shown in Figure 3.19. There is a clear distortion of the signal from one sample to the next. The most important thing to note is that the amplitude of the signal is reduced and the peak tends to spread over several spectral lines rather than being concentrated at one spectral line. It is important to recall that the amplitude of the frequency response function is directly related to the mode shapes, which will be affected by this leakage.

The spreading of the peak over several spectral lines will give the appearance of damping, so the mode shape and damping will be affected by leakage. These are two very important parameters of interest when performing an experimental modal test.

Leakage is probably the most common and most serious digital signal processing error. Unlike aliasing, the effects of leakage cannot be eliminated. Leakage effects can only be reduced. These effects can be partially reduced by

- averaging techniques
- increased frequency resolution
- use of periodic/special excitation
- use of window functions.

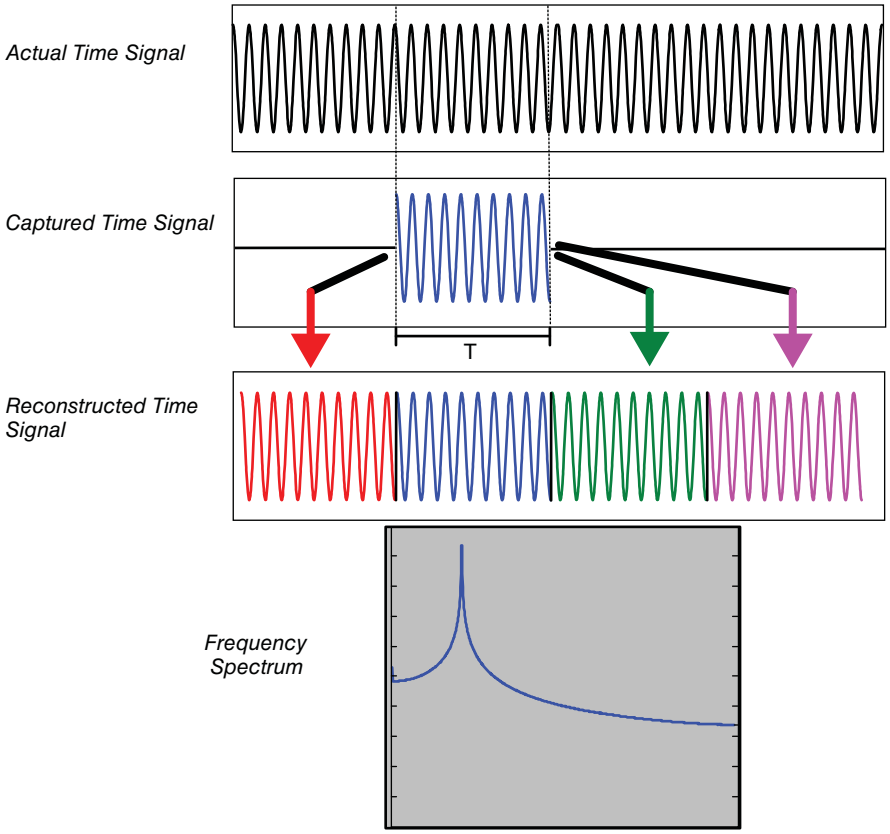

Figure 3.18 Actual time signal, sampled and reconstructed, along with the resulting frequency spectrum from the FFT for improperly sampled data.

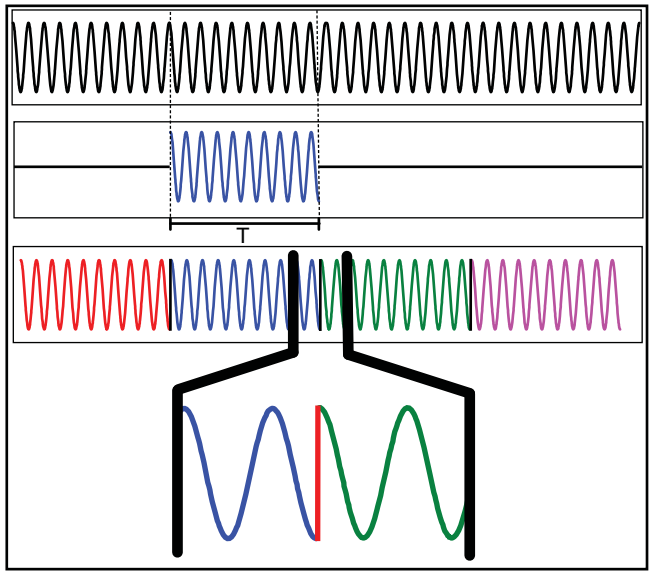

Figure 3.19 Sampling clearly showing discontinuity from sample to sample.

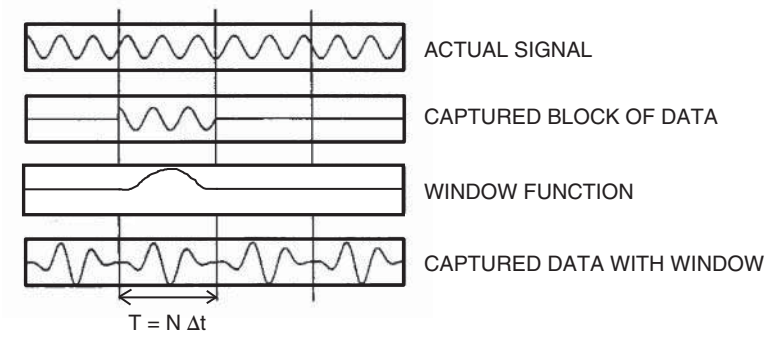

Figure 3.20 Conceptualization of windows weighting functions to reduce leakage.

3.10.1 Minimization of Leakage

A window is a weighting function that is applied to the measured signal. The function of the window is to make the measured signal appear more periodic in the sample interval, thereby reducing the effects of leakage. There are many different windows that could potentially be used and too many exist to list and describe herein.

Some of the more common window types used for experimental modal analysis are:

- rectangular
- Hanning
- flat top
- force
- exponential.

The intended process of a general window function is to attempt to weight the function so that it better satisfies the periodicity requirement of the Fourier transform process. This is conceptually shown in the four frames in Figure 3.20.

For the most part for experimental modal applications, a Hanning window is used for random signals, a flattop is used for calibration, a rectangular window is used when the signals are guaranteed to satisfy periodicity, and force/exponential windows are used for impact testing. Each of the windows is discussed next.

3.11 Windows and Leakage

Window functions typically employed for experimental modal analysis testing are the Hanning, flat top, rectangular, force, and exponential windows. A rectangular window (or uniform window or boxcar window) is used only when the signal is known to contain an integer number of sinusoids making up the time signal or when the captured time signal is totally observed within one sample interval of the analyzer; this is basically uniform weighting of the data. A Hanning window is normally applied for random excitations, where the contents of the signal measured are completely unknown. The Hanning window offers reasonably good frequency resolution while the amplitude accuracy of the measured signal can contain as much as 16% error. The flat top window is normally employed on signals that are sinusoidal in nature and it offers measured signal amplitude accuracy to within 0.1% but lacks significant frequency resolution; generally this is a good window for calibration purposes. The force and exponential windows are typically employed in impulsive excitation testing; the exponential window is applied to the response

of the system in an attempt to weight the time response to ensure that the entire transient is observed within one sample interval of the analyzer.

Windows, while a necessary requirement for minimizing the signal processing error of leakage, distort the measured time data to some degree. The distortion will always appear as a loss in accuracy in the measured peak amplitude in the frequency domain, and will always give the measured frequency data the appearance of larger damping in the system.

The rectangular, Hanning, and flat top windows will be described next. Basically, all windows are evaluated based on the width of the main lobe (which controls the amplitude accuracy) and the roll off of each of the side lobes (which controls frequency discernibility). These effects are schematically shown in Figure 3.21.

For each of the windows described next in Figures 3.22–3.24, the frequency representation of the window is shown in a log mag plot with $\pm 15\Delta f$ on either side of the main lobe centered at 0 and also in a magnitude plot with $\pm 3\Delta f$ on either side of the main lobe. When a single frequency sinusoidal signal is involved, there are two important special cases. The first is when the signal is periodic in the sample interval and there is no distortion of the signal due to the Fourier transform process. The second is when the signal is such that the signal is not periodic within the sample interval; this will create leakage and the worst case of leakage will be discussed.

3.11.1 Rectangular Window

The time window shape for a rectangular window is a unity gain for the entire T seconds of data required to acquire the signal. The rectangular window is also referred to as a box car, uniform window or no window. The rectangular window function is shown in Figure 3.22. The main lobe is narrow, but the side lobes are very large and roll off quite slowly. The main lobe is quite rounded and can introduce large measurement errors. The rectangular window can have amplitude errors as large as 36%.

In looking at the log mag plot in Figure 3.22a, there are several things to note. Each major tick mark on the plot is $2\Delta f$. This means that every $1\Delta f$ the function drops to zero. That implies that if the signal is periodic in the sample interval then the only frequency component that will be observed is the main lobe; every Δf away from the main lobe, the value drops to zero so that only one frequency is observed. Now looking at the magnitude plot in Figure 3.22b, the major tick mark on the plot is $0.5\Delta f$ and again the function drops to zero $1\Delta f$ away from the main

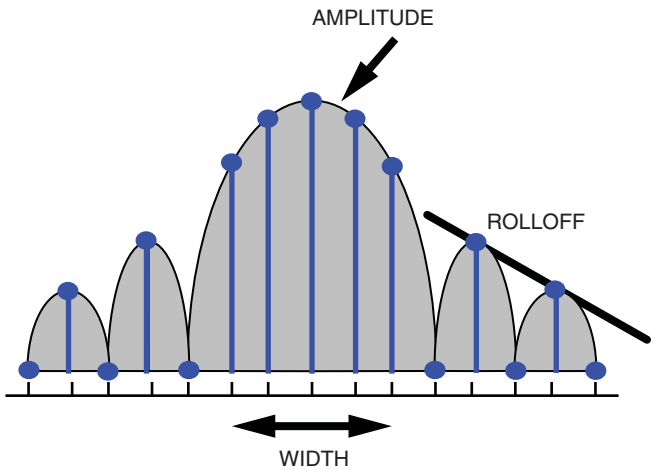

Figure 3.21 Distortion effects of windows to reduce leakage.

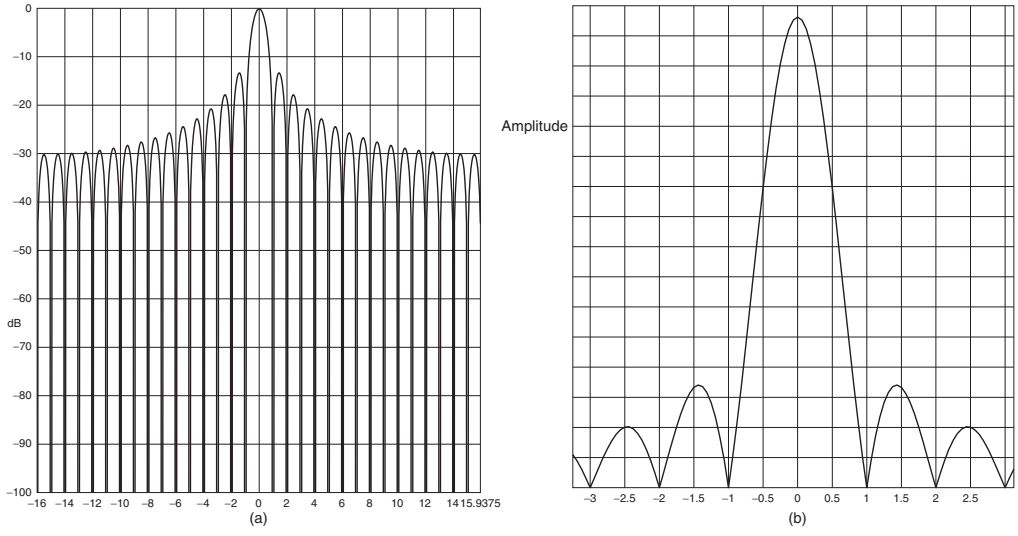

Figure 3.22 Rectangular window frequency signature for (a) log mag and (b) linear mag.

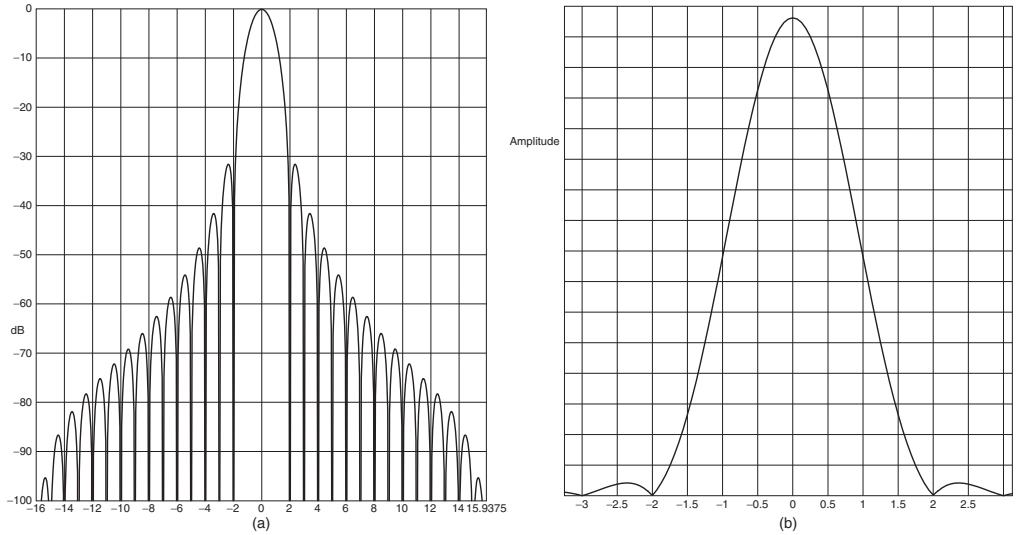

Figure 3.23 Hanning window frequency signature for (a) log mag and (b) linear mag.

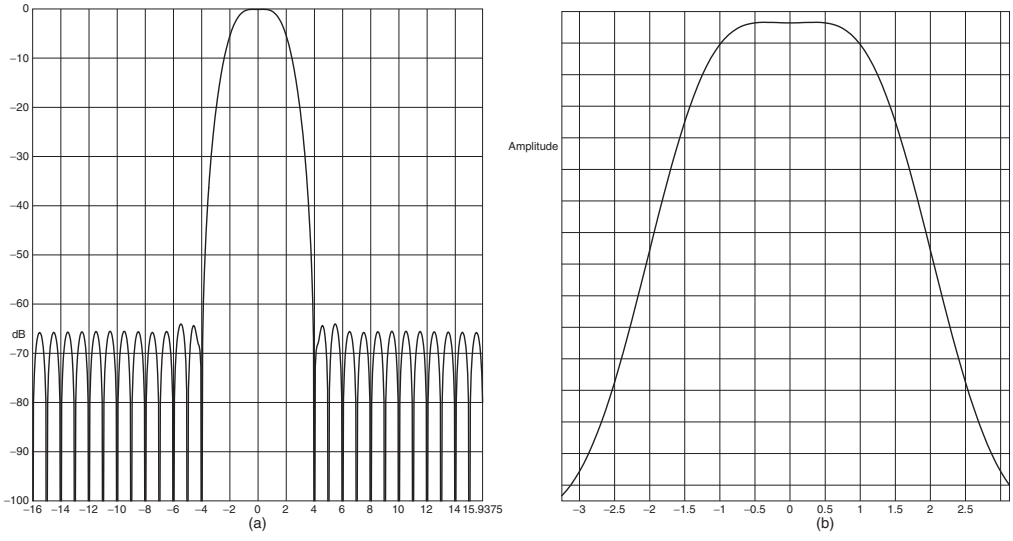

Figure 3.24 Flattop window frequency signature for log mag (a) and linear mag (b).

lobe. This works well if the signal satisfies the periodicity requirement of the transform. But if it doesn't then there is a distortion of the signal. And the worst distortion will occur when the frequency to be measured is exactly between two Δf; this will be shown shortly.

3.11.2 Hanning Window

The time representation of the Hanning window is a half cosine curve. The Hanning window function is shown in Figure 3.23. The first few side lobes are rather large, but a 60 dB/octave roll off rate is good. This window is most useful for searching operations where good frequency resolution is needed, but amplitude accuracy is not important; the Hanning window will attenuate the signal by as much as 1.5 dB (16%).

In looking at the log mag plot in Figure 3.23a, there are several things to note. Each major tick mark on the plot is 2Δf. Previously, for the rectangular window, every 1Δf the function drops to zero. But for the Hanning window almost all of the Δf drop to zero, except on either side of the main lobe where the spectrum has significant amplitude. Now in the magnitude plot in Figure 3.23b, the major tick mark on the plot is 0.5Δf and again the function does not drop to zero on either side of the main lobe. So right away it is seen that the window, applied to a completely periodic signal that satisfies the periodicity requirement, is affected by the Hanning window and results in at least 3Δf observed in the resulting frequency representation of the signal. And if the signal doesn't satisfy the periodicity requirement then there is a distortion of the signal. The worst distortion will occur when the frequency to be measured is exactly between two Δf; this will also be shown shortly. The Hanning window is a good window, which balances the frequency discernibility with the amplitude accuracy.

3.11.3 Flat Top Window

The time representation of the flat top or P301 window is a series of four sine waves. The flat top window function is shown in Figure 3.24. The main lobe is very flat and spreads over several frequency bins. While this window suffers from frequency resolution, the amplitude can be measured very accurately with less than 0.1% error.

In looking at the log mag plot in Figure 3.24a, there are several things to note. Each major tick mark on the plot is 2Δf. Previously, for the rectangular window, every 1Δf the function drops to zero. However, for the flat top window almost all of the Δf drop to zero except for several values on either side of the main lobe, where the spectrum has significant amplitude. Now the magnitude plot in Figure 3.24b, the major tick mark on the plot is 0.5Δf and again the function does not drop to zero on either side of the main lobe. So right away it is seen that the window applied to a completely periodic signal that satisfies the periodicity requirement is affected by the flat top window and results in at least 7Δf observed in the resulting frequency representation of the signal. If the signal doesn't satisfy the periodicity requirement then there is a distortion of the signal, and the worst distortion will occur when the frequency to be measured is exactly between two Δf; this will also be shown shortly. But the advantage of the flat top is that while the frequency may not be easy to identify, the amplitude is measured very accurately. This makes the flat top window an excellent choice for measuring amplitudes very accurately.

3.11.4 Comparison of Windows with Worst Leakage Distortion Possible

Now if a sinusoidal signal is exactly halfway between the frequency resolution then the worst leakage will result. In Figure 3.25, the rectangular, Hanning and flat top windows are shown with no leakage and the worst leakage possible, in order to show the distortion of the signal. The upper portion of the figure shows the leakage free measurement in the log mag display, spread

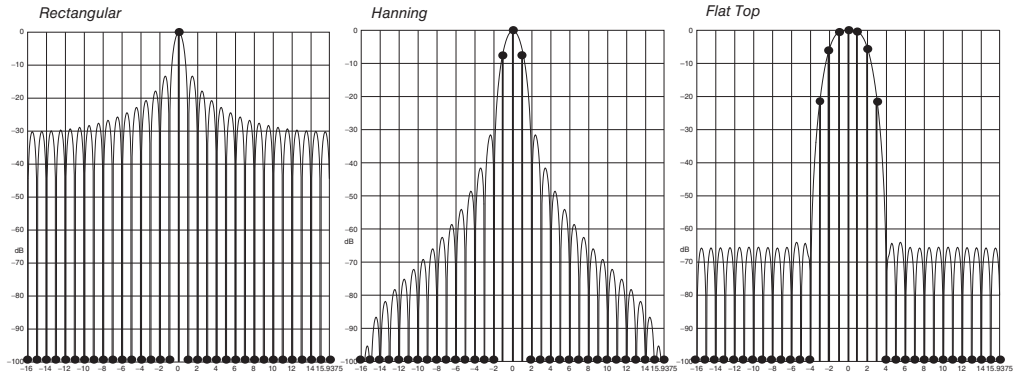

Figure 3.25 Comparison of the rectangular, Hanning and flat top windows with periodic signals satisfying and not satisfying the periodicity requirement of the Fourier transform process.

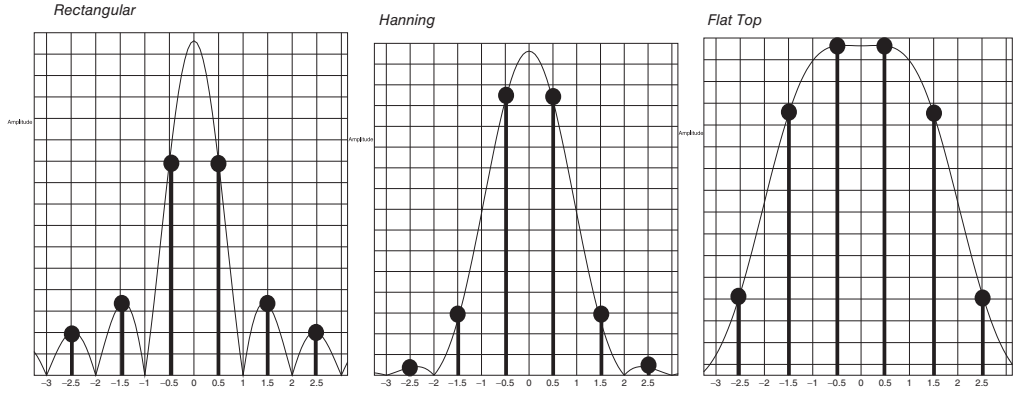

Figure 3.25 (*Continued*)

over 16Δf. Clearly the windows have an effect, even if the signal actually satisfies the periodicity requirement of the Fourier transform process. And the distortion is more pronounced in the lower portion of the figure, where the signal does not satisfy the periodicity requirement of the Fourier transform process.

3.11.5 Comparison of Rectangular, Hanning and Flat Top Window

An overlay plot for the comparison of the rectangular, Hanning and flat top windows is shown in Figure 3.26. Notice how the rectangular window has very little rolloff of the side lobes when compared to the Hanning and flat top windows.

3.11.6 Force Window

In many applications, measurements are acquired through impact tests. When acquiring data in this fashion, noise may be present on the input channel and the use of a Hanning or flat top window is not appropriate. The force window has unit amplitude over a specified portion of the sample interval and zero over the balance of the sample interval. The force window is an effective mechanism for reducing noise on the input channel for an impulsive type of excitation.

3.11.7 Exponential Window

In many applications where impact excitation is used, the response of the system is the summation of damped sine waves. As in the case of the excitation force, a Hanning or flat top window is not appropriate for this type of signal. An exponential window can be used to force the response of the system to be periodic within the sample interval. There are instances when the time sample is long enough to allow the system to naturally decay within the sample interval. In this case, there is no reason to apply any window. A signal that has this characteristic is referred to a *self-windowing* function.

The force and exponential windows are shown in Figure 3.27 and are discussed in much more detail in the application portion of this text.

3.11.8 Convolution of the Window in the Frequency Domain

While windows are applied in the time domain by multiplying the actual captured time signal by the window time shape, the effects of the window can be more clearly seen in the frequency domain. In the frequency domain, the window line shape is actually convolved with the actual signal in the frequency domain. These effects are shown simply in Figure 3.28, where a three spectral line window shape is shown with a single discrete sine wave. The effect of multiplication of a window with measured data in the time domain results in what is called *convolution* in the frequency domain. The theoretical window shape is multiplied by the actual signal to form a summation at each value at each Δf. So we can see in this example, the actual signal at the seventh Δf is multiplied by this assumed three lobe window. The value at the first Δf is zero because each of the corresponding terms of the window times the signal sum to zero when we consider the first Δf. Actually, the value is zero until the window center lobe is located at the sixth Δf and also has values when the center lobe is located at the seventh and eighth Δf, after which the value is zero.

3.12 Frequency Response Function Formulation

Several frequency response function formulations exist for the formulation of measured frequency response functions in the presence of noise. In all formulations of the frequency

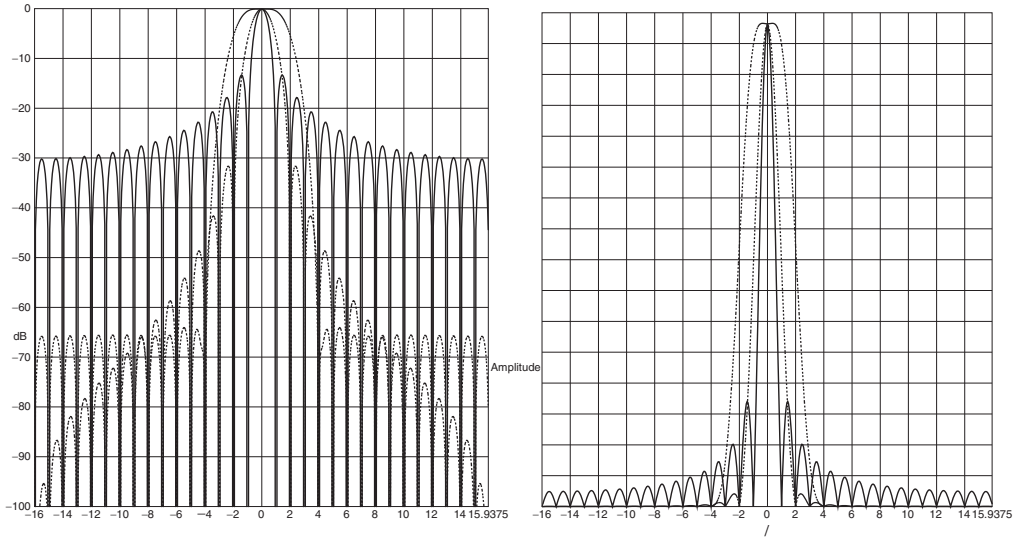

Figure 3.26 Overlaid plot of the rectangular, Hanning and flat top windows.

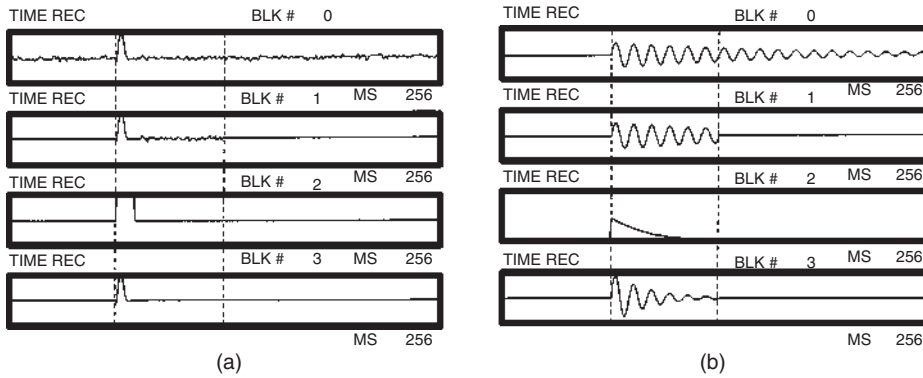

Figure 3.27 Illustration of (a) force and (b) exponential windows.

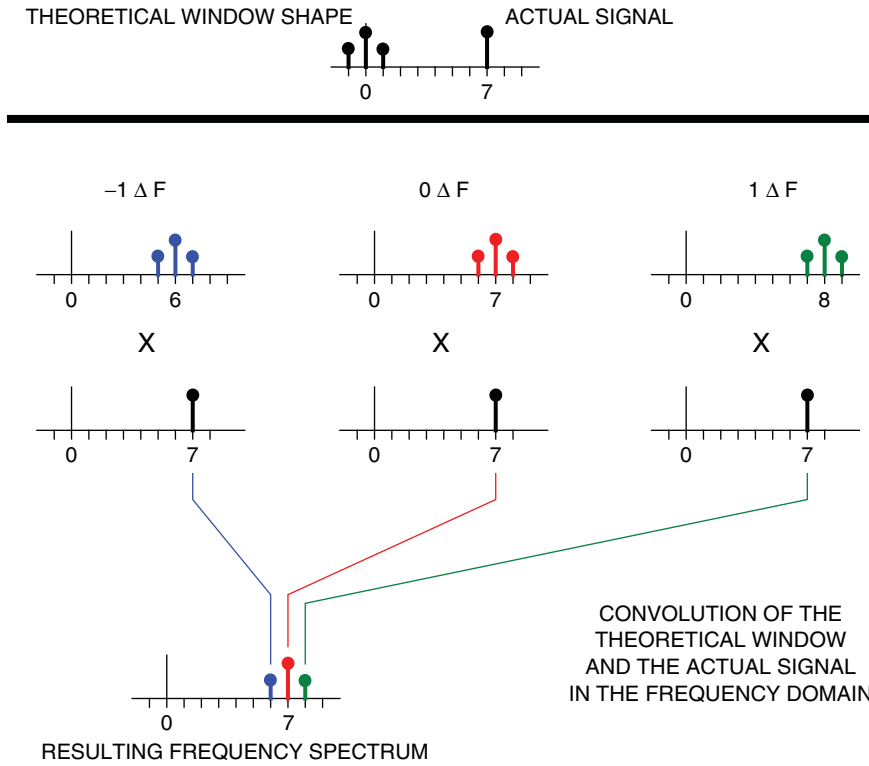

Figure 3.28 Schematic of the convolution of the theoretical window with the actual signal in the frequency domain.

response function, if the noise is minimized then all the different forms of the measured frequency response function will approach the same value in the limit. While several approaches exist, two common approaches are identified below. Figure 3.29 shows a typical input–output measurement situation.

First, let's define an input–output model. If we define x(t) as the input signal and y(t) as the resulting output signal, then performing an FFT on these signals will produce:

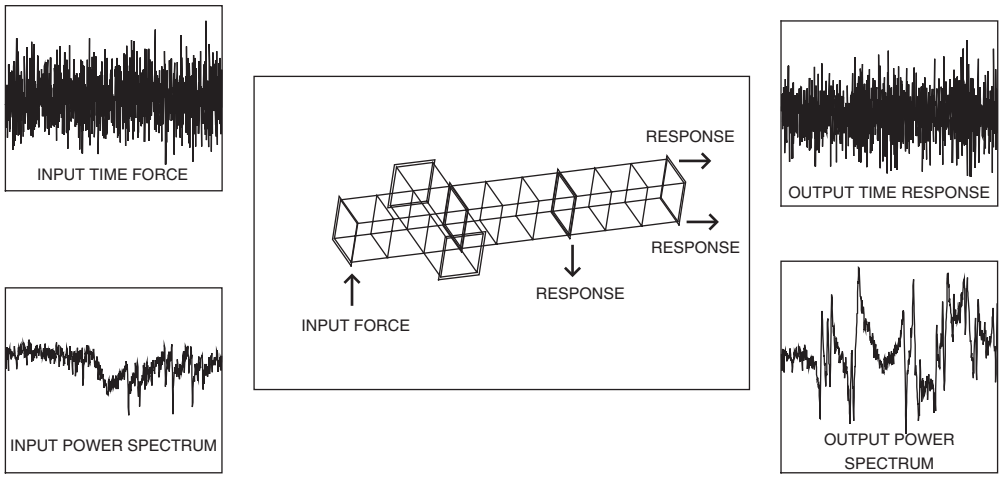

Figure 3.29 Typical input–output measurement situation.

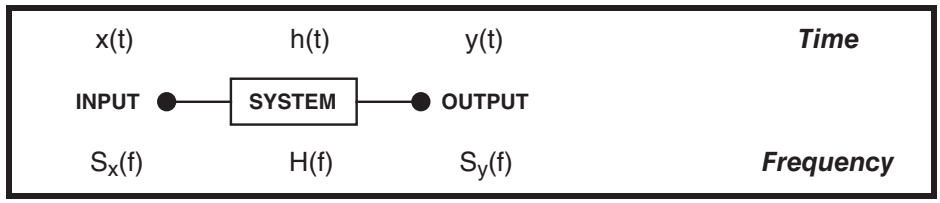

where S_x and S_y are the linear Fourier spectra of the input signal x(t) and y(t), respectively. These frequency domain signals are related to the frequency response function as

$$S_y = H\, S_x$$

Generally, most analyzers will measure averaged power spectrum of time signals to minimize noise on the measurement. These computed power spectra are related to the linear spectra as:

G_{xx}	Input power spectrum	$S_x\, S_x^*$
G_{yy}	Output power spectrum	$S_y\, S_y^*$
G_{yx}	Cross power spectrum	$S_y\, S_x^*$

With these definitions, two relations can be written by post-multiplying the input–output relationship by S_x^* in one case and by S_y^* in the other case to give

$$S_y S_x^* = H\, S_x S_x^* \quad \Rightarrow \quad H_1 = \frac{G_{yx}}{G_{xx}}$$

$$S_y S_y^* = H\, S_x S_y^* \quad \Rightarrow \quad H_2 = \frac{G_{yy}}{G_{xy}}$$

The first formulation of H tends to minimize noise on the output and is generally an underestimate of the measured frequency response function. The second formulation of H tends to minimize noise on the input and is generally an overestimate of the measured frequency response function. A third formulation, called H_v, is computed in a vector least squares sense

and minimizes noise on both the input and output simultaneously and is a better approximation to the true H of the system.

The *coherence*, or ordinary coherence, function is defined as

$$\gamma^2 = \frac{G_{yx}G_{xy}}{G_{xx}G_{yy}} = \frac{H_1}{H_2}$$

The coherence function is a scalar value, which ranges between 0 and 1. When the coherence is zero, none of the output signal is coherently related to the input signal and there is no causal relationship; when the coherence is one, all of the measured output signal is coherently related to the input signal. The coherence is a valuable tool to assess the adequacy of the measured frequency response function.

3.13 Typical Measurements

3.13.1 Time Signal and Auto-power Functions

Both input and response time signals are captured in the FFT analyzer. If needed, windows are applied to the discretized data. Once this is done the signal is transformed to the frequency domain as linear Fourier spectra. These linear spectra are complex valued functions having real and imaginary parts, or magnitude and phase. In order to compute the auto-power spectra, the two signals are multiplied by their respective complex conjugates. Once these functions are changed from linear spectra to power spectra, the functions become real valued with no phase relationship. Typical time signals and power spectra are shown in Figure 3.30 for the input excitation and the output response.

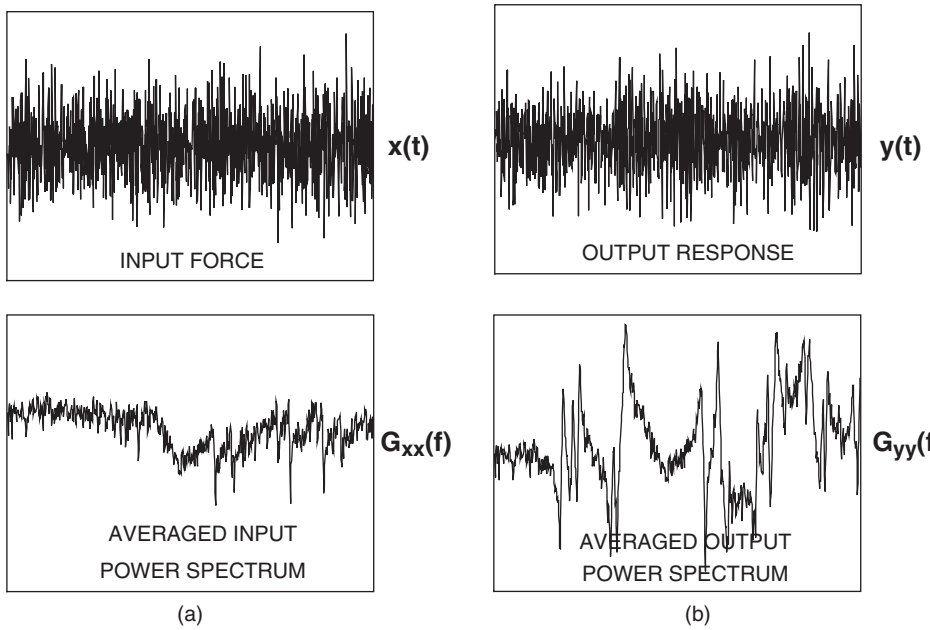

Figure 3.30 Time signal (top) and power spectra (bottom): (a) input; (b) output.

3.13.2 Typical Measurement: Cross Power Function

Once the input and response linear Fourier spectra are computed, then the cross power spectrum can be computed. The cross power spectrum is a complex valued function having real and imaginary parts, or magnitude and phase. The cross spectrum is shown in the lower half of Figure 3.31, along with the input spectrum (top left) and output spectrum (top right)

3.13.3 Typical Measurement: Frequency Response Function

Once the input and response auto-power spectra and the cross power spectrum are averaged, then the frequency response function is generated from these spectra, as shown in Figure 3.32. The frequency response function is a complex valued function because in all of the formulations of H, the cross power spectrum is used; the cross spectrum is a complex valued function.

3.13.4 Typical Measurement: Coherence Function

At the same time the frequency response function is computed, H, the coherence function is also evaluated. A typical coherence plot is shown in Figure 3.33, along with the frequency response function. Notice that the coherence appears to be very good, with values approaching 1.0. There are a few frequencies where the coherence drops most noticeably. These coherence drops occur close to anti-resonances, which is not a problem because there is very little output, if any, at these locations. Thus it is expected for the coherence to drop here. Overall this is a fairly good measurement.

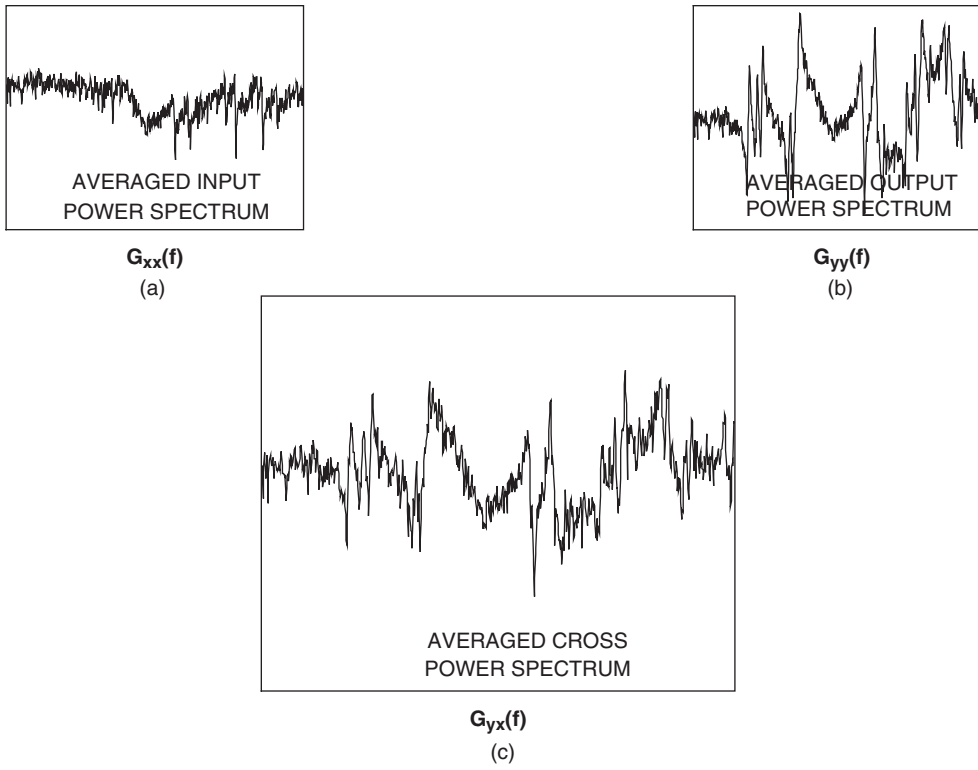

Figure 3.31 Power spectra: (a) input; (b) output; (c) cross power spectrum.

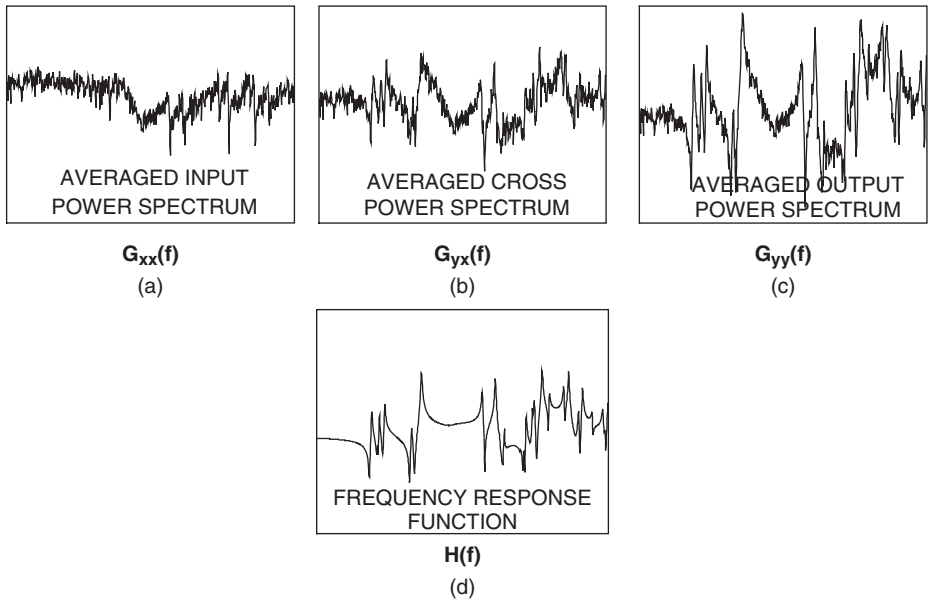

Figure 3.32 Power spectra: (a) input; (b) cross power spectrum; (c) output; (d) computed frequency response function.

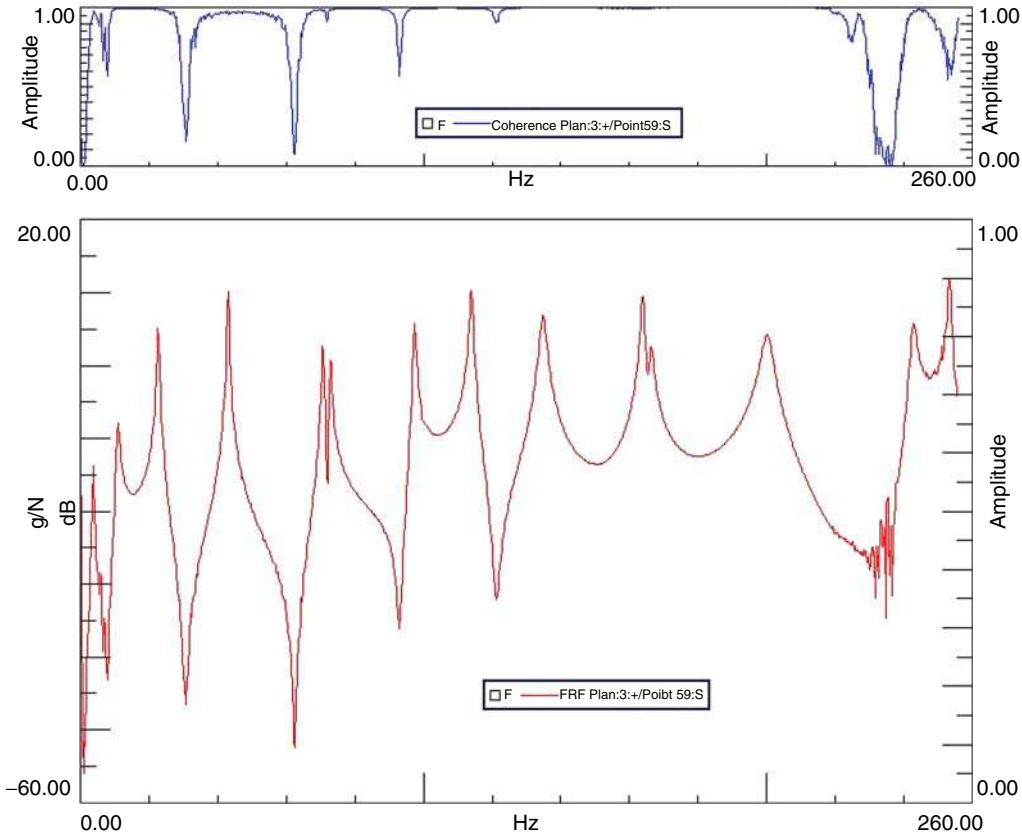

Figure 3.33 Computed frequency response function (bottom) with coherence (top).

3.14 Time and Frequency Relationship Definition

Generally measurements are acquired and averaging is done to reduce the amount of variance seen on the measured data when there is noise present. The input–output model and definition of linear and square law relationships is:

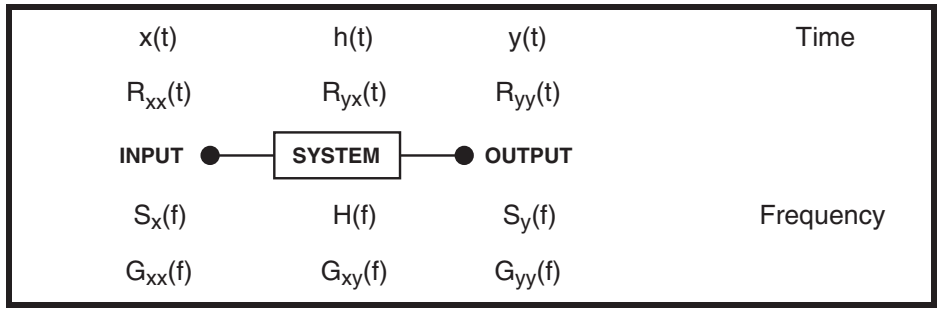

where

x(t)	time domain input to the system	y(t)	time domain output to the system
$S_x(f)$	linear Fourier spectrum of x(t)	$S_y(f)$	linear Fourier spectrum of y(t)
H(f)	system transfer function	h(t)	system impulse response
$R_{xx}(t)$	autocorrelation of the input signal x(t)	$R_{yy}(t)$	autocorrelation of the output signal y(t)
$G_{xx}(f)$	autopower spectrum of x(t)	$G_{yy}(f)$	autopower spectrum of y(t)
$G_{yx}(f)$	cross power spectrum of y(t) and x(t)	$R_{yx}(t)$	cross correlation of y(t) and x(t)

The general Fourier transform pairs are defined here; these are the measurements typically obtained from the FFT.

$$x(t) = \int_{-\infty}^{+\infty} S_x(f)\, e^{j2\pi ft}\, df \qquad S_x(f) = \int_{-\infty}^{+\infty} x(t)\, e^{-j2\pi ft}\, dt$$

$$y(t) = \int_{-\infty}^{+\infty} S_y(f)\, e^{j2\pi ft}\, df \qquad S_y(f) = \int_{-\infty}^{+\infty} y(t)\, e^{-j2\pi ft}\, dt$$

$$h(t) = \int_{-\infty}^{+\infty} H(f)\, e^{j2\pi ft}\, df \qquad H(f) = \int_{-\infty}^{+\infty} h(t)\, e^{-j2\pi ft}\, dt$$

$$R_{xx}(\tau) = E[x(t), x(t+\tau)] = \lim_{T \to \infty} \frac{1}{T} \int_T x(t)\, x(t+\tau)\, dt$$

$$G_{xx}(f) = \int_{-\infty}^{+\infty} R_{xx}(\tau)\, e^{-j2\pi ft}\, d\tau = S_x(f) \bullet S_x^*(f)$$

$$R_{yy}(\tau) = E[y(t), y(t+\tau)] = \lim_{T \to \infty} \frac{1}{T} \int_T y(t)\, y(t+\tau)\, dt$$

$$G_{yy}(f) = \int_{-\infty}^{+\infty} R_{yy}(\tau)\, e^{-j2\pi ft}\, d\tau = S_y(f) \bullet S_y^*(f)$$

$$R_{yx}(\tau) = E[y(t), x(t+\tau)] = \lim_{T \to \infty} \frac{1}{T} \int_T y(t)\, x(t+\tau)\, dt$$

$$G_{yx}(f) = \int_{-\infty}^{+\infty} R_{yx}(\tau)\, e^{-j2\pi ft}\, d\tau = S_y(f) \bullet S_x^*(f)$$

3.15 Input–Output Model with Noise

The general input–output model shown in Figure 3.34, used earlier, is augmented with both noise on the input and output as possibilities.

Using the input–output noise model above, the formulation of H is as follows.

$$H = G_{uv}/G_{uu}$$

The formulation can be used to identify noise on either the input or output and the effects on the measured frequency response function can be determined; this is presented in the next cases, which detail the noise evaluation. But there is a general observation that can be made for the measured frequency response functions; this is simply shown in Box 3.2.

Box 3.2 General effect of noise on measured frequency response functions

sensitive to noise on input	sensitive to noise on output
underestimate of true H	overestimate of true H
$H_1 = H\left[\dfrac{1}{1+\dfrac{G_{nn}}{G_{uu}}}\right]$	$H_2 = H\left[1+\dfrac{G_{mm}}{G_{vv}}\right]$

3.15.1 H_1 Formulation: Output Noise Only

Using the basic input–output model and adding noise S_m on the output, gives:

$$S_m + S_v = H\, S_u$$

Post-multiplying by the conjugate of the input spectrum S_u^*, gives:

$$(S_m + S_v)\, S_u^* = H_1\, S_u S_u^*$$
$$S_m\, S_u^* + S_v\, S_u^* = H_1\, S_u S_u^*$$

If the output noise is incoherent with input signal (uncorrelated), then $S_m S_u^* = 0$ as more averages are taken. Then the following can be written:

$$H_1 = S_v\, S_u^* / S_u S_u^* = G_{uv}/G_{uu}$$

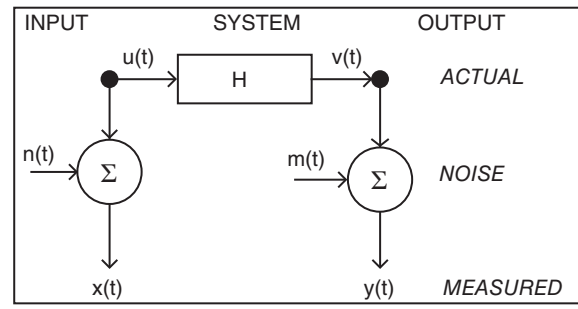

Figure 3.34 General input–output noise model.

3.15.2 H_2 Formulation: Output Noise Only

Using the basic input–output model and adding noise S_m on the output, gives:

$$S_m + S_v = H\, S_u$$

Post-multiplying by the conjugate of the output spectrum $(S_m^* + S_v^*)$, gives:

$$(S_m + S_v)\,(S_m^* + S_v^*) = H_2\, S_u(S_m^* + S_v^*)$$
$$S_m\, S_m^* + S_v\, S_v^* + S_v\, S_m^* + S_m\, S_v^* = H_2\, S_u S_m^* + H_2\, S_u S_v^*$$

If the output noise is incoherent with input and output signal (uncorrelated), then as more averages are taken, the following can be written:

$$S_m\, S_m^* + S_v\, S_v^* = H_2\, S_u S_v^*$$
$$G_{mm} + G_{vv} = H_2\, G_{uv}$$
$$H_2 = (G_{mm} + G_{vv})/G_{uv} = H + G_{mm}\,/\,G_{uv}$$
$$H_2 = H\,(1 + G_{mm}\,/\,G_{vv})$$

3.15.3 H_1 Formulation: Input Noise Only

Using the basic input–output model and adding noise S_n on the input, gives:

$$S_v = H(S_u + S_n)$$

Post-multiplying by the conjugate of the input spectrum $(S_u^* + S_n^*)$, gives:

$$S_v\,(S_u^* + S_n^*) = H_1(S_u + S_n)\,(S_u^* + S_n^*)$$
$$S_v\, S_u^* + S_v\, S_n^* = H_1(S_u S_u^* + S_n S_n^* + S_n S_u^* + S_u S_n^*)$$

If the input noise is incoherent with input and output signal (uncorrelated), then as more averages are taken, the following can be written:

$$S_v\, S_u^* = H_1\,(S_u S_u^* + S_n S_n^*)$$
$$G_{vu} = H_1\,(G_{uu} + G_{nn})$$
$$H_1 = G_{uv}\,/\,(G_{uu} + G_{nn}) = (G_{uv}/G_{uu})/(1 + G_{nn}/G_{uu})$$
$$H_1 = H/(1 + G_{nn}/G_{uu})$$

3.15.4 H_2 Formulation: Input Noise Only

Using the basic input–output model and adding noise S_n on the input, gives:

$$S_v = H(S_u + S_n)$$

Post-multiplying by the conjugate of the output spectrum S_v^* gives:

$$S_v\, S_v^* = H_2\,(S_u + S_n)\, S_v^*$$
$$S_v\, S_v^* = H_2\,(S_u S_v^* + S_n\, S_v^*)$$

If the input noise is incoherent with input and output signal (uncorrelated), then as more averages are taken, the following can be written:

$$H_2 = G_{vv}/G_{uv}$$

3.16 Summary

Digital signal processing concepts were reviewed. Digitization, aliasing, quantization, sampling, and aliasing of measured signals were reviewed. The concept of leakage and the use of weighting functions (windows) were described. Different techniques for estimation of frequency response functions were discussed. Only digital data acquisition and signal processing concepts directly related to experimental modal testing were described.

4

Excitation Techniques

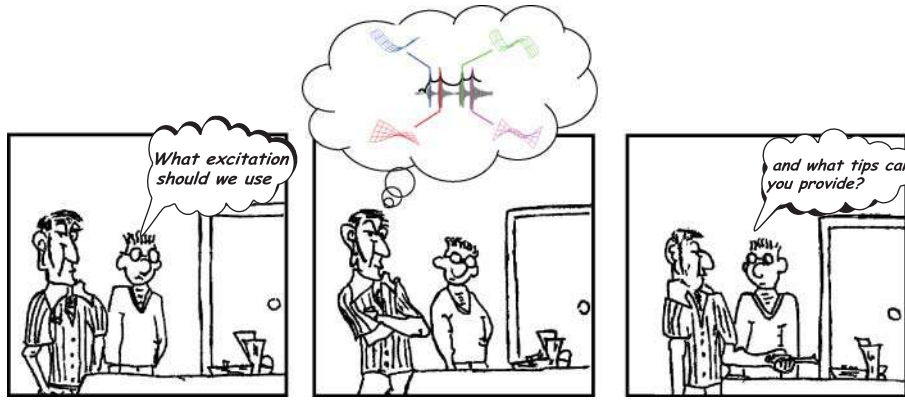

4.1 Introduction

From the development of general modal theory, it is clear that measured frequency response functions are needed in order to extract a modal model. Several alternatives exist for exciting a structure in order to measure response characteristics. However, in order to obtain a set of calibrated measurements, the response of the system due to an applied known input force is required. This limits the type of excitation that can be used for obtaining frequency response functions. Generally, two categories of applied forcing functions are used for experimental modal testing: impact and shaker excitation. While there are numerous other types of excitation, generally they do not provide a known or measured input force. Therefore, the discussions here will be limited to impact and shaker excitation methods, which are the most common methods used.

The most common of the impact techniques involves the use of an impact hammer that is fitted with a force transducer at the head, with a variety of tips that can be used to impart impulsive type of excitation to the structure.

In regards to shaker testing, there are several commonly used techniques for the development of an experimental modal model using force shakers. The force inputs to the system can have two general categories: random or deterministic. Each of these categories of signals can be used to determine the character of the system: both the generation of the frequency response function and an assessment of the linearity of the system under test.

Modal Testing: A Practitioner's Guide, First Edition. Peter Avitabile.

Companion Website: www.wiley.com/go/avitabile/modal-testing

Random excitations have properties that can only be described by some statistical character of the signal. The signal can be described as having some overall level, with some statistical confidence concerning the signal as time progresses. Generally, a mathematical relationship cannot be written to describe the signal at any point in time. These classifications of signals generally have varying amplitude, phase, and frequency content at any point in time. Some random signals commonly used in modal testing are pure random and burst random.

Deterministic signals, on the other hand, conform to a particular mathematical relationship and can be described exactly at any instant in time. As such, the response of the system can also be exactly defined if the system character is known. Some deterministic signals commonly used in modal testing are swept sine, pseudo-random, digital stepped sine and sine chirp.

For all of the measurement techniques, the input/output signals are sampled and the time data is digitized. If necessary, these sampled signals are windowed to minimize leakage in the measured spectrum; some of the excitation techniques considered are specifically designed such that there will not be any leakage associated with the measurement process and therefore they do not need a window weighting function to be applied to the signal. The resulting input power spectrum, output power spectrum, and cross power spectrum are averaged in order to obtain confidence in the measured characteristic. These averaged functions are then used to compute frequency response functions.

The overall measurement process for impact testing is shown in Figure 4.1 and for shaker testing in Figure 4.2; these are intended to show the overview of the process. The flow charts were discussed in the chapter covering signal processing.

First, some of the aspects of impact testing will be discussed, and then of shaker testing. Impact testing items are discussed, followed by an example of some data collected on a simple structure to illustrate some key points. Shaker testing techniques are described, followed by some typical data collected for a simple structure; multiple-input, multiple-output shaker testing is also covered.

4.2 Impact Excitation Technique

Impact testing has become a very popular method of acquiring frequency response functions for experimental modal testing. The portability and simplicity of equipment required make it a valuable test technique for troubleshooting applications and for conducting experimental modal tests. Several issues need to be addressed concerning impact technique, with regards to the input force and resulting output response of the system. A typical impact response measurement is shown in Figure 4.3 for a single degree of freedom system. Notice that while the input force is totally observable within one sample interval T of the analyzer, the response of the system is not; the response continues to exponentially decay well beyond the sample block recorded. This will introduce significant distortion of the signal due to leakage unless a window is used.

There are many items to discuss relative to impact testing. Aspects of hammer tip selection, use of force window, pre-trigger delay, double impact and use of exponential response windows are discussed next, along with several other related issues. There are also many additional examples of impact testing and issues that need to be considered and these are presented in the applications section in Part 2 of the book.

4.2.1 Impact Hammer

Generally, impact testing is performed using an impact hammer and is the most common way this testing is conducted. While there are other novel ways to perform this impulsive type of excitation test, only hammer impact is considered here.

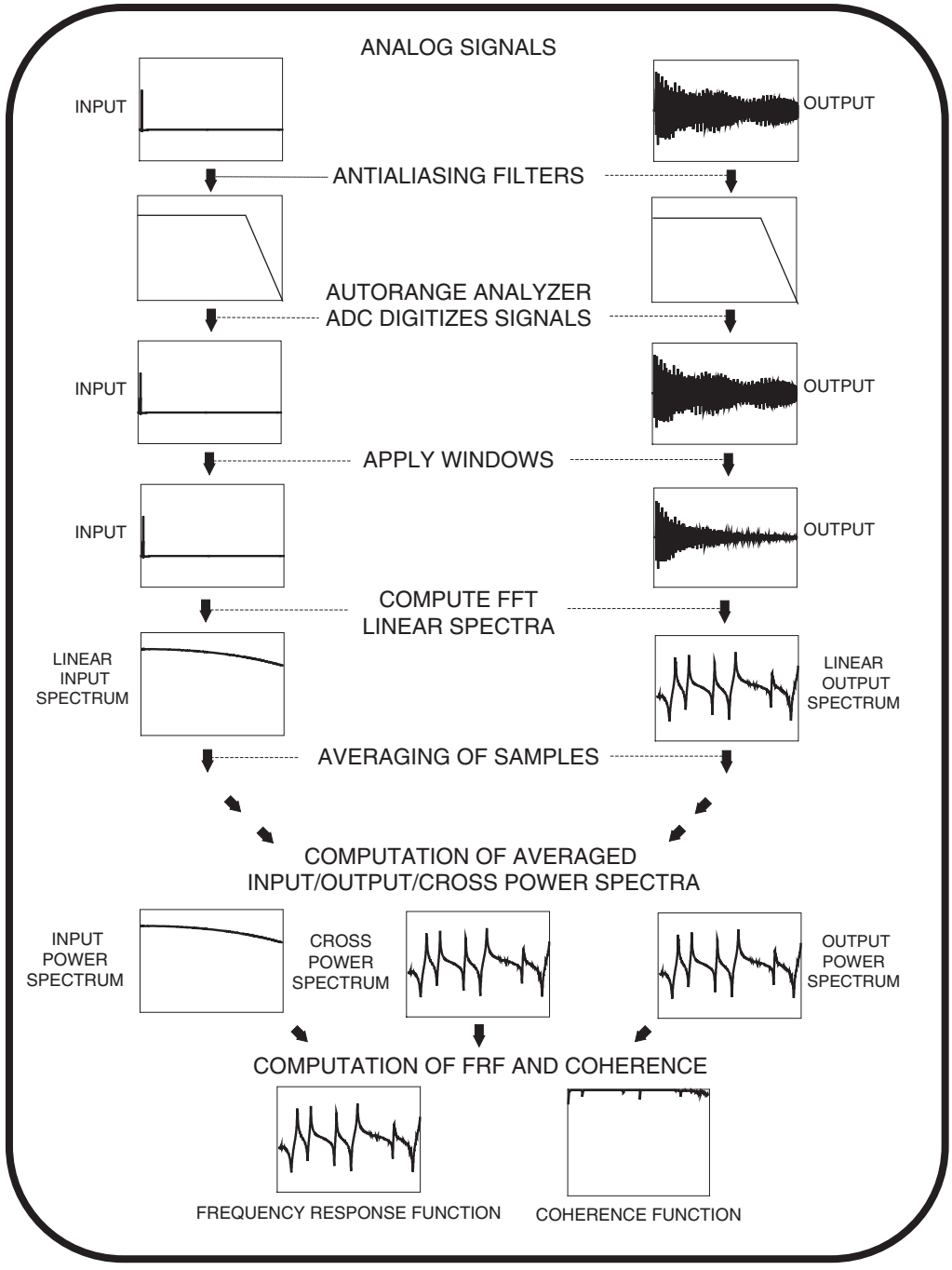

Figure 4.1 Overall measurement process for impact test.

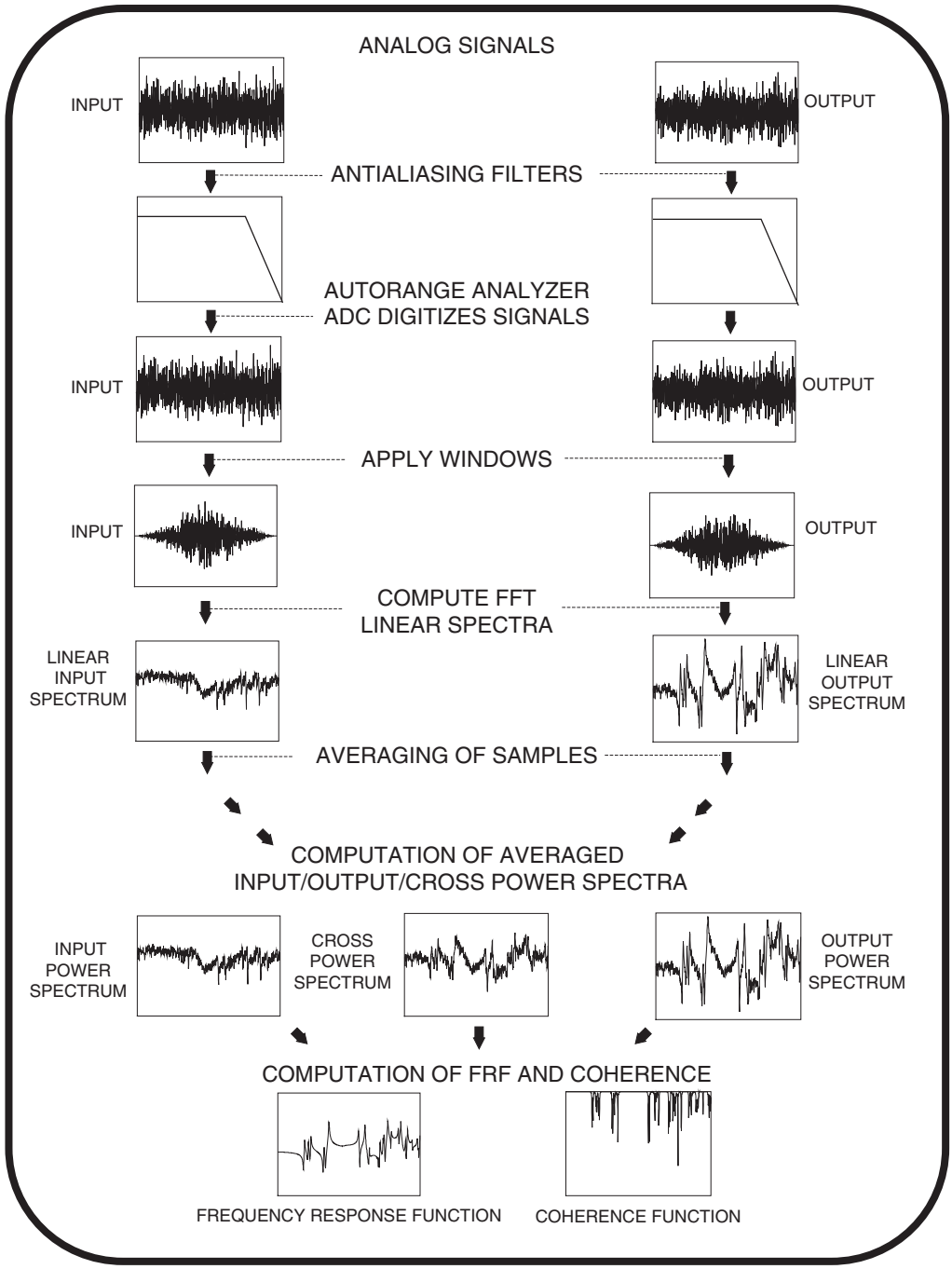

Figure 4.2 Overall measurement process for shaker test.

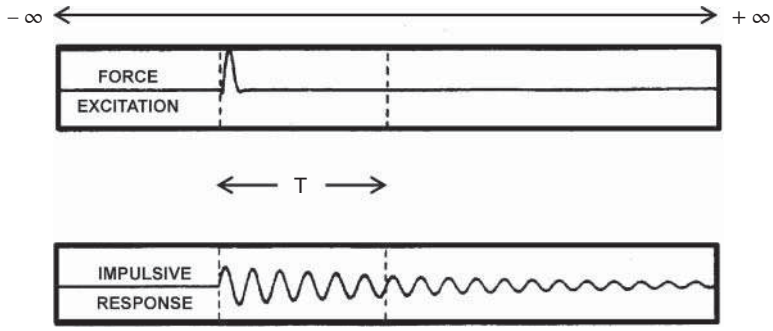

Figure 4.3 Impact and response shown over sample block T.

The impact hammer generally consists of a hammer with a force gage mounted into the head of the hammer; the force gage can be fitted with different impact hardness tips to provide some customization of the frequency band of excitation. There are many different hammer tips that can be deployed, enabling very low frequency ranges as well as very high frequency ranges. The tips range from very soft rubber, to air capsules, to plastic tips, to metal tips. Several common hammers commercially available are shown in Figure 4.4, ranging from small to large, with a few variations such as the modal punch and an electric hammer. The hammer is used to impact

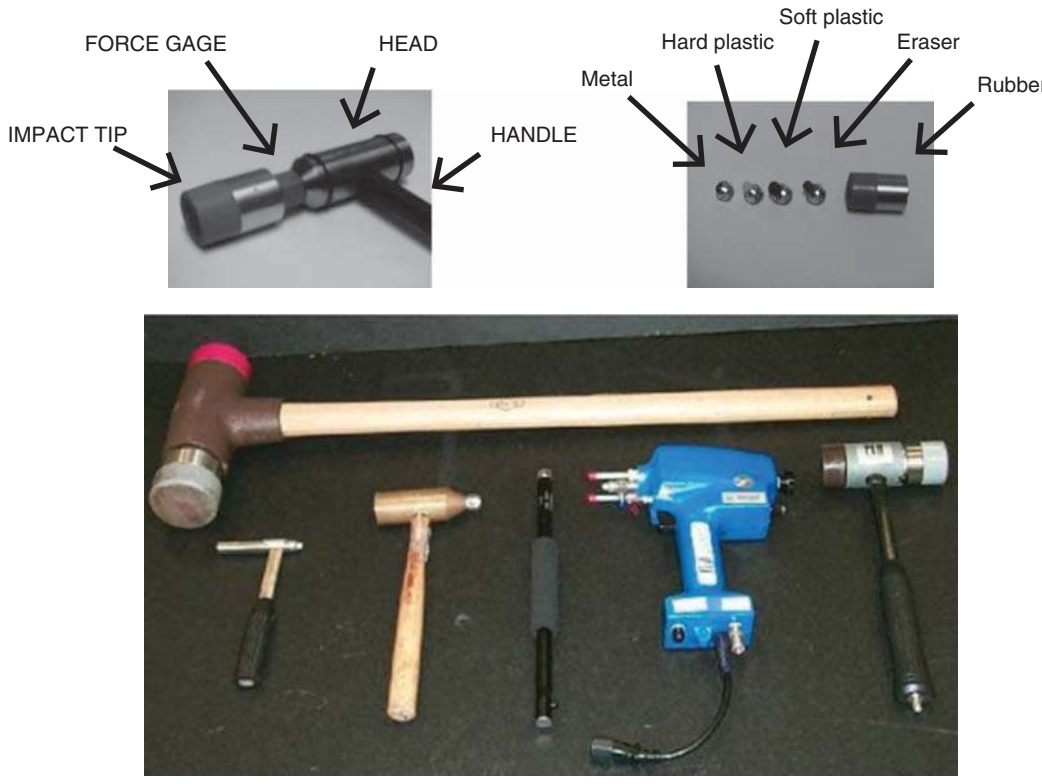

Figure 4.4 Several common impact hammer configurations. Courtesy of PCB Piezotronics, Inc.

the structure under test to cause an impulsive excitation such as that shown in the upper trace in Figure 4.3. The force time pulse directly controls the frequency range that is excited.

4.2.2 Hammer Impact Tip Selection

One very important area for consideration is that of the hammer tip selection. The input force spectrum frequency content is controlled to a large degree by the length of the time pulse (time of duration of impact) applied to the system. This is controlled largely by the stiffness of the hammer tip (although the input force spectrum can at times be controlled mainly by the local flexibility of the structure under test). In general, the harder the tip, the wider the frequency spectrum that is excited; the softer the tip, the narrower the frequency spectrum that is excited. This is shown in Figure 4.5 for four tips of different hardnesses. Now there is always discussion as to how much roll off of the hammer force spectrum is acceptable before the force is insufficient to excite the structure. Some people will state that 3 dB is the limit, while others may state that it is as much as 10 to 20 dB roll off before the force is not adequate to excite the structure. There is really no clear value, and it is most reasonable to look at the frequency response measurement and the coherence in order to define the acceptability of the measurement made; more will be discussed on this in the next sections, as well as in the application portion of the text. Another critical item to note is that the published curves for hammer tip

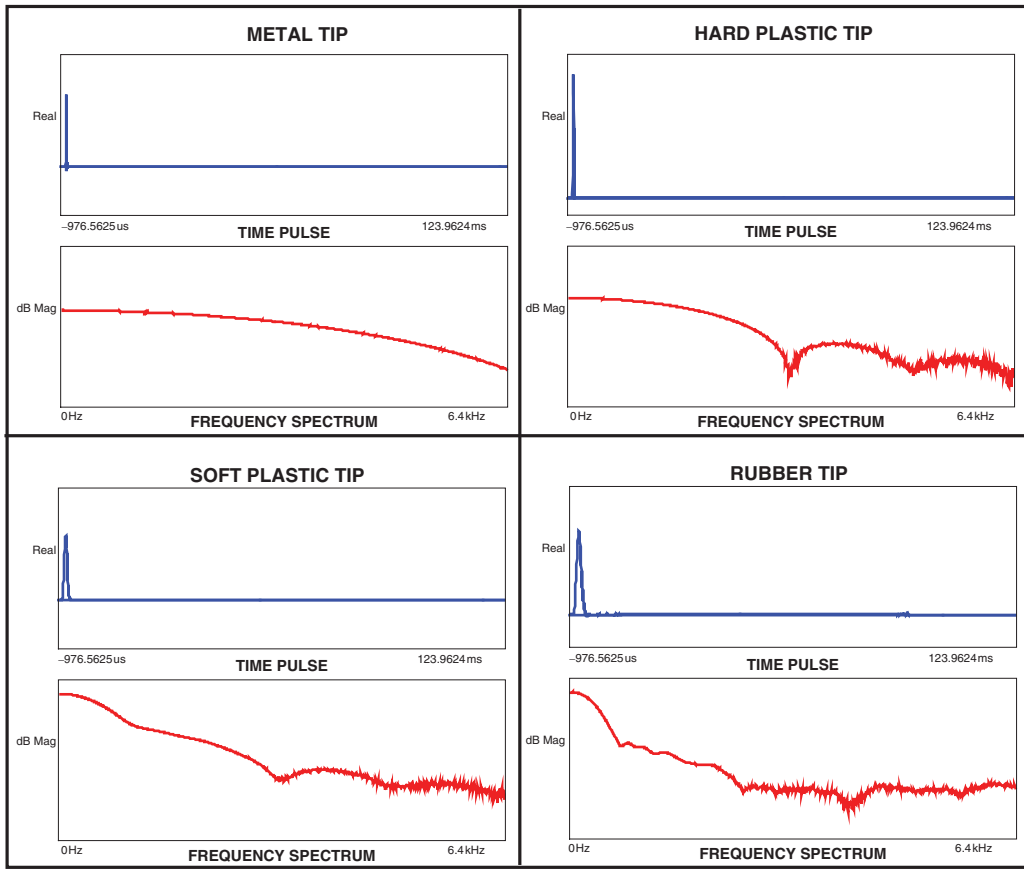

Figure 4.5 Input time pulse (blue) and resulting frequency spectrum (red) for a metal tip, hard plastic tip, soft plastic tip, and rubber tip.

frequency ranges of excitation are for a hammer impacting a massive steel block; those will not be the force spectra that will be observed when testing actual structures.

4.2.3 Useful Frequency Range for Impact Excitation

In order to better understand the useful frequency range from an impact excitation, a typical measurement can be used. Figure 4.6 shows a frequency response function from an impact measurement. In general, the measurement looks acceptable in the 400 Hz band but there appears to be variance above 400 Hz, which may be the result of noise or nonlinear behavior or a range of other possibilities.

But this measurement cannot be evaluated without looking at the coherence. Figure 4.7 shows this same measurement of the frequency response functions with the coherence overlaid for comparison. Now the coherence confirms that the measurement quality looks acceptable up to 400 Hz, but then degrades above 400 Hz.

But upon reviewing Figure 4.8, which shows the measurement with the frequency response functions and coherence along with the input force spectrum, it becomes very clear that the cause of the poor measurement above 400 Hz is most likely the fact that the impact excitation does not excite frequencies above 400 Hz. So the question is whether or not this is a good measurement. Over the full 800 Hz bandwidth, the frequency response function measurement is not good. But if only frequencies up to 400 Hz are of interest, then this is a good measurement. Looking at the input force spectrum, it is clear that the measurement and coherence are very good up to 350 Hz, even though the input force spectrum has rolled-off by approximately 30 dB. The actual measurement and all the important parts need to be examined in order to determine if the measurement is adequate or not. When impact testing, it is sometimes very difficult to pick a hammer tip that will excite exactly the frequency range of interest. So there needs to be some flexibility in the actual excitation frequency range and the measurement must be assessed.

Now Figure 4.9 shows another frequency response function and coherence, with the input force spectrum, which is the typical measurement that would be desired for all measurements. But, in reality, this is not a measurement that can typically be achieved in a real practical application; being able to have a force spectrum that excites the exact frequency range of interest usually is not possible. However, it is presented to show what an optimum condition may look like.

4.2.4 Force Window for Impact Excitation

Because there may be some unwanted noise on the impact channel, the use of a force window may be needed to minimize the effect. The use of a force window is shown in Figure 4.10. This window is typically implemented as a rectangular window that exists over a portion of the block or it may be a cosine wave taper on the input, depending on the particular implementation. The main use of the force window is to minimize the effect of spurious noise on the input channel. If an ICP force transducer is used, then the ICP signal conditioner essentially employs a high pass filter, removing any DC bias on the force signal. However, if this is not the case then some care needs to be exercised to ensure that the time sampled signal has no DC distortion of the impact signal.

4.2.5 Pre-trigger Delay

Another feature common to impact testing is the need for pre-trigger delay in acquiring frequency response measurements. Because the analyzer needs to measure some voltage in

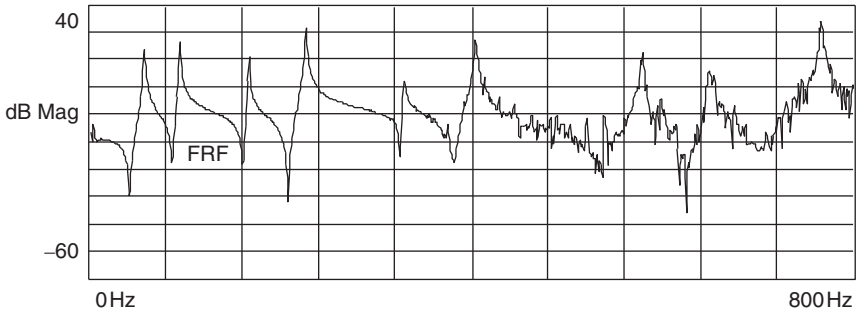

Figure 4.6 Typical FRF from an impact measurement.

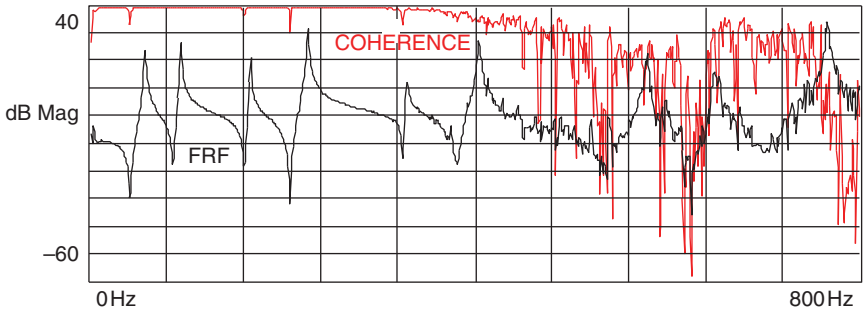

Figure 4.7 Typical FRF with coherence from an impact measurement.

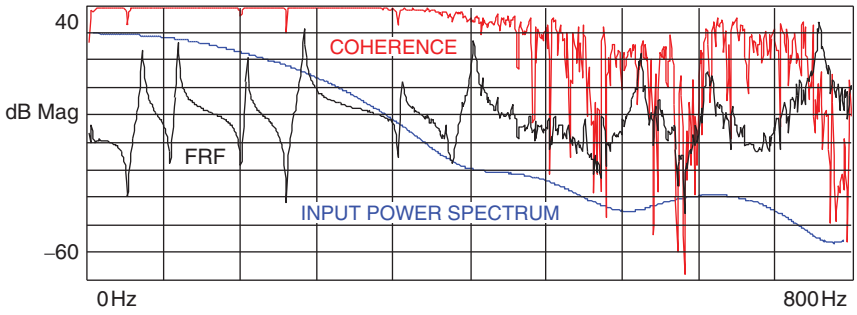

Figure 4.8 Typical FRF and coherence with the input force spectrum from an impact measurement.

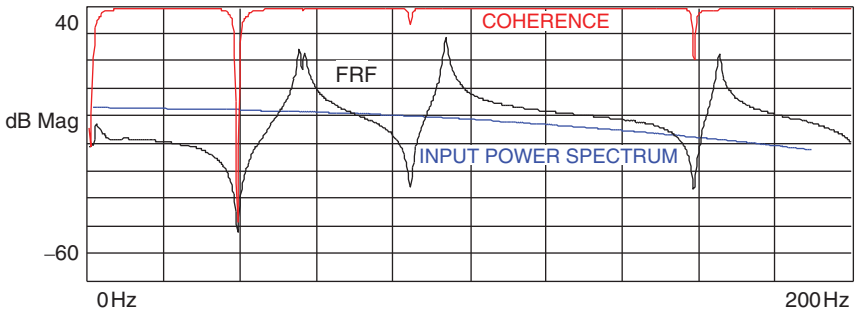

Figure 4.9 Ideal FRF and coherence with the input force spectrum from an impact measurement.

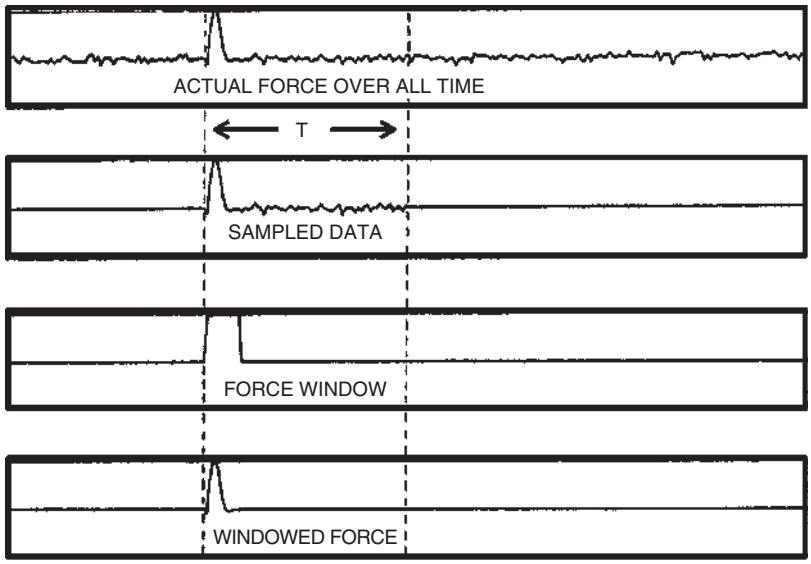

Figure 4.10 Sampled force with force window applied.

order to trigger the start of the acquisition, part of the impact measurement is lost if the zero time is set based on the trigger time, as depicted in Figure 4.11 in the upper left time pulse (red). In reality, the pulse that the system is exposed to can be significantly different, as depicted in the lower left time pulse (blue). The resulting force spectrum from these two different time pulses can be seen overlaid on the right of Figure 4.11. A much wider frequency range is shown than what would typically be used in the FFT; only the area near the main lobe is actually

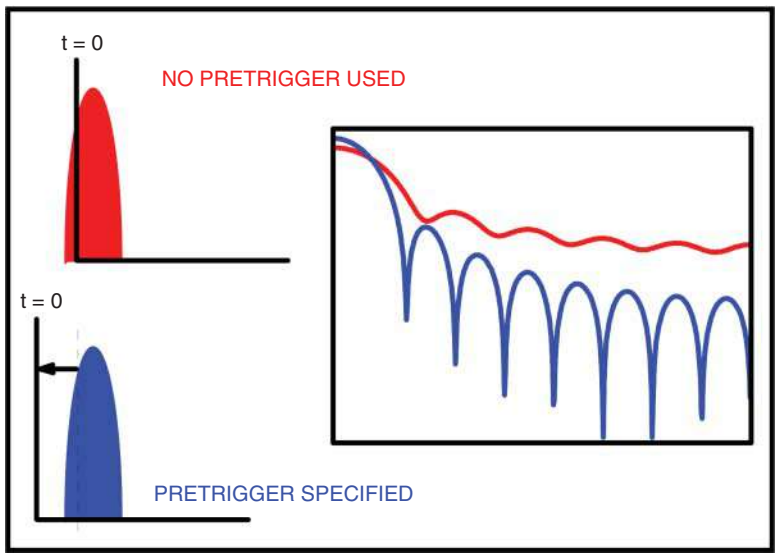

Figure 4.11 Comparison of force spectrum, with and without pre-trigger delay.

useful for the impact test. Over the frequency range of interest, the two input force spectra are not substantially different, but they do cause a different scaling of the frequency response functions computed. Most software packages and FFT analyzers incorporate pre-trigger delay to eliminate this problem. But it is important to note that the pre-trigger delay needs to be applied to all the response channels, otherwise a phase lag will exist in the measurement. However, care should be exercised to determine if the "pre" trigger is labelled as either a plus or a minus (which depends on the specific system used).

4.2.6 Double Impact

A common problem in impact testing is double impacts that often occur. Often the double impact occurs due to improper excitation using the hammer. Other times, however, the structure may be very lightly damped and extremely responsive in certain locations. In these cases, the structure is excited with the impulsive excitation and the structure responds and impacts the impact hammer before the hammer can be moved away from the structure. While double impacts are undesirable and should be avoided, there are situations where double impacts cannot be prevented. This is only a serious situation when the resulting input force spectrum is distorted as a result of the double impact causing serious dropout of the force spectrum. However, in no case should a force window be used to window out the effects of the double impact. The double impact is truly the input that is seen by the structure, and the response of the system is due to all of the impacts that occur during the time sample. Figure 4.12 shows two different double impact measurements. The tell-tale sign of the double impact can usually be seen best in the force spectrum measurement. Generally, a single impulsive force will generate a smooth force spectrum, as shown in Figure 4.5. The resulting force spectrum, in both cases in Figure 4.12, shows some variation over the frequency range; this is a direct result of the double impact in the time domain signal. Double impacts can be difficult, but in some situations they are unavoidable. Later, some measurements will be shown in which double and multiple impacts are intentionally applied on the structure, and useful frequency response functions and mode shapes can still be extracted.

4.2.7 Response due to Impact

The response of the system due to the impact excitation will be the result of the damped exponential response of all of the modes that are activated by the input. For lightly damped structures, the response of the structure often does not die out by the end of the sample interval and thus the signal is not totally observable within one sample interval, as shown in Figure 4.13 for a single degree of freedom system. In this case, leakage will be a serious concern and an exponential window may potentially be required, as shown in Figure 4.13. The use of the exponential window will minimize the effects of leakage, but it brings its own distortion of the signal. Two options to circumvent the need for the use of the window would be to lengthen the time block (by narrowing the bandwidth) or increasing the number of time samples to acquire data; both of these steps will have the effect of making the signal more observable within one sample of data and should be considered before an exponential window is used. This is shown in Figure 4.14, where the time trace in the lower portion of the figure (blue) requires the use of an exponential window, whereas the signal in the upper portion of the figure (red) has a longer time record, either due to a change in the bandwidth or an increase in the number of spectral lines, thereby making the time record longer and minimizing the need for the exponential window to be applied. In extremely lightly damped structures, however, this is not always possible or practical and the use of the exponential window cannot be avoided. The

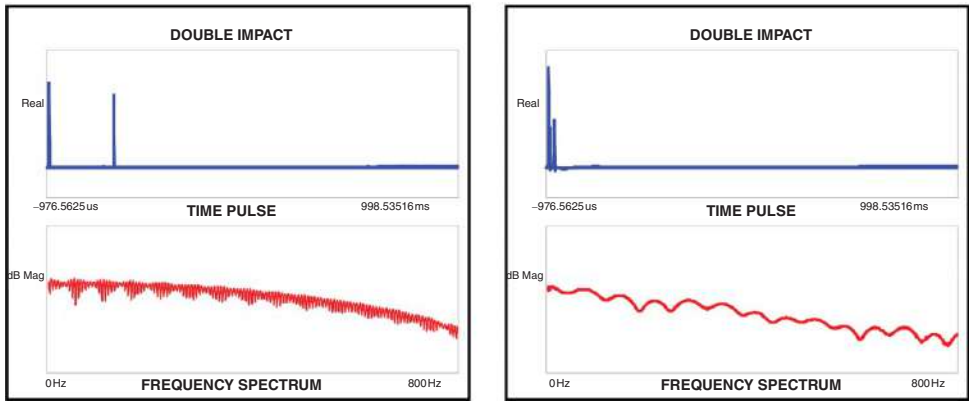

Figure 4.12 Two different double impact time pulses and corresponding frequency spectra.

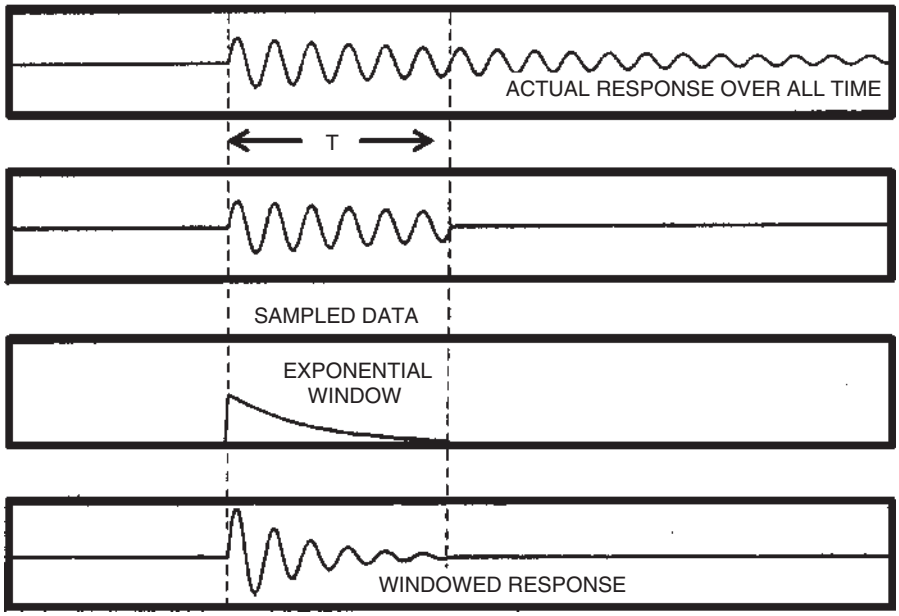

Figure 4.13 Time response due to an impact excitation requiring an exponential window.

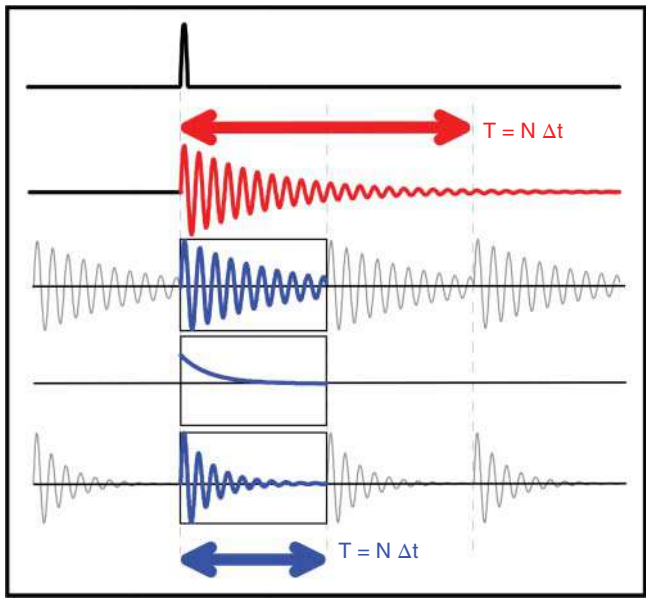

Figure 4.14 Time response due to an impact excitation with two time response blocks: one requiring an exponential window and one not requiring an exponential window.

use of the exponential window can at times mask the presence of closely spaced modes and should be used cautiously.

4.2.8 Roving Hammer vs Stationary Hammer and Reciprocity

The impact test can generally be conducted two different ways. One way is with the hammer roving to all the points to be measured and a stationary accelerometer (or set of accelerometers). The other way is with the hammer stationary at one point, with accelerometers mounted on the structure (or with a set of accelerometers that rove across the structure) to measure all the points. The roving hammer approach will measure one row of the frequency response matrix, whereas the stationary hammer will measure one column of the frequency response matrix. From a theoretical standpoint, there is really no difference between these two tests because reciprocity is true. Figure 4.15 shows the reciprocal frequency response functions that would be measured from each approach.

In the example above, only one row or one column of the frequency response matrix was identified. Now let's consider extensions of each of these cases, in which multiple reference data is collected. This is advantageous because multiple reference data can be used to extract frequencies and mode shapes using redundant information contained in the frequency response matrix.

Figure 4.16 shows a frame structure with three separate components attached to the frame, and with each component mounted with isolator mounts. This is typical of many practical applications, in which components are connected together to form a system. The isolation mounts make it very difficult to excite the structure from only one location and to be able to measure responses for all the modes that may be of interest from each of the components. So, in Figure 4.16, there are three separate accelerometers mounted on each of the three separate components. A roving impact hammer approach is used to measure all of the points specified for the modal test. As each point is impacted, there are three separate frequency response functions that are measured; each represents one measurement in each of the rows of the frequency response matrix, as shown in Figure 4.16 in blue, red and green. As the hammer roves to each separate point, a new set of three separate frequency response functions is measured in each of the three separate rows. Each of the rows represents one reference location associated

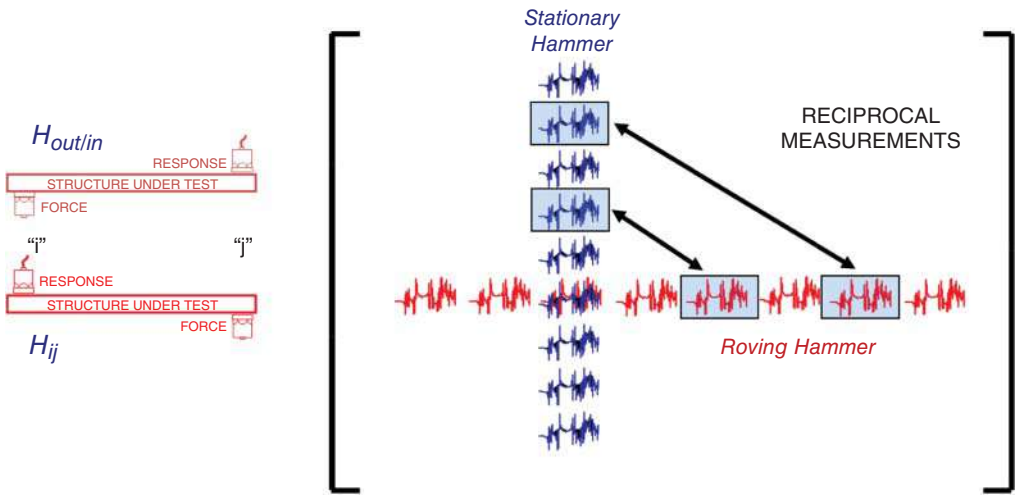

Figure 4.15 Frequency response matrix data collected for a roving hammer (row, red) and a stationary hammer (column, blue) shown with reciprocal FRF measurements schematically depicted.

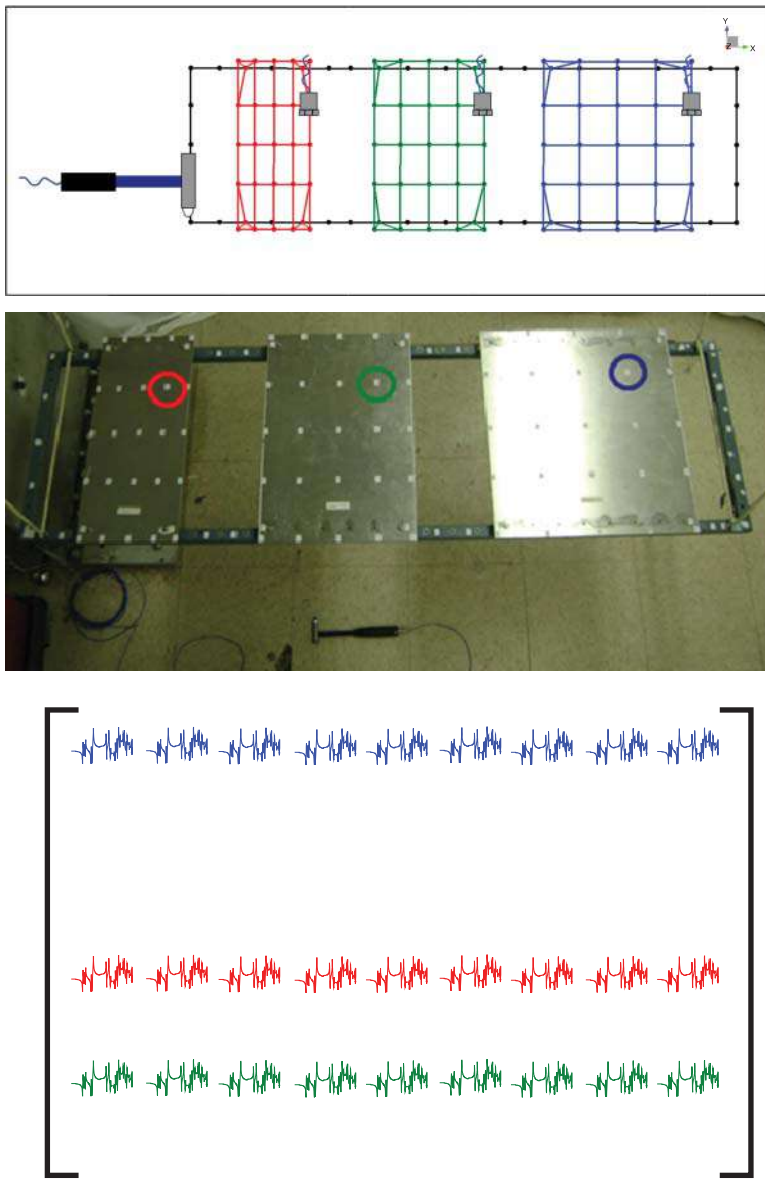

Figure 4.16 Roving hammer modal test with three separate accelerometer reference locations.

with the fixed accelerometer location. Once all measurement points are acquired, then there will be three separate, complete rows of the frequency response matrix available. This test technique is commonly referred to as the multiple reference impact technique (MRIT). The rows can be used separately or together to identify the frequencies and mode shapes. The collection of redundant data is extremely useful; further discussion is contained in the modal parameter estimation discussions.

Now in the second case, all the accelerometers are mounted on the structure, on all of the components, for all the measurement points. Figure 4.17 shows this test setup. The advantage here is that operating data is often collected with all of the accelerometers mounted on the

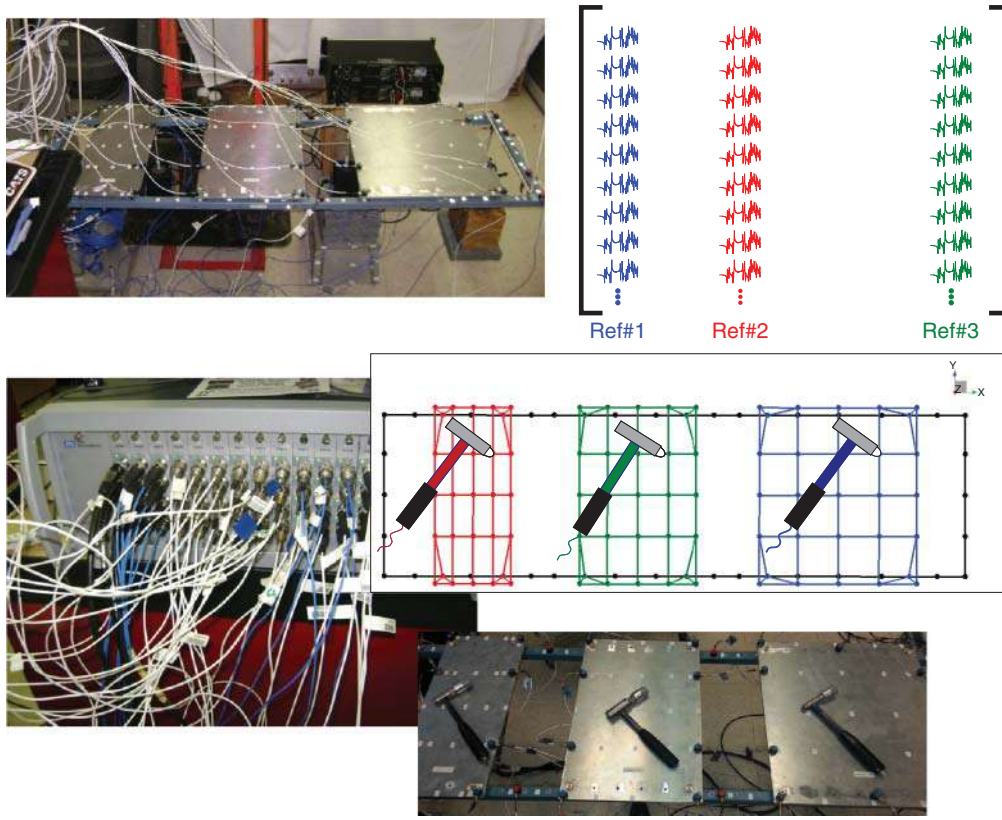

Figure 4.17 Three separate hammer input reference locations with all accelerometers fixed.

structure for that operating test. When this is the case, the experimental modal test will result in one complete column of the frequency response matrix when one point is impacted, such as when the hammer impacts on any one of the components shown in Figure 4.17. When more than one hammer location measurement is made, then additional columns of the frequency response matrix are measured. This then provides multiple reference data similar to what was just described above. Of course, there is a lot more setup involved in this second case, and a need for a large number of acquisition channels as well as a large number of accelerometers. But the time to collect all of the data is much shorter, and inconsistencies are less likely to occur than in the previous configuration with the roving hammer, which required a longer time to collect the data. The second approach is preferred because consistency of the data is more likely to occur and the modal parameter estimation process will be more straightforward.

One additional item that should be mentioned is that when all the transducers are mounted on the structure, the data can easily be streamed to disk and then processed afterwards with different signal processing parameters to find the best set of measurements possible. This is shown in Figure 4.18 for a large 8m optical telescope that was tested with over 100 accelerometers mounted on the structure. Each impact location yielded a separate column of the frequency response matrix. Figure 4.18 shows only three of the 100 accelerometer locations, along with the impact force. Twenty-five separate impacts were acquired and then later processed to give 25 measurement averages for each of the 100 accelerometer locations and for each of the separate hammer impact locations.

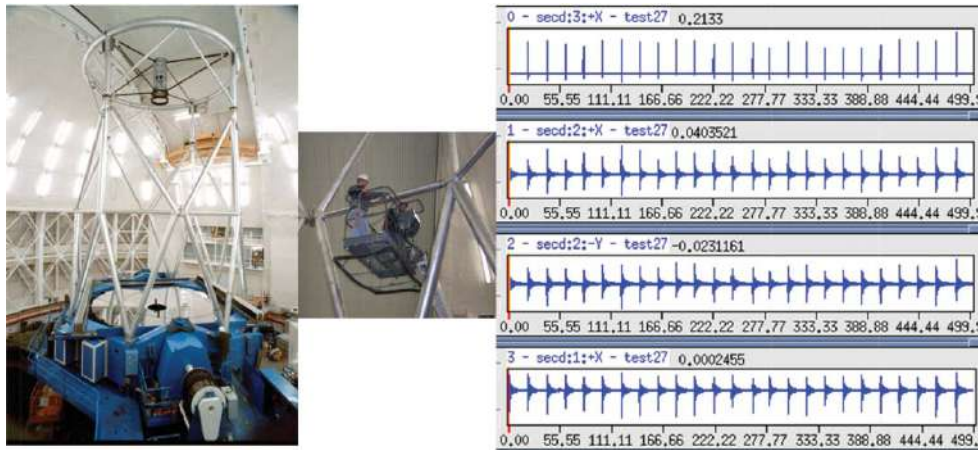

Figure 4.18 Optical telescope modal test with 100 accelerometers and multiple impact locations, showing time streamed data collection for three accelerometers and 25 samples acquired.

4.2.9 Impact Testing: an Example Set of Measurements

Now let's look at taking some measurements on a simple structure, the effects of different analyzer settings, and their effect on the resulting frequency response functions. An investigation of frequency bandwidth, lines of resolution, and the use of different impact tips will be made. Note that some of the frequency response functions were obtained by using HPGL output files for presentation and unfortunately suffer from some screen resolution problems but nonetheless exhibit some very important features. The test structure is a rectangular frame that has been used on numerous occasions over the past few decades. The structure and FFT analyzer with impact hammers is shown in Figure 4.19 for reference.

Now let's impact using the soft plastic tip first. Figure 4.20 shows an 800 Hz BW with 400 spectral lines. Notice that the input is fairly sharp and that there is quite a bit of time response that does not decay by the end of the block. Clearly if no window is used then there will be leakage in this measurement.

Now leakage can be seen in the measurement, but notice that at higher frequencies the measurement does not look particularly good either. This is because the input force spectrum drops off quite substantially, by 400 Hz. This is due to the fact that the impact tip used does not excite this frequency range very well at all. Either a harder tip or a different frequency range must be used.

Now still using the soft plastic tip, a 200 Hz BW with 800 spectral lines is used and is shown in Figure 4.21. Notice that the input is fairly sharp and that there is quite a bit of time response. But notice that the time response tends to decay much closer to zero than in the previous case. This is because that time record is much longer than the previous case so that the time response has more time to naturally decay to zero but the signal does not decay enough to eliminate the leakage problem. Now leakage can be seen in the measurement as a distortion of the frequency response function in the region at the base of the peaks of the frequency response function. It may not be clear just yet what a good frequency response function should look like so let's look at a few more parameters to change.

Figure 4.19 Typical impact measurement setup for blue frame structure.

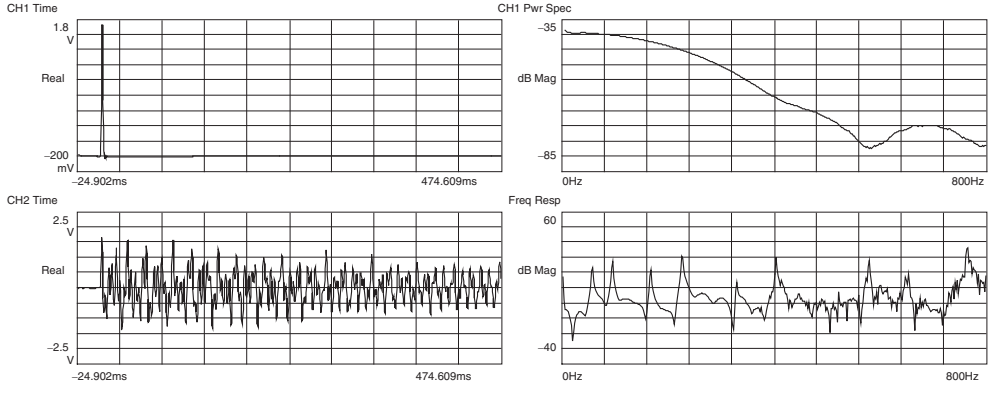

Figure 4.20 Measurements for 800 Hz with 400 spectral lines impact force (top left); input force spectrum (top right) time response (bottom left); FRF (bottom right).

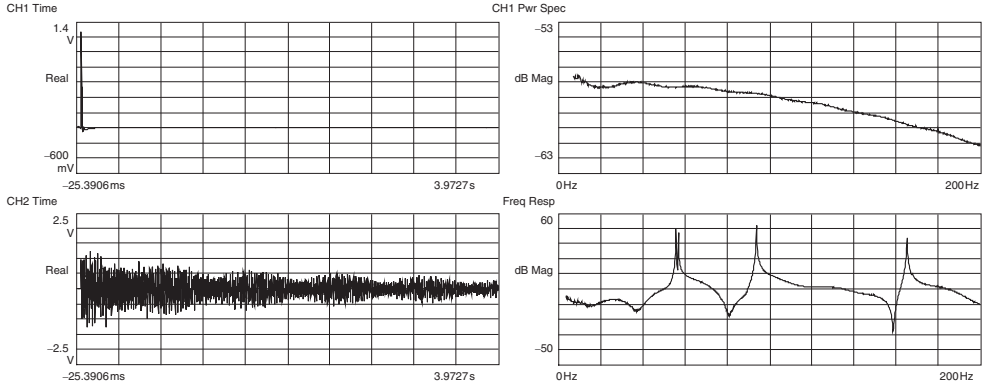

Figure 4.21 Measurements for 200 Hz with 800 spectral lines: impact force (top left); input force spectrum (top right); time response (bottom left); FRF (bottom right).

Now still using the soft plastic tip, a 400 Hz BW with 400 spectral lines is used, and with a damping window on the time data. This is shown in Figure 4.22. Notice that the input is fairly sharp and that the response seems to die out by the end of the time block. Because a damping window is applied to the data, the unwindowed data is not seen. For now, let's just note that the signal appears to be totally observable within one sample interval of the analyzer.

Now this measurement looks fairly good. Notice that the input power spectrum is fairly flat, but does have some roll off by the end of the frequency block. The frequency response function also has some distortion at the end of the frequency block. Take a close look at the last measurement and notice that there appear to be two closely spaced modes at that first frequency, but these are not seen in this measurement. Let's look at this a little closer.

Now still using the soft plastic tip and using a 400 Hz BW with 800 spectral lines along with a damping window on the time data, the measurement is shown in Figure 4.23. Now see both the unwindowed time data and the windowed data to see what's going on. Notice that the time signal appears to be totally observable within one sample interval of the analyzer now.

Now this measurement looks fairly good. Notice that the input power spectrum is fairly flat but does have approximately 20 dB of roll off by the end of the frequency block. The frequency response function also has some distortion at the end of the frequency block. Notice that there are two peaks at that first frequency now. That's because more lines of resolution were used, which enabled the use of less damping window. In the last measurement, a fairly heavy damping window was applied, so the two peaks were smeared together in what looked like one peak when in fact there were two peaks. This is a very important concern when impact testing and using the damping window.

Now just to confirm what is happening, let's put on a very heavy damping window to see the effect (Figure 4.24). The soft plastic tip is still used, but now with a 400 Hz BW with 400 spectral lines, again along with a damping window on the time data. Again, both the unwindowed time data and the windowed data are shown to show what's going on. Notice that the time signal appears to be totally observable within one sample interval of the analyzer, but the damping applied to the signal is quite significant.

Now this measurement looks fairly good. Notice that the input power spectrum is fairly flat but does have some roll off by the end of the frequency block. But those two closely spaced peaks at that first frequency are not seen. So that means that too much damping applied may mask some of the modes of the system. So what should be done here when testing using impact? Generally, try to add as little damping to the measurement as possible; this can be accomplished by adding more spectral lines or by changing the bandwidth. Let's do both of these next.

Now the soft plastic tip is still used (the tip has not been changed up to this point). Now let's use a 100 Hz BW with 800 spectral lines along with a very light damping window on the time data. This is shown in Figure 4.25. Now look at both the unwindowed time data and the windowed data to see what's going on. Notice that the time signal appears to be totally observable within one sample interval of the analyzer, but a little bit of damping window needs to be added to the response signal.

Now the frequency response function looks very good. Notice that there are two closely spaced modes in the 50 Hz range. If inappropriate analyzer settings are used then these closely spaced modes could be missed; attention to carefully reviewing the data and using appropriate measurement settings is critical to clearly see those two modes. Care needs to be exercised when taking these measurements.

Now that the measurement process is understood, let's look at some different tips on the impact hammer.

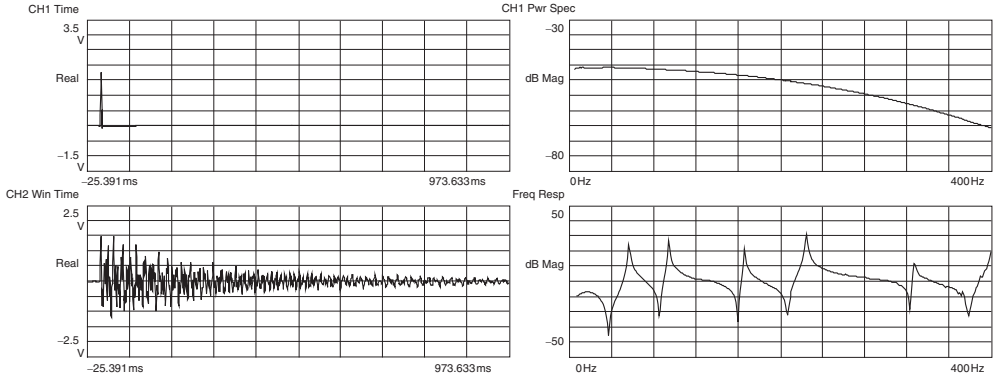

Figure 4.22 Measurements for 400 Hz with 400 spectral lines: impact force (top left); input force spectrum (top right); time response (bottom left); FRF (bottom right).

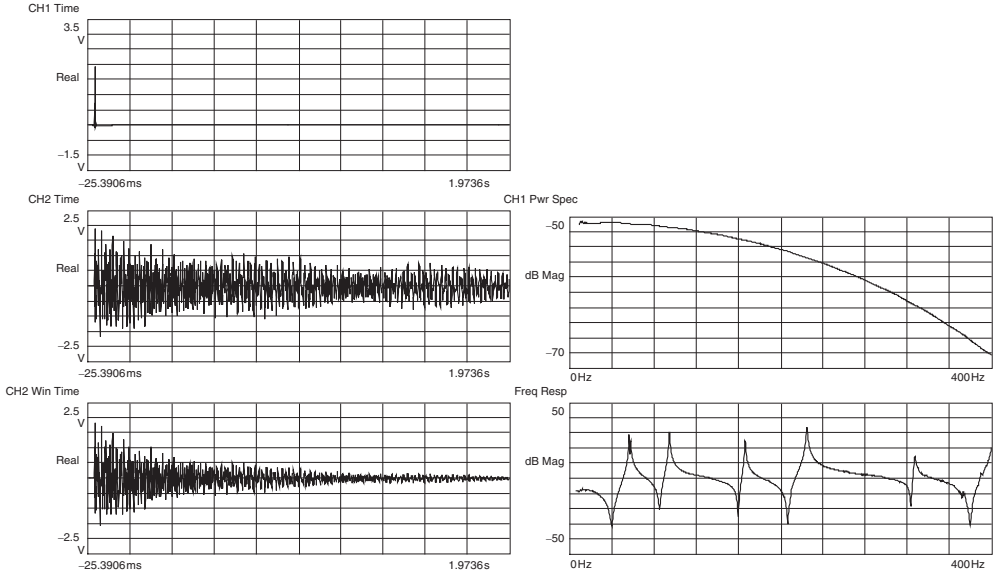

Figure 4.23 Measurements for 400 Hz with 800 spectral lines with damping window: impact force (top left); input force spectrum (top right); raw time response (middle left); windowed time response (bottom left); FRF (bottom right).

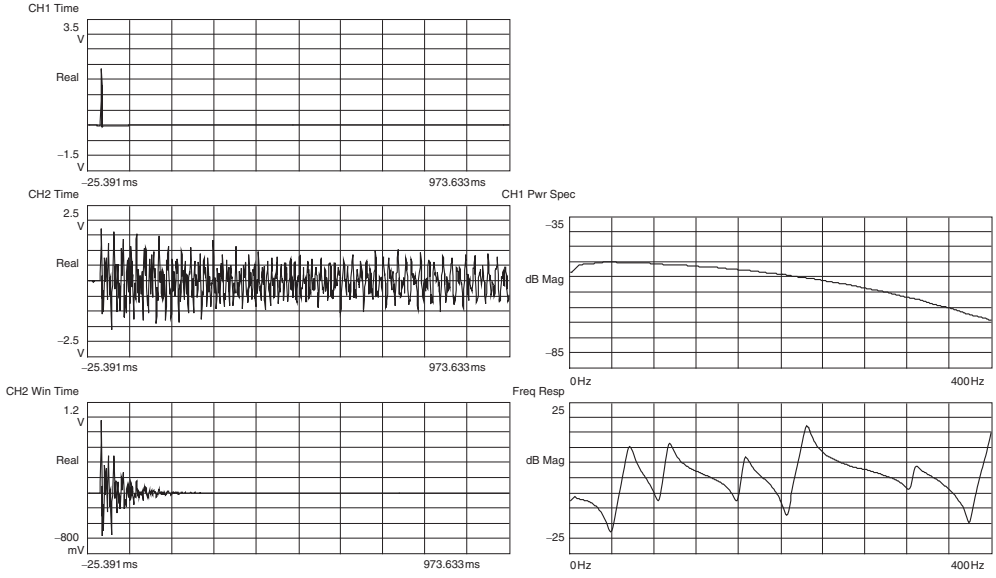

Figure 4.24 Measurements for 400 Hz with 400 spectral lines with heavy damping window: impact force (top left); input force spectrum (top right); raw time response (middle left); windowed time response (bottom left); FRF (bottom right).

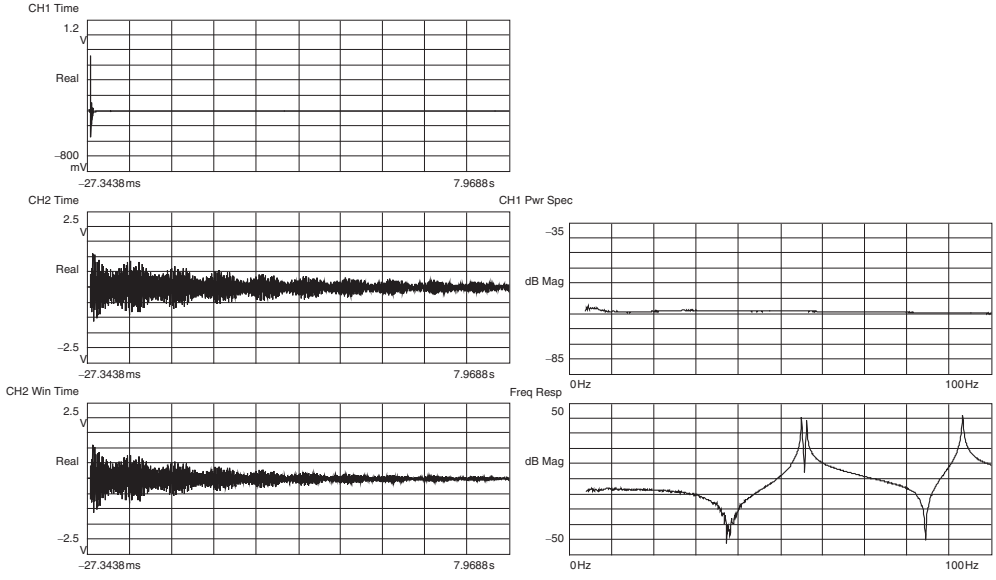

Figure 4.25 Measurements for 100 Hz with 800 spectral lines with very light damping window: impact force (top left); input force spectrum (top right); raw time response (middle left); windowed time response (bottom left); FRF (bottom right).

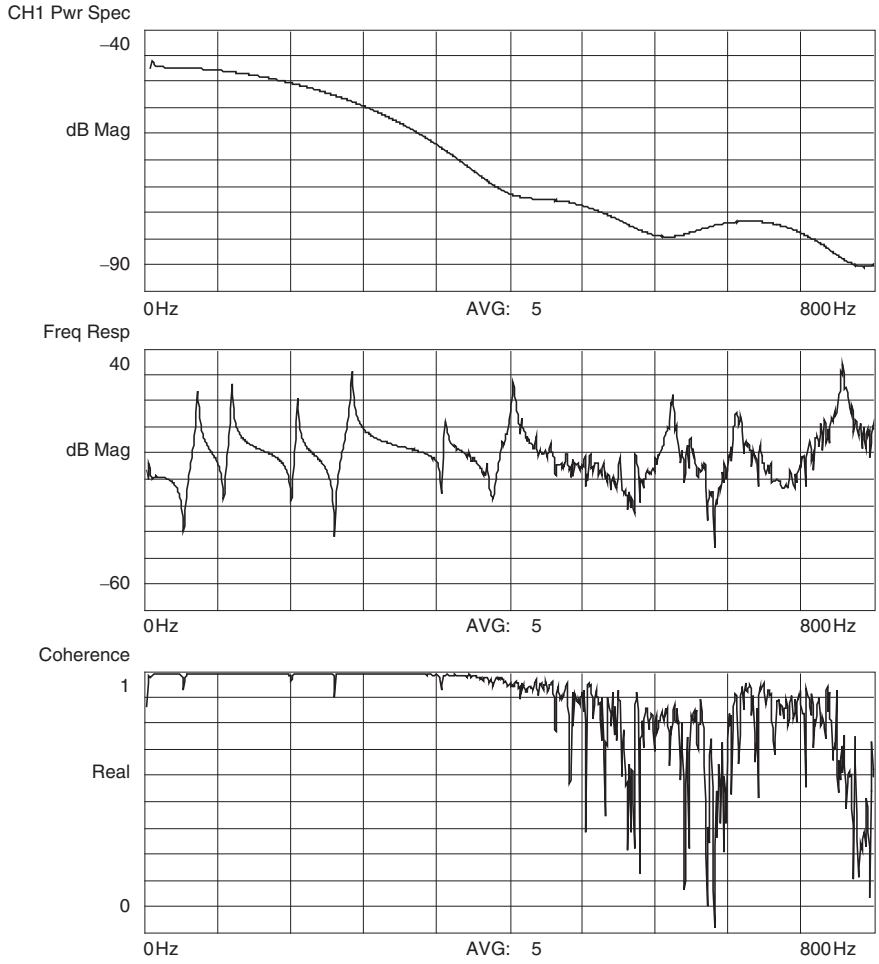

Figure 4.26 Measurements for 800 Hz with 800 spectral lines: input force spectrum (top); FRF (middle); coherence (bottom).

Now let's try using a soft eraser tip with an 800 Hz BW and 800 spectral lines, as shown in Figure 4.26. Only the input power spectrum, frequency response function, and coherence will be reviewed. Notice that the input force spectrum rolls off quite rapidly and that there is insignificant energy halfway through the frequency range. The frequency response function also looks poor for the higher frequencies and, looking at the coherence function, it is very obvious that the measurement is inadequate in the second half of the frequency block.

Now let's try using a hard metal tip with a 200 Hz BW and 800 spectral lines, as shown in Figure 4.27. Only the input power spectrum, frequency response function, and coherence are shown. Now because a hard tip is used, a very flat input spectrum is expected. But the frequency response functions and coherence don't seem to look as good as expected when compared to other good measurements. Well the input certainly is flat; so flat that it excites many modes well outside the frequency range of interest. Certainly, the accelerometer measures that response and the ADC settings must be setup for the total energy that the accelerometer sees, even though only the energy associated with the lower frequencies is of interest. This measurement suffers from quantization error. Always pick the hammer tip to excite just the right frequency

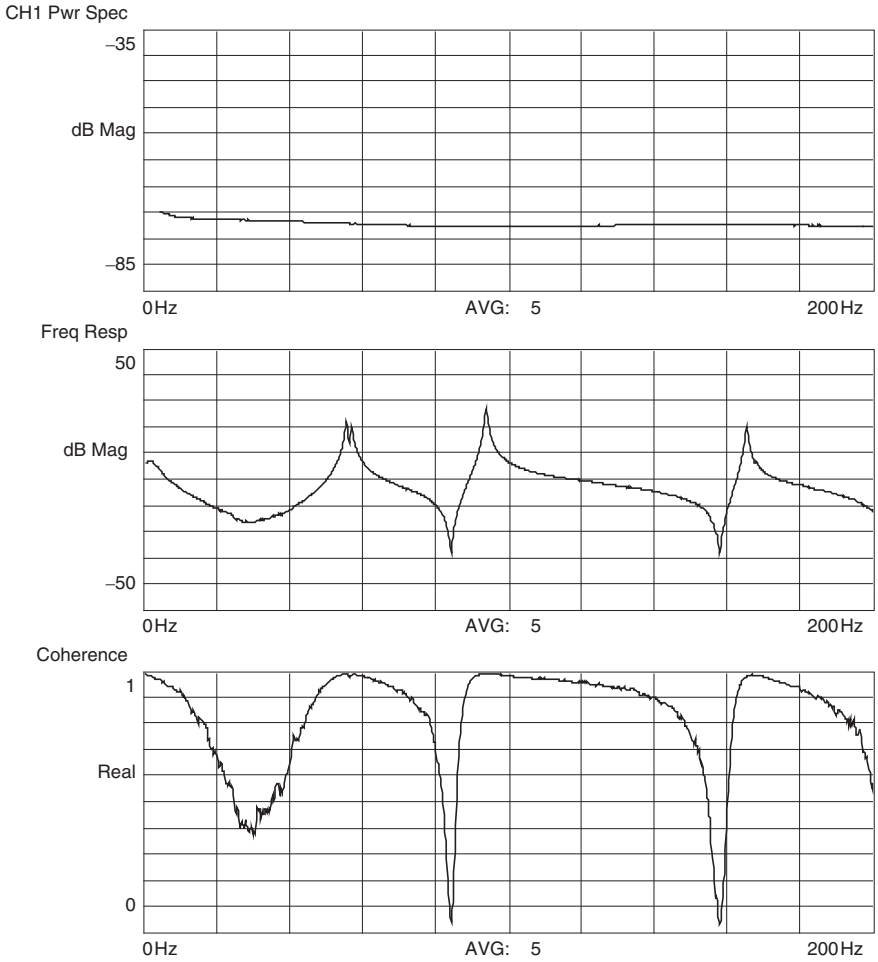

Figure 4.27 Measurements for 200 Hz with 800 spectral lines with metal tip: input force spectrum (top); FRF (middle); coherence (bottom).

range. Basically, there is balancing act that needs to be performed here: large hammer roll off and lack of exciting modes vs small hammer roll off and exciting modes that are not of interest.

Now let's try using that soft tip again, with a 200 Hz BW and 800 spectral lines, as shown in Figure 4.28. Only the input power spectrum, frequency response function, and coherence are shown. Now there is slightly less than 10 dB roll off in the input force spectrum for this condition. This is probably acceptable. The frequency response function is very good and the closely spaced mode can been seen. The coherence function also looks very good; it is close to unity at all frequencies except some minor dropouts at the antiresonances, which is expected and tolerable. This seems to be an acceptable measurement.

Now go back and look at all the steps just covered to get to this point and all the things done to get to this measured data. This is a typical measurement sequence that is used all the time when making impact measurement to make sure nothing is missed. And just to re-cap what was observed, Figure 4.29 shows the three most critical pieces in the entire measurement process covered above. The three panels show the measurement with slightly too much damping on the left, definitely too much damping in the middle, and a good measurement on the right.

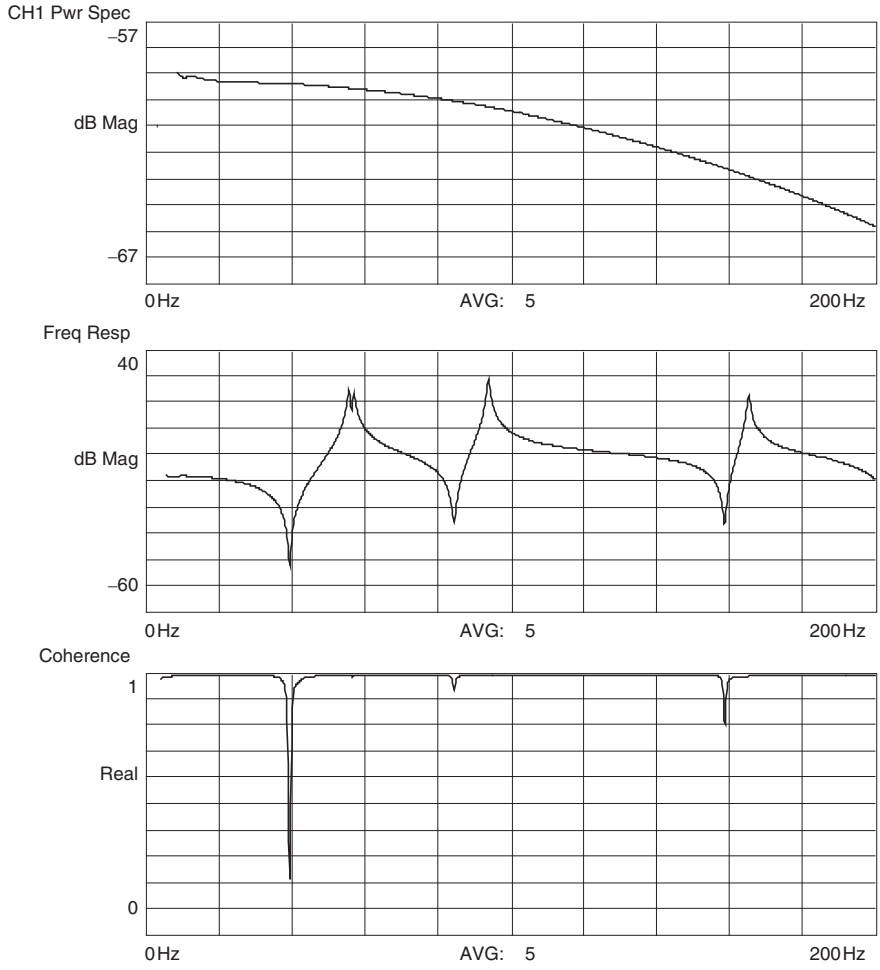

Figure 4.28 Measurements for 200 Hz with 800 spectral lines with very soft tip: input force spectrum (top); FRF (middle); and coherence (bottom).

Increased time and frequency resolution allows all the modes to be seen without distortion; the top trace is the impact time force, the middle trace is the time response, and the bottom trace is the frequency response function. All the measurements were made over the same bandwidth but with different damping windows applied to all three measurements to show the effect of the damping window, which may mask some of the modes in the measurement. This is critical. Generally, try to always take a measurement without any damping window at all, even when a damping window will ultimately be necessary. With no damping window applied there will be leakage, but at least there is a better chance that all the modes will be observed. Many FFT analyzers and software packages have default parameters set when the force/exponential window is specified for a measurement. This is very bad because a novice may not think or realize that the damping window may hide some critical information. The first measurement should always be taken with no window applied. This will enable a good view of the modes in the data. After that first measurement, the window can be applied but with an understanding of how many modes are expected to be in the measurement. If the first measurement were the left panel in Figure 4.29 (which is also Figure 4.22) then the user may perceive it to be a good measurement,

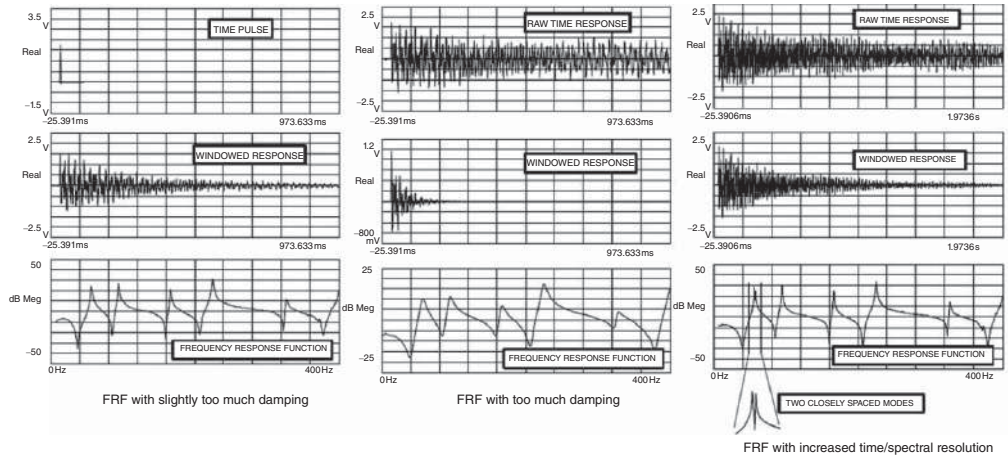

Figure 4.29 Impact time force (upper traces), time response (middle traces) and FRF (bottom traces) for a measurement with slightly too much damping window applied (left), definitely too much damping window applied (middle) and improved resolution with little damping window applied (right).

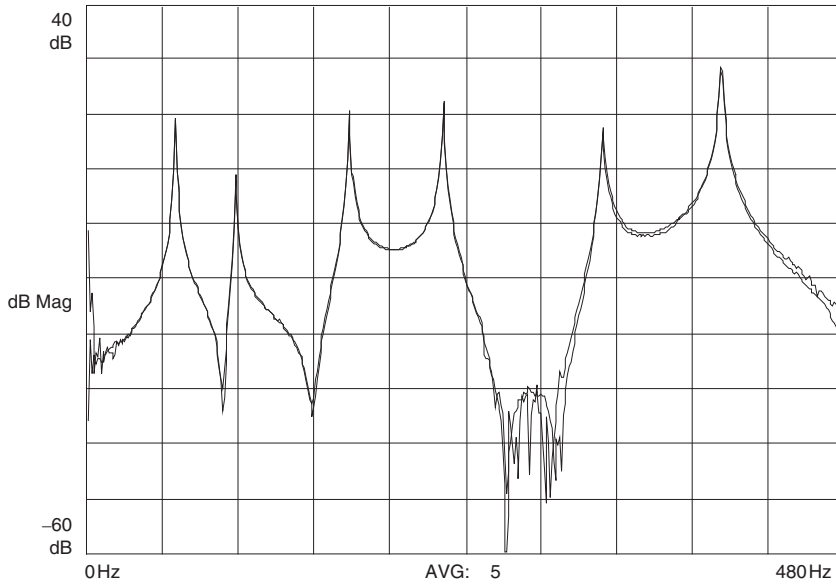

Figure 4.30 Reciprocity measurement.

with good frequency response and good coherence. However, they might not realize that there were two modes at that first peak. This also would get confusing later during parameter estimation, when the stability diagram might be hard to interpret: issues of mass loading and time variance and nonlinearities might all be identified from the poor stability diagram information, when in fact there might really be two modes in the structure at what appeared to be just one peak. While the exponential window may ultimately be required, never apply it before an unwindowed measurement is made, so as to make sure the window is actually needed.

One last thing to check is the reciprocity of the system. The measurement in Figure 4.30 shows this check. This is a fairly good measurement, with only a small variation in the antiresonant regions, which is tolerable.

4.3 Shaker Excitation

Shaker testing that is used for equipment qualification is very different to shaker testing, as it is used for experimental modal testing. This needs to be discussed. With conventional vibration testing, a test article is normally hard mounted to the top surface of the shaker armature and then some base excitation is applied, usually monitored by controlling some prescribed acceleration. The device under test (DUT) is normally subject to some operating environment, generic spectrum, or some excessive environment to determine if the equipment is suitable for the intended service. Traditional shaker testing is widely used to expose a structure, test article, or device under test to high level forces and loads to determine the suitability of equipment for specific operating environments. Figure 4.31 shows a typical shaker configuration that is often encountered.

In the early days of modal testing with shaker excitation, smaller shakers were used to apply some low level excitation, so as to be able to measure a frequency response function. Usually the shaker was attached to the structure with a long rod, commonly referred to as a stinger or

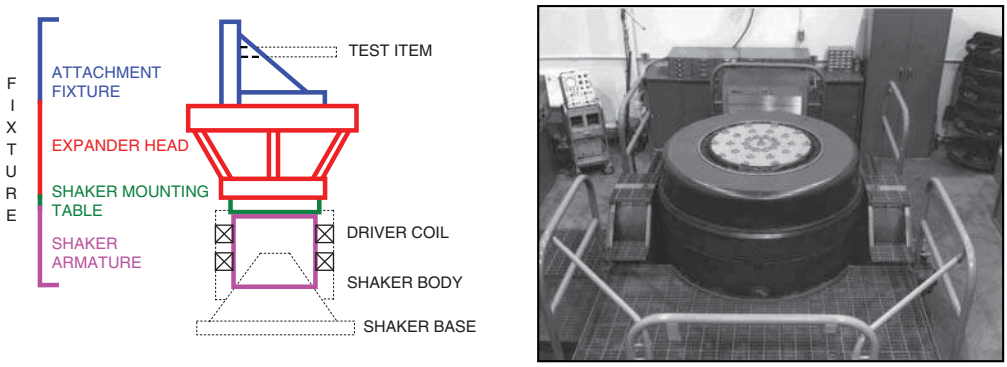

Figure 4.31 Typical shaker configuration used for vibration qualification testing.

quill, in order to impart force to the structure. The purpose of the quill was to try to dynamically decouple the shaker from the structure.

Because these shakers were traditionally used for base excitation, the armature attachment configuration was not optimal. Usually, some type of left–right thread arrangement was made or some type of collar was designed to enable an easier attachment to the shaker. It was really a very difficult arrangement, no matter how the connection was made. In addition, there had to be some thought given to what actual length of quill was needed. If a different length quill was needed, then the shaker needed to be reoriented and realigned, as different quill lengths were used for the modal test. Overall, the setup of the shaker for a modal test was very difficult and cumbersome.

Due to all these problems, some thought was given to specific design configurations that were better suited for modal testing. This gave rise to the through-hole armature, with a collet design (as on a hand drill) that enabled very easy attachment of the shaker to the modal test article. This design also allows for very easy adjustment of quill length if needed. The arrangement is so simple that it is difficult to imagine having to set up a test without it.

For experimental modal testing, the shaker is used in a very different way. The excitations are generally at a much lower level than that needed to characterize the structure. A typical modal shaker test setup configuration is shown in Figure 4.32. The signal is generated, usually from the data acquisition system, and fed into the shaker amplifier. The head of the shaker is attached using a stinger (or quill), which is attached to a force sensor (or impedance head), which is attached to the structure at the excitation location. The actual signals will be discussed separately after some discussion of the shaker's physical attachment to the structure.

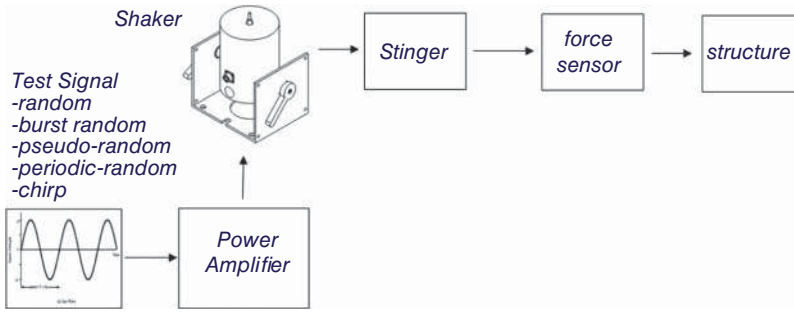

Figure 4.32 Typical modal shaker system configuration.

4.3.1 Modal Shaker Setup

Before the actual excitation techniques are discussed, let's describe a typical shaker test setup, as shown in Figure 4.33. A force shaker is usually attached to the structure through a long rod called a stinger or quill. This stinger is intended to transmit force only in the direction of thrust of the actuator and impose as little stiffness effect as possible in the other directions; the quill

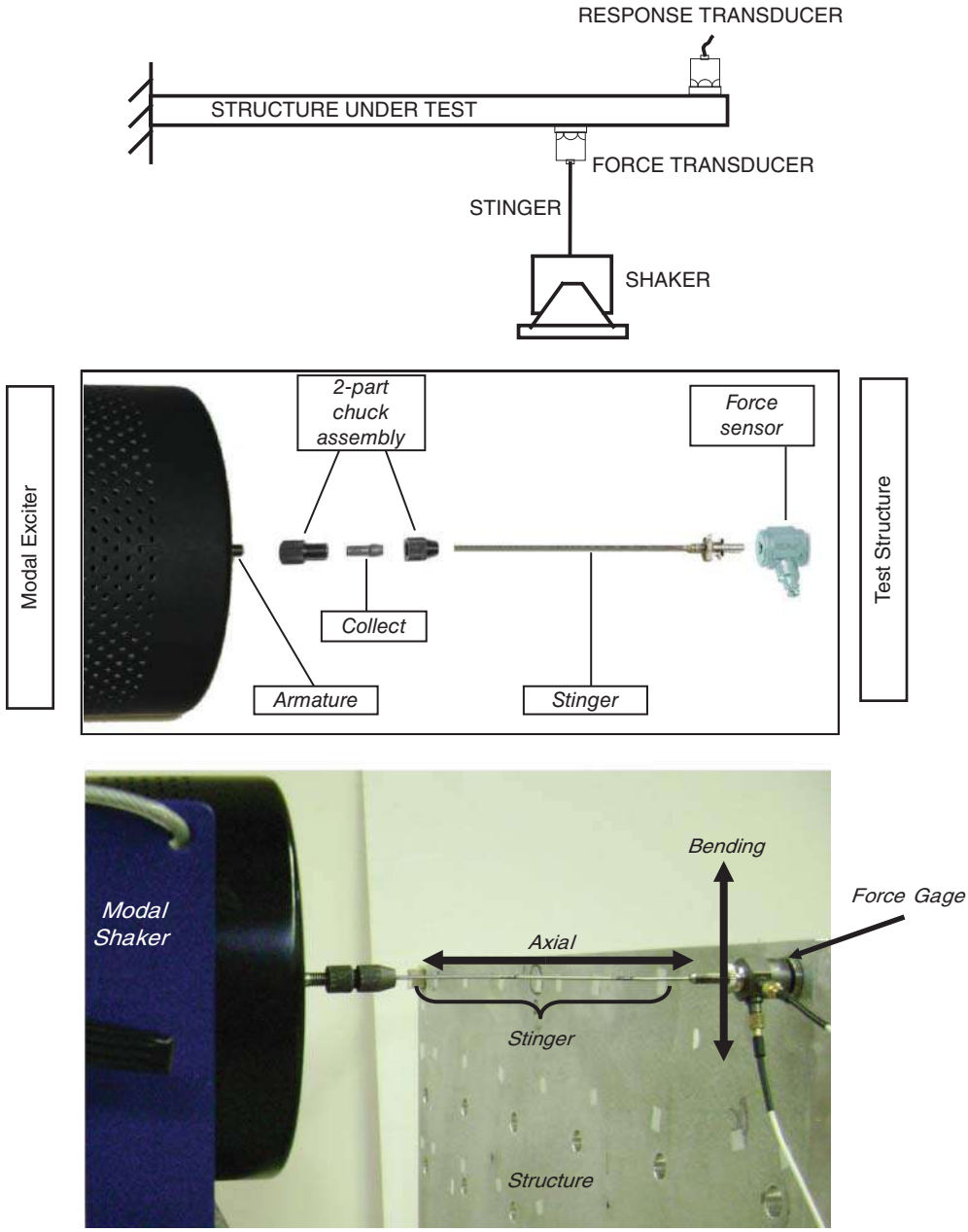

Figure 4.33 Typical shaker setup schematic (top) with pieces of the modal shaker/stinger (middle) and an actual shaker (bottom) attached to a test structure in the lab. *Source:* Image courtesy of PCB Piezotronics, Inc.

acts as a mechanical fuse. A force transducer is mounted on the structure side of the quill to measure the force imparted into the system. A response accelerometer is mounted at one or several locations on the structure to measure the frequency response function. The excitation signal is fed to the shaker system (shaker and amplifier) through the data acquisition system.

The stinger acts as a mechanism to impart force only along the length of the rod and is very flexible in shear or bending. This is necessary because the force transducer only measures force in tension or compression and does not measure (nor is it intended to measure) the bending moment that may be imparted to the structure. The alignment of the force shaker and stinger to the structure is very important; any skew or misalignment will distort the force applied to the structure. Care must be exercised to ensure that this alignment is as accurate as possible.

There are many different stingers that are employed, ranging from piano wire to thin drill rods to thin metal rods to threaded plastic or metal rods, as shown in Figure 4.34. Generally, the smaller stingers are used on smaller, more flexible structures, whereas bigger and stiffer stingers are used on larger structures.

4.3.2 Historical Development of Shaker Excitation Techniques

Rather than describe each of the excitation techniques by its category – deterministic vs. random – a clearer perspective can be obtained if each of the different excitation techniques is presented in chronological order of development. But in general each of the excitation techniques will fall into a category of either deterministic or non-deterministic (random) excitation. In general, deterministic signals are very good for determining if the system is linear or has slight (or significant) nonlinear behavior. Non-deterministic signals, on the other hand, tend to be very good for smoothing some of the variance and noise that may be seen on a system. Both have their place in modal testing, as will be seen in the following discussions on each of the different signals typically employed for experimental modal testing. Figure 4.35 shows a general categorization of each of the two general categories.

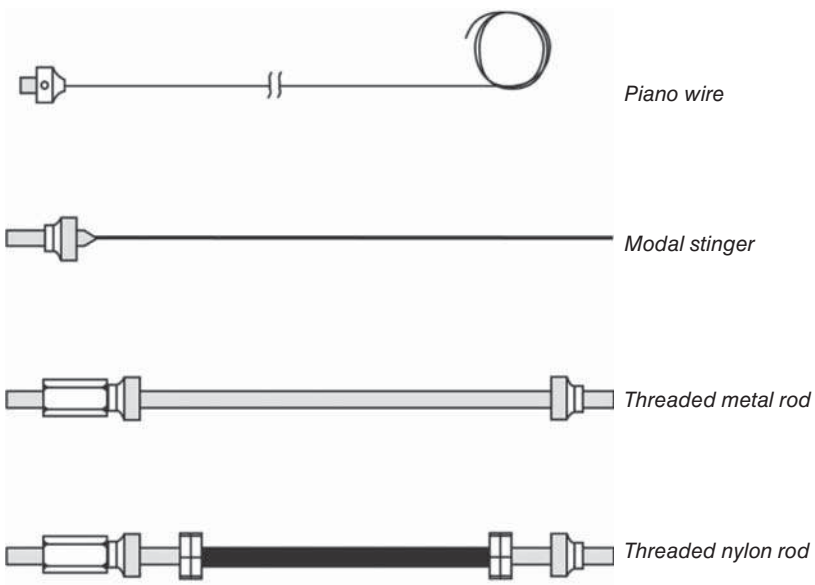

Figure 4.34 Assortment of shaker stingers. *Source:* Image courtesy of PCB Piezotronics, Inc.

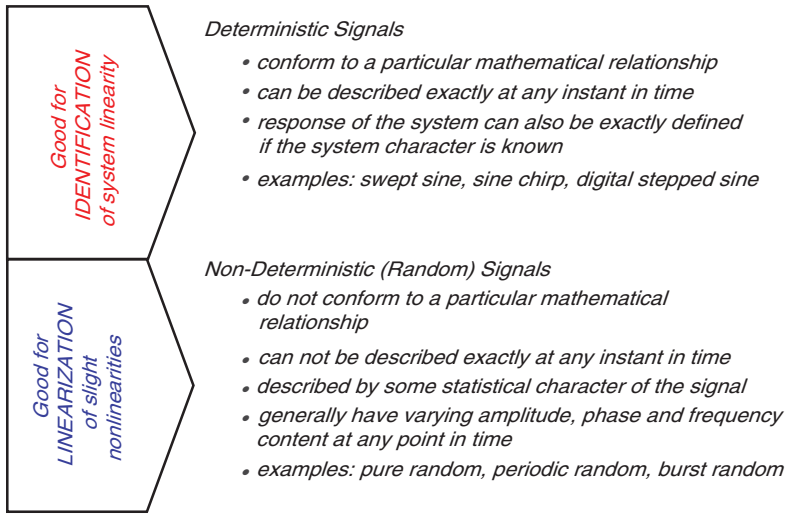

Figure 4.35 Comparison of deterministic and non-deterministic excitation.

4.3.3 Swept Sine Excitation

Historically, swept sine testing was used by the aerospace industry for ground vibration testing for many years. As a testing technique, it has a very long history of usage and is widely accepted by many in the industry. Basically, a sine wave is swept from a low frequency to a high frequency over a very long time. During the sweep, the output response is measured. This testing technique has very good signal to noise and overall RMS levels are very good.

However, swept sine testing was developed for analog instrumentation applications and its direct application in standard form using digital signal processing techniques has some limitations. Due to the nature of the extremely slow sweep, the time for testing is very long and does not take advantage of the speed and processing power of the FFT process; leakage is also a very serious concern. The obvious advantage of this test technique is that the signals obtained are always very good, with excellent signal to noise ratios and excellent overall RMS levels. Swept sine testing is excellent for characterizing the nonlinear character of a system.

4.3.4 Pure Random Excitation

One of the first shaker excitation techniques utilized for experimental modal testing was pure random excitation. Pure random excitation is a stationary, ergodic process. As such, the specific excitation cannot be defined at any instant in time but, rather, only the statistical properties of the signal can be assessed. Such a signal has randomly varying amplitude and phase and is a good general purpose excitation method. The basic measurement process for acquiring frequency response functions is shown in Figure 4.36; each individual sample is different from every other sample due to the random nature of the signal and is the reason why each sample is shown in a different color in the figure. Typically, a signal is started and the data acquisition system is started to auto-range the levels for each channel before averaging is started.

As a general test technique, random excitation was very easy to implement and was one of the first general excitation techniques used. However, a significant problem associated with a random excitation is that both the input and output response signals will always suffer from leakage. This is the most serious of all the signal processing errors associated with pure random

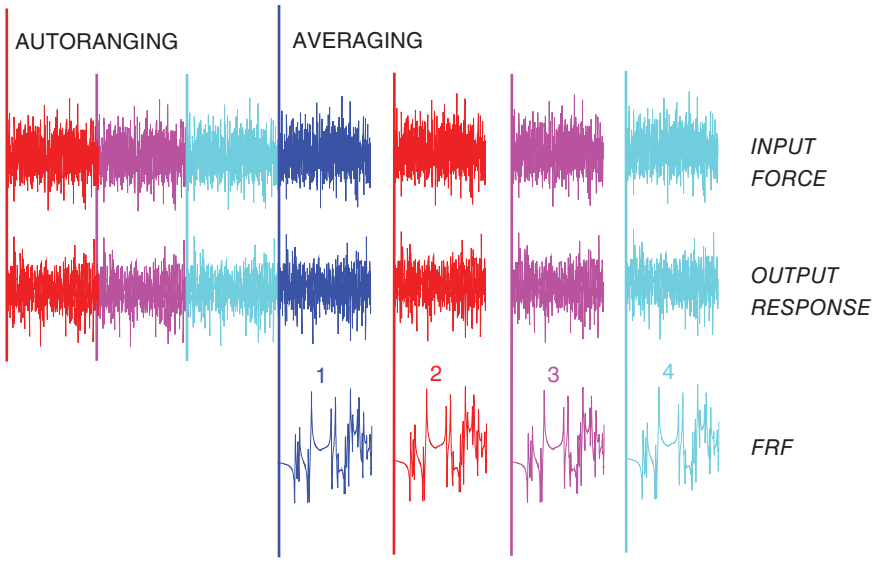

Figure 4.36 Schematic of typical input force (top), output response (middle), and FRF (bottom) for random excitation.

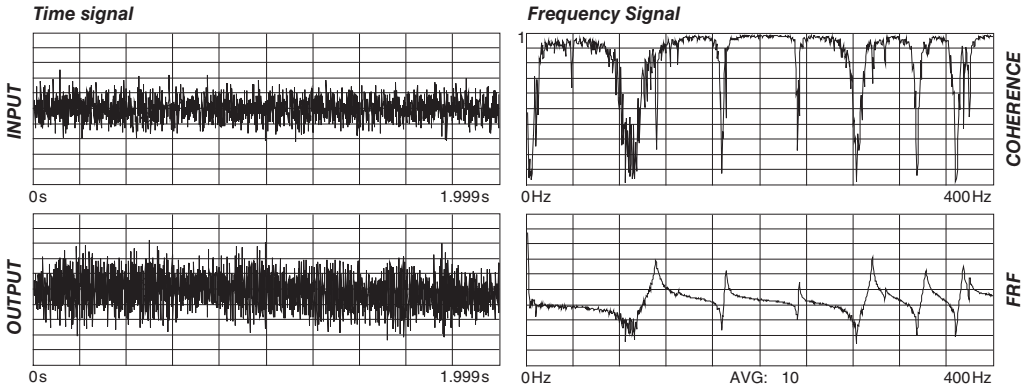

Figure 4.37 Input force (top) and output response (bottom) on left and coherence (top) and FRF (bottom) on right for random excitation.

excitation. The leakage error will cause a serious degradation of the quality of the measured frequency response function, with significant error resulting, particularly at the resonant peaks of the system. The time domain input excitation and output response for a typical measurement are shown in Figure 4.37.

The frequency response function along with coherence for a measurement taken with pure random excitation is also shown in Figure 4.37. The coherence is poor at many frequencies and the frequency response function shows some variance on the data. This is a normal characteristic of a frequency response function acquired using pure random excitation. In general, the quality of the measurement will improve as more averages are acquired, but when compared to other excitation techniques, no amount of averaging will improve the measurement to a point where pure random excitation would be considered a viable technique for most modal testing performed today.

4.3.5 Pure Random Excitation with Windows Applied

The random excitation data previously shown was acquired with no window or weighting functions applied to the measured data. From digital signal processing considerations, a window is necessary in order to minimize the effects of this leakage phenomenon. Now, if a Hanning window is added to the same data, the window tends to make the signal appear to better meet the periodicity requirement of the FFT process. The measurement process is shown in Figure 4.38 for the same random excitation previously shown, except that a weighting function (in this case a Hanning window) has been applied to the data.

Figure 4.39 shows the time signals with the Hanning window applied, along with the frequency response function, which appears much cleaner, with dramatically improved coherence. While the measurement is generally much better with the use of a window on the measured data, leakage is still a concern and causes degradation of the measured frequency response function. Leakage is mostly a concern at the resonances of the system.

Due to the varying amplitude and phase of the input signal, system nonlinearities will generally be averaged out as more and more averages are taken. This is a very important advantage of using random excitation. Slight nonlinearities will tend to be averaged away with more averages. Due to leakage considerations and the fact that slight nonlinearities need to be averaged out of the measured frequency response function, many averages should routinely be acquired when using random excitation. This will tend to cause the testing time to increase significantly.

4.3.6 Pure Random Excitation with Overlap Processing

One method used to reduce testing times with pure random excitation is overlap processing. Because the Hanning window tends to weight the first and last quarters of the time block to zero, this data is not effectively used in the normal averaging process. Overlap processing effectively uses the portion of the block that has been heavily weighted to zero as a result of

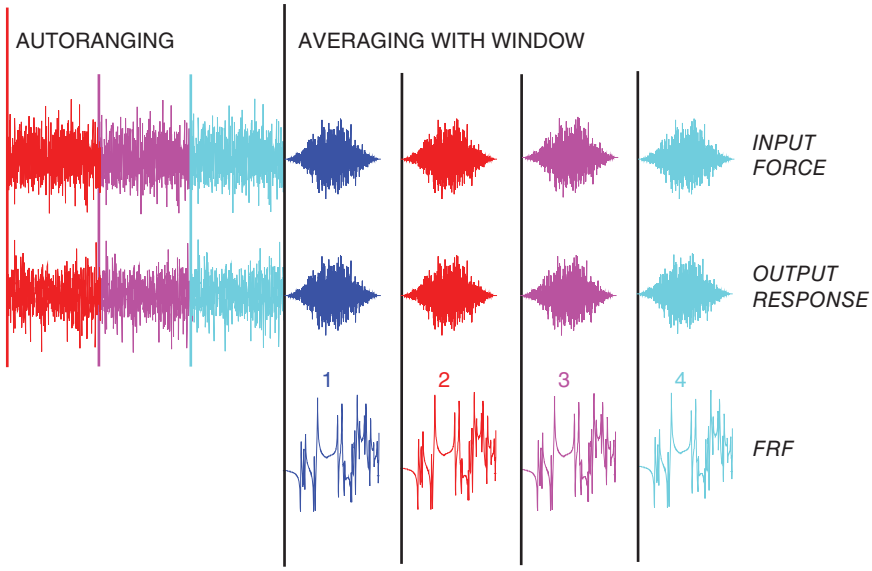

Figure 4.38 Schematic of typical input force (top), output response (middle), and FRF (bottom) for random excitation with Hanning window.

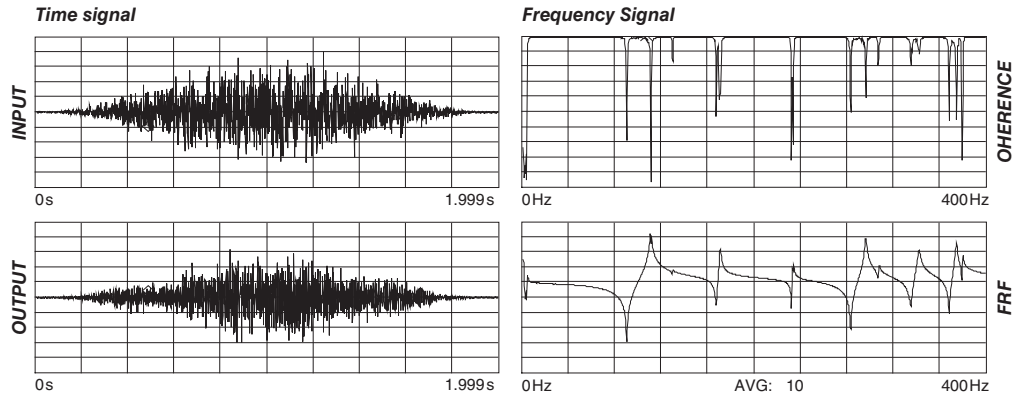

Figure 4.39 Input force (top) and output response (bottom) on left and coherence (top) and FRF (bottom) on right for random excitation with Hanning window.

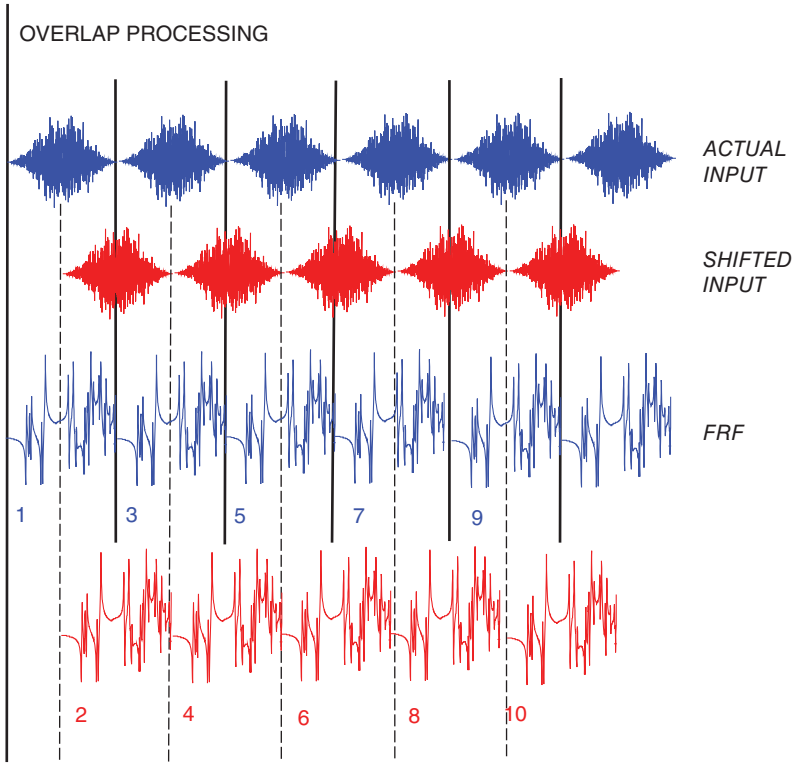

Figure 4.40 Schematic showing effective use of data with 50% overlap processing.

the application of the Hanning window. Overlap processing allows for almost twice as many averages with the same data when a 50% overlap is used. The overlap process with 50% overlap is shown in Figure 4.40, illustrating how averaged data is acquired. In this schematic, only six samples of data are acquired, but with overlap processing eleven averages are computed from the measured data.

4.3.7 Pseudo-random Excitation

Considering the leakage problem using a pure random excitation, as described above, efforts were made to try to reduce the error associated with the measured frequency response function. The error described above is directly due to violation of the periodicity requirements of the FFT process. Let's consider the development of a signal whose general characteristic does not violate this requirement.

Take a particular spectral line in the frequency domain and take the inverse FFT; the resulting time response will be a sinusoid and the time signal will contain an integer number of cycles of the signal. Because this time signal does not violate the periodicity requirement of the FFT process, no windows are necessary in order to transform this signal without distortion. Now take a second spectral line at a different frequency and take its inverse FFT; the resulting time signal will also be a sinusoid, with the same character as the previous signal described above. If these two sinusoids are added together, then the resulting time signal will also satisfy the periodicity requirements of the FFT process and no windows will be required in order to transform this data.

If each spectral line in the FFT analyzer is assigned a particular value, and an inverse FFT were taken, the resulting signal would be the summation of all the sinusoids making up the discrete spectral values of the signal in the frequency domain. The resulting time signal would look very much like a random signal, but would be made up of the summation of sinusoids; this signal is referred to as a pseudo-random signal. It would also satisfy the periodicity requirement of the FFT process and no windows would be required in order to transform this data.

If this signal is used for excitation of the system, the response of the system also satisfies the periodicity requirement of the FFT analyzer once the system reaches steady state. This occurs because the response of the system is made up from the sinusoidal responses of many sinusoids. Because the basic signal then contains an integer number of cycles of the signal over the sample interval, no window is required on the input or output signals and leakage is not a problem. This now eliminates one of the biggest contributors to the distortion of the measured frequency response function: leakage.

Of course, this approach comes with some side effects. Because the same signal is continually used as input to the system, the system will respond the exact same way to each input block of data once the steady state response is reached. Therefore, a serious disadvantage of using pseudo-random excitation is that this excitation will not have the ability to average away any slight nonlinearities that may exist in the system. Therefore, rattles and slight nonlinearities will not be averaged out of the data as more averages are acquired.

The pseudo-random measurement process can be seen in Figure 4.41; it is very important to note that the signal that is used for excitation is the same signal that is repeated over and over; this is shown in one color to highlight that fact. The excitation is input to the structure and the response is measured. The analyzer is set to autoranging, such that optimal ADC settings can be achieved at the same time the structure is reaching its steady state response. Once this is achieved, averaging is initiated for the desired number of averages. Again, it must be emphasized that the same excitation is used over and over and therefore the structural response will be the same once the steady state response is achieved.

4.3.8 Periodic Random Excitation

Considering the problems associated with pseudo-random excitation, further enhancements were made to this excitation technique in an excitation technique referred to as *periodic random excitation*. Basically, periodic random excitation is the same as pseudo-random excitation except that for each measurement a new input spectrum is generated and an inverse

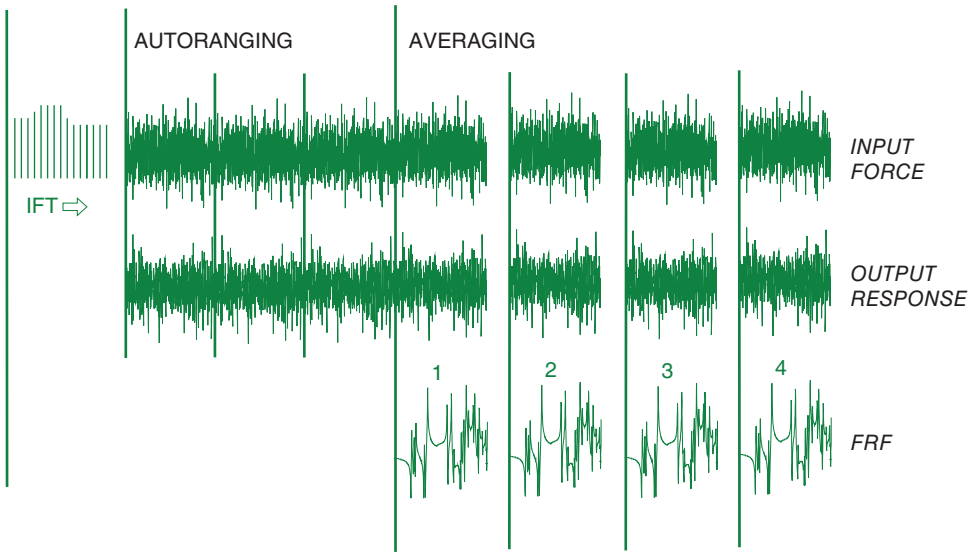

Figure 4.41 Schematic of typical input force (top), output response (middle), and FRF (bottom) for pseudo-random excitation.

FFT is taken to create a new time signal for each average of the measurement process. Again, the signal is used to excite the system and the system is allowed to come to its steady state response while the autoranging process of the acquisition is under way. Once this is achieved, then only one average is taken. At this point, another spectrum is generated (different from the first spectrum), inverse transformed. This is used to start the process again to acquire the next average of the frequency response function. In this way, each measurement will excite the structure differently, and then with averaging, nonlinearities will be removed from the measurement as more and more averages are taken. As with pseudo-random excitation, no windows are necessary for this measurement process because the input excitation signals and the output response signals will all satisfy the periodicity requirement of the FFT process. While very high quality frequency response functions are obtained from this approach, a significant amount of time and hardware is required to perform this measurement technique.

The basic measurement process for periodic random excitation is shown in Figure 4.42; here it is important to note that the same signal is repeated for the collection of data for the first average, as highlighted in blue, but the second average collected uses a different random signal, highlighted in red: each average uses a different random signal.

4.3.9 Burst Random Excitation

Due to the time and cost considerations of pseudo-random and periodic random excitation techniques, easier to implement techniques were needed in order to make the measurement of high quality frequency response functions feasible. Again, realizing that the main concern was the distortion of the measured frequency response function due to leakage resulting from violation of the periodicity requirement of the FFT process, transient signals whose total duration could be observed within one sample interval of the block of data acquired were considered. One signal that offered great potential was the *burst random* signal. Burst random excitation has become one of the more popular excitations available for experimental modal testing today. This special excitation technique offers all the advantages of random, pseudo-random, and periodic random excitations without the disadvantages associated with these techniques.

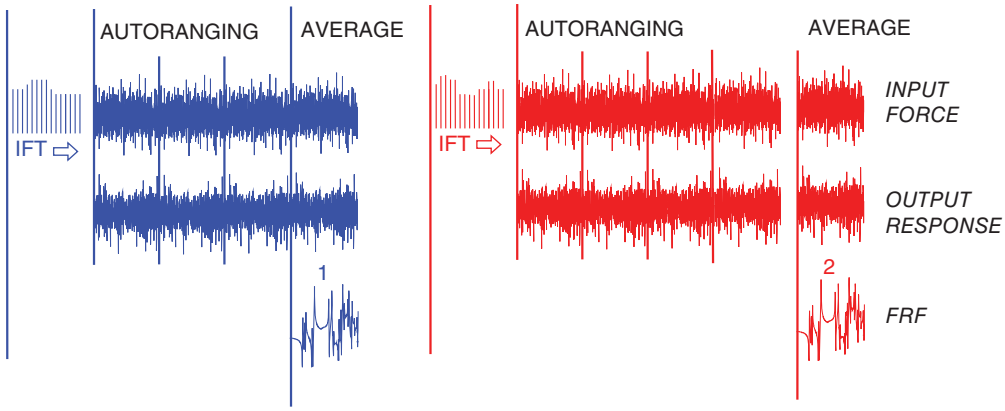

Figure 4.42 Schematic of typical input force (top), output response (middle), and FRF (bottom) for periodic-random excitation.

Burst random is formed as follows. A random excitation is generated but is only output for a portion of the data block. In this way, the excitation signal is totally observable within one sample interval of the FFT analyzer; there is no need for the use of windows because there is no leakage associated with the captured signal. In addition, a pretrigger delay is often used with this excitation so that there is no excitation signal within the first several time bins of the captured data. The burst random signal is shown in Figure 4.43.

Providing that the response measured on the structure is also totally observable within one sample interval of the FFT analyzer, there is no need for the use of windows because there is no leakage associated with the captured signal. However, once the excitation is turned off, the structural response will die exponentially, at a rate depending on the damping associated with the structure. If the response of the structure does not die out within one sample interval, then the burst should be shortened such that the response does end before the end of the sample interval. The burst can be controlled by specifying the percentage of the block over which the excitation is to be applied. Generally, this can be accomplished with most structures.

The burst random measurement process can be seen in Figure 4.44. The excitation is input to the structure and the response is monitored to ensure that the response dies out before the end of the sample interval. The burst length can be adjusted so that this is accomplished. During this time the analyzer can be autoranging, such that optimal ADC settings can be achieved. Once this is achieved, then averaging is initiated for the desired number of averages.

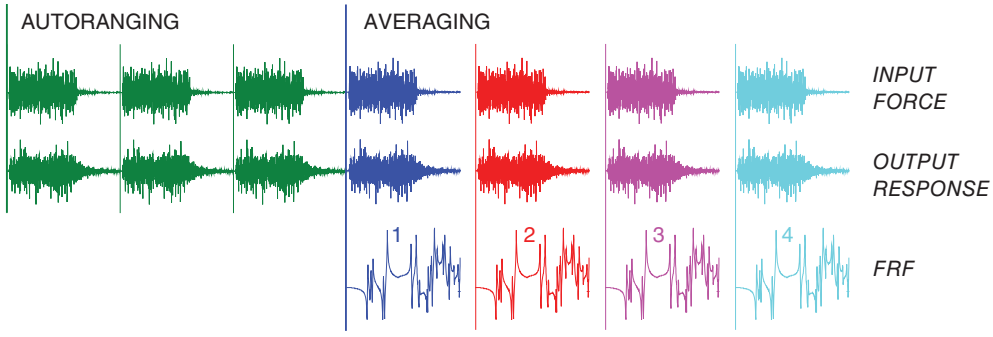

Figure 4.43 Schematic of typical input force (top), output response (middle), and FRF (bottom) for burst random excitation.

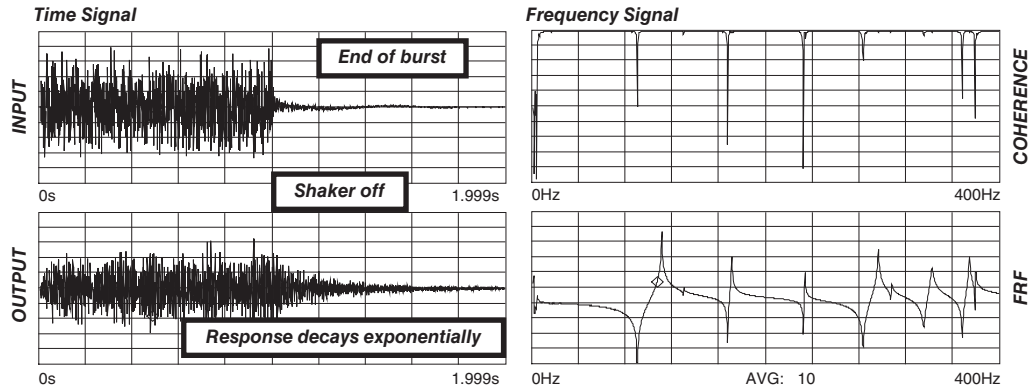

Figure 4.44 Input force (top) and output response (bottom) on left and coherence (top) and FRF (bottom) on right for burst random excitation.

Because the basic excitation technique comprises a random function, all of the advantages of random excitation to linearize slight nonlinearities that exist in the data will be retained. In addition, none of the disadvantages associated with random excitation – in particular, leakage – are seen with burst random excitation because the transient nature of the signal prevents this from happening. The frequency response function and coherence functions for the measured time data are shown below and it is clearly seen that the measured frequency response function and coherence are greatly improved relative to the measurements previously shown, which were acquired with random excitation.

4.3.10 Sine Chirp Excitation

Sine chirp excitation has become a very popular technique for efficient testing of linear structures for development of a modal model. Basically, the sine chirp is very similar to the traditional swept sine test that has been performed for many years; the only difference is that one whole sweep of the frequency range occurs within one sample interval of the FFT analyzer. Because the input signal is totally observable from one sample of the signal, the periodicity requirement of the FFT process is not violated and no windows are required. The basic measurement process is shown in Figure 4.45; note that the same signal is played over and over, which allows the structure to reach its steady state response such that both the input and output are then periodic in the sample interval and no window is required.

This signal is input to the structure and, while the analyzer is autoranging, the system response will eventually reach steady state response. Therefore, the output response is also totally observable within one sample interval and no window is required for this excitation type.

Sine chirp provides all the advantages of traditional swept sine testing along with the speed of the FFT process. The resulting frequency response function is one of the best acquired measurements for linear systems other than digital stepped sine excitation. Also, note the coherence values for this measurement. These are shown in Figure 4.46. Sine chirp is also a good test technique for identifying nonlinear system character.

4.3.11 Digital Stepped Sine Excitation

Due to the excellent nature of swept sine testing, an alternative technique that utilizes the speed of the FFT analyzer was developed. This is referred to as *digital stepped sine*. Basically, sine waves are generated at discrete frequencies, which correspond to the digital values of the FFT analyzer for the frequency resolution available.

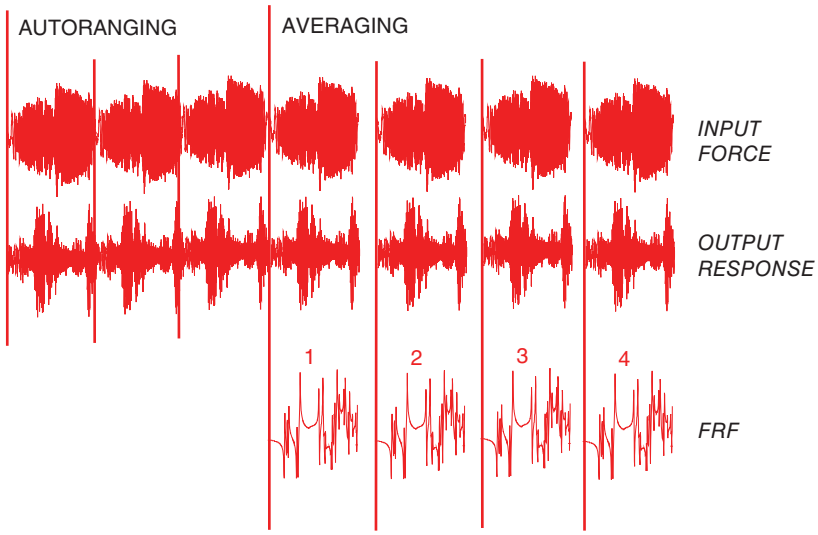

Figure 4.45 Schematic of typical input force (top), output response (middle), and FRF (bottom) for sine chirp excitation.

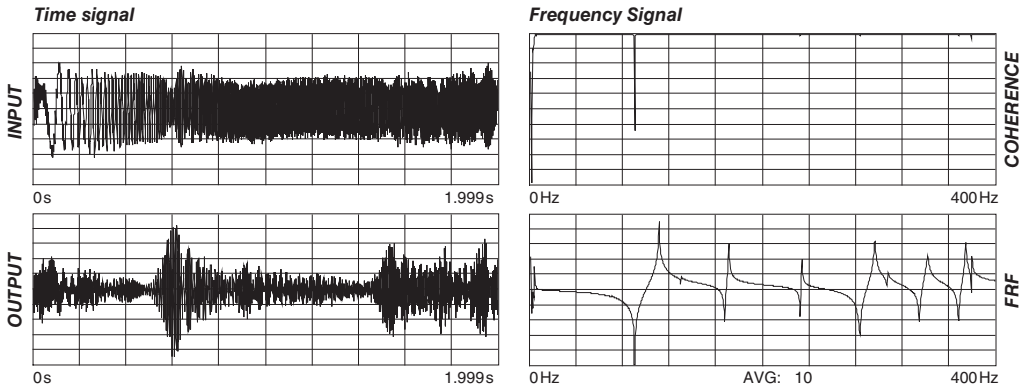

Figure 4.46 Input force (top) and output response (bottom) on left and coherence (top) and FRF (bottom) on right for sine chirp excitation.

The system is excited with a single sine wave and the steady state response is measured. Because the input frequency coincides with one discrete spectral line of the FFT analyzer, the measured time signal will always contain an integer number of cycles of the signal and is considered to satisfy the periodicity requirement of the FFT process. The measurement process is shown in Figure 4.47.

Once an acceptable measurement is achieved, the excitation is digitally stepped to the next discrete frequency available in the FFT analyzer. This process is repeated until all discrete frequencies have been measured.

This test technique retains all the advantages of swept sine testing and combines all the advantages of the FFT analysis process. Obviously, the test time to acquire a wide frequency band with fine frequency resolution will require a significant amount of time, but the accuracy and resolution of the data make it an excellent test technique. Like swept sine, digital stepped

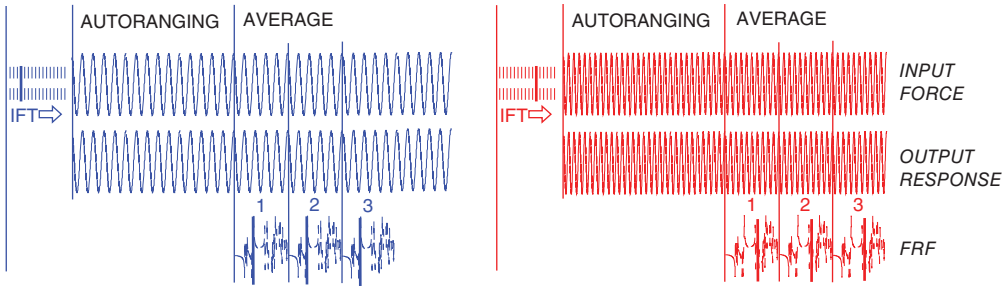

Figure 4.47 Schematic of typical input force (top), output response (middle), and FRF (bottom) for stepped sine excitation.

sine is excellent for characterizing any nonlinear character of a system. If all the transducers are mounted on the structure, the length of time to collect the data is not significant

4.4 Comparison of Different Excitations for a Weldment Structure

Several of the more commonly used excitation techniques were used for the development of a frequency response function for a weldment structure. The results are presented in this section for comparison purposes. In particular, random excitation with and without a Hanning window, and burst random and sine chirp excitation were used on the weldment structure shown in Figure 4.48. Also, a linearity check was performed using sine chirp to illustrate the effects of non-linearities in a structure. In this way, a clear assessment of the advantages and disadvantages of the different excitation techniques can be made.

For all measurements made, a frequency range of 400 Hz was used, with 800 spectral lines of resolution. Typically, ten averages were calculated in order to compute the H_1 frequency response function. Input and output time histories are shown, along with the resulting frequency response function and coherence.

4.4.1 Random Excitation with No Window

Figure 4.49 shows the input/output time histories on the left and the coherence/frequency response on the right. Viewing the results in the time domain, the input and output signals are

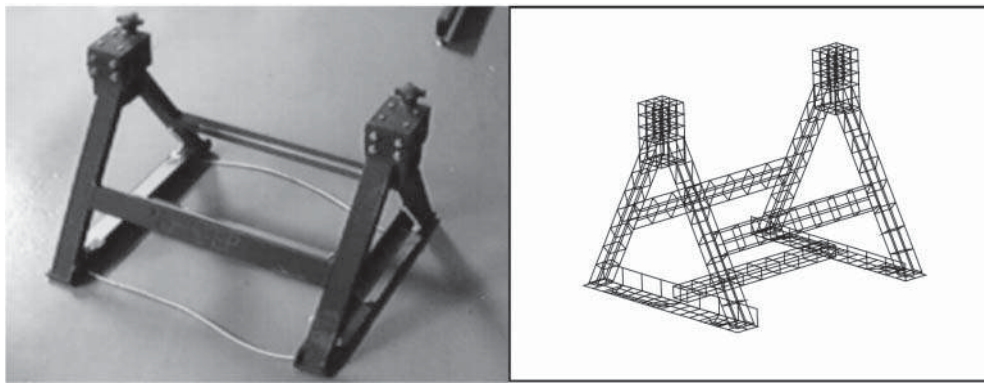

Figure 4.48 Weldment structure used for comparison measurements.

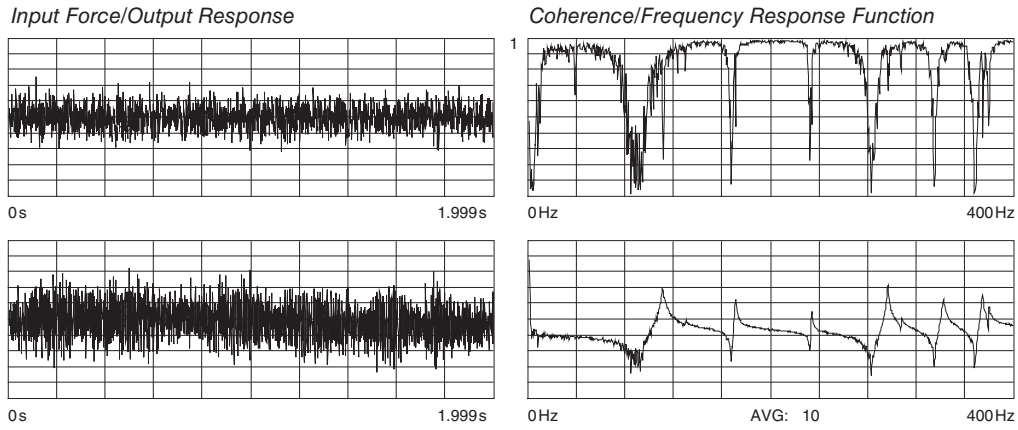

Figure 4.49 Input force (top) and output response (bottom) on left and coherence (top) and FRF (bottom) on right for random excitation.

random in nature but there is no useful information that can easily been seen in the data. In the frequency domain, however, the frequency response function shows several modes that exist. The frequency response measurement shows quite a bit of variance on the measured function. Many more averages would be required in order to reduce the variance on this measurement. Even with excessive averaging and overlap processing, however, the variance would not be able to be reduced to acceptable levels. The main reason for the distortion of this measurement is leakage. This is always a problem with random excitation techniques.

4.4.2 Random Excitation with Hanning Window

Figure 4.50 shows the input/output time histories on the left and the coherence/frequency response on the right. With a Hanning window applied the situation is somewhat improved. Viewing the results in the time domain, the input and output signals are again random in nature but there is no useful information that can easily been seen in the data; the effects of the Hanning window, however, are clearly seen in the data. In the frequency domain, the frequency response function shows several modes that exist. The frequency response measurement still shows quite a bit of variance on the measured function. Many more averages would be required in order to reduce the variance on this measurement. It is very important to note that the coherence function has fairly low values, particularly at the resonant peaks. Even with the Hanning window applied, excessive averaging is still necessary in order to reduce the variance to acceptable levels. Again, the main reason for the distortion of this measurement is leakage. This will always be a problem with random excitation techniques, even with the Hanning window applied. The Hanning window reduces a good deal of the leakage but does not eliminate the problem.

4.4.3 Burst Random Excitation with No Window

Figure 4.51 shows the input/output time histories on the left and the coherence/frequency response on the right. Viewing the results in the time domain, the burst random excitation signals still contain no useful information that can be easily seen. However, both the input and output signals are now completely observed within one sample interval of the time block. Because this is the case, the signal does not violate the basic periodicity requirement of the FFT process and there is no need to apply any window in this case. This will produce a leakage free measurement that will not be distorted by leakage. The frequency response function is considerably better than the random case, with significantly improved coherence values,

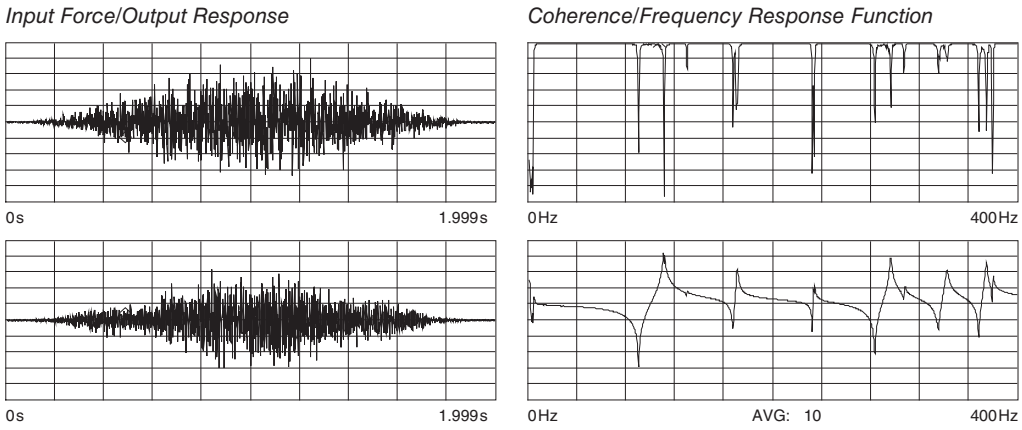

Figure 4.50 Input force (top) and output response (bottom) on left and coherence (top) and FRF (bottom) on right for random excitation with Hanning window.

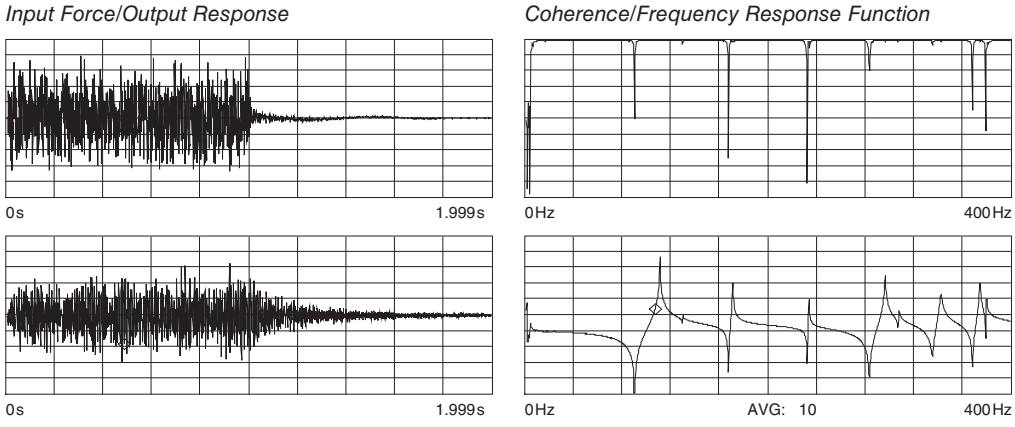

Figure 4.51 Input force (top) and output response (bottom) on left and coherence (top) and FRF (bottom) on right for burst random excitation.

particularly at the resonant peaks. Also, note that the resonant peaks are much sharper than in the random case because leakage and windows tend to smear data, causing an appearance of higher damping than actually exists.

4.4.4 Sine Chirp Excitation with No Window

Figure 4.52 shows the input/output time histories on the left and the coherence/frequency response on the right. Viewing the results in the time domain, the sine chirp signals show some useful information. Because the chirp sweeps from low to high frequency within one sample interval, the time response will contain amplification, as the chirp sweeps through each of the resonant frequencies. Again, both the input and output signals are completely observed within one sample interval of the time block. Because this is the case, the signal does not violate the basic requirement of the FFT process and there is no need to apply any window in this case. This will produce a leakage free measurement that will not be distorted by leakage. The frequency response function is considerably better than the random case, with significantly improved coherence values, particularly at the resonant peaks. Also, note that the resonant peaks are much sharper than in the random case because leakage and windows tend to smear data, causing an appearance of higher damping than what actually exists.

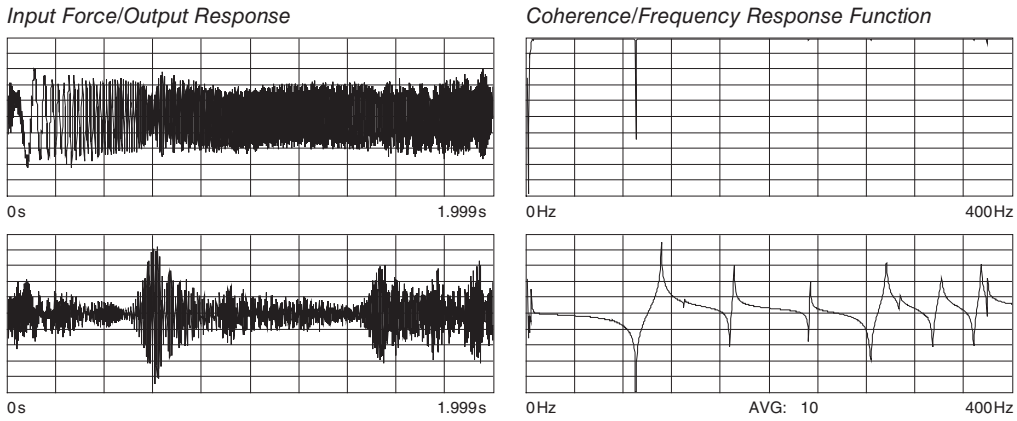

Figure 4.52 Input force (top) and output response (bottom) on left and coherence (top) and FRF (bottom) on right for sine chirp excitation.

4.4.5 Comparison of Random, Burst Random and Sine Chirp

Figure 4.53 shows a comparison of the random, burst random and sine chirp. The burst random and sine chirp produce very similar results. The resonant peaks are well defined and there is very little variance on the measured data. Comparing these two results to the random measurement, it can be seen that the random measurement has considerably more damping at the resonant peaks than in the case of burst random and sine chirp. Also, notice that there appears to be a double peak at the first frequency in the random measurement; this is due to leakage and will be looked at closer.

4.4.6 Comparison of Random and Burst Random at Resonant Peaks

Let's compare the results with random and burst random excitation, as shown in Figures 4.54 and 4.55.

On the surface, it appears that both measurements are same on the left, but taking a closer look on the right, there appears to be some distortion at the peaks. With even a closer look in Figure 4.56, it becomes very apparent that there is a severe distortion of the frequency response function, particularly at the resonant peak. Even with the use of a Hanning window on the random data, there is still a serious effect of leakage!

4.4.7 Linearity Check Using Sine Chirp

The frequency response function shown in Figure 4.57 was measured using different force levels and sine chirp excitation to document the linearity of the system. Clearly there is nonlinear behavior, but not all of the modes are affected equally by whatever nonlinearity exists in the system. Some modes show very little change due to an increase in force level; other modes show some slight differences due to increases in force level, and a few other modes show a dramatic change in the dynamic characteristics of the system.

4.5 Multiple-input, Multiple-output Measurement

Multiple-input, multiple-output (MIMO) testing has become very popular and offers several advantages over single-input, single-output testing (SISO) methods. This technique allows for a better energy distribution, so as to excite large structures more uniformly. The simultaneous

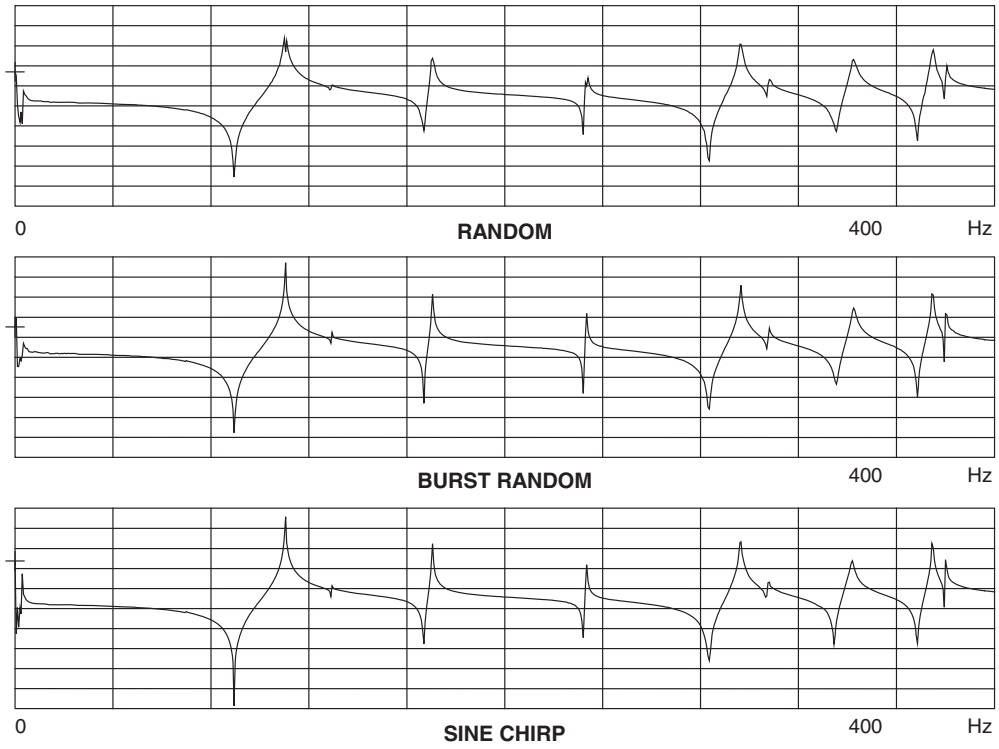

Figure 4.53 Comparison of FRF with random with a window, burst random, and sine chirp excitations.

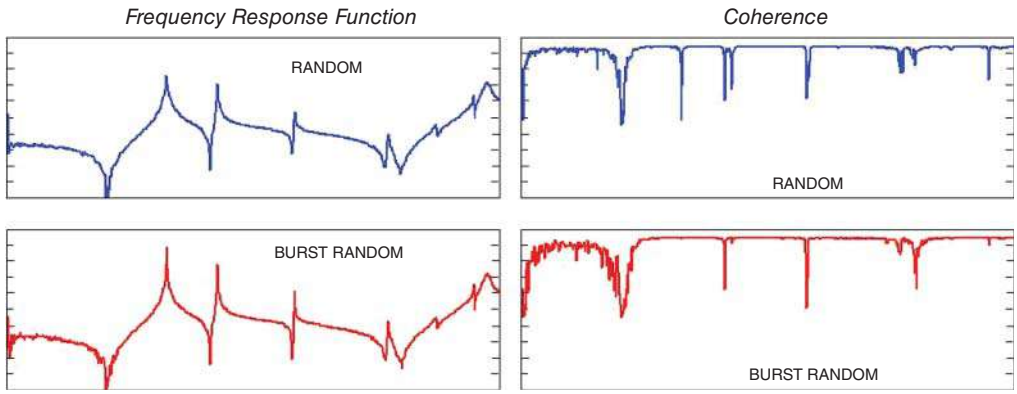

Figure 4.54 Comparison of FRF and coherence with random and burst random excitations.

input also allows for nonlinearities to be excited differently, such that a better linear approximation of the system can be obtained. In addition, the simultaneous collection of multiple columns of the frequency response matrix allows for a more uniform and consistent definition of the frequency response functions that will be used to develop the experimental modal model of the system. The data collection time for MIMO is the same as SISO.

Instead of computing frequency response functions as scalar quantities, matrix processing of the data is required. The input output model is the same and is defined as:

$$[G_{XF}] = [H][G_{FF}]$$

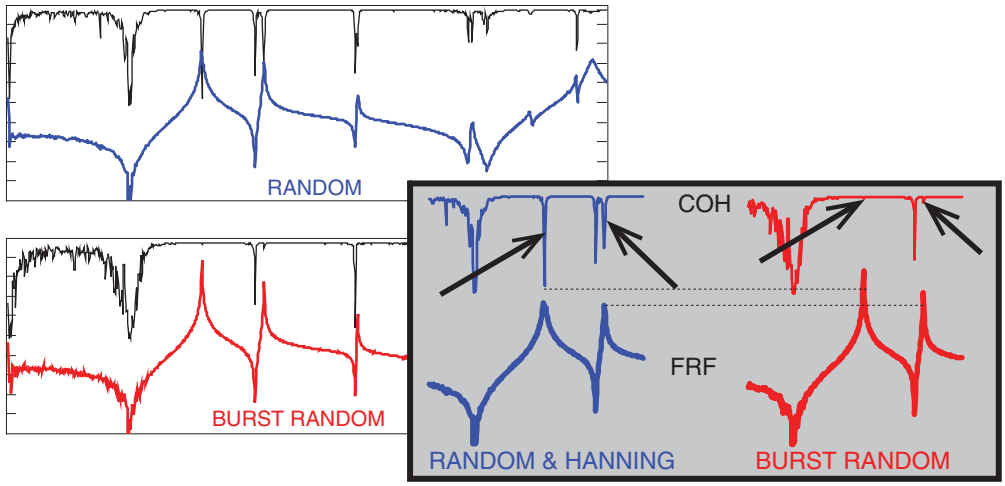

Figure 4.55 Comparison of FRF overlaid with coherence with random and burst random excitation.

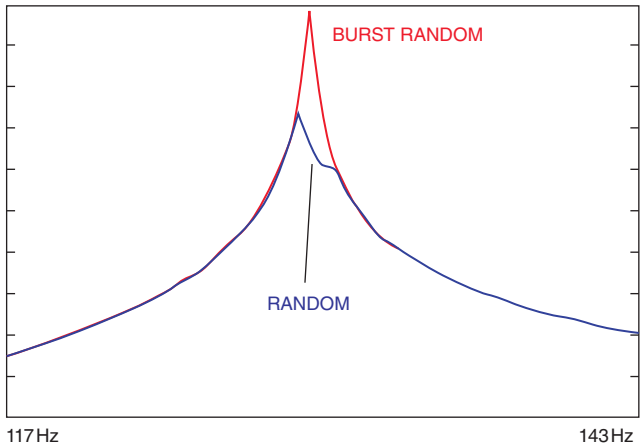

Figure 4.56 Zoomed in FRF on mode 1, showing difference between FRF from random and burst random excitations.

where

$$[H] = \begin{bmatrix} H_{11} & H_{21} & \cdots & H_{1,Ni} \\ H_{21} & H_{22} & \cdots & H_{2,Ni} \\ \vdots & \vdots & & \vdots \\ H_{No,1} & H_{No,2} & \cdots & H_{No,Ni} \end{bmatrix}$$

where No is the number of outputs and Ni is the number of inputs. Solving for [H] then

$$[H] = [G_{XF}][G_{FF}]^{-1}$$

4.5.1 Multiple Input vs Single Input Testing

Due to the effects of shaker mass and stiffness, there may at times be differences between the results from different single input tests. However, the theory of modal analysis implies that

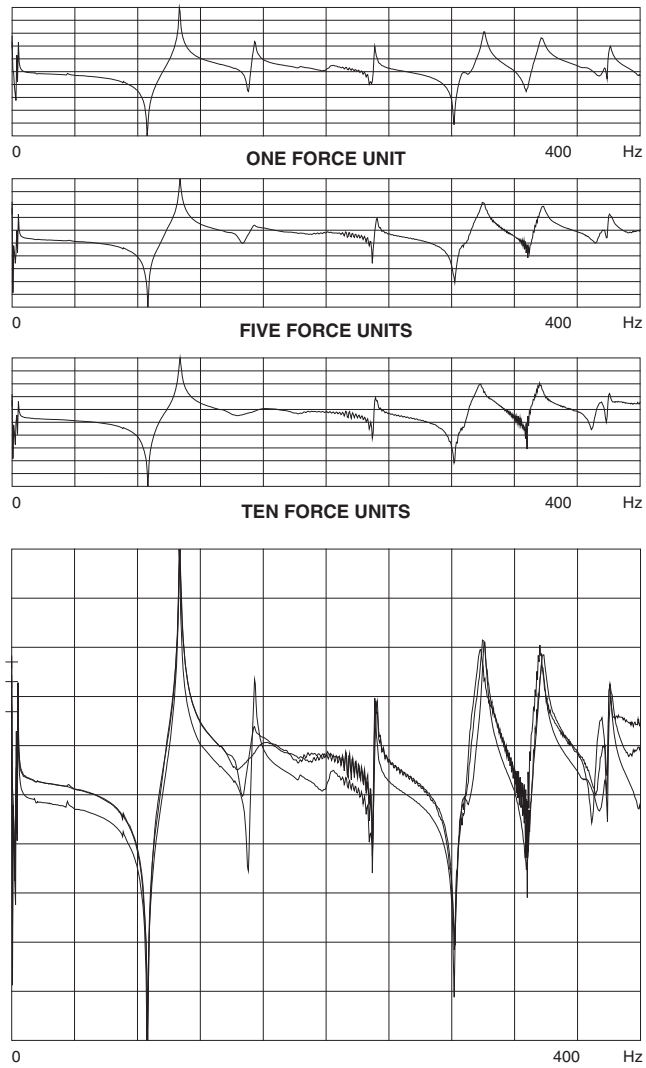

Figure 4.57 Linearity check with sine chirp excitation (FRFs).

reciprocity must hold true. From a practical standpoint, this is often not the case in an actual test condition. Single input excitation can, however, provide very good results if only one input reference is needed. When trying to combine different SISO shaker reference tests, there is always the possibility of inconsistencies. This can result from the total time that it takes to acquire the data, to environmental changes that affect the system modes, or from many other difficulties that can cause the data to be inconsistent when attempting to merge several different SISO tests that have been performed. Usually, just the moving of the shakers to different reference locations may be enough to cause inconsistencies from one SISO reference to another SISO reference. Often, test labs will attempt such moves due to a lack of shakers, or lack of data acquisition sources, or for many other reasons.

The best way to perform a MIMO test is to have many shakers attached to the test structure simultaneously. Usually, the MIMO test will require much lower force levels overall, thereby not exciting the structure's nonlinearities if they exist. Using multiple input testing, the resulting data will also better satisfy the reciprocity requirement.

An early test from the 1980s is shown next. This is a comparison of SISO data and MIMO data on the same structure and also includes both random excitation and burst random excitation; the reciprocal measurements are shown for the two shaker configuration. Figure 4.58 shows these measurements; the full bandwidth is not shown, but rather a zoom into a very tight band around two very closely spaced modes to show the measurement differences and allowing several observations to be made. The top two plots show the SISO measurements with random

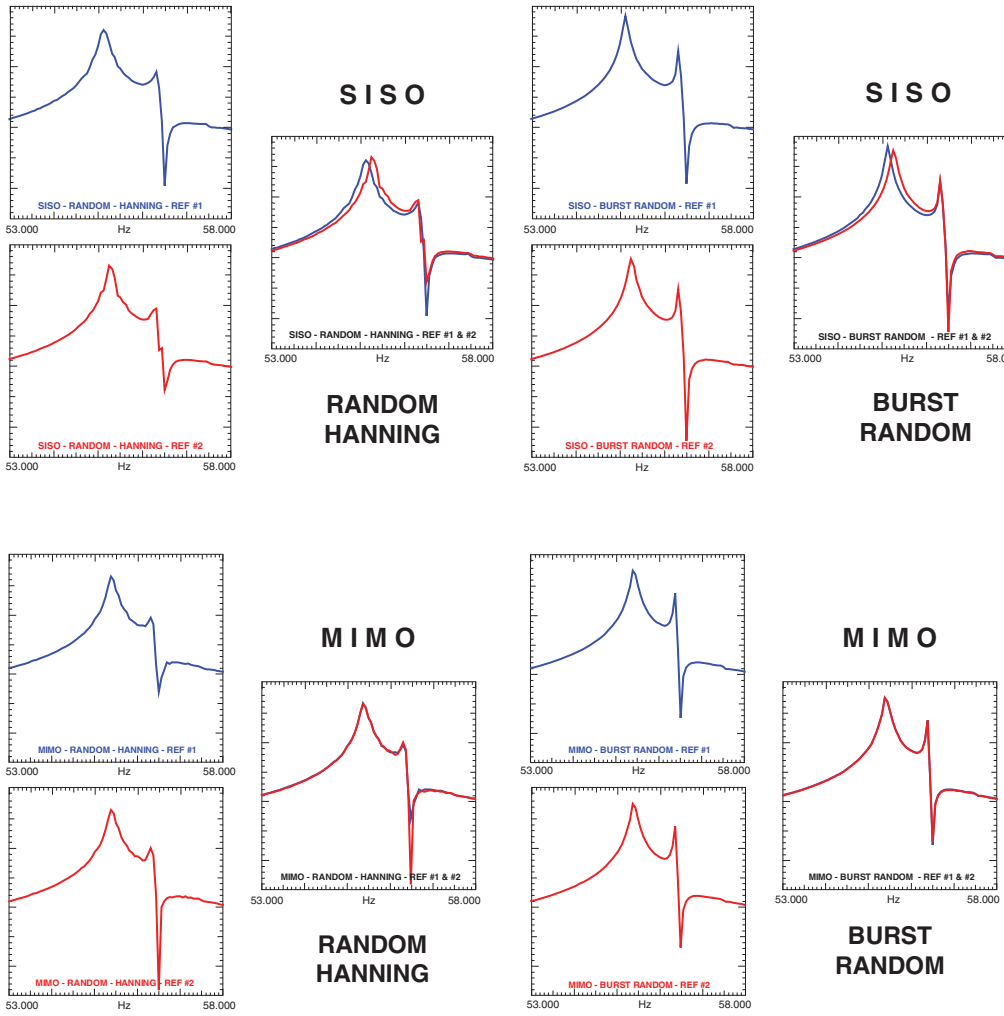

Figure 4.58 Comparison of SISO and MIMO reciprocal data sets collected with random excitation with a Hanning window and burst random excitation.

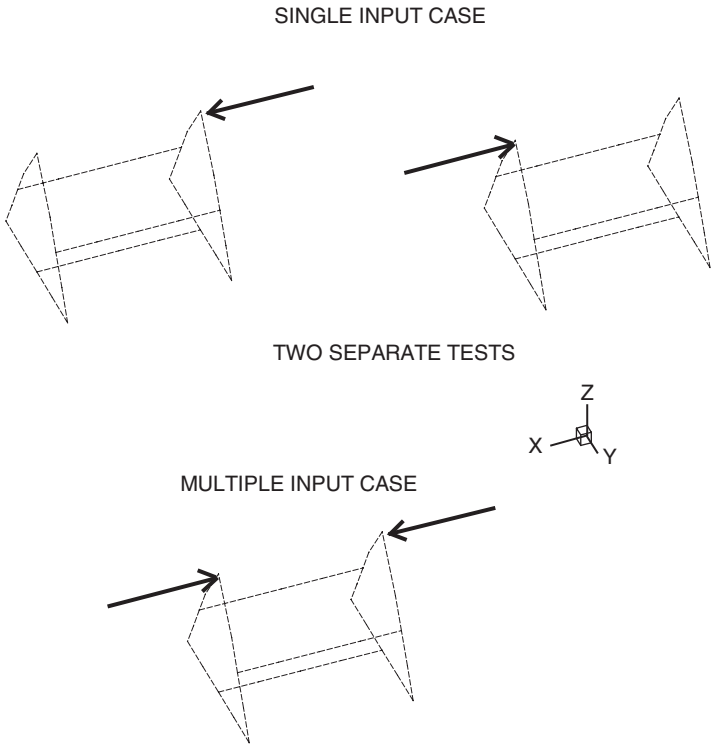

Figure 4.59 Schematic for two separate SISO tests (top) vs MIMO test (bottom).

excitation and burst random excitation, with the measurements separated and overlaid; the bottom two plots show the MIMO measurements.

Now if a baseband measurement was shown over the 1000 Hz bandwidth, the measurements would look very good and the perception would be there wasn't much difference. But narrowing in to the two closely spaced modes, there are differences that are very clear. First looking at the SISO measurements, there is a mismatch between the peaks in the measurements. Now the random signal with the Hanning window shows some variance in the measurement, as well as poor overlap of the two modes. While the burst random measurement is a much better measurement overall, there is an inconsistency in the peaks. This is due to the shaker hardware being attached at two different locations on the structure. This measurement inconsistency will cause difficulties in interpreting the stability diagram; there will certainly be two peaks identified where the first mode is located. The problem is that in half of the measurements the pole will appear at one frequency and for the other half of the data the pole will appear at a slightly different frequency. This will almost always be the case when trying to combine different SISO tests to form a multiple reference set of data. Now looking at the MIMO data, the inconsistencies between the two references is no longer a problem. But looking at the random excitation data, there is some variance between the two reciprocal measurements overlaid. Clearly the burst random excitation data is, overall, the better of the sets of data presented here.

4.5.2 Multiple Input vs Single Input for a Weldment Structure

Due to effects from shaker mass and stiffness, there may at times be differences between the results from different single input tests. Using the same structure used for demonstration of different excitation techniques, reciprocity measurements were made using single input and multiple input approaches for comparison.

4.5.3 Multiple Input vs Single Input Testing

For multiple input testing (Figure 4.59), each of the inputs must be uncorrelated with the other inputs to the system. This is necessary because the input power matrix must be inverted. If the inputs are correlated to each other, the inverse is not accurate. While the signal generated from the digital to analog converter may be mathematically uncorrelated, the actual forces may be slightly different. This can be because of the amplifier but more importantly if there is any structure/shaker dynamic coupling. Generally, a principal component analysis is performed and the input power to all of the force shakers is checked to ensure sufficient input to the system is available, as shown in Figure 4.60.

Basically, the input force spectrum matrix is decomposed using a singular value decomposition (SVD). Each spectral line of the frequency spectrum is decomposed to identify how many linearly independent pieces of information make up the information at that spectral line. Each of the spectral lines is evaluated and the singular values are plotted as a function of frequency. The SVD plots on the left in Figure 4.60 show that there are indeed two independent inputs applied to the structure. If there was only one independent input to the system, only one of the plots of the SVD would have a significant value and the other singular value would be substantially less. This is a critical check that needs to be made when performing a MIMO test. At times, there can be situations when testing larger structures where the shakers are dominated by the structure response at a mode(s) and so the input forces cannot maintain their independent characteristic due to the dominating structural response. The principal component plot (or SVD plot)

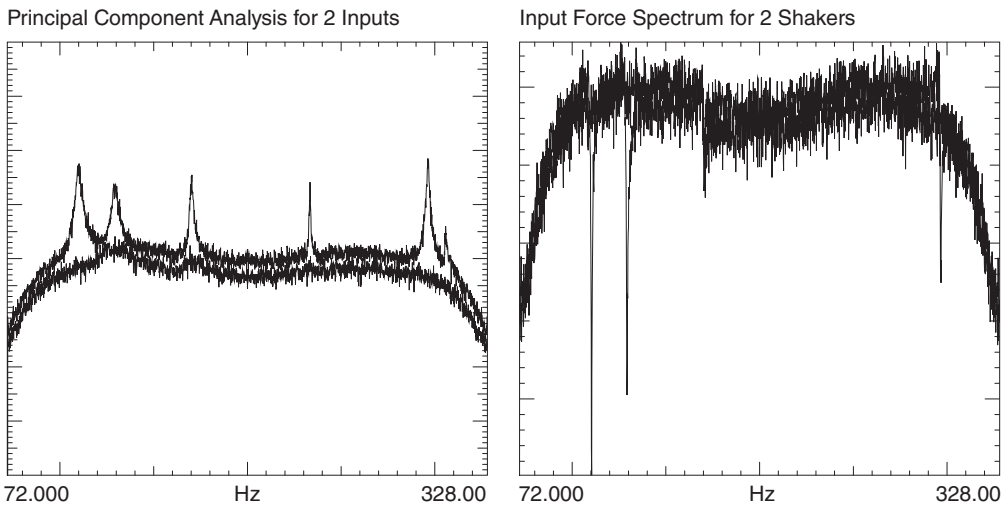

Figure 4.60 SVD for two shaker inputs (left) and two force spectra overlaid (right).

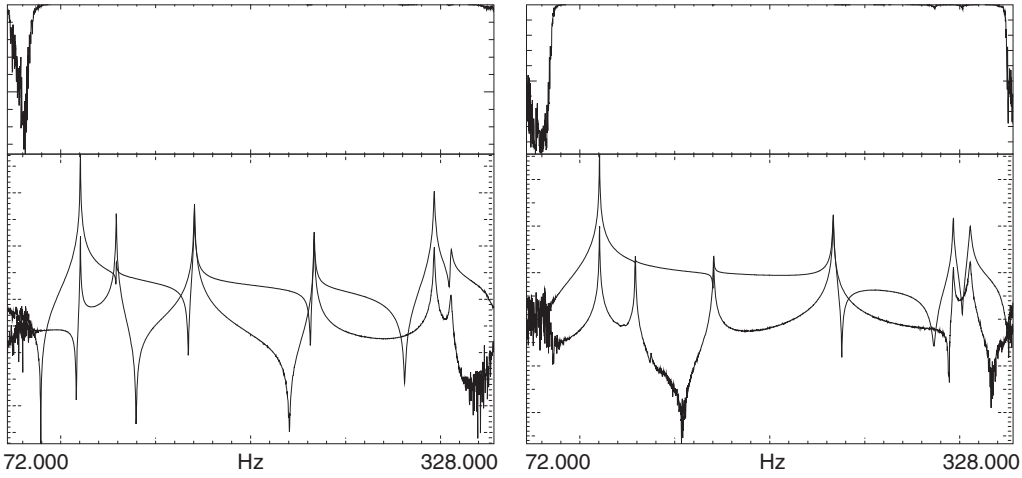

Figure 4.61 Multiple coherence (top) related to two FRFS (bottom) for two input locations.

will show this. If this happens, different shaker locations may be required to circumvent the structure/shaker dynamic interaction.

Once the inputs have been checked for the system, measurements are acquired in the usual fashion. But there are a few different measurements that are necessary. One is the multiple coherence and the other is the partial coherence. The multiple coherence is similar to the ordinary coherence and is interpreted in a similar fashion. Because there are multiple inputs, the coherence of an output response due to all the measured inputs must be evaluated (similar to the ordinary coherence). If all of the output is linearly related to all the measured input forces, then the multiple coherence will be close to 1.0; values less than 1.0 indicate that there are other, unmeasured inputs that are contributing to the measured response. The partial coherence is an indication of the coherent relationship between the output response and one of the inputs (with the effects of the other input removed); the sum of all the partial coherences will give the multiple coherence. The interpretation is essentially the same as in the single input scenario. Figure 4.61 shows two sets of frequency response functions and their companion multiple coherence; both measurements show very good multiple coherence, except at very low and high frequencies where the shaker input spectrum is trimmed at the ends of the spectrum. Overall the frequency response functions and multiple coherence are very good for these measurements.

4.5.4 Comparison of Multiple Input and Single Input for Weldment Structure

While the particular structure under test is fairly linear, there is very little difference between the multiple input and single input cases. This is not generally the rule in most testing situations. However, there are some differences seen in the comparison measurement in Figure 4.62.

4.5.5 MIMO Measurements on a Multi-component Structure

Often, systems are comprised of components assembled to form a system. The components are generally isolated from each other to some degree through isolation mounting systems.

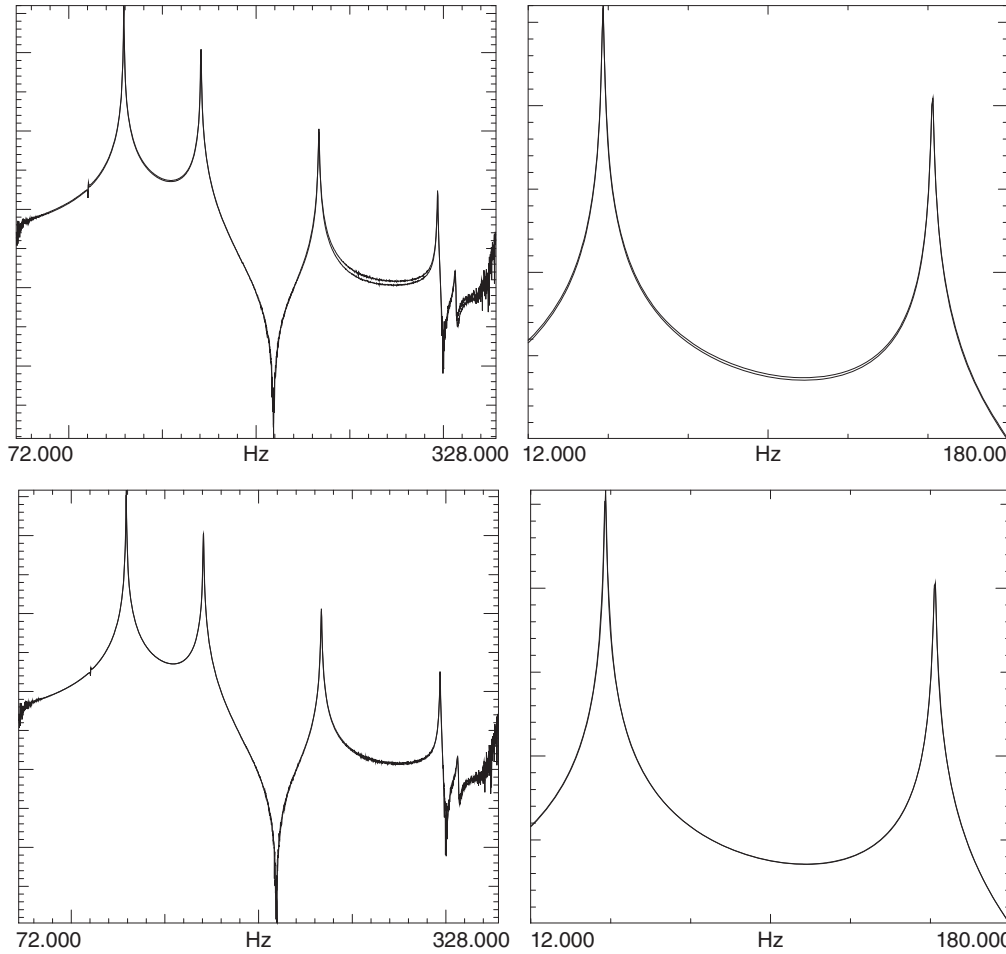

Figure 4.62 SISO measurement (top) and MIMO measurement (bottom) with broadband FRF shown on left and expand into first two modes on right.

In these cases, multiple input, multiple out measurements are usually crucial to the success of generating frequency response measurements for an experimental modal test. One such structure was specifically designed to illustrate some of these difficult measurement situations for academic use. For this structure, it was clearly demonstrated that a single input, single output methodology did not produce measurements that were of sufficient quality for a modal test. Subsequently, a MIMO test was performed and some of the drive point and, in particular, reciprocal measurements were obtained to show the usefulness of the MIMO approach.

The structure is shown in Figure 4.63 and in reviewing the mode shapes it becomes very clear that there are some modes that are global in nature (and can be seen anywhere on the structure) but that there are also very local modes (where the mode shape response is localized to one or two components and not easily seen from every location on the structure). MIMO testing approaches are critical for these types of systems.

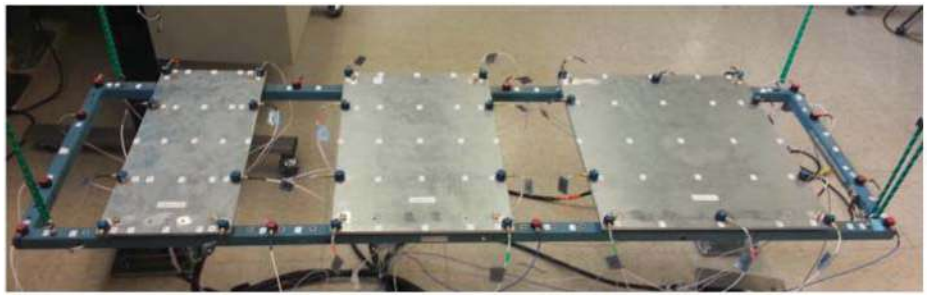

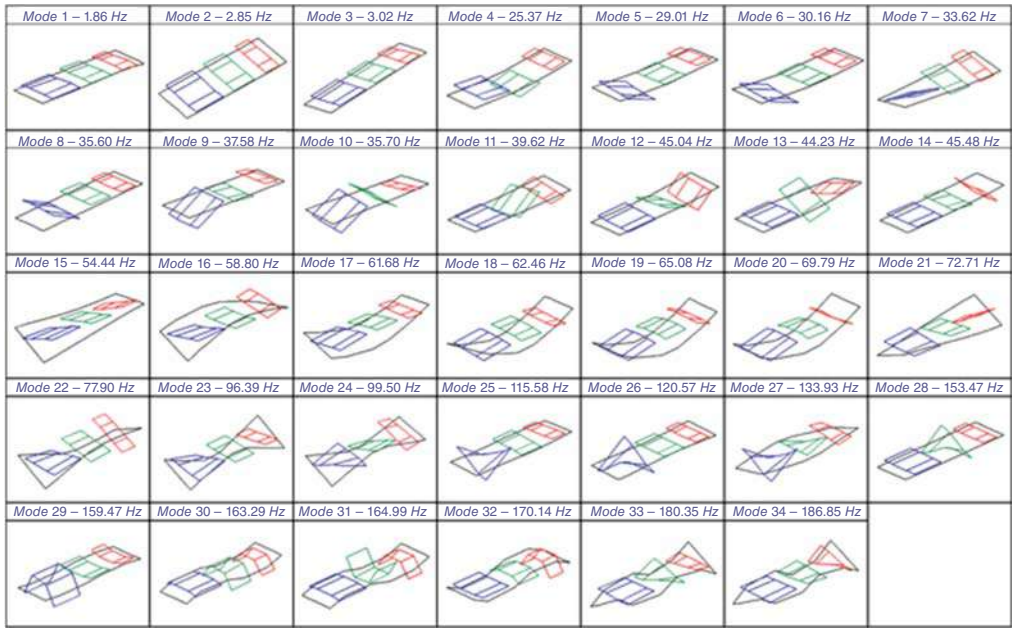

Figure 4.63 Frame structure with separate attached modally active components.

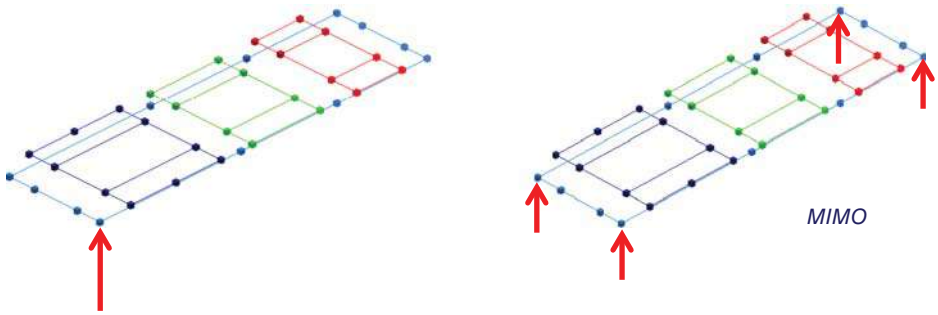

Figure 4.64 SISO and MIMO test setup configurations.

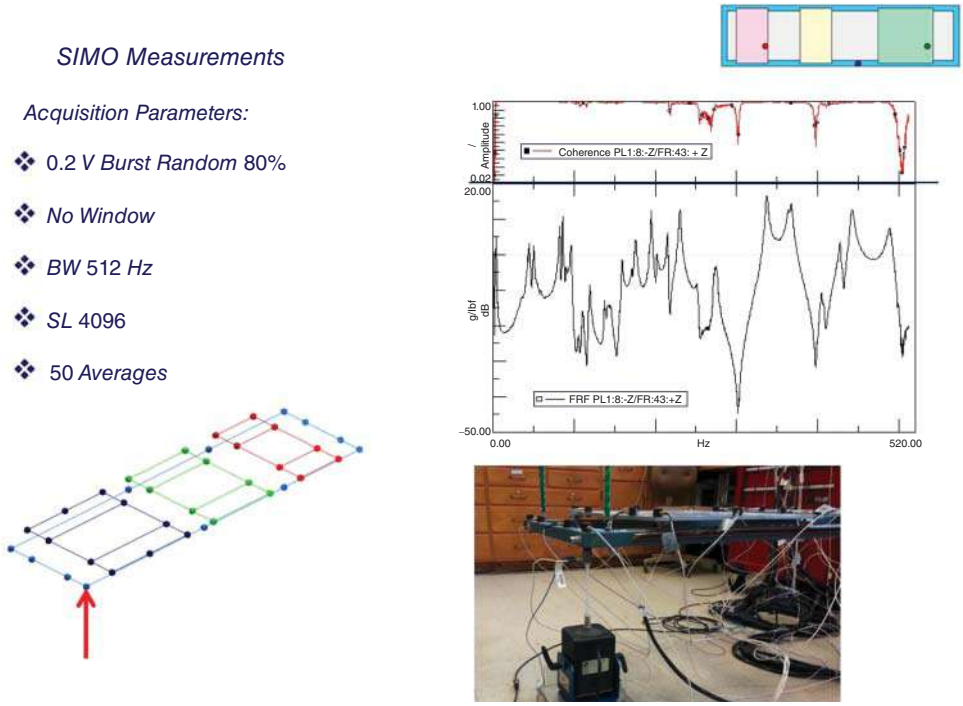

Figure 4.65 SISO test setup and results for one shaker location.

Figure 4.64 shows the typical setup for a SISO and MIMO test. There were 38 accelerometers mounted at all the measurement locations needed for the modal test. All testing was performed over a 512 Hz bandwidth with 4096 spectral lines. Only burst random excitation was utilized; previous studies with other excitation techniques clearly showed that burst random provided the best results overall. There were 50 averages taken and no windows were required because burst random excitation was used. Tests were conducted with SISO and MIMO configurations. The SISO tests were conducted with the shakers located at the four MIMO locations shown in Figure 4.64.

The SISO measurement is shown in Figure 4.65. Overall, the measurement looks good, with well-defined peaks in the frequency response function and a good coherence. This measurement is shown for reference; all four SISO tests had similar results. However, when the single shaker is moved from one reference location to another reference location, the resulting measurements show differences in the reciprocal frequency response functions from the SISO acquired data; this causes an inconsistency in the data when modal parameters are extracted from the data and makes the stability diagram difficult to interpret.

Figure 4.66 shows the MIMO test setup along with three separate reciprocal frequency response functions that were acquired from the MIMO test configuration. In each subplot, the reciprocal measurement is shown, noted by the arrows located on the structure. In all three measurements, the comparison of the reciprocal measurement is extremely good. This is attributed to the MIMO arrangement and data collection process. Clearly, the measurements are much better and more consistent when compared to the four separate SISO tests performed.

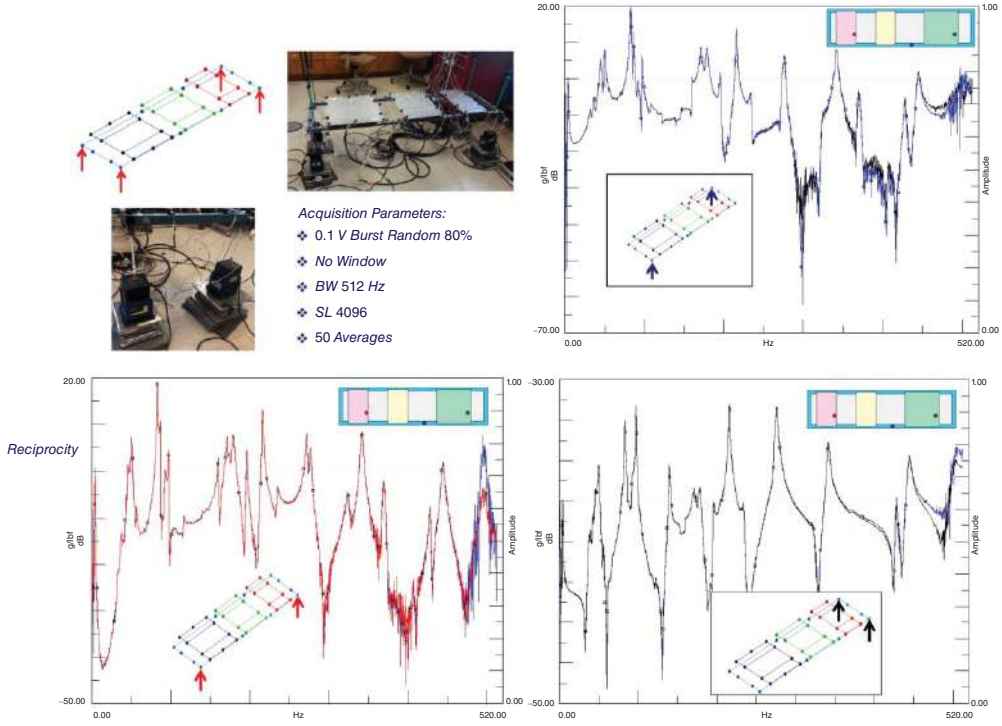

Figure 4.66 MIMO test setup and results for MIMO configuration.

4.6 Summary

Impact techniques for acquiring frequency response measurements were reviewed. All the basic considerations for hammer tip selection, useful frequency bandwidth, triggering and pre-trigger delay, force and response windows, and roving vs stationary hammer were all presented and discussed. An example structure was used to step through an entire impact test to illustrate the methodology needed to set up any impact test.

Shaker setup and shaker excitation techniques using a variety of different excitation signals were reviewed. All the commonly used (and some not so commonly used) excitations were presented, along with their strengths and shortcomings. Many of these techniques were shown and compared for a common structure.

Multiple input, multiple output testing techniques were also presented and used for a modal test structure to illustrate some of the additional measurements related to this type of testing.

5

Modal Parameter Estimation Techniques

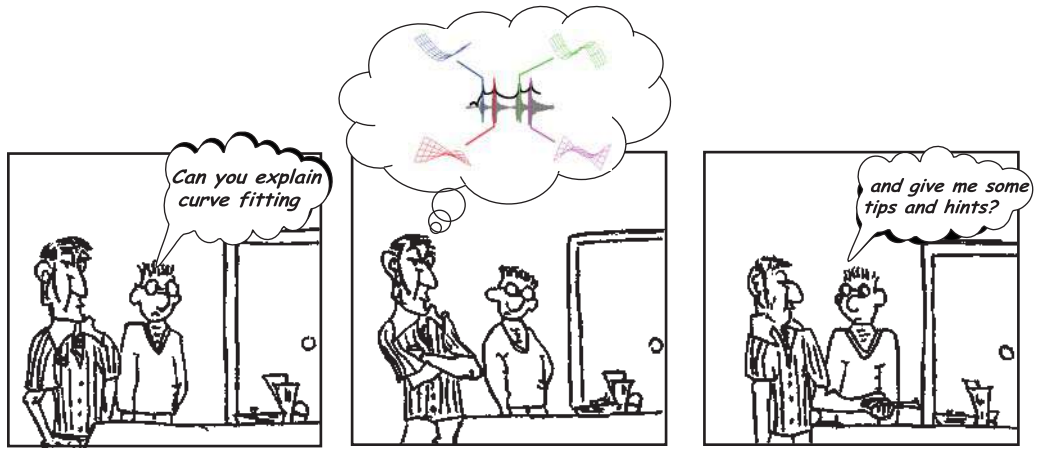

5.1 Introduction

From the development of general modal theory, it is clear that all that is needed in order to generate frequency response functions are the poles and residues of the system. It should be equally clear that if a point-to-point frequency response function is measured, then it should be possible to extract the system parameters of poles and residues from the measurement. The process of extracting this information is referred to as *modal parameter estimation*. Because a mathematical function expressing the frequency response function is used to fit the measured data to this relationship, the process is often referred to as *curvefitting*. The problem faced by the test engineer is the determination of the order of the model (number of modes) and the form of the model (time or frequency domain). These are not trivial problems, especially when the data collected is not perfect. In the following sections, some traditional approaches and definitions for estimating modal parameters will be addressed. The general theory of all of the modal parameter estimation approaches is far beyond the scope of this book. Here, the approaches will be discussed with a focus on the forms of the different methods and considerations when using different techniques. However, before any in-depth treatment of particular curvefitting techniques is performed, some simplistic concepts of least squares approximation of data will be discussed; this is followed by introduction of some rudimentary concepts to help readers understand the modal parameter estimation process. Then the commonly used techniques are described. A separate chapter addressing some of the practical aspects of extracting data is included to show some of the issues related to extraction of data.

Modal Testing: A Practitioner's Guide, First Edition. Peter Avitabile.

Companion Website: www.wiley.com/go/avitabile/modal-testing

5.2 Experimental Modal Analysis

5.2.1 Least Squares Approximation of Data

A least squares approximation for data, probably utilizing a linear relationship to characterize the dataset, is often used. Consider Figure 5.1, which shows some data collected for a force gage; actually any dataset could be considered, but here a simple force gage is used for illustration.

Assuming that there is no voltage when there is no force, then a straight line describing the force transducer must pass through zero. The dotted line in Figure 5.2 (left) shows the best possible straight line to fit the data (minimization of error on a least squares basis). However, looking at this straight line, there is a lot of variance between the measured data and the straight line describing the data and the confidence in the accuracy of the predicted line is not good. But the data doesn't seem to have a trend to pass through zero and that does not seem reasonable for this curvefit.

Now let's suppose that there is no restriction that the straight line pass through zero and fit the data again with the line shown in Figure 5.2 (middle). Notice that the resulting best fit line does not pass through zero and there is an offset from zero. This would assume that the force gage could actually have a load with no voltage reading; this could correspond to a preload situation, for instance. While this curve appears to better fit the data, there is still some significant variance between the data and the straight line. But some consideration needs to be given to the inclusion of all the data for the fit. Possibly, some of the force measured may be less than what the transducer can accurately measure and may be in the noise floor of the measurement.

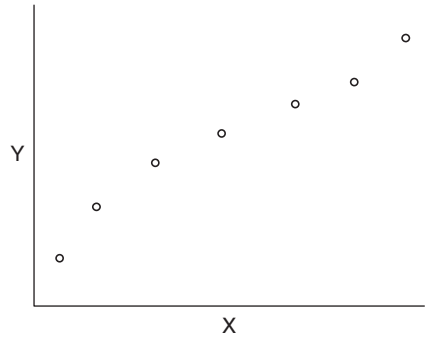

Figure 5.1 A typical set of data used for a least squares analysis.

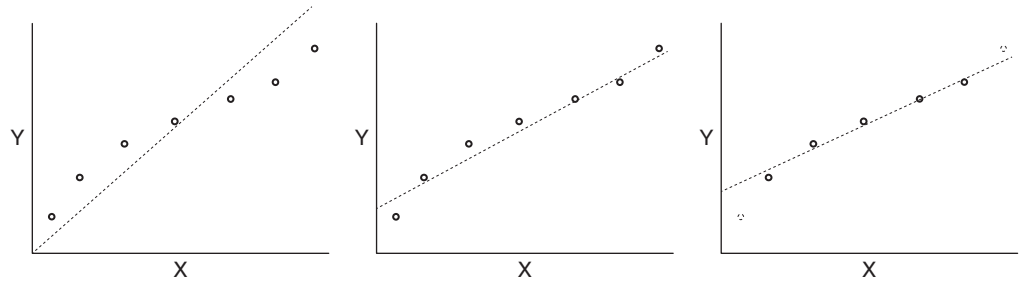

Figure 5.2 Straight line fit passing through zero (left), straight line fit with offset (middle) and straight line fit with some data removed (right).

Likewise, some of the force measured may be well above the range of the transducer and may be corrupt.

Now what if the fit were to exclude the lowest reading and the highest readings, as shown in Figure 5.2 (right)? Exclusion of these readings might be warranted if there were a minimum threshold voltage before a valid reading could be obtained, or if there were an upper limit of useful data obtained from the transducer. This curve seems to even better fit the measured data. Notice that three different straight lines have been obtained from this estimation process, all of which are approximations of the actual phenomenon. Exact answers are rarely obtained, but the analyst must be sure that the data used is representative of the phenomena expected.

In fact, there is no basis for an assumption that the line is a first order mathematical relationship. The data could possibly be better characterized with a higher order model to better describe the measured data. Notice that there is some discretion for the analyst to decide the order of the model, whether to allow for compensation for other effects, and which data points to include in the estimation process. These judgments result in very different approximations of the system to be characterized. This will also be the case in modal parameter estimation.

When performing modal parameter estimation, the analyst must decide on several items pertinent to the extraction of modal data from the measured frequency response function, as shown in Figure 5.3. The analyst must decide:

- the order of the model
- the amount of data to be used
- the need for compensation for residual effects.

The order of the model is very important in order to identify how many modes might exist in the frequency band selected. The amount of data to be used is identified when the cursor band is selected; these data points are included in the parameter estimation process. And the last item to specify is whether or not to include the effects of modes outside the band that have a contribution within the band for estimation.

And going back to the straight line fit for the force gage just discussed, the same steps were taken for the estimation of the line to fit the data. The analyst needs to decide on whether to

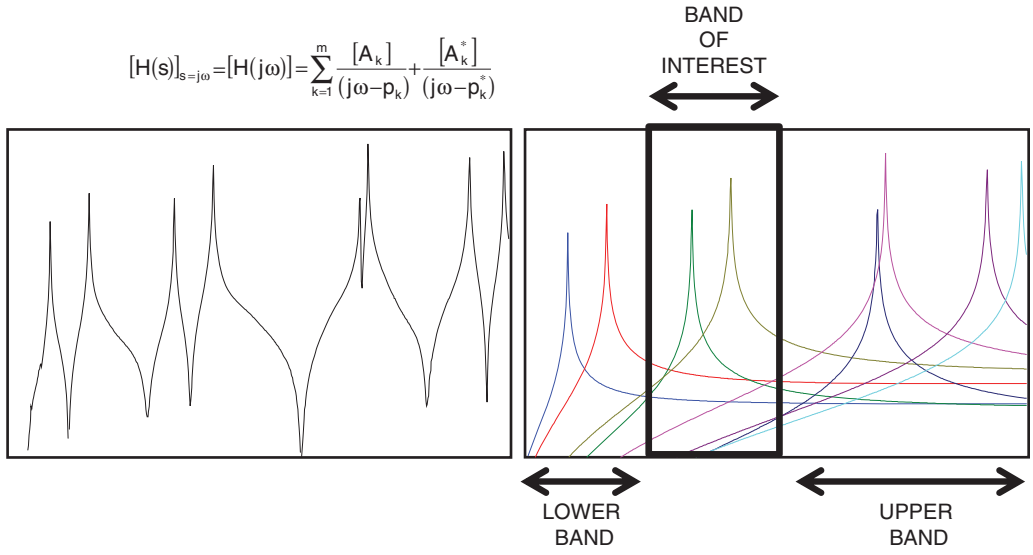

Figure 5.3 Illustration of curvefitting with band of interest and adjacent bands.

fit a straight line or polynomial to the data (the order of the model). They also need to define how much of the data to include (amount of data to be used). And they need to decide if any outside effects, such as an offset, need to be considered (compensation for residual effects). So the exact same steps used to least squares fit data are the same ones used in the modal parameter estimation process to extract modal parameters (except that the functions used to fit the data are more complicated).

This observation starts a discussion on several very basic concepts regarding individual modes, their overlap, and the relationship between them. The basic equation can be written in the frequency domain in partial fraction form as:

$$[H(s)]_{s=j\omega} = [H(j\omega)] = \sum_{-\infty}^{\infty} \frac{[A_k]}{(j\omega - p_k)} + \frac{[A_k^*]}{(j\omega - p_k^*)} \tag{5.1}$$

It is written here to include all modes of the system. For the discussion here, only one particular ij measurement is presented:

$$h_{ij}(s)_{s=j\omega} = h_{ij}(j\omega) = \sum_{-\infty}^{\infty} \frac{a_{ijk}}{(j\omega - p_k)} + \frac{a_{ijk}{}^*}{(j\omega - p_k^*)} \tag{5.2}$$

However, it is illustrative to break the function up into three pieces related to the bandwidth over which parameters are to be extracted (k = 1 to m) and then the lower band and upper band on either side of the band of interest as

$$\begin{aligned} h_{ij}(j\omega) = & \sum_{\text{lower band}} \frac{a_{ijk}}{(j\omega - p_k)} + \frac{a_{ijk}{}^*}{(j\omega - p_k^*)} \\ & + \sum_{k=1}^{m} \frac{a_{ijk}}{(j\omega - p_k)} + \frac{a_{ijk}{}^*}{(j\omega - p_k^*)} \\ & + \sum_{\text{upper band}} \frac{a_{ijk}}{(j\omega - p_k)} + \frac{a_{ijk}{}^*}{(j\omega - p_k^*)} \end{aligned} \tag{5.3}$$

This is illustrated in Figure 5.3, where the magnitude of the measurement is shown on the left (as measured) and the individual modal contributions are shown on the right, along with the three regions related to the equation. The equation describing the complete measurement is essentially the summation of all the modes but is broken down into these three distinct regions. Of course, when estimating modal parameters over the band of interest, the effects of the modes outside the band (below the band of interest and above the band of interest) do have an effect in the band of interest. In order to account for those modes outside the band, residual effects are often included. The modes below the band of interest essentially have a mass effect and the modes above the band of interest essentially have a stiffness effect. (These mass and stiffness effects were discussed in the theory section and were referred to as mass and stiffness lines when the single degree of freedom model was discussed.) These same effects are included here to account for the out of band effects of the other modes when attempting to identify modal parameters in the band of interest.

Now that the equation has been written in terms of these three bands, the equation can be used to introduce the residual terms:

- the mass effect of the lower order modes below the band of interest
- the stiffness effect of the higher order modes above the band of interest.

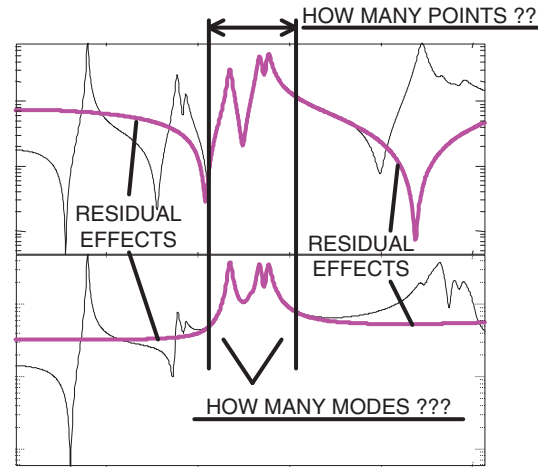

Figure 5.4 Typical FRF with selected band for estimation of parameters.

The equation to represent this is given as

$$h_{ij}(j\omega) = \text{lower residuals} + \sum_{k=1}^{m} \frac{a_{ijk}}{(j\omega - p_k)} + \frac{a_{ijk}^{*}}{(j\omega - p_k^{*})} + \text{upper residuals} \tag{5.4}$$

Figure 5.4 shows the band of interest along with the effects of the residuals. When fitting data in the band of interest, the effects of the out of band modes are important to the success of the fit in the band of interest. Typically, residual modes (not modal modes) are estimated as part of the process. These residual modes are important for the extraction of the modes in the band but they are also critical when synthesizing or recreating the measurement from the modal parameters selected. While all the commercial software packages include residuals as part of the curvefitting process, not all allow the residual modes estimated to be saved for future use along with the synthesis of the measurements from the modal parameters. This can cause a mismatch between the measured data and synthesized data from the measured parameters.

5.2.2 Classification of Modal Parameter Estimation Techniques

The basic theory for development of the modal model can be written in many different forms, but in essence all of the techniques are the same. Differences occur mainly due to less than perfect measured data.

In the most basic approximation, a frequency response measurement can be broken down into the modal components that make up the measurement derived from equivalent single degree of freedom systems. Therefore, it would stand to reason from an analytical standpoint that only a single degree of freedom approximation would be required. However, from a measurement standpoint, there may be significant modal overlap between two closely spaced modes, which would prevent the accurate extraction of modal parameters using a single degree of freedom technique. Therefore, often it is necessary to utilize a multiple degree of freedom model in order to extract valid parameters when the modes are closely spaced, with significant modal overlap. Thus, at a first level of approximation, there may be the need for both single degree of freedom curvefitters and multiple degree of freedom curvefitters in order to handle a range of situations.

Figure 5.5 is a plot of a 2DOF system with different types of modal overlap due to different reasons. The first plot shows well-separated, lightly damped modes. The second plot shows two lightly damped modes with coupling that is the result of the closeness of the modes to

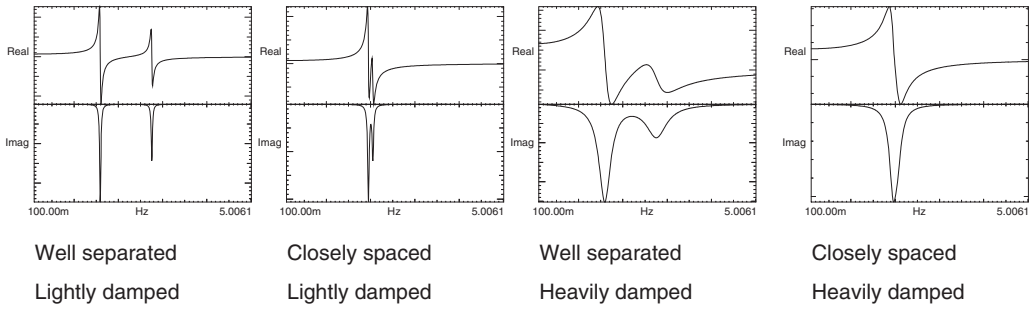

Figure 5.5 FRF for a 2DOF system with different damping and frequency closeness.

each other. The third plot shows two heavily damped modes with overlap that results from the damping on the system as opposed to the closeness of modes in the previous case. The fourth plot shows two heavily damped, closely spaced modes which could easily be misconstrued as a single degree of freedom system if the plot was not reviewed carefully. Now each of the four different cases shown in Figure 5.5 are discussed next, one at a time, with the actual measurement and the decomposed measurement showing each mode's contribution. In each case, mode 1 is in blue and mode 2 in red.

Figure 5.6 shows the frequency response measurement for the 2DOF system; as one measurement on the left and then with the measurement broken down by the contribution of each mode on the right, allowing us to understand the relationship between the two modes in the frequency domain plot. Notice that the two modes are well separated and each is clearly defined and separate from the other. Notice that the imaginary part of the measurement for mode 1 starts at zero, rises to a peak, and then comes back to zero before there is any indication of mode 2. And similarly for mode 2, the imaginary part of the measurement starts to rise from zero well after the mode 1 response, reaches a peak, and then returns to zero. There is no real overlap of these two modes at all. In this case, a single degree of freedom curvefit of the data can easily be performed due to the separation between the two modes.

Figure 5.7 shows the frequency response measurement for the 2DOF system, as one measurement on the left and then with the measurement broken down by the contribution of each mode on the right, to enable us to understand the relationship between the two modes in the frequency domain plot. For this measurement, each mode has the same damping as the previous case but the frequencies are closer to each other. Immediately upon reviewing the imaginary

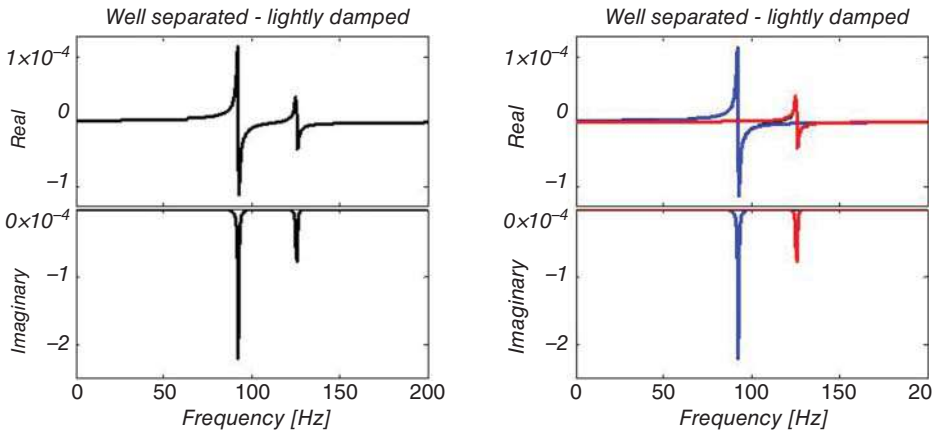

Figure 5.6 FRF for a 2DOF system: well separated and lightly damped.

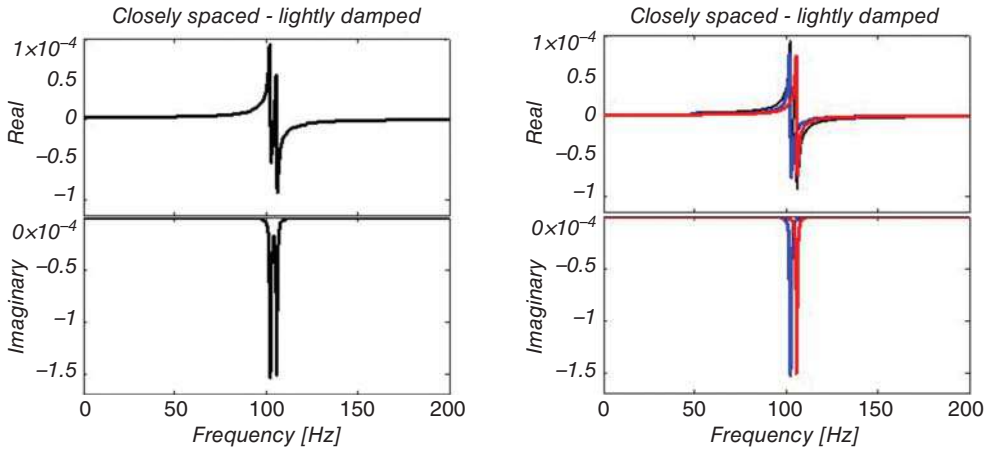

Figure 5.7 FRF for a 2DOF system: closely separated and lightly damped.

part of the measurement, the measurement is seen to have an overlap between mode 1 and mode 2. There is clearly overlap in the measurement. In this case, a single degree of freedom curvefit can be attempted, carefully selecting the cursor bands, but the reality is that a multiple degree of freedom curvefit with two modes specified as the order of the model may provide a better approximation for the fit. Substantiating a single degree of freedom model to fit this data is difficult.

Figure 5.8 shows the frequency response measurement for the 2DOF system; as one measurement on the left and then with the measurement broken down by the contribution of each mode on the right, as done in the previous cases. The frequencies have the same separation as the first case but the damping for each mode was increased to highlight modal overlap. Now in this case the modes are separated from a frequency standpoint, but there is modal overlap because the damping is much higher than in the previous case. The plot on the left clearly shows the overlap in the measurement and the plot on the right shows the significant modal overlap of mode 1 and mode 2. In this case, a single degree of freedom can be used to try to estimate parameters but due to the modal overlap a multiple degree of freedom curvefit may ultimately be needed to extract valid parameters. A comparison of the two different approaches is highly recommended, so as to determine if significant differences exist.

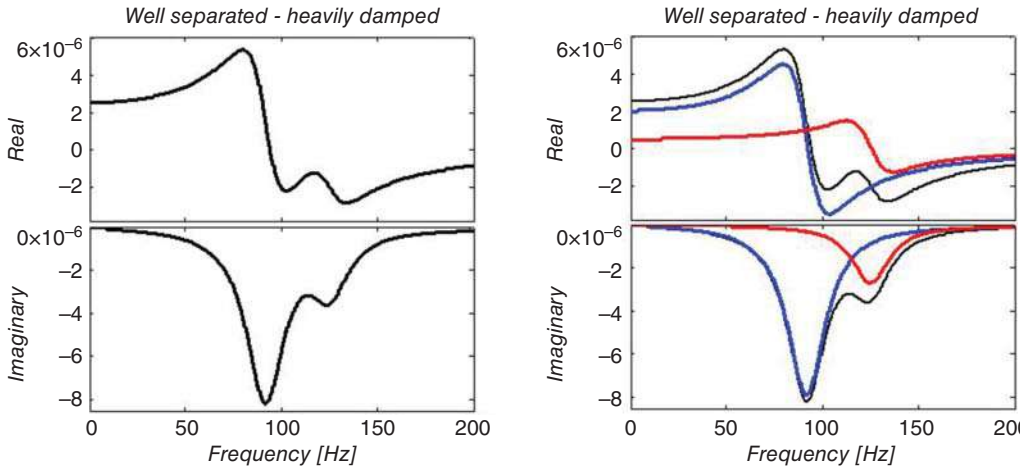

Figure 5.8 FRF for a 2DOF system: well separated and heavily damped.

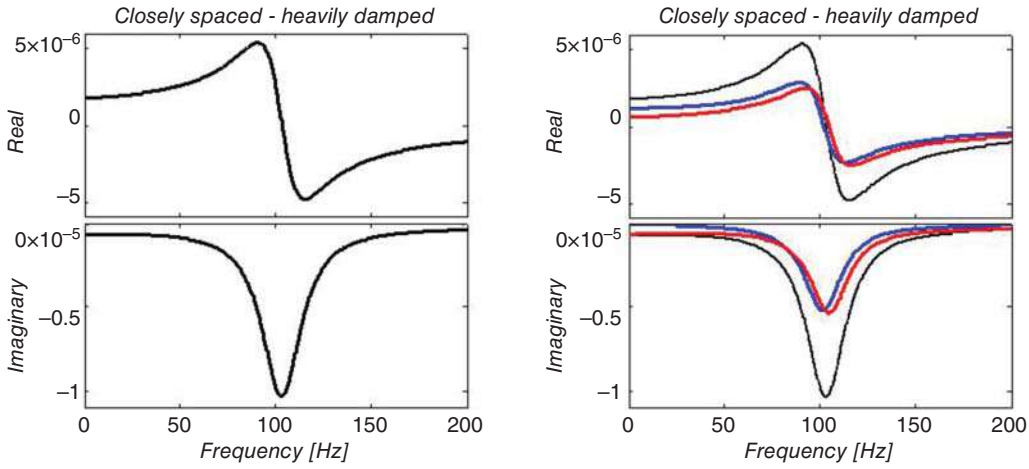

Figure 5.9 FRF for a 2DOF system: closely separated and heavily damped.

Figure 5.9 shows the frequency response measurement for the 2DOF system; as one measurement on the left and then with the measurement broken down by the contribution of each mode on the right, as done in the previous cases. The frequencies have the closeness of the second case, along with the heavy damping of the third case. Now the significant damping and closeness have brought the measurement to the point where it is difficult to tell that there are two modes in the measurement. Now this case is very interesting because there appears to only be one mode. So what if, when curvefitting, only one mode was specified for the order of the model? In this case, only one mode would result from the parameter estimation process; the results would likely be some average of the two modes in that band.

Now what if two modes were specified for the cursor band when curvefitting? The modal parameter estimation process would produce two modes and would likely produce two accurate residues. This data has been used with most of the commercially available curvefitters and generally all of them produce good results *if and only if* two modes are selected for the band; that is critical because the curvefitters cannot guess for the analyst how many modes are in the band. The bottom line here is that the modal parameter estimation algorithms *can* extract valid data from this type of measurement *if* the data measurement is done well. The curvefitters are generally not the problem. Generally, the measurements collected are not accurate enough or contain too much variance and noise to enable valid parameters to be extracted.

The next consideration would be whether to fit the data in the time domain or the frequency domain. Because the equations can be cast in either domain, the modal parameter estimation phase can be carried out in either domain. When using the time domain, the equations can be represented as a damped, exponentially decaying, sinusoidal response. When using the frequency domain, the equations may be cast in partial fraction form, pole-zero form, polynomial form, or some other equivalent form. Both domains are depicted in Figure 5.10. Basically, the equations will be cast into a form that offers some numerical advantage or mathematical "gimmick" that will enable the equations to be processed more efficiently or with greater speed. In both representations of the single degree of freedom system, the system time or frequency characteristic can be defined by the pole and residue of the system, regardless of the domain in which it is presented. And given infinite resolution in the frequency domain, time domain, and amplitude, there is no difference in either form of the data; with infinite resolution the parameters will be extracted equally well in either domain. But as a general rule, very lightly

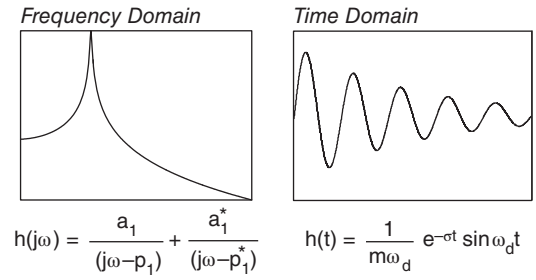

Figure 5.10 Frequency domain representation (left) and time domain representation (right).

damped systems may be best represented in the time domain whereas more heavily damped systems may be better represented in the frequency domain.

Additionally, the measured frequency response data can be measured one measurement at a time, or one column of data at a time, or several columns of data at a time, depending on how it is acquired. The data can also be reduced in the same manner: one measurement at a time, or one column at a time, or multiple columns at a time. These are referred to as *local*, *global* or *polyreference* curvefitting, respectively. Each is briefly described next. Local curvefitting was mainly done in the early days of modal testing and is rarely, if ever, used today. Today global curvefitting and polyreference curvefitting dominate in the modal testing community, but these techniques impose a significant requirement, namely that the data must be collected in a very consistent manner due to the way the data is reduced.

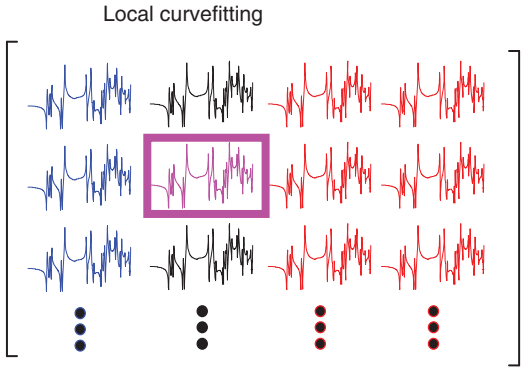

In *local curvefitting*, the poles and residues are extracted for each measurement independent of other measurements in the frequency response matrix. This is shown in the frequency response matrix on the left. This is useful when the frequency and damping are not constant from one measurement to the next.

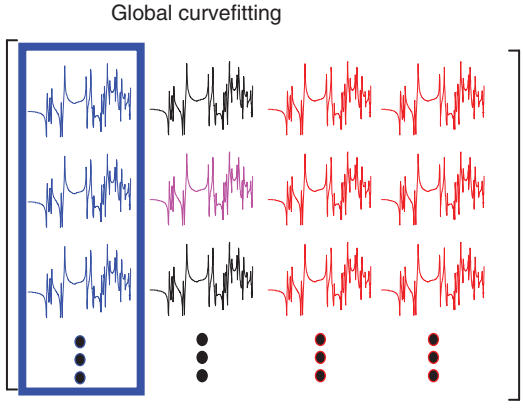

In *global curvefitting*, an estimate is made of the poles from a global standpoint using all or a selected set of measurements that are available from a single row or column of the frequency response matrix as shown on the left. The residues are then extracted in a second pass using the fixed global poles found in the first pass.

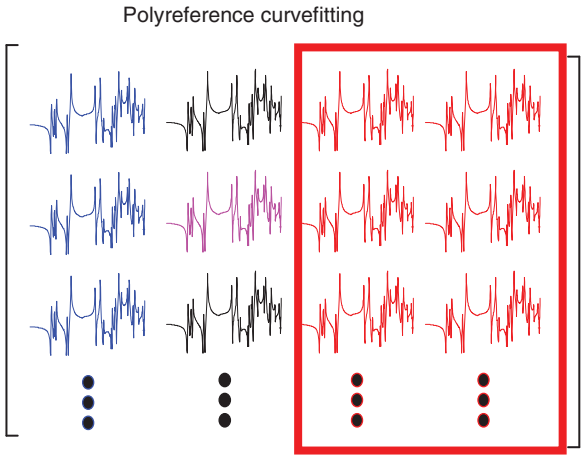

In *polyreference curvefitting*, an estimate is made of the poles from a global standpoint using all or a selected set of measurements that are available from a multiple rows or columns of the frequency response matrix as shown on the left. The residues are then extracted in a second pass using the fixed global poles found in the first pass.

5.3 Extraction of Modal Parameters

With some of the basic terminology defined above, some of the more elementary techniques for estimation of parameters will now be addressed, after which commonly used approaches will be outlined. Note that only summary equations and concepts are included here; detailed theoretical developments are beyond the scope of this book. The interested reader should look to published papers for specific details of each of the commonly used techniques.

5.3.1 Peak Picking Technique

One of the first parameter estimation techniques developed involved the use of peak picking to obtain a rough estimate of the residue of the system. Providing there is sufficient separation between the modes of the system, this provides a reasonably good estimate of the residue of the system. The frequency is determined by the location of the peak and the damping is estimated by the half power method. If the frequency response function is evaluated at the natural frequency of the system, the residue can be approximated for a single degree of freedom system by:

$$h(j\omega)\,|_{\omega\to\omega_n} = \frac{a_1}{(j\omega_n + \sigma - j\omega_d)} + \frac{a_1^*}{(j\omega_n + \sigma + j\omega_d)} \tag{5.5}$$

Because the damped natural frequency and natural frequency are approximately equal for lightly damped systems, the residue can be approximated by

$$a_1 = \sigma\, h(j\omega)\,|_{\omega\to\omega_n} \tag{5.6}$$

Basically this implies that the peak of the frequency response function is directly related to the residue (to within a scale constant of the damping of the system). The peak picking process is shown schematically in Figure 5.11. If all the points on the structure are evaluated, then a good estimate of the shape can be obtained as a first pass on the data. While peak picking is not the most accurate approach by any means, a good overall depiction of the shape can be made. Often, the approach is very useful to identify misplaced sensors or sensors that are incorrectly oriented. At times, an abbreviated set of points can be measured and the shape quickly identified

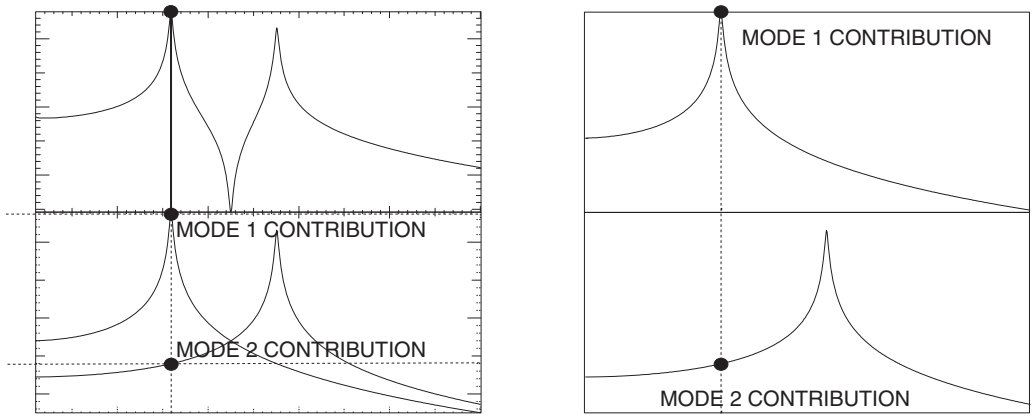

Figure 5.11 Schematic showing peak picking technique.

with peak picking before a more complete set of points is measured and a more complete data reduction performed.

5.3.2 Circle Fitting – Kennedy and Pancu

For lightly damped, well-separated modes, a single degree of freedom approximation is accurate. If the frequency response function is cast in complex form, then in the complex plane (Nyquist plane), the frequency response function appears as a circle, as shown in Figure 5.12; this is the same plot as in the theory section, where response measurements were introduced. In this form, the equation of a circle can be used in a least squares fashion to extract the parameters of interest, namely the pole and residue. The frequency is found to be bounded by the two data points which have the widest separation when displayed in the Nyquist plot. The damping

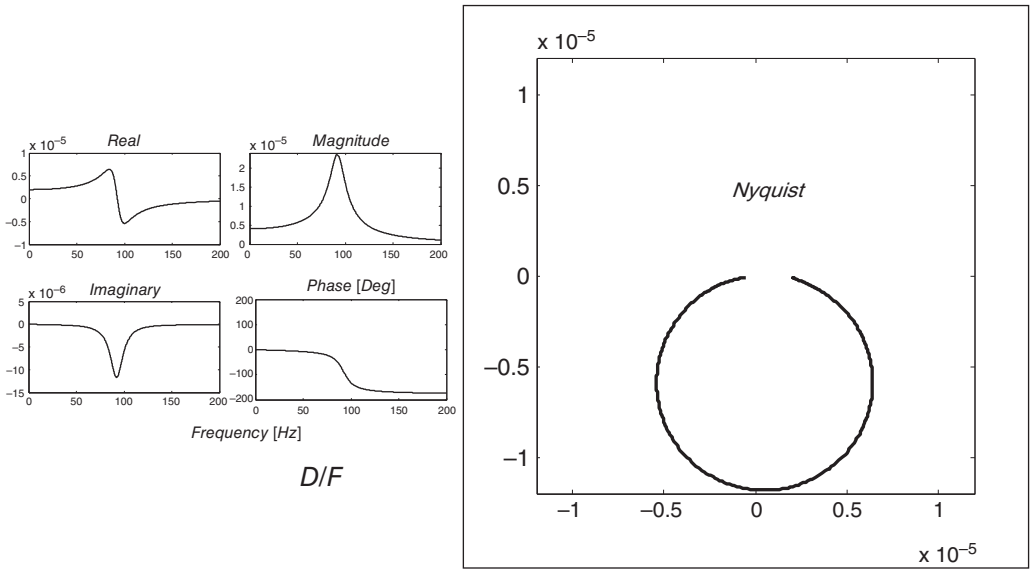

Figure 5.12 Schematic showing circular representation in the Nyquist plot (right) for SDOF system.

of the system can be determined by the half power point method. The residue can be approximated by the diameter of the circle, a_{ij}. The circle fit was one of the first mathematical extraction techniques developed due to the simplicity of the equation for a circle. Extensions of the circle fit can be made to account for overlap from adjacent modes, as well as complex mode characteristics. While the circle fit is simple, this approach is not often used in modal tests because generally there is a closeness of modes that renders the circle fit unsuitable for most systems.

5.3.3 SDOF Polynomial

An extension of the circle fit technique is the single degree of freedom polynomial frequency domain approach. This is used to estimate parameters using

$$h(s) = \frac{1}{ms^2 + cs + k} \quad \text{or} \quad h(j\omega) = \frac{1}{m(j\omega)^2 + c(j\omega) + k} \tag{5.7}$$

With this technique, the parameters to extract are the pole and residue. This approximation for the SDOF system is shown schematically in Figure 5.13.

5.3.4 Residual Effects of Out of Band Modes

The residual effects of other adjacent modes can be included in the model as a mass effect of the lower modes and as a stiffness effect due to the higher modes:

$$h(j\omega) = \frac{1}{m\omega^2} + \frac{1}{m(j\omega)^2 + c(j\omega) + k} + \frac{1}{k} \tag{5.8}$$

The curvefitting with residual effects is best illustrated in Figure 5.14. The full equation describing the frequency response is shown in the upper portion of the figure with the contribution of each mode over the entire frequency range. However, when parameters are estimated, only the band of interest is used to estimate parameters. In this illustration, mode 2 in red is the mode of interest but there is an out of band effect of mode 1 (in blue) and mode 3 (in green). Recall from single degree of freedom theory that the portion of the response below that of the resonance is considered as a stiffness effect and the portion of the response above that of the resonance is considered a mass effect. So, over the band of interest shown in the lower portion of the figure, the effects of mode 1 (in blue) over the band where mode 2

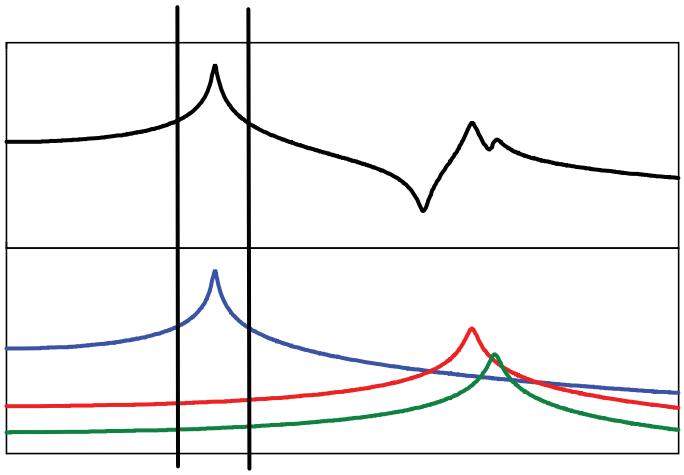

Figure 5.13 Schematic showing curvefit for an SDOF system.

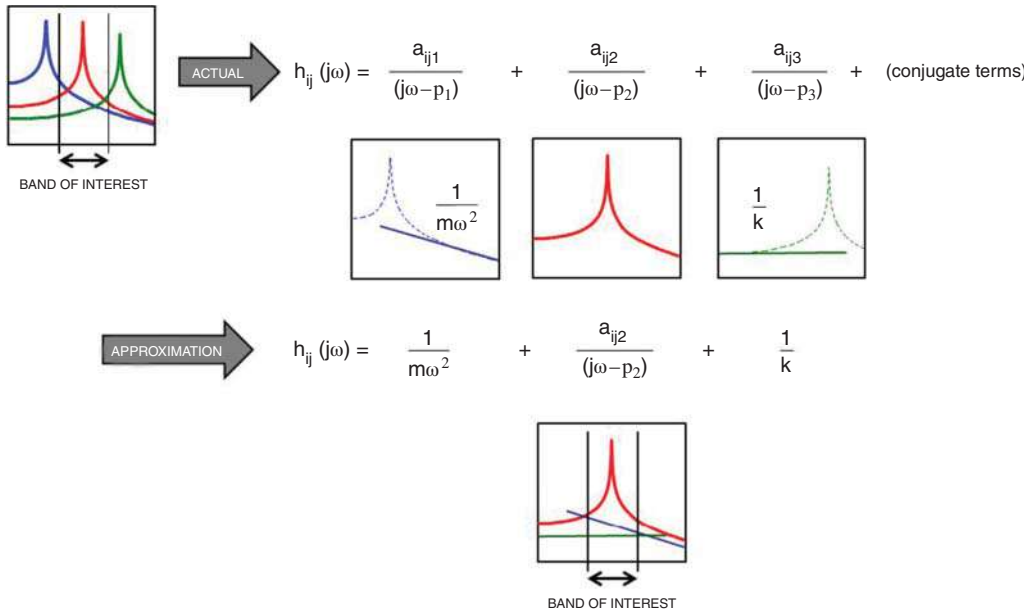

Figure 5.14 Schematic showing mass and stiffness residual effects used for curvefitting.

is predominant, are primarily a mass effect whereas the effects of mode 3 are predominantly a stiffness effect. So the effects of out of band modes can be easily handled with these simple effects. However, this is just an approximation and the closer the modes are to each other, the less accurate this approximation becomes.

5.3.5 MDOF Polynomial

An extension of the SDOF polynomial technique was developed to handle more than one mode. Early work used a variety of different forms of the equation involved in order to handle numerical issues; this results from the wide dynamic range of numbers due to the power associated with the polynomial terms. In its simplest form, the equation can be written in partial fraction form as:

$$h_{ij}(j\omega) = \frac{a_{ij2}}{(j\omega - p_2)} + \frac{a^*_{ij2}}{(j\omega - p^*_2)} + \frac{a_{ij3}}{(j\omega - p_3)} + \frac{a^*_{ij3}}{(j\omega - p^*_3)} \tag{5.9}$$

where only two modes (modes 2 and 3 in this example) are shown in Figure 5.15; residual terms can also be added to this equation if needed.

Obviously, this equation can be extended to deal with a number of modes over a variety of different bands. Variations of this polynomial equation have been created and the most popular is the rational fraction polynomial, which is cast in polynomial form in both the numerator and denominator. This technique generally works best with only a few modes in the band of interest. The method uses orthogonal polynomials to better condition the numerical processing of the data. This is a very popular approach, which is still widely used for estimating modal parameters in commercially available software packages.

5.3.6 Least Squares Complex Exponential

One very popular approach uses time domain data in the form of the damped exponentially decaying sinusoidal response for a system. This was one of the original time domain techniques,

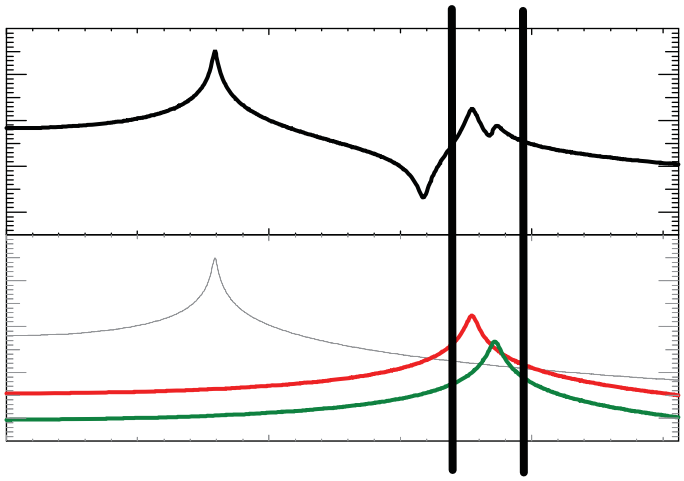

Figure 5.15 Schematic showing curvefit for an MDOF system.

which used only time response measurements. Time data was captured and was decomposed to extract modal parameters. The *least squares complex exponential* can be written as

$$h(t) = \sum_{k=1}^{m} \frac{1}{m_k \omega_{dk}} e^{-\sigma k t} \sin \omega_{dk} t \tag{5.10}$$

This equation was adopted by the modal community in a slightly different form. Because frequency response measurements are typically collected, the measured frequency data had to be inverse Fourier transformed to obtain time data for the approach. Figure 5.16 schematically shows the transform from the frequency to time domain to utilize this approach.

The transform essentially provides time data for the least squares complex exponential modal parameter estimation procedure, and the equation can be written in summation form as

$$h(t) = \frac{1}{m_1 \omega_{d1}} e^{-\sigma l t} \sin \omega_{dl} t + \frac{1}{m_2 \omega_{d2}} e^{-\sigma 2 t} \sin \omega_{d2} t + \frac{1}{m_3 \omega_{d3}} e^{-\sigma 3 t} \sin \omega_{d3} t + \ldots \tag{5.11}$$

Normally, the complex exponential is written in exponential form. In this form, with sampled data, the solution can be written as linear finite difference equations with constant real coefficients of order 2m. The resulting characteristic equation can be solved using a least squares approach for the highly overdetermined set of equations. In the process of manipulating the equations into normal form, a compact coefficient matrix, the *covariant matrix*, is formed; the rank of this matrix is used to determine the number of modes using a *least squares error chart* or *singular values diagram*.

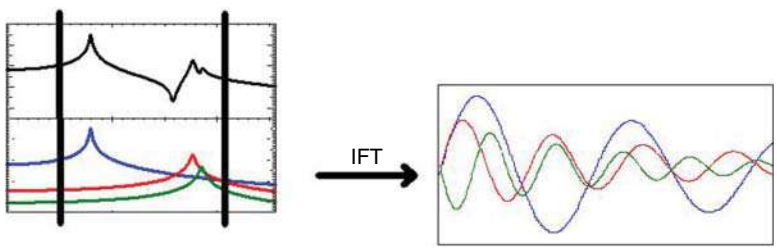

Figure 5.16 Transform of FRF measurement to obtain equivalent time domain data.

This approach was one of the first multiple degree of freedom techniques that was used in the early days of modal testing and it is still used today in several of the different curvefitting techniques. The approach uses the Prony algorithm to solve the set of equations. The Toeplitz equations are used to form the characteristic polynomial after which mode shape extraction takes place using the Vandemonde equation formulation.

The technique is numerically fast and stable, as opposed to frequency domain techniques, which can suffer from numerical issues. It can generally handle many modes. In contrast to frequency domain techniques, time domain techniques cannot include residual terms and for the numerical procedure to perform properly, additional modes need to be specified in the numerical process; these extra modes must be sifted from the true poles of the system. One other difficulty in the early days of modal analysis was that the inverse Fourier transform needed to be performed with data that had the number of points specified to be a power of 2. At times, the inverse transform could contain time domain leakage, which had an effect on the results. However, with faster computers today, a DFT can be used and reduces this time domain leakage effect.

5.3.7 Advanced Forms of Time and Frequency Domain Estimators

The modal parameter estimation techniques presented above help to put some of the simple concepts into context and are the underlying basis of the more advanced techniques deployed today in commercially available software packages. Understanding these basics helps readers to understand the more advanced techniques without getting too deeply involved in the math and theoretical development. There is a large body of research and papers that expound on these techniques for the interested reader.

5.3.8 General Time Domain Techniques

Other time domain techniques exist that extend the complex exponential described above. Techniques such as the Ibrahim time domain and the polyreference least squares complex exponential utilize variants of the impulse response equation:

$$[h(t)] = [V]\begin{bmatrix} \ddots & & \\ & e^{\Lambda t} & \\ & & \ddots \end{bmatrix}[L] \tag{5.12}$$

In general, these techniques provide global parameters for the poles of the system and can use either single reference or multiple reference data for the estimation process. This equation has the same basic information as the least squares complex exponential approach and all the same issues discussed above are applicable to it.

5.3.9 General Frequency Domain Techniques

Other frequency domain techniques exist that extend the polynomial techniques described above. Techniques such as least squares frequency domain, orthogonal polynomial, frequency domain parameter identification utilize some variant of the rational fraction, partial fraction, or reduced equation of motion to formulate the problem. The basic equation can be given as:

$$[h_{ij}(j\omega)] = \sum_{k=1}^{m}\left[\frac{u_{ik}L_{kj}}{(j\omega - p_k)} + *\right] + UR_{ij} + \frac{LR_{ij}}{\omega^2} \tag{5.13}$$

This is essentially the same equation written in partial fraction form, with upper and lower residuals to compensate for out of band effects. Notice that the equation is written in terms of

mode shapes rather than residues (and this is essentially equivalent to that discussed in the theory section of the book). But another thing to notice is that residue in the numerator is written in a slightly different form. However, it is equivalent to the equation in the theory section except that the value of the reference mode shape and the q scaling constant are grouped together to form a new term, which is called the *modal participation factor*:

$$u_{ik}L_{jk} = q_k u_{ik} u_{jk} = u_{ik}(q_k u_{jk}) \tag{5.14}$$

The modal participation factors identify the strengths of each reference relative to each other.

Due to the nature of the higher order polynomials used in the process, the equations may suffer from ill-conditioning. Many different classes of orthogonal polynomials are used to better condition the numerical processing.

5.3.10 General Consideration for Time vs Frequency Representation

Some of the basic differences between the time and frequency domain curvefitters can be best understood by writing the time and frequency equations that are generic to each.

The time domain representation consists of impulse response functions and the order (or power) is first order for all of the terms used to describe the set of equations:

$$h_{ij(n)}(t) + a_1 h_{ij(n-1)}(t) + \cdots + a_{2n} h_{ij\ (n-2N)}(t) = 0 \tag{5.15}$$

In the frequency domain representation, all the terms describing the set of equations are raised to a power and this can cause a very wide dynamic range, which has a direct effect on the numerical processing of the data.

$$[(j\omega)^{2N} + a_1(j\omega)^{2N-1} + \cdots + a_{2N}]h_{ij}(j\omega) = [(j\omega)^{2M} + b_1(j\omega)^{2M-1} + \cdots + b_{2M}] \tag{5.16}$$

So in looking at these equations, the numerical issues and dynamic range of the frequency domain techniques are easier to understand. The frequencies are raised to a power of 2N, so for a wide band with many modes, the terms become very large and cause difficulties when numerically processing the data; numerical conditioning of the equations is necessary and different curvefitters deploy different methods to do this. While the time domain techniques do not have this complication, the inclusion of residual effects is not possible as it is with frequency domain techniques.

5.3.11 Additional Remarks on Modal Parameter Estimation

While the approach is commonly called "curvefitting", a better expression is "modal parameter estimation". Curvefitting generally involves some system identification and arbitrary polynomials can be used to fit data. This is different to what is done in modal parameter estimation. There is a basic assumption that the equations to describe the system can be written from a second order differential equation (or a Laplace transform). The basic characteristics can be written in terms of the poles and residues (or frequency, damping, and mode shape) that come from a modal space approximation in which all of the modes can be written as separate/individual contributions to the measured response function, while assuming a linear, time invariant set of equations. Therefore, the use of either a single degree of freedom approximation or a multiple degree of freedom approximation, either in the time or frequency domain, is a very good approximation of the measured system response. This is best characterized in the schematic shown in Figure 5.17. The equations can be written in partial fraction form (or any manipulation) with the poles and residues, or they can be written as mode shapes (instead of residues). The poles define the frequency and damping for the system. When written in mode shape form, the amplitude of the response function is directly related to the value of the mode shape at the

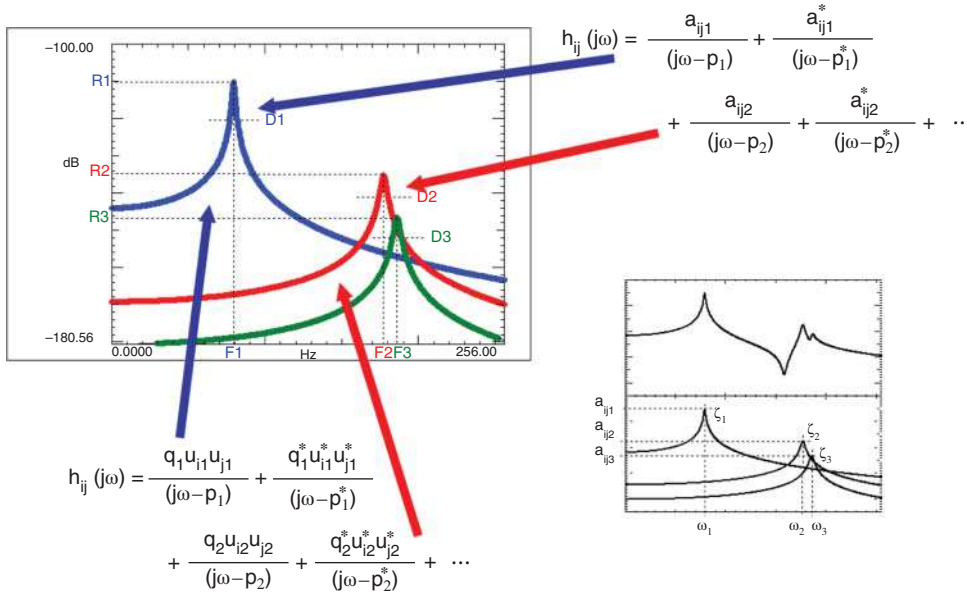

Figure 5.17 FRF broken down by mode, showing FRF both in residue equation form and shape equation form.

input location multiplied by the value of the mode shape at the output location, for each mode of the system. The goal of the modal parameter estimation process is to extract the poles and the residues (or the mode shapes) from this measured data using the equation that describes the second order differential equation from a linear time invariant system.

5.3.12 Two Step Process for Modal Parameter Estimation

The commonly used approach for estimating modal parameters today, is a two step process. In the first step, the set of measurements is used to obtain the poles for the system. Once the pole has been identified, then this pole is used in the equation as a fixed or global quantity for the system. The theory indicates that there is one value that represents the pole for the frequency response equation, and this value is independent to the particular input–output measurement location. So it stands to reason that this pole value should be estimated first and its value then locked. In the second pass, using the pole identified in the frequency response equation, the residues are evaluated, giving the mode shapes from the measurements. Of course, the implication here is that the pole really does need to be a global quantity for each of the modes from the measured data. This then places a very strict requirement that the measured data should be acquired in a manner that will capture this effect. This is the approach taken in essentially all the commercially available software today.

The main approaches commonly used today for a traditional experimental modal analysis are:

- time domain complex exponential
- polyreference time domain
- rational fraction polynomial
- orthogonal rational fraction polynomial
- polyreference frequency domain.

5.4 Mode Identification Tools

Modal parameter estimation is not always an easy task, especially when the data measured is not the best possible data. Measured data of the highest quality is always highly recommended. But even with the best of data, sometimes the task of identifying modes can be difficult, especially when there are closely spaced modes or complicated responses with many modes over tight bandwidths. Several tools exist to facilitate the identification of modes in the data. The summation function, multivariate mode indicator function, complex mode indicator function and the stability (or consistency) diagram are commonly used tools. These are discussed next, and then the tools to validate the parameters extracted from the data.

5.4.1 Summation Function

In terms of determining the number of poles to extract from the measured data, several indicator functions exist. The first approach is to review the measured frequency response functions and look for peaks in the measured data. However, the presence of closely spaced or repeated roots makes this difficult.

A summation of all the measured frequency response functions, referred to as the *enhanced frequency response function* or *summation function*, will tend to accentuate modal peaks that exist in the data. However, closely spaced or repeated roots will tend to add to the power of the summation function, thereby meaning this tool is only useful when the modes are spaced reasonably far apart. The summation function is shown in Figure 5.18.

5.4.2 Mode Indicator Function

Another function is referred to as the *mode indicator function* (MIF) and can be expressed in terms of the real and imaginary parts of the frequency response function:

$$\text{MIF} = \frac{F^T H_R^T H_R F}{F(H_R^T H_R + H_I^T H_I)F} \tag{5.17}$$

This function can be used with multiple referenced datasets and there will be one MIF for each of the references included in the dataset; if only one reference exists, then there will only be one MIF. Dips in this function are indicators that a mode exists at that frequency. The MIF has a much sharper and more discerning indication of modes than the summation function.

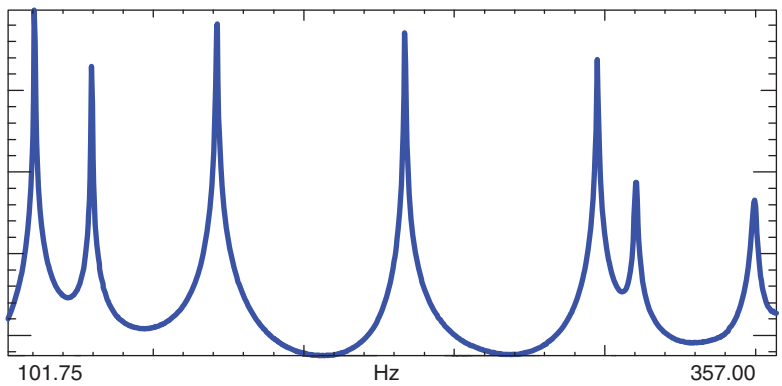

Figure 5.18 Summation function showing several peaks over a limited bandwidth.

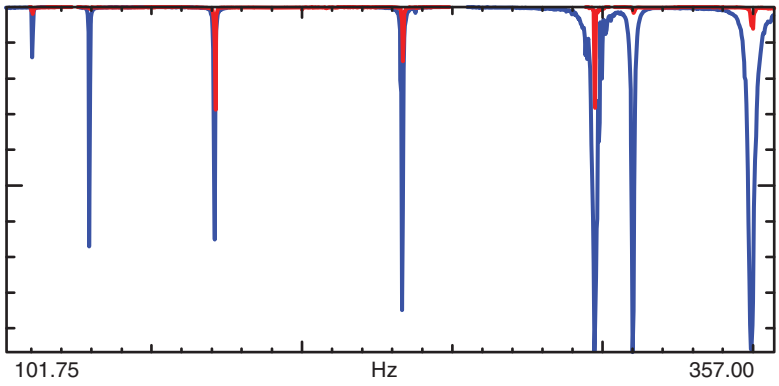

Figure 5.19 MMIF showing several dips over a limited bandwidth with primary MIF in blue and secondary MIF in red.

This is because the formulation uses the real part of the measured response; the real part of the frequency response function exhibits a very rapid change in the region of the resonance.

If multiple references exist, there with be several MIFs and the function is referred to as the *multivariate mode indicator function* (MMIF) The primary MIF will have minima at each of the structural natural frequencies. The secondary and other MIFs will only have minima in the case of repeated or pseudo-repeated roots. A higher MIF will not have a dip at a frequency unless the primary MIF has a dip. Figure 5.19 shows a MMIF with two references, so that there are two MIFs; notice that the secondary MIF has a several dips where the primary MIF also has a dip at the same frequency, indicating that there are potentially two modes at that frequency.

The MMIF is a much more accurate tool for indication of modes. However, the assumption is that the real part of the frequency response function is zero at resonance. If the measurements have some distortion or if there is some phase information in the measurements (associated with non-real normal or complex modes) then the MMIF may not be able to accurately identify the modes accurately.

5.4.3 Complex Mode Indicator Function

Another function referred to as the *complex mode indicator function* (CMIF) is determined by the singular value decomposition of the frequency response matrix and is given as

$$[H] = [U]\begin{bmatrix} \ddots & & \\ & S & \\ & & \ddots \end{bmatrix}[V^h] \tag{5.18}$$

The CMIF is a plot of the singular values at each frequency line and will rise to a peak where there is a mode of the system. There will be one curve for each reference that is included in the frequency response matrix. The first or primary CMIF will rise to a peak for each mode in the system; repeated roots or pseudo-repeated roots can be observed in the secondary and higher CMIF curves. Figure 5.20 shows a CMIF for a set of data where there is repeatedness, or very closely spaced modes. These are indicated by the arrows in the figure. There is sometimes confusion when the second or higher CMIF appears to have a peak, but is not at one of the frequencies where the first CMIF has risen to a peak; these are not an indication of a mode and are a numerical result of what is called the crossover frequency, which is further discussed in Part 2 of this book, on the practical application of these techniques.

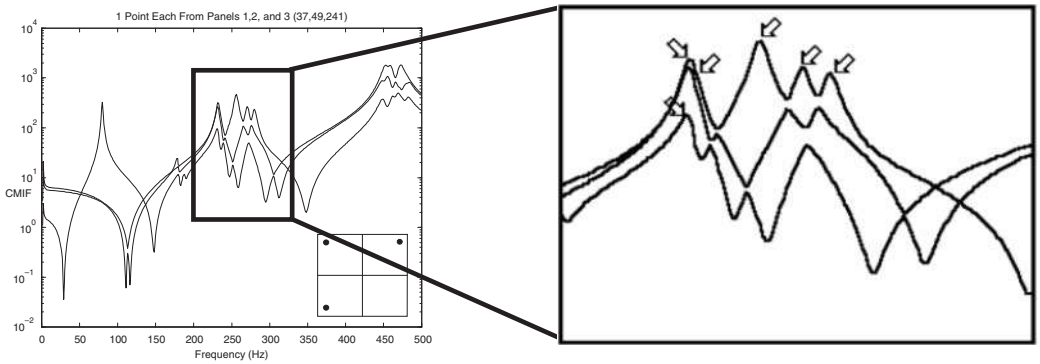

Figure 5.20 CMIF plot with three references indicating multiple roots.

5.4.4 Stability Diagram

Since the early days of modal testing and extraction of modes, once the number of modes has been estimated for a certain band then one of the tools available for fitting a model in the time domain to the band of interest is the *least squares error chart*. As the number of modes assumed to exist in the model is increased, a least squares error can be observed as a function of the number of assumed modes in the model. The number of modes in the data is determined by the knee of the curve, where there is a pronounced change in the number of modes versus the error. The *covariance matrix* generated in this process can also be spectrally decomposed using singular valued decomposition to determine the rank of the set of equations and plotted either as an error chart or as a *singular values diagram*. The interpretation of the singular values diagram is much more straightforward than the error chart. As higher and higher order models are assumed, the true structural modes will converge to a stable number whereas noise or computational modes will appear in an inconsistent or random fashion in the plot.

Today a more popular approach is to use the *stabilization diagram* of this information. The approach is to fit models with higher and higher orders and to incorporate all this information in one plot. As the poles converge to "stable roots" the plot contains markers to identify a variety of information as to the progression of the root or pole. Generally, a selection on the accuracy of the frequency, damping, and vector can be selected. Usually the stabilization diagram is shown along with the summation function, mode indicator function, or complex mode indicator function. Figure 5.21 shows a stability diagram from the 1990s as an example. But before this is discussed a much simpler discussion is needed to put this diagram in perspective.

The stability diagram was a major step forward towards a clear concise presentation of the poles of the system. In the 1990s and early 2000s, the stability diagram was used with either frequency domain curvefitters or with time domain complex exponential curvefitters. The basic idea is that an order of the model to fit the data is selected and poles are computed. (Note: the nomenclature used here is consistent with notation used by LMS and other software packages use other notation but all have the same general approach.)

If poles are found then they are marked with an "o". Then the order of the model is increased and the poles are recalculated. If the same poles are found, then that pole was flagged as follows:

- If the frequency was the same as the frequency of the previous mode to within 1%, then it was flagged with an "f".
- If the modal vector was the same as the modal vector of the previous mode to within 2%, then it was flagged with a "v".

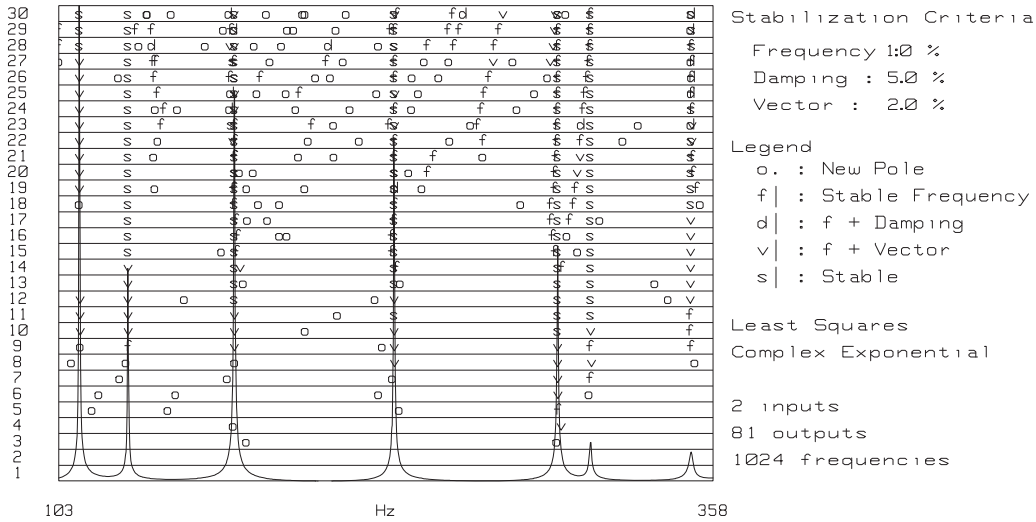

Figure 5.21 Stability diagram from the 1990s with summation function.

- If the damping was the same as the damping of the previous mode to within 5%, then it was flagged with a "d".
- If the frequency, vector and damping were all the same as the frequency, vector, and damping of the previous mode to within 1%, 2%, and 5% respectively, then it was flagged with an "s" indicating that it has reached a stable value to within the stated tolerance.

The tolerances of 1%, 2%, and 5% are ones that are generally considered reasonable but can be changed if desired.

So in order to first introduce the stability diagram, a simpler case is shown in Figure 5.22. Now the modes in this structure are well spaced but there is a very closely space root that is contained in the data. The summation, MIF, and CMIF are shown separately on the right of the figure, alongside the stability diagram in the middle of the figure; the pseudo-repeated root was observed in the MMIF and CMIF and the zoom into that region of stability, shown on the left of the figure, clearly shows that there are two distinct roots observed in the data. On closer investigation, the summation shows all the peaks but cannot distinguish the closely spaced modes. However, both the MMIF and CMIF show the presence of the very closely spaced modes in the data. Now the stability diagram with the CMIF overlaid has very convincing poles, which are stable. Even the zoom-in area, where there are two very closely spaced modes, has a very clear depiction of the stable poles in the system. This is good data and the selection of the poles is not difficult at all. This dataset came from a multiple reference impact test and all the data is obtained in a very consistent fashion.

Often there is confusion in regards to which "s" in the stability diagram is the correct one to pick. There are many "urban legends" in this regard. The simplest answer is that any of the "s" values will be the same to within 1%, 2%, and 5%, which are the tolerances identified. So any "s" will fit those criteria. Often there are certain rules of thumb that people have made up, but they generally have no technical substance whatsoever.

Back in the 1990s, a typical stability diagram provided useful information but the techniques still had some indication of other modes. While the approach for displaying the data was a major step forward, there was still a great deal of sifting and processing of data in subsets over different bands. This was still a chore when extracting modes. A complicated stability diagram used for processing the data from the Canadian Space Agency Radarsat satellite required significant

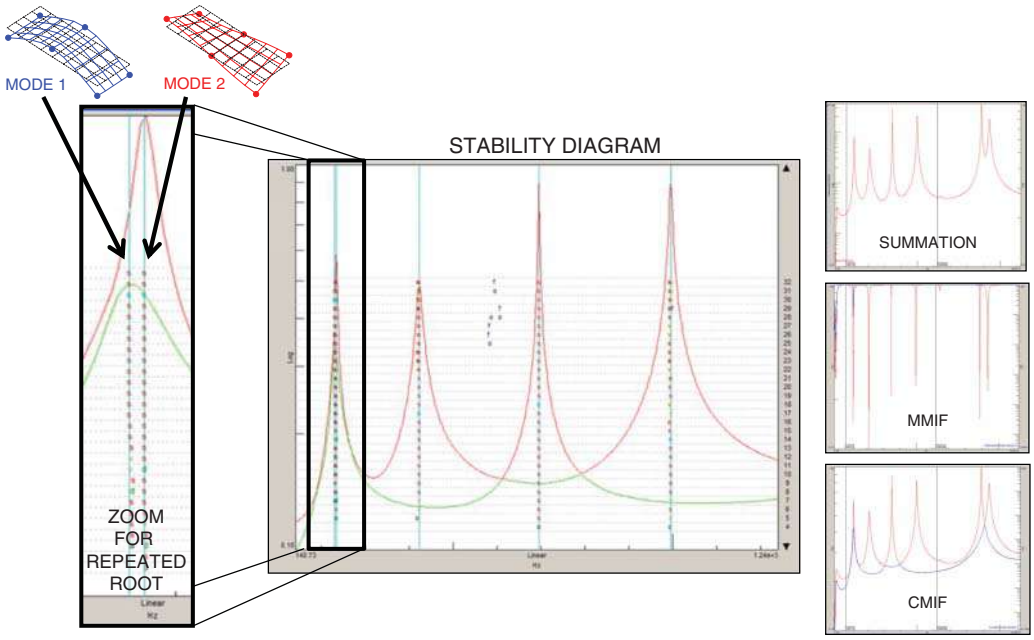

Figure 5.22 Stability diagram with summation, MMIF, and CMIF with a pseudo-repeated root.

interrogation in order to extract all the valid modes for the structure. This stability diagram is shown in Figure 5.23. Clearly there are many modes that are obvious in this plot, but there are also many modes that are not as evident. Back two decades ago, the methodology was to break the data into several smaller bands and to sift the data, so as to only include the best measurements related to the modes in that band. For instance, the first 20–30 modes of that structure were primarily horizontal bending modes, with little vertical response. Including all the vertical measurements tended to corrupt the pole extraction because the measurements themselves had significant variance. Once these vertical measurements were removed and the data sifted to include only horizontal related measurements and references, the data became much more manageable and the poles were slightly more obvious. But in the mid-2000s, several improvements were made to better handle the noise and variance in the data and this led to a significant improvement in the process.

5.4.5 PolyMAX

The modal parameter estimation process made some groundbreaking strides with the introduction of a new set of procedures and processes for the extraction of modal parameters. LMS was the first to introduce the technique referred to as "PolyMAX", and within a few years all the major commercially available software packages had similar implementations. While the basic set of equations remain essentially the same, the processing and understanding of which parts of the equations were more or less sensitive to noise allowed for a much clearer picture when using the stability diagram. For the interested reader, there have been many papers on this topic.

To be able to show the dramatic contrast of the PolyMAX approach, the same Canadian Space Agency Radarsat dataset was used to extract modal parameters. Figure 5.24 is the stability diagram, which is based on exactly the same dataset as that presented in Figure 5.23. The clarity of

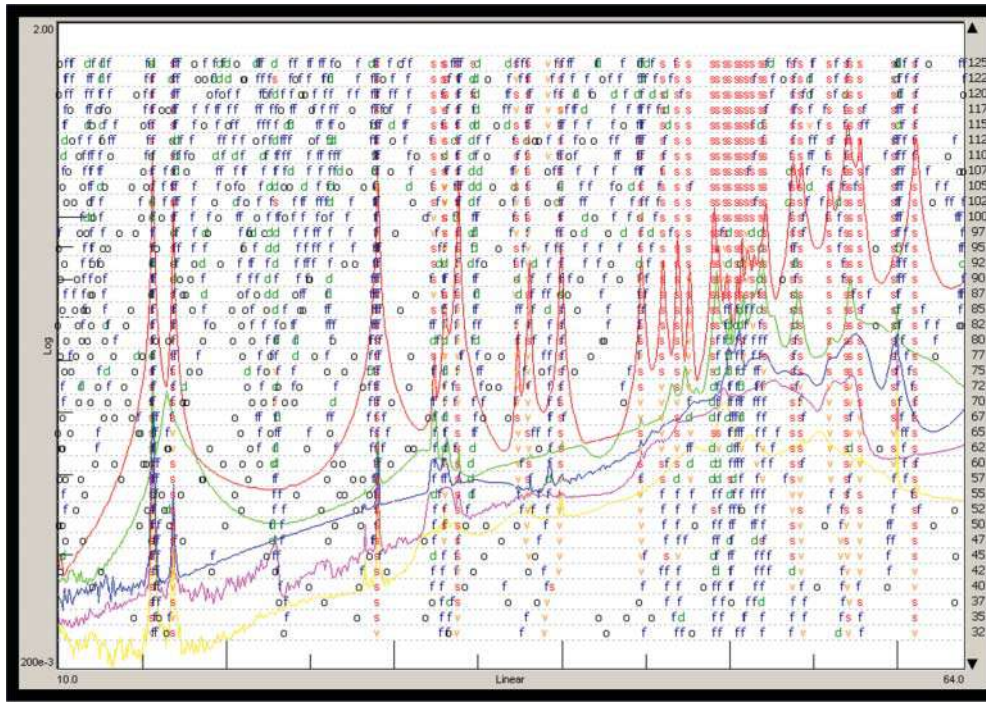

Figure 5.23 Stability diagram for Canadian Space Agency Radarsat satellite test in 1993.

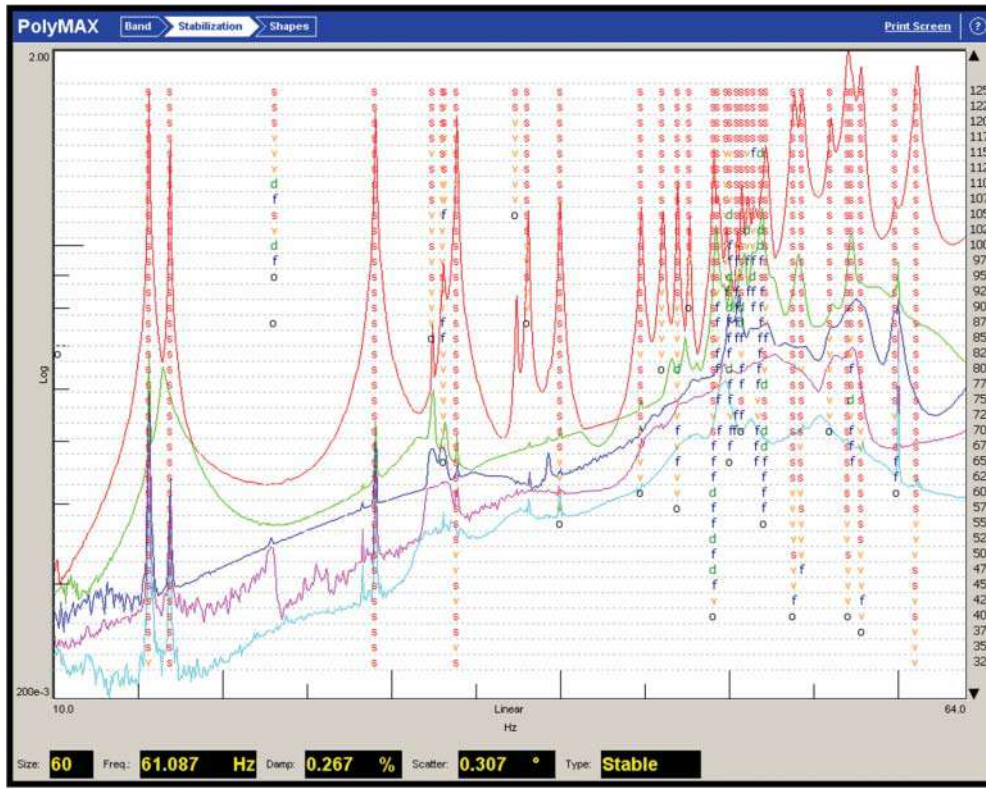

Figure 5.24 Stability diagram for Canadian Space Agency Radarsat satellite test in mid-2000 using PolyMAX.

the poles is outstanding when compared to the previous techniques. Since their introduction, PolyMAX approaches have come to dominate the modal parameter estimation community.

The PolyMAX modal parameter estimation procedure has been a tremendous groundbreaking tool that is widely used and dominates modal data reduction, at least for this researcher. In fact, the presentation of the poles is so clear that now there are many other artifacts in the data. Previously, these were hidden behind the computational modes and were not considered important, mainly because they were rarely obvious to the test engineer.

5.5 Modal Model Validation Tools

Once modal parameters have been extracted, the data needs to be further processed to help validate the extracted parameters. Several techniques exist to aid in the validation of the modal model and these are discussed next. The two biggest tools are the recreation of the measured data from the parameters extracted (synthesis) and the correlation of the vectors with the modal assurance criteria.

5.5.1 Synthesis of Frequency Response Functions using Extracted Parameters

Once parameters have been extracted over several smaller bands, then the extracted pole and residue information is used to synthesize a frequency response function, which is then compared to the actual measured data in order to ensure that the extracted parameters are accurate.

In the first stage, it is important, when the curvefitting is performed, to ensure that the model used is adequate to represent the measured data. Figure 5.25 shows two measurements from a structure that has very directional modes. The particular synthesized measurements are from cross-measurements between two directions where the synthesis is expected to be more difficult. While there is noise and variance in the data, overall the measurement and synthesized measurement are in very good agreement, even in the presence of noise and cross-axis mode effects).

This is just the results from the curvefitting process. However, when small bands are selected in order to completely cover a wider frequency range, the modes from several bands and the residual terms all need to be included in order to synthesize the original measured function. Figure 5.26 shows schematically the overall process when combining modes over several bands. The modes from each of the bands need to be assembled into one complete set, along with the lower residual modes from the first band and the upper residuals from the last band, in order to properly synthesize the entire measured function.

To illustrate this, the Canadian Space Agency Radarsat modal dataset was used to synthesize two different measurements from the parameters extracted from the measured data. These are

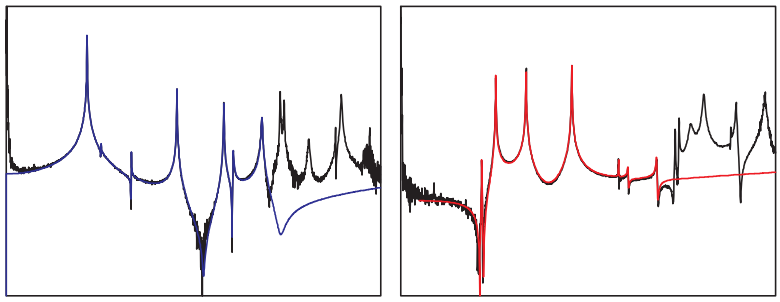

Figure 5.25 Synthesis comparison for two cross measurements for a structure with very directional modes.

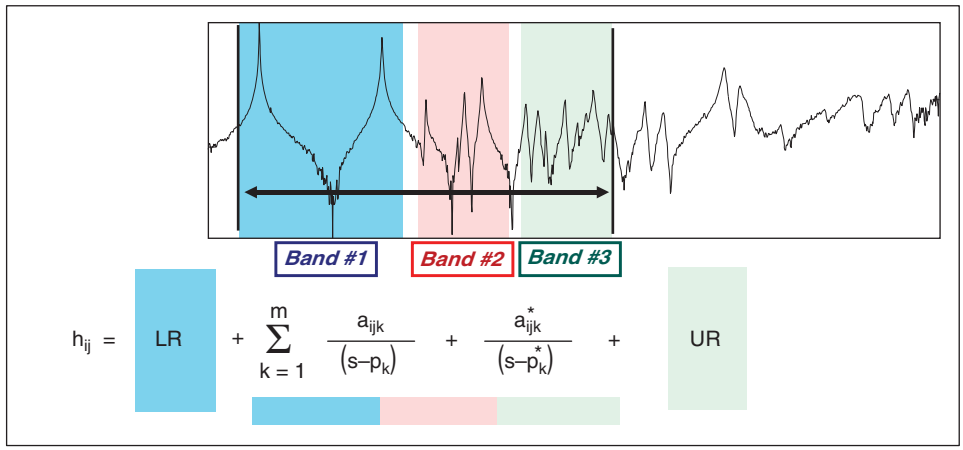

Figure 5.26 Modes (poles and residues) combined from band #1, band #2, and band #3, along with the lower residual from band #1 and upper residual from band #3 to synthesize the frequency response function.

shown in Figures 5.27. Figure 5.27a shows a synthesized measurement in which many of the local and global modes of the system can be observed. Figure 5.27b shows a synthesized measurement where mainly global modes are observed. For both measurements, the synthesized measurement compares very well with the measured data.

5.5.2 Modal Assurance Criterion

The modal assurance criterion was developed as a vector correlation tool to check the similarity or consistency between different modal vectors estimated from an experimental modal test; this tool has been widely used for several decades and has been extended to cover comparisons with analytical models as well. Here, the application is restricted to only comparing experimental modal vector results.

Because different experimental modal vectors can be extracted from different modal parameter estimation techniques, or from different rows or columns of the frequency response matrix, or from entirely different modal tests, the *modal assurance criterion* (MAC) was developed to determine the amount of correlation (or lack thereof) between different modal vectors. The MAC is computed as:

$$MAC_{ij} = \frac{[\{e_i\}^T\{e_j\}]^2}{[\{e_i\}^T\{e_i\}][\{e_j\}^T\{e_j\}]}; \; MAC_{ij} = \frac{[\{e_i\}^H\{e_j\}]^2}{[\{e_i\}^H\{e_i\}][\{e_j\}^H\{e_j\}]} \tag{5.19}$$

One formulation is used for real normal vectors and the other is used for data that is comprised of complex vectors with both magnitude and phase. As the MAC approaches 1, there is a high indication that the two vectors are very correlated. As the MAC approaches 0, there is a high indication that the two vectors are very uncorrelated. Notice that the MAC is formulated in the same way as the coherence function.

There are many reasons why the MAC may be less than 1.0. Some typical reasons may be:

- The modal vectors extracted are different from each other.
- There may be noise that contaminates the vectors being compared.
- The vectors may be affected by nonlinearities in the measured data.
- There is an insufficient number of measured points to characterize the shape.

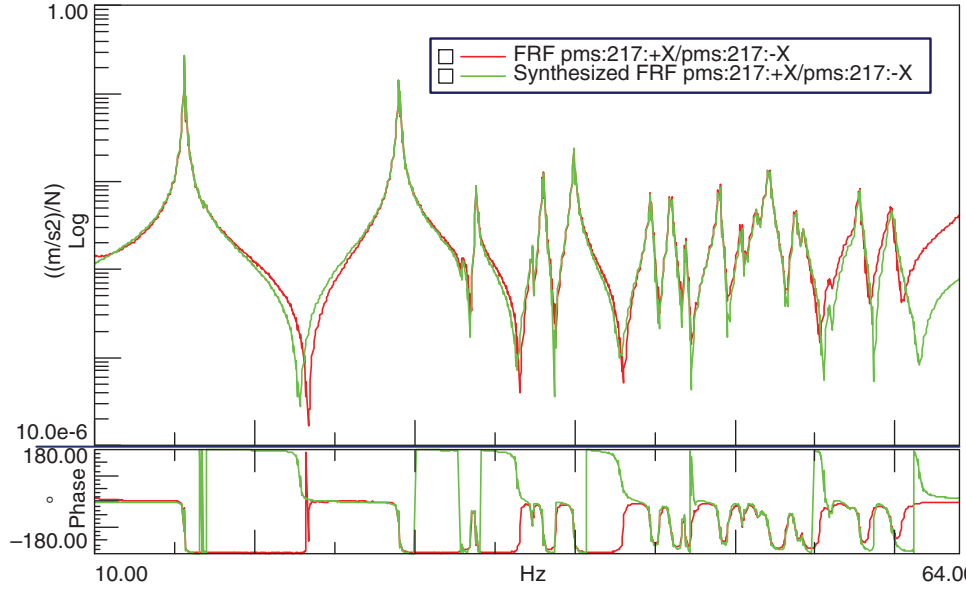

(a)

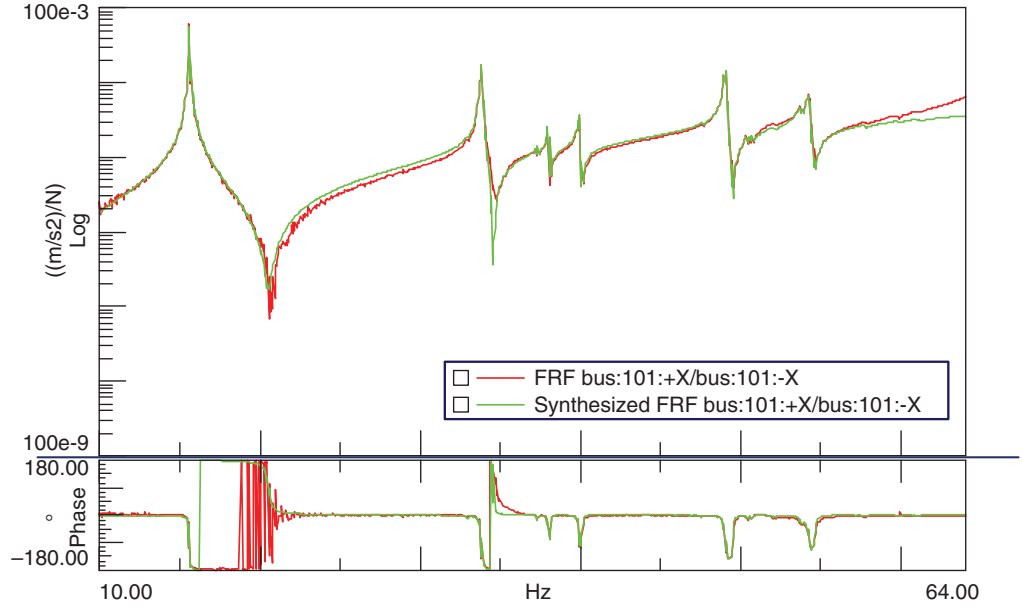

(b)

Figure 5.27 Synthesis comparison for drive point measurement for the Canadian Space Agency Radarsat satellite: (a) with both local and global modes; (b) with mainly global modes.

The MAC is an excellent tool and should always be used, but the interpretation of the data needs to be done carefully. Further discussions of the MAC are contained in some of the application examples in other parts of the text.

As one example, the MAC was performed for two modal tests, where the structure was supported slightly differently between the two tests to illustrate some of the features of the MAC. The two sets of modal data collected were compared with a cross-MAC. Notice that the first two modes have swapped order between the two tests, which shows the results of the correlation; the MAC is shown in Figure 5.28. Clearly, the boundary condition had a significant effect on the order of the modes for this case.

5.5.3 Mode Participation Factors

The mode participation factors are related to the reference degree of freedom for each reference and are only meaningful with multiple references. This is a weighted function, with values between 0 and 1. When looking at the factors, the strength of a reference degree of freedom relative to each mode is seen. This helps to determine if appropriate references have been selected. This also shows which references are primarily exciting which modes. References that have low participation for all modes may not be useful for the parameter estimation process and, more importantly, may have detrimental effects when using the mode indicator tools; they may need to be excluded from the dataset when estimating the poles of the system.

5.5.4 Mode Overcomplexity

The mode overcomplexity (MOV) is a weighted percentage of the response degree of freedom for which a mass addition yields a negative shift in frequency. Therefore, an MOV of unity is

			Corner				
	Mode No.		1	2	3	4	5
		Frequency	231.82 Hz	232.11 Hz	423.44Hz	694.33 Hz	996.99 Hz
Midpoint	1	230.11 Hz	0.47	**96.18**	0.19	0.04	0.43
	2	233.32 Hz	**97.12**	0.01	0.02	0.37	0.03
	3	422.16 Hz	0.02	0.30	**99.73**	0.00	0.31
	4	695.12 Hz	0.33	0.04	0.00	**99.83**	0.11
	5	995.69 Hz	0.01	0.23	0.37	0.09	**98.93**

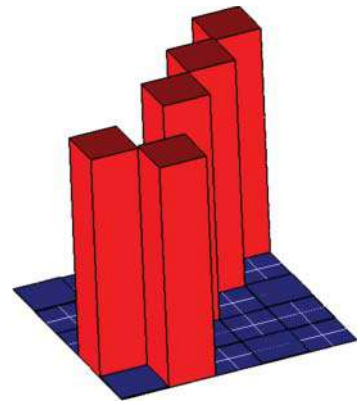

Figure 5.28 MAC table and 3D matrix comparing mode shapes from two different modal tests with two different boundary conditions.

the desired value and low MOV indicates less than desirable results, which may be caused by a noisy modal vector or be an indication that the mode is not actually a mode of the system.

5.5.5 Mean Phase Co-linearity and Mean Phase Deviation

The *mean phase co-linearity* (MPC) is an assessment of how much phase scatter exists in the modal vectors; remember that real normal modes have components of the mode shape that are either totally in phase with other components of the mode shape or totally out of phase with other components of the mode shape. Therefore, real normal modes should have a MPC close to unity; lower values indicate that there is a phase lag. The *mean phase deviation* (MPD) indicates the amount of phase scatter that exists in the modal vector; real normal modes should have a mean phase deviation close to zero. However, it is very important to note that both the MPC and MPD are really only useful for systems where the modes are actually real normal modes. They are not really very useful for systems where the modes will have some complexity to them and where relative phasing is expected in the mode shapes.

5.6 Operating Modal Analysis

Up until this point, only traditional experimental modal analysis techniques have been discussed. To just put everything in perspective, a general input–output configuration is presented in Figure 5.29 in matrix form and in Figure 5.30 with the measurements acquired. This shows the input forces, output responses, and resulting frequency response functions that are acquired from a traditional modal test; the schematic is shown with two references. This shown in a matrix schematic as well as in a measurement schematic as an overview.

Over the last decade, there have been determined efforts to use operating data, with a structure in its operating configuration, in order to extract modal parameters. These types of models are often called "output only" systems. Measurements can be obtained from transducers mounted on the structure, but there is no measured force with which to compute a frequency response function, as typically done in a conventional modal test. In order to collect frequency data, a reference response transducer is used to compute cross-spectra from either a single reference or from multiple references. So a matrix of cross-spectra, similar to a matrix of frequency response functions, can be acquired while the structure is in its ambient or operating condition. Figure 5.31 shows a typical configuration, in which there are many measurement

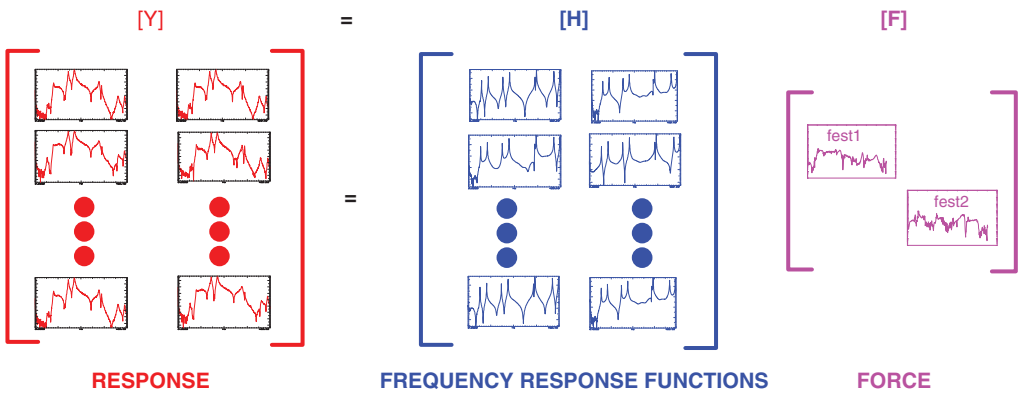

Figure 5.29 Typical experimental modal test measurements in matrix form.

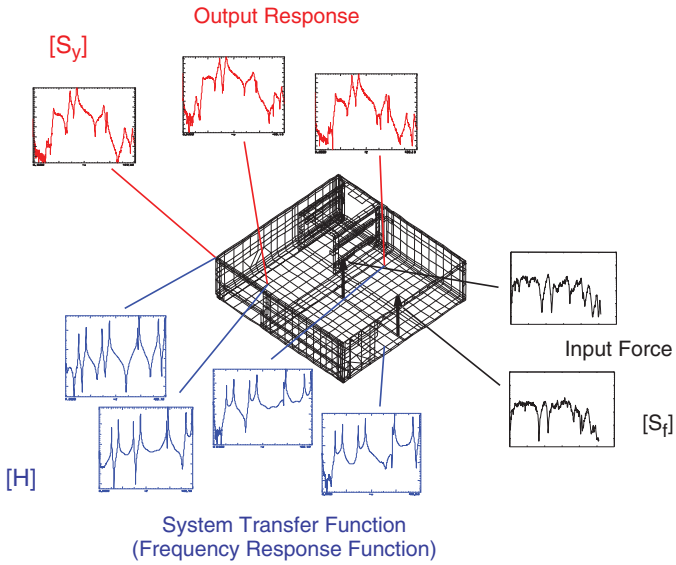

Figure 5.30 Typical experimental modal test configuration.

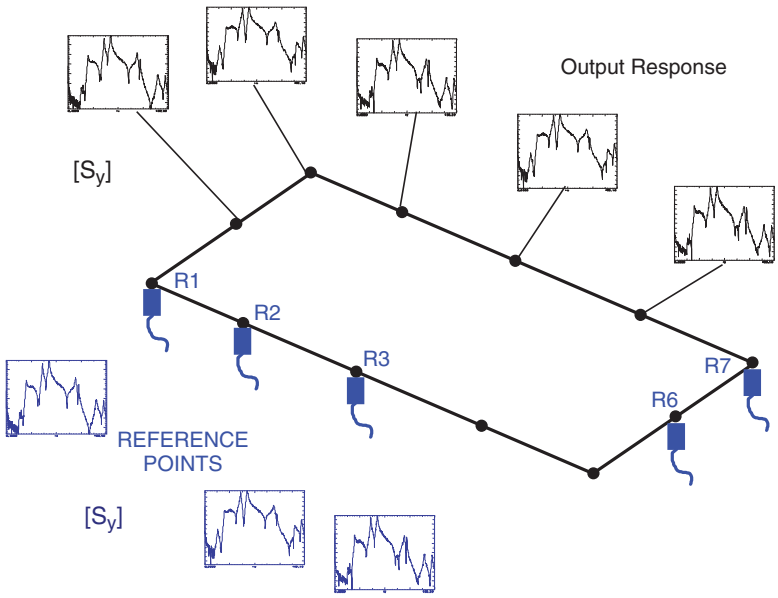

Figure 5.31 Typical operating modal test configuration.

points that are designated as output points (in black). A subset of those points is designated as references (in blue); note that only a few spectra are shown for illustrative purposes.

Operating modal analysis has several significant advantages. It analyzes the structure in its most natural state, with actual boundary conditions of the in-service condition, and with the actual excitations in the real environment. Certainly, this is an advantage over a laboratory test. For very large structures, it may be the only way possible to obtain these parameters because the structure cannot be excited with conventional techniques. The structure does not have to

be brought to the laboratory to be tested with simulated boundary conditions and set ups and with excitation forces that are not the actual forces that will be seen in the real application. These are compelling reasons to perform a test in this way.

However, one important consideration is that there is no practical way to determine if all the modes of the system have been excited, so as to extract all the modes of the system. Of course, many argue that if a mode is not excited because the operating forces don't excite it then those modes aren't important. But if the data is to be used for other simulations or correlations, then all of the modes of the system are necessary, not just a subset that responds in a particular set of operating conditions. Another difficulty is that the same "apparent" operating conditions can often produce different deformation patterns that are unexplained. So there are a few underlying assumptions with operating modal analysis that need to be stated first so that a clear understanding of the approach, with its advantages and deficiencies, can be reached.

The measured response is due to some unknown force that excites the structure either at discrete locations (such as mounting points) or across a large portion of the structure (such as wind loading). The response due to this unknown force is measured and cross-spectral measurements (relative to a fixed response point or multiple fixed response points) can be obtained by averaging the responses. But only responses can be measured. Figure 5.32 shows a measurement of a cross-spectrum; the unmeasured force spectrum and unmeasured frequency response functions are shown to clearly illustrate that the unknown force needs to be able to adequately excite the response of all the modes; if not, then the response may not be clearly seen for all the modes of the system. Notice that the output spectrum has several significant peaks, corresponding to the third and fourth modes, but there is very small output response due to the small input force excitation to the system in this lower frequency range. Clearly, if the force does not have adequate frequency content then significant modes of the system

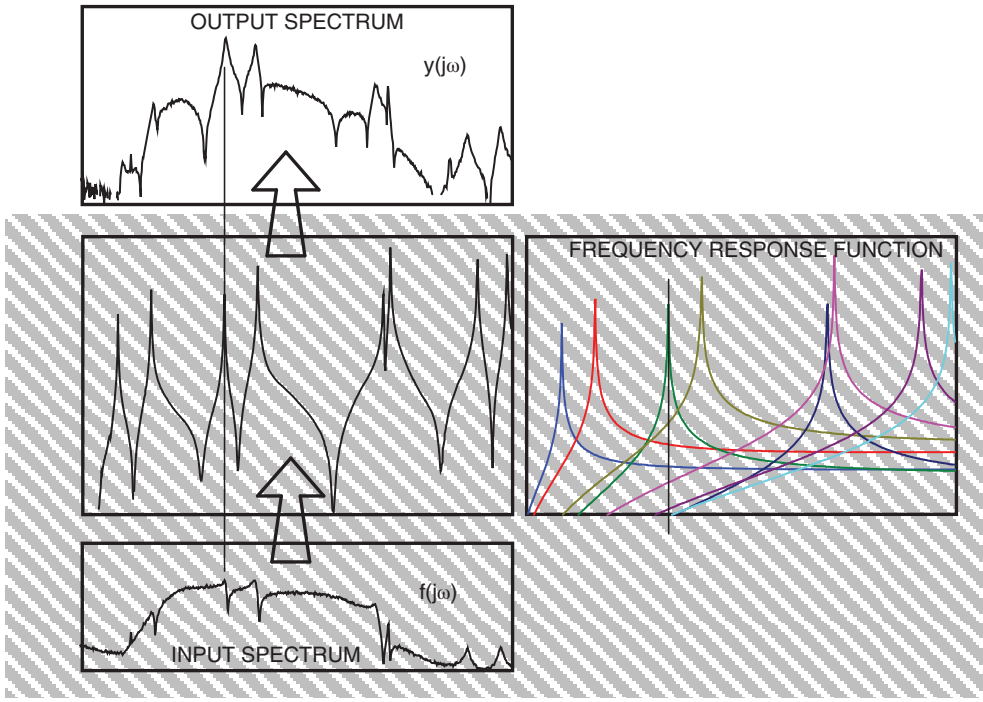

Figure 5.32 Schematic showing output only response scenario with unknown force and FRF shown.

may not be adequately excited and observed in the data. And of course, if any of the forces are applied at the node of a mode of the structure then certainly those modes will not be observed in the response. Of course, this is all very obvious from the traditional modal testing discussed throughout this book.

Now let's identify the basic premise for output only systems in terms of the anticipated force.

The basic assumption for any output only system in regards to the force exciting the system is:

- The force spectra are broad and smooth.
- The force spectra are uncorrelated or weakly correlated.
- The forces act over the entire structure.
- The force is assumed to be a Gaussian white noise approximation.
- The force needs to be random in space and time.

This set of assumptions is hard to meet in practice, and there is no way to really verify that all these conditions are met.

So what these assumptions imply is that the force spectrum needs to look essentially like the force that is typically used for an experimental modal test when shaker or impact excitations are used. This is also a very important assumption because the output response from all the transducer measurement points can be normalized to this assumed force spectrum and then the data starts to look very much like traditional frequency responses. This is very good because then all of the traditional modal parameter estimation techniques can be easily morphed into all the existing time and frequency domain modal parameter estimation techniques. So if the unknown force satisfies the conditions, then the measured response can be decomposed using most of the typical decomposition techniques used in traditional modal testing. If all these conditions are met then the operating modal analysis can produce very good approximations of the modes of the system.

Some of the common parameter extraction tools used today for operating modal analysis are:

- Ibrahim time domain technique
- eigensystem realization algorithm
- stochastic subspace identification
- frequency domain decomposition technique
- auto-regressive frequency domain models
- polyreference frequency domain technique.

There is no doubt that as more research is performed, these output only approaches will become better and better. Some data on operating analysis and reduction of data for output only systems is contained in Part 2 of this book, on the applications.

5.7 Summary

Basic concepts of modal parameter estimation were introduced. Differences between single degree of freedom and multiple degree of freedom techniques were discussed by example for a simple 2-DOF system. The similarity of using time and frequency domain representations was described, along with a description of local, global, and polyreference techniques. Finally, commonly used techniques were briefly described. Mode identification tools and model validation tools were also presented.

Part II

Practical Considerations for Experimental Modal Testing

6

Test Setup Considerations

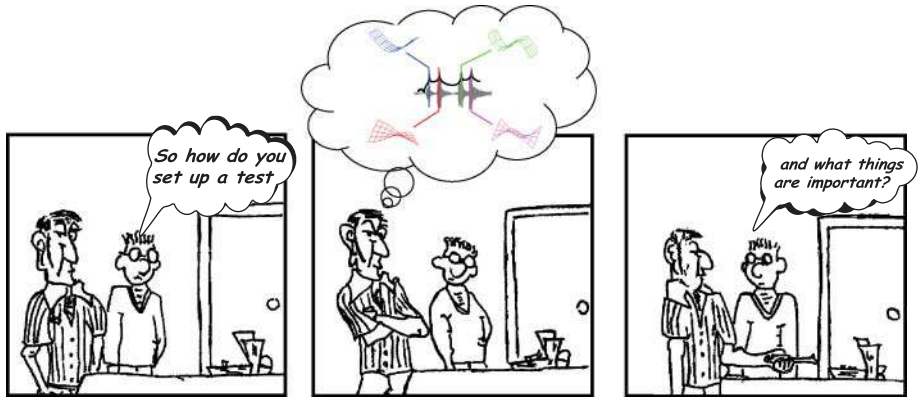

An experimental modal test can be performed for many different reasons or purposes. Often, the modal test is conducted to identify the modal characteristics for comparison to an existing finite element model. Or the test may be performed to identify critical characteristics needed by the design team in generating new designs or improving existing ones. Sometimes the experimental test data is needed to perform simulation analyses. At other times, the test may be part of a requirement for a particular contract. But often the experimental test is conducted because there may not be a model for a structure where there is some operating problem; the modal test is performed to gain insight into the different frequencies and modes that may be present in the structure, whether it be a prototype or a piece of equipment in service. Suffice it to say that there are many reasons for performing a test and often those reasons may drive the test to be performed in a fashion that is not typical of the modal tests that are generally performed. But understanding why the test is being conducted is sometimes more important than the test itself. And it is critical that everyone requesting the test clearly understand what the test can and cannot be used for in solving the problem at hand. This is sometimes where things break down; many people may say they have an understanding of the modal test, but may not have a *deep* understanding of the modal test.

But important issues will be the availability of the test hardware, costs to perform the test and other physical constraints that may require the test to be performed a certain way. However, then the test may be performed with not all of the desired tests, measurements, configurations, and so on that that might be considered necessary in order to perform the test properly. Often there are administrative constraints that do not allow for all the tests that are desired. Or the people to run all the tests may be absorbed with other projects and other tests; there is no one

Modal Testing: A Practitioner's Guide, First Edition. Peter Avitabile.

Companion Website: www.wiley.com/go/avitabile/modal-testing

to conduct all the tests that are needed. Sometimes there is a lack of data acquisition system channels to run all the test configurations as desired and a piecemeal set of tests may have to be performed to acquire the data. And most importantly, is there a sufficient budget to run the tests desired?

While these considerations may seem outside the scope of the technical discussion in this book, the practical reality is that a critical subset of possible tests may have to be chosen. This is a serious issue to consider when performing a modal test. But the main thing for everyone to ask is "Why are we running this test?" And you may ask "Why ask why?" and the answer to that is sometimes you find out that some people may have a completely different understanding of what can be gleaned or extracted from the test.

And one of the most basic questions is what is really the most important output from the test:

- Is it the frequency of the modes?
- Is it the mode shape of the modes?
- Is it the damping of the modes?

Maybe only one of these outputs is really important and the others are just useful information. Or maybe all of them are equally important. This consideration can have a very important impact on the test that is conducted, the instrumentation used, and the data to be reduced.

Another critical question that often is very difficult to answer is how the results of the modal test integrate with the system level response and performance of the complete system. Often, an extreme amount of detail is provided for the modal test yet the overall performance of the system is not significantly affected by the specific results of the modal test of a subcomponent, yet this is not known when the test is performed. The level of accuracy needed at the system and component levels may be different; that is, sometimes the modal test results could be sufficient using less stringent requirements for subcomponent, so that a much simpler test could be conducted (and lower costs achieved).

All participants should discuss the test goals and objectives so that there is no misunderstanding when the test data is reduced and results provided. There are several items that can be mentioned here. These are presented in no particular order and some topics may appear under multiple headings below. Some of the very simple topics that need to be addressed are:

- the frequency range of concern
- the transducers to be used
- the number of modes to be extracted
- the type of excitation to be used
- the number of points to be measured
- the level of detail of internal components
- how the structure is to be configured for testing.

As each of these topics is discussed, examples of scenarios that have caused difficulties or strange results from personal experience over four decades will be presented. Some of the topics may be directly related to the test setup considerations but there may be several topics that are discussed here that contain general information that is not easily included in other chapter sections.

6.1 Test Plan?

A test plan is a vital part of the modal test. It helps to guide the steps in the test and to ensure that all measurements and data desired are collected. The test plan is a mutually agreed upon

scope of the test. Even routine tests should have a test plan so that everyone is in agreement that the data to be collected will be sufficient for the project needs or contractual requirements; at times, mandated tests may change slightly in scope and "that's the way we always do it" cannot be the mode of operation, especially on modal tests that are performed as part of a contractual obligation.

The test plan is useful to identify:

- the scope of the test
- the frequency range of interest and resolution required
- the number of modes to be obtained
- the number of measurement points to be acquired
- the sequencing of collection of data
- specific/unique measurements to be acquired
- identify the format of data to be provided to a customer
- scope of which organizations are providing which services (when multiple groups are involved)
- specific stop points during the test to review data collected
- critical items that need to be completed prior to leaving the test site
- specific information to be included in the test report.

This may seem to be extra work, and a waste of time, but test plans have proven to be very valuable documents, even for the simplest of experimental modal tests. A test plan helps to get everyone on board with the test, its scope, and the results expected. While not specifically part of the test plan submitted to a customer, additional documentation should be developed locally to make sure the engineers and technicians all work in unison to conduct the test.

6.2 How Many Modes Required?

Often, people just really don't know how many modes may need to be identified for a modal test. All too often too few modes are identified and often too many are requested "just to be on the safe side". But there are many tests that are run with very clear and sometimes mandated numbers of modes to be acquired; these are often for parts that have contractual requirements about the number of modes to be identified. While the number of modes may be clear from a contract, it does not mean they are really needed. If there are no clear guidelines then the engineer must really understand the application and the loading scenarios in order to make a judgment call. Some understanding of the excitation frequency range is necessary in order to determine the frequency range and the modes that make a significant contribution to the overall response.

While the total number of modes to be collected is very important, a bigger question (actually a much bigger question) is how the test article is to be mounted for testing:

- in a fully fixed condition
- in a free–free condition
- in an actual installation or fixture simulating the installation.

This can have a dramatic effect on the test and the frequency range that must be considered for the test. This consideration then raises several important questions that need to be answered.

- How free is free, because 0 Hz doesn't really exist?
- How fixed is fixed, because an infinitely stiff boundary is impossible to achieve?

- How well does the fixture replicate the installation?
- How much does the fixture dynamically interact with the test article?

Many modal tests are performed in a so called "free–free" condition, but the reality is that this is not possible to achieve in a practical sense. Usually, there is an attempt to provide a test setup that tries to achieve modes that are close to 0 Hz. However, the finite element models that were generated can have pure 0 Hz rigid body modes defined when the model is generated. But the main thrust is to try to obtain a test setup where the six low frequency rigid body mode approximations are separated from the flexible modes of the system so that there is no substantial dynamic coupling. But there are many systems where the flexible modes are close to the rigid body modes and there is no way to separate them. If a finite element model is available, then the model can be used to study the effects of the support system on the measured rigid body mode approximations. This is extremely useful when trying to understand any dynamic interaction that may exist between the flexible modes and the rigid body modes. And while the model is being mentioned here, there really should never be a finite element model generated with pure free–free conditions because that is not a realistic test configuration. If anything, the finite element model should model the support condition that is to be used to conduct the experimental modal test, so as to provide the most realistic configuration of the system. This is imperative if the test data is to be compared to the finite element model, when a correlation study is to be performed as part of the work.

If a model is not available, then some preliminary work should be performed to understand the effects of the support system on the flexible modes. If the structure is supported by bungee cords, then two tests can be performed: one with single bungee cords and one with "doubled up" bungee cords. In this way, there should be a definite shift in the rigid body modes. More importantly there may be an effect of the stiffness change in the bungee cord with respect to the flexible modes of the system. If there is no appreciable shift in the flexible frequencies then the rigid body modes may not have a significant effect on the flexible modes and the results can be used with more confidence that there is little effect on the flexible modes to be measured.

But even with the softest of support conditions, the physical placement of the supports can have an effect on the mode ordering. One very simple illustration is for an academic structure that is often used, which has closely spaced lower order bending and torsion modes that can be affected by the method of support. While the boundary condition shown next is very non-traditional, the effects of mode swapping can be seen in two test setups that could be used to test the structure. Very soft supports were located at the corners of the structure in one test setup and at the mid sides of the structure in the second test setup. The first bending and first torsion modes were shifted in frequency by about 1% but, more importantly, the order of the modes was switched between the two tests. So the way the same boundary condition was applied to different locations on the structure had an effect on the frequencies and ordering of the modes. The two structure setups are shown in Figure 6.1 and the cross-MAC is shown in Table 6.1, revealing the effects of the same boundary condition placed in two different configurations.

Figure 6.1 RR frame structure with two different boundary condition setups.

Table 6.1 Cross-MAC illustrating boundary condition effects.

			Corner				
	Mode No.		**1**	**2**	**3**	**4**	**5**
		Frequency	231.82 Hz	232.11 Hz	423.44 Hz	694.33 Hz	996.99 Hz
Midpoint	1	230.11 Hz	0.47	**96.18**	0.19	0.04	0.43
	2	233.32 Hz	**97.12**	0.01	0.02	0.37	0.03
	3	422.16 HZ	0.02	0.30	**99.73**	0.00	0.31
	4	695.12 Hz	0.33	0.04	0.00	**99.83**	0.11
	5	995.69 Hz	0.01	0.23	0.37	0.09	**98.93**

In another instance, a large shock plate was tested before it was installed on its air-ride system to give some validation for the model. Because the final support system was not available, the 250 lb plate was supported with three rubber mounts (corresponding to the air-ride support locations) and with six other rubber mounts. The rigid body modes were less than 20 Hz for all six modes and the flexible modes were all above 200 Hz. So the separation would seem to be appropriate. But, as it turned out, when the structure was tested on each of the two support systems, not only were the rigid body modes slightly different but the flexible modes also saw an effect, shifting the modes by 1%. Figure 6.2 shows the results of the two tests.

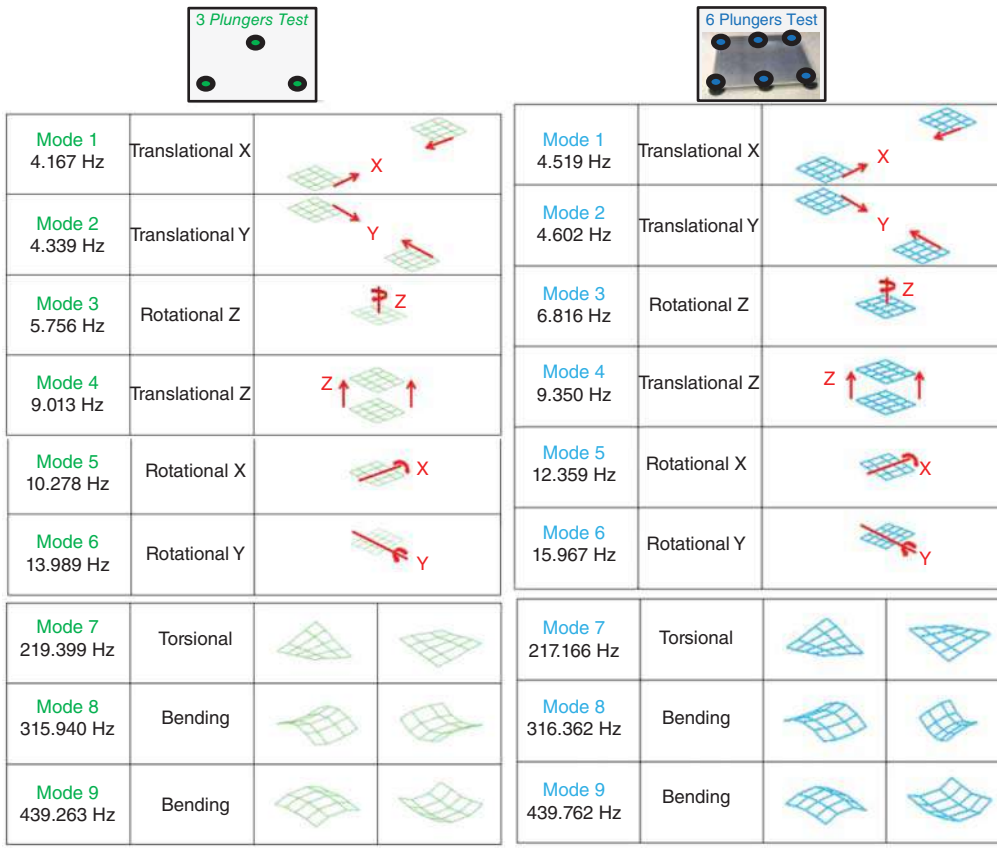

Figure 6.2 Shock plate tested with two different support conditions.

So from these two cases, care must be exercised to ensure that the test setup and boundary conditions are well understood. And again, if a finite element model is developed as part of the work, then the model should have boundary conditions applied that mimic the true test setup and not use pure free–free conditions. But the bottom line is that there is no such thing as a truly free–free boundary condition and even if there is a significant frequency difference between the rigid body modes and the flexible modes, there can still be effects on the modes due to the boundary conditions applied. Even with a 10:1 ratio between the rigid body modes and flexible modes, there was still an effect due to the boundary conditions for the case just shown.

Another way that an experimental modal test can be run is with the structure constrained or built in at an interface. To create this built-in condition is even harder than the free–free condition. Generally, people totally underestimate the size and mass of an appropriate anchor to simulate a built-in condition. The main reason why this test is even considered is because of the way some finite element models are created using Craig Bampton component mode synthesis techniques, which require modes with a fixed interface in order to create the system model. So at times, this is required. The easiest way to attempt to achieve this is with a seismic anchor that is large and massive. But as structures get larger, this becomes more and more difficult to achieve. And this problem becomes amplified when the structures are long and slender, for example wind turbine blades. One study showed that the weight and inertia to create a suitable seismic anchor to achieve a built-in condition was much more than anyone envisioned. Figure 6.3 shows the summary of that study, giving an idea of the mass ratios required, especially for rotary inertia, to achieve an appropriate interface.

An experimental modal test is often set up with a fixture that replicates the dynamic interface in the actual installation using only a portion of the actual structure. While this sounds like a good way to conduct an experimental modal test, many attempts have ended with the realization that the fixture dynamics do not mimic that actual installation well enough and therefore the dynamics are different to those that exist in reality. At times this approach may produce an acceptable test result, depending on the accuracy needed or desired. Caution should be used with this approach to ensure that the actual dynamic response is achieved.

One area where people often can fall into difficulty is when a test structure is mounted to a fixture to run an experimental modal test. If the fixture has any modes of its own in the frequency range of interest, then there can be a pronounced effect on the test structure, rendering the modes of the test article useless. Often the modes of the test fixture can be higher than the modes of the test article and there can still be significant dynamic coupling between the test fixture and test structure, rendering the modes from the experimental modal test questionable.

If the actual installation configuration is available, the test could be conducted in that configuration and then the results would be expected to be as true to the installation as one could envision. However, if the goal of the experimental modal test is to validate a finite element model of the component, then the finite element model needs to include the full configuration, otherwise the model will not be representative of the configuration.

6.3 Frequency Range of Interest?

In terms of the test, two very important considerations are the frequency range of interest and the types of modes that need to be extracted from the experimental modal test. Sometimes only the lower order modes are of interest, but higher modes may be needed depending on the application and reason for the test. Someone needs to identify the frequency range for the input forces that excite the system so that the analysis bandwidth and modes to be extracted can be

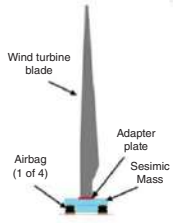

	CX-100 Blade properties	Fixture properties
Weight [1b]	380	21,740
Mass Inertia [1b-in^2]	—	10,435,200

	MATLAB Results [Hz]	
	Built-in	On seismic mass
Mode 1	4.36	5.29
Mode 2	11.76	12.44
Mode 3	24.35	24.78

Properties of Anchor		Freq. of Mode 1 (Hz)		Curvature of Mode 1
Mass	Inertia	With Anchor	Truly built in	
M	MR	5.29	4.36	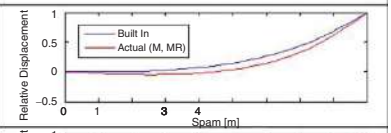
2*M	MR	4.87	4.36	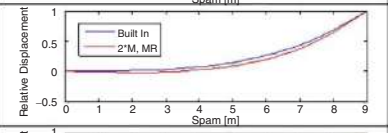
M	2*MR	4.87	4.36	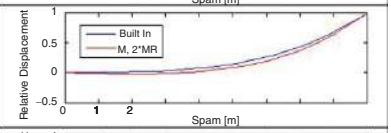
M	10*MR	4.47	4.36	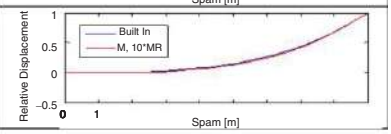

Figure 6.3 Mass and inertia ratios to achieve a built-in boundary condition for a CX-100 turbine blade.

identified. Each test is different, and there is no hard and fast rule for the frequency range to be addressed. But there may be cases where a contractual specification or standard has been imposed and then there may be some predefined ranges that must be addressed. However, if the experimental modal test is being conducted to solve some operating difficulty or to identify modes of interest to improve the overall system performance, then the frequency range may not be clearly identified and then the bandwidth to make measurements may be unknown or not clearly defined.

At times, there may be a collection of modes that need to be acquired. Maybe only the rigid body modes are needed for multibody dynamic response studies, or maybe only the lower order flexible modes are needed for fundamental characteristics to be identified, or maybe some higher frequency characteristics are needed for acoustic response purposes. The reason for the test needs to be understood in order to know what types of modes or frequency range are to be considered.

First it is important to define what is meant by "low frequency" and "high frequency", and that will depend on what type of structure is being considered. For a large wind turbine blade, the first several modes of bending and torsion will be much lower than 10–20 Hz for instance. But for a jet engine turbine blade (which has the same types of modes), the first frequency may be 300–400 Hz, depending on the size of the blade. The first dozen modes may go as high as 10,000 Hz or higher. So the first thing that must be stated is that consideration has to be given to the lower order modes of the system and the frequency range they cover. All too often, people may incorrectly state that experimental modal analysis doesn't work at high frequencies. However, that is not true and consideration needs to be given to the types of modes and waveforms that need to be captured. The first ten modes of the wind turbine blade and the jet engine turbine blade can certainly be obtained from experimental modal analysis, but there may be very different frequencies at which those modes occur. So there certainly needs to be some consideration of the frequency range and types of transducers that are used, and these will be very different depending on the frequency range to be considered. Three different frequency ranges are considered for three different structures in Figures 6.4–6.6.

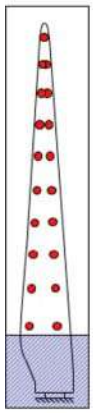

Mode #	Mode Shape	Flap	Edge
1	1st Flap		
2	1st Edge		
3	2nd Flap		
4	2st Edge		
5	3rd Flap		
6	4th Flap		
7	3rd Edge		

Figure 6.4 Very large wind turbine blade low frequency experimental modal test.

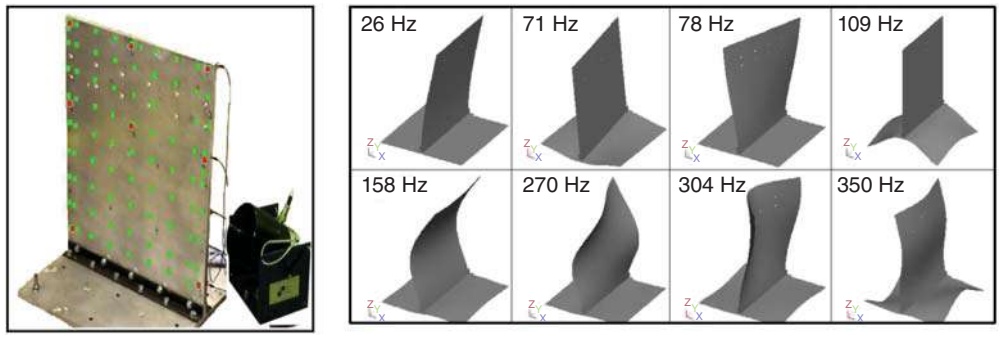

Figure 6.5 Medium sized academic structure experimental modal test.

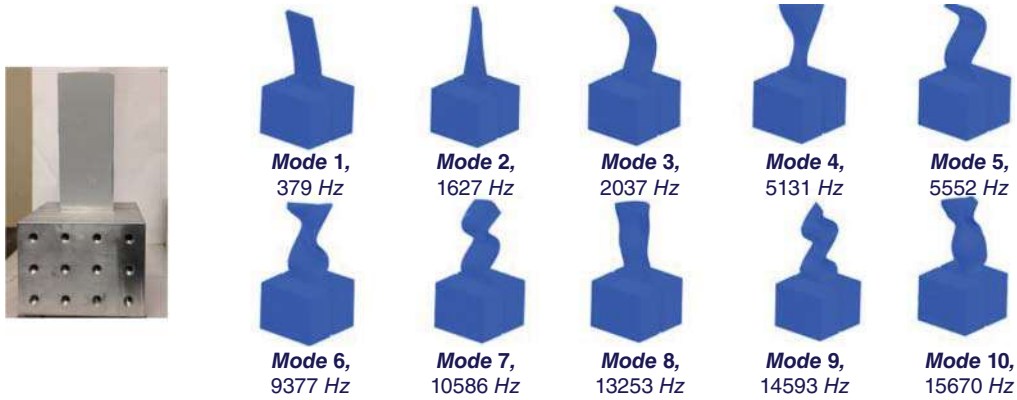

Figure 6.6 Very small jet engine turbine blade simulation, high frequency experimental modal test.

Figure 6.4 shows a large wind turbine blade, where the first several modes are beam bending, with all modes below 10 Hz. Figure 6.5 shows an academic structure called BU (base-upright) where the first eight modes span 20–400 Hz. Figure 6.6 shows another academic structure, which is used to mimic higher frequency characteristics seen in small jet engine turbine blades; the first ten modes span from 300–15,000 Hz. In all three structures, the first set of lower order modes are all identified. While the mode shapes are very similar low order bending and torsion modes, the frequencies of the modes themselves are very, very different.

So two things need to be pointed out here. First, the knowledge of the actual mode shape for each of the modes to be identified is extremely important in deciding how many points are needed and where to locate the transducers to capture each of the modes to be considered. Second, each of these three structures may need very different transducers to collect the data because of the drastic differences in frequencies to be considered. In the first low frequency modal survey, very low frequency accelerometers could be used, especially considering that the frequencies to be measured will be less than 10 Hz and some modes may actually be at less than 1 Hz. As an alternative, an optical system using dynamic photogrammetry might also be considered. In the second case, accelerometers could likely be used to make the measurements needed. In the third case, however, the structure is very small and lightweight and most likely a noncontact measurement such as a laser vibrometer may be needed due to the higher frequencies to be measured and the need for a lightweight solution due to mass loading considerations for an accelerometer.

So this is a case where the determination of the distribution and number of measurement points may deploy the same methodology but the actual transducers to be used could be vastly different due to the extremely wide frequency range for each of the three tests. This ultimately identifies that the experimental test lab may need a very wide range of measurement systems depending on the types of structures and frequency ranges involved. A wide range of different accelerometers, with different sensitivities, may also be needed to allow for different test circumstances.

6.4 Transducer Possibilities?

So there are many different transducers and measurements that can be deployed to conduct the experimental modal test. Acceleration, velocity, or displacement are the likely measurements. Some tests are conducted with strain gages but these will not be discussed here. Also, various novel approaches using sand patterns have been used but also are not discussed here.

Obviously, consideration of the transducers to be used is needed, depending on the frequency range and types of modes involved. But accelerometers are probably the most common transducer used for modal tests and lasers are probably the next most common measurement approach. Other techniques, such as digital image correlation and dynamic photogrammetry, are starting to be used more as the cost of cameras reduces and resolution increases. At the time of writing, motion magnification is starting to appear as another alternative.

Of course, the useful frequency range and sensitivity of the transducer needs to be selected to suit the tests to be performed. Often, there is really no information regarding the response expected from the structure to be tested and this can make transducer selection very difficult, to say the least. Generally, an assortment of transducers and sensitivities is the best approach when there is no information regarding the structure's expected response. And even if the structure is stated to be similar to ones previously tested, there are usually differences from previous tests and therefore being prepared with an assortment of transducers is still advisable. Often, a brief test on a similar structure can provide a tremendous insight into the response levels to be expected. For example, when tests were needed for the Gemini telescope under construction in Chile, a trip to the operating sister telescope in Mauna Kai was requested to obtain rough data so that accelerometers could be identified for the tests, which ultimately used over 100 permanently mounted accelerometers for both operating and modal tests. Some of the accelerometers needed to be very sensitive, with very low frequency requirements to acquire all the data of interest.

In a test on a large wind turbine blade (more than 60 m in length), previous test results on a slightly smaller blade were used to estimate the maximum voltages that might be observed for the first experimental modal test performed. The customer wanted to purchase accelerometers rather than rent them; the voltage setting from the previous test helped to define the sensitivity of the accelerometers to be purchased. Using 1000 mV/g as opposed to 100 mV/g made a significant difference in the quality of the measurements on the turbine blade. Table 6.2 shows the channels and voltages recorded from the previous test; this was very useful to define the sensitivities for the procurement of accelerometers.

6.5 Test Configurations?

In many tests, accelerometers are used but often there may not be enough accelerometers or enough channels of data acquisition to support the entire test. In most scenarios, the concern is

Table 6.2 Maximum channel voltage distribution.

Pt. #	Direction	Channel	Serial	Sensitivity (mV/g)	Voltage Ranges at Reference (V)								
					11:X	13:X	15:X	17:X	2:Z	11:Z	13:Z	15:Z	17:Z
1	X+	5	104009	980.4171	0.2	0.5	0.2	0.2	0.5	0.1	0.2	0.5	0.2
	Z+	6		947.5198	0.2	0.2	0.05	0.1	0.2	0.2	0.5	0.5	0.5
2	X+	7	104010	966.5479	0.2	0.5	0.2	0.2	0.5	0.2	0.2	2.0	0.2
	Z+	8		973.4251	0.1	0.2	0.2	0.5	0.2	0.5	0.5	5.0	0.5
3	X+	9	83168	995.4277	0.1	0.5	0.2	0.5	0.5	0.1	0.2	0.2	0.2
	Z+	10		1013.5176	0.1	0.2	0.1	0.2	0.2	0.2	0.5	0.5	0.5
4	X+	11	83169	1011.4053	0.1	0.2	0.2	0.5	0.2	0.2	0.2	0.5	0.2
	Z+	12		1007.5164	0.2	0.5	0.2	0.5	0.5	0.5	0.5	2.0	0.5
5	X+	13	83170	980.595	0.1	0.5	0.2	0.5	0.5	0.1	0.1	0.2	0.1
	Z+	14		1002.9363	0.05	0.1	0.1	0.1	0.1	0.2	0.5	0.5	0.5
6	X+	15	83172	1013.7888	0.1	0.5	0.2	0.5	0.5	0.1	0.2	0.2	0.2
	Z+	16		1073.6235	0.1	0.5	0.2	0.5	0.5	0.5	1.0	1.0	1.0
7	X+	17	83173	983.2784	0.1	0.5	0.2	0.5	0.5	0.1	0.1	0.2	0.1
	Z+	18		954.6505	0.05	0.1	0.1	0.1	0.1	0.2	0.5	0.5	0.5
8	X+	19	83174	1019.4618	1.0	0.5	0.2	0.5	0.5	0.5	0.5	0.5	0.5
	Z+	20		988.5574	1.0	0.5	0.2	0.2	0.5	0.5	0.5	0.5	0.5
9	X+	21	83175	973.8487	0.2	0.5	0.2	0.5	0.5	0.2	0.1	0.2	0.1
	Z+	22		1014.5338	0.05	0.2	0.1	0.1	0.2	0.5	0.5	0.2	0.5
10	X+	23	83176	1000.1573	0.2	0.5	0.2	0.5	0.5	0.2	0.2	0.2	0.2
	Z+	24		985.1972	0.1	0.5	0.2	0.2	0.5	0.5	1.0	0.5	1.0
11	X+	25	83180	1002.247	0.5	0.5	0.2	0.5	0.5	0.5	0.2	0.5	0.2
	Z+	26		1019.3975	0.5	0.2	0.1	0.2	0.2	1.0	0.5	0.5	0.5
12	X+	27	102913	1039.2945	0.5	0.5	0.2	0.5	0.5	0.5	0.2	0.2	0.2
	Z+	28		1019.6451	0.1	0.5	0.2	0.2	0.5	0.5	1.0	0.5	1.0
13	X+	29	102922	989.381	0.2	1.0	0.5	0.5	1.0	0.2	0.2	0.5	0.2
	Z+	30		959.5634	0.1	1.0	0.1	0.2	1.0	0.5	1.0	0.5	1.0
14	X+	31	102924	1004.0335	0.5	2.0	0.5	0.5	2.0	0.5	1.0	0.5	1.0
	Z+	32		1029.681	0.2	1.0	0.5	0.5	1.0	1.0	1.0	1.0	1.0
15	X+	33	102926	978.0894	0.2	1.0	0.5	1.0	1.0	0.2	0.5	0.5	0.5
	Z+	34		1024.9489	0.05	0.5	0.5	0.2	0.5	0.5	1.0	0.5	1.0
16	X+	35	102927	977.7977	0.2	1.0	1.0	0.5	1.0	0.5	2.0	0.5	2.0
	Z+	36		1025.615	0.1	0.5	0.5	0.5	0.5	1.0	2.0	1.0	2.0
17	X+	37	102929	950.6447	0.5	1.0	0.5	1.0	1.0	0.2	5.0	0.5	5.0
	Z+	38		950.953	0.2	0.5	0.5	0.5	0.5	0.5	1.0	0.5	1.0
18	X+	39	102930	1049.7952	0.2	1.0	0.5	1.0	1.0	0.2	2.0	0.5	2.0
	Z+	40		980.8092	0.2	0.5	0.5	0.5	0.5	1.0	2.0	1.0	2.0
19	X+	41	102931	988.3253	0.5	1.0	0.5	1.0	1.0	0.2	1.0	0.5	1.0
	Z+	42		1019.6261	0.1	0.5	0.5	0.5	0.5	2.0	2.0	1.0	2.0
20	X+	43	102932	1009.0189	0.5	1.0	0.5	1.0	1.0	0.2	1.0	0.5	1.0
	Z+	44		1014.2949	0.5	1.0	0.5	2.0	1.0	2.0	5.0	2.0	5.0

that the mass of the accelerometers may change the modes of the structure as they are repositioned to acquire all the measurements needed for the test. If the mass of the accelerometers is significant then there may be an inconsistency in the data from one bank of data to the next. This can cause extreme difficulties when modal parameter estimation is performed. Care should be exercised to prevent this at all costs and appropriate measures taken to mitigate this common difficulty.

The best way to run the test is to have all the accelerometers mounted on the structure and companion data acquisition channels available so that all the data is collected together in a consistent fashion. But often there are fewer data acquisition channels and the measurements need to be made in "banks", with subsequent banks of measurements made until all the measurement points have been covered. One way to check to see if mass loading is a problem is to mount two accelerometers next to each other (or piggyback mounted to each other) and make a measurement to see if there is a significant shifting of the modal frequencies. If there is an effect then there are several remedies available. Mounting all of the accelerometers on the structure is one easy way to do this, even though there are many fewer data acquisition channels available; the mass loading is consistent but the problem is that there is more total mass on the structure. If there is a finite element model then this mass loading effect can easily be included and adjustments made.

The next scenario is that there are fewer accelerometers and fewer data acquisition channels than required measurement points. Often people will move the accelerometers from one set of points to the next set of points until all measurements are made. But this can often result in a mass effect on the structure and therefore an inconsistency in the data collected when going from one set to another. An approach to mitigate this mass loading effect is to mount dummy masses equal to the weight of the accelerometer, so that a fairly consistent mass is maintained as measurements are made. While this is not the best solution, it will make the mass loading problem less severe. So consideration is needed in the test plan of the availability of hardware and instrumentation.

But sometimes clever tricks can be used to help the situation. In one test, years ago, there was a requirement for 50 triaxial accelerometer measurements with a 60 channel data acquisition system. So rather than mount 50 triaxial accelerometers and then have them rove on the structure, small mounting cubes were used, with uniaxial accelerometers screwed into the mounting blocks. All the accelerometers were oriented in the x-direction for the first bank, in the y-direction for the second bank, and then in the z-direction for the third bank. In this way the mass was fairly consistent, and the accelerometers and the cabling just needed to be reoriented and not moved to other measurement locations, thereby minimizing the mass loading problem. The point numbering remained the same and only the direction of response needed to change. This was a much better solution to adding dummy masses on the structure for the test. More information on mass loading effects and some examples are contained in the application chapters of this book.

But one extra step should always be specified if there is collection of different banks of data. If a test is conducted in steps of roving transducers, always check drive point frequency response functions between different sets of tests, especially when testing over several days or when the environment is not stable over time, since this may affect results.

And another measurement problem that is often encountered is when both operating and modal tests are conducted. Often there is a request to use one set of transducers to perform the two tests. Unfortunately, the operating loads are typically higher than the forces induced during an experimental modal test, so the sensitivities of the transducers are not comparable for the operating and modal tests. Often project managers may impose a restriction, requiring the same set of transducers to be used for the two tests to save time and expense. This

will almost always mean use of accelerometers that are not sensitive enough for the modal test, and the measurements will be negatively impacted by noise due to low amplitude signals to be measured with inappropriate sensitivities. Many tests run in this fashion have ended up with measurements that are not very good overall, and the modal results have not been satisfactory.

6.6 How Many Measurement Points Needed?

Certainly this is one of the hardest questions to answer, especially when there are no prior modal tests and a model is not available. But the answer to this question is actually very simple. You need enough measurement points to see the shape defined, which implies that the measurement points need to be sufficient to see the waveform of the mode shape. The problem is that you need to know what the waveform is, and often that is unknown. So the distribution of measurement points needs to be defined very carefully if the actual mode shape is needed. But there are some cases when the entire mode shape is not necessary, especially when the experimental modal model is to be used for simulation of the response due to a variety of different input excitations. In these cases, the only points needed are locations where inputs are to be applied and where response is to be measured; all other points are really just for viewing pleasure only and do not change the simulation of the input–output points needed for response. In Figure 6.7, a space frame structure is shown with three different sets of points. The structure in black shows a larger set of points, which depicts the entire structure and allows the viewer to see the motion of the mode shape at all points. However, the two structures shown in red have a very abbreviated set of points. But if these are all the points needed for the input–output problem then they are totally adequate; it may just be that the viewer cannot understand the complete motion of the entire structure.

In Figure 6.8, the plate structure does not need the 45 points shown in black if there is no need to see the mode shapes. If only two input locations and three response locations are needed to describe the input–output problem, then there are really only five points needed. The 45 point measurement model is only needed because the viewer needs the definition to describe the mode shapes for the structure.

So the definition of points really depends on the purpose for the model or simulation. However, if mode shapes are needed then the points need to be sufficient to describe all the modally active portions of the structure. Often there are portions of the structure that are not of specific concern (or are hidden) and instrumenting these points are not possible. In order to illustrate this, the structure in Figure 6.9 shows two components that are both modally active. If measurements are only made on one part of the structure, it will be very unclear as to what the mode shapes are. The mode in blue looks exactly the same as the mode in red in the upper left portion of the plot. However, when the rest of the structure is added, the two

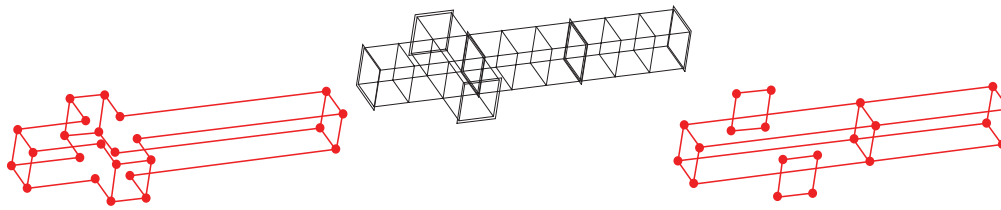

Figure 6.7 Space frame structure with various combinations of measurement locations.

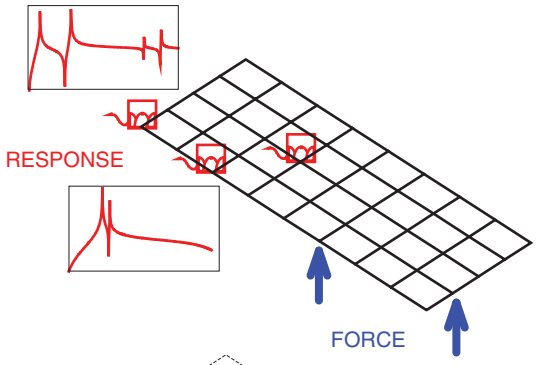

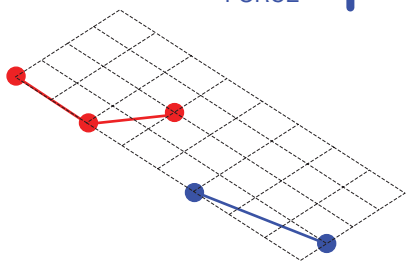

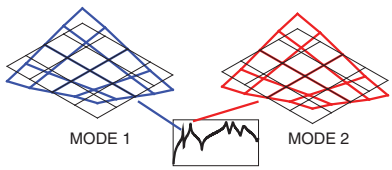

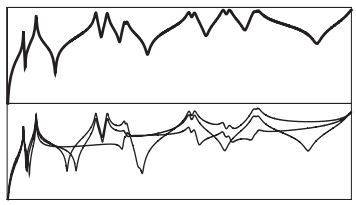

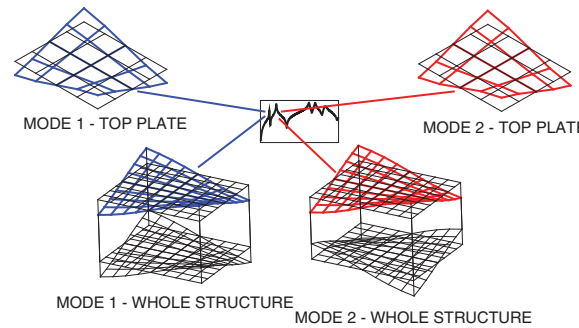

Figure 6.8 Plate model with two input and three output locations.

Figure 6.9 Coupled plate model with one component not measured.

modes clearly have differences because there is a phase relationship that can only be seen if the entire structure is measured. When too few points are measured then a phenomenon called *spatial aliasing* results. Care is very much needed in order to avoid this problem. However, if the modes of the structure are not known then it can become a problem that is not easy to solve.

To illustrate this for another case, the simple plate will be used again. In Figure 6.10, if the measurement points are not distributed to completely see the mode shape then a misunderstanding of the shape could result where mode 1 and mode 3 look the same but in reality are different. And in Figure 6.11, if the measurement points are only at the four corners, a higher order mode may be misunderstood to be a rigid body motion. So a proper distribution of points is critical to the overall understanding of the mode shapes of the system.

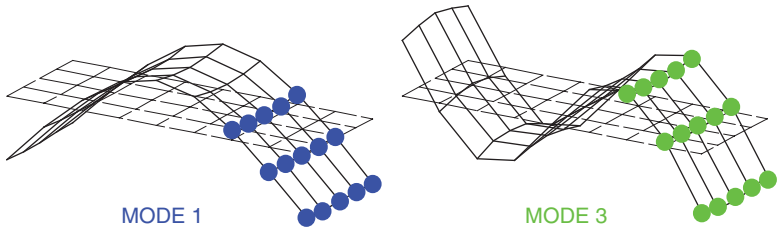

Figure 6.10 Poor distribution of points: mode 1 and mode 3 not distinguishable.

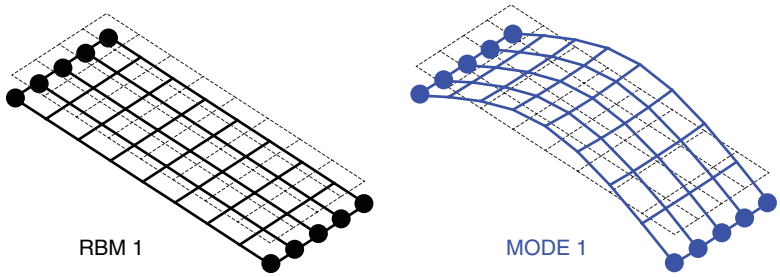

Figure 6.11 Poor distribution of points: RBM 1 and mode 1 not distinguishable.

Often a larger set of reference accelerometer locations might be specified for a roving hammer, which on the surface would already appear to be sufficient. One case of a large composite plate produced results with 9 reference accelerometers and 81 impact locations, but missed one of the lower order modes. Everyone was shocked how this could happen until a finite element model was used to see where there might be problems. Figure 6.12 shows the 9 reference locations and 81 roving impact points. Looking at this figure, it is very clear how a mode was missed: all 9 reference accelerometers were located at the nodes of the mode shown, so it was clear that they were not sufficient to identify this mode.

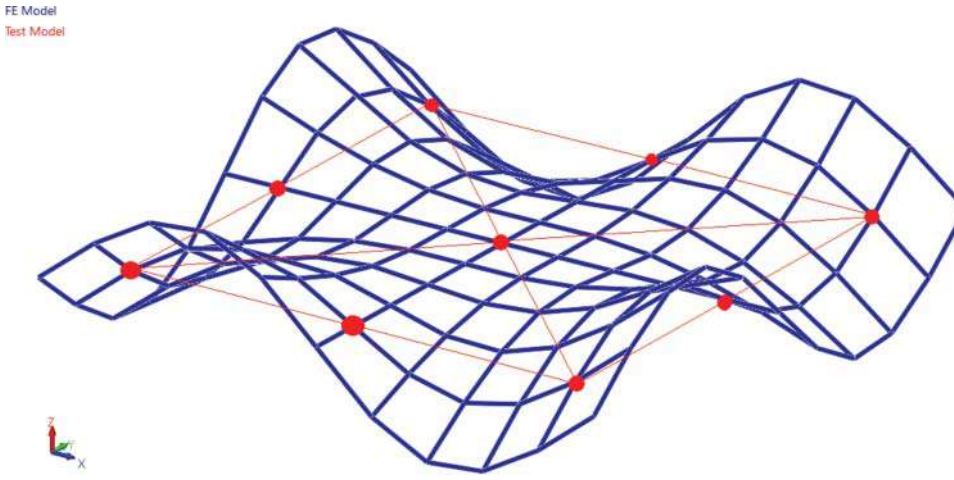

Figure 6.12 Poorly selected reference locations for nine reference accelerometer locations.

6.7 Excitation Techniques

Today most experimental modal tests are conducted using either impact excitation with a calibrated hammer or shaker excitation, with the shaker configured with a force gage or impedance head on a stinger connected to the shaker. These techniques will be briefly described here and further discussed in their respective chapters in this book. While impact and shaker excitation are the most popular techniques, there are many other unusual excitation methods that can be used to obtain the modes of vibration. But it is important to note that many of these excitation techniques do not measure the force applied to the structure and therefore a calibrated frequency response function cannot be obtained and so the mode shapes cannot be scaled. Therefore, unscaled shapes are obtained.

Often, the operating conditions or ambient vibration can be used as a natural excitation to the system, and response measurements can be made and modal parameters can be extracted. These types of systems are often referred to as "output only" systems because there is no applied force that is measured during the process. Often the modes can be captured adequately, but the underlying assumption is that all of the modes are excited. However, if the force is not measured then there is no way to know the energy distribution over frequencies and if all the modes are adequately excited. This can be an important consideration. Of course, there is a benefit to these types of tests because the structure is usually installed in its in-service configuration and the loads are similar to those found in service. The system can be run at different operating levels and in different configurations to determine system performance.

Other types of excitation are used sometimes. For instance, loudspeakers have been used to acoustically excite structures and measure response; this works well for discrete sine testing when trying to excite a particular mode of a small jet engine turbine blade for instance. And a pluck test can often be used to excite larger structures where the lower order modes are of interest. However, for the most part impact hammer excitation is the most popular method to make experimental measurements for modal testing, followed by shaker excitation. These approaches are covered in two separate chapters because there is so much to discuss; only some brief introductory remarks are made here. Impact testing is by far the most common and most popular way in which experimental modal tests are conducted. This is a very easy and portable approach for acquiring experimental measurements for a modal test. Shaker testing, which is the next most popular approach to modal testing, requires more hardware and is much less portable than impact testing. But shaker testing has a few very important benefits when compared to impact testing. Shaker testing allows for a much more uniform and controllable excitation of the structure, which is very important when testing larger structures and structures that may have some slight nonlinear characteristics that need to be identified. But shaker testing requires more hardware and more equipment setup, which is very important to consider especially when performing troubleshooting tests, where time is at a premium.

6.8 Miscellaneous Items to Consider

While the old days of a paper logbook may be gone, there is a critical need to maintain a sequential logging of the events that occur during a test. An individual's memory may not be sufficient to recall all the steps that were taken, especially small details that seem to be insignificant at the time. In addition, there are circumstances in which data may be collected by one group and reduced by another group. While this is not considered to be an ideal situation, the fact remains that this sometimes occurs in larger organizations that perform bigger modal tests. In one test on a large optical telescope, there was one operating test (Test 25) out of a series

of 57 different operating configurations of the telescope where the modal data extracted from the test appeared to correlate to the traditional impact modal tests much better than any other dataset, even though that particular configuration was considered to be one that should have the least correlation. Each of the datasets was reviewed several times and there didn't appear to be a reason for the good correlation. The people who collected the data were not the same ones who reduced the data. After some considerable time was invested, the logbook revealed that Test 25 was conducted and requested specifically by the project engineer responsible for the test. It included a new windscreen that had been designed by the project engineer, and for that one particular test he had halted all construction at the site while measurements were made. Because of this, the data collected had much less noise than for the other tests, where all the data was all collected in a noisy construction environment. So that one dataset was actually better than most of the other datasets, which was likely the reason for the improved data. This would have never been known if it hadn't been captured in the paper logbook.

During a test, many things should be checked and monitored to ensure that there is a stable environment and that all the equipment used to perform the test remains in a constant state throughout the testing. A test of a large piece of mining equipment took place over a series of days. The equipment was freely supported with an air bag system. What no-one noticed (or even thought to check) was that the pressure in the air bag system was not held at a constant pressure. One SISO test was run on one day and then a second SISO test was run on a different day once the shaker had been moved to a different excitation location. The different sets of measurements were collected over several days and upon initially reducing the data and reviewing the mode shapes, there were results that seemed to be inconsistent. All the frequency response functions were compared and there was an obvious shift in the peaks of the flexible modes, but the cause was not readily known. However, upon inspecting the lower frequency range, where the rigid body modes reside, there was much clearer evidence that there was a shifting of the peaks in the frequency response functions. While the low frequency rigid body modes were not the focus of the test, these modes provided the needed information that there was an inconsistency in the data. The frequency response functions are shown in Figure 6.13 and clearly show the inconsistency in the datasets. One set of data was collected with the accelerometers all mounted with one shaker excitation (blue, upper left) and a second set of data was collected with all the accelerometers mounted with the shaker at a different excitation location (red, lower left); all of the data is shown combined into one dataset on the right of the figure. Each dataset contained useful data because all the accelerometers were mounted to collect all the data at the same time. However, merging the two datasets created an inconsistent set of data. Digging deeper, the cause of the problem was that one of the air bag support devices had air pressure of only 20 psi; all of the air bags were initially pressurized to 40 psi and no-one had checked the pressure during the test. Fortunately, this was caught at the end of the test when initial data reduction was performed and the discrepancies in the data could not be explained.

In another test on some computer cabinet equipment, there was a very distinct difference in the mode shapes that caused some concern. The test was collected with a roving set of accelerometers that was moved into six or seven different parts of the structure. While the test was only to look at the overall computer cabinet arrangement, the large 19 inch computer rack needed well over 200 measurements, which were recorded with a 40 channel data acquisition system. Mass loading of the accelerometers was not a critical issue in the roving of the accelerometers but there was a very distinct difference in the mode shapes in certain portions of the structure. On the surface, there was no apparent reason why this could have happened. However, upon reviewing the logbook with the sequence of events, there was a time during the test where one of the engineers opened one of the cabinet doors between one of the roving sets of tests. Apparently when the door was closed, the latch was not properly reseated and this

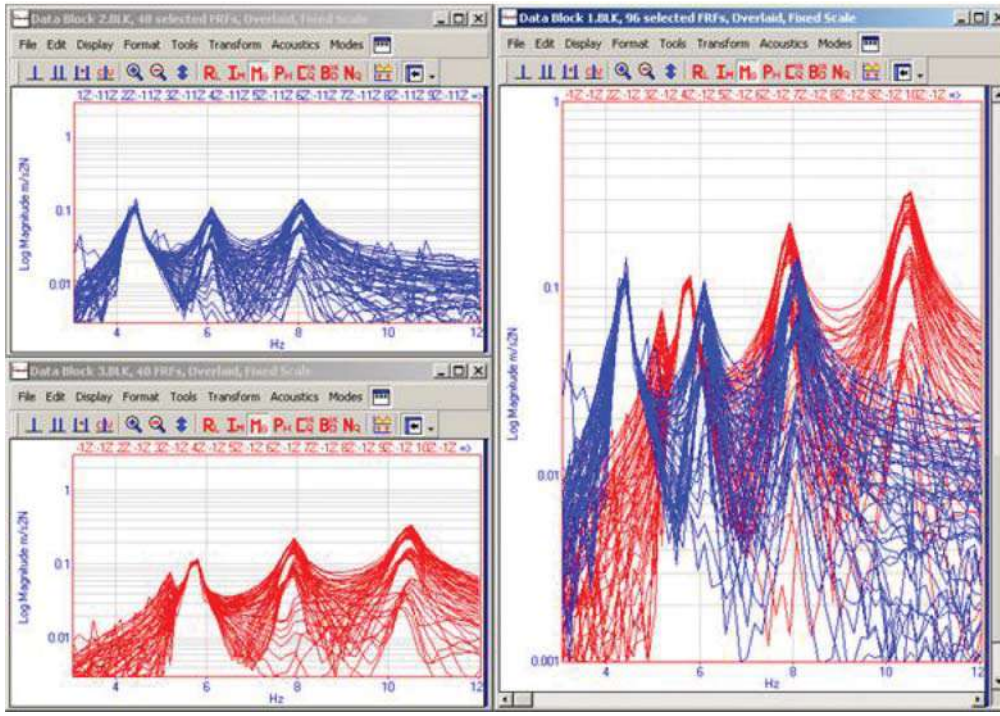

Figure 6.13 Mode shifting due to air bag pressure changes during SISO shaker testing.

gave rise to a change in the system characteristics and had a direct effect on the frequencies and mode shapes of the system. Because the data was collected in an odd sequence, the log-book helped to identify which measurements were taken at which points in time and when the computer cabinet door was opened and closed. Once this had been determined then the data made much more sense.

And one other test, many years ago, involved testing six vehicles subjected to a wide variety of NVH testing, one of which was an experimental modal test. The goal was to identify how much variability of modal parameters might exist, since this would help with the analytical model predictions. The initial results of the modal tests were confusing and no-one could believe some of the test results obtained. What was unknown to everyone was that modifications were made to each of the six different vehicles during the course of the testing due to the nature of all the different NVH tests performed. So in reality, each of the cars was not exactly what might come from a typical production line due to all the different tests that were performed. There was so much variation as each vehicle was received for modal testing that the comparisons were not useful for the intended study regarding variability. This is not a statement about the ability to conduct a good modal test; the differences found were due to each of the different NVH groups making what appeared to be as small modifications to conduct each of the different types of tests they needed, thereby rendering the six vehicles sufficiently different to prevent meaningful results being obtained from the study.

It is always important to perform some preliminary data reduction to make sure that all the data collected appears to have the modes expected before the test site is vacated. This step is extremely useful, especially when all the data collected is streamed to disk and only time data is collected. Often a quick data reduction will reveal if the data is acceptable or not. At times, a test structure may only be available for a short period and if the data collected is not adequate then

there may not be another chance to retest the structure and obtain the data needed. A quick look at the data before leaving the test site will at least provide some sense of whether it is adequate or not. One test, a few years ago, produced unacceptable results and no one looked at the data before they left the test site. Unfortunately no one set the accelerometers to the ICP setting on the data acquisition system and all the data collected was essentially useless; it contained no information that could help solve the problem at hand. In another test, decades ago, data on an aerospace structure was collected with a compression approach involving 128 channels of data on a 14 channel analog tape recorder. The data was collected and the structure was released to the next phases of the project before it could be reviewed. The data collected was not the best and unfortunately there was very little good data to be extracted from this complicated structure; any hopes of correlating the data to the finite element model were quickly dropped. Upon first reviewing the data, requests to recollect better data were not approved because the structure was no longer available to the organization. In both of these cases, some preliminary review would have been able to quickly identify that the data was not of sufficient quality for the needs of the project.

Taking photos of test setups and their different configurations for the modal tests provides invaluable information when a year or two has passed (or even a week) and when there is discussion regarding the results and what the actual test configuration looked like at the time: shaker setups or test support condition setups and any of the other items regarding how the actual test was performed. Today, with digital cameras in abundance, many pictures can be taken, with zoomed out and close-up pictures of all details of the test setup. Photos should be routinely taken for all accelerometer locations, with clearly visible cables for tri-axial accelerometers and serial numbers if possible. This information was very helpful in one test where, after the test was complete, the modal shape data had unusual features. It turned out that two cables had been switched. The photo helped to resolve the concerns about the data collected. Figure 6.14 shows a collection of unrelated photos taken during different modal tests. Notice in the upper left picture that there is an identifying feature of the strain gage that was mounted for the test on a wind turbine blade as part of a qualification test; this was a large 60 m wind turbine blade,

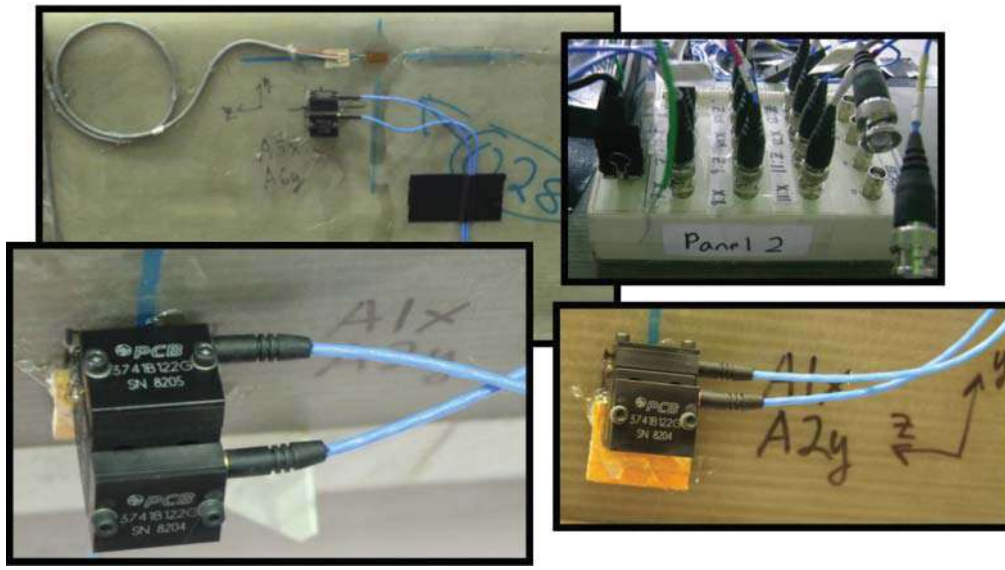

Figure 6.14 Typical accelerometer test locations.

so the accelerometer and strain gage are considered to be at the same point because of the size of the wind turbine blade. However, the picture helps to locate the accelerometer and strain gage with respect to each other.

The selection of a coordinate system and the location of the origin are often overlooked. Now this may sound like a silly thing to worry about, but there have been many tests where the finite element model uses one coordinate system and the test uses a different coordinate system. Even simple things such as what is positive and negative can create issues when discussing the results following the test. Selecting a common coordinate system is very easy to do and can eliminate confusion later on, when discussing the results and explaining the test data. the selection of consistent units is also important. Within one company there is usually a commonality of units, but this is not always the case when different entities are involved.

Structures with symmetry can also cause difficulties when trying to correlate with a finite element model and test data. While the structure may appear to be symmetric, there may be some internal components or mass distributions that cause the modes to not be symmetric, leading to confusion when describing the modes and correlating to the model. Figure 6.15 illustrates a structure that had all of these complications. The structure on the left was a housing for a payload for an F-15 fighter, which had a distribution of mass that made the modes asymmetric; correlation to the model required the proper orientation. The panel on the right was also difficult because there were no defining locators in the test data to ensure that the structure was properly aligned to the finite element model in scale, node location, and rotation. All these factors caused difficulties.

Mass loading of accelerometers is sometimes considered a small problem. But at the times, small shifts in frequency can have dramatic effects, especially when structures are coupled together. In order to understand this effect, a review of the tuned mass absorber in Figure 6.16

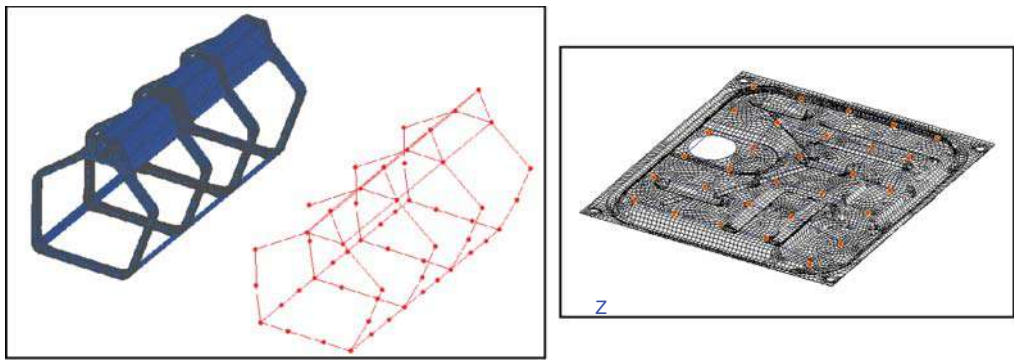

Figure 6.15 Symmetric configurations: orientation necessary.

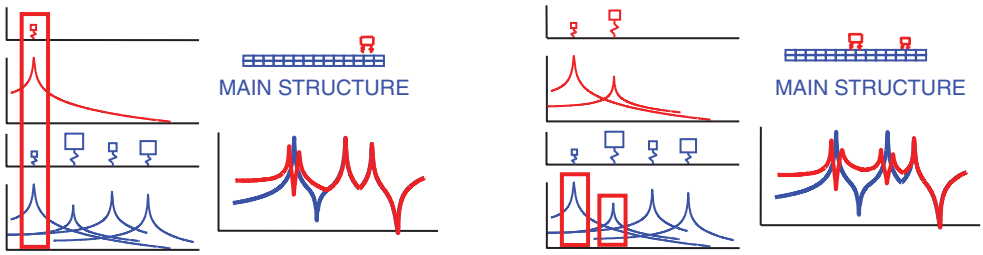

Figure 6.16 Illustration of simple tuned mass absorber.

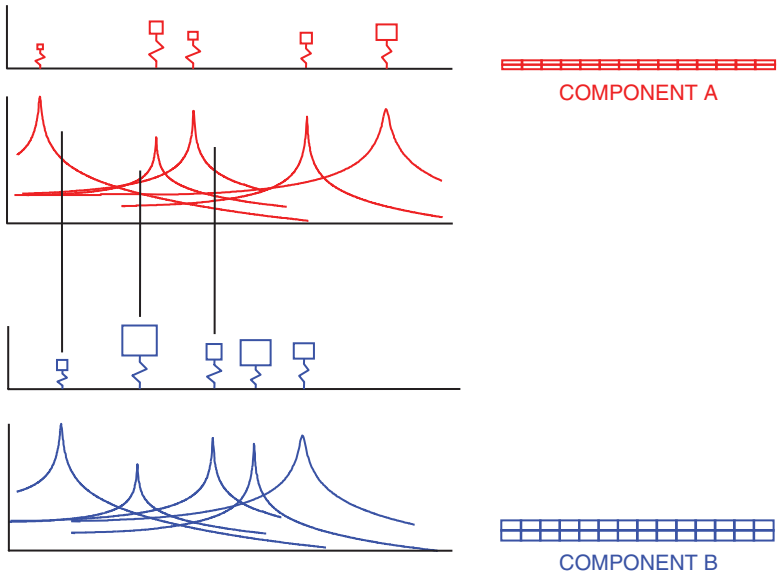

Figure 6.17 Schematic of dynamic coupling effects of modes.

will bring several points into focus. On the left is the application of a simple mass–spring system (in red) to the structure (in blue); notice that the first mode splits into two modes because the added tuned mass absorber is designed to have the same frequency as the structure. On the right, two tuned mass absorbers are applied for mode 1 and mode 2 and the first two peaks are split into four peaks again because the tuned absorber is designed to do that.

So now Figure 6.17 shows two components that are tied together and it needs to be understood that both components are nothing more than a collection of single degree of freedom systems and if the modes of component A line up with the modes of component B then there will be dynamic coupling between the two components. That will have the same effect as the tuned mass absorber but on multiple modes simultaneously if the frequencies of both components line up with each other. So if a small mass loading effect shifts the modes of one of the components then the modes may line up differently and a completely different dynamic coupling will result. The figure illustrates this possibility. So small mass loading effects can be quite dramatic and produce entirely different system characteristics.

The setup can also have some serious consequences if care isn't taken when conducting a test. A series of tests was conducted on six small wind turbine blades for a comparative study. The blades were clamped to a large anchor at three blade mounting hole locations. However, the bolting rods were a little long and, at the end of testing three blades on a Friday afternoon, someone suggested adding some lightweight packing foam on the exposed studs to prevent injury to people in the lab. When testing resumed on Monday, the last three blades were tested and in consideration of safety the foam was retained for the test. However, when the results were compared there was a dramatic 40 Hz shift. Ultimately it was determined that the very light foam on the cantilevered stud had a natural frequency close to the fifth mode of the blade and acted like a tuned mass absorber, causing a significant change in the frequency measured for the turbine blade. Had this not occurred, the effect might have gone unnoticed. This illustrates the importance of having a proper test setup. Very small, seemingly unimportant aspects of the test setup can have a significant effect on the results. Figure 6.18 shows this dramatic shift due to what appeared to be an insignificant change in the test setup.

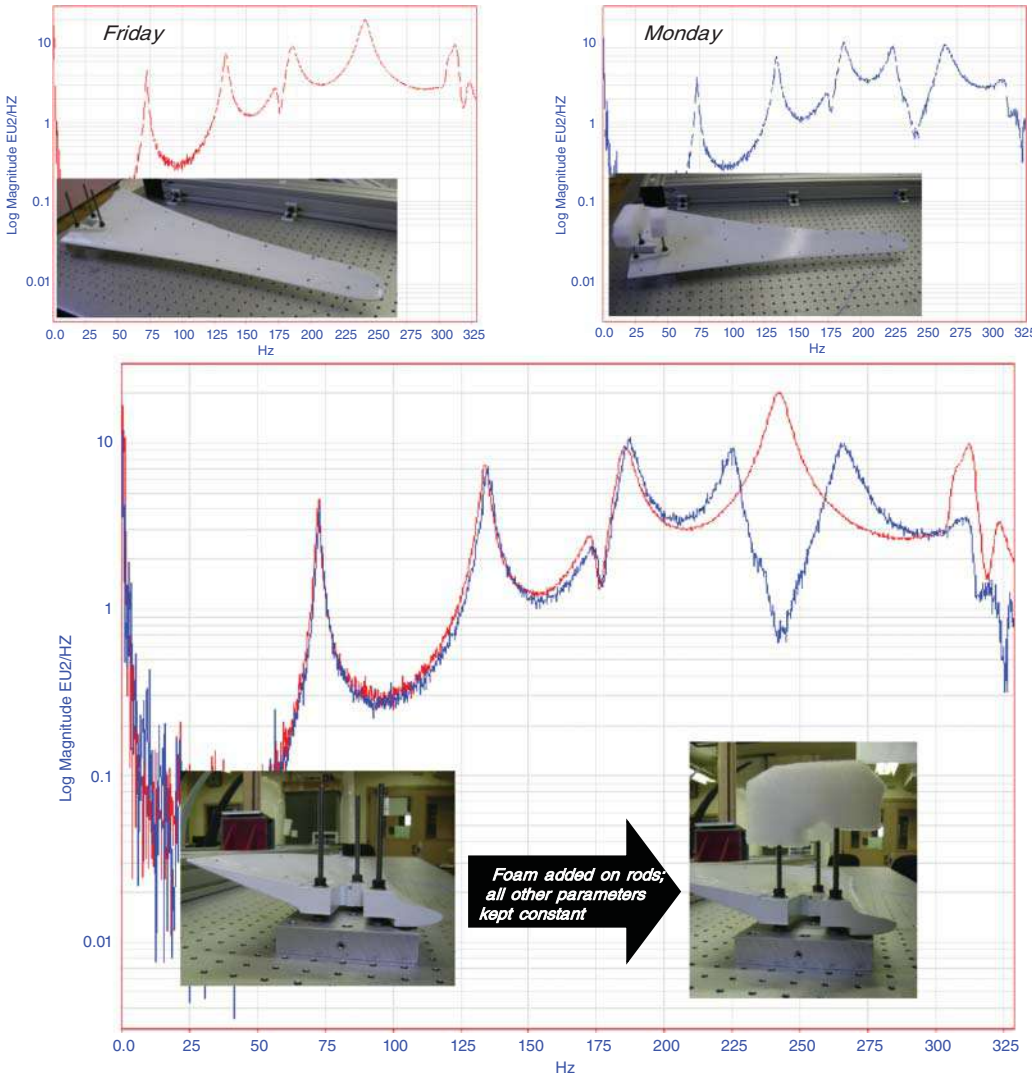

Figure 6.18 Effect of very small change to test setup.

Of course, backing up data as the test progresses is always a good thing to do and should be done every few hours, between different tests, or on some other regular basis. Years ago, a test engineer was not backing up data as his test progressed. No one was aware of this. On the third day of testing there was a need to transfer the data to the analytical group. The test engineer copied the dataset but wasn't sure if the correct database had been copied. So the incorrect dataset was deleted and when the data was selected to be recopied, only an empty dataset remained. Inadvertently, the test engineer had deleted the data and there were no back-ups; all the data was lost. It is therefore vital to make duplicate copies of datasets on separate devices so this does not happen. And as a general rule, the original virgin datasets should never be manipulated; only copies should be used for analysis and manipulation so as to prevent any unintended mishaps.

And as a general rule, all data should be written out to a universal file format that can be read into any software package. This is critical as software packages are changed as time progresses. Test data might be collected with Company A's software and saved in Company A's proprietary format. Several years later, however, Company A's software might have been replaced with Company Z's software, meaning that none of the earlier data can be accessed. Now this may seem like a small issue, but as decades pass access to old databases may become impossible. The use of old computer platforms should also be considered. Decades ago, data was collected on Digital Equipment or HP1000 or HP Unix hardware. The binary files from that time are not necessarily accessible with current computer platforms. While universal files are not perfect, at least they are accessible, unless stored on floppy disks or zip disks which may no longer be readable. A few small extra steps can really save time later. Consider specifying the data backup mechanism carefully.

So, these are a few items that need to be considered when performing a modal test.

6.9 Summary

This chapter has reviewed some of the very basic things to consider when conducting an actual modal test. Very basic information that is always needed, such as a test plan, was discussed. This was followed by items such as the scope of the test, the frequency range required, the modes to be extracted, the number of points to be acquired, excitation approaches and many other items that can easily be forgotten but are usually needed for modal tests.

7

Impact Testing Considerations

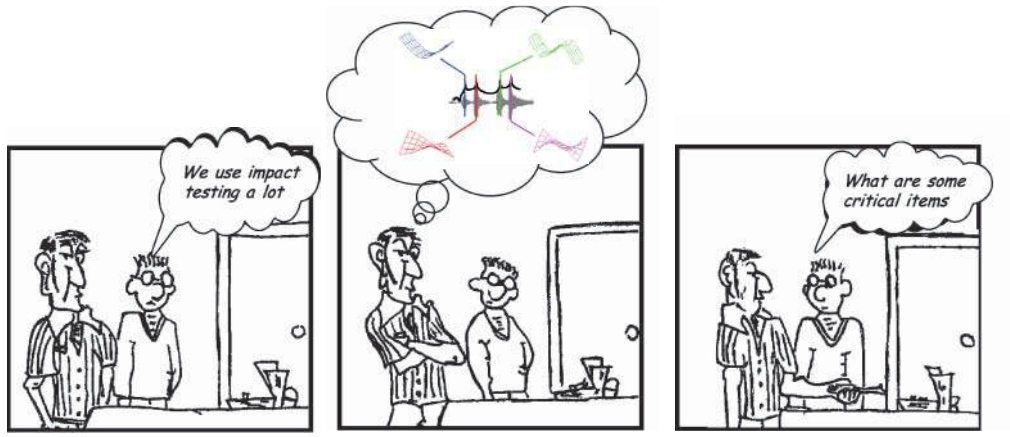

In an earlier chapter, some of the basics of impact testing were discussed. This included a basic discussion of the hammer configuration and the hammer tips. Some discussion on the different hammer tips and the input force spectrum was presented, along with the typical structure exponentially decaying response that is observed. Force and exponential windows and the use of pre-trigger delay were presented, along with some discussion of double impact difficulties. An example was also presented. This chapter presents a wide variety of additional practical considerations with regards to impact testing and has examples to show the results if care is not exercised when collecting data. There is also discussion of some misconceptions regarding this commonly used excitation technique.

7.1 Hammer Impact Location

If the impact test is going to be conducted with a roving hammer, then the hammer location is not of concern. The reference point where the accelerometer is mounted is the key. The reference location should be at a location where all of the modes can be clearly seen. But the chances of this happening are slim in typical structural systems. So then the key is to use several different accelerometer locations from which, in total, all of the modes can be observed.

However, if the hammer is going to be stationary, then the location is very important. The hammer is now the reference location and it should be located at a point where all of the modes can be observed. Of course, this too may not be possible and then several different impact locations may be required, from which, in total, all of the modes can be observed.

Modal Testing: A Practitioner's Guide, First Edition. Peter Avitabile.

Companion Website: www.wiley.com/go/avitabile/modal-testing

In either case, knowledge of the expected modes of the structure is critical in conducting the modal test. Extreme care needs to be exercised if the mode shapes of the structure are not known. Placement of the reference can easily occur at a node of a mode if the mode shapes are not known and care is not taken.

7.2 Hammer Tip and Frequency Range

Earlier, the hammer and tip and useful frequency range were discussed. It is critical to re-emphasize this important fact: Typically the harder the tip, the wider the frequency range that will be excited; the softer the tip, the lower the frequency range that will be excited. A few hammer tips and the typical frequency ranges they excite are shown in Figure 7.1. Of course, this data comes from impacting the tip on a large steel block that has no local deformation; if these tips were used to excite a more flexible structure then the frequency range excited would be heavily dependent on the structure's local flexibility and the location where the structure was excited. Don't ever rely on the published curves that are provided with impact hammers; the input spectrum to the structure may not have the same overall frequency range excited. This must always be checked. Some of the examples here will shed more light on this topic.

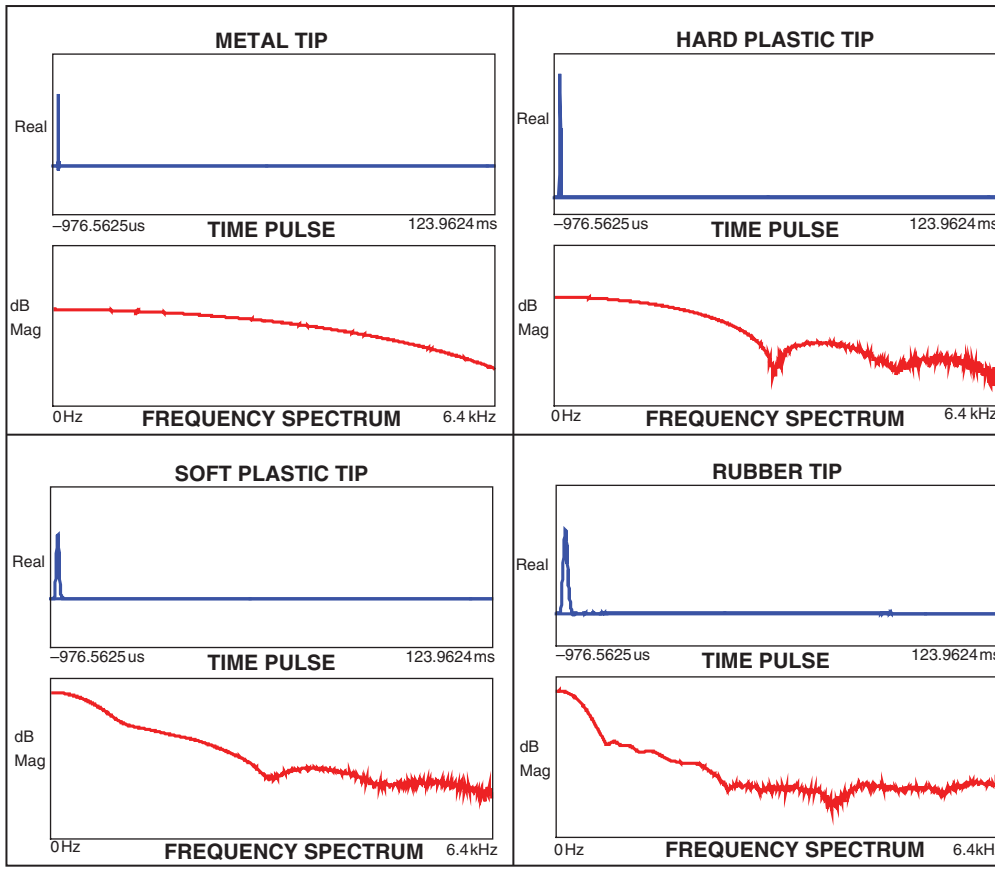

Figure 7.1 Time pulse and frequency spectrum for several hammer tips.

Now before any other aspects of impact testing are discussed, a quick set of measurements is provided, with a soft, medium, and hard tip but the impact is also varied, from a soft hit, to a medium hit, and then a hard hit. This is very important to see the variability in the input force spectrum and frequency range excited. An impact was made on a very large and massive steel block. The force level applied to the block was kept to a softer level, a medium level, and a harder level. In addition, an air capsule tip was evaluated, then a plastic cap on top of a hard plastic tip, and then a hard plastic tip on its own. The results of these impacts (time pulse and input spectrum) are shown in Figure 7.2.

The air capsule tip shows a dramatic change in the time pulse and resulting force spectrum depending on the force level applied. Notice that the frequency spectrum excited with an attenuation of 20 dB changes significantly (and the hardest hit excites a much wider range overall). So if an impact test is performed and every hit for an average has a different level of force, the spectrum excited by that impact is significantly different each time. This could have a significant effect on the coherence for the higher frequency ranges.

A plastic cap on top of a hard plastic tip can exhibit the same behavior in many cases. For this particular test, the plastic cover was slightly longer than the hard plastic tip so that there was effectively a small air pocket included. Again, depending on the level of excitation applied, there may be a significantly different input force spectrum/frequency range excited.

A hard plastic tip shows relatively little variation in the spectrum force characteristics over the frequency spectrum excited. There is the same small variation but, relative to the previous two tips, it is very small. So the frequency range excited with this tip will be relatively constant even with relatively different impact levels applied.

This effect is very important when testing structures where the frequency range to be excited is critical. For the first two tips, the frequency range excited is dependent on the level of excitation used. Care must be exercised to ensure that a fairly consistent force strike is applied with every impact, for every average, and for every measurement. This is not so easy to do all the time. So take care when using some of those special tips in your impact hammer kit.

7.3 Hammers for Different Size Structures

Impact testing can be performed on very large structures such as bridges and buildings, very small structures such as jet engine turbine blades and computer disk drives, and everything in between. Of course the size of the hammer will vary depending on the size of the structure. A very large three foot sledgehammer can be used to test large trucks, busses, and larger framed structures. A miniature hammer can be used to test small lightweight structures such as computer disk drives, golf club face plates, and small jet engine turbine blades. Of course, there may be some extremely small structures or very large structures that are not be suitable for commercially available hammers and sometimes custom impact excitation devices may need to be designed. These will not be discussed here because they are very problem specific, however, a large pendulous mass with a force gage could be devised to impact a large structure or a small metal ball bearing could be used to excite a very small structure. But these are specialty situations.

A recent test of a large 60 m wind turbine blade used a large sledgehammer to provide excitation for determination of some very low modes at less than 10 Hz. The measurements obtained were very good for this structure. Of course, care was taken to ensure that a good input frequency spectrum was obtained and the resulting frequency response functions and associated

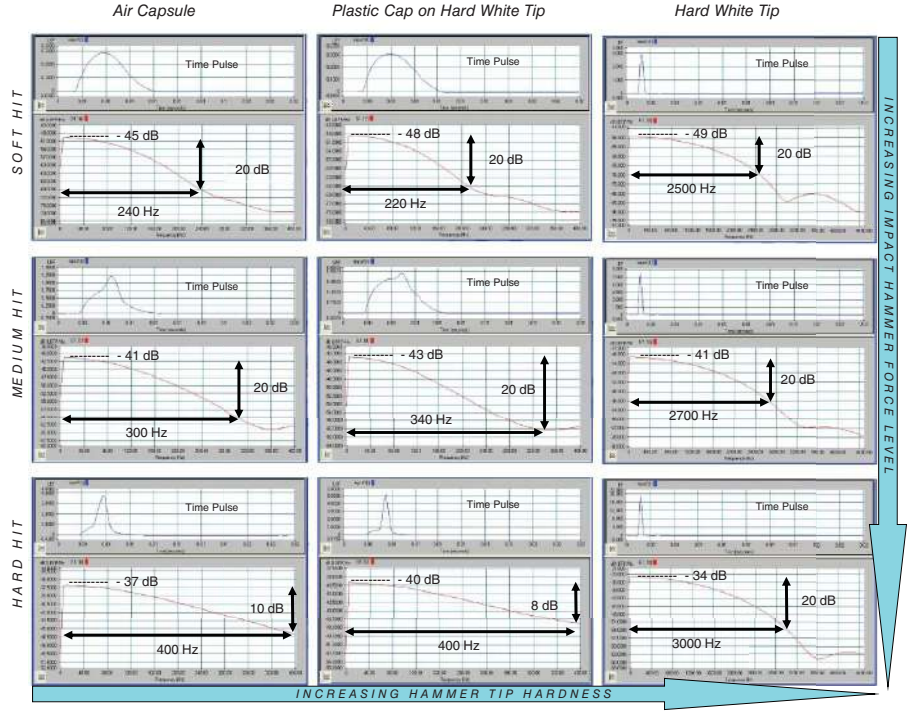

Figure 7.2 Comparison of tips of different hardnesses with different impact strengths.

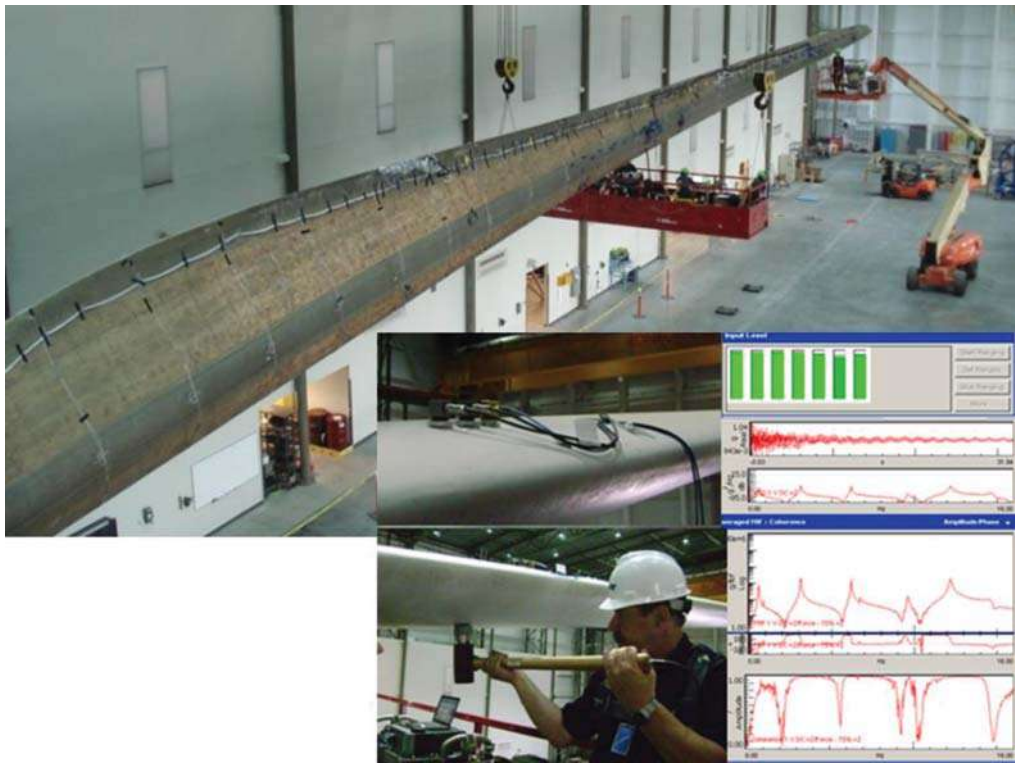

Figure 7.3 Impact test setup for a large wind turbine blade.

coherence were all acceptable. Figure 7.3 shows the turbine blade with test equipment setup for the modal test.

But for a test of a structure of this size, consideration needs to be given to the wiring and cables associated with the test. In this test, the accelerometers were grouped in three separate patches and then all routed to a common point where the data acquisition system was located. This is shown in Figure 7.4. The cable for the hammer needed to be long enough to reach all the potential impact locations. The data acquisition system was located at the midpoint between the accelerometer patches. Because the accelerometers were all mounted on the structure, the hammer was not roved to all the measurement locations; only four separate impact locations (in two directions) were used for the modal test for a total of eight separate references. And in fact, all references were needed because for many modes only two references were actually useful, with significant modal participation factors. At least two of the references (not the same ones) had poor modal participation factors for certain modes but were definitely needed for other modes. So while theory says that only one reference is needed to identify the modes, trying to select one reference point that is good for all the modes is often very difficult.

To illustrate this, an example set of modes for a generic large wind turbine blade are shown in Figure 7.5. Now as the mode shapes are reviewed, there are four reference locations shown in red. Notice how, for several modes, two of the references are very close to nodes for certain modes but at very good locations for other modes. When this test was conducted, the customer did not want to reveal either the frequencies of the turbine blade or the mode shapes of the turbine blade. Without any knowledge of the mode shapes of the structure (other than experience or "gut feel"), the selection of the reference points was not an easy task. While in

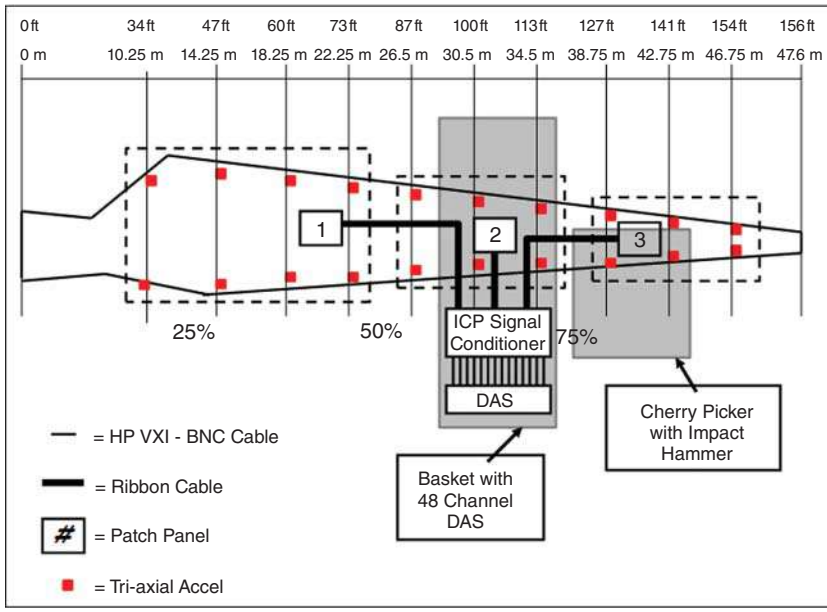

Figure 7.4 Wiring layout for modal test of a large wind turbine blade.

this case a total of eight references (four in each of the two primary mode directions of flap bending and edge bending) might seem excessive, selection of this many references turned out to be wise once the final mode shapes were reviewed. While at first glance the modes of the wind turbine blade may seem to be very simple cantilever beam bending modes, this may not be the case; the actual mode shapes of the blade are very strongly affected by the composite blade layup, which is not obvious when looking at the exterior of the blade.

And in another test of a large structure – an optical telescope – all 100 accelerometers were mounted on the structure because operating tests were going to be conducted with a wide variety of different configurations studied and with whatever actual wind conditions existed at the site. While the customer was not interested in a modal test (and didn't want the extra time required for the test), a modal test was actually performed between the times when the wind had died down and there was no useful operating data to collect. So a strategy (which should be part of the test plan) as to how to alter the procedure for conducting the test and the layout of all the instrumentation so as to facilitate moving from an operating test to a modal impact test needed to be well planned. The test was performed while construction was underway and the impact modal test needed to have the best data possible. The appropriate time for the modal tests was at lunchtime, when the crews stopped working and went to the canteen for lunch. A quick reconfiguration of the test setup was clearly identified in the test plan and enabled the impact tests to be conducted at a quiet time and without disruption to the operating data collection. Following the test, the customer asked if there was any additional data beyond the operating tests to confirm the modal information, and luckily that data had been collected and was available, even though that was not originally requested as part of the test.

Figure 7.6 shows the Gemini telescope during testing at a remote mountain top in Chile. One difference between this test on the telescope and the test on the turbine blade was that all the data collected for the telescope was streamed to disk for later processing. During the week of testing, some of the data was reduced at night, enabling the testing staff to be sure

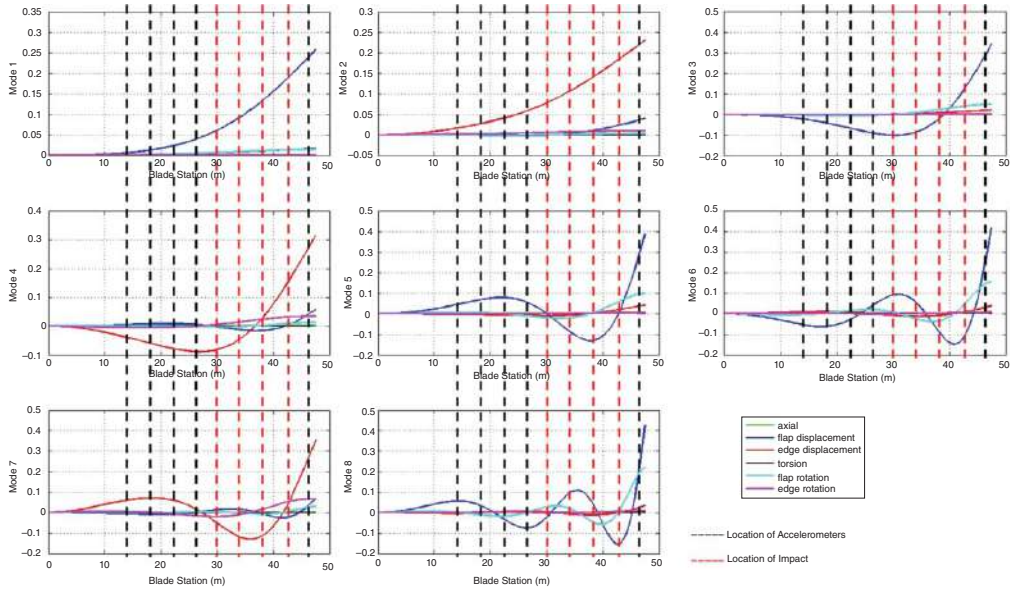

Figure 7.5 Typical flap and edge mode shapes for large wind turbine blade tests.

Figure 7.6 Modal and operating testing on a large optical telescope.

that useful data was being collected. In fact, two impact modal tests were conducted because the first test was actually conducted during the ongoing construction during the day; initial evaluation revealed that while the data was useful, there was enough background noise that recollection of the impact data was necessary. This highlights the important point that some preprocessing of the data collected should always be performed, because the structure may often not be available for additional testing if some of the data is inadequate for extracting useful information. Certainly, once the Chile telescope test site had been vacated and the test team returned home, retesting the structure for any additional data would have been very expensive, time consuming and in some cases just not possible.

Now big structures pose a completely different set of practical issues when compared to very small structures. In the case of modal tests performed for dynamic characterization of natural frequencies in golf club face plates, the ability to repeatedly impact exactly the same point, in the same direction, is a very big concern. So for the golf club testing, a special tripod hammer holder was configured with a small coffee straw. The swivel head of the small tripod enabled a very precise location to be selected. Then, with the swivel locked in place, a small flick of the straw allowed the hammer to impact the golf club face in a consistent and repeatable fashion. This arrangement is shown in Figure 7.7, in which 3 laser vibrometers are used to make several measurements at a time (along with a microphone and accelerometer mounted on the back of the club head).

So, in the big telescope test or big wind turbine test, small deviations of the actual input location are not critical; if the impact is off by a small amount of one half inch or so, it is of no consequence because of the large size of the structure. But for a golf club face plate, small deviations can have a much more pronounced effect, as can be imagined. Actually, this simple impact hammer configuration has been used in the lab since 2000, when this testing was first done, and has proven to be invaluable when testing smaller structures in which the precision of the impact location is of concern.

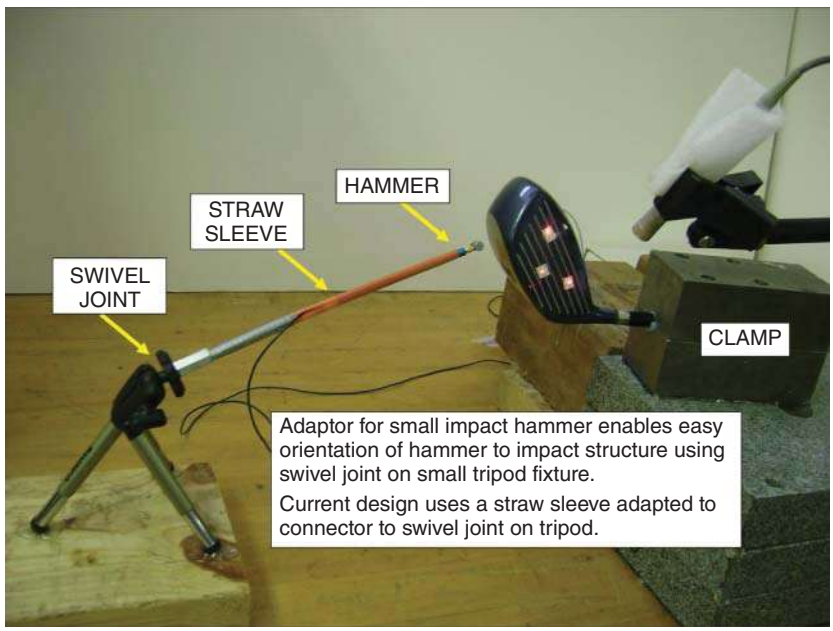

Figure 7.7 Schematic of golf club testing with small impact hammer configured with a small camera tripod.

7.4 How Does Impact Skew and Deviation of Input Point Affect the Measurement?

The effects of consistently impacting the same point and impacting in the same direction are very important and become more important when smaller structures are tested. Two cases are presented here to evaluate this.

7.4.1 Skewed Impact Force

A frequency response measurement is made and for each of the averages and the hammer is intentionally skewed so that the impact force is not exactly in the same direction for each impact. This can easily happen in a test when care is not exercised for each measurement made; this may happen when a long day of testing occurs or when the point to be impacted is not in an easily impacted location. The problem is that for each measurement made, the impact force is not in the same direction and then there is an inconsistency from one impact to the next. This will result in a degradation of the coherence for that measurement. Figure 7.8a shows a good set of results, where each measurement was made with care to impact the same point and in the same direction. Figure 7.8b shows the result of a lack of care in ensuring that each impact is made in the same direction; the same point was hit but the angle of impact was not the same for each measurement made for the averages obtained. While the measurement in Figure 7.8b is not terrible, it is not as good as the more accurate measurement in Figure 7.8a. This is most clearly seen in the coherence of the measurement. Obviously, care needs to be taken to obtain the best possible measurement.

7.4.2 Inconsistent Impact Force Location

A frequency response measurement is made and, for each of the averages, the hammer is intentionally impacted close to the desired point but not exactly at the same point for each measurement. While the direction is kept the same, the actual point is slightly different for each measurement. This then makes each measurement inconsistent with every other measurement of the average. Figure 7.9a shows a good set of results, where each measurement was made with care to impact the same point and in the same direction. Figure 7.9b shows the result of a lack of care in ensuring that each impact is made at the same point; the angle of impact was the same for each measurement but the actual point of impact was slightly different for each measurement for the averages made. While the measurement on the right is not terrible, it is not as good as the more accurate measurement on the left. Again, this is most clearly seen in the coherence of the measurement. Obviously, care needs to be taken to obtain the best possible measurement.

7.5 Impact Hammer Frequency Bandwidth

The selection of the hammer tip for an impact test and selecting the proper bandwidth for the test are two very important factors that need careful consideration. At times, too hard a hammer tip may be selected and then the actual excited frequency range may be well beyond the selected bandwidth for the measurement. At first, this may not seem to be a problem because the FFT analyzer will only address the bandwidth selected. But the problem is that the energy of the impact is well outside the bandwidth and, more importantly, the actual accelerometer response will be due to all of the modes excited by the impact and the accelerometer output voltage will

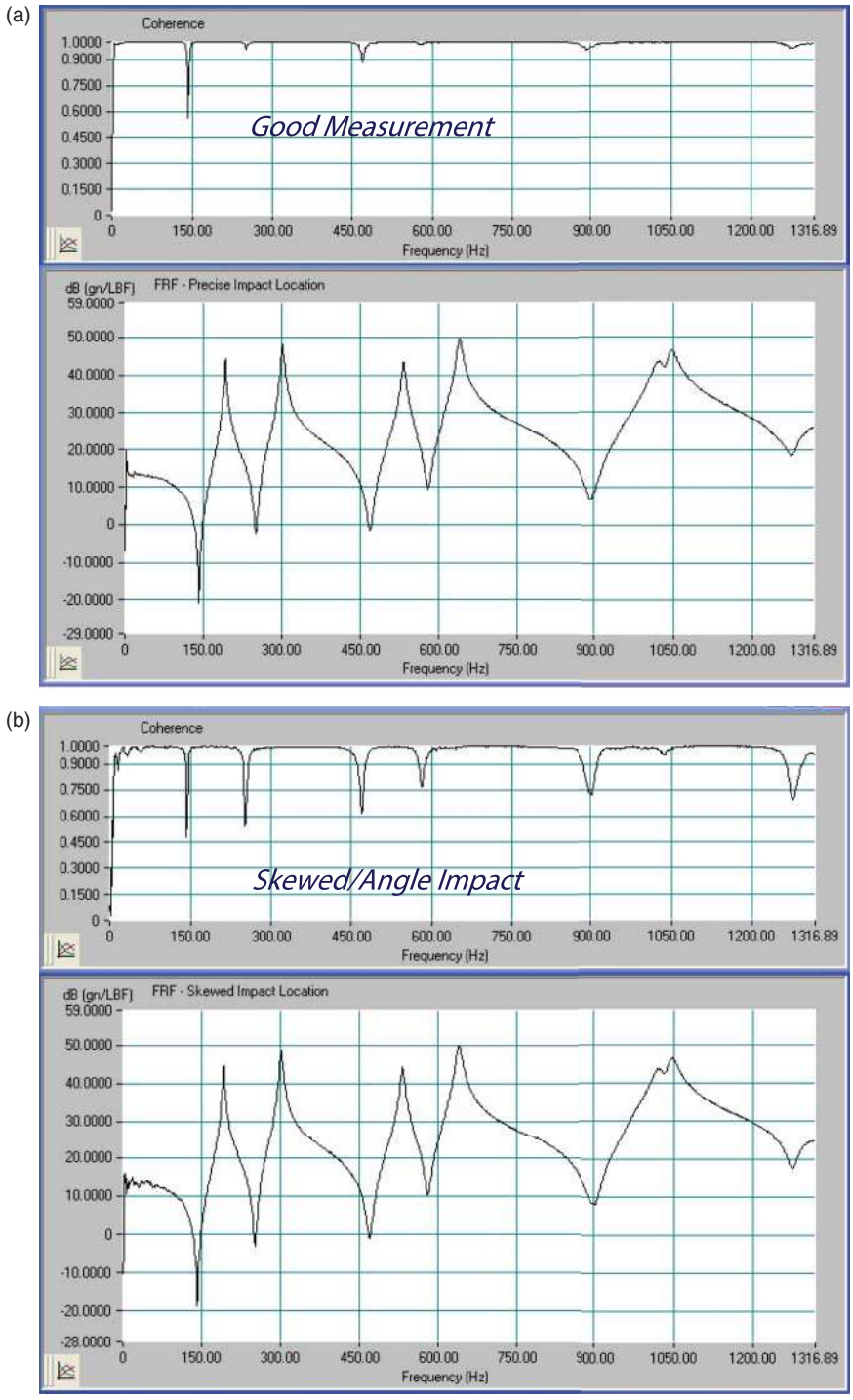

Figure 7.8 Measurement for (a) a good impact excitation (b) a skewed impact excitation.

(a)

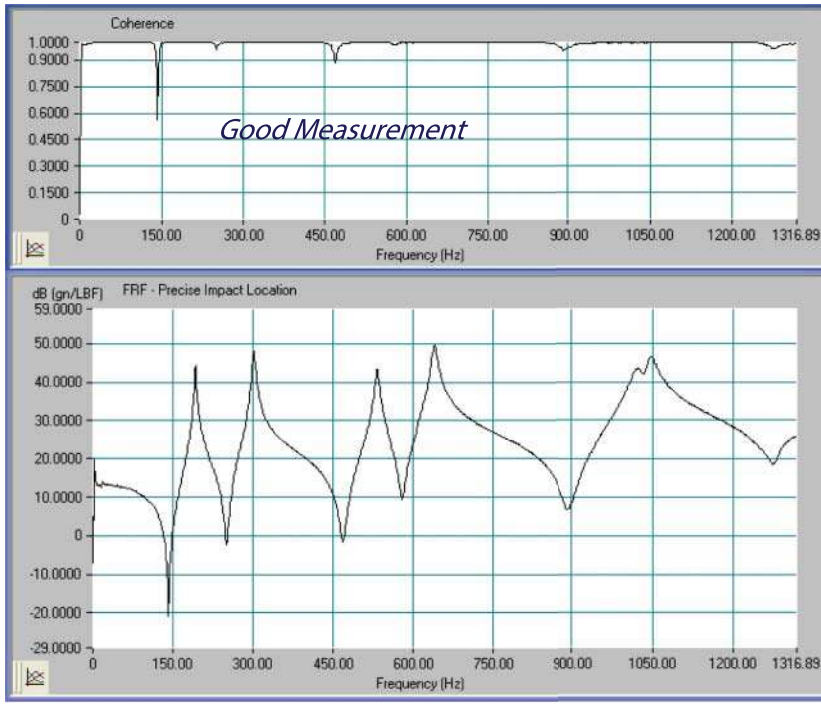

(b)

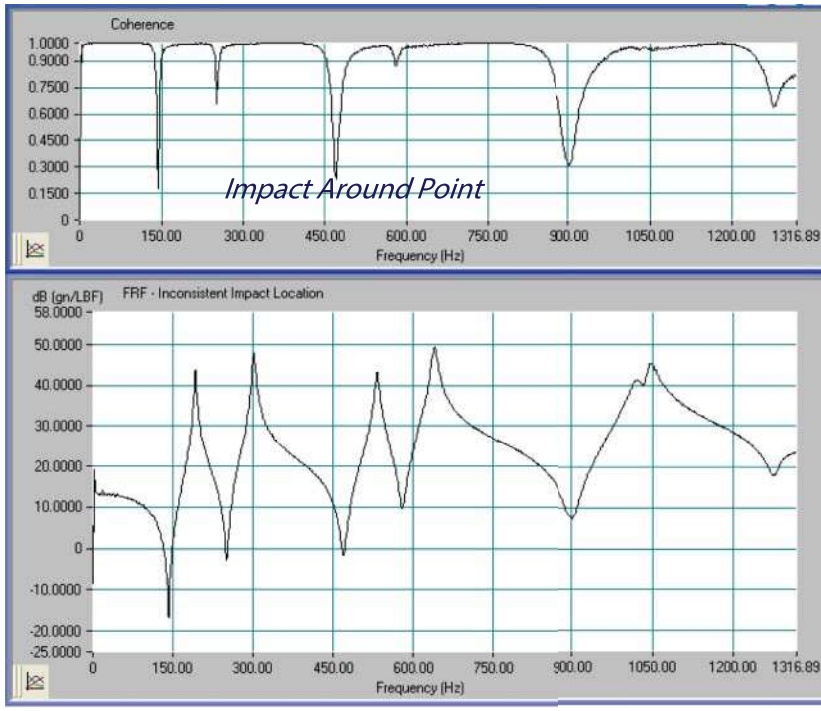

Figure 7.9 Measurement for (a) a good impact excitation (b) an inconsistent impact excitation.

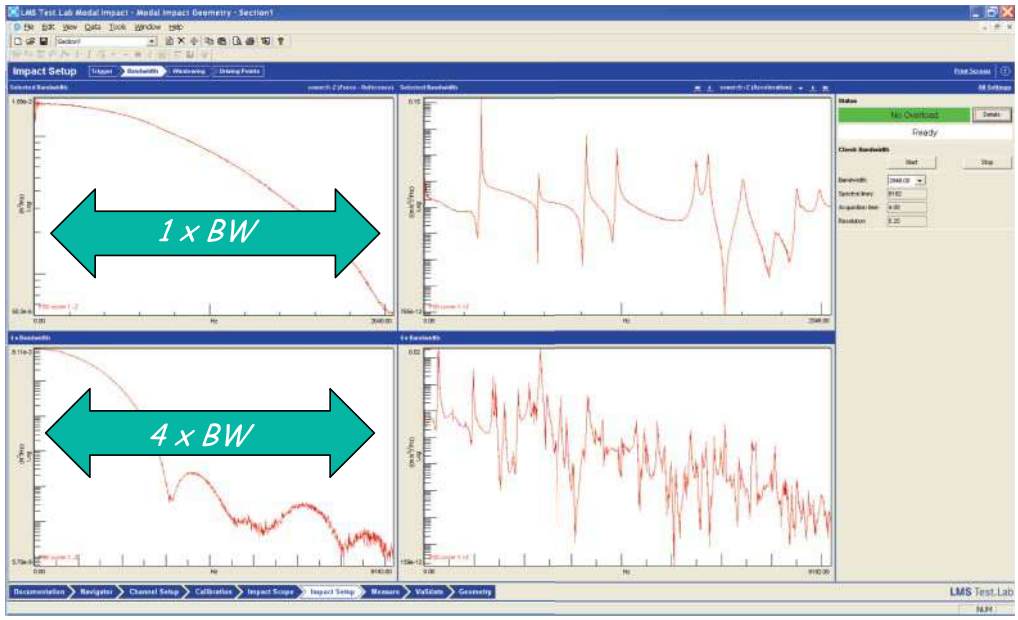

Figure 7.10 Comparison of impact force spectrum for specified bandwidth and four times the specified bandwidth.

be over that same bandwidth. Actually, some of the DAQ range will be used for the energy of the modes excited outside the desired bandwidth and will have a detrimental effect on the measurement overall. But the FFT bandwidth selected has no effect whatsoever on this. So it is critically important to use several different analysis bandwidths with the same impact hammer tip to make sure the excited frequency range is well understood. This must be checked by the test engineer when the test is initially set up, so that the effect can be understood. This may need to be done manually with the FFT analyzer or it may be embedded in the test software, as is shown in Figure 7.10, which shows the frequency bandwidth desired and also shows four times that bandwidth to understand the actual frequency band excited.

To further illustrate this phenomenon, Figure 7.11 shows several impact hammer force spectra with several impact tips over different frequency ranges. This helps to show this effect more clearly. Obviously, the proper impact hammer tip to excite the bandwidth desired for the particular application needs to be well understood for each test to be performed.

First of all, let's remember that the input force spectrum exerted on the structure is a combination of the stiffness of the hammer/tip as well as the stiffness of the structure. Basically, the input power spectrum is controlled by the length of time of the impact pulse. A long pulse in the time domain results in a short or narrow frequency spectrum. A short pulse in the time domain results in a wide frequency spectrum. Let's look at some examples and see what this means from a measurement standpoint. In Figures 7.12–7.14, black is the frequency response function, blue is the input spectrum and red is the coherence.

Let's use a very soft tip to excite a structure over an 800 Hz frequency range. As shown in Figure 7.12, the input power spectrum (blue) has some significant roll off of the spectrum past 400 Hz. Also, notice that the coherence (red) starts to drop off significantly after 400 Hz and the frequency response function (black) does not look particularly good past 400 Hz. The problem here is that there is not enough excitation at higher frequencies to cause the structure to respond. If there is not much input, then there is not much output. Then none of the measured

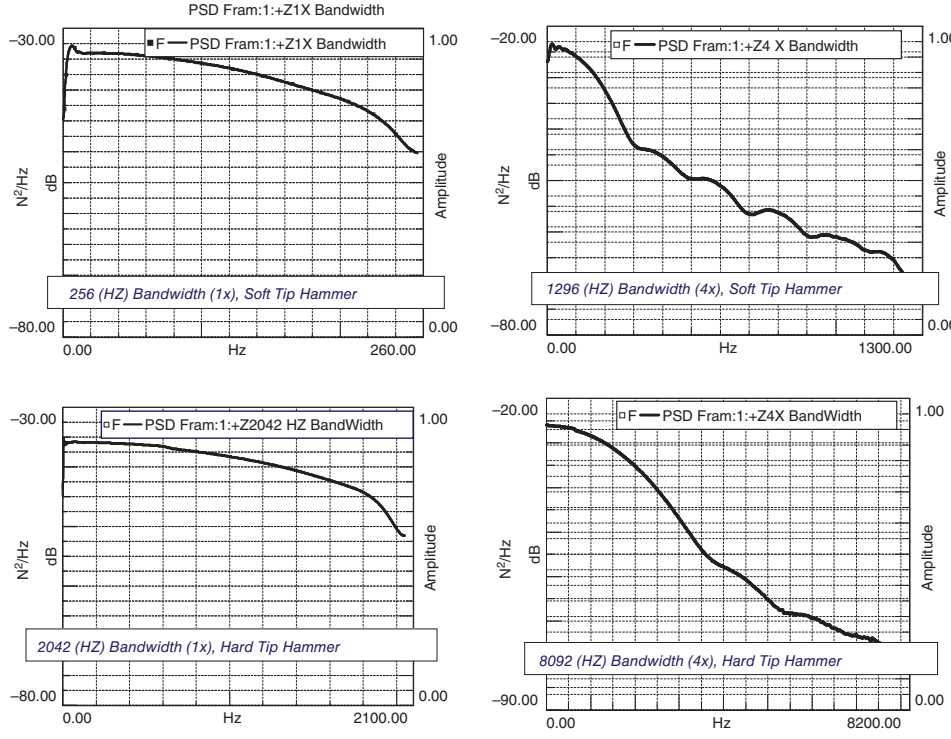

Figure 7.11 Comparison of two bandwidth settings with two different tips over two different frequency ranges.

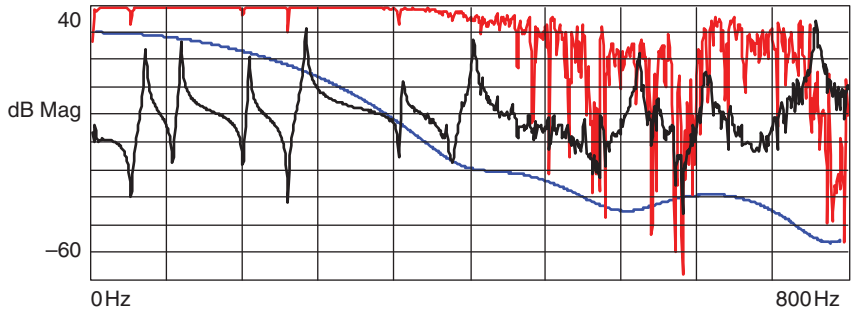

Figure 7.12 Soft hammer tip used for wider frequency range.

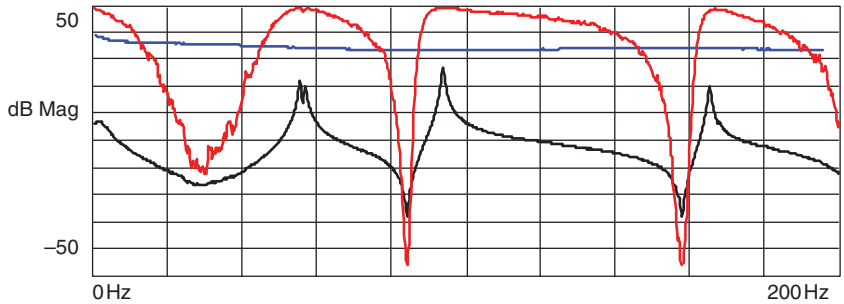

Figure 7.13 Very hard hammer tip used for narrow frequency range.

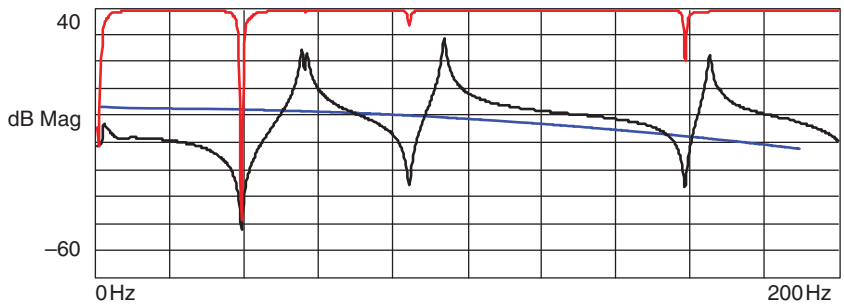

Figure 7.14 Suitable hammer tip used for desired frequency range.

output is due to the measured input, and the frequency response function and the coherence are not acceptable.

Now let's use a very hard tip to excite a structure over a 200 Hz frequency range. As shown in Figure 7.13, the input power spectrum (blue) is extremely flat over all frequencies of interest. Also, notice that the coherence (red) is not particularly good for this measurement. The problem here is that there is too much excitation at higher frequencies, causing all the modes of the structure to respond.

Now let's use a medium hardness tip to excite a structure over a 200 Hz frequency range, such that the input force spectrum does not drop off significantly by the end of the frequency range of interest. As shown in Figure 7.14, the input power spectrum (blue) rolls off by 10–20 dB by 200 Hz. Also, notice that the coherence (red) looks especially good at all frequencies over

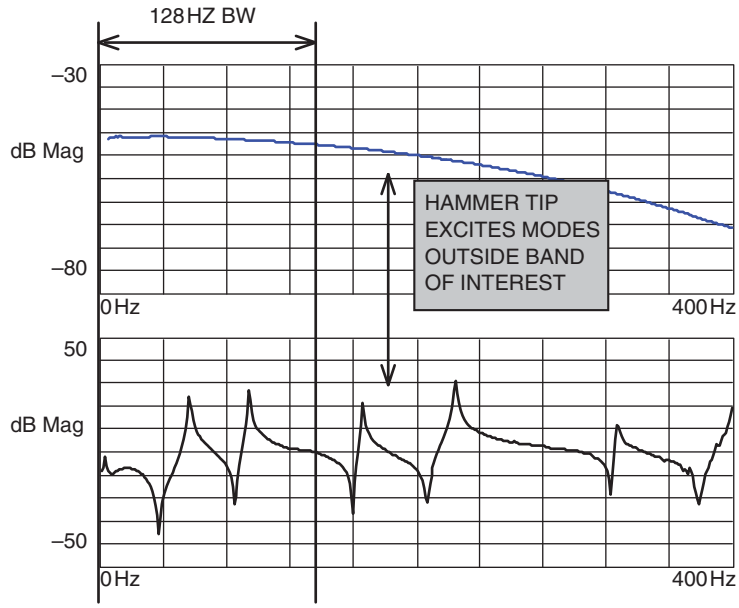

Figure 7.15 Illustration of hammer energy distribution beyond the bandwidth of interest.

the 200 Hz band with the exception of anti-resonances. The drop off of the coherence is fully acceptable at these frequencies because the structure is non-resonant (anti-resonant) at these frequencies. This means that there is no appreciable response to measure so the coherence is expected to drop here. This is a good measurement overall.

Notice that the input spectrum is not perfectly flat, as may be desired. In fact, when the input is almost perfectly flat, as shown in Figure 7.13, the measurement is not as good. Let's explain why this happens. Consider the measurement shown in Figure 7.15. This measurement was taken over a 400 Hz bandwidth. The hammer tip used had approximately 20 dB roll off over the 400 Hz band, which is probably acceptable for this measurement.

Now let's say only 128 Hz bandwidth is desired and that the input spectrum cannot roll off by more than 3 dB. Look at Figure 7.15 with the 128 Hz bandwidth specified. The input force spectrum rolls off by approximately 2–3 dB over this 128 Hz frequency band. So the measurement should be acceptable. But what really happens is that while the analysis frequency band is only 128 Hz, the response of the structure is based on the energy imparted to the structure. So the structure responds well past 128 Hz because the input force excites all of those modes, even though these frequencies may not be of interest.

The accelerometer, mounted on the structure, measures all of that response and outputs a voltage that is input to the analyzer. Just doing a quick eyeball of the total area under the curve of the frequency response function, it appears that only one third of the energy is associated with the bandwidth of interest. The rest of the energy is associated with something that is outside the bandwidth of interest. But the accelerometer senses all that energy. The ADC on the analyzer may need to be setup such that an overload does not occur due to the total response of the structure.

If the signal is not analog filtered before it reaches the analyzer, then the ADC may need to set excessively high to avoid a potential overload. Remember, most of the energy of the signal

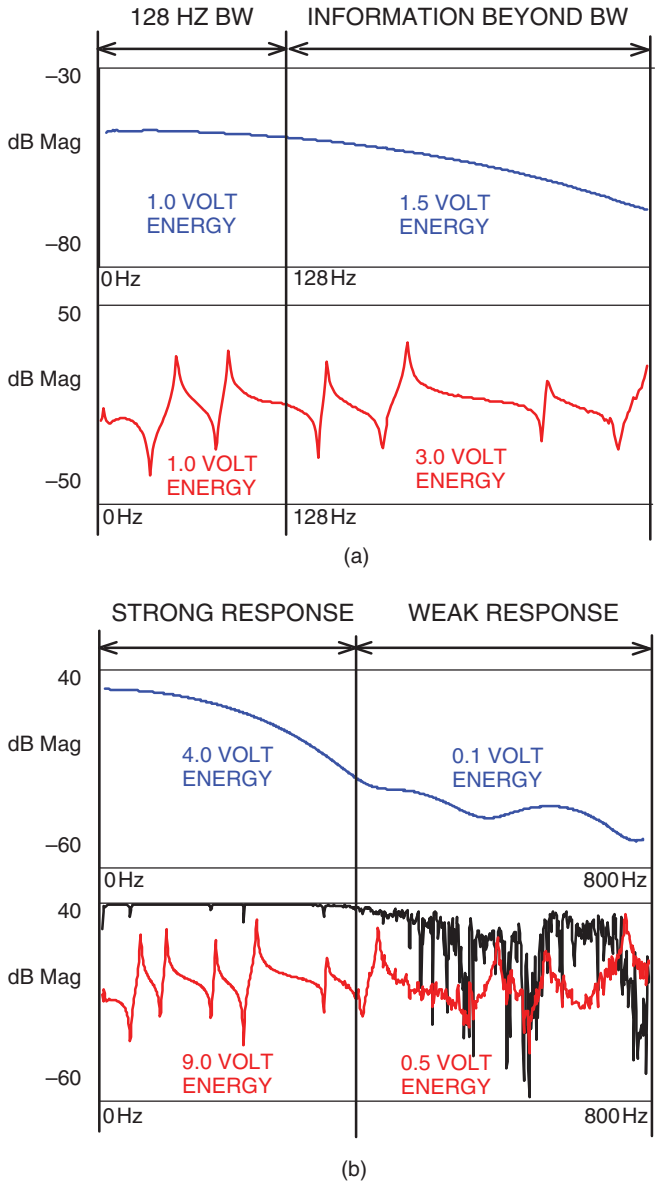

Figure 7.16 Illustration of hammer energy distribution beyond the bandwidth of interest with (a) hard and (b) soft tip.

is probably outside the 128 Hz bandwidth of interest. This results in a quantization problem in the ADC. This can easily be corrected through the use of an impact tip that does not needlessly excite modes outside the bandwidth of interest. Figure 7.16 illustrates this point. In Figure 7.16a, the input excitation has substantial energy well above the desired bandwidth for analysis. In Figure 7.16b a softer hammer tip is used. This does not excite higher frequencies above the bandwidth of interest and overall gives a much better measurement.

7.6 Accelerometer ICP Considerations for Low Frequency Measurements

Generally the accelerometers used for modal testing are of ICP type. The nature of ICP is that accelerometer measurements at low frequency are not possible because the ICP signal conditioner prevents a DC measurement. This type of accelerometers is mainly useful for oscillatory or frequency measurements. So often these accelerometers are used to measure frequencies well above DC and typically are intended for higher frequency measurements. But there are some very sensitive accelerometers that can measure very low frequencies close to DC and with high sensitivity at 100 mV/g and 1 V/g, but they are not intended to measure at DC. Actually, the ICP signal conditioning has attributes that make it very much like a high pass filter; the frequencies measured above the cut-off frequency of the filter are relatively unaffected by the conditioner, but the frequencies below that of the cut-off frequency are very much affected by the filter. So this needs to be well understood when attempting to make measurements at or below the effective cut-off frequency of the ICP signal conditioner. And it is critical to know exactly how low in frequency a measurement can be made and be expected to be unaffected by this high pass filter characteristic. In order to illustrate this, some very low frequency measurements were made on a large wind turbine blade using a high sensitivity ICP accelerometer and two DC accelerometers of different sensitivities that can measure to DC frequencies. Figure 7.17 shows the three different accelerometers and the resulting frequency response measurements. Notice that the DC accelerometers can measure fairly well and consistently with each other down to DC frequency but the ICP accelerometer tracks well down to about 0.3 Hz before the measurement is affected by the ICP signal conditioner high pass filter effect. This information is critical if very low frequencies are to be measured with an ICP accelerometer.

7.7 Considerations for Reciprocity Measurements

The effects of reciprocity are very important to modal testing. This reciprocity is basically the reason why only one row or one column of the frequency response matrix needs to be measured in order to extract modal parameters (mode shapes) from a modal test. But reciprocity is also a critical measurement for many other reasons. During the modal test, there may be a need to make the reciprocal frequency response measurement. Figure 7.18 shows this reciprocal measurement in a schematic sense. Because the system matrices are square symmetric, then the frequency response measurement is also square symmetric.

While this seems like an easy test to perform, to actually make a reciprocal measurement is actually quite involved; it requires very careful testing to make a very good reciprocal measurement. Figure 7.19 shows a simple structure on which a reciprocal measurement was made with a force impact from a pendulum impacting the structure. While this measurement looks very good from a broadband measurement perspective, the measurement has some variation, as revealed as each peak is enlarged to show the actual peaks and how they compare. In order to improve on the reciprocity, the structure has very small ball bearings glued to the structure to ensure that the input force is precisely located on the structure, as shown in Figure 7.20. Once this has been done, the measurement improves dramatically, but only after extreme care was taken, ensuring that the best possible measurement was made. This extreme accuracy was later needed for a procedure that was developed to calibrate some non-standard transducers and to obtain good calibration values.

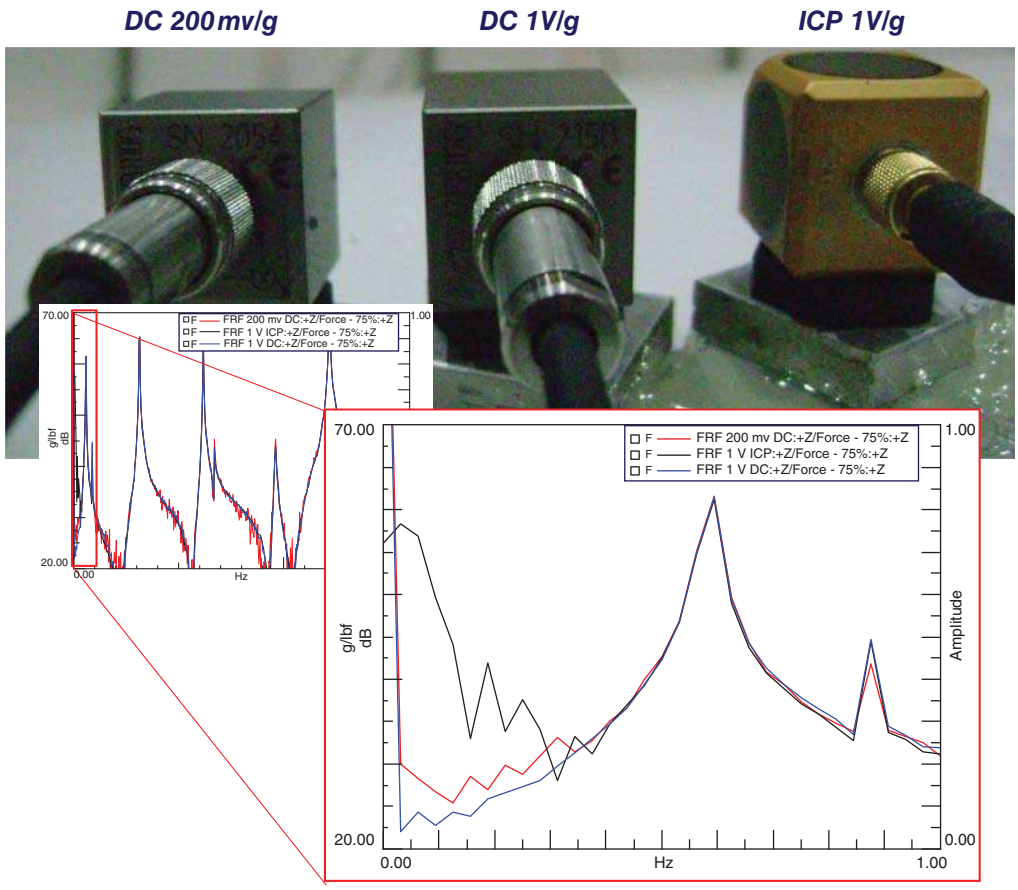

Figure 7.17 Comparison of two DC accelerometers and an ICP accelerometer for very low frequency application.

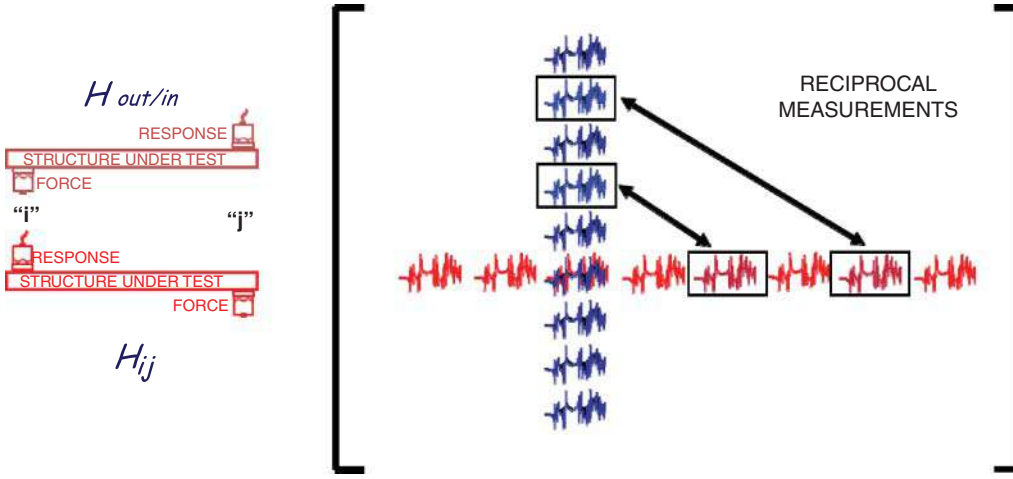

Figure 7.18 Schematic showing reciprocal measurements from shaker test and roving impact test.

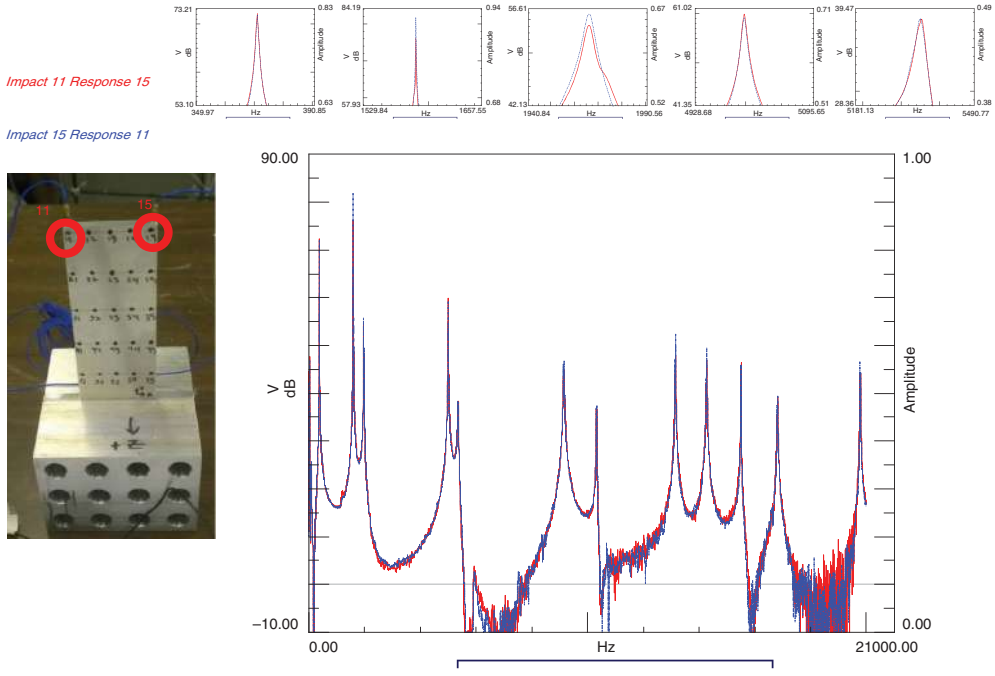

Figure 7.19 Small structure setup for reciprocal measurements.

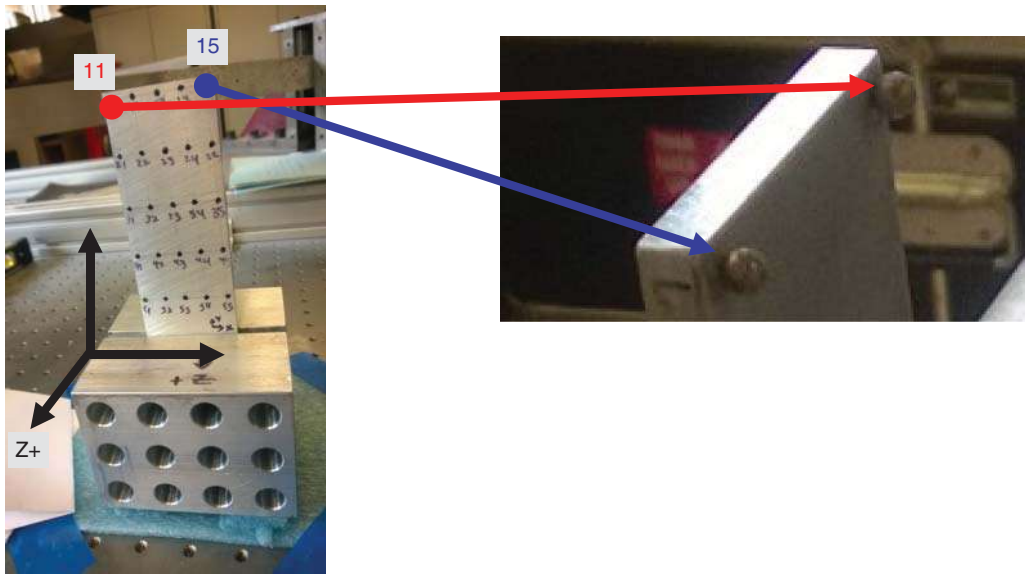

Figure 7.20 Close-up of ball bearings used to improve accuracy of reciprocal measurements.

7.8 Roving Hammer vs Roving Accelerometer

There are two ways that impact tests are normally conducted. One way is to have the accelerometer at a fixed or stationary location, and the impact hammer is then roved around the structure to obtain all the measurements. The other way to run a modal test is to have the hammer impact the same location and the accelerometers are roved around the structure to perform the modal test. However, when the accelerometers are roving around the structure there may be a mass loading effect, which can cause inconsistency between the measurements due to the roving mass of the accelerometers. When a roving hammer test is performed then the frequency response matrix is populated with rows of the matrix and the rows filled depends on where the reference accelerometer is located. When the hammer is stationary (which is similar to a shaker test) then columns of the frequency response matrix are filled and the columns filled depends on where the impact hammer is located; in this case, all of the accelerometers may be mounted on the structure so that one complete column(s) of the matrix will be filled and then the roving mass is not an issue. Figure 7.21 shows these two test setups, with the roving hammer on the left and the stationary hammer on the right. It is very important to note that if a roving hammer is used and several reference accelerometers are placed on the structure, then multiple reference data will result in one row for each reference accelerometer used. If a stationary hammer test is performed and the hammer is moved to several different points then one column will result for each impact location. These data can be used as multiple input, multiple output data for the modal parameter estimation process. While this is not actually multiple input, multiple output data, as might be collected with multiple shakers, the data will have the same consistency as that collected with multiple shaker testing. Otherwise difficulty may be experienced when reducing the data collected.

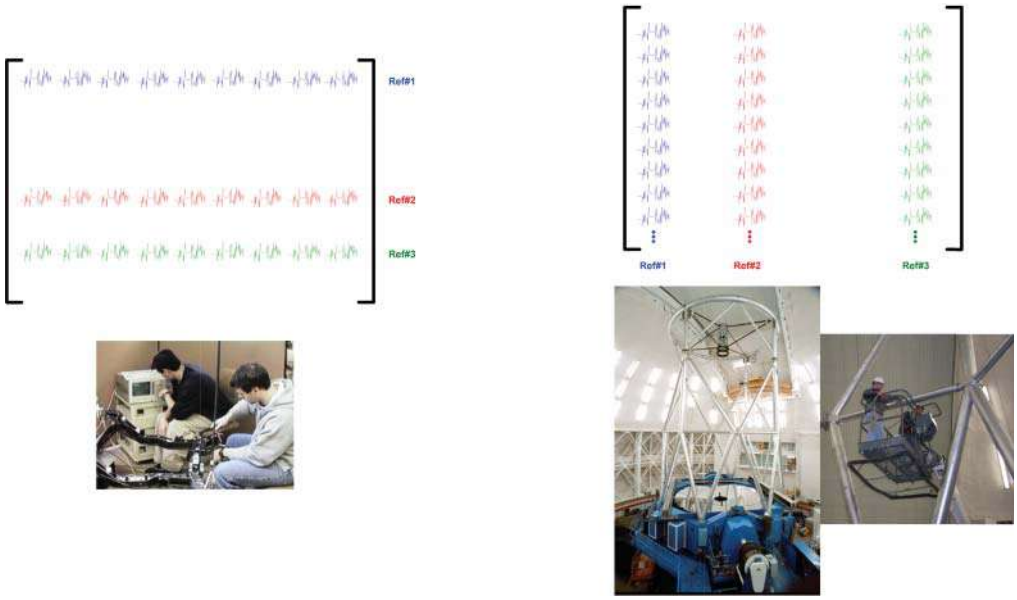

Figure 7.21 Multiple reference impact test: roving hammer test (left) and stationary hammer test (right).

7.9 Picking a Good Reference Location

In any modal test, the selection of the reference location is of paramount importance. If a finite element model is available then this should be used to help with the selection of the reference. However, often a modal test may need to be performed and there is no information (or a model of any type) as to the expected frequencies and mode shapes. In these tests, extreme care must always be exercised to ensure that the reference accelerometer is not located at the node of a mode. Usually, several different measurement locations need to be explored to ensure that modes are not missed. Figure 7.22 shows a very simple structure, for which selection of one point to be used as a reference for all the modes to be obtained is very difficult, to say the least. Several frequency response measurements are shown and it is very clear that all of the modes cannot be easily seen in all of the measurements. In addition to making several survey-type measurements to identify all the modes and selecting a possible reference location, the test should be conducted with a few references to ensure that modes are not missed.

7.10 Multiple Impact Difficulties and Considerations

At times, multiple impacts may occur and sometimes there is little that can be done to circumvent this problem. Double impacts should be avoided if at all possible, but there can be situations where multiple impacts can actually be used to perform an impact measurement. The real concern is that the input force spectrum should be relatively flat over the frequency spectrum and there should be no significant dropout in the force spectrum and the frequency response/coherence should look good. If this is true, then most likely the measurement will be adequate to identify the frequencies and mode shapes. But how flat does the force spectrum need to be and how much of a drop in the force spectrum is tolerable? These are good questions to ask. A force spectrum drop of more than 5–10 dB should be avoided, but as long as

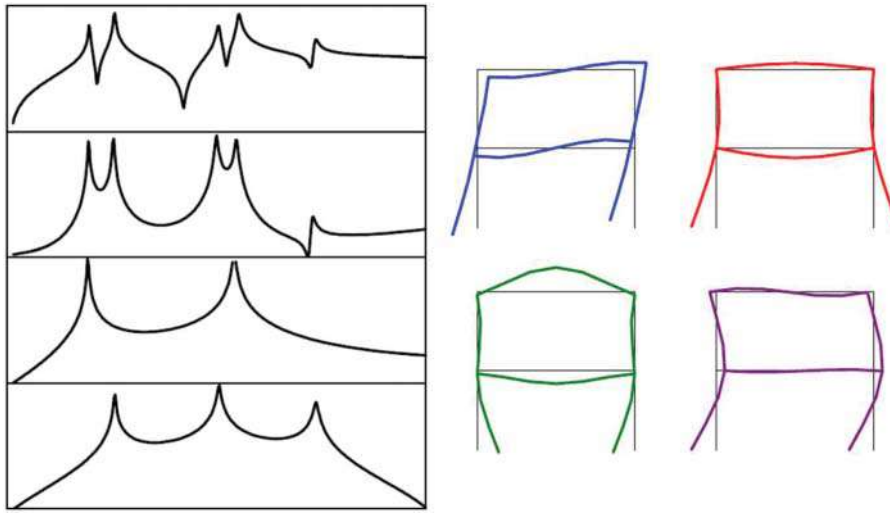

Figure 7.22 MACL frame with directional modes: FRFs (left) and shapes (right).

the coherence is good then the frequency response may be acceptable for a measurement. Two examples are now discussed in which multiple impacts were intentionally used.

7.10.1 Academic Structure

Several measurements are made on a simple plate structure, starting with a single impact and then with a series of randomly applied impacts. A series of pulses is applied to the structure but some care needs to be used here. The impulses must be applied in a very incoherent fashion in terms of their timing and spacing. The pulses should also not be applied for the entire sample period. They should be applied for a portion of the sample interval; 50–75%, for instance. But it is also important for the response to be totally observed within the sample interval so that no leakage will occur. In this way, all the requirements of the Fourier transform are satisfied. In fact, the signal will start to approach a broadband excitation, with characteristics similar to that of a random signal such as a burst random signal. A simple plate structure was used to illustrate the technique. Due to the responsive nature of the structure, double impact measurements were unavoidable, but they were not so serious as to corrupt the measurement overall.

First, a single impact is applied; or least the intent is to apply a single impact. Figure 7.23 shows the time signals for the impact and response. Figure 7.24 shows the input power spectrum with the frequency response. Figure 7.25 shows the frequency response function along with the coherence. Overall, the measurement is good but the effects of a double impact are seen in the input time excitation and the input spectrum in the shape of a varying input spectrum. The variation of the input spectrum is sufficiently small to not distort the overall measurement for the system, as evidenced by the coherence. In the second test, a series of impact measurements was applied to the structure. Figure 7.26 shows the time signals for the impact and response. Figure 7.27 shows the input power spectrum with the frequency response. Figure 7.28 shows the frequency response function along with the coherence. While multiple impacts were applied, the overall measurement is very good. The resulting frequency response and coherence are very good. Multiple impacts definitely gave some improvement in the measurement overall for this academic structure.

The first measurement (Figures 7.23–7.25) was made with a single impact and clearly the variance in the frequency response function and the coherence show that the measurement

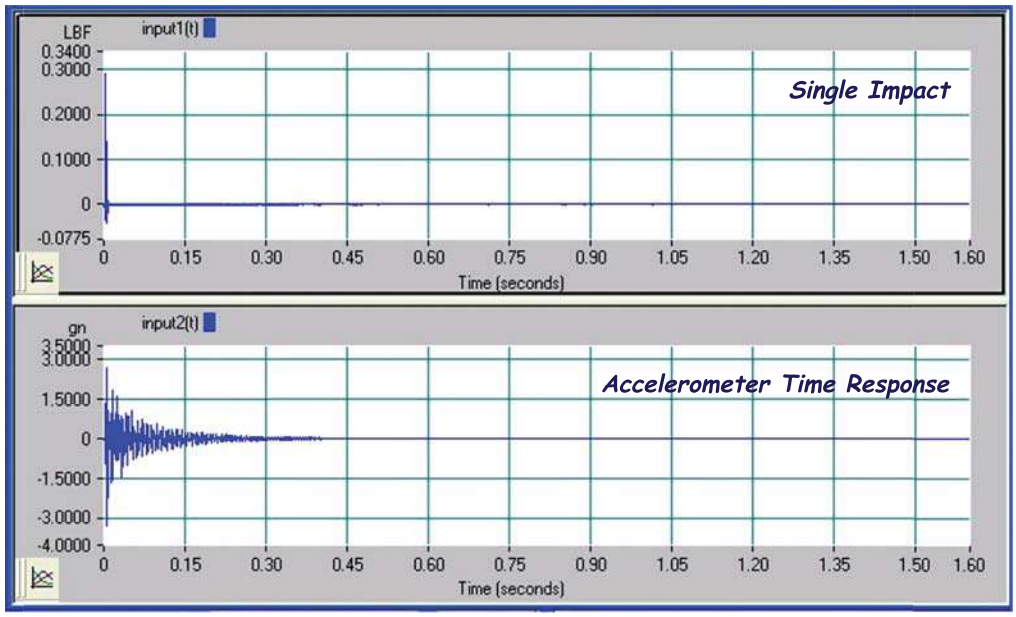

Figure 7.23 Single impact excitation: excitation (top) and response (bottom)

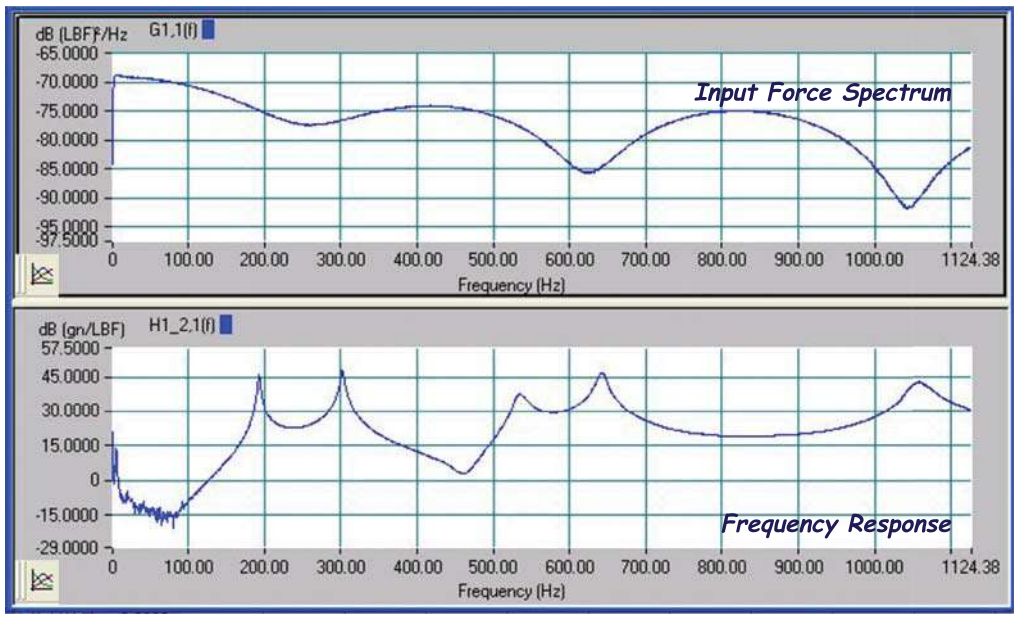

Figure 7.24 Single impact excitation: input spectrum (top) and FRF (bottom)

is contaminated with noise. But the next measurement (Figures 7.26–7.28) shows the results for multiple impacts, and it is very obvious that the frequency response and coherence are dramatically improved with the multiple impact test technique used. Of course, care must be made to ensure that the entire input and output are observed within one sample interval of the FFT time window, but if that is done then the measurement can be very much improved.

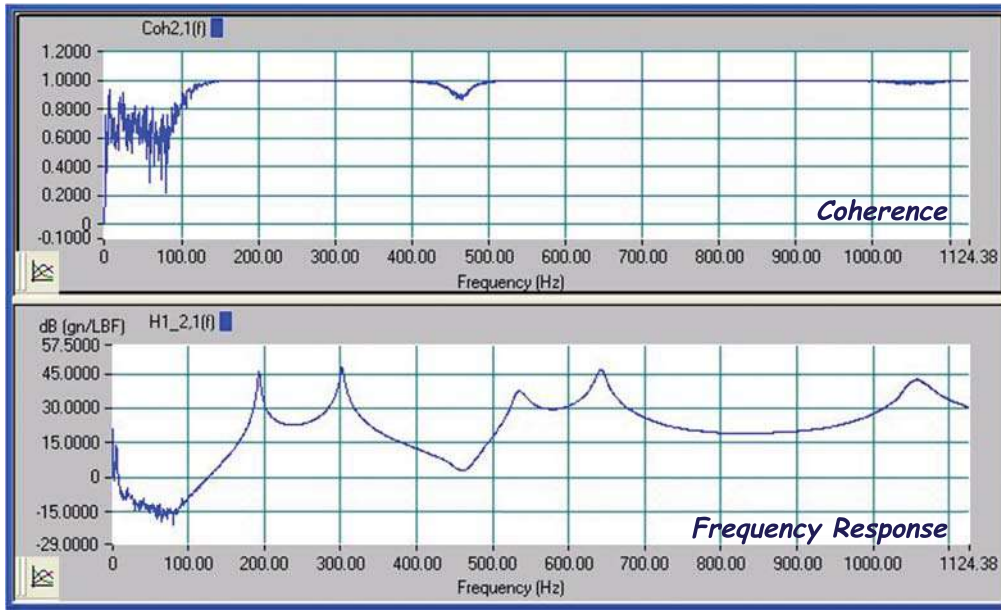

Figure 7.25 Single impact excitation: coherence (top) and FRF (bottom)

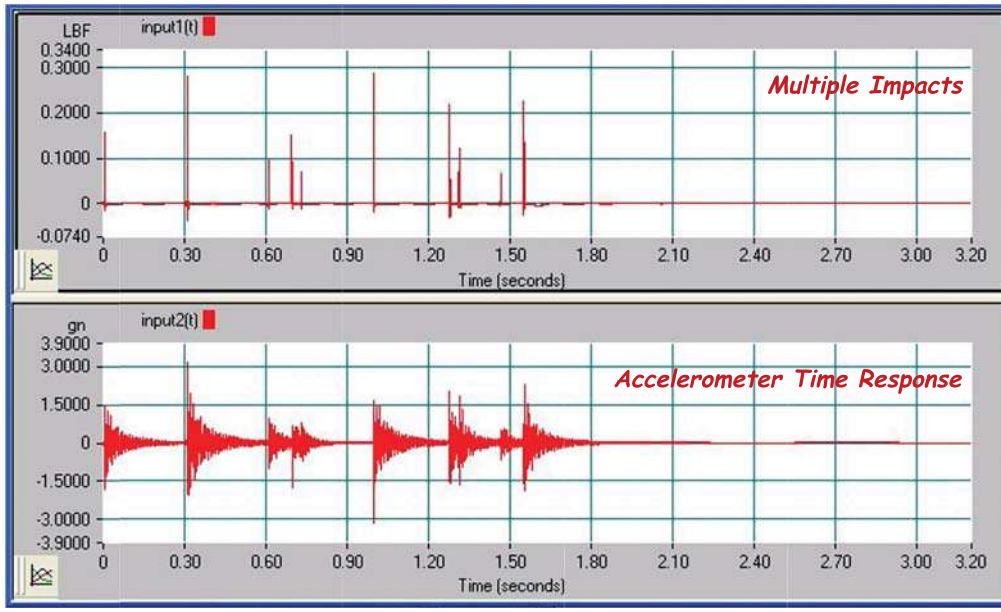

Figure 7.26 Multiple impact excitation: excitation (top) and response (bottom)

7.10.2 Large Wind Turbine Blade

Several years ago, there was a test on a wind turbine blade. When performing a test with a single impact, the long time record suffered from noise. A decision was made to try a set of multiple impacts in a random pattern lasting for about 50% of the time block. Two measurements are shown in Figures 7.29 and 7.30, with a 200 mV/g accelerometer and a 1000 mV/g accelerometer,

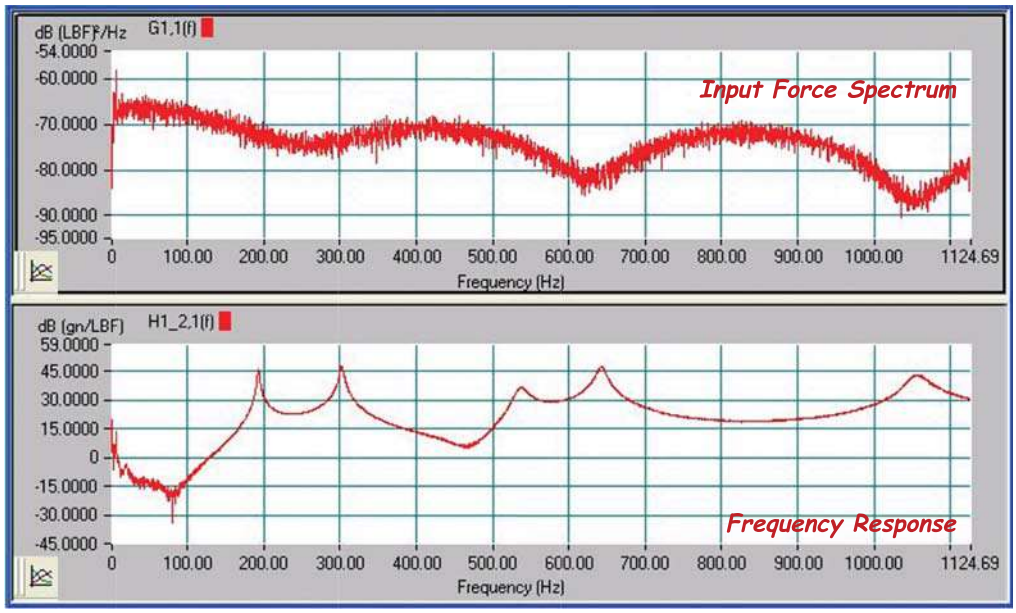

Figure 7.27 Multiple impact excitation: input spectrum (top) and FRF (bottom)

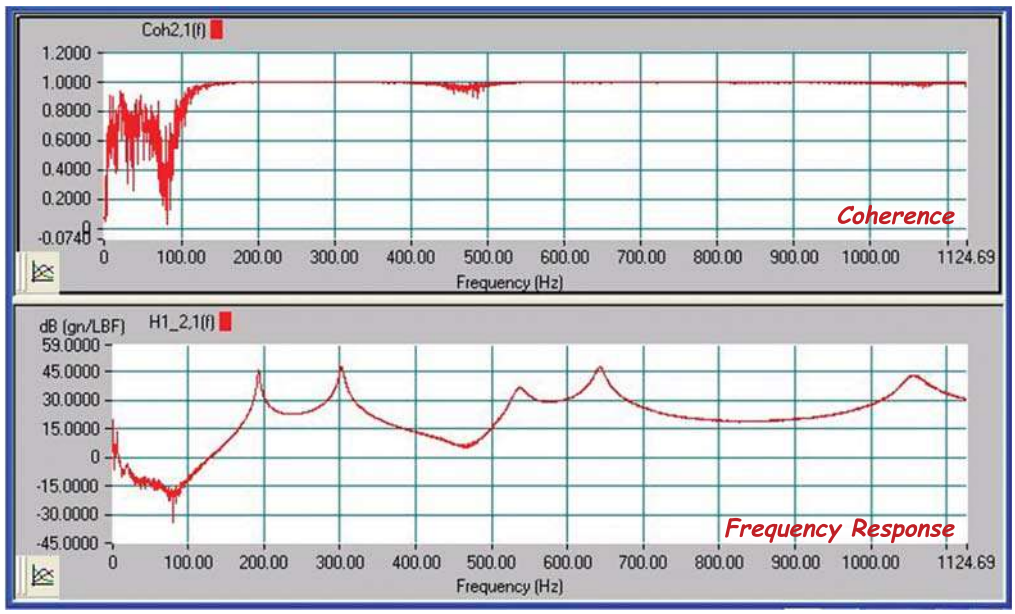

Figure 7.28 Multiple impact excitation: coherence (top) and FRF (bottom)

respectively. In both figures, the input impact excitation, accelerometer time response, coherence, and frequency response for the single impact are shown on the left in the figure and for the multiple impacts are on the right. In both cases the frequency response is seen to be improved, as is with the coherence for each measurement. Clearly the multiple impact excitation produced a better measurement for this very large structure. Of course, care must be exercised to make

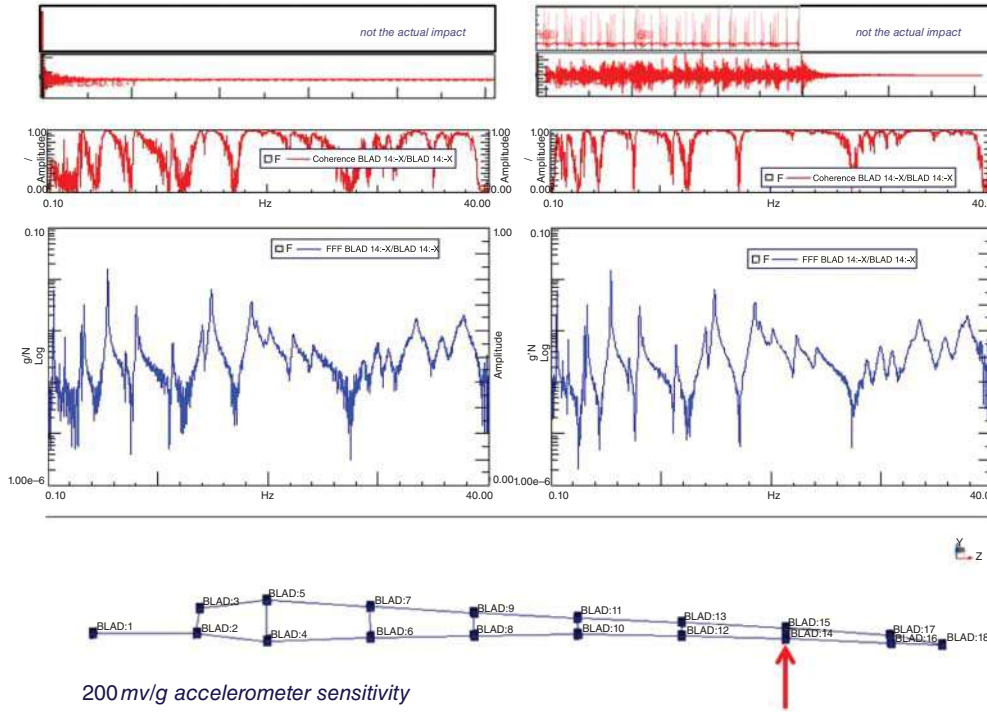

Figure 7.29 Frequency response and coherence for 200 mV/g accelerometer for single impact (left) and multiple impact (right).

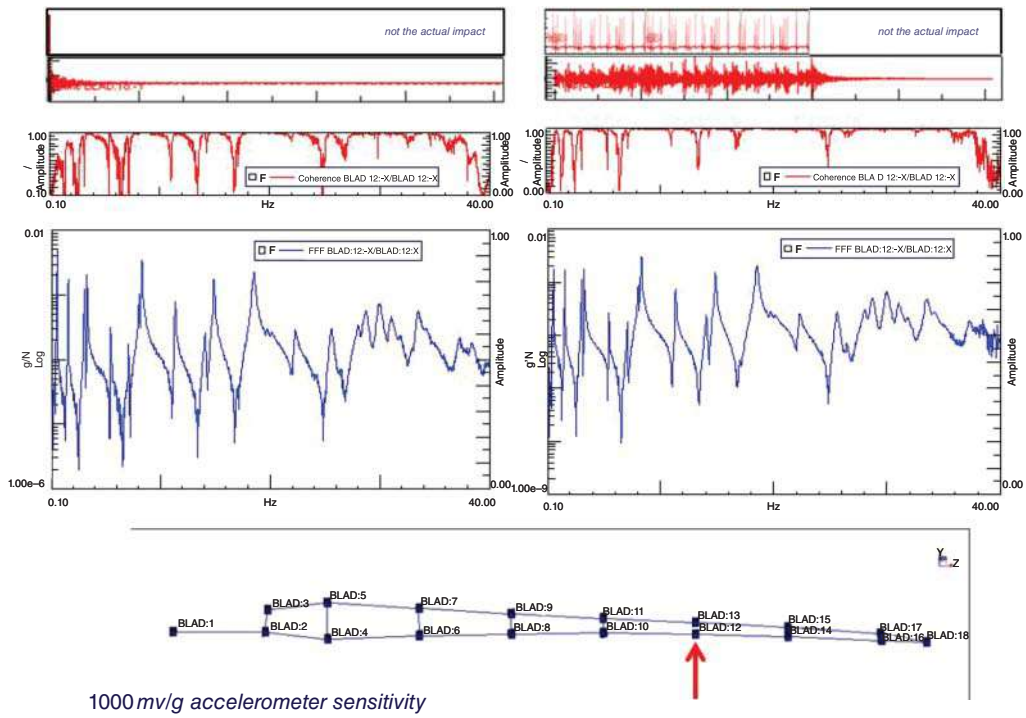

Figure 7.30 Frequency response and coherence for 1 V/g accelerometer for single impact (left) and multiple impact (right).

sure that the entire input and output are observed within one sample interval of the FFT time window, but if that is done then the measurement can be very much better than with a single impact, as seen in this very large "real world" structure test.

7.11 What is "Filter Ring" during an Impact Measurement?

Often when performing impact testing, the force pulse appears to be very regular in shape, with a pulse that resembles a half-sine wave. The event starts at zero, followed by the pulse, and returns to zero at the end of the measurement event. However, often the force pulse seems to oscillate about zero after the initial half-sine pulse. Why does this happen? Is it possibly a double impact and should a window be used to minimize the effect? This problem is referred to as "filter ring". Let's start out with some simple measurements to show this problem, which is often seen. Just by taking a few sample measurements, the effect can be observed. Hopefully, it can be better understood through some simple examples and illustrations.

Filter ring is a problem that can be seen on many FFT analyzers. For the measurements and discussion here, a general "Brand XYZ" FFT analyzer is used. A measurement will be made on a typical structure with an impact force hammer and response accelerometer. However, only the force input will be discussed here. Some of the force pulses will be very regular in shape, just as in the textbook case. But other measurements will have a force pulse that has an oscillation towards the end of the time pulse, as if it were the response of a simple single degree of freedom system. This problem is often referred to as "filter ring". It happens because the analog anti-aliasing filters on the front end of the analog to digital converter (ADC) may show a response at their own natural frequencies, which are possibly excited by the force pulse. This is actually what occurs. The force pulse will excite different frequency ranges depending on the tip that is used to excite the structure, as is well understood by most people.

But here is the problem. Depending on what frequency range (bandwidth) is selected, this filter ring may or may not be noticeable on the analyzer. Now on the surface this doesn't seem reasonable, until the actual inside workings of the FFT analyzer are considered. Usually, FFT manufacturers have different sets of anti-aliasing filters: one for low frequency work and one for high frequency work. Typically, when measuring lower frequency ranges, the lower frequency filter is employed. If a soft impact tip is used then this will not significantly cause any filter ring. But if a slightly harder tip is used, then the upper frequency range of the hammer excitation may excite the low frequency analog anti-aliasing filter. The filter gets excited and has a dynamic response characteristic that manifests itself on the force pulse as this so called filter ring.

So let's take some measurements to illustrate this filter ring characteristic and see how setting different frequency bandwidths may have an effect on the filter ring observed. An impact hammer will be used with four different tips over two different frequency ranges. The hammer tips will consist of a very soft red air capsule, a medium blue plastic tip, a harder white plastic tip, and a metal tip. In each case, the hammer is used to impact a structure to acquire a time trace. In one set of measurements, the frequency bandwidth is set at 400 Hz and in the second set of measurements the bandwidth is set to 1600 Hz. Figure 7.31 shows the results of the different impacts over the two frequency bands. The tips range from softest to hardest from top to bottom. Notice that the 400 Hz bandwidth has significantly more filter ring as the hammer tips go from softer to harder. This is because the harder tip excites a wider frequency range and has a great possibility of exciting the low frequency analog anti-aliasing filter. Comparing 400 Hz bandwidth to 1600 Hz bandwidth, there is a noticeable change in the filter ring: there is hardly any ring at all for 1600 Hz bandwidth. And the only difference was the selection of the bandwidth. On this particular FFT analyzer, a particular anti-aliasing filter is used depending

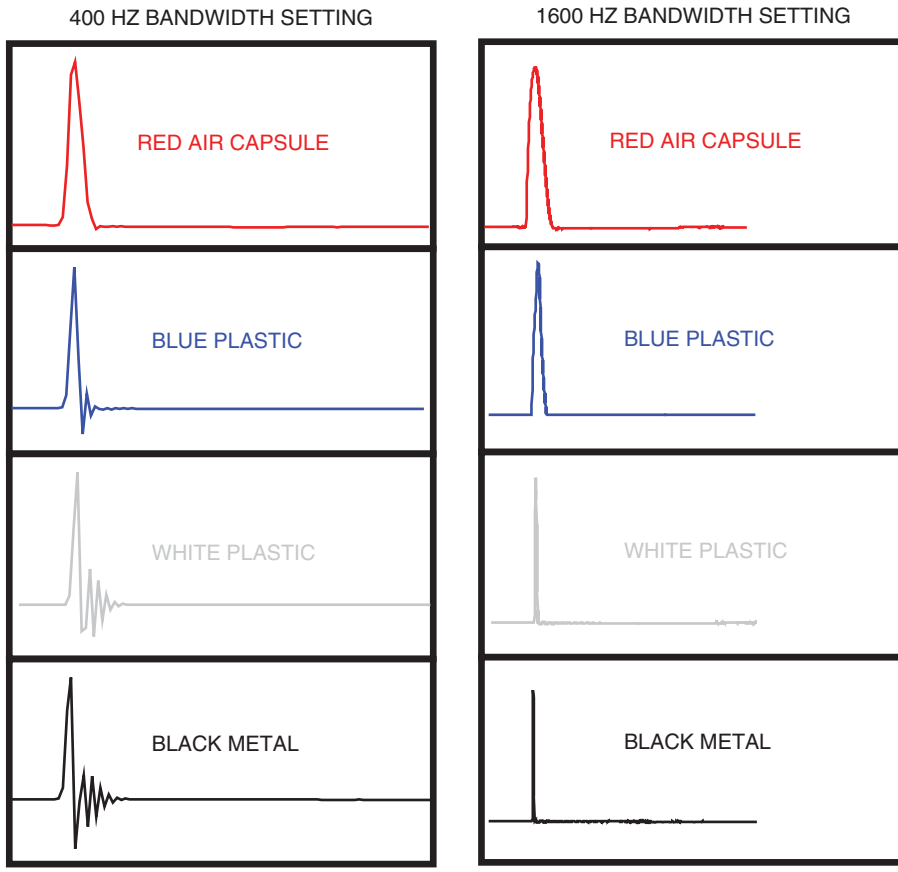

Figure 7.31 Effects of filter ring depending on bandwidth selected: 400 Hz BW (left) and 1600 Hz BW (right).

on which bandwidth is selected. Clearly, the filter ring is much more obvious when the harder tip is used over the lower frequency range. This is because the harder tip has significantly more energy at the higher frequencies, which excites the filter dynamic characteristics. Notice how the softer tip doesn't excite this filter very much at all. Generally, a softer tip is a better selection to ensure that filter ring does not occur. If there is filter ring, it makes sense to select a higher frequency range so that filter ring is minimized. Then it is not a serious issue and the problem is resolved.

7.12 Test Bandwidth Much Wider than Desired Frequency Range

At times in a test lab, there may be many different reasons to run structural dynamic tests over different frequency ranges. Sometimes, there is a desire to run one test and have the data be used by several different groups in a company for all the data that is needed by all the different groups. Let's say that a company would like to conduct several tests at frequencies as high as 2 kHz but that the modal test may only need to be performed to 500 Hz. In order to minimize costs, a company may suggest running one test to 2 kHz and then each group within the company just uses the portion of the data that is pertinent to them.

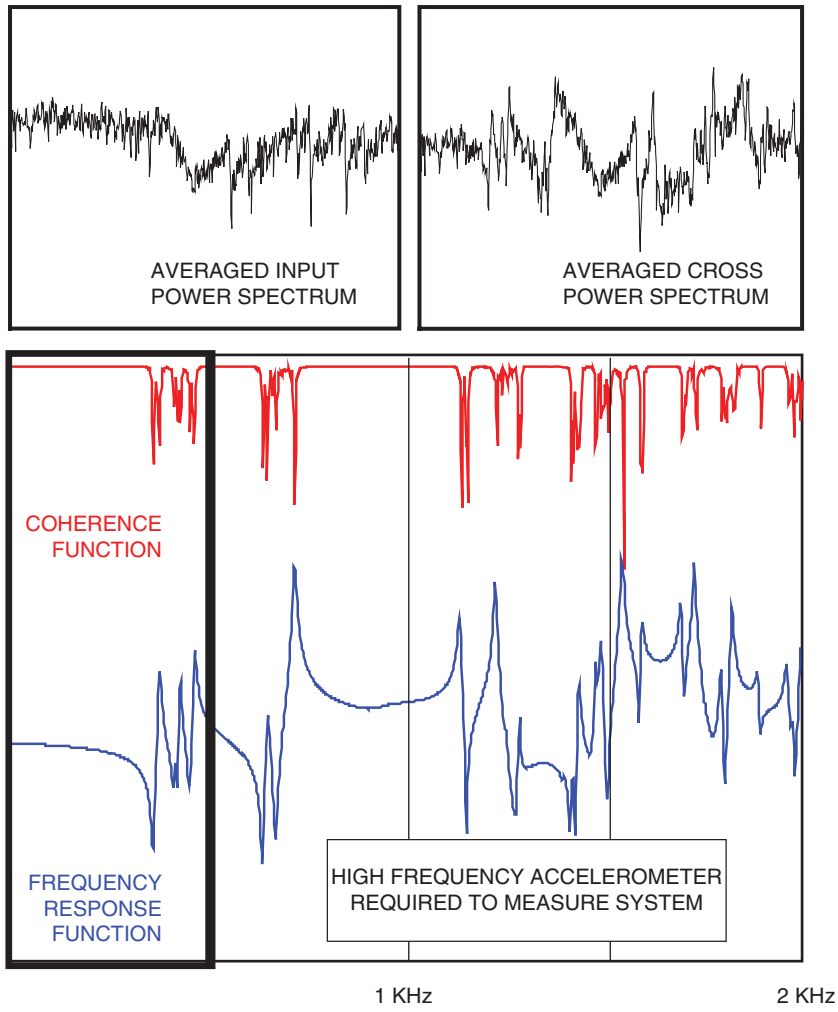

Figure 7.32 Measurement over 2 kHz with 500 Hz range to be analyzed.

Now this is an interesting scenario and there are several issues to be discussed relative to this. The important question is why one would want to run a test in this fashion in the first place and then discuss some of the issues that might have an effect on the overall measurement and then possibly some alternate things to consider. Let's consider the measurement shown in Figure 7.32. The measurement would be acquired over a 2 kHz range but only the range up to 500 Hz is to be analyzed, as suggested by the team leaders.

There is really no right or wrong answer here, but there are some strong reservations regarding the adequacy of this measurement as shown. Without any very specific details, this measurement, as requested, may not be the best measurement. Looking at the input power spectrum, cross power spectrum, frequency response function, and coherence, there is definitely excitation and response to 2 kHz. There appear to be considerably higher response levels in the higher frequency range as well as many more modes of the system. This measurement looks acceptable overall, but is it really the best possible measurement over the 500 Hz frequency range of interest?

The first thing to consider is why is there only a need to extract model information up to 500 Hz when the excitations cover a much higher frequency range. Well, the analysis or design

to be considered may only involve lower order frequencies. It may be that the model to be developed is only needed to address responses up to 200 or 400 Hz and there is no need to consider the contribution of higher frequencies for the aspects of the design to be considered. That implies that the higher modes do not significantly participate in the overall response of the system and can be excluded from the analysis.

If this is the case, the excitation need not extend to a high frequency to extract the measurements and model the system dynamics appropriately. But possibly the excitation may have come from an operating condition at which the input excitation is broadband and excites this wide frequency range. But because it is an operating condition, it may be considered a better excitation than an artificially generated excitation, but this is definitely debatable.

But there may also be a dual purpose need for the test. While one group may only be concerned with frequencies up to 500 Hz, there may be others that need to use and analyze the data up to 2 kHz, with regard to other applications. This is always a problem when one test is to be used for multiple purposes and analyses. This is not the optimum way to conduct a test but may be used purely in consideration of time aspects when a test article is not available for long durations or is an expensive piece of hardware on a tight production schedule. In any event, there may be multiple reasons for this type of test scenario.

But what might be the issues that might affect the overall measurement? Well, there needs to be some consideration of the transducers used to acquire the measurement. If the excitation extends to well beyond 500 Hz (and up to 2 kHz) then the transducers selected must be suitable for responses at this high frequency range. Of course, this implies that the accelerometers selected should be suitable for high frequency and, as such, may not be as sensitive at lower frequencies as an accelerometer that is selected specifically for a lower frequency range. So the issue that is of concern is the selection of a transducer that is going to provide a suitable measurement below 500 Hz while not being overloaded or saturated by the higher frequency excitation. This can cause inappropriate transducer selection.

As another issue, the excitation up to 2 kHz will cause a high frequency response that may not be of interest or may excite other problems (such as nonlinearities) that might contaminate the overall measurement. A preference might be to measure only the frequency range of interest, as shown in Figure 7.33. It seems much wiser to limit the excitation used with a low pass filter and not ever excite the higher frequency modes of the system. This would then possibly allow the use of more sensitive lower frequency accelerometers, which would provide a much better measurement overall. This approach also allows for a better utilization of the analog to digital converter in the acquisition system. But the bottom line is that the instrumentation and its associated signal conditioning must also be considered. Unnecessary loading of the transducer makes no sense at all. Why excite and measure something that isn't of concern?

But looking at the measurement, there may be some concern as to the contribution of the modes just beyond 500 Hz and up to 1 kHz. At some time in the future there may be a reason or need to evaluate beyond what was required today. And looking at that next band in Figure 7.34, it is clear that there are some dominant modes that may be of interest (if not today, then maybe tomorrow). So often, there is not a clear-cut answer as to what frequency range might be appropriate. But one thing is clear: the transducers selected for making the measurements need to be very sensitive to the actual frequency range to be tested and this consideration needs to be well thought out before a test is conducted.

So what if this test is forced to run with a 2 kHz excitation but is only analyzed to 500 Hz. It might be best to run a test with 2 kHz excitation and a second test with 500 Hz excitation. Both measurements should provide equivalent information if all the issues identified above have been properly addressed. And if forced to excite the structure to 2 kHz, then it would be wise to run both tests and analyze both sets of data to see if there are any significant differences. Of course, this still would imply that the instrumentation would have to be suitable for both frequency ranges and therefore may not be optimum for the lower frequency range.

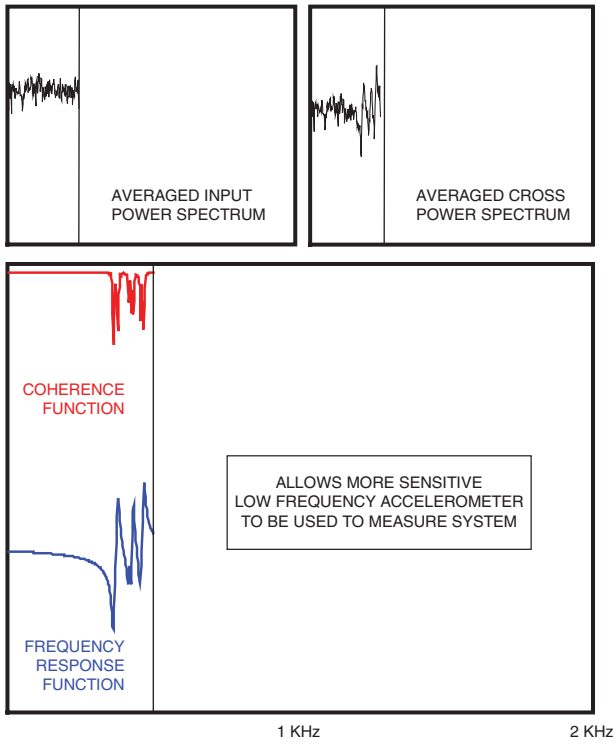

Figure 7.33 Frequency excitation to 500 Hz.

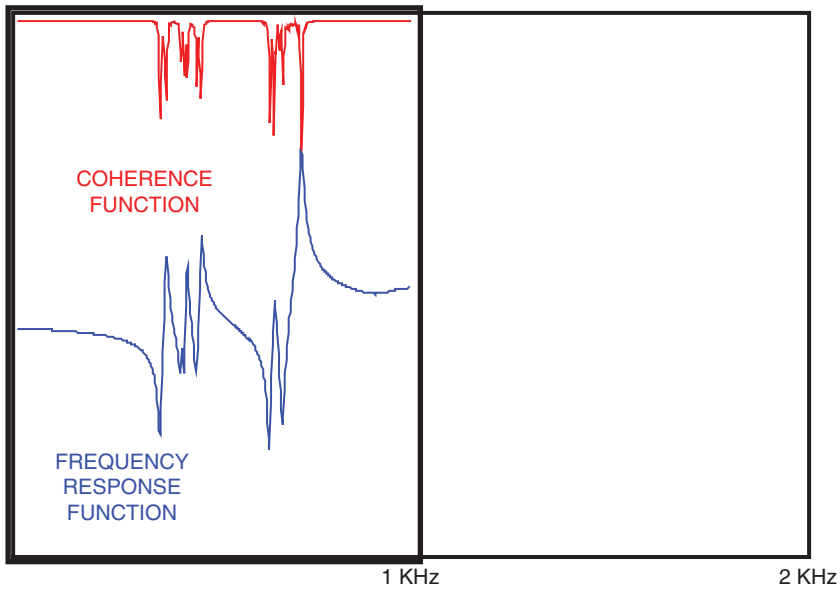

Figure 7.34 Measured response to 1 kHz.

7.13 Why Does the Structure Response Need to Come to Zero at the End of the Sample Time?

So now let's talk a little bit about what kind of problems can result from the measurement if the structure response doesn't die out before the start of the next measurement. The measurement presented here was on a very lightly damped structure and in order to prevent leakage most likely an exponential window is needed. This measurement is likely to look like what is shown in Figure 7.35. The upper trace shows the time response for a much longer sample than what was used for acquisition. The middle trace is what was actually captured from the FFT for the T seconds of data collected. And the lower trace is the time response with the window

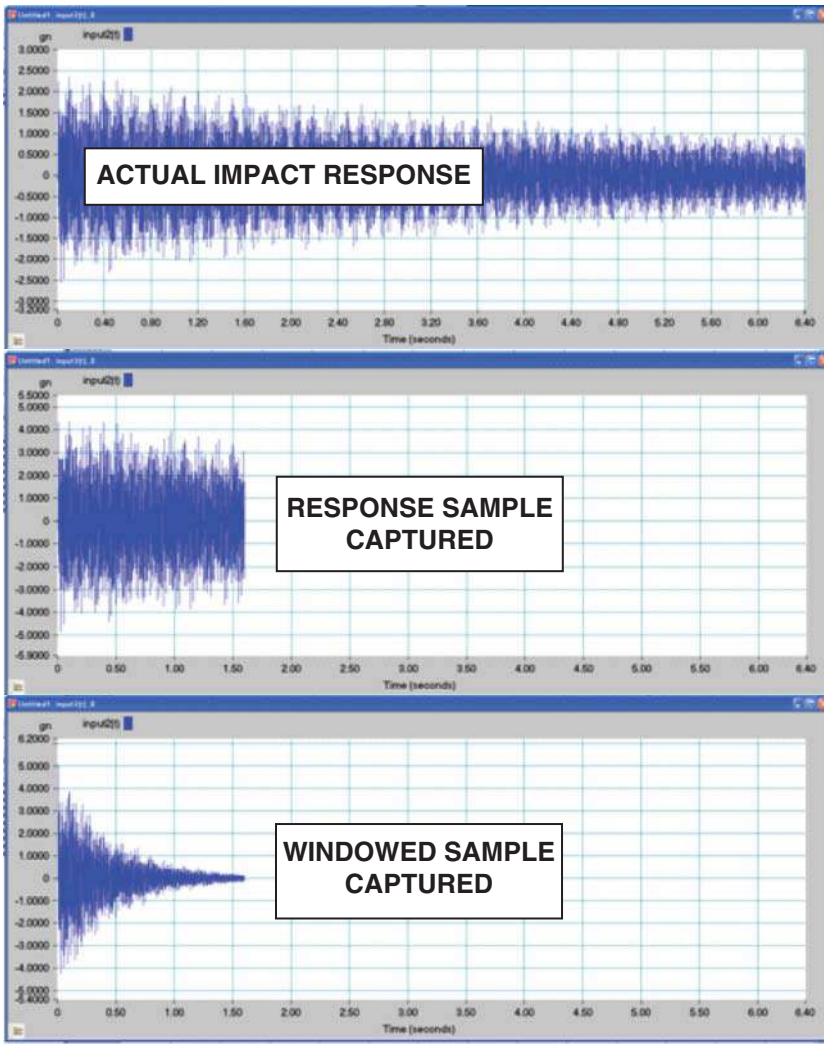

Figure 7.35 Impact response for one sample.

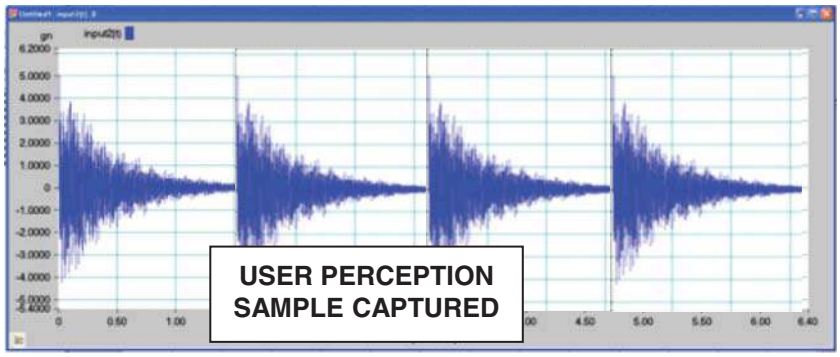

Figure 7.36 User perception of impact averaged response.

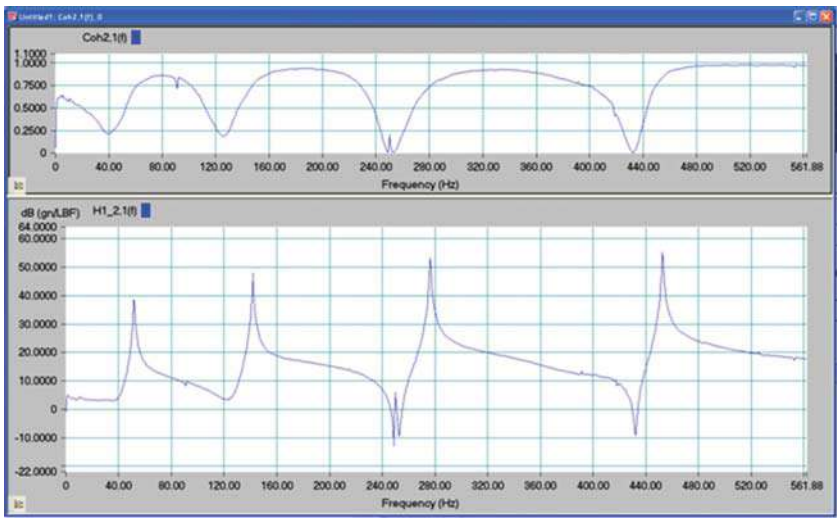

Figure 7.37 FRF and coherence from initial measurements.

applied to the output response. So up until this point everything looks reasonable. The averaging was performed by impacting the structure and measuring the response for a series of many averages.

A sample of these averages is shown in Figure 7.36. The window was applied and the response was measured and averaging was performed to obtain the data described – at least from the user's perspective. However, the frequency response measurement that resulted, as shown in Figure 7.37, did not look very good overall and the coherence was not very good either. In addition, this drive point frequency response measurement lacks the measurement characteristics that are typically expected with strong resonant and anti-resonant frequencies.

So what could possibly have gone wrong here? To understand what happened, go back to the formulation of the system transfer function. When the equation of motion is written and the

Laplace transform is taken then:

$$(ms^2 + cs + k)X(s) = f(s) + (ms + c)x_0 + m\dot{x}_0$$

And the system transfer function is

$$H(s) = \frac{X(s)}{F(s)} = \frac{1}{ms^2 + cs + k}$$

But in order to do that the extra terms on the right-hand side of the equation are eliminated; these are the initial conditions for the transformation and are then considered to be zero.

So ignoring those terms assumes that the initial conditions are zero. But the problem is that the way that the original measurement was acquired, the structure's response in between each individual impact was assumed to be zero. While a damping window was applied to the data and it looks like the response has decayed to zero, that is only with respect to the software used to acquire the data.

Actually, what most likely happened is that the measurements were taken in close succession and the actual response of the structure never actually died out before the next sample was taken. This is schematically shown in Figure 7.38. So what happens is that the response of the second average is contaminated by the remaining response of the first impact. And the third average is contaminated by the remaining response of the first and second averages. And this continues for all the averages taken. So basically the measured response of each average (after the first average) is not the result of the impact excitation for that particular average, and it

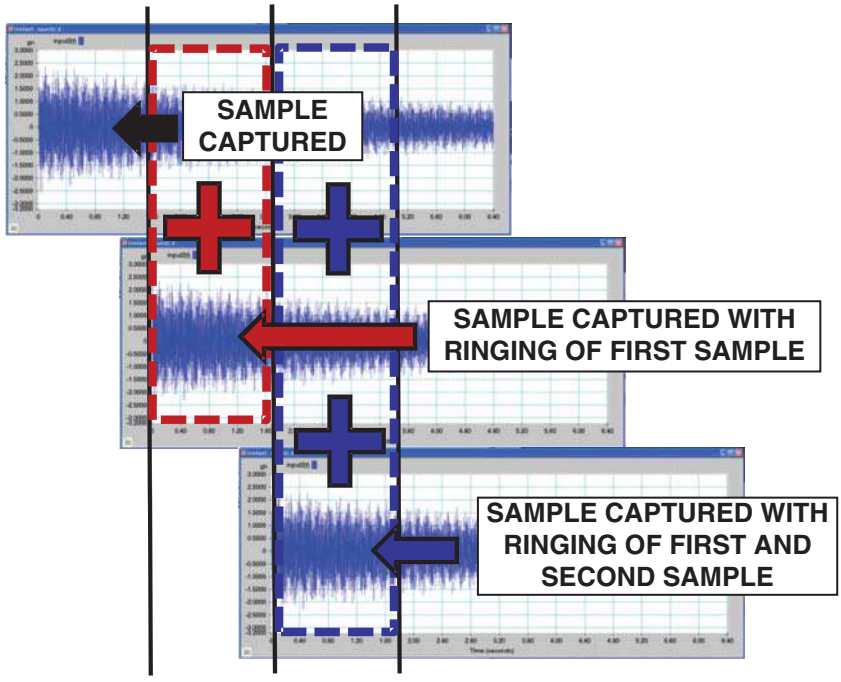

Figure 7.38 Impact response from structure standpoint.

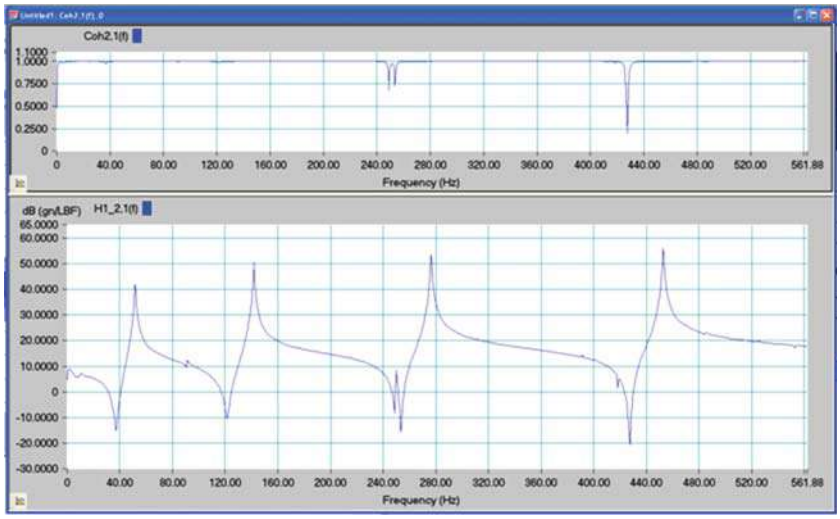

Figure 7.39 Good FRF and coherence from proper technique.

is not the response due to the measured force for that particular average. So that is why the coherence is so poor.

To confirm that this is the case, another measurement was made, with sufficient time given to allow the structure to return to a steady state (no response) condition. The resulting frequency response function and coherence is shown in Figure 7.39 and it is very clear that this measurement is far superior to the one shown in Figure 7.37.

7.14 Measurements with no Overload but Transducers are Saturated

There can be times when there is no overload on the ADC but the measurements may not be very good. This is especially true when the transducers themselves become saturated and therefore distort the measurement. There can be many things that might cause this problem. The measurements can be contaminated by a variety of sources. Many different types of problems may be encountered in different situations. But in the example shown next, there is a very strange problem in the measurement that was made. At first glance, the structure seems to be one that can be tested with little problem. The measurement will be intentionally distorted by transducer saturation, which may not cause an overload in the ADC. For the measurement here, a simple plate was instrumented with an accelerometer and subjected to impact testing. Three different cases will be shown to show what could happen with such a measurement.

7.14.1 Case 1: Sensitive Accelerometer with Exponential Window

In the first measurement, an impact excitation was used. A very sensitive accelerometer was used and because leakage may be a problem, an exponential window was used for this measurement. Figure 7.40 shows the input excitation and the response from the accelerometer. Also shown in the figure are the ADC range settings that resulted from the measurement. The measurement looks reasonable and there doesn't appear to be any problem with the time measurement.

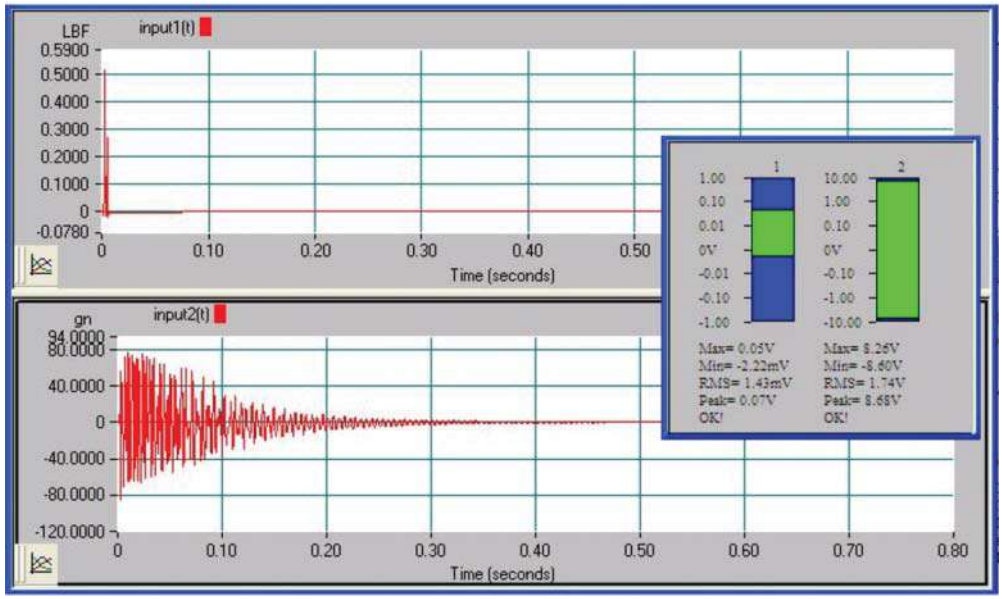

Figure 7.40 Excitation (top) and response (bottom) with sensitive accelerometer and exponential window for case 1.

However, looking at the frequency response function and the coherence in Figure 7.41, the measurement looks terrible. The measurement has no real useful information anywhere in the frequency range shown. Clearly, this measurement is not good at all.

7.14.2 Case 2: Sensitive Accelerometer with No Window

In the second measurement, an impact excitation was used again, but no window was applied to the response window, so that it could be seen if any additional information could be seen. Figure 7.42 shows the input excitation and the response from the accelerometer. Also shown in Figure 7.42 are the ADC range settings that resulted from the measurement. There doesn't appear to be any overload with the time measurement. Looking at the frequency response function and the coherence in Figure 7.43, the measurement still looks terrible.

But looking at the time trace, the response does not appear to be what would be expected for a second order exponentially decaying system. What has actually occurred here is that the accelerometer response was so large that it saturated the accelerometer response, causing it to respond in a nonlinear fashion. During the first 0.05 s of time response, the system does not appear to respond in an exponential fashion. But the interesting part is that the total accelerometer voltage output was not greater than 10 V and therefore did not overload the ADC of the acquisition system!

7.14.3 Case 3: Less Sensitive Accelerometer with No Window

In the third measurement, an impact excitation was used again, but no window was applied and a less sensitive accelerometer was used for the measurement. Now the time response in Figure 7.44 and frequency response in Figure 7.45 looks like what was expected. The problem in this case was that when too sensitive an accelerometer was used for the impact test. While the FFT analyzer ADC did not overload, the accelerometer was saturated by the large response;

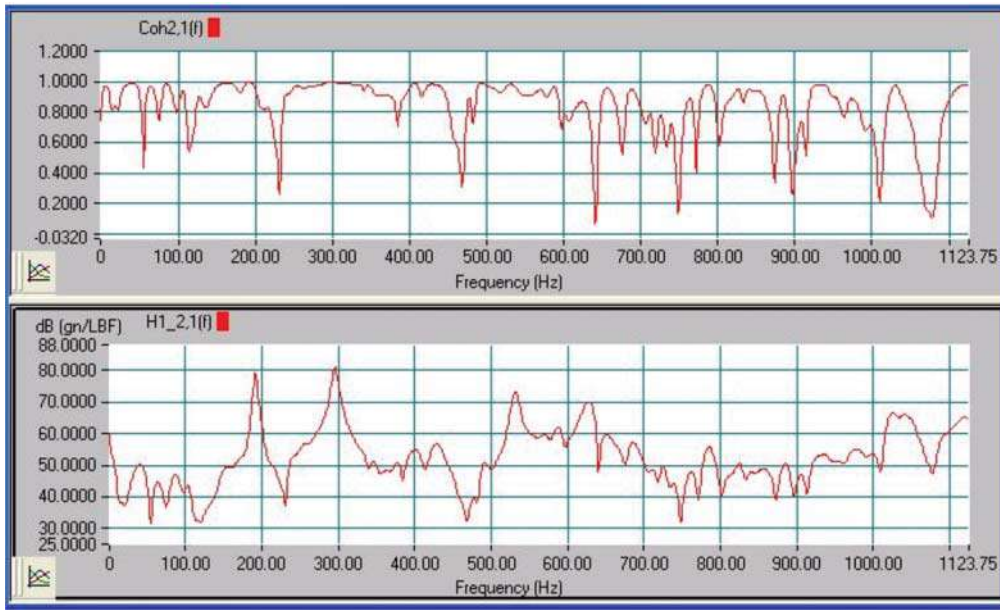

Figure 7.41 FRF (bottom) and coherence (top) with sensitive accelerometer and exponential window for case 1.

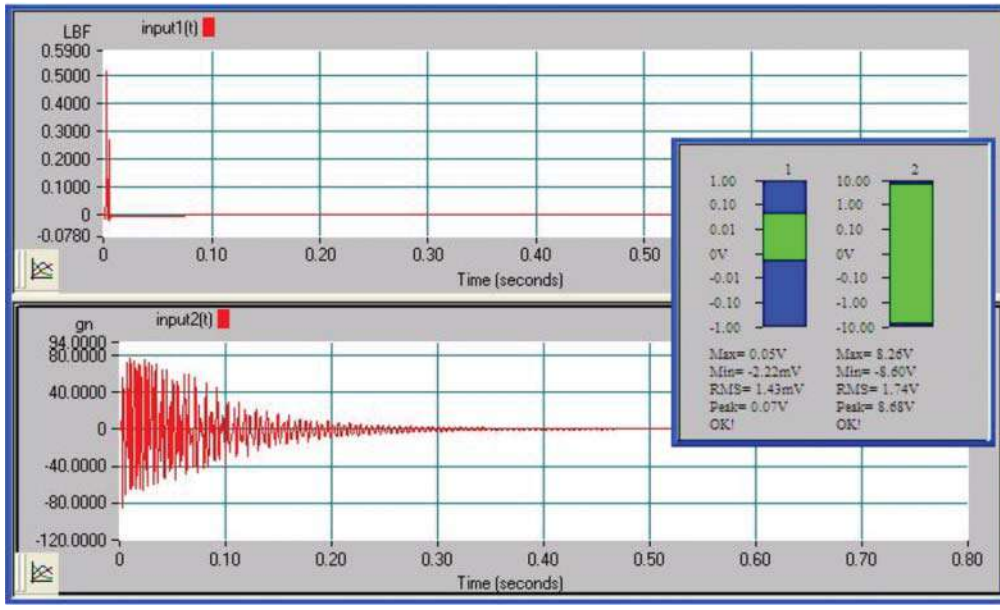

Figure 7.42 Excitation (top) and response (bottom) with sensitive accelerometer and exponential window for case 2.

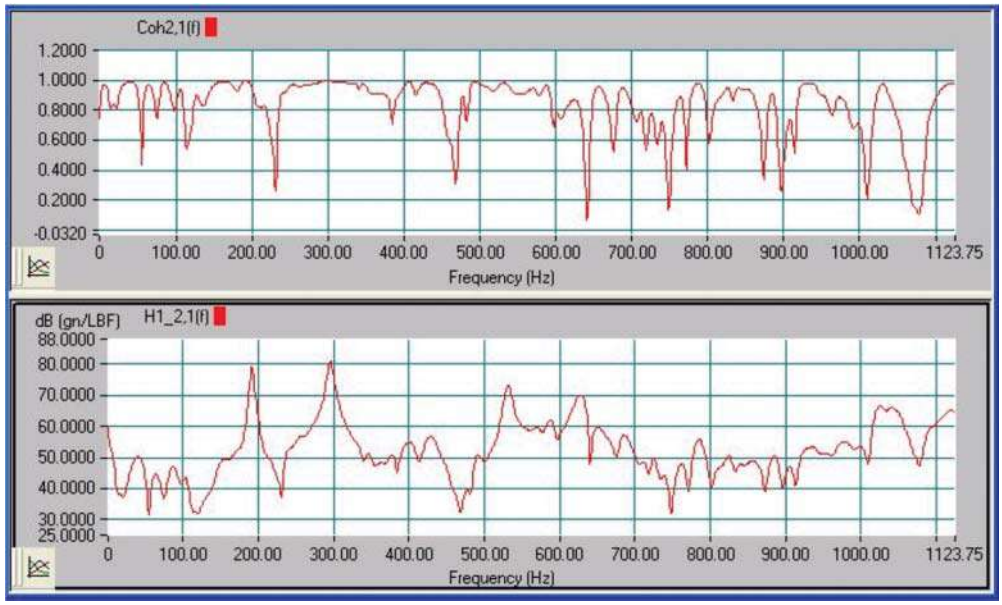

Figure 7.43 FRF (bottom) and coherence (top) with sensitive accelerometer and exponential window for case 2.

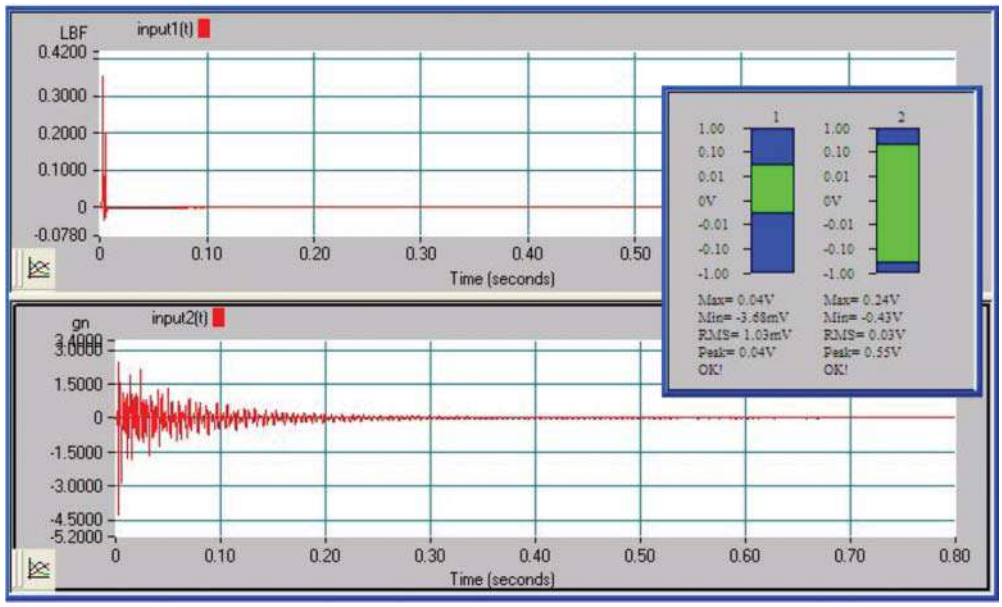

Figure 7.44 Excitation (top) and response (bottom) with sensitive accelerometer and exponential window for case 3.

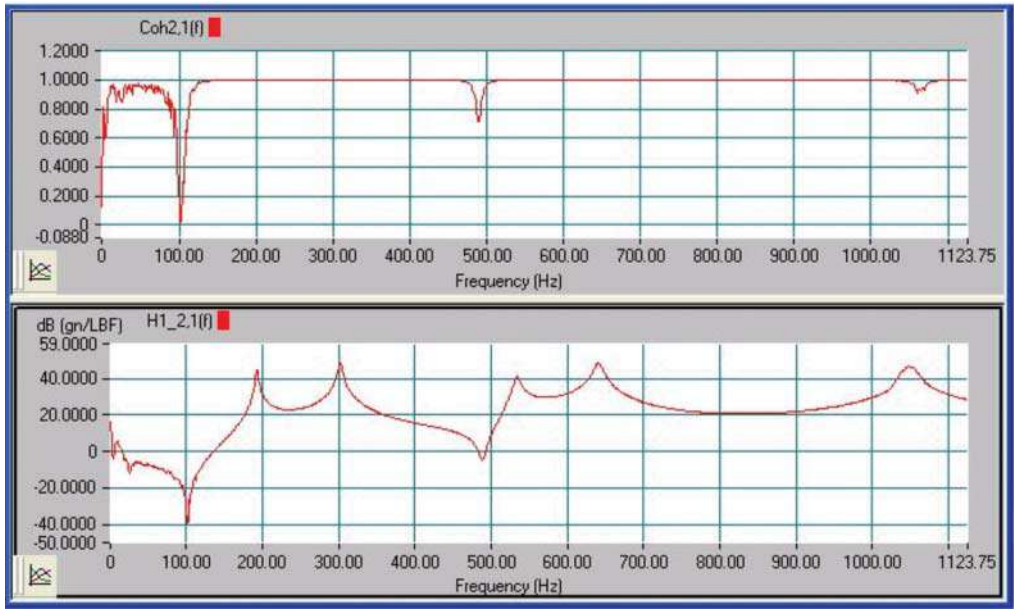

Figure 7.45 FRF (bottom) and coherence (top) with sensitive accelerometer and exponential window for case 3.

this caused a response that was very different from the damped exponential response expected. So it is very important to look at all the pieces of the time and frequency measurements made.

7.15 How much Roll Off in the Input Hammer Force Spectrum is Acceptable?

This is a controversial topic with many people. At one point in time people claimed that there could be no more than 1 dB roll off on the input spectrum. This was a very harsh criterion and in fact the result of this actually excited many modes well outside the band of interest, potentially saturating the accelerometers and thereby causing a poor measurement. Now let's understand why rules exist in modal testing. Often guidance is necessary about how to conduct a test. This guidance is intended to protect users from making measurements that may not be particularly useful in some testing scenarios. But the problem is that some of these "guidelines" get interpreted as if they were unbreakable rules. And maybe the "guidelines" were set out 20 or more years ago, when instrumentation was not as good as it is today and back when 12 bit acquisition systems were very commonplace. But maybe those rules are not as critical today, with much better instrumentation and 24 bit acquisition systems commonly used. So while guidelines are clearly needed, users need to realize that they are suggestions and they need to understand how to interpret if a measurement is useful or not.

So to illustrate this point, a simple plate structure was tested with an impact excitation technique. Two tests were performed. The first test used a harder tip and with an input spectrum with a 10 dB roll off over the frequency range of interest. The second test was with a softer tip, with 30–35 dB roll off; approximately 10 dB over the first third of the spectrum, approximately 25 dB over the next third of the spectrum, and the remainder over the last third of the spectrum. The hard tip and soft tip input force spectra are shown in Figure 7.46.

The drive point frequency response function for the modal test with the harder hammer tip is shown in Figure 7.47 and the drive point frequency response function for the test with the

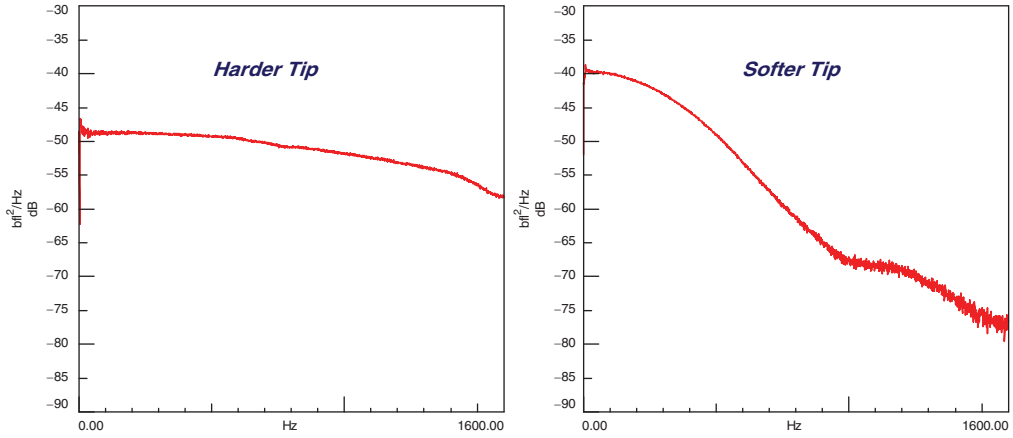

Figure 7.46 Comparison of hard tip and soft tip force spectrum.

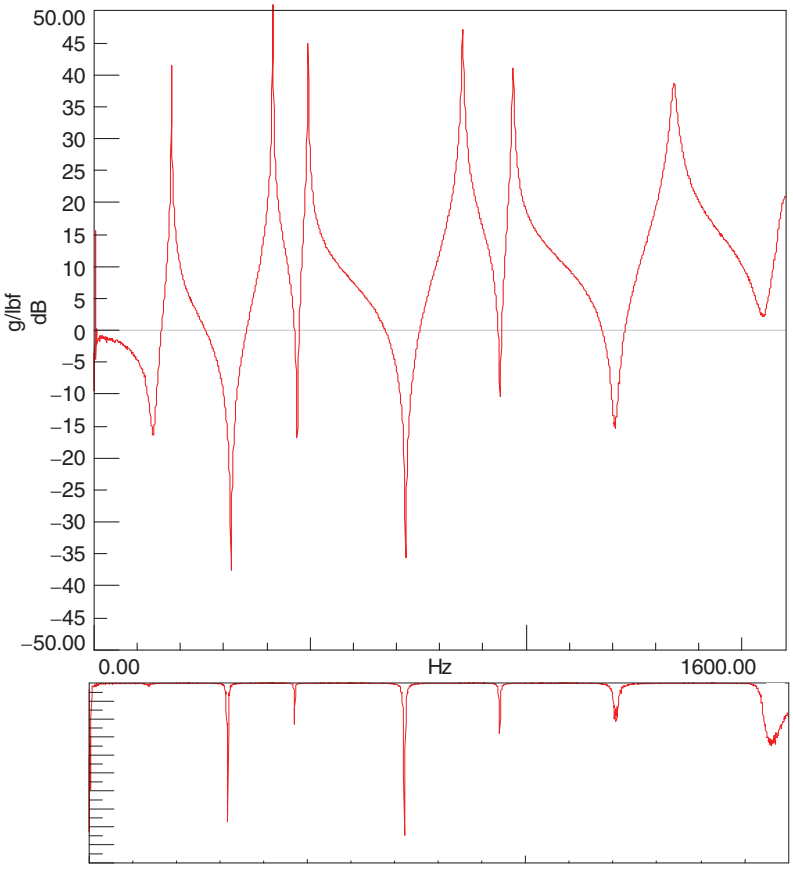

Figure 7.47 FRF and coherence for hard tip.

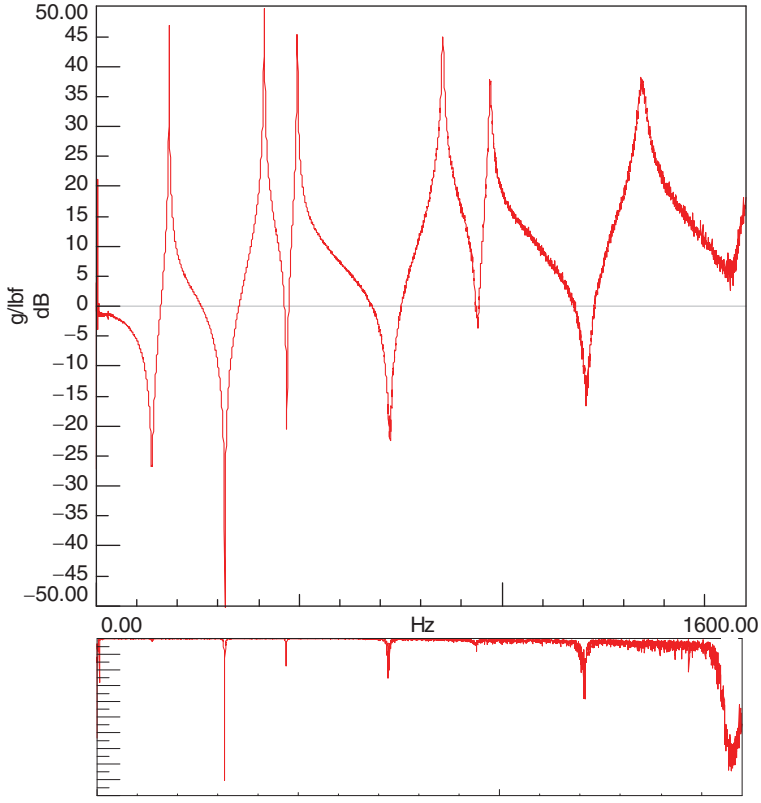

Figure 7.48 FRF and coherence for soft tip.

softer tip is shown in Figure 7.48. Now clearly, the frequency response function with the harder tip is overall a much better measurement, as evidenced by the coherence. One thing to notice in the frequency response function with the softer tip is that the measurement at the higher frequency shows some variance in the frequency response function overall and there is a slight degradation of the coherence at the higher frequencies.

Now why is the measurement is needed and what is the measurement used for? Sometimes tests are performed to obtain very high quality measurements for very specific applications. But sometimes measurements are made to get a general understanding of the generic characteristic mode shapes for the structure and maybe do not need to have the same high quality as some other tests that need to be performed. Think of it like buying lumber for a home building project; knot-free wood is not needed for the entire project; sometimes wood of a lower quality is more than adequate for the project undertaken.

Now it is desirable to take high quality measurements all the time, but sometimes the cost involved in doing that makes the test prohibitively expensive. So let's see just how good or bad these measurements are. Modal parameters were estimated from both sets of measurements. The generic mode shapes are shown in Figure 7.49 for reference. A MAC was also computed for the two sets of mode shapes and is also shown in the figure. Now the mode shapes from both tests are seen to be essentially the same, so the frequency response function measurements seem to be adequate for the simple assessment of mode shapes for the structure.

Now this does not show that this type of input force spectrum roll off is acceptable, but sometimes there is still useful information that can be obtained from data. So while there are

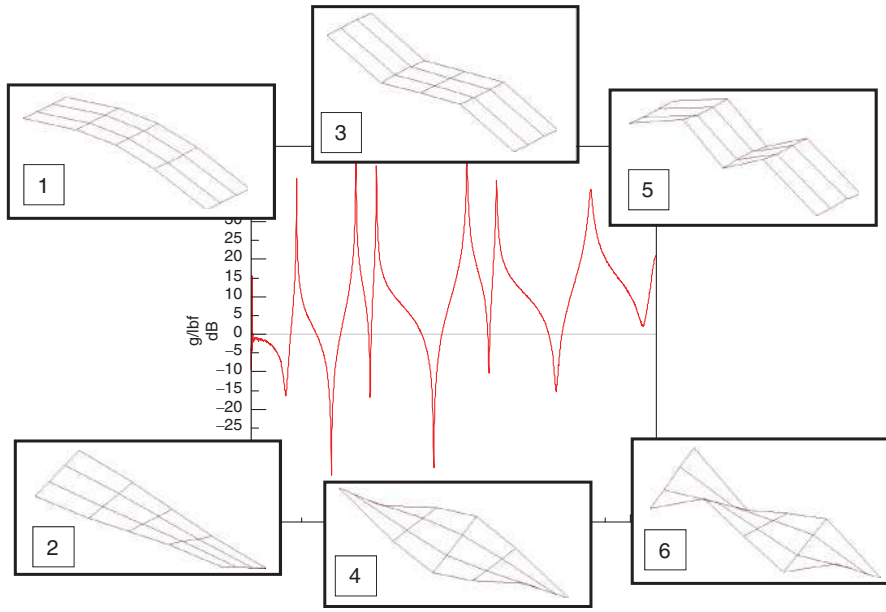

Frequency	179.3 *Hz*	413.5 *Hz*	495.1 *Hz*	853.7 *Hz*	970.6 *Hz*	1345.2 *Hz*
179.3 *Hz*	100	0.006	0.152	0.048	32.868	0.006
413.5 *Hz*	0.006	100	0.015	0.123	0.002	9.974
495.1 *Hz*	0.152	0.015	100	0.001	0.165	0.075
853.6 *Hz*	0.048	0.124	0.001	100	0	0.179
970.6 *Hz*	32.873	0.002	0.165	0	100	0
1345.2 *Hz*	0.006	9.975	0.075	0.179	0	100

Figure 7.49 Typical mode shapes shown with MAC comparing both sets of data collected.

guidelines to follow, that doesn't necessarily mean that the data is not useful. But care as to how to collect the data and interpret the results is critical.

7.16 Can the Hammer be Switched in the Middle of a Test to Avoid Double Impacts?

Double impacts have been discussed earlier, but this section considers a different scenario. Superficially, switching the hammer might appear to be a way to mitigate the double impact, but there may be some ramifications as a result of doing so. So let's take some measurements on the same structure just to see what impact this has (no pun intended). In the previous section, there was discussion about the roll off of the hammer; it was shown that the roll off itself didn't significantly degrade the resulting mode shapes of the system but that there was some degradation of the frequency response functions measured as expected.

Now during that original test, care was taken to avoid any double impacts (with the harder tip). But using that same structure, some additional measurements were acquired and some of

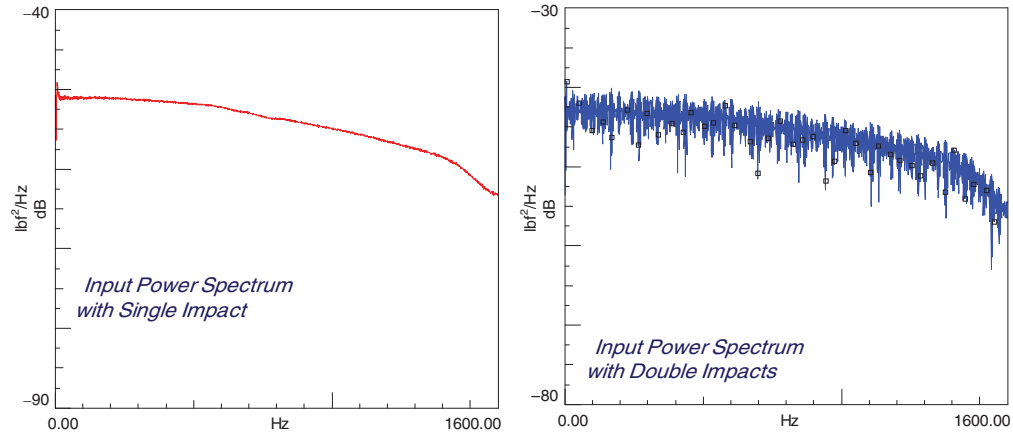

Figure 7.50 Comparison of single and double force spectrum.

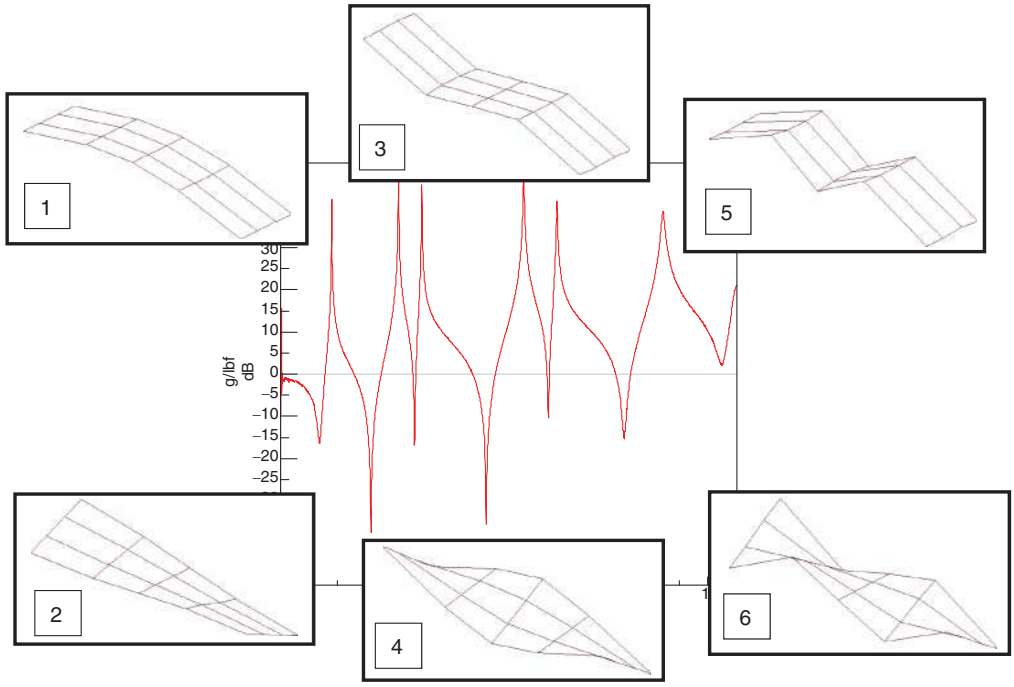

Figure 7.51 Mode shapes for structure.

the measurements were intentionally acquired with double impacts. And in fact another whole set of data was collected and it was specifically ensured that every one of the frequency response functions acquired came from an impact excitation where double impacts were applied. For reference, the typical input force spectra for a single impact and a double impact are shown in Figure 7.50. While the double impact shows variation of the input force spectrum over the entire frequency band, it is important to note that there are no large drops in the input spectrum, which would be the major concern. For reference, Figure 7.51 shows the typical mode shapes for the structure tested.

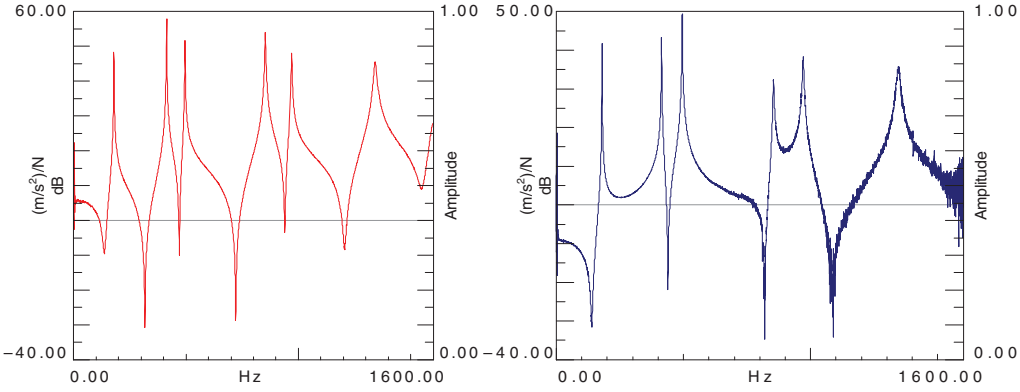

Figure 7.52 Typical FRF for harder impact tip (left) and for softer tip (right).

Now one data set is collected with the harder tip and no double impacts. This will be the reference for the comparisons that will be considered here. And a second data set to acquire some measurements in locations of the structure where double impacts could possibly occur was performed with the use the softer tip to acquire those measurements. To document this properly, the outer ten frequency response functions of the structure are measured with the harder tip and the inner ten frequency response functions are measured with the softer tip.

For comparison, two frequency response functions from each hammer tip are shown in Figure 7.52, for the harder tip (left) and the softer tip (right).

Now for the first comparison, the MAC was computed for the reference modal data set and the "hybrid" set of modal data where some of the measurements were made with the harder tip and some were made with the softer tip; the original idea was to minimize the double impact with the softer tip. The MAC for this case is shown in Table 7.1. Notice that the MAC for the diagonal terms ranges from about 95 to 99 for the corresponding modes; the off-diagonal terms are not as critical to this evaluation because spatial aliasing is the main difficulty with such a limited set of data points.

But remember from the previous section, when the harder tip modal data set was compared with the softer tip modal test, there was essentially no difference between the modes. So what has happened here? Basically, as the tip on the hammer was switched, there was an effective change in the input spectrum that essentially changed the calibration for the hammer. Because all the measurements were not collected with the same hammer tip, there is a bias on some of the measurements relative to the balance of the measurements. This means that an imbalance exists in the scaling of the frequency response functions. So this directly implies that during a

Table 7.1 MAC comparing reference data with "hybrid" data.

Frequency	*179.270 Hz*	*413.356 Hz*	*495.121 Hz*	*852.661 Hz*	*970.418 Hz*	*1341.456 Hz*
179.304 Hz	*98.547*	*0.207*	*0.048*	*0.17*	*30.453*	*0.114*
413.501 Hz	*0.052*	*98.088*	*0.007*	*0.253*	*0.149*	*10.311*
495.105 Hz	*0.114*	*0.189*	*99.798*	*0.144*	*0.173*	*0.216*
853.646 Hz	*0.107*	*0.573*	*0.002*	*97.825*	*0.121*	*0.31*
970.634 Hz	*33.247*	*0.144*	*0.09*	*0.082*	*95.881*	*0.126*
1345.196 Hz	*0.122*	*9.725*	*0.07*	*0.431*	*0.132*	*97.921*

Table 7.2 MAC comparing reference data with softer hammer tip data.

Frequency	*179.454 Hz*	*414.166 Hz*	*495.463 Hz*	*855.208 Hz*	*972.122 Hz*	*1346.707 Hz*
179.304 Hz	*99.634*	*0.014*	*0.085*	*0.093*	*33.183*	*0.024*
413.501 Hz	*0.024*	*99.823*	*0.004*	*0.137*	*0*	*12.293*
495.105 Hz	*0.039*	*0.036*	*99.906*	*0.034*	*0.093*	*0.058*
853.646 Hz	*0.1*	*0.175*	*0*	*99.475*	*0.065*	*0.341*
970.634 Hz	*33.476*	*0.01*	*0.117*	*0.072*	*99.579*	*0.051*
1345.196 Hz	*0.018*	*11.365*	*0.06*	*0.216*	*0.009*	*99.292*

test the hammer tip shouldn't be switched in the middle of the test or else there can be a bias in the frequency response functions collected, unless calibration to normalize that effect in the data acquired is included when the hammer tip is switched.

Now let's take this just one step further and use another set of data. While using double impact data is not desirable, sometimes data might be collected with double impacts and maybe that data is not difficult to use, as long as care is used to make sure that all the data is reasonable, with good coherence. Now using the data set where all the frequency response functions were measured with some type of double impact but all frequency response functions were acquired with the same hard tip for all measurements, modal parameters were extracted. Now another MAC was computed for the reference modal data and the modal data with some type of double impact at all measurement points. The MAC is shown in Table 7.2 for this case. Now notice that the MAC for all the diagonal terms is all above 99. This shows that the data was actually very good overall and the frequency response functions collected with double impacts are actually better than the data where effort was made to minimize the double impact by using a softer tip at a subset of locations on the structure. This might not be expected, but it makes sense considering that the double impact data was collected with a somewhat consistent input excitation whereas the "hybrid" dataset was not.

7.17 Closing Remarks

A variety of different impact test scenarios were identified and various issues were presented and discussed. Some examples of improper hammer excitation were presented to show the distortion of the FRFs obtained. Assorted issues of transducer saturation, reciprocity, selecting a reference location, hammer bandwidth, multiple impacts, hammer tips, and filter ring were all discussed, with examples to illustrate issues of concern. Several examples were presented from a variety of different questions that have been posed as possible ways to conduct a test when one or more of the problem issues were encountered; these examples show how the data may be distorted when attempting to rectify a problem that often occurs during a modal test. Each of these items discussed has been seen time and time again, but they are easily rectified. These examples are useful and will help those with problems similar to those presented.

8

Shaker Testing Considerations

The general shaker test setup was briefly discussed in an earlier chapter. The basic force gage and stinger/quill arrangement was briefly discussed and was followed by a description of some of the typical excitation techniques employed for making frequency response measurements with a shaker system. Here some of the more practical issues and experiences of testing with single and multiple shakers are discussed. Some good techniques and some bad techniques will be illustrated in the material presented here.

8.1 General Hardware Related Issues

8.1.1 General Information about Shakers and Amplifiers

The shaker and amplifier form a set of hardware that is typically used for shaker excitation testing. This is really just a voice coil with an amplifier, similar to a speaker on a stereo system. A signal is fed to the amplifier and the amplifier sends that signal to the shaker. The signals can be simple sine waves or sine sweeps. But for modal testing these signals are normally either random or deterministic in nature. Common signals are:

- random or burst random for non-deterministic signals
- sine chirp, pseudo-random, or digital stepped sine for deterministic signals.

These signal types were all discussed in an earlier chapter. Figure 8.1 shows the typical arrangement for the shaker and amplifier system along with the ultimate force, which is

Modal Testing: A Practitioner's Guide, First Edition. Peter Avitabile.

Companion Website: www.wiley.com/go/avitabile/modal-testing

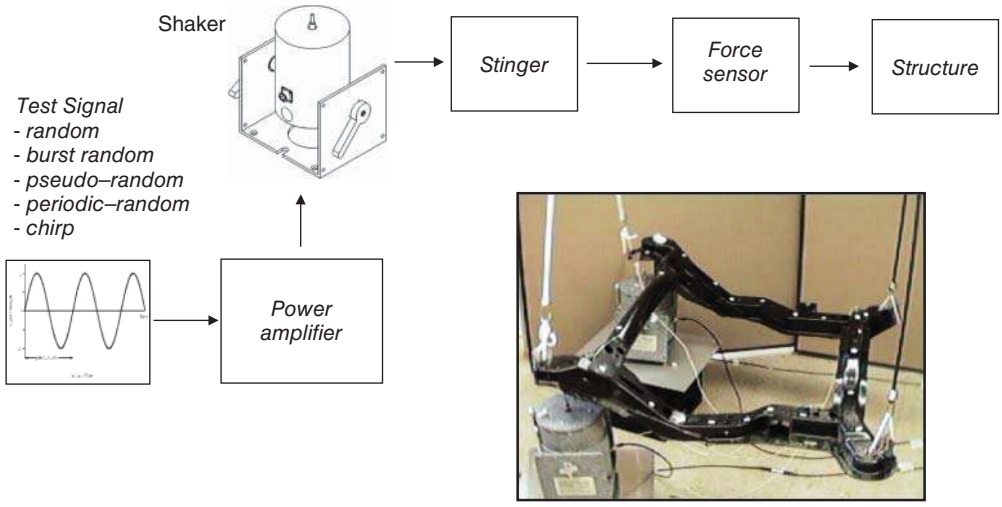

Figure 8.1 Typical shaker/amplifier configuration for experimental modal testing.

measured at the structure interface. Generally, a force gage or impedance head is used as the transducer at the structure side of the measurement.

8.1.2 What is the Difference between the Constant Current and Constant Voltage Settings on the Shaker Amplifier?

Most shakers for general use are set up with current amplifiers. When using some of the more common shaker excitation techniques used today for modal testing, this does not provide for good frequency response measurements. This is especially true for burst random excitation, which is very widely used in modal testing with single or multiple shakers. When using burst random excitation, the response of the system needs to decay to zero before the end of the sample interval of the FFT analyzer time capture. With current amplifiers, the armature of the shaker coil is allowed to freely float after the excitation is terminated. For very lightly damped systems, sometimes the excitation and response lingers on well beyond the sample interval.

However, when the amplifier is set up as a voltage amplifier then the back EMF effect provides resistance to the armature and helps to cause the system response to die out more quickly. This may seem to be inappropriate because it seems that the shaker system is then supplying damping to the measurement. But this is not really an issue as long as the force is measured for the entire measurement. Then the correct input–output relationship is measured. (It is also important to note here that the force needs to be measured and not the electrical parameters of the amplifier in order to make the correct measurement.)

8.1.3 Some Shakers have a Trunnion: Is it Really Needed and Why Do You Have It?

The trunnion is actually a bracket to support the shaker; it allows the shaker to be rotated into different positions. The trunnion is a very important feature of the shaker system. Without a trunnion, it is very difficult to set up a shaker for modal testing. The trunnion allows the shaker to be configured in different orientations and angles for excitation. The trunnion is also beneficial when aligning the shaker to the structure for modal testing. The structure often has multiple modes in different directions, which may be orthogonal with respect with each other. In these cases, the excitation may need to be provided in the x- and y- and z-directions to get each of the different modes adequately excited. An alternative is to mount the shaker at a skewed

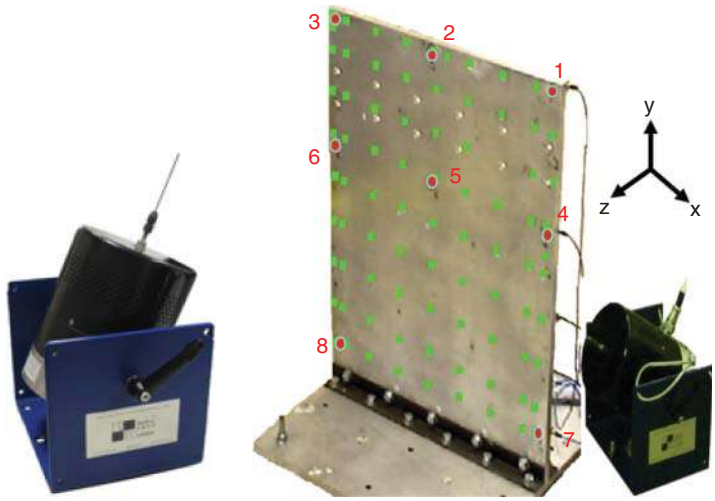

Figure 8.2 A typical modal shaker with trunnion (left) and a test setup with skewed excitation input (right).

angle to the structure such that all the different modes in the different directions can be equally excited. The shaker trunnion is absolutely necessary for these types of test situations. A typical shaker with trunnion and a testing application with a skewed shaker configuration are shown in Figure 8.2.

8.1.4 Where is the Best Location to Place a Shaker for a Modal Test?

The question of the location of the shaker is a little bit different than that of where the reference accelerometer should be located, but some of the same thought process is appropriate. Earlier in the theory section (as well as in some of the application sections), the need to have the reference location at a point on the structure in motion for each of the modes was clearly stated. For the impact test where the hammer is roving, the location of the reference accelerometer should be at a location where the response is large for all of the modes. In general, the same can be said for a shaker reference location, but with a few extra things that need to be considered. Generally, shakers have limited stroke and limited velocity along with maximum force rating which controls the maximum acceleration. So, if a shaker is mounted to the structure at a point where the displacement is large or the velocity response is high, then the shaker will not be able to "keep up" with the structure response; the shaker will then not be forcing the structure but rather just following along with the response. This is referred to as an *impedance mismatch*. When this happens then there will be a force drop out in the force spectrum at one or more of the resonances of the structure, and the frequency response and coherence may not be good for the measurement. This is not a good situation for making a good measurement. In this situation, the shaker needs to be located at a different location on the structure; one where the structure has less overall response and then the shaker can force the structure with a good, broad, reasonably flat input force spectrum over the frequency range of interest. Of course, in order to do this there needs to be some understanding of the anticipated mode shapes for the structure, but without any prior knowledge of the structure's mode shapes, this can prove to be very difficult. Typically, before a shaker test is performed, a very preliminary impact modal test provides useful information that can help provide an understanding of the mode shapes if no other information is available.

8.1.5 How Should the Shaker be Constrained when Testing?

When setting up for shaker testing, the shaker must be aligned with the structure in order to excite the structure in the desired direction. The shaker force levels used are often very low in amplitude and there is no need to firmly affix the shaker to the floor or mounting arrangement. However, there may be some vibration that transmits back through the base to the floor. In these cases, it is critical that the shaker be firmly affixed to the floor. For low levels of force, hot glue around the base may be more than adequate. But in some instances the hot glue may not be sufficient and some type of mounting arrangement may be required. The shaker may need to be attached to the floor with a bolting arrangement. Another possibility is to sit the shaker trunnion onto sand bags prior to attaching/aligning the shaker to the system. This approach doesn't always work, but is another variation to minimize the vibration motion of the base of the shaker. If shaker base vibration is observed, make sure that the shaker alignment is checked during the sequence of testing to ensure that misalignment does not occur. In addition, the drive point frequency response functions should be routinely checked to make sure that no significant change in the system has occurred.

8.1.6 What's the Best Way to Support a Shaker for Lateral Vibration When it is Hung?

Usually, a shaker stand such as the lateral shaker stand as shown in Figure 8.3 or its equivalent is used. The shaker needs to be supported at four separate points to allow appropriate horizontal motion of the shaker as shown. At times an inertial weight is added to enhance the performance of the shaker system.

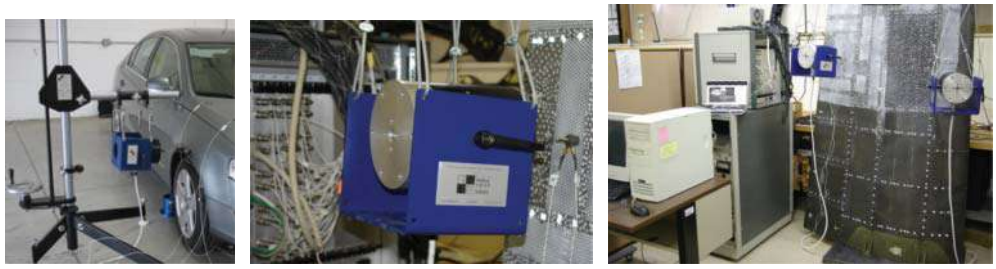

Figure 8.3 Typical shaker measurement setup. *Source*: Image courtesy of PCB Piezotronics, Inc.

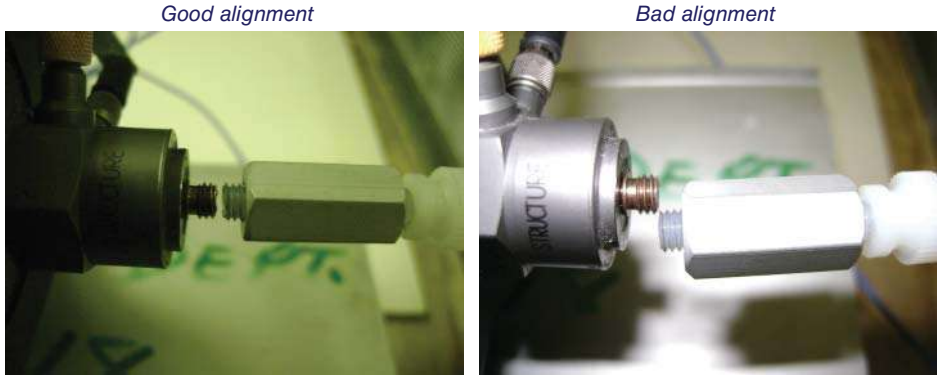

Figure 8.4 Good alignment (left) and bad alignment (right) for a shaker stinger attachment.

8.1.7 What are the Most Common Practical Failures with Shaker Setup?

Misalignment of the quill is often a real problem in modal testing. While nothing really breaks as a result of this, the measured frequency response functions will not be good representations of the system characteristics. At times this will cause difficulties in estimating modal parameters from data that has been contaminated as a result of poor shaker alignment. Often people do not even realize that their measurement has been contaminated by these effects because they are obscured by the fact that their structure is complicated and has many inconsistencies due to noise, nonlinearities, and other effects. It is all too easy to overlook these simple measurement issues due to other commonplace factors.

The main problem with shaker misalignment is that the force gage or impedance head sees loads that are other than normal to the surface. This can cause a distortion of the actual measured force that is applied to the structure. It is very important to make the best possible measurement, and alignment is an important part of that process.

Another problem will result when the structure is too compliant at the point of shaker attachment. Several issues will result from this problem. For one, the shaker may not have enough stroke for the actual structure displacement observed during testing. While displacement is one effect, often people forget that the shaker coil also has velocity limitations, typically around 70 ips for commercial electrodynamic shakers. What happens in these cases is that the structure wants to deflect (especially at resonant frequencies) and the shaker can't "keep up" with the actual displacement/velocity of the structure. So rather than applying a force to the structure, the shaker armature is trying to push the structure, which is moving faster than the coil is moving. This causes a "force dropout" in the input force spectrum, especially at resonant frequencies. Often this will be referred to as impedance mismatch between the shaker and structure. In order to remedy this, typically the shaker will need to be moved to another location of the structure where the structure is not as compliant.

8.1.8 What is the Correct Level of Shaker Excitation for Modal Testing?

The excitation levels for modal testing are usually very low. There is no need to provide large force levels for conducting a modal test, especially if appropriate response transducers (accelerometers) are selected, namely those with good sensitivity. The force level only needs to be sufficient to make good measurements. In fact, large force levels tend to overdrive the structure and can excite nonlinear characteristics of the structure and provide overall poorer measurements than with lower level force tests.

8.1.9 How many Shakers should I use in my Modal Test?

The number of shakers required is often a difficult question to answer. Basically, there are never enough shakers when conducting a large modal test. Often the limit is the total number of shakers available in the test lab for modal testing. Two shakers are sufficient for many tests. Sometimes three or four shakers are needed for much larger structures. But generally, more than five shakers are rarely used. The main point is that there needs to be enough shakers acting as reference locations that are positioned so that all of the modes of the structure are adequately excited and good frequency response measurements are obtained.

8.1.10 Shaker and Stinger Alignment Issues

The alignment is extremely important and some simple discussions on how to set up the shaker are appropriate. These just describe some simple steps that are commonly taken when setting

up the attachment or the shaker to the structure. This is followed by some guidance about the stinger alignment issues that are often faced when setting up a shaker test.

In setting up a shaker test, typically the shaker and quill are set up first, with the quill extended to the desired length and the force gage or impedance head attached to the end of the quill. With the shaker collet loosened, the quill can be extended in and out of the armature to obtain the desired length. Once this is done, the force gage or impedance head mounting pad can be affixed to the structure; the mounting pad can be attached with superglue If the alignment is correct, then the shaker quill should be able to be very easily unthreaded from the force transducer or impedance head *and* it should also thread right back in without any binding (resistance to threading the stinger) or difficulty whatsoever. This is one way to assure that the shaker and quill are properly aligned.

However, at times there may be a threaded mating hole in the structure for mounting the force gage or impedance head and attaching the shaker. Alignment in these situations is much more difficult. The main point is that the shaker must be aligned such that the quill can be very easily threaded in to the force gage or impedance head, with no difficulty or binding whatsoever. Figure 8.4 shows two situations: one in which the stinger is aligned well and one where it is not aligned well. The threading of the quill to the force gage should have no binding whatsoever.

Figure 8.5 shows three pictures of the sequence of attaching the stinger. Once the stinger is aligned correctly, the lock nut on the impedance head or force gage should be tightened. Next, the collet on the shaker should be tightened, making sure that the shaker head is held in place to minimize loads on the armature.

8.1.11 When should the Shaker be Attached to the Structure?

Generally, all the accelerometers are attached to the structure and cabling run from the structure to the acquisition system before the shaker is attached to the system. The shaker/stinger attachment/alignment is usually the last step in the process. If it is attached before all the instrumentation is set up, then there may be some settling of the structure or shifting of the structure during the course of test setup. This is especially true when performing free–free testing. If there is any shifting or settling of the structure, then this may cause misalignment of the shaker/stinger setup, which may lead to incorrect measurements. This may not be noticed until after the test is completed and the shaker disassembled from the structure. Because of this, the shaker is generally the last item to be set up when performing modal testing. Figure 8.6 shows a test with all the instrumentation attached to the structure, with the shaker attachment about to be performed.

8.1.12 Should I Disconnect the Stingers while not Testing?

Generally, the shakers are disconnected from the structure when testing is not being performed. During the setup of the test, there may be some shifting or settling of the test article. At times,

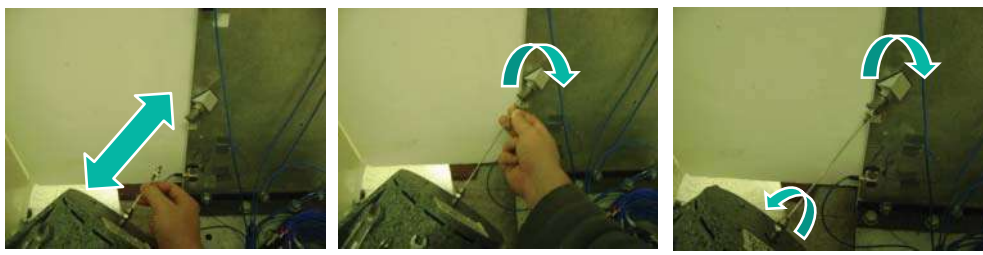

Figure 8.5 Stinger installation sequence: extend stinger (left), screw into force gage (middle), tighten lock nuts (right).

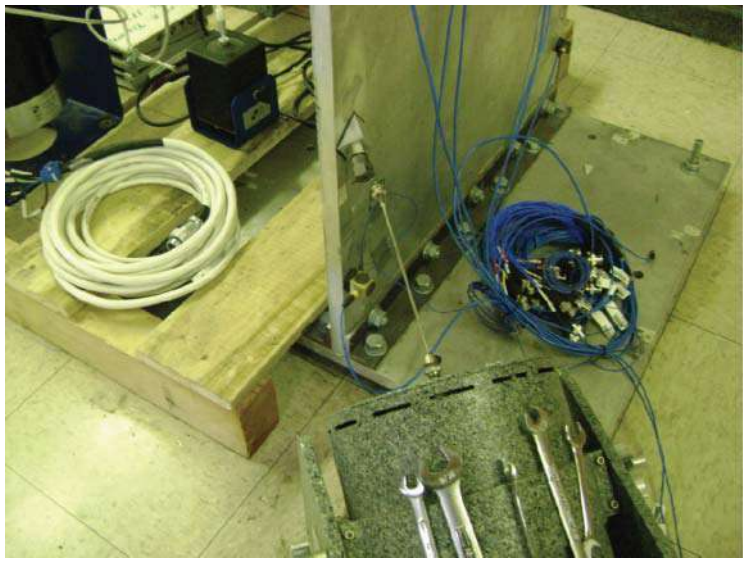

Figure 8.6 Stinger attachment: last step after structure setup and instrumentation attached.

airbag support systems may lose air and cause shifting of the structure. Or there may be reconfiguration of the test article during tests. For instance, a gas tank may be empty in one test and then full in another test. There are many reasons why the system may need to be reconfigured during the test.

Because this is the case, there may be a general shifting or redistribution of mass in the system, which in turn causes shifting in the test article relative to the original alignment of the shakers to the structure. If the shakers are attached during these reconfigurations, there may be side loads applied to the quill attaching the shaker to the structure; the alignment of the system may be disturbed in these cases. If the shakers are still connected, side loads on the shaker armature can result and may cause damage to the shaker system. In addition, it may become difficult to disassemble the stinger from the structure once the alignment has been disturbed. Figure 8.7 shows the original alignment of the shaker prior to attaching all the instrumentation. Due to the addition of the instrumentation and other related setup issues, the structure is seen to shift slightly and the original shaker alignment is no longer appropriate. If the shaker was attached prior to the complete instrumentation, there would be side loads on the shaker

Initial shaker set up before all test set up complete

After adding all instrumentation

Figure 8.7 Shaker settling: initial setup (left) and sag in system after several hours (right).

Figure 8.8 Structure shaker misalignment requiring shaker adjustment.

and force gage that might go unnoticed; these side loads could have an effect on the measured frequency response functions.

If the shakers are disconnected, then upon reattaching the shakers for the next set of tests, it will be obvious if any misalignment has occurred. If the original shaker alignment is disturbed, then the shakers must be realigned in order to provide a proper attachment to the system. Figure 8.8 shows a misaligned stinger and impedance head; the shaker must be repositioned to provide the appropriate alignment. At times this can be difficult, but suffice it to say that the measured frequency response functions will degrade if this alignment is not performed properly.

8.1.13 Force Gage or Impedance Head must be Mounted on Structure Side of Stinger?

The force transducer should always be mounted on the structure side of the stinger and not on the shaker side of the stinger, as shown in Figure 8.9. This then measures the force that

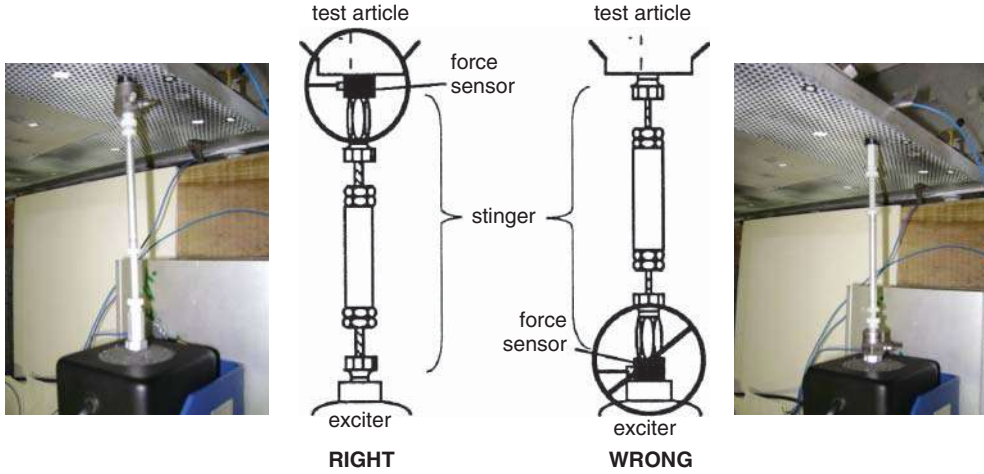

Figure 8.9 Correct force gage configuration (left) and incorrect force gage orientation (right). *Source*: Image courtesy of PCB Piezotronics, Inc.

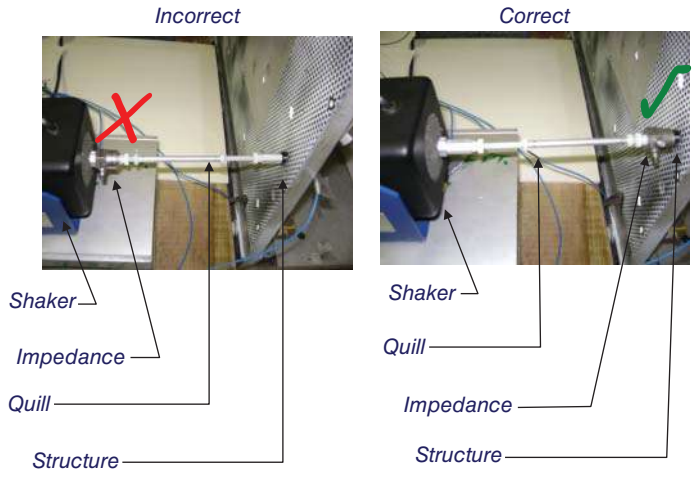

Figure 8.10 Incorrect orientation (left) and correct orientation right for measurement.

is imparted to the structure, information which is needed to properly compute the frequency response function, which is the ratio of response to applied force.

If the force gage is mounted on the exciter side, then the dynamics of the stinger become part of the measured function and this is improper. Figure 8.10 shows the two mounting approaches. Figure 8.11 shows the difference in the two frequency response measurements: one taken with an incorrect and one with a correct mounting arrangement. The figure shows the significant difference in the two measured functions, illustrating the importance of this mounting arrangement.

8.1.14 What's an Impedance Head? Why use it? Where does it go?

An impedance head is a transducer that measures both force and response in one device. Typically today, an impedance head consists of an accelerometer and force gage, but in the old days

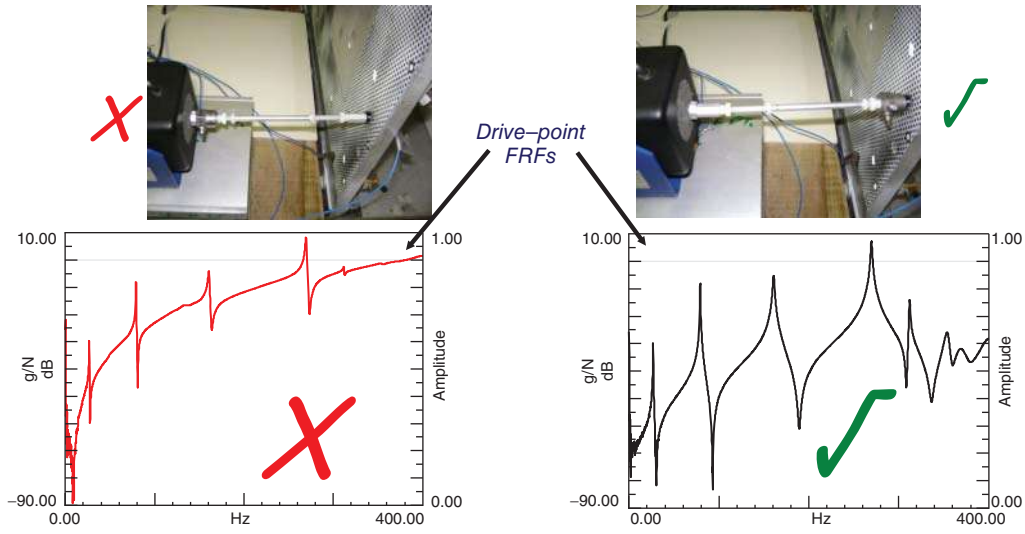

Figure 8.11 Resulting measurement with incorrect configuration (left) and correct measurement (right).

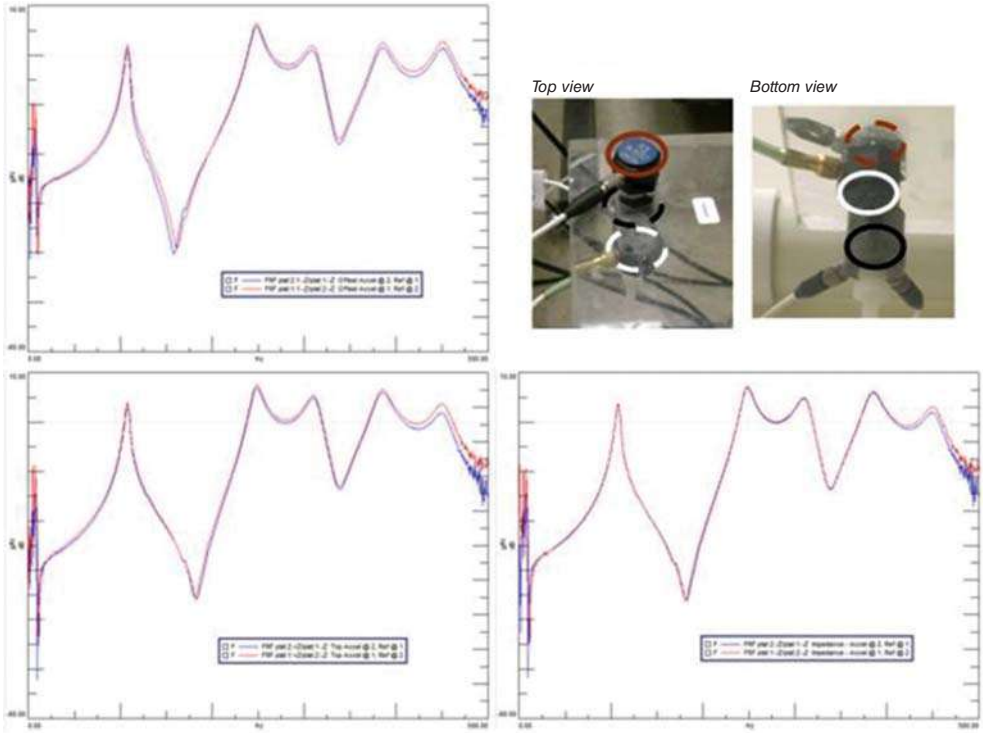

Figure 8.12 Comparison of FRF with: offset accelerometer (top left); accelerometer aligned as well as possible (lower left); impedance head (lower right).

it was a velocity transducer and force gage (which is where the name "impedance head" comes from; the usage has lingered on until today, even though velocity is no longer measured). This drive point frequency response function is a critical measurement for the structure and it is strongly advised that impedance heads be used in all cases. In Figure 8.12, three scenarios are shown. In the upper left frequency response function, the accelerometer is intentionally misaligned with respect to the force gage to illustrate the differences that can result. In the lower left frequency response function, the accelerometer is aligned as well as possible but differences can still be seen. In the lower right frequency response function, an impedance head is used to minimize the alignment issues that can possibly result. Clearly, the measurement with the impedance head is the preferred measurement for these critical frequency response function measurements. A combination of a separate force gage and accelerometer is often used, but time and time again this measurement has been shown to be worse than that obtained with an impedance head.

8.2 Stinger Related Issues

8.2.1 Why should Stingers be used?

Stingers, also called *quills*, are required to perform modal testing with shakers. The shaker head should never be directly attached to the structure for modal testing. This would not provide good frequency response measurements for modal testing. If the shaker were to be directly attached to the structure, then dynamic effects of the shaker would be imposed onto the structure. The frequency response function could be dramatically affected by this.

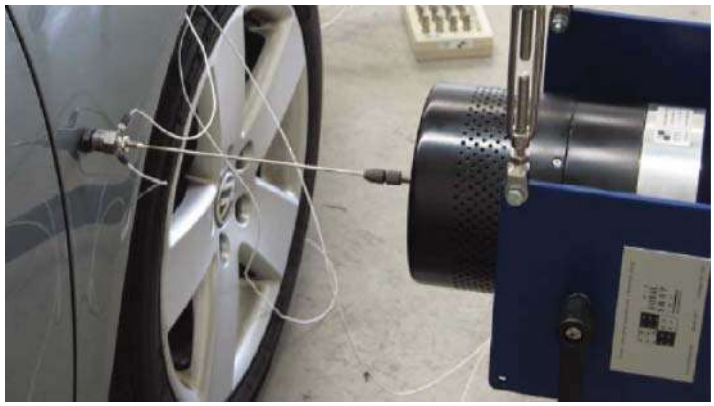

Figure 8.13 A typical shaker measurement setup with stinger. *Source*: Image courtesy of PCB Piezotronics, Inc.

Basically, the stinger allows the shaker to be decoupled from the structure and allows force to be applied only along the direction of the quill; at least this is the concept of the setup of the shaker with a stinger illustrated in Figure 8.13. With this setup, force is only applied along the axis of the quill and the only force measured by the force transducer or impedance head is in the intended direction for measuring the force through the piezoelectric crystal. It is important to remember that the force sensing element is only sensitive to motion in one direction; the force sensing element is not designed to measure lateral loads or moments.

Of course this arrangement is never going to be perfect and there will always be some slight effect of the shaker on the structure. The intention of using the quill is that it should be very stiff in the axial direction and extremely compliant to lateral loads. Now this is very easy to say and sometimes not so easy to achieve. In practice, the intention is to make the stinger very stiff in the axial direction to allow force to be transmitted (and measured) to the structure. The effect of the lateral stiffness on the overall system is very dependent on the structure being tested. If the structure is very stiff, then lateral stiffness is often not a serious concern. However, when the structure is very flimsy or has a significant amount of rotational effect at the attachment point of the stinger, lateral loads can become very important. In addition, these rotational effects generally become more important at higher frequencies, so it is always difficult to determine the actual impact on the overall results. One easy way to determine the effects of stinger lateral and rotational effects is to make several test runs, with the length of the quill varying by ±10% and observe the change in the measured drive point frequency response.

8.2.2 Can a Poorly Designed Shaker/Stinger Setup Produce Incorrect Results?

Shaker testing for experimental modal analysis can cause some special difficulties if care is not taken in setting up the shaker and attachment device. The idea of the stinger is to allow for axial motion to be imparted into the structure, which is then measured by the force gage for simple compression and tension type loads. The purpose of the stinger is to allow for loads in the direction of excitation but to minimize the lateral loads that may be imparted into the system. Essentially, a free body diagram concept allows us to know the force imparted into the structure at the attachment point. Therefore, all the dynamic effects of the shaker system and stinger are not included in the dynamic characterization of the structure under test. At least that's what is happening from a theoretical standpoint. Of course, this assumes that the stinger has essentially no lateral stiffness and does not make any significant contribution to the overall dynamic characterization of the system. This consideration is extremely important because the

force gage only measures the axial load applied; if there are any other loads (lateral or moment), the force gage does not measure them.

The measurement that was made is described next. (This measurement was received from an outside source.) A relatively flexible beam was set up for testing with a shaker. However, the stinger was relatively short and there was a possibility that the rotational stiffness of the stinger might affect the beam's flexible modes. So now let's take a look at some of the measurements that were made. Figure 8.14 shows a frequency response function measurement that was taken, with a shaker system attached to the structure with a stinger that was possibly too short. This then caused the rotational stiffness of the stinger to be more pronounced, especially relative to the flexible beam that was being measured. A modal test revealed that there were classical first and second bending modes for the first two peaks, as expected. However, the next two peaks revealed essentially the same classical third bending mode of the beam. Frequency response function measurements were obtained only for the structure under test, but there were none on the stinger.

Subsequent tests (and additional measurements on the stinger itself) revealed that the two peaks were actually the result of a tuned absorber effect. The stinger was actually in phase with the structure mode shape at third peak of the frequency response function and out of phase with the structure motion at the fourth peak of the frequency response function. The force gage only accounted for the axial motion imparted by the shaker excitation; there was no measurement of the rotational effects associated with the beam rotary stiffness introduced by the stinger in the test setup. But the stinger actually looked like a rotational spring relative to the beam at the attachment point. In order to confirm the observation, a longer stinger was utilized in a second test of the structure. The longer stinger effectively minimizes the effect of the rotational stiffness imparted to the structure under test. Figure 8.15 shows the frequency response function with the longer stinger attached. It is clear that the frequency response function is much cleaner and follows the expected pattern of a beam-like mode response. A brief modal survey was conducted and the first three peaks correspond to the first three classical mode shapes for a cantilever beam.

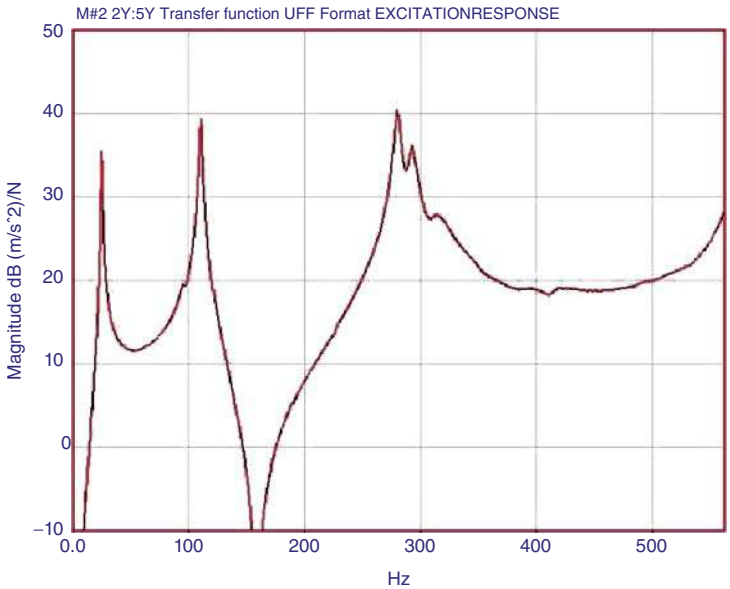

Figure 8.14 FRF with short stinger.

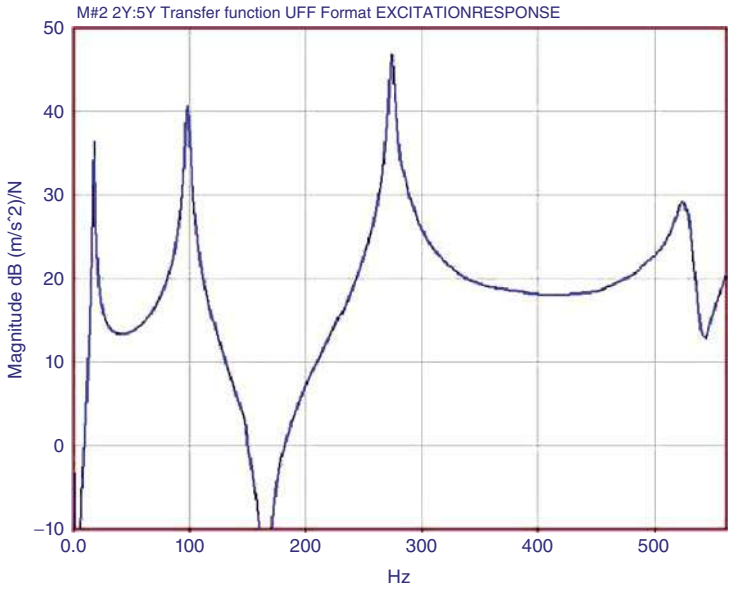

Figure 8.15 FRF with longer stinger.

Clearly, the first two modes see a shifting of frequency due to the different stinger configurations. This can be due to a variety of factors: mass loading effect, stinger effect, different test setup, and so on. These are measurements that were provided by an outside source so the actual test setup is unknown, but the effect is very clear. The third peak is significantly different. There is a splitting of the main peak, as is typically seen in tuned absorber applications. There is also a significant reduction in the overall amplitude of the measured response, as is seen in tuned absorber theory.

Figure 8.16 shows the expected shape that would result if this stinger acted as a tuned absorber to the measurement system. Again, these measurements were provided from an outside source and are used to illustrate the effect that is expected to exist here. Obviously, the rotational effects of the stinger at the attachment point on the structure will be more pronounced as the stinger is shortened. If the stinger happens to have the same frequency as one of the modes of the main structure, then the coupling would definitely produce frequency response functions like those shown in Figure 8.14.

Clearly, the effect of the shaker stinger length plays a very important role in the measurement of accurate frequency response functions. If the stinger is too short then there is a general stiffening effect that can be seen in the measured response function. For this particular case, there is a general tuned absorber effect that can be easily seen. This tuned absorber effect may not occur in every stinger application, but was observed in this particular measurement setup.

Figure 8.17 shows an overlay of the two frequency response function measurements acquired: one with the short stinger and one with the longer stinger. Comparing the two measurements shows significant differences on all the modes of the system measured. Notice that the frequencies of the beam with the shorter stinger are higher in frequency, indicating that the test setup had an added stiffness effect on the frequencies of the system. The effects of the stinger (or quill) can be very important and may render frequency response measurements inaccurate if care is not taken. The next section has several different cases studied relative to stingers on a candidate structure.

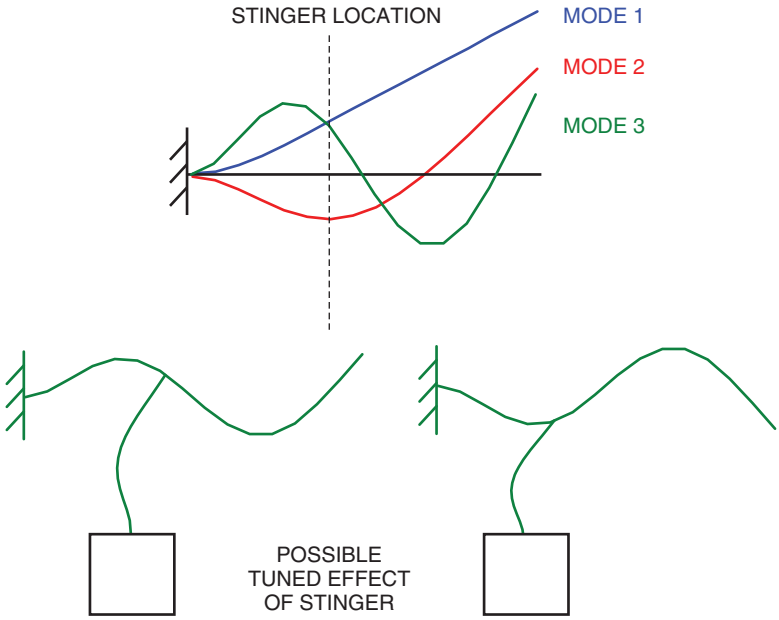

Figure 8.16 Stinger tuned absorber effect. Shapes not to scale and sketched to show expected effect of stinger rotational stiffness coupled to main structure.

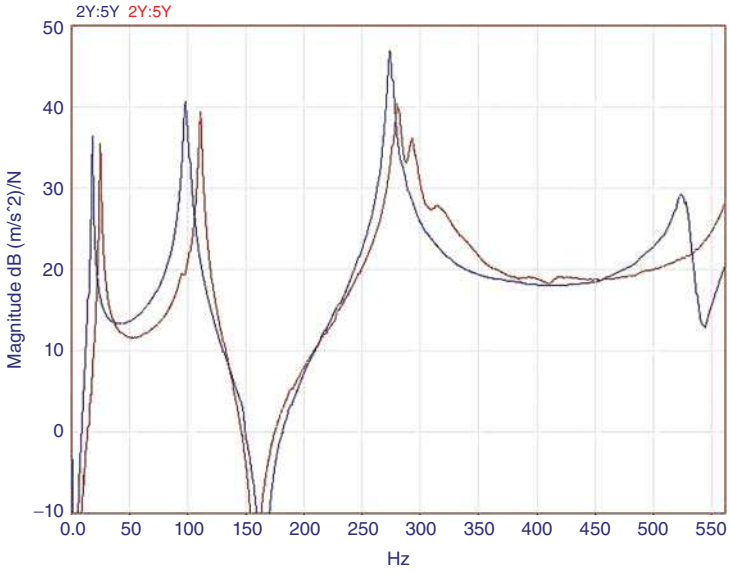

Figure 8.17 Comparison FRF for different stinger lengths.

8.2.3 Stingers and their Effect on Measured Frequency Response Functions

Shaker excitations are often utilized for the development of high quality frequency response functions for use in any structural dynamic modeling scenario. There are a variety of test situations that have an effect on the adequacy of the measurements obtained. Issues related to stingers, impedance transducers, force level, reciprocity, single excitation and multiple excitation are a few of the critical areas. The following sections are broken down to address

measurements and considerations in each of these areas. These findings are measurements from many different structures, as experienced over the years. Each subsection will describe some of the issues related to the particular test setup and the results obtained, while also providing some insights on making improved measurements.

8.2.3.1 Stinger Location

The function of the stinger (or quill) is to decouple the shaker from the test structure. While all stingers have some bending stiffness, if a suitable location is chosen on the structure this stiffness will not contribute to the stiffness of the structure. This can be a major issue when the structure is very compliant, as these structures can have large displacements; there can be corresponding rotations in the structure's response. The most problematic situation is rotational stiffness at the location of stinger attachment, which may affect higher frequency mode shapes.

A candidate structure, shown in Figure 8.18, was used for SISO measurements; frequency response functions were taken at three different heights. While no specific discrepancies were consistent at any one of the heights considered, a reciprocity check between upper and lower measurements revealed differences, as shown in Figure 8.18. The inconsistency in the measurements indicated that there were effects from adding the shaker at different locations on the structure. Clearly some of the frequencies are different with different shaker height locations. This can be due to the stinger stiffness, which may have a more significant effect on the higher modes as they exhibit greater curvature than the lower order modes of the upright portion of the structure. Note that not all measurements taken are shown to reduce clutter in figure; this figure is typical of results obtained for all heights investigated.

One very important item to note is that the stinger is intended to impart motion only in the axial direction; the force imparted is intended to only be in that direction. However, any rotation of the structure causes bending in the stinger and is not accounted for in the frequency response function measurement; this then introduces stiffness in the structure, which affects the frequencies of the structure to some degree. In addition, the force gage does not measure any moments imparted from these rotations and is only designed to measure axial motion.

8.2.3.2 Stinger Alignment

Often the setup of the shaker and stinger can be difficult. The alignment of the shaker and stinger is a very important concern when the structure and shakers are set up for testing. Misalignments are a cause for concern. The effects of stinger misalignment are examined in this subsection.

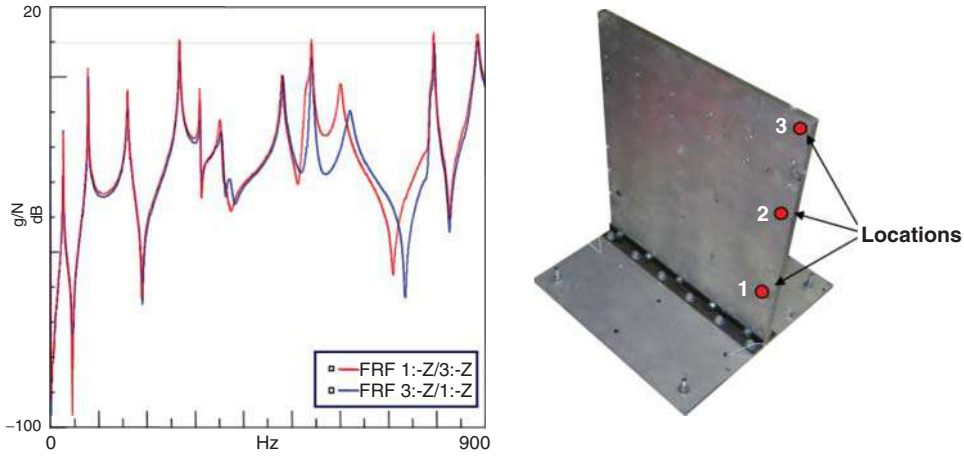

Figure 8.18 Reciprocity measurement between upper and lower SISO measurements.

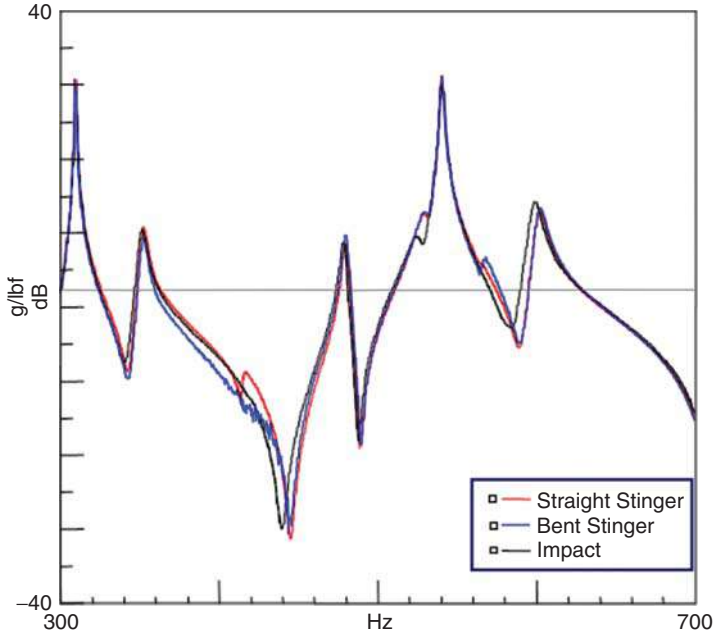

Figure 8.19 Intentional stinger misalignment.

A 5 inch (127 mm) long stinger (from the shaker head to the structure) was attached to the structure and the shaker was shifted to have approximately 10° of misalignment. Figure 8.19 displays this measurement compared to the aligned shaker and impact measurements.

With the shaker misalignment, measurement differences are clearly seen in the frequency response function in the 400–450 Hz region. The specific reason for the differences may be a combination of effects, including the intentional misalignment that was introduced into the measurement. With a better aligned shaker, this frequency band also had an extra peak, possibly due to a resonance of the stinger. While these results are not completely conclusive, one clear statement that can be made is that care needs to be exercised to ensure that the alignment is correct. Misalignment can cause distortion of the measured frequency response function.

Another misalignment issue lies in the stinger itself. This can result from misalignment of the shaker (as just presented) or can result from poor fabrication of the stinger system. Any misalignment can result in the possibility of bending of the stinger. Figure 8.20 shows a damaged stinger used for testing and a comparison of the measured frequency response functions with those taken using a good stinger. As shown in the figure, the mode at approximately 1130 Hz is completely distorted when the damaged stinger is used.

8.2.3.3 Stinger Length

While the location of stinger attachment may already be predetermined, the stinger length can be adjusted. This parameter can have a significant effect on measured frequency response functions. If care is not taken in a shaker test setup, measured frequency response functions can be easily corrupted. A quick preliminary impact test is recommended, in order to confirm the accuracy of the shaker test.

In this case, three different quills (supplied by The Modal Shop) were used:

- 2150G12: a 1/16 inch (1.59 mm) diameter steel rod
- 2155G12: a 3/32 inch (2.38 mm) diameter steel rod
- K2160G: a 0.028 inch (0.07 mm) steel piano wire.

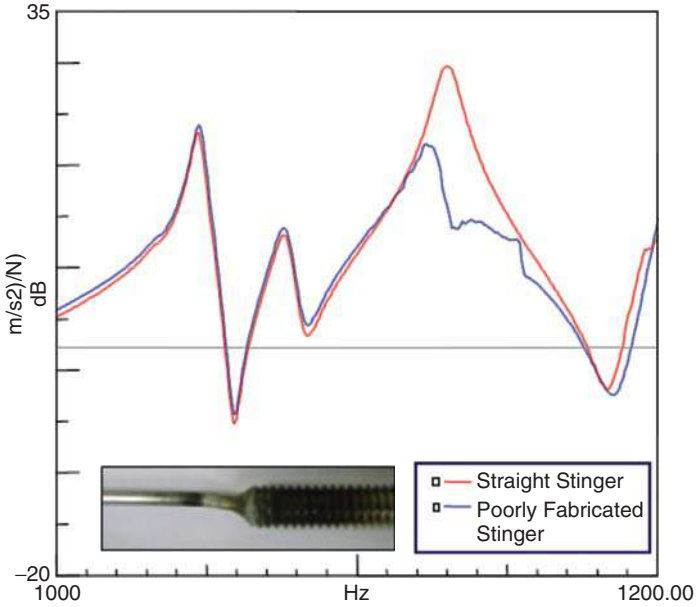

Figure 8.20 Poorly fabricated stinger assembly.

Lengths were varied from 1 to 7 inches (25.4–178 mm), as shown in Figure 8.20, and the shaker was used in both fixed and hanging positions. Figure 8.21 shows the measured frequency response functions of the 1/16 inch (1.59 mm) drill rod at different lengths. For these measurements, the shaker was fixed at the lowest attachment point, although similar results were obtained with all the stingers.

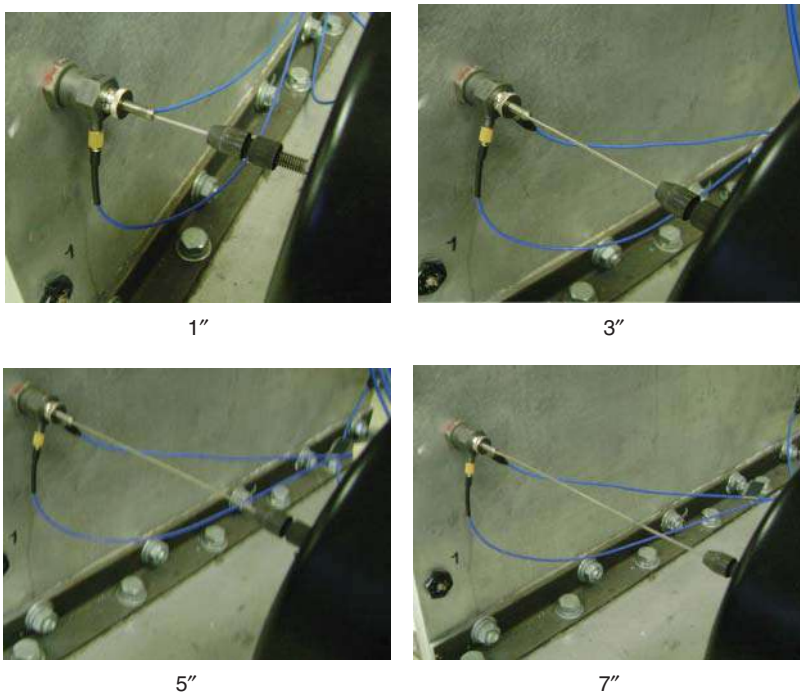

Figure 8.21 Four stinger lengths shown.

The discrepancies in the measured frequency response functions are clearly illustrated in Figure 8.22. No stinger length matched the impact measurement exactly, although a 3 inch (76.2 mm) stinger length seemed to be ideal for this structure. While a 3 inch (76.2 mm) stinger is ideal, a 5 inch (127 mm) stinger yields differences in the frequency response functions. Piano wire gave accurate frequency response functions at shorter lengths than the quills, typically at around 1 inch (25.4 mm). Generally, if the stinger is too short, the structure will have increased stiffness, which can lead to shifts in mode frequencies. On the other hand, a stinger that is too long can introduce additional peaks due to stinger resonances.

8.2.3.4 Stinger Type

While steel threaded and drill rods are the most commonly used stingers, piano wire and nylon threaded rods are also available. This subsection will compare these stingers to show what effects each can have on the test structure. Five different types of quills supplied by The Modal Shop were used:

- 2150G12: a 1/16 inch (1.59 mm) diameter steel rod
- 2155G12: a 3/32 inch (2.38 mm) diameter steel rod
- 2120GXX: a 10-32 threaded steel rod with three different lengths of 9, 12 and 18 inches (228.6, 304.8, 475.2 mm)
- 2110G12: a(10-32 12 inch (304.8 mm) threaded nylon rod
- K2160G: a 0.028 inch (0.07 mm) steel piano wire.

Ideal lengths, as determined in the last subsection, were used with the steel rod and piano wire, whereas the threaded rod was at set lengths. The shaker was used in both fixed and hanging positions. Figure 8.23 shows typical frequency response functions, comparing the measurements obtained with the various stingers.

While the overall measurements compare well, closer examination shows discrepancies in the threaded steel rod measurement. The discrepancies were not surprising, because the 2120GXX stingers are much thicker and stiffer compared to the thinner and lighter 2150G12 and 2155G12 steel rods. An extra mode appears around 520 Hz and the amplitude is slightly decreased in the following two modes. With all stingers, a common frequency shift occurs and increases with frequency. When setting up the test, the effects of each stinger can vary dramatically depending on the mass and stiffness of the test structure and must be considered.

8.2.3.5 Sleeved Stingers

Sleeves can often be added to the stinger to stiffen the stinger in an attempt to impart more force to a higher frequency and prevent the stinger from buckling. It is important to realize that this may have an effect on the measured response function, especially when the structure has local flexibility at the shaker attachment point. Figure 8.24 shows a comparison of the measurement of a system with and without sleeves attached to the stingers. When comparing the sleeved and unsleeved stinger setups, the first thing to notice is that the higher frequency portions of the frequency response functions are very different. The sleeves have an obvious effect.

However, at a lower frequency range the two frequency response functions show very few differences. In the mid-frequency range, the results show some change in the measured frequency response functions, especially when looking at the zoomed-in portion of the measurement. The sleeves tend to stiffen the stinger arrangement. As the frequencies and mode shapes at higher frequencies have more curvature, the effect of the sleeves on the stingers becomes more and more pronounced. The effects of the sleeve stiffening becomes more pronounced as the local flexibility of the structure becomes smaller and smaller. This may not be readily apparent when performing the test. The easiest way to identify if this is a concern is to test the structure with and without the stiffening sleeves on the stingers.

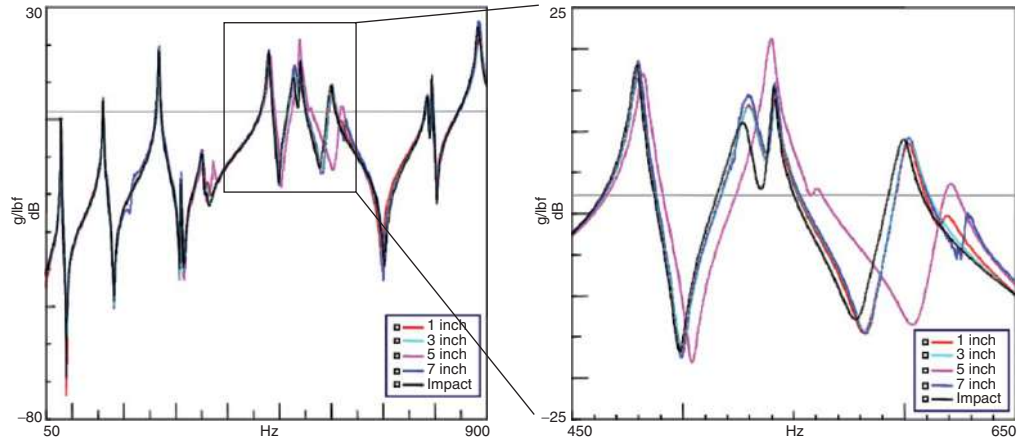

Figure 8.22 Stinger length comparisons.

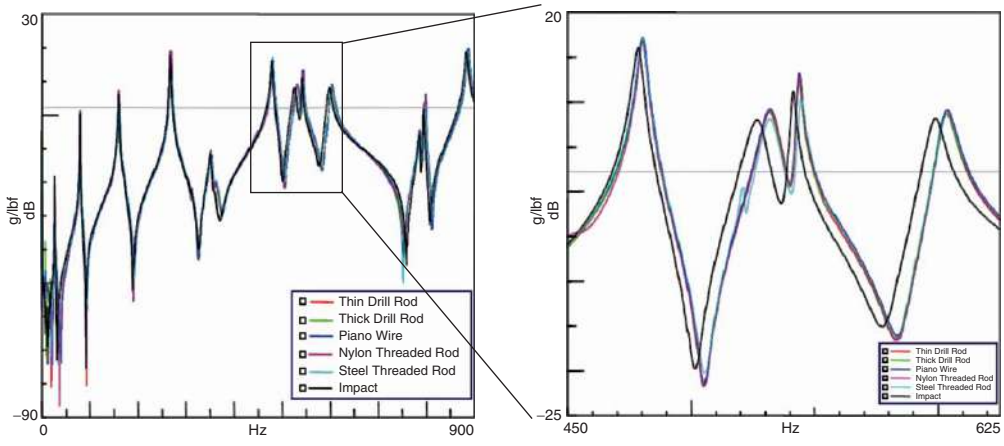

Figure 8.23 Stinger type comparison.

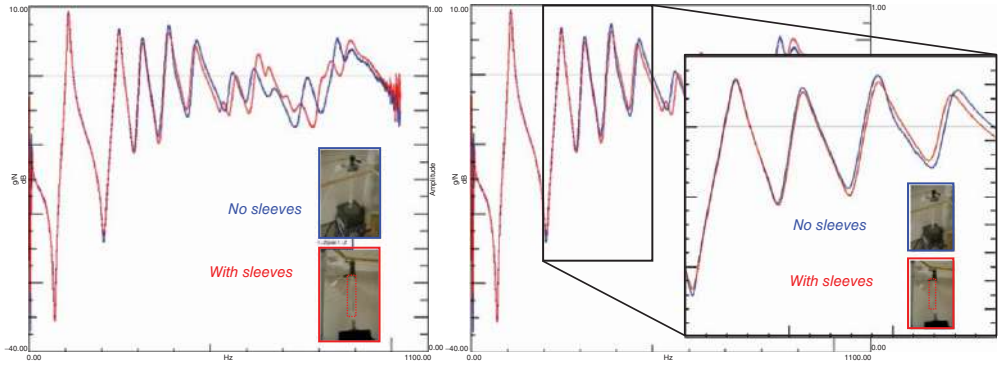

Figure 8.24 Sleeved vs unsleeved stinger comparison.

8.2.3.6 How do Piano Wire Stingers Work? How are they Pretensioned??

Piano wire stingers are an excellent way to circumvent the problems with lateral stiffness associated with conventional stingers. Essentially the piano wire has no lateral stiffness. The piano wire is pretensioned with a load that is greater than the alternating load to be applied; a preload of 3–4 times the range is considered reasonable. The piano wire is fed through the core of the shaker armature, so it is critical to have a modal shaker that is designed to do this. A simple preload can be applied with weights. With the weight applied, the collet is used to clamp the piano wire, with the piano wire pretensioned. As long as the applied load during shaker excitation is less that the preload, then the piano wire is an excellent way to conduct a modal test and eliminate the effects of lateral stiffness in conventional stingers. Of course, this testing doesn't always work well with systems that are supported in a very free condition. Piano wire is usually used for systems that are tested in an existing configuration (like a car or motorcycle).

8.3 Shaker Related Issues

8.3.1 Is MIMO needed for Structures with Directional Modes?

Structures often have modes that may be very directional in nature. The portal frame used in several examples is a good example of this type of behavior. Figure 8.25 shows the first six modes of the frame and it is clear that there are some modes that have predominant motion in the setup horizontal direction and other modes that have predominate motion in the setup vertical direction. If the shakers used to excite the structure are set up in the x- and/or y-directions, the frequency response measurements will only see a subset of modes from each shaker and it may be necessary to use multiple shakers for this test to obtain all the modes. Figure 8.26 shows the frequency response measurements that would be obtained from this type of test. But while two shakers could be used to excite the structure in the x and y-directions separately, the test could also be conducted with just one single shaker that would be set at a skewed angle to the x- and y- directions, as shown in Figure 8.27, such that the first four modes could be excited; if the next two modes were of interest, the shaker would need to be moved to a different skewed location so as to not be at the node of the mode.

Now there is a feature in all modal software to rotate coordinates to make this measurement, but there is a much easier way to do this test without any coordinate transformations. This involves making an additional drive point measurement that is not included in the geometry mapping of the measurements. One measurement, a drive point measurement, can be made at an arbitrarily named point such as "point 99s", as shown in Figure 8.28.

Then all the measurements that are made in the x- and y-directions are made relative to the point at 99s. The collection of measurements would look like this

$$\begin{Bmatrix} a_{1x99s} \\ a_{1y99s} \\ a_{2x99s} \\ a_{2y99s} \\ a_{3x99s} \\ a_{3y99s} \\ a_{4x99s} \\ a_{4y99s} \\ \vdots \\ a_{99s99s} \end{Bmatrix} = q\, u_{99s} \begin{Bmatrix} u_{1x} \\ u_{1y} \\ u_{2x} \\ u_{2y} \\ u_{3x} \\ u_{3y} \\ u_{4x} \\ u_{4y} \\ \vdots \\ u_{99s} \end{Bmatrix} \text{ and } a_{99s99s} = q\, u_{99s} u_{99s}$$

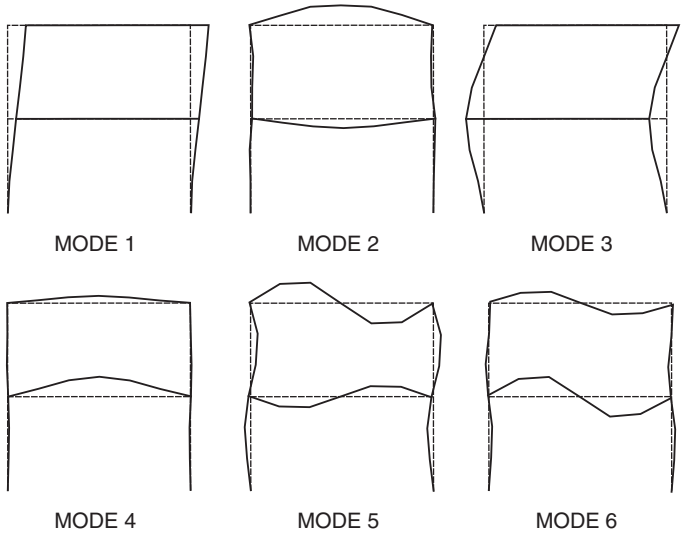

Figure 8.25 MACL frame mode shapes.

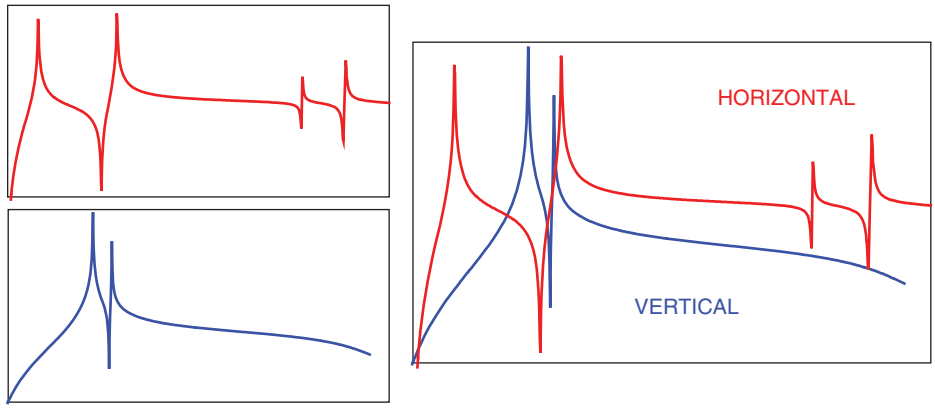

Figure 8.26 Horizontal and vertical drive point measurements, showing the directional nature of the modes.

Figure 8.27 Skewed input excitation to overcome directional shape characteristics.

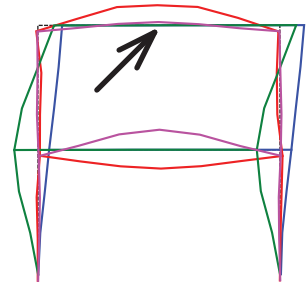

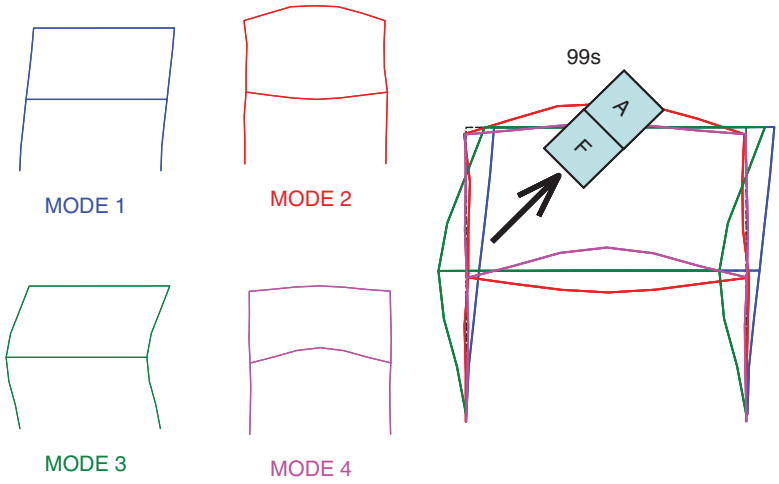

Figure 8.28 Skewed impedance measurement with geometry notation.

The skewed drive point is used as a reference and is used to scale all the other measurements made. This is a very simple and easy way to handle this skewed coordinate issue. Point 99 does not actually need to be included in the geometry and should not be included in the geometry.

8.3.2 Shaker Force Levels and SISO vs MIMO Considerations

There is often consideration of running a modal test with a single shaker with a higher force amplitude to excite the system adequately to make good frequency response measurements. This leads directly into the question of using SISO or MIMO approaches when running an experimental modal test. This section discusses some of the considerations around this issue.

8.3.2.1 High Shaker Force Levels

In modal testing, the intent is to use lower levels of excitation and identify system characteristics; the test is not intended to provide operating level input excitations. In fact, if higher levels are used, nonlinear characteristics of the structure are sometimes excited. The overall measurement becomes distorted and not particularly useful for modal parameter estimation. This is also dependent upon what kind of structure is being testing. If it is a very simple component of a larger system and the component itself is fairly linear, using a single shaker with an appropriate force level specified will not present problems.

But when the structure becomes more complicated (with many components assembled to form a system), then the ability to provide a force excitation to measure all the locations on the structure to identify the mode shapes can become more difficult. This difficulty can then be compounded when the various components are attached with mounting devices; it can be hard to isolate all the components from each other. It becomes difficult to provide an adequate excitation from one shaker location while making adequate frequency response function measurements at all the specified response points. It then becomes necessary to "crank up the signal" to obtain measurable vibration at all the response locations. When this is done, nonlinearities will likely be excited and the overall measurement will be degraded.

A recent test on a large propulsion system had a system intended to isolate all components for vibration transmission purposes. Specific data cannot be shown, but a similar laboratory structure with several components attached through an isolation system illustrates the problem

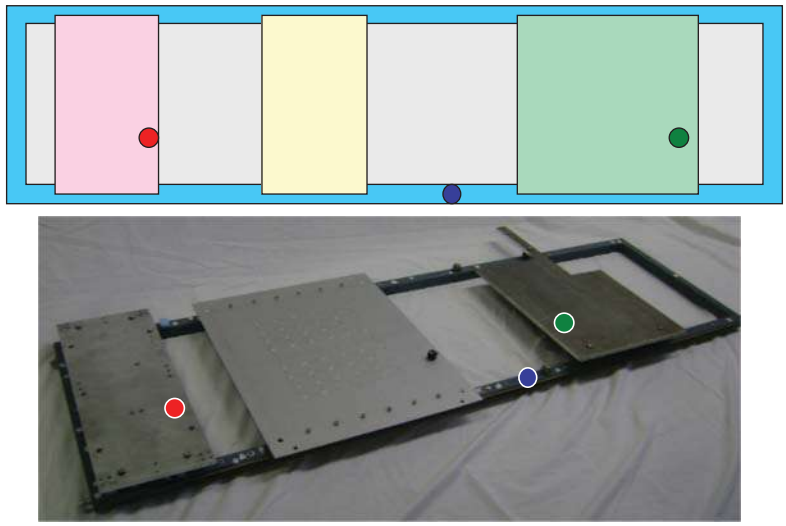

Figure 8.29 Laboratory structure with isolated components.

of using just one shaker to excite the system. The laboratory structure is shown in Figure 8.29. There are three plate components attached with isolators to a larger frame structure.

A single shaker was attached on the main frame and frequency response function measurements were made. In addition, a three shaker MIMO test was also conducted to compare the measurements obtained. Figure 8.30 shows a typical drive point measurement (on the main frame in this case). The frequency response function in red is related to the SISO test.

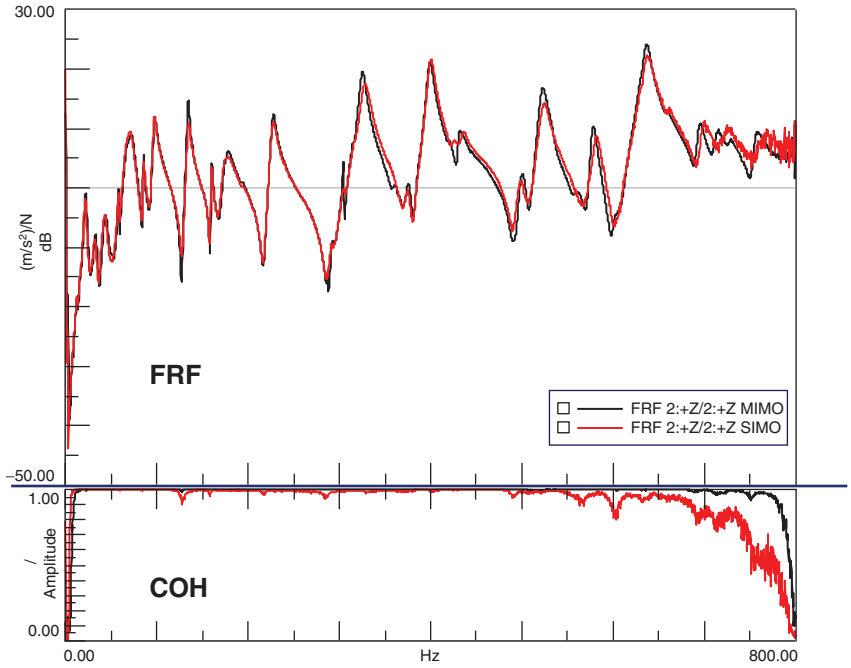

Figure 8.30 SISO vs MIMO FRF drive point measurement.

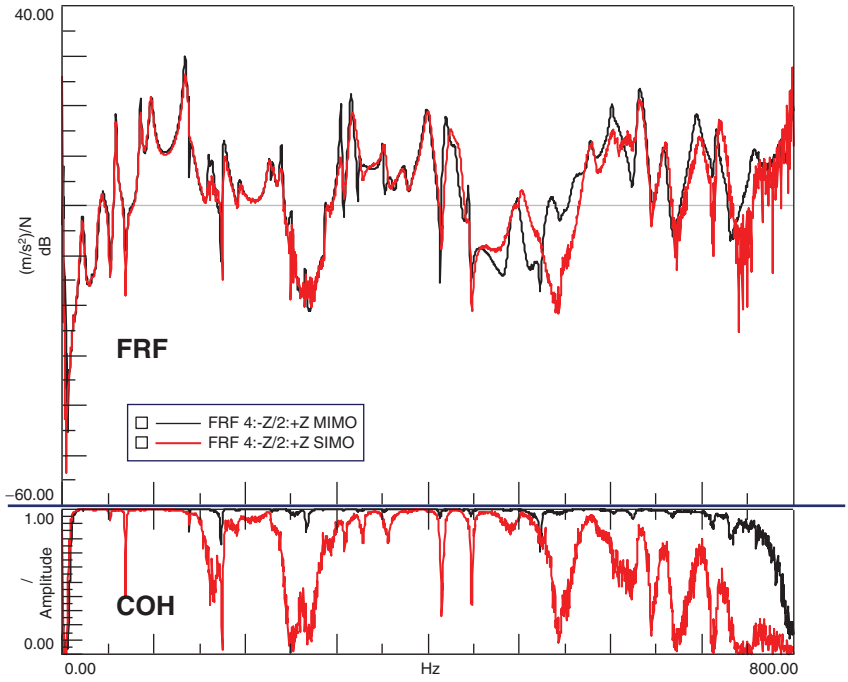

Figure 8.31 SISO vs MIMO FRF cross measurement.

Figure 8.30 also shows the same frequency response function (black) obtained from the three shaker MIMO test, which was conducted with much lower overall excitation.

In looking at the frequency response function, it is clear that the SISO frequency response function obtained is not the same quality as the MIMO frequency response function, which was obtained using lower overall shaker excitation levels. This is especially true when looking at the coherence. A cross measurement of even poorer quality is shown in Figure 8.31. Again, the frequency response function and coherence are seen to be much worse from the SISO test.

8.3.2.2 High Shaker Force Levels

In the previous case, the single shaker input with a high force level clearly showed that the frequency response function was distorted and coherence was poor. Sometimes the multiple reference data is obtained from a single shaker and then the shaker is moved to other locations to obtain the multiple referenced data. This may seem to be a viable solution but there are limitations to this approach. The first problem has already been discussed: the level of force with one shaker will need to be much higher in order to get an adequate response at all the measurement locations in the structure, and this will cause measurement distortions.

A single shaker may work for structures that are uncomplicated. Structures of many components and substructures attached in a manner to minimize the flow of energy through the subsystems can cause difficulties. The situation is very different when the components are isolated from each other. In these situations, it is very hard to get an adequate response throughout the structure with just one excitation source. Multiple references are needed. A comparison of a SISO and a MIMO test setup will be made here.

A laboratory structure is shown in Figure 8.32. This structure had three components mounted to a frame. Each of the components was attached with a very soft mount, an intermediate mount, and a very hard mount. The main frame and the attachments do have some of the

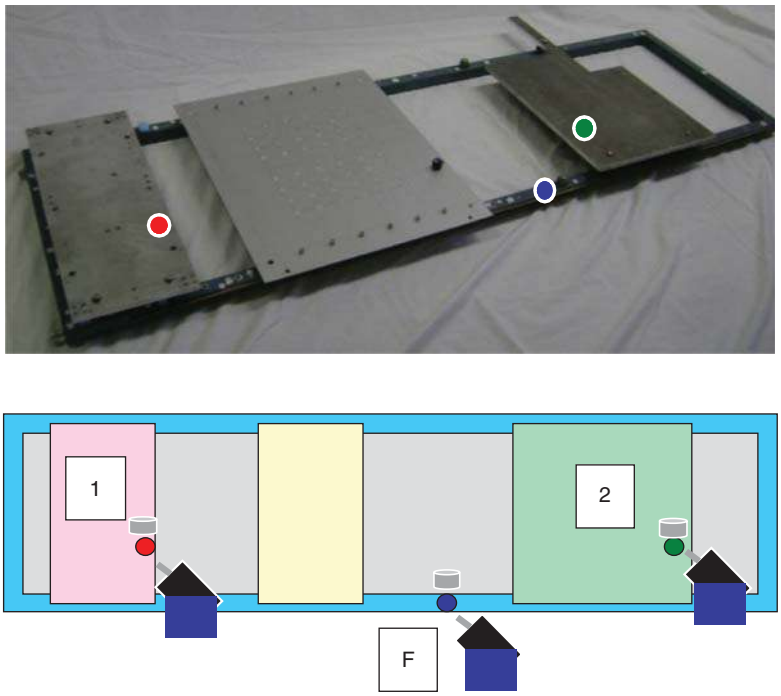

Figure 8.32 Laboratory structure with isolated components.

typical irritating rattles and noise that plague the collection of frequency response function data. No attempt was made to minimize any of these noise sources. They are welcome here, as they illustrate a typical structure measurement.

The structure was tested in many different configurations. Only a few are presented here to show the problem with the frequency response functions collected with single shaker setup and with a multiple shaker setup. The three shaker reference locations are shown in Figure 8.32.

Separate tests were run with each of the individual shakers used to collect frequency response function data from the structure as well as a multiple reference MIMO set of data. In order to make the best possible measurements, the individual SISO shaker tests needed a higher force excitation level to make suitable measurements. The MIMO configuration needed lower force levels in order to make acceptable frequency response function measurements.

In order to evaluate all the measurements, several frequency response functions in the 0–800 Hz range were compared. In all frequency response functions the reference was made to the shaker mounted on the frame. The other references could be used and yielded essentially the same results as those presented next. In Figures 8.33–8.35, the frequency response function in red was obtained from the SISO test and the frequency response function in black was obtained from the MIMO test. Two measurements are shown from the frame to the attached components and one of the measurements was a drive point on the frame itself.

So at first glance, the data in Figures 8.33–8.35 does not look terribly different and many might actually say the data is acceptable. But in looking more closely at some of the reciprocal frequency response functions, it becomes clear that the peaks of the frequency response functions from the SISO tests are inconsistent with the others performed. This causes a discrepancy between the different datasets. A few are shown in Figure 8.36. The reciprocity criterion between the different datasets is not satisfied. This will have a significant effect when modal parameters are extracted (and will be discussed in the next section).

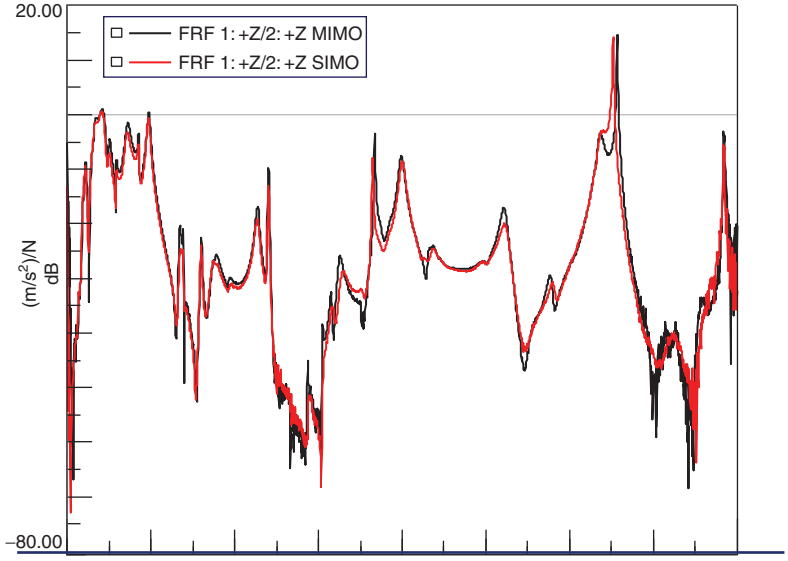

Figure 8.33 FRF component (1) to frame (F) reference.

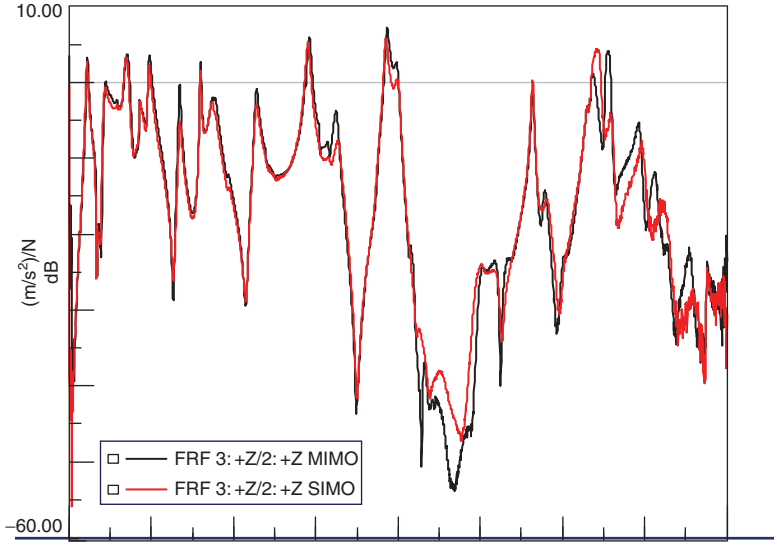

Figure 8.34 FRF component (2) to frame (F) reference.

8.3.2.3 Effects of FRF Measurements in the Modal Parameter Estimation Process

From a purely theoretical standpoint, modal parameters can be extracted from any reference location as long as it is not at the node of a mode. But of course, practicality of the measurements possible on a real structure needs to be evaluated. In the last two sections, several aspects of the measurements were discussed. The frequency response function measurements are always much better overall when the data is collected simultaneously in a MIMO test. If a single shaker is used, two issues arise that tend to provide frequency response functions that are not of the best quality for modal parameter estimation.

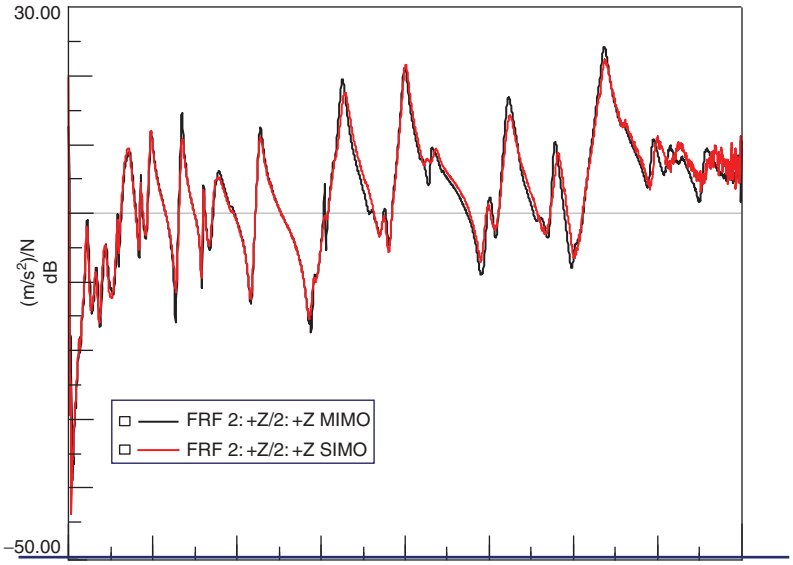

Figure 8.35 FRF frame (F) to frame (F) reference.

In one case, a single shaker needs to have a higher excitation level in order to make adequate measurements, but this invariably causes nonlinearities to be excited and generally tends to increase the variance in the measurement. The frequency response function measurements are not as good as one would like. The second issue is that when multiple referenced data is formed from single reference tests, generally the frequency response functions are likely to be related in an inconsistent fashion. The frequency response function peaks may show some slight variations in frequency. While the structure may be time invariant, the test setup can have an effect on the measured frequency response functions when the tests are obtained from separate tests. Another source of variability is when data is collected at different times. Slight environmental changes can compound this problem.

For the sake of continuity with the two previous test cases, the test data for this discussion will be the same as used previously. Shifting of the frequencies was noted for some modes. The reciprocity criterion was not satisfied for all the SISO data collected and used to form the multiple reference dataset.

The laboratory structure is schematically shown in Figure 8.37. Three reference sets of data were collected using SISO methodology in three separate tests. Data was also collected for all three references simultaneously using a MIMO methodology.

The previous cases discussed some inherent measurement issues. This data will be processed to show the difficulties in identifying modal parameters. In all cases, the stability diagram will be used to show how some of the variance in the data presents challenges in identification of the system poles.

The first challenge is to take all three separate SISO test frequency response functions and form one multiple reference dataset for processing. Note that this is absolutely not MIMO data, because it was collected separately. The first step in the modal parameter estimation process is to identify the system poles. This is usually done using the stability diagram with an overlay of one of the mode indicator functions; for the plots here, the CMIF is used in all cases.

Figure 8.38 shows the stability diagram for this case. While this diagram may be acceptable to many, there is definitely some variation in the system poles and there is not a strong, stable

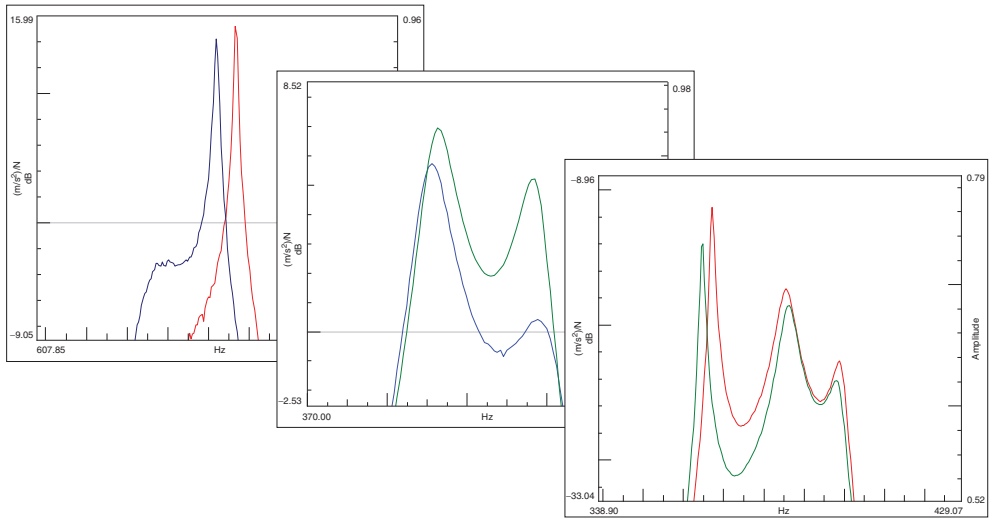

Figure 8.36 Close-up of several FRFs, showing inconsistency.

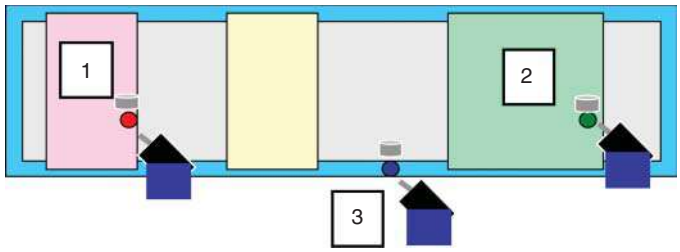

Figure 8.37 Laboratory structure with isolated components.

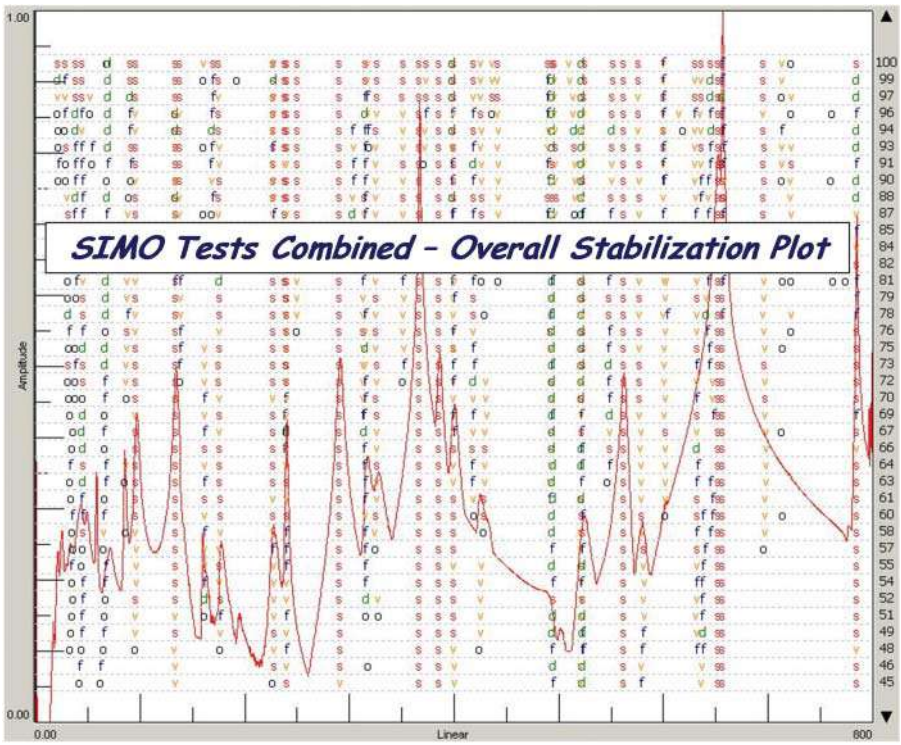

Figure 8.38 Stability diagram for combined SISO FRFs.

pole identified for every one of the system poles. As the data is processed, the improvement in the stability diagram will be seen when considering different subsets of data.

Before the MIMO dataset is evaluated, it is important to look at the individual SISO datasets. Figure 8.39 shows the three separate SISO test datasets processed individually before being combined into one multiple referenced dataset. The stability diagram for each of the separate test cases produces very consistent stable system poles. There is no question what the system poles are with this data; the poles are identified very clearly.

The individual datasets (Figure 8.39) clearly show the system poles but the situation is not as clear (Figure 8.38) when all the datasets are combined. Remember that SISO data was collected consistently for each of the individual SISO tests. Even in the light of some of the noise and nonlinearities that were discussed in the previous two cases, the identification of the system pole is not difficult here. But when all the individual SISO datasets are combined, there is no

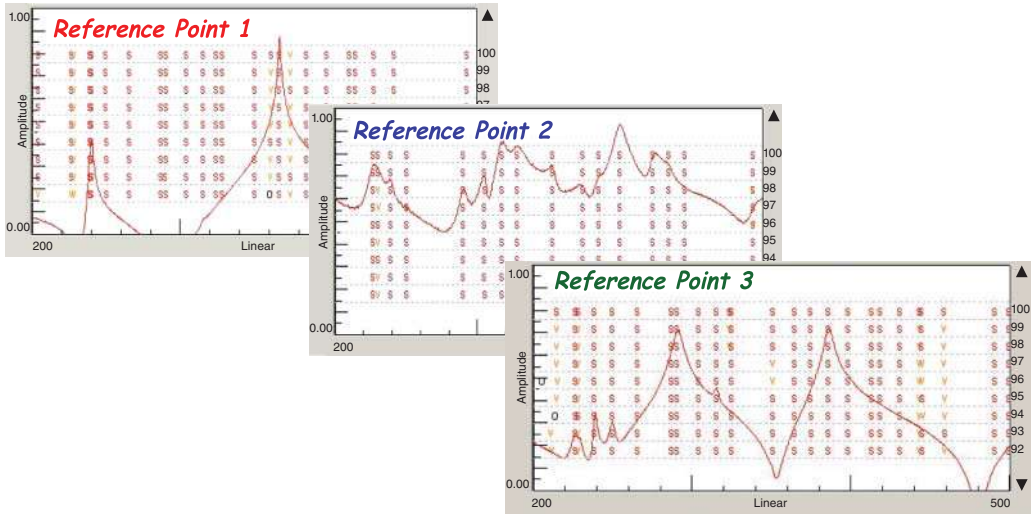

Figure 8.39 Stability diagram for three separate SISO tests.

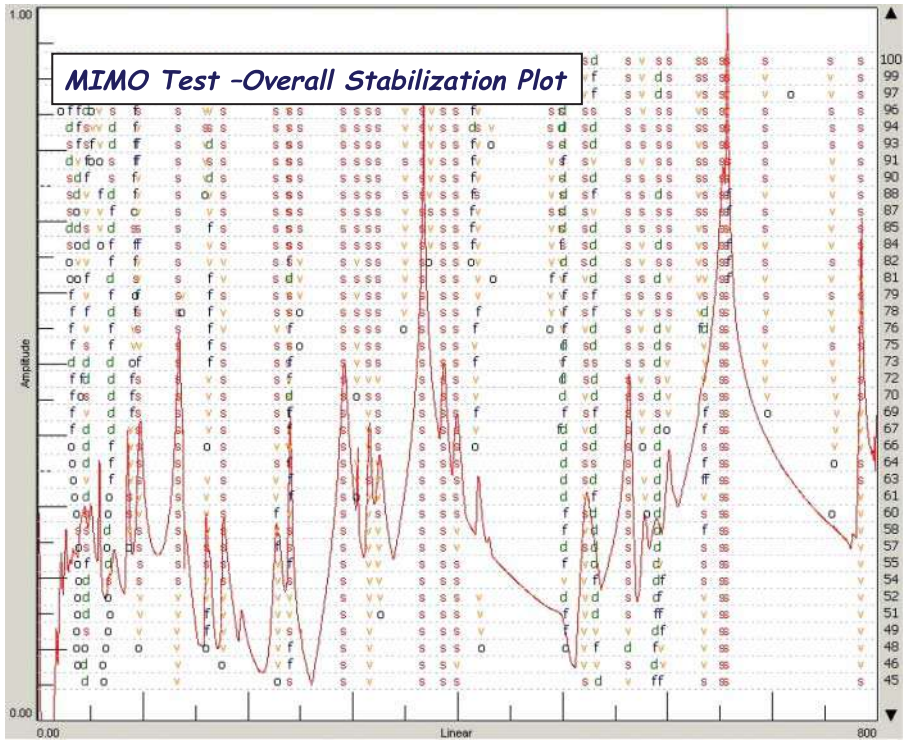

Figure 8.40 Stability diagram for MIMO FRFs.

guarantee that the data will be consistently related between the three different SISO tests that were performed. The shifting of the peak of the frequency response function measurements was pointed out in the previous case. This shifting was noted in several measurements, such as the reciprocal frequency response functions. The main problem is that the data was collected in three separate tests and the data was not guaranteed to be consistently related. This is why the stability diagram in Figure 8.38 becomes more difficult to interpret and the system pole identification is not as straightforward.

To confirm this, the MIMO dataset (where all data is collected simultaneously in a consistent fashion) is used to generate a stability diagram. This is shown in Figure 8.40. This stability diagram is much better than the one shown in Figure 8.38. Some frequencies remain imperfect, but this is much better than the previous scenario. Previously the data was collected separately and the consistency could not be guaranteed.

The real problem here lies with the data. The frequency response functions must be collected in a consistent manner. The SISO test cannot provide data with this consistency, but the MIMO test generally does due to the nature by which data is collected.

8.4 Concluding Remarks

Many different aspects of shaker testing were addressed. Some very basic and practical considerations for the setup of the shaker and stinger were discussed to provide some tips and considerations for this. Some additional attention was given to the stinger and measurement issues that can arise. These were presented with several examples. Both SISO and MIMO were discussed and compared. Some problems that can result during data reduction were also presented, with consideration of the way a modal test might be arranged. All of the examples drive home to the point that the data must be collected in an accurate and, most of all, a consistent fashion, otherwise difficulties will be encountered in the modal extraction process.

9

Insight into Modal Parameter Estimation

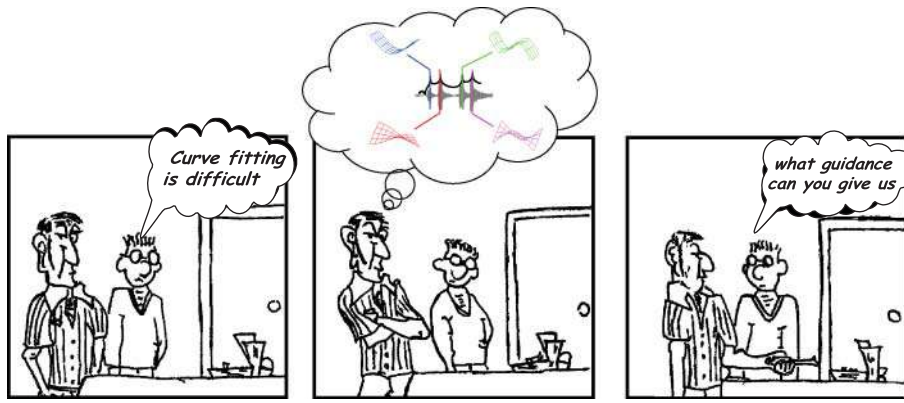

9.1 Introductory Remarks

The task of modal parameter estimation can be complicated, especially when the data collection has been performed haphazardly and without consideration for all the important steps necessary to make good measurements. The process gets very difficult when the measurements have many contaminants that could have been prevented in the data collection phase; care at the measurement phase makes the parameter estimation process much smoother. Of course, there may be measurement difficulties that are difficult to overcome, but time and time again, it has been clearly shown that care and effort spent at the measurement phase always makes the parameter estimation phase easier.

This cannot be over-stressed; the best possible measurements are needed in order to extract the best possible modal parameters from the data. The modal parameter estimation phase cannot fix measurement errors, and poor measurements can cause confusion with the mode indicator tools and in extraction of accurate poles and residues.

People often request help to extract modal parameters from sets of data collected and expect that an "expert" can create miracles with data that is riddled with common measurement issues, such as leakage, windows, poorly excited modes, improper excitation, inappropriate transducer sensitivities, poor dynamic range, and a list of other items that all relate back to bad measurement procedures when the data was collected. People often rush to collect data, likely due to some schedule deadline or administrative need to complete a test by a certain date, and

Modal Testing: A Practitioner's Guide, First Edition. Peter Avitabile.

Companion Website: www.wiley.com/go/avitabile/modal-testing

this forces a collection of data without the care and effort needed to obtain the best measurements possible.

In this chapter, a set of different modal parameter estimation scenarios are described, in order to help highlight some of the difficulties when the data is collected improperly or in an inconsistent fashion or just when overall the data is poor. This will show some of the problems faced when extracting modal parameters. There are also very simple examples that show some of the features that need to be understood when extracting data. There are also examples to help demystify the "urban legends" that have come to be accepted as truth but really have no technical substance whatsoever. Examples are also given to illustrate the differences between local and global curvefitting. In addition, there will be some very frank, candid statements, based on over four decades growing up with this technology and performing a wide variety of tests over the years.

9.2 Mode Indicator Tools Help Identify Modes

Generally, all the mode indicator tools should be investigated. Never use just one of the tools. The SUM, MMIF, and CMIF are all useful and together they help to identify modes. The stability diagram, while really a mode selection tool as part of the modal parameter estimation process, is also a very good indicator of the quality and consistency of the data used for the parameter estimation process. For years, a simple rectangular plexi-plate structure has been used for testing and parameter estimation studies, because its design contained a pseudo repeated root for the first bending and torsion mode. So, generally, when data is evaluated, the first step is to look at all of these tools. This will be done for the plexi-plate structure. Let's talk about each of the most common tools to show their strengths and weaknesses and how to interpret data from each.

Of course, the measured frequency response function (FRF) can be viewed also, but with only one frequency response function it may very difficult to identify how many modes exist. This is a problem because all of the modes may not be active in the particular frequency response function measured. The modes may be directional, and from one measurement all the modes may not be easily observed. This might also be true of the drive point measurement, where all the peaks will have the same phase; two very closely spaced modes may be very difficult to observe. Using a two shaker MIMO test with 15 accelerometer measurements for the plexi-plate structure, the tools used are:

- summation function (SUM)
- multivariate MIF (MMIF)
- complex mode indicator function (CMIF)
- stability diagram.

The first tool discussed is the summation function, SUM. This is a very simple formulation. Basically, it is the sum of all of the frequency response functions measured (or sometimes only a subset of all the frequency response functions is used). The SUM will reach a peak in the region of a mode of the system. The idea is that if all the frequency response functions are considered, all of the modes will be seen in the majority of the measurements. As more and more frequency response functions are included, there is a greater chance that all of the modes will be seen in the collection of frequency response functions summed together. This is obviously better than one particular measurement, in which not all the modes may be present.

A SUM function for all the measured response functions is shown in Figure 9.1. The SUM function will identify modes reasonably well, especially if the modes are well separated. In the

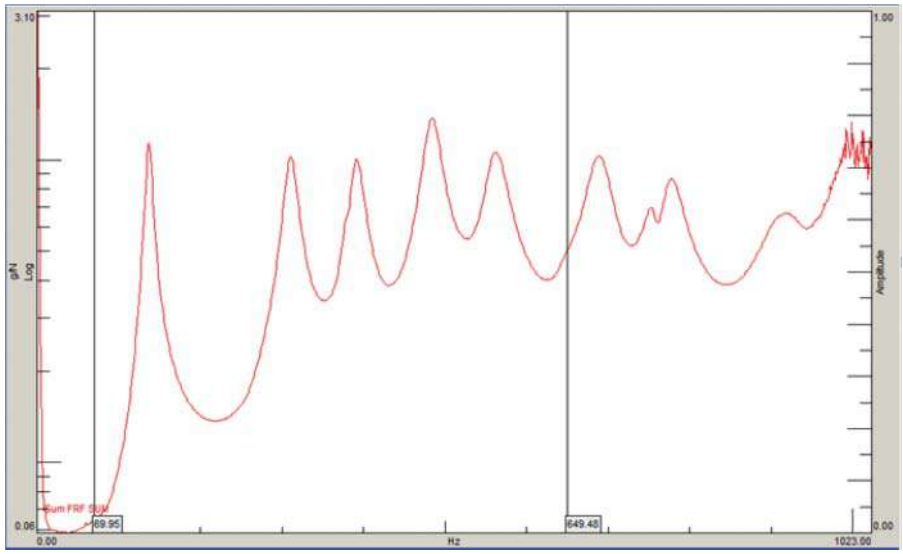

Figure 9.1 SUM for 2 references and 15 accelerometers.

figure, there are five peaks observed in the cursor band, which indicates that there are at least five modes in the frequency band shown. Another important feature of the SUM function is that each of the peaks is generally fairly wide and, if closely spaced modes exist, then this may not show all the modes well.

While the SUM function is useful, it is not always very clear when modes are closely spaced. The original mode indicator function (MIF) was formulated to provide a better tool for identifying closely spaced modes. Basically, the mathematical formulation of the MIF is that the real part of the frequency response function is divided by the magnitude of the frequency response function. Because the real part rapidly passes through zero at resonance, the MIF generally tends to have a much more abrupt change across a mode. The real part of the frequency response function will be zero at resonance and therefore the MIF will drop to a minimum in the region of a mode. An extension of the MIF is the multivariate MIF (MMIF), which is an extended formulation of MIF for multiple referenced frequency response function data. The MMIF follows the same basic description as a single MIF. The big advantage is that multiple referenced data will have multiple MIFs (one for each reference) and can detect repeated roots. This is shown in Figure 9.2 for the same dataset as used in Figure 9.1.

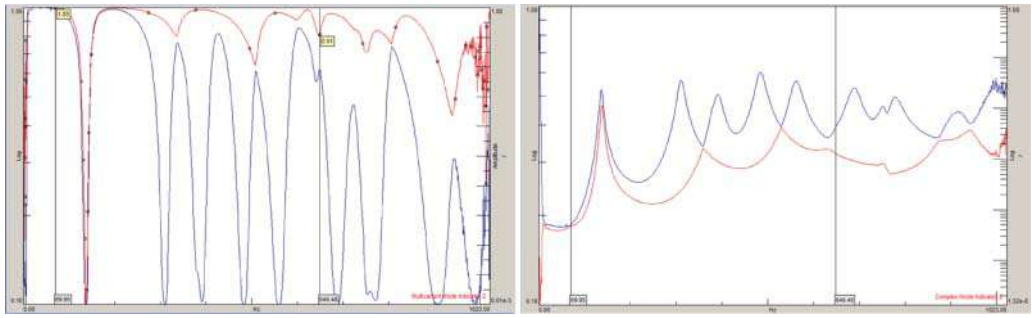

Figure 9.2 MMIF (left) and CMIF (right) for 2 references and 15 accelerometers.

If the first MIF (blue) drops, then there is an indication that there is a pole of the system at that frequency. Every one of the drops in Figure 9.2 for the first MIF (shown in blue) indicates a mode of the system. Notice that there are six dips in the function in the cursor band shown; one more than was observed in the SUM function. Clearly, there is one mode that is closely spaced close to 140 Hz, which was not clearly identified in the SUM function.

Now if the second MIF also drops at the same frequency as the first MIF, then there is an indication that there is a repeated (or pseudo-repeated root). Clearly, the second MIF in Figure 9.2 (shown in red) indicates that there is a repeated root at the first dip in the MIF, close to 100 Hz. Note that the SUM only indicated one mode in this range. However, the other small dips in the second MIF close to 300 Hz and 500 Hz is not an indication of a mode because the second MIF does not dip at the same frequency as the first MIF. In order to have an indication of two roots, both MIFs must dip at the same frequency.

The MMIF is a much more accurate tool for indication of modes. However, the assumption is that real part of the frequency response function is zero at resonance. If the measurements have some distortion or if there is some phase distortion in the measurements (associated with non-real normal or complex modes) then the MMIF may not be able to accurately depict the modes.

The complex mode indicator function (CMIF) is a better tool if this is the case. The CMIF is based on a singular valued decomposition of the frequency response function matrix, which can determine all the principal modes that are observed in the set of measurements. The plot of the singular values also helps to identify poles of the system. The CMIF will peak where maximum values exist, indicating poles of the system. There will be one CMIF curve for each reference. Figure 9.2 also shows the CMIF for this same dataset. Clearly, the two CMIF curves peak close to 100 Hz, indicating that there are two peaks at that frequency. In the 350 Hz and 520 Hz frequency range, there is an indication of peaks in the second CMIF, but these are not an indication of modes because they do not coincide with the peaks in the primary CMIF. The CMIF function provides some additional insight into the number of poles in the frequency band of interest.

All of the tools assist in the selection of poles during the extraction process. The last tool is the stability diagram, SD. The basic philosophy is that poles that are extracted from an increasing order mathematical model will repeat or be consistent as the order is increased if the pole is a global characteristic of the system. Other indications of roots will not maintain a consistent indication as the order of the model is increased. A plot of these characteristics when a pole migrates to a stable configuration provides yet additional insight into the poles of the system. Figure 9.3 shows a stability diagram over a narrower frequency range than previously shown. Notice that there is an indication of a repeated root near 100 Hz and another pair of roots close to 300 Hz.

Now the pair of roots close to 300 Hz was not completely observed at first glance. But looking back at the MMIF and the CMIF, the peak in the 300 Hz region seemed asymmetric and to the left of the peak an additional mode could be possible. So the stability diagram helped to further clarify the poles of the system. Clearly, all the tools are needed in order to identify all the important modes of the system.

9.3 SDOF vs MDOF for a Simple System

In order to help guide the novice, a simple two degree of freedom model with known mass, damping and stiffness matrices is used to determine the poles and residues as well as the partial fraction form of the frequency response function in the appendix. Because the model is

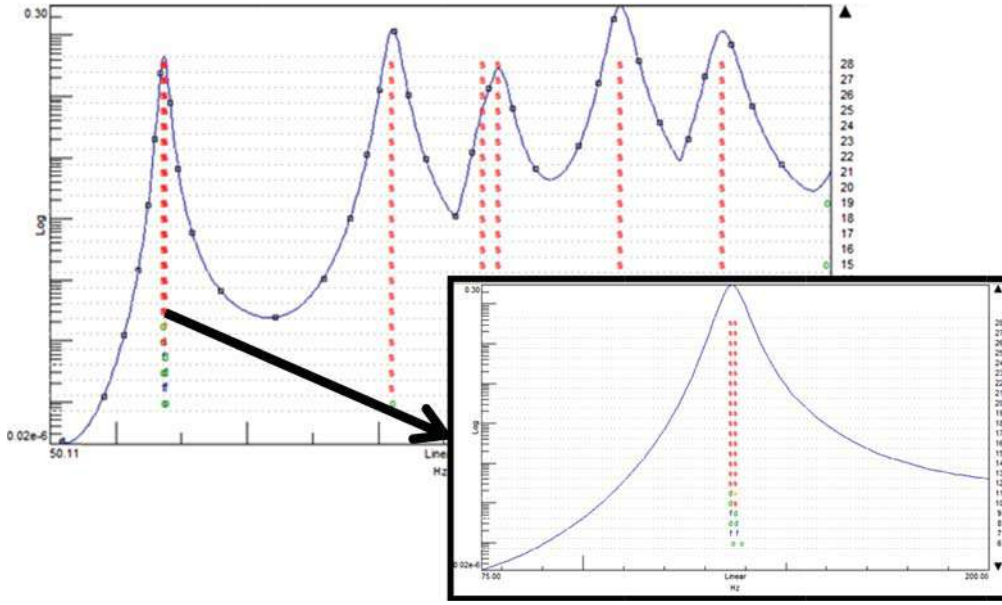

Figure 9.3 Stability diagram for FRF data.

analytically derived, the frequency response functions are not affected with any noise or other contaminants. Here these measurements will be used in a commercial software package to extract the poles and residues (which are actually known) for comparison to the analytical model used to generate the functions. A simple single degree of freedom model and a multiple degree of freedom model are both used with a local curvefitting approach. The main idea here is to just show some differences, even with a simple two degree of freedom system with well-spaced and lightly damped modes. The model is described in the appendices.

Table 9.1 shows the results of modal parameter estimation using a local curvefitting approach with the rational fraction polynomial and using a single degree of freedom approximation for each mode separately. The frequency is estimated fairly well, but the damping and the residue are not as accurate; this is most likely the result of modal overlap, even though the two modes appear to be fairly well separated. Table 9.2 also uses a local curvefitting approach with the rational fraction polynomial, but uses a multiple degree of freedom approximation and fits the

Table 9.1 Modal parameter comparison for SDOF polynomial curve-fit.

H11	Mode 1			Mode 2		
	Analytical	SDOF Poly	% Diff.	Analytical	SDOF Poly	% Diff.
Freq. [Hz]	92.16	92.06	0.11%	125.40	125.37	0.02%
Damp. [% Crit.]	8.60%	8.30%	3.49%	6.33%	7.39%	16.75%
Residue	0.00059	0.00055	6.18%	0.00020	0.00026	28.65%
H21	**Mode 1**			**Mode 2**		
	Analytical	**SDOF Poly**	**% Diff.**	**Analytical**	**SDOF Poly**	**% Diff.**
Freq. [Hz]	92.16	92.29	0.14%	125.40	125.13	0.22%
Damp. [% Crit.]	8.60%	9.48%	10.23%	6.33%	5.97%	5.69%
Residue	0.00040	0.00049	21.62%	0.00030	0.00027	7.10%

Table 9.2 Modal parameter comparison for MDOF polynomial curve-fit.

H11	Mode 1			Mode 2		
	Analytical	MDOF Poly	% Diff.	Analytical	MDOF Poly	% Diff.
Freq. [Hz]	92.16	92.16	0.00%	125.40	125.41	0.01%
Damp. [% Crit.]	8.60%	8.60%	0.00%	6.33%	6.33%	0.00%
Residue	0.00059	0.00059	0.67%	0.00020	0.00020	0.52%
H21	**Mode 1**			**Mode 2**		
	Analytical	**MDOF Poly**	**% Diff.**	**Analytical**	**MDOF Poly**	**% Diff.**
Freq. [Hz]	92.16	92.16	0.00%	125.40	125.41	0.01%
Damp. [% Crit.]	8.60%	8.60%	0.00%	6.33%	6.33%	0.00%
Residue	0.00040	0.00040	0.71%	0.00030	0.00030	0.51%

two modes together. The frequency and damping are estimated very accurately, but there is a slight error in the residues computed.

9.4 Local vs Global: MACL Frame

In the early days of modal testing, only local curvefitting was possible. This was mainly due to the very limited computational capabilities available. But as the field matured and developed, there was a trend to curvefit with a two step process, in which the poles are estimated first to find the best poles to represent the system. Those poles are then used in the second pass to find the residues. Generally, the resulting mode shapes were represented much better overall, especially in the depiction of nodes of modes and local modes (where a portion of the structure was very active but the balance of the structure was very inactive). These areas that were inactive had very small responses, and when performing a local curvefit, the pole would often be estimated poorly. This then had a direct effect on the residue extracted. The global curvefitting approaches tended to give a much better representation of node points and structures when some regions of the structure were more active than others. The reason is that the pole, according to modal theory, is supposed to be one value and not be different from one measurement point to the next. But of course this then demands that the measurements need to also have that same global characteristic when measurements are made. At times, the measurement setup, procedure, or process can violate this need to obtain consistent data and this then creates an inconsistency with the theory invoked. But the benefits far outweigh the problems. So these global techniques have become standard in just about all modal parameter estimation approaches.

In order to understand this idea better, a simple planar frame structure (which has very clear node points) is used to show the difference between the local and global curvefitting approaches. The structure's first six modes are shown in Figure 9.4, along with a typical measurement showing the modes. For this structure a simple single degree of freedom fit for each of the modes is sufficient to extract the modes; a local curvefit is used.

Figure 9.5 shows three of the modes that had very distorted mode shapes due to local curvefitting. Notice that the points are located where there should be node points on the structure. The data was refit with a local multiple degree of freedom curvefit, with the same results. However, once the global curvefitting approach is used, this problem does not occur. And to be sure that this is not related to measurement noise, the data used was synthesized from a finite element model to ensure that the local curvefitting technique is the culprit in this distortion.

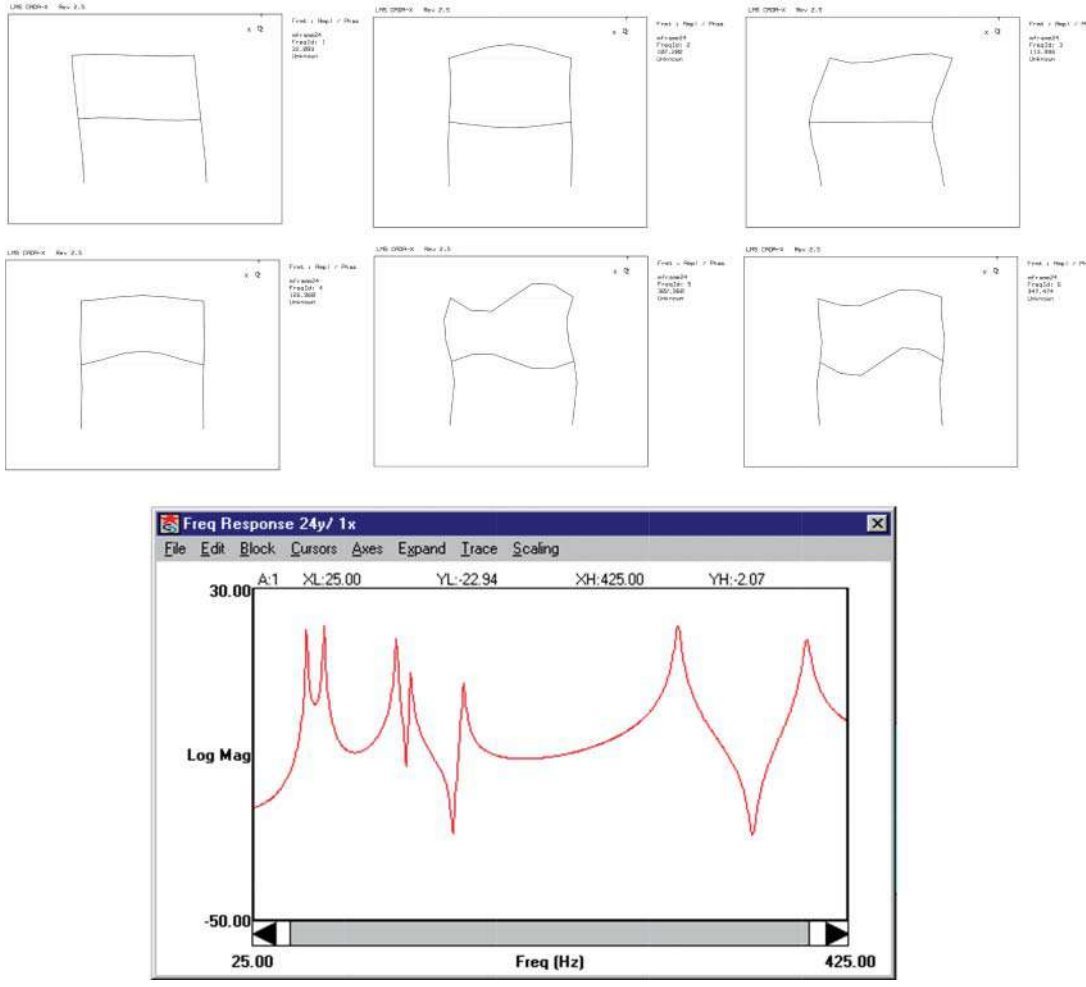

Figure 9.4 First six planar modes of MACL frame with a typical FRF measurement.

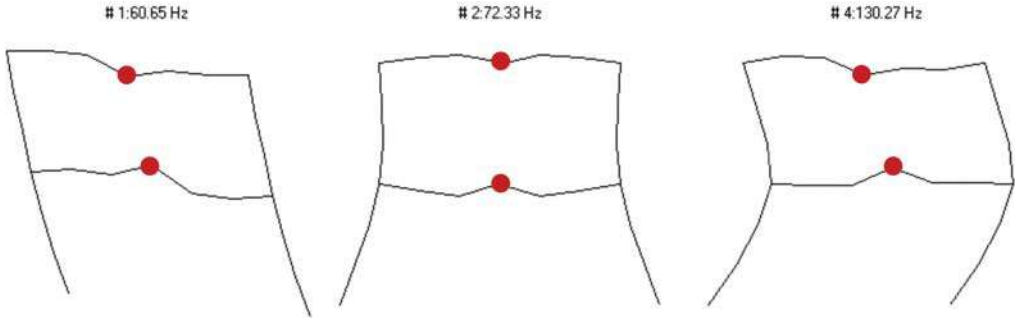

Figure 9.5 Three modes with distortion due to local curvefitting.

9.5 Repeated Root: Composite Spar

Repeated roots are not often observed in test data, but they do certainly exist and can be difficult to deal with when attempting to extract parameters. If repeated roots occur, then multiple reference measurements are needed to extract the repeated root. While truly mathematically repeated roots are not often seen, pseudo-repeated roots are often seen in test data. These are not mathematically repeated but occur in close proximity to each other, so they are often referred to as "repeated". Many have then extended the need for multiple references when the roots are pseudo-repeated. While multiple referenced data is always welcome, there may not be a critical need to use MIMO data for pseudo-repeated roots. This example will show such a case of a pseudo-repeated root; the modes will be extracted with a single reference. More importantly, the pseudo-repeated root will be extracted with an assumption that there is only one mode in the band, so as to clearly show what happens when poor decisions are made in the modal parameter estimation process. The structure is a composite beam, which is a spar for some structure of unknown origin. The composite spar is shown in Figure 9.6, along with the modal test geometry for reference on the left of the figure. The spar looks like an I-beam, with one flange that is a traditional T-section and with the other flange as an L-section; the entire spar has a taper along the long length of the spar and there is no symmetry in the geometry. Impact measurements were made for approximately 100 points with one reference transducer. In reviewing all the measurements, there appeared to be single modes at all the peaks of the summation function. As a first cut, only one mode was selected, at the second major peak in the summation. Modal parameters were extracted and the mode extracted seemed very reasonable

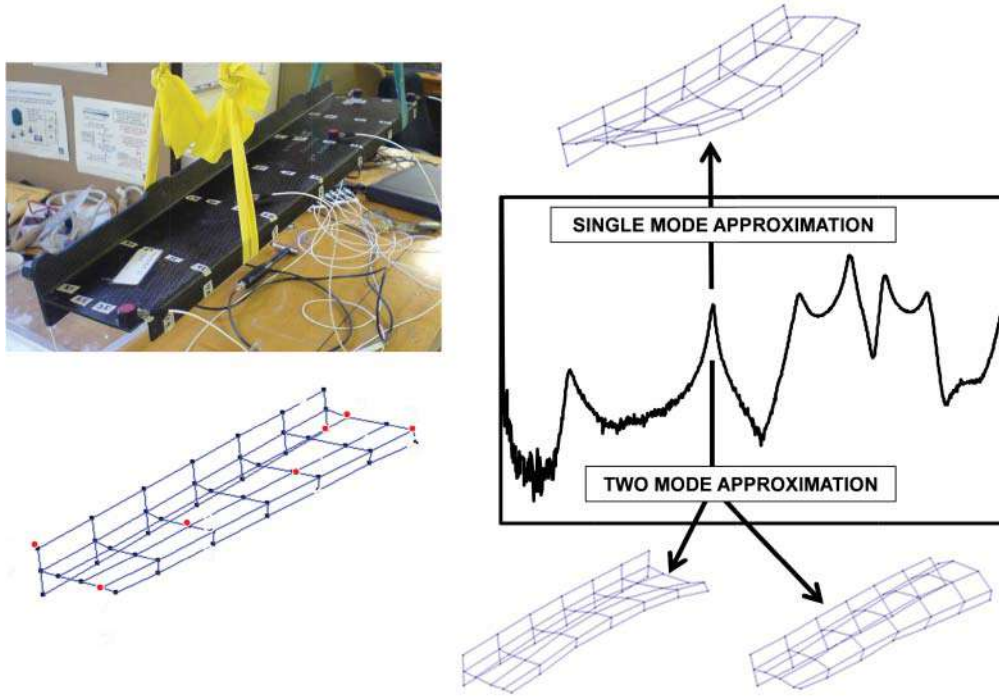

Figure 9.6 Composite spar structure and test geometry (left), summation function with single mode approximation (top), and two mode approximation (bottom).

and there was no reason to suspect any repeatedness. The mode shape is shown above the summation function in Figure 9.6.

There was no finite element model, so there was no other information available to question the shape extracted; the mode appeared very believable. But there appeared to be some measurements (less than five total measurements) that were cross-directional measurements in the x- and y- directions that seemed to indicate there might be an additional mode. While the measurements appeared noisy and were not strong, a second pass on the data revealed two modes at the second peak in the summation function. The two modes extracted are shown at the bottom of the summation function in Figure 9.6. One mode is a bending mode along the long axis of the flange, and the other mode is a bending mode along the short axis of the flange. The frequencies were within 2 Hz of each other and due to the damping in the structure along with the closeness of the modes relative to the frequency resolution of the FFT analysis, the two modes were difficult to identify from the data collected. But modal parameter estimation (rational fraction polynomial) was easily able to identify the two modes that were in the measured data.

This particular structure has since been tested many times with many references and, time and time again, the data has been able to extract multiple modes. And the mode indicator tools have clearly identified that multiple modes exist when multiple references are utilized. Now the important inference to draw from all this is that the original single reference data was more than sufficient to extract the pseudo-repeated root. Many will insist that multiple reference data is absolutely required to extract a pseudo-repeated root but this study clearly shows that only the single reference methodology is needed to extract this pseudo-repeated root. Of course, multiple reference data is always preferred, but this case shows that it is not actually required as long as the analyst recognizes that multiple roots exist at essentially the same frequency.

9.6 Wind Turbine Blade: Same Geometry but Very Different Modes

The composite spar example above demonstrates the need to understand what the basic mode shapes of the structure might be. Without that knowledge, assumptions as to the mode shapes can be incorrect and may lead the test down a path that produces incorrect results. The geometry of the structure led the analyst to believe the first single mode extracted. To extend on this case, there were two recent tests of large turbine blades. The customer had requested a test on a large turbine blade and the results produced the typical expected cantilevered bending modes. The modes were organized in the typical arrangement: first bending in the flap direction, first bending in the edge direction, second bending in the flap direction, second bending in the edge direction, and so on. Note that flap and edge modes are the terminology used for the turbine industry but these are essentially cantilevered beam bending modes in the two perpendicular directions.

A year or two later, the customer requested a second modal test on a different blade that had the same exact dimensions and geometry (at least from the viewpoint of an outsider looking at the exterior of the blade). The modal test group gave no second thoughts to the fact that it was essentially the same turbine blade as had previously been tested. But when the test was completed and the data reduced, several modes were dramatically different, and two modes were very closely spaced, which was not what had been seen in the earlier tests.

Now of course multiple references were used and the modes were all extracted properly for both tests. However, the second test had two very closely spaced modes, which were not the traditional flap and edge modes seen in the first test. A MAC comparison is shown in Figure 9.7, along with the summation function for the two blades; clearly there are two closely spaced modes in the second configuration and the mode shapes are different to the first test. If the tests

MAC		BLADE B						
		1	2	3	4	5	6	7
BLADE A	1	98.71	1.45	34.70	5.64	4.82	2.93	0.10
	2	0.18	99.01	0.03	21.04	17.28	0.57	10.81
	3	24.68	0.49	98.95	15.25	15.66	10.30	0.33
	4	0.04	27.98	0.04	59.38	41.68	1.44	33.82
	5	9.06	0.03	34.68	39.30	58.02	24.81	2.04
	6	3.17	0.73	13.49	24.75	11.30	98.44	0.00
	7	0.44	8.54	1.18	8.28	27.46	1.01	98.91

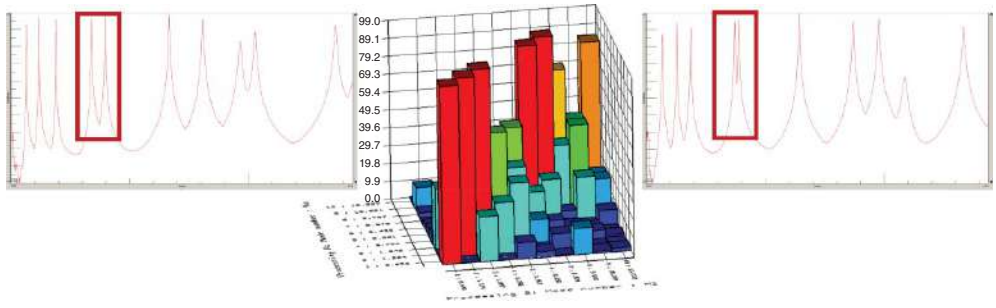

Figure 9.7 Comparison of two large turbine blades.

were assumed to have the same results and if only one reference was used to save some time and expense in running the test, then there could easily have been some difficulties with the data, especially if the designers changed the blade and the roots became pseudo-repeated. The point here is that while a structure may look the same as another structure from an exterior viewpoint, care must be exercised on every test performed because system properties or characteristics might be altered and this can have a significant effect on the modes of the system overall. Never become complacent when performing tests because there are many things that can easily make a test become a disaster.

9.7 Stability Diagram Demystified

The parameter estimation process is a very important part of the extraction of a model (poles and residues). Usually this is broken down into two parts: the extraction of the poles in the first step and then the estimation of the residues in the second step. The stability diagram is a tool that is used in the process of the extraction of the pole from the data. Let's discuss the estimation of poles and the use of the stability diagram. A few simple examples are included here to emphasize the critical issues in the estimation process.

Let's assume that a set of data as shown in Figure 9.8 exists. As a starting point, a third order fit will be assumed to describe the phenomena well. In general, the fit is reasonable, as evidenced by the R^2 coefficient, which is large. But when the variance tolerance is included (dotted lines), there is a fair amount of variation possible. One point is clearly seen as an outlier to the fit of the data. If this outlier point is removed from the dataset, as seen in Figure 9.9, then the R^2 coefficient increases. So, from the set of data shown here, it becomes very clear that the data quality is very important to the extraction of a valid set of parameters. It is of paramount importance to have good quality data for the estimation process.

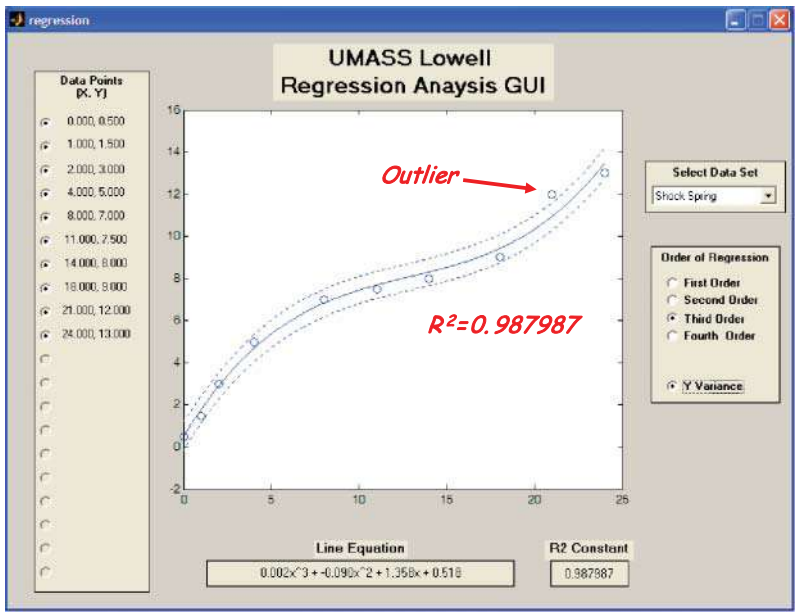

Figure 9.8 Fit of data with obvious outlier.

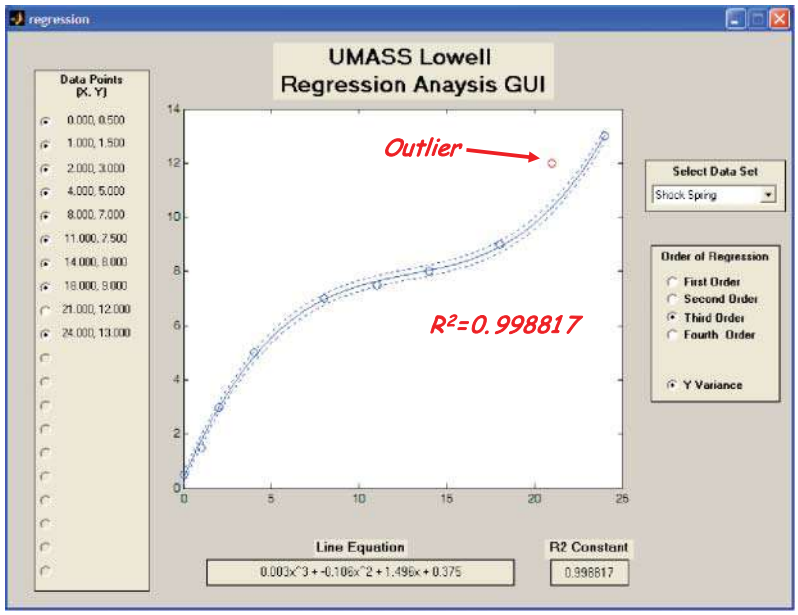

Figure 9.9 Fit of data with outlier removed.

From this simple example, it is clear that good data is important. Now consider the dataset shown in Figure 9.10. This is a very simple set of data that appears to have a very simple first order characteristic. Let's study the estimated parameters as the order of the model is increased.

The plots in Figure 9.11 show the progression of the estimation of the slope as the order of the model is increased from first order to fourth order. In Figure 9.11a, the first order fit produces

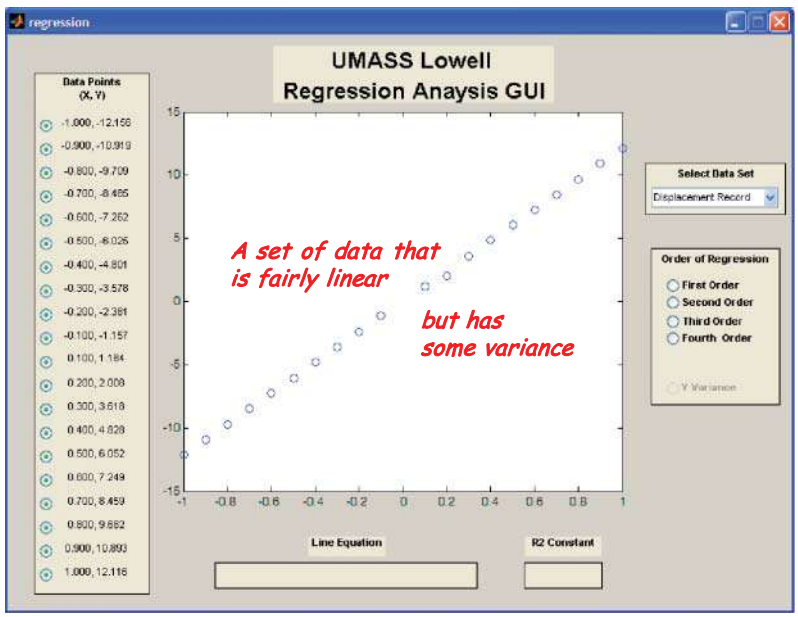

Figure 9.10 Set of fairly linear data.

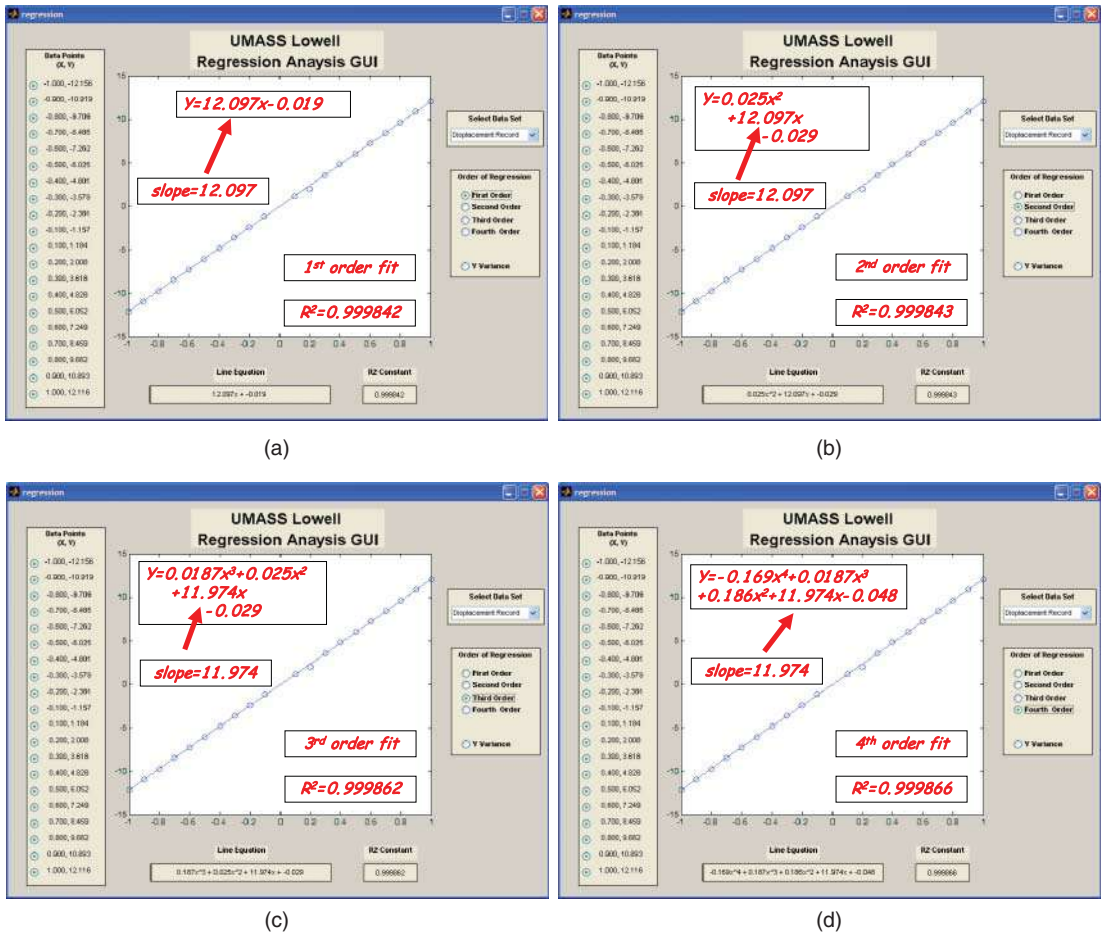

Figure 9.11 Estimates of the slope for: (a) first order; (b) second order; (c) third order; (d) fourth order fit of data.

a slope of 12.097, with a very good R^2 value. As the order of the model is increased to second order in Figure 9.11b, the slope is still 12.097, with a good R^2 value. So increasing the order of the model to second order has not produced a change in the estimate of the slope. Of course, the higher order terms are basically making adjustments to account for the variance on the measured data.

As the order of the model is increased to third order in Figure 9.11c, the slope is 11.974, which is very close to the slope previously computed from the first order and second order models. In fact, the slope is only 1% different. So an argument can be made that the slope is basically the same and has not changed significantly from the previous estimates. And as the order model is further increased to a fourth order model in Figure 9.11d, the slope is again estimated to be 11.974, which is unchanged.

So after this process is complete, the general consensus would be that the parameter of the slope of the data is approximately 12.0 and that very little change occurs as the order of the model is increased. Also, note that it doesn't matter which order model is used because, to within the tolerance of 1%, all orders produce essentially the same slope!

This simple example provides an understanding of exactly what goes on behind the scenes in the development of the stability diagram. As the order of the model is increased, there will

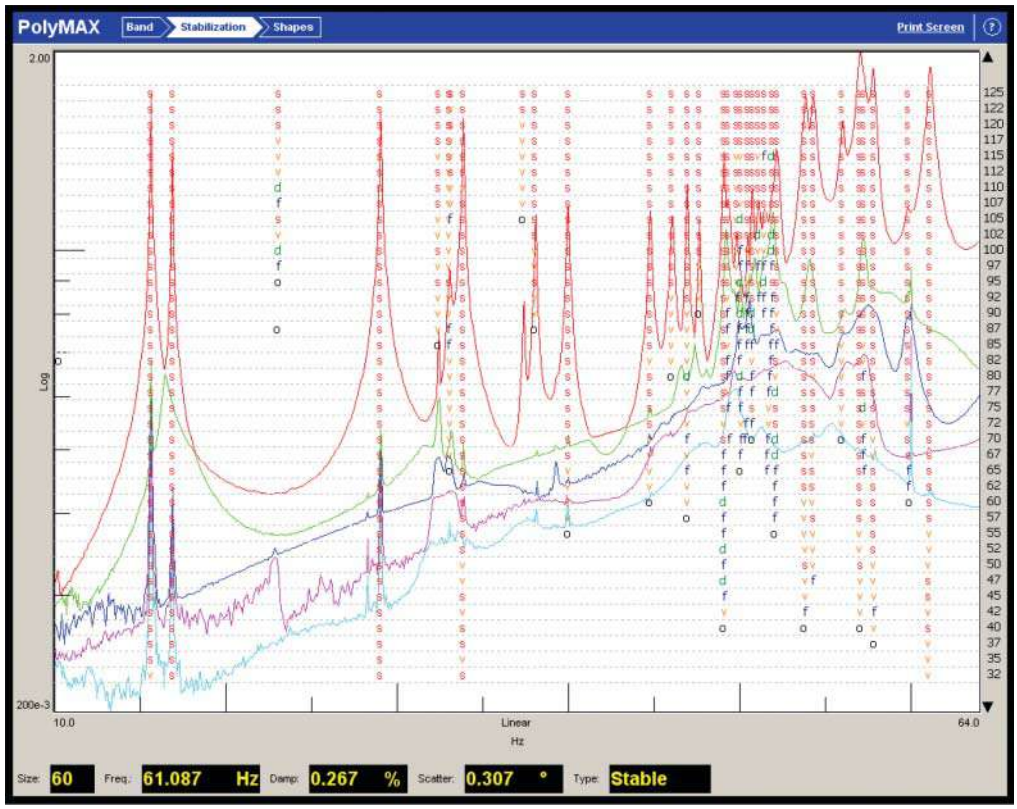

Figure 9.12 Typical stabilization diagram.

be estimates of poles. If the pole estimated only changes very slightly from one order of model to the next, then the software will provide a flag (or indicator) to help demonstrate if the pole has reached some "stable value" within some specified tolerance; these tolerances might be set to 1% on frequency and 5% on damping to identify pole stabilization. There are usually some indicators that will be provided and superimposed on a SUM, MMIF, or CMIF plot. A typical stability plot is shown in Figure 9.12. The stability diagram helps to identify which poles are "consistent" or stable as the order of the model is increased. The "s" indicator clearly shows the location of the poles.

9.8 Curvefitting Demystified

Curvefitting might look like black magic at first, but let's make a few simple analogies to help demonstrate that it is really fairly straightforward. The example below is very simple indeed. Some information was discussed regarding the system transfer function and the frequency response function in the theory. The system transfer function was written in partial fraction form for a single degree of freedom system as

$$h(s) = \frac{a_1}{(s - p_1)} + \frac{a_1^*}{(s - p_1^*)}$$

and the frequency response equation was written as

$$h(j\omega) = h(s)|_{s=j\omega} = \frac{a_1}{(j\omega - p_1)} + \frac{a_1^*}{(j\omega - p_1^*)}$$

Now these two equations show that the independent variable is "s" in the first equation and in the second equation it is "ω" and that the value of "h" depends on these values. Also, notice that there are two constants, or parameters: the residue "a" and the pole "p". So these are the parameters that define "h" given some value "ω"; these are called modal parameters.

Now look at the system transfer function or a piece of the system transfer function called the frequency response function. The only thing to realize is that the surface of the system transfer function and the curve of the frequency response function are defined by only two parameters for the single degree of freedom system, namely the pole "p" and residue "a". So, looking at Figure 9.13, realize that only two parameters define that surface and line, which is pretty amazing.

Now let's take a step back to something a little simpler and more commonly understood. Let's look at a very simple straight line fit of some measured data. Let's perform a least squares error minimization for the data presented in Figure 9.14. Now any line can be fit to the data, but for this set of data it seems that a first order fit makes the most sense. Of course, the model to use is $y = mx + b$ and there are two parameters that define the line, namely the slope and y-intercept.

So, for instance, in Figure 9.14, the resulting least squares fit of the data resulted in two parameters with a slope of 12.097 and a y-intercept of −0.019. Also, realize that this data was obtained

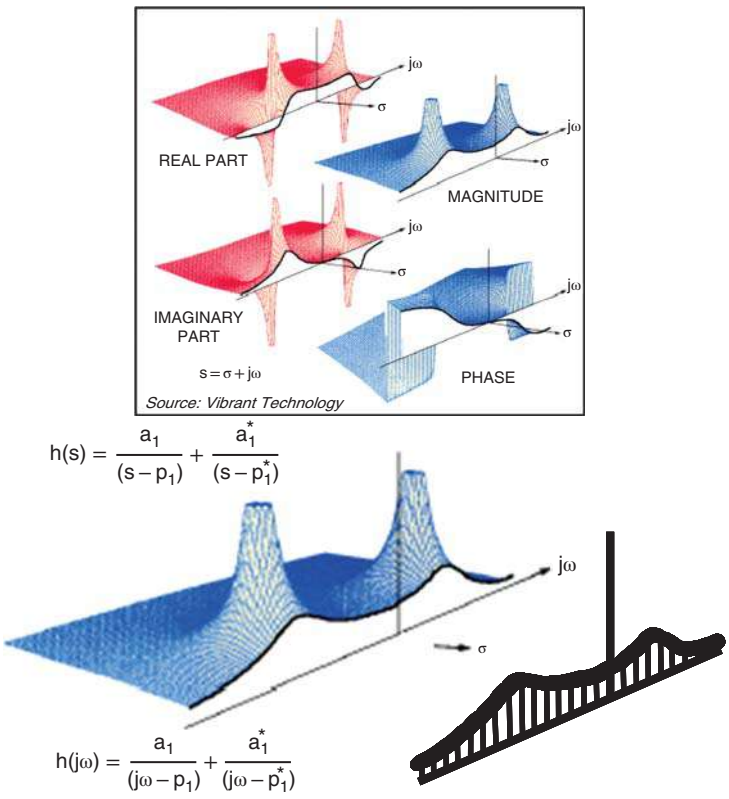

Figure 9.13 System transfer function and FRF. *Source*: Image courtesy Vibrant Technology, Inc.

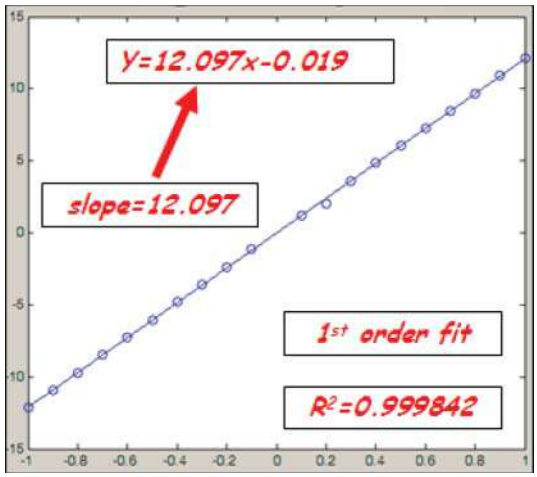

Figure 9.14 Example of simple straight line fit.

from a set of measured data that had some variance and that the least squares regression analysis identified the best parameters to represent this data with these two parameters of slope and y-intercept.

So, if this same logic is applied to a single degree of freedom frequency response function then a fit of a second order model of the form of a frequency response function (as written above) to the data presented in Figure 9.15 can be performed. And looking at this schematic, it is very easy to see that there is a set of data and curvefit from which two parameters are obtained, namely the pole and residue. It is really the same as the straight line fit except that the data is complex and the line is a little more complicated. But in principle, it is the same methodology. The frequency response function measured is at discrete data points (with complex data). A line is fit to the frequency response function to find the parameters that best describe the data in a least squares fashion.

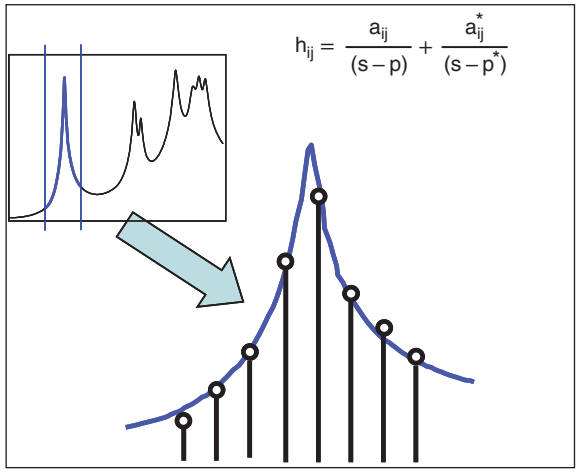

Figure 9.15 Conceptual SDOF curvefit.

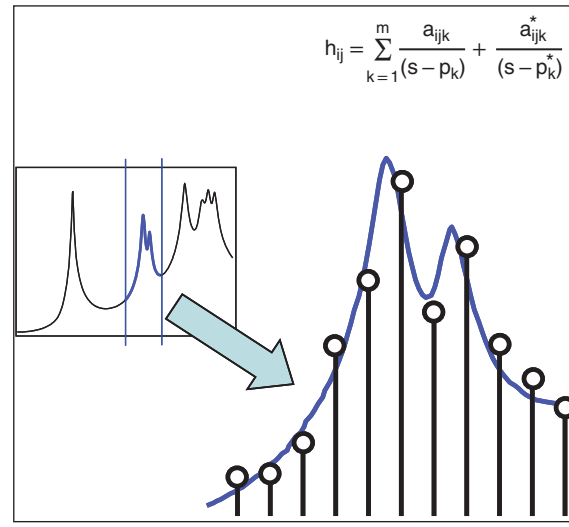

Figure 9.16 Conceptual MDOF curvefit.

Now of course the data in Figure 9.15 is for a single degree of freedom system. This same approach can be extended to a higher order function, as shown in Figure 9.16. So, in this way, multiple modes (or essentially a higher order polynomial) can be fit to the data described by the discrete complex data measured from the frequency response function. And all the same arguments relating to the estimation of modal parameters can be made again here with the data in Figure 9.16.

So, accepting the procedure that is always performed for the simple straight line, the same procedure can be applied to the modal parameter estimation process (but of course the data is complex and the line is slightly more complicated). Essentially, in both cases, parameters that describe the function are extracted in a least squares fashion.

So there really isn't any black magic at all to the curvefitting process. It is really the same process that we all perform with simpler straight line regression analyses. Modal parameter estimation is just an extension of simpler curvefitting of data.

9.9 Curvefitting Different Bands for the Poles and Residues

Generally, when performing modal parameter estimation, small bands with few modes are generally desirable. But the curvefitting process is a two stage procedure and there are two different ways that the poles and residues can be extracted. In one approach, the poles can be extracted in separate smaller bands and the residues are also extracted in each of those same bands, defined as shown in Figure 9.17. However, in the second stage of the process to get the residues, at times, people will use one larger band that encompasses all the smaller bands, as shown in Figure 9.18. The real thing to be concerned about is whether or not the synthesized frequency response function compares to the actual measured data or not. Both approaches are acceptable providing the synthesized frequency response compares well to the measured function.

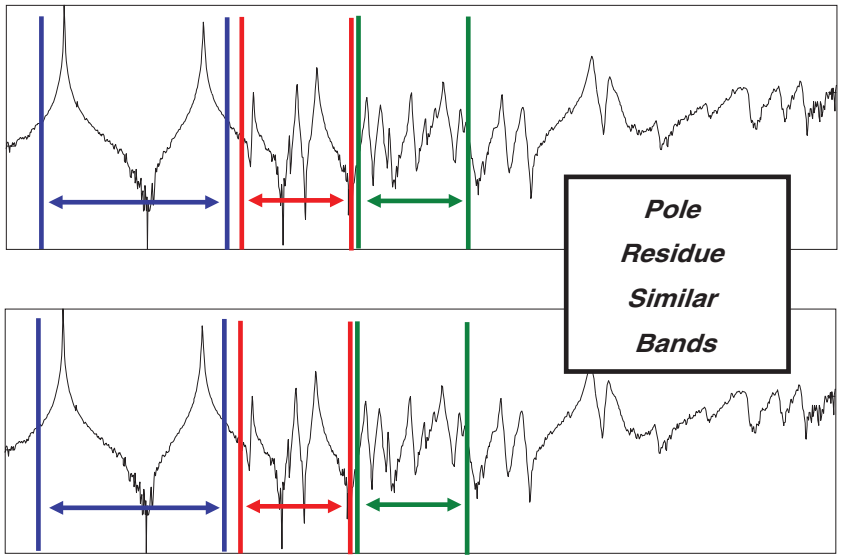

Figure 9.17 Similar bands used for curvefitting for poles and residues.

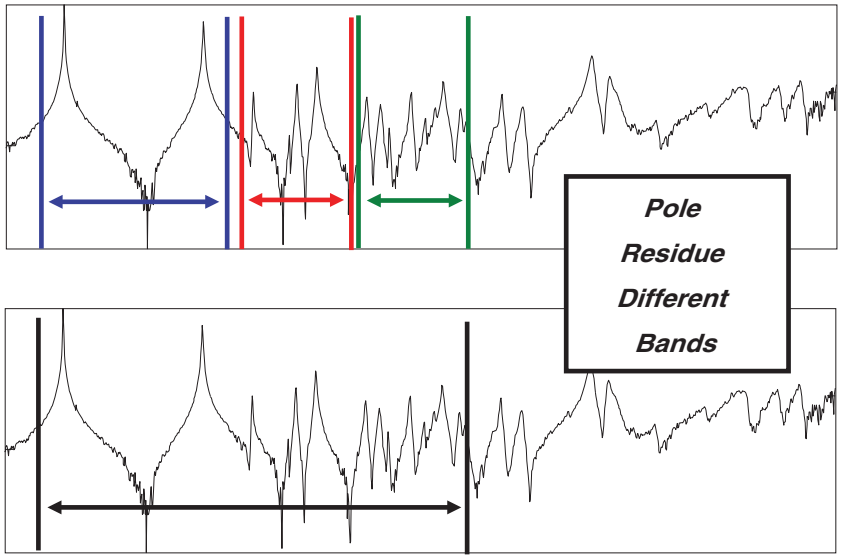

Figure 9.18 One all encompassing band used for curvefitting for residues.

9.10 Synthesizing the FRF from Parameters from Several Bands Stitched Together

Of course once all the data is processed, the frequency response function should be re-created or "synthesized" from the extracted poles and residues and compared to the original data to ensure that a good fit of the data was obtained. Now if all the modes (poles and residues) are fit in one band, this is a very straightforward process. But if smaller bands are used, then the data needs to be pieced together to recreate or synthesize the frequency response function.

So let's say that the data was fit in three separate bands, as shown in Figures 9.19–9.21. Each band would have the set of modes fit in that band, as well as the upper and lower residuals

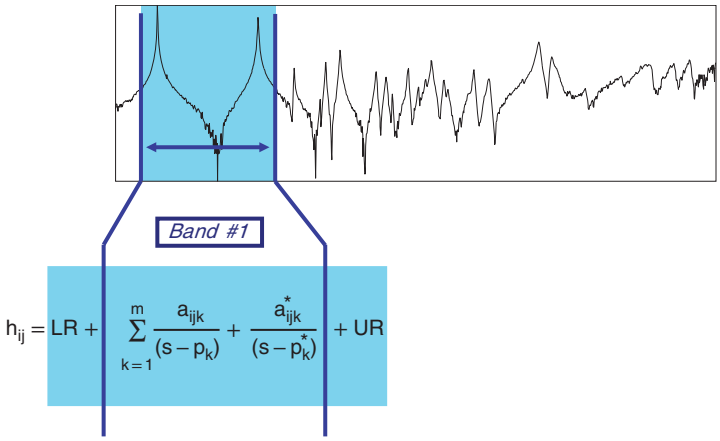

Figure 9.19 Band 1 fit data.

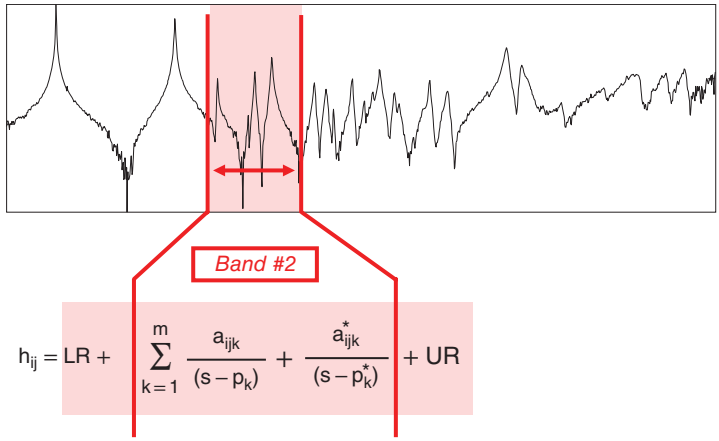

Figure 9.20 Band 2 fit data.

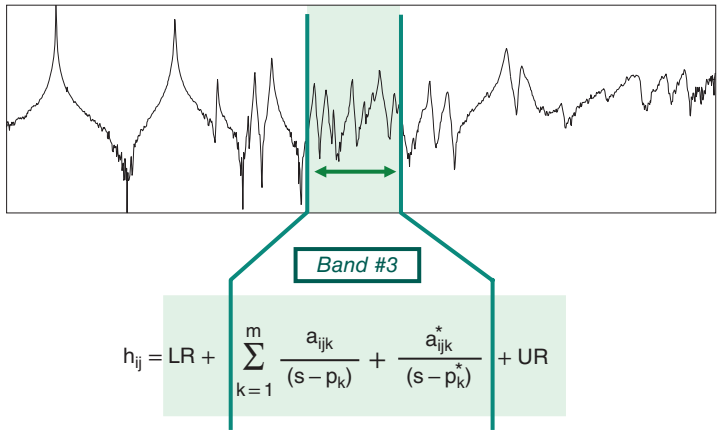

Figure 9.21 Band 3 fit data.

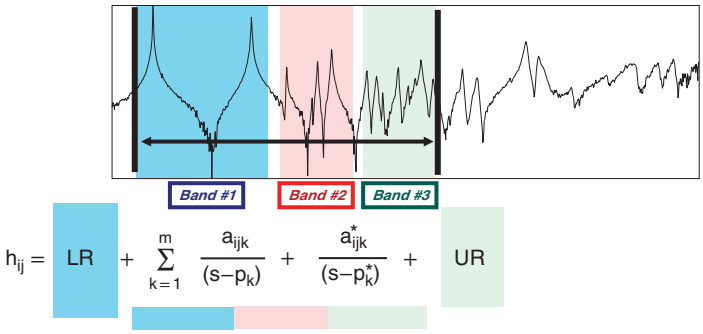

Figure 9.22 Modes (poles and residues) combined from band 1, band 2 and band 3, along with the lower residual from band 1 and upper residual from band 3 to synthesize the frequency response function.

for each band. Now when the combination of the three separate bands are fit together, the modes for each of the bands need to be combined, but the lower residual of the first band and the upper residual of the last band need to be included with the modes in order to generate a proper synthesized function, as illustrated in Figure 9.22.

9.11 A Large Multiple Reference Modal Test Parameter Estimation

Back in the early 1990s, there was a test of a large satellite for the Canadian Space Agency. At the time, the RADARSAT satellite involved one of the largest modal tests ever conducted. The dataset is contained on the website and the appendix contains a more recent data reduction using PolyMAX. The two stage process was becoming more popular in the 1990s. This section discusses the modal parameter estimation performed at that time and gives an insight into the modal parameter estimation process for a more complicated system.

The test geometry of the RADARSAT experimental modal test configuration is shown in Figure 9.23. This structure was tested with five separate shaker excitation locations, with 250 measurement points. The main structural modes of interest for this structure were in the 10–60 Hz band. Several different modal parameter extraction scenarios were performed to show the degradation of the extracted modes when all of the measured degrees of freedom were used, as opposed to a more selective set of degrees of freedom for the generation of poles and extraction of residues. The dataset was then processed using the PolyMAX technique to show the ease with which this difficult dataset can be efficiently processed.

9.11.1 Case 1: Use of All Measured FRFs

The frequency response measurements were evaluated over eight different bands between 30 and 60 Hz. Poles were extracted using a time domain complex exponential curvefitting technique. The typical mode indicator tools were used for the identification of modes of the system: the summation function, the multivariate mode indicator function, and the complex mode indicator function were all used for the identification of modes and are shown in Figure 9.24 for the entire bandwidth. Figure 9.24 also shows the first stability diagram using the entire bandwidth for evaluation. Clearly, the stability diagram is very difficult to interpret when using the entire bandwidth for all of the references.

Figure 9.25 shows three separate stability diagrams, over three separate bandwidths, where all the references and all measured DOFs are used for the extraction process. The stability diagram was also used for the identification of the poles of the system. For this case, all the references and all the measured DOFs were used to extract modal parameter estimates. The mode indicator tools produced adequate identification of the modes of the system, but the stability diagram

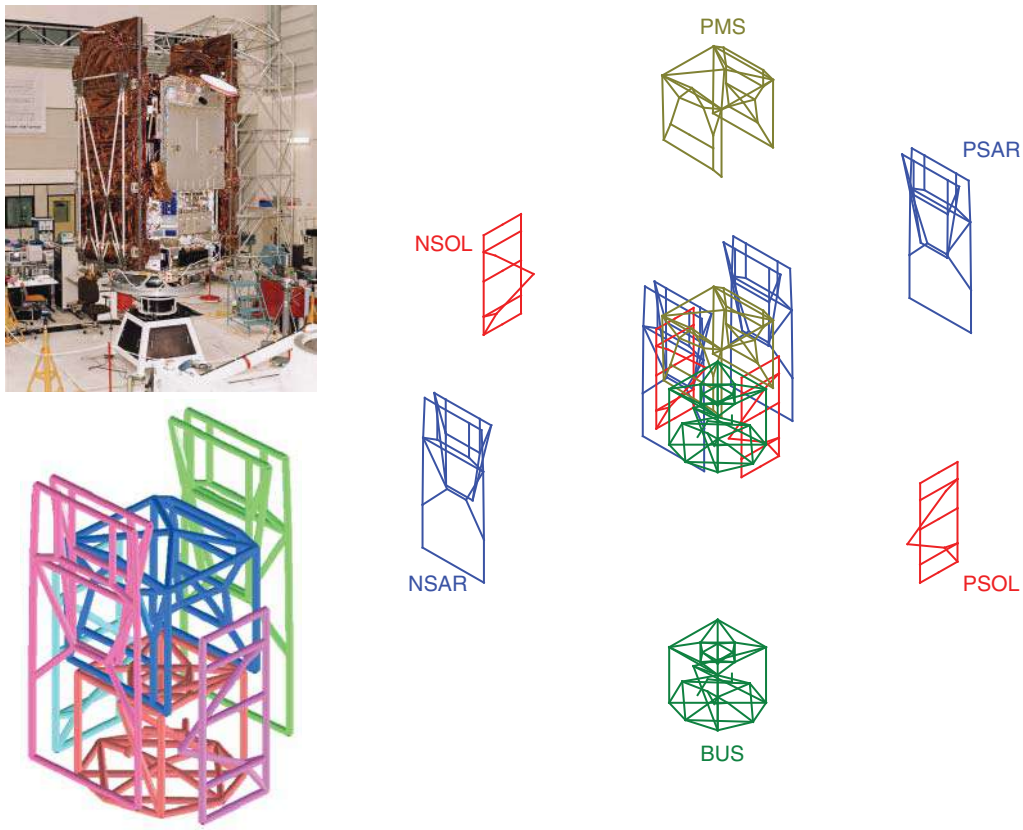

Figure 9.23 RADARSAT1 test geometry.

produced only marginal identification of the poles of the system. The selection of poles from these plots was fairly difficult due to the variance of the estimated pole parameters. Due to the large number of measurements that were obtained from references that did not adequately excite the modes, the stability diagram results are not particularly good. The pole selection adequacy is very questionable.

Once mode shapes were extracted, the frequency response functions were synthesized and compared to measured data. Two different synthesized functions are shown in Figure 9.26. These are not particularly good synthesized comparisons. This is due to the poor extraction of modal parameters from the modal extraction process. These two plots are typical of the synthesized functions for other measurement locations on the structure.

In addition, the modal assurance criterion (MAC) was used for the assessment of the modes extracted. The matrix plot of the MAC values is shown in Figure 9.27. The majority of the off diagonal terms are reasonably low, and the extracted data from this perspective appears acceptable, even though the synthesized frequency response functions are not very good at all. The first 25 modes extracted from the measured data are shown in Figure 9.28. Many of these modes are primarily local modes of the main radar and solar panels of the satellite. While the modes appear reasonable from mode shape plots and from the MAC, the synthesized frequency response functions clearly show that the extracted parameters need further scrutiny.

In order to further evaluate this data, the modal participation factors are plotted in matrix form in Figure 9.29. The participations seen in Figure 9.29 clearly show that the first 25 modes are primarily excited by the x shaker reference location and the y shaker reference location. The higher frequency modes are activated more significantly from the z shaker reference location.

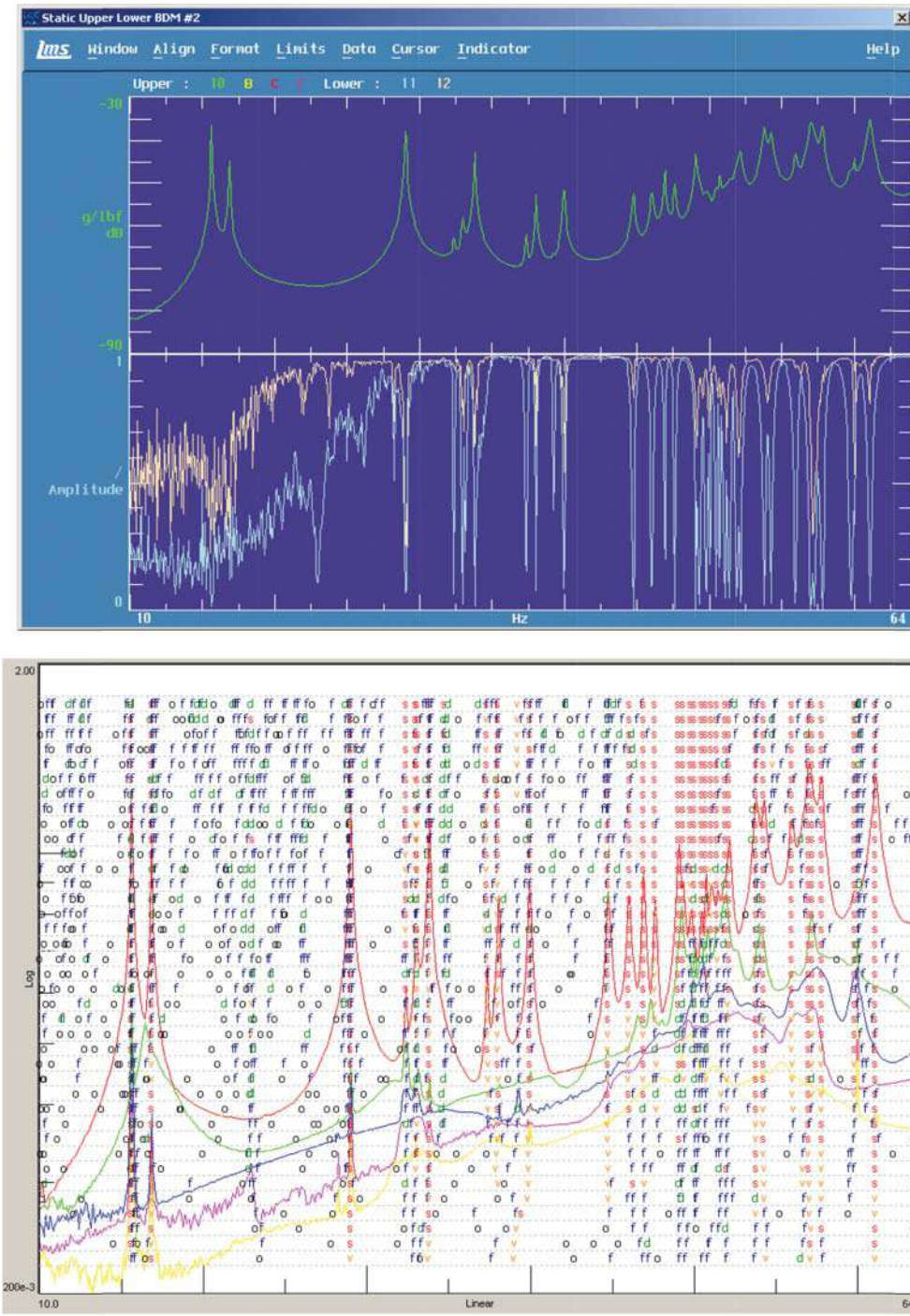

Figure 9.24 Summation function and mode indicator function using all references along with stability diagram over the entire band.

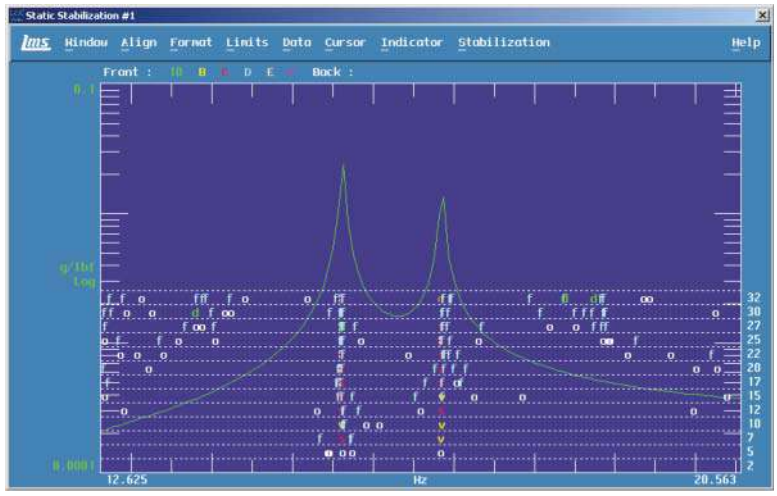

(a)

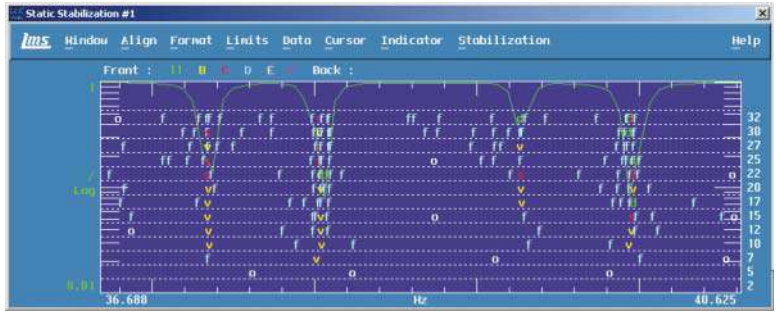

(b)

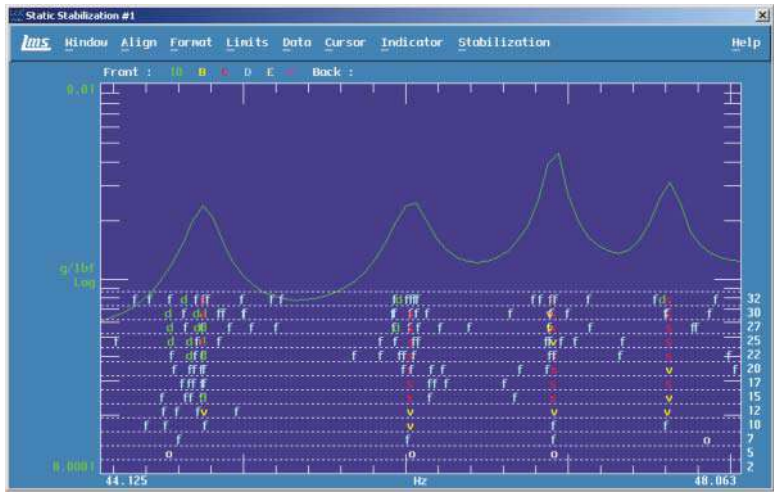

(c)

Figure 9.25 Stability diagram for three different bandwidths using all references: (a) 12.6–20.6 Hz; (b) 36.7–40.6 Hz; (c) 44.1–48.1 Hz.

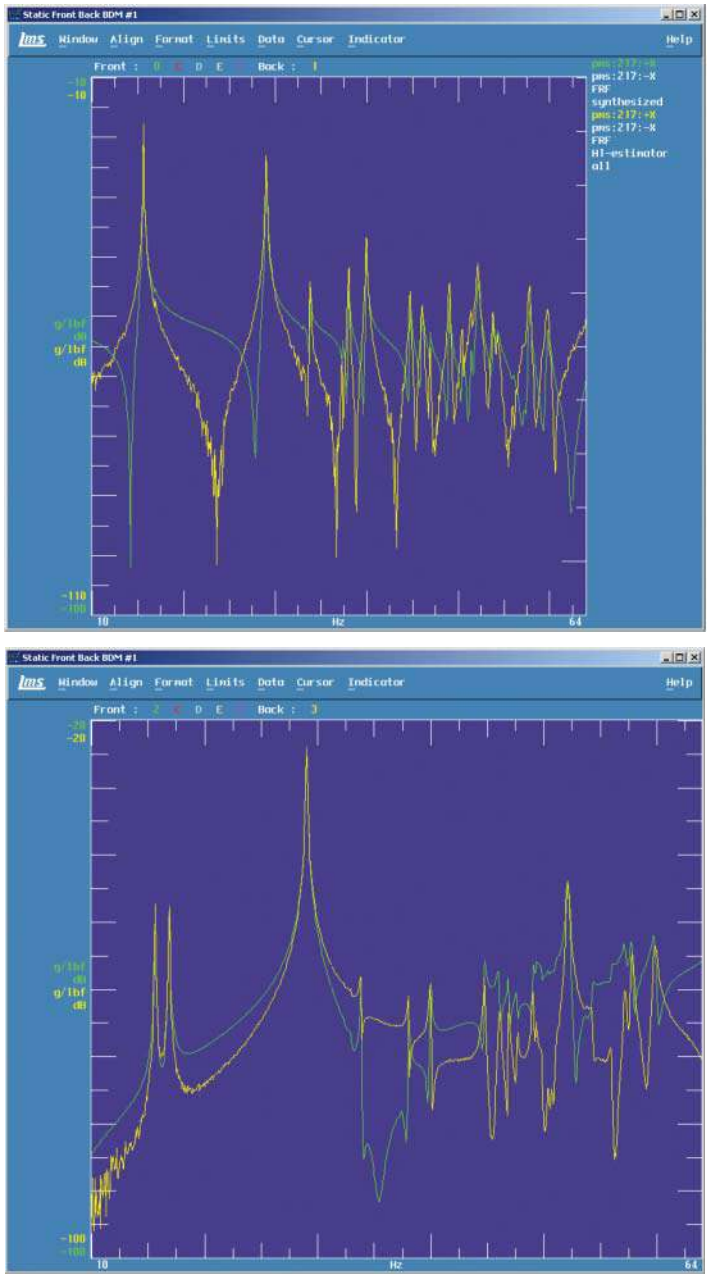

Figure 9.26 Typical synthesized FRF using all references.

In order to show the detrimental effects of using all the references and all the measured DOFs, a selective set of references and measurement locations was used to determine the modal parameters of the system in Case 2.

9.11.2 Case 2: Use of Selected Sets of Measured FRFs

For this evaluation, only the x shaker excitation location and the y shaker excitation location were used; the z shaker excitation locations were not used as references in the evaluation. Again,

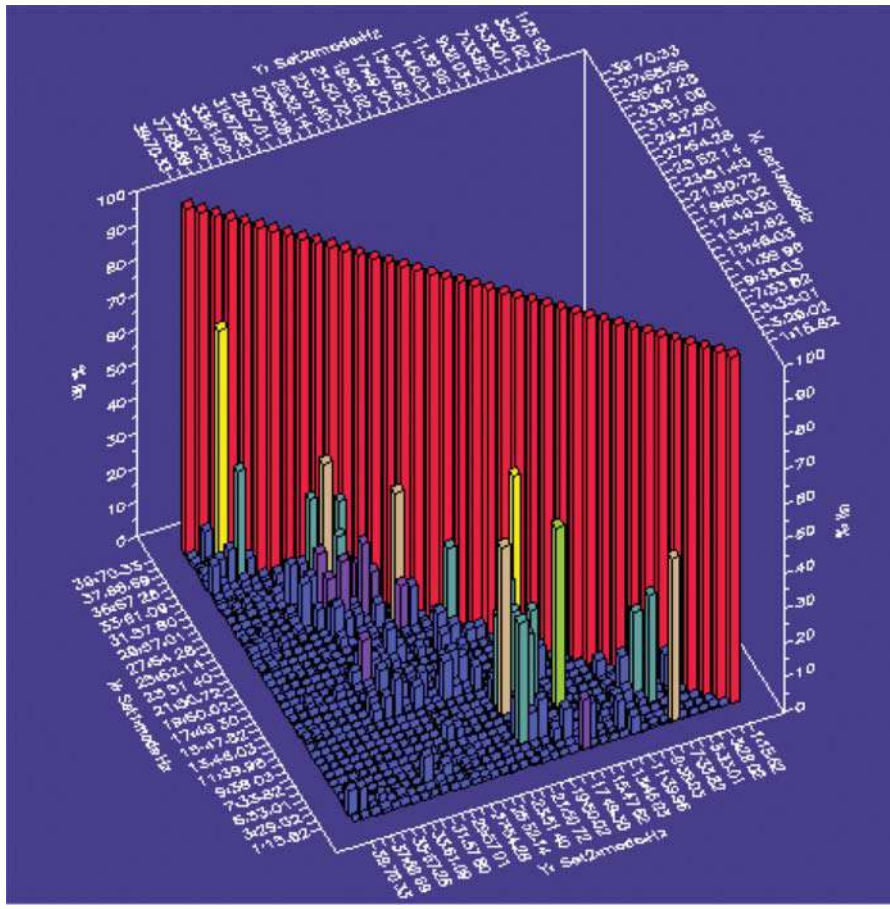

Figure 9.27 MAC of modes using all references.

the frequency response measurements were evaluated over several different bands between 30 and 60 Hz. Poles were extracted using a time domain complex exponential curvefitting technique. The typical mode indicator tools were used for the identification of modes of the system: the summation function, the multivariate mode indicator function, and the complex mode indicator function were all used for the identification of modes and are shown in Figure 9.30 for the entire bandwidth. Comparing Figure 9.30 with Figure 9.24, the indicator tools are much easier to interpret because only pertinent (rather than all) references were used.

Figure 9.31shows three separate stability diagrams over three separate bandwidths where a selected set of references and a selected set of measurements were used for the evaluation. Comparing Figure 9.31 to Figure 9.25 clearly shows the improved situation for the selection of poles from the stability diagram. The careful selection of references and measurements for the determination of poles clearly has an impact on the extraction process and improves the selection of poles for the system. The selection of poles is definitely improved through the selection of reference locations.

Once mode shapes were extracted, frequency response functions were synthesized and compared to measured data. Two different synthesized functions are shown in Figure 9.32. Both of these show very good correlation with the actual measured data and are better than the results shown in Figure 9.26. These two plots are typical of the synthesized functions for other

Figure 9.28 Modes of the RADARSAT1 satellite: first 25 modes of the structure.

measurement locations on the structure. Clearly, the selection of references and measurement locations for the extraction of modal parameters has a significant effect on the extracted modal parameters.

In addition, the MAC was used for the assessment of the modes extracted. The matrix plot of the MAC values is shown in Figure 9.33. The majority of the off diagonal terms are reasonably low. Some of the off-diagonal terms may be an indication of spatial aliasing; additional measurements would minimize this. The MAC is not a particularly good tool for the detailed evaluation of the extracted results. The MAC heavily weights the largest values of the shape and is not a particularly good tool for detailed overall assessment of the extracted parameters. It is shown mainly for reference.

9.11.3 Case 3: Use of PolyMAX

With the advances in modal parameter estimation using the PolyMAX approach introduced in the mid-2000s, wide bands of frequency response measurements can be effectively processed

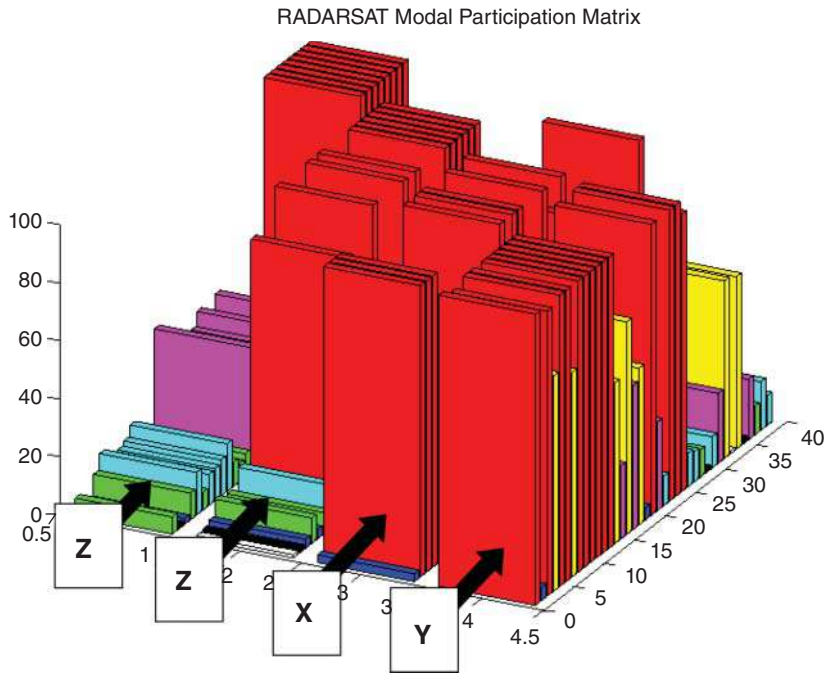

Figure 9.29 Modal participation matrix of the RADARSAT1 satellite.

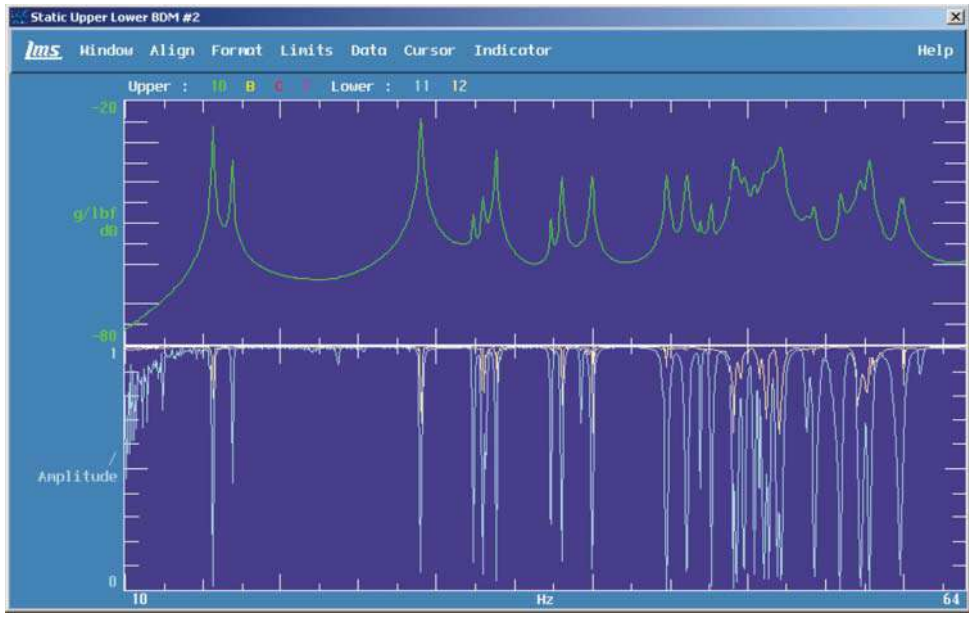

Figure 9.30 Summation function and mode indicator function using selected references.

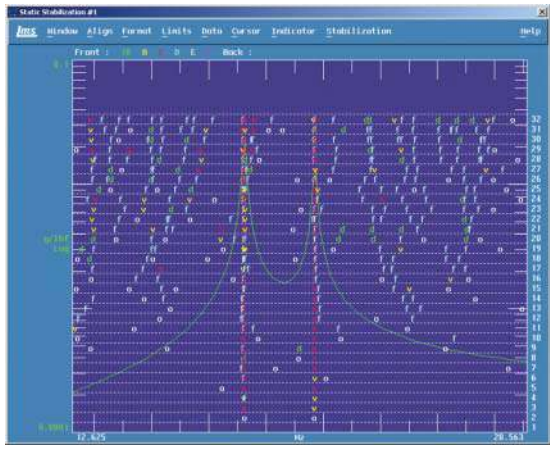

(a)

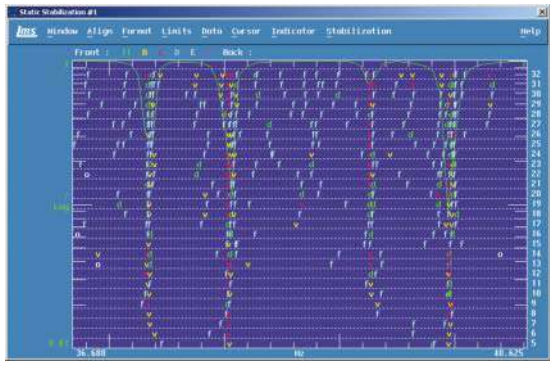

(b)

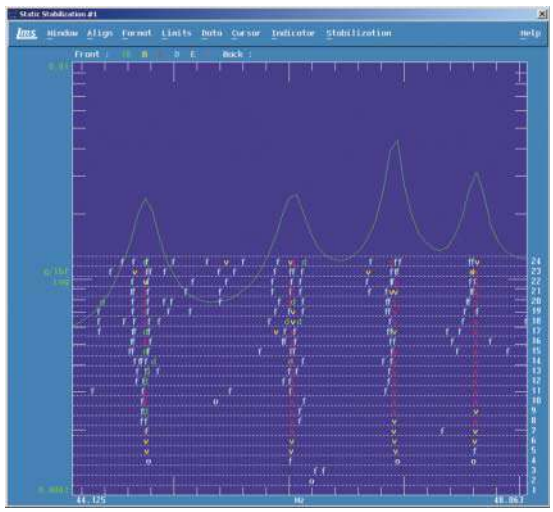

(c)

Figure 9.31 Stability diagram for three different bands using selected references: (a) 12.6–20.6 Hz; (b) 36.7–40.6 Hz; (c) 44.1–48.1 Hz.

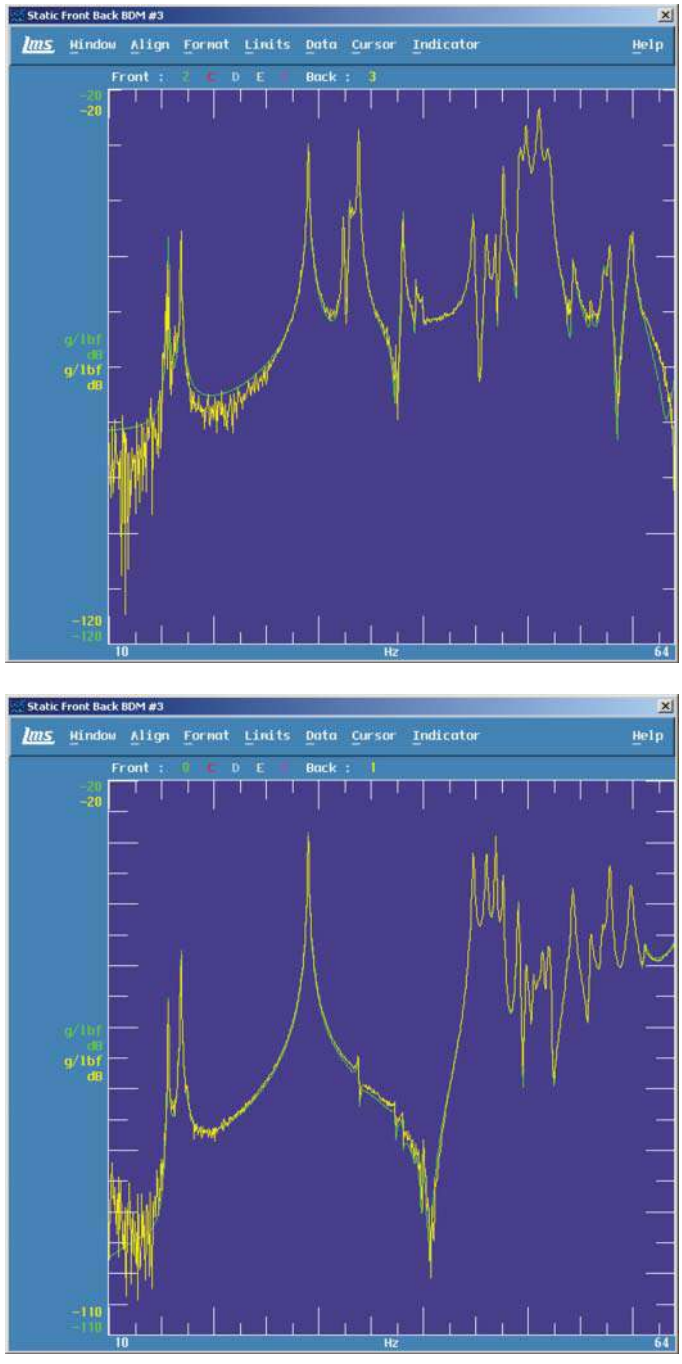

Figure 9.32 Typical synthesized FRF using selected references.

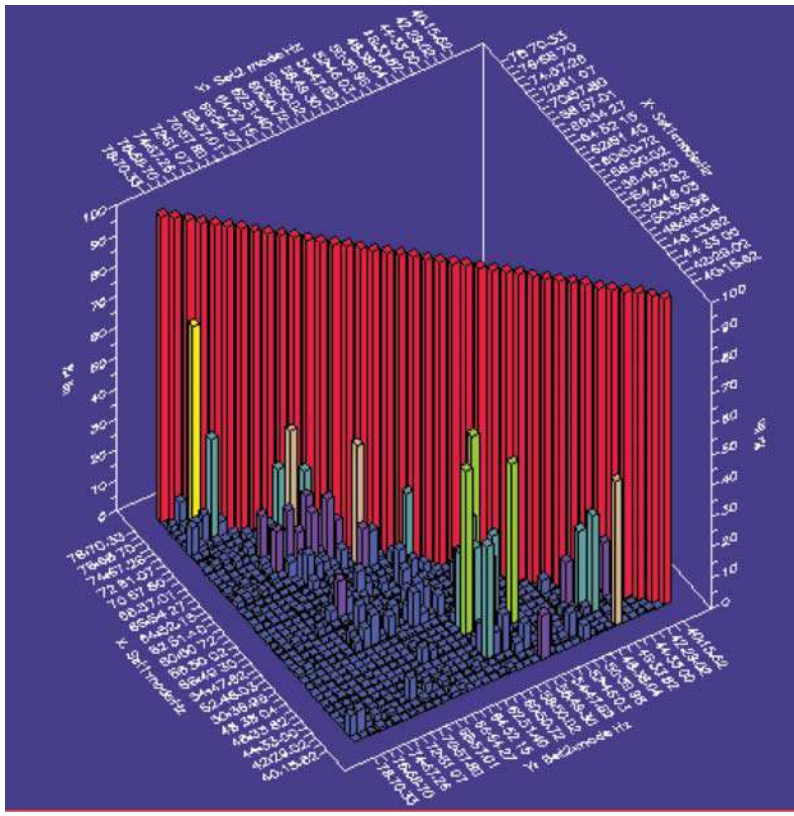

Figure 9.33 MAC of modes using selected references.

with little restriction on bandwidth and little need to sift the large set of measurements to produce good pole estimates. The PolyMAX approach to modal parameter estimation has revolutionized the modal parameter estimation process. The same datasets described above were reprocessed using all measured degrees of freedom for all references. The mode indicator function and complex mode indicator function are shown in Figure 9.34. The stability diagram is presented in Figure 9.35. The stability diagram is very easy to interpret. Clearly the poles extracted appear to be very well identified over this wide frequency range. Figure 9.36 shows a comparison of some synthesized frequency response functions for selected measurements. These synthesized measurements show very good correlation to the actual measurements acquired. In addition, the MAC was used for the assessment of the modes extracted. The matrix plot of the MAC values is shown in Figure 9.37. The majority of the off diagonal terms are reasonably low. The MAC off diagonal terms are comparable or lower than those extracted using other techniques.

The parameters extracted using traditional approaches are plagued by noise and mode participation considerations in the estimation process. A significant amount of work is required to sort the datasets into selective bands that are reasonably well excited by the various reference shaker locations in order to extract acceptable modal parameters. This involves significant time and effort to accomplish. The newer PolyMAX technique simplifies this process and extracts equivalent parameters using wide bandwiths and without having to sift through the datasets

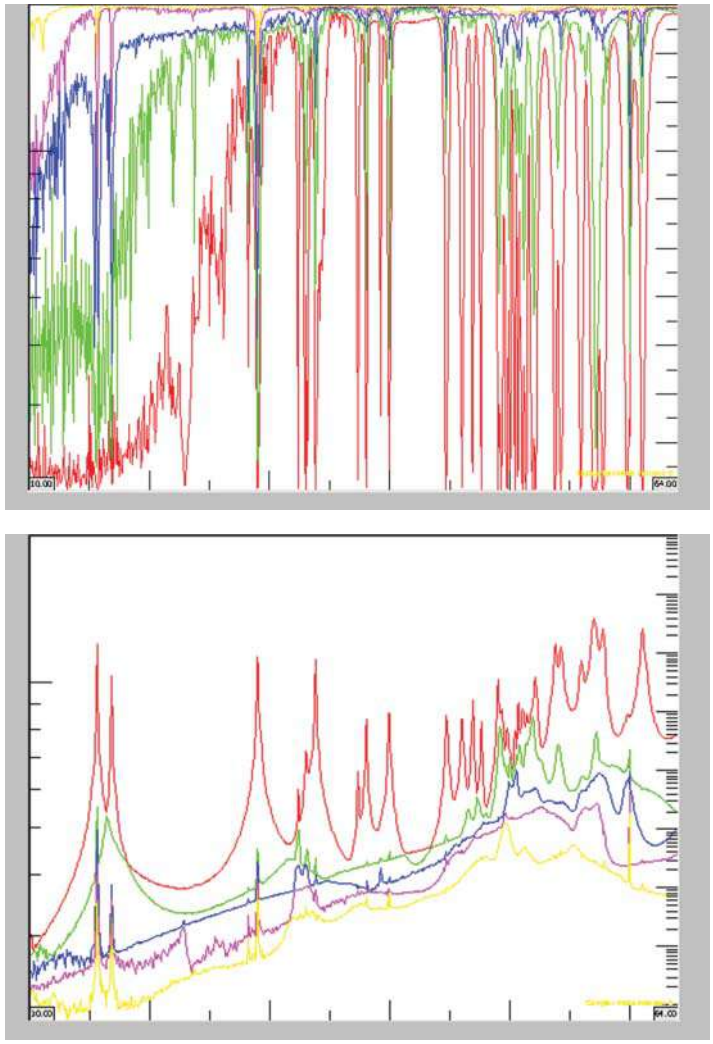

Figure 9.34 Multivariate mode indicator function and the complex mode indicator function using all references.

for the best references to excite all of the modes. PolyMAX is a significant tool for reducing the effort involved in the reduction of frequency response functions for modal parameter extraction.

9.12 Operating Modal Analysis

In order to illustrate data extracted from the cross-spectra typically employed in operational modal analysis, a small frame structure was used here. For reference, a traditional modal test was performed to obtain reference modes shapes; a test verified finite element model was also available to further substantiate the results. The MIMO data was processed and the stability

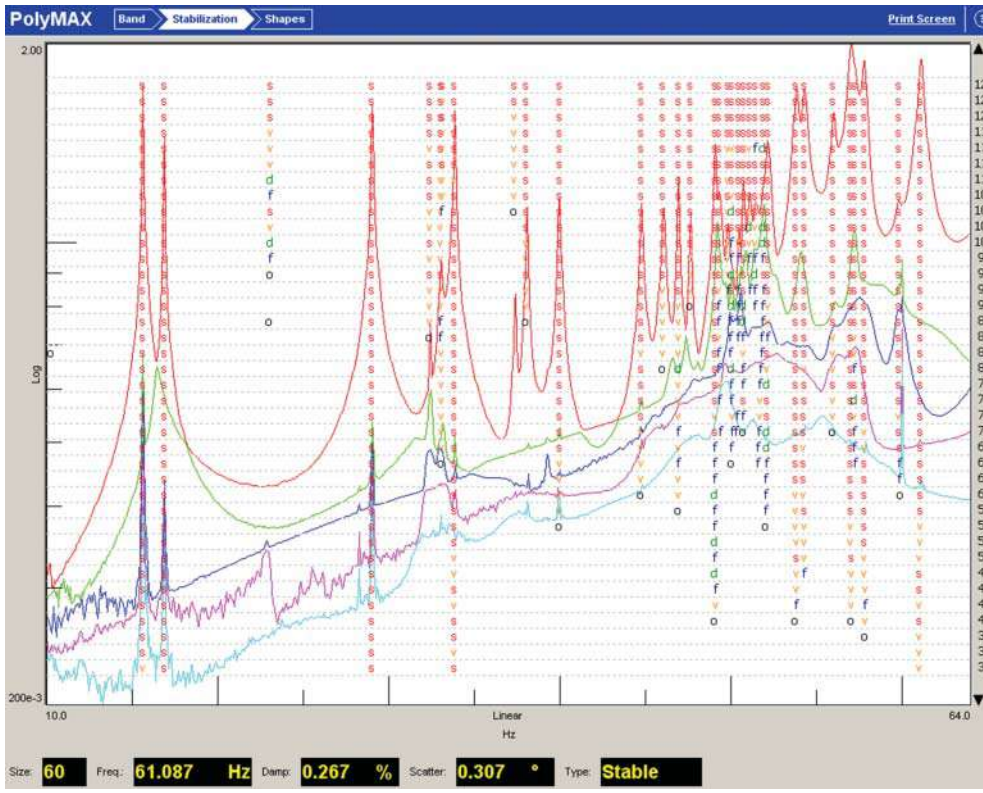

Figure 9.35 Stability diagram using PolyMAX and all references.

diagram with the SUM and four CMIF functions are shown in Figure 9.38 along with the mode shapes extracted.

With the frame structure freely suspended, an arbitrary set of response measurements was collected while the structure was impacted with several impact hammers that were distributed randomly around the structure. There were random timings between all the impact hammers. In this way, the excitation was spatially broad across the entire structure, with a frequency spectrum that excited all the modes of interest. Obviously, this is an external unmeasured excitation that satisfies all the conditions necessary for operating modal analysis. Time data from the test was streamed to disk and used to calculate auto and cross spectra from selected reference accelerometers. Curvefitting was done using LMS Operational Polymax; the characteristic mode shapes of the frame can be seen in Figure 9.39 along with the stability diagram. The results were further processed and mode shapes were compared using the MAC, which is shown in Table 9.3. The results show that the modes are all extracted well, but with some degradation of mode 3.

Following this operating test, a second test was performed in which the excitation was only applied at locations where the structure would be attached to a mating attachment point on its companion structure. Now these mounting locations happen to occur at nodes of some of the modes of the structure; this is realistic because in some design configurations for automotive and truck structures (as well as propulsion systems for shipboard applications and large structure configurations), the attachment of components is designed to be at nodes of modes to minimize the flow of vibrational energy. Now the same excitation is used for the operating

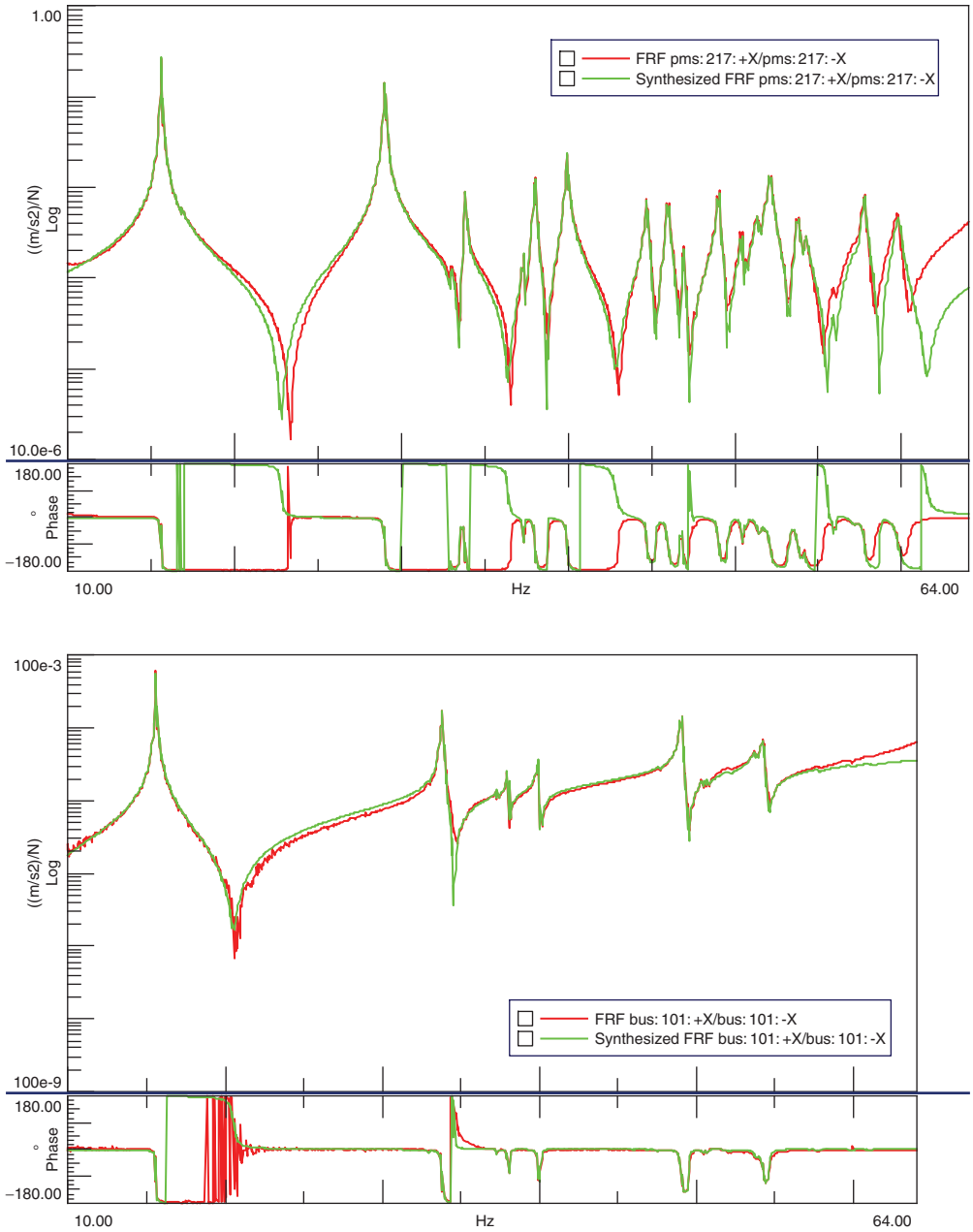

Figure 9.36 Selective synthesized frequency response functions.

data but it is restricted to specific points on the structure. Time data from the test was streamed to disk and used to calculate auto- and cross-spectra from selected reference accelerometers. Curvefitting was again performed using LMS Operational Polymax and the characteristic mode shapes of the frame can be seen in Figure 9.40. The modes extracted from the operational modal analysis were compared to the traditional modal test results using MAC, and are shown in Table 9.4.

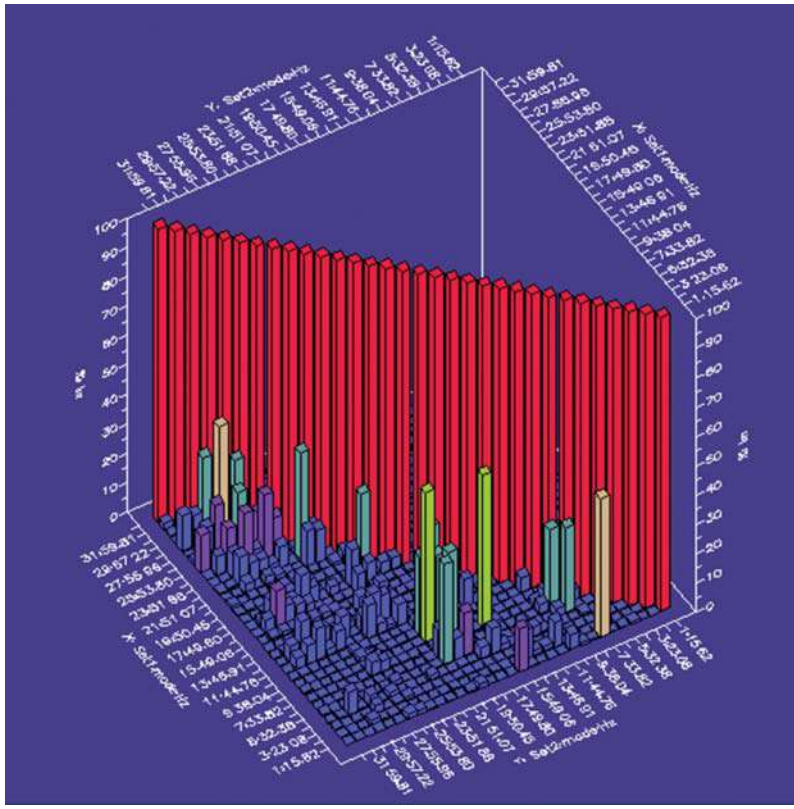

Figure 9.37 MAC of modes using PolyMAX.

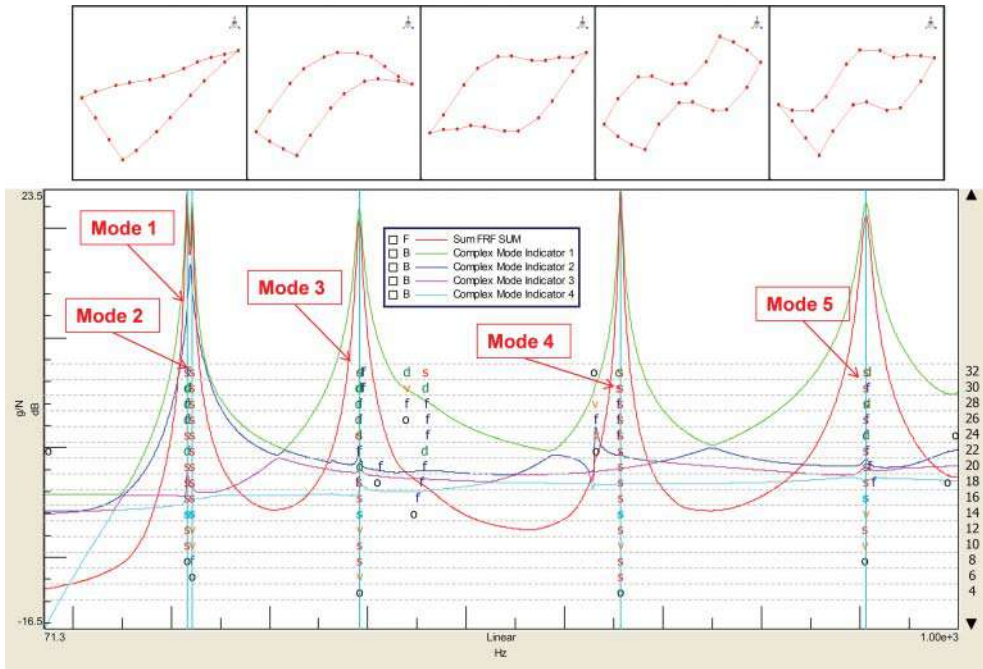

Figure 9.38 Stability diagram and first five modes of frame from a MIMO shaker test.

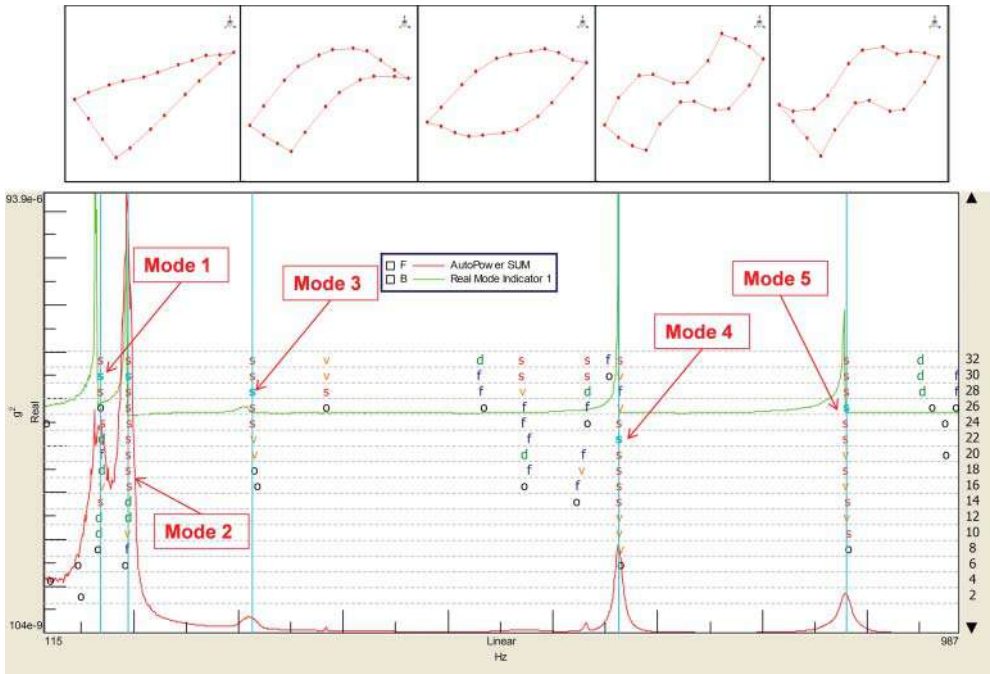

Figure 9.39 Stability diagram and first five modes of frame from an OMA spatially broad excitation with wide frequency band.

Table 9.3 MAC of MIMO modal test and operational modal test with spatially broad excitation.

	Mode No.	Operational modal test				
		Mode 1	Mode 2	Mode 3	Mode 4	Mode 5
MIMO test	Mode 1	98.99	1.23	0.07	0.02	0.50
	Mode 2	0.48	93.84	5.40	0.00	0.15
	Mode 3	0.02	0.10	73.65	0.07	0.08
	Mode 4	0.01	0.00	0.00	99.50	1.44
	Mode 5	0.03	0.06	0.00	0.12	98.16

Table 9.4 MAC of MIMO modal test and operational modal test with localized excitation.

	Mode No.	Operational modal test				
		Mode 1	Mode 2	Mode 3	Mode 4	Mode 5
MIMO test	Mode 1	—	1.45	0.08	0.00	0.05
	Mode 2	—	94.61	0.61	0.04	0.58
	Mode 3	—	0.08	50.07	0.19	0.15
	Mode 4	—	0.01	0.01	0.46	0.02
	Mode 5	—	0.06	0.01	0.01	1.01

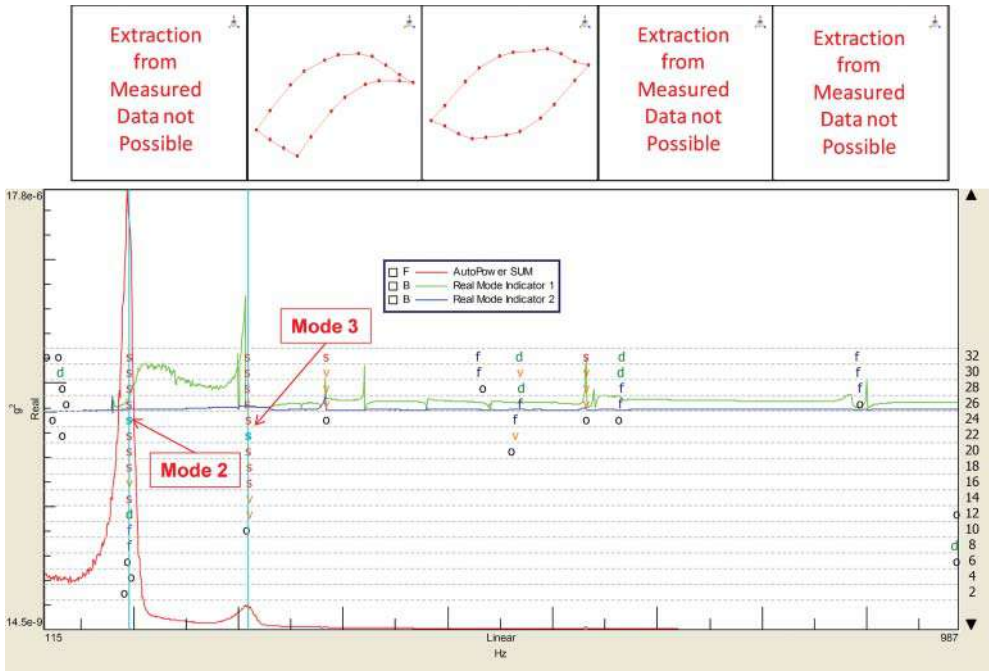

Figure 9.40 Stability diagram and two modes of frame from an OMA localized excitation with wide frequency band.

These results clearly show some of the shortcomings of operational modal analysis. Whenever the operating forces do not have adequate spatial or frequency richness, then the reduction of the data is likely to miss modes or misrepresent modes. However, one easy way to overcome this deficiency is to always add additional excitation to the structure in order to ensure the richness of the unmeasured excitation. This is easily accomplished by adding small portable shakers to the structure while it is in its operating condition. The location of the shakers will follow the same rules as those used for running a traditional modal test. In this way, the excitation from the shakers combined with the operating response will be better suited to adequately exciting all modes and extracting useful modal data. This was in fact done with the frame structure considered here; small shakers were attached on the structure and added to the operating excitation applied. Using this new set of data, time data from the test was streamed to disk and used to calculate auto- and cross-spectra from selected reference accelerometers. Curvefitting was again performed using LMS Operational Polymax and the characteristic mode shapes of the frame can be seen in Figure 9.41. The modes extracted from the operational modal analysis were compared to the traditional modal test results using MAC and are shown in Table 9.5.

These results clearly show that, even with an operating excitation that cannot adequately excite all the modes, the additional of extra shaker excitation allows for the operating modal analysis approach to adequately identify the modes of the system. So, while operating modal analysis can have some shortcomings, there are alternatives for the way the structure is excited, with supplemental excitation giving a much better chance that all the modes can be observed.

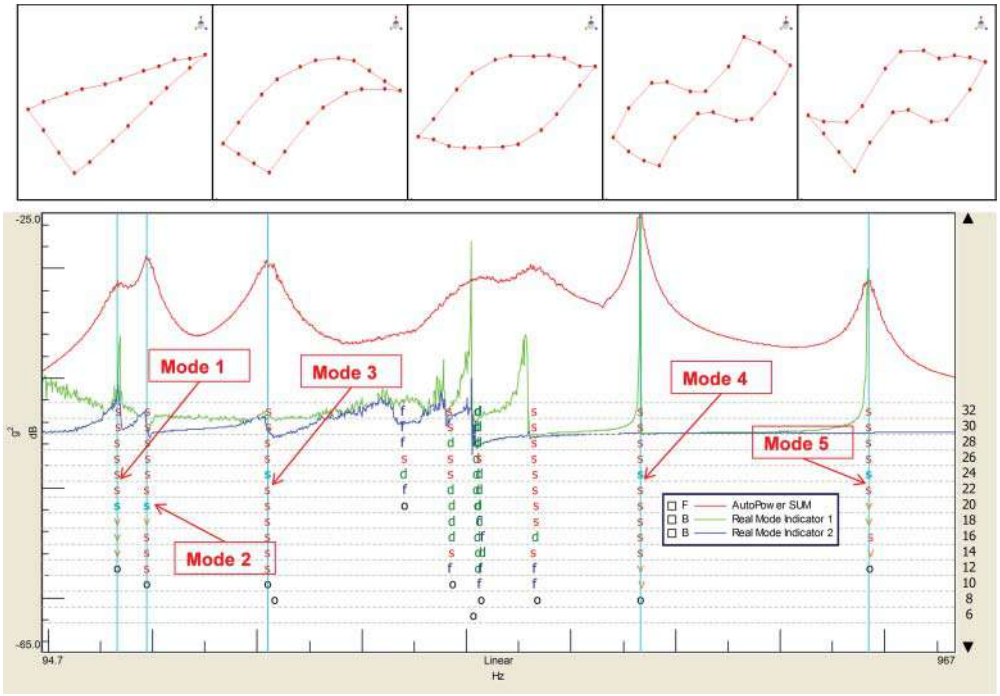

Figure 9.41 Stability diagram and five modes of frame from an OMA localized excitation complemented with additional shaker excitation with wide frequency band.

Table 9.5 MAC of MIMO modal test and operational modal test with localized excitation.

	Mode No.	Hybrid modal test				
		Mode 1	Mode 2	Mode 3	Mode 4	Mode 5
MIMO test	Mode 1	98.53	1.28	0.02	0.06	0.90
	Mode 2	0.39	91.16	0.01	0.02	0.13
	Mode 3	0.05	0.21	81.69	0.07	0.20
	Mode 4	0.01	0.05	0.01	99.54	0.72
	Mode 5	0.14	0.12	0.00	0.03	98.47

9.13 Concluding Remarks

Some very simple modal parameter estimation cases were shown, in order to clearly illustrate the power of the curvefitting process. The simple cases clearly show that the modal parameter estimation process is very accurate. The SDOF and MDOF curvefitting for a simple 2DOF system shows the accuracy of the parameters extracted, even with simple analytical models. Several intermediate level cases were shown to further describe the process. Use of local and global curvefitters were demonstrated to illustrate the differences in the parameters extracted. In addition, some repeated root cases were described, to show the accuracy of the extraction

process when care is exercised. The stability diagram, which is used extensively in modal extraction, was explained using a very simple example to demystify this powerful tool. Some examples of modal extraction in which different bands are utilized were described, along with a resynthesis of the measured data to further explain the process. The last example outlined a very large modal test for the Canadian Space Agency, whose RADARSAT test was used to show the modal extraction process and set out some issues to take note of when curvefitting. This was followed by the description of an operational modal data reduction set, illustrating some of the issues associated with using this approach for extraction of modal parameters. The appendices contain several of these datasets so that parameter extraction can be performed and compared to the data available on the book website.

10

General Considerations

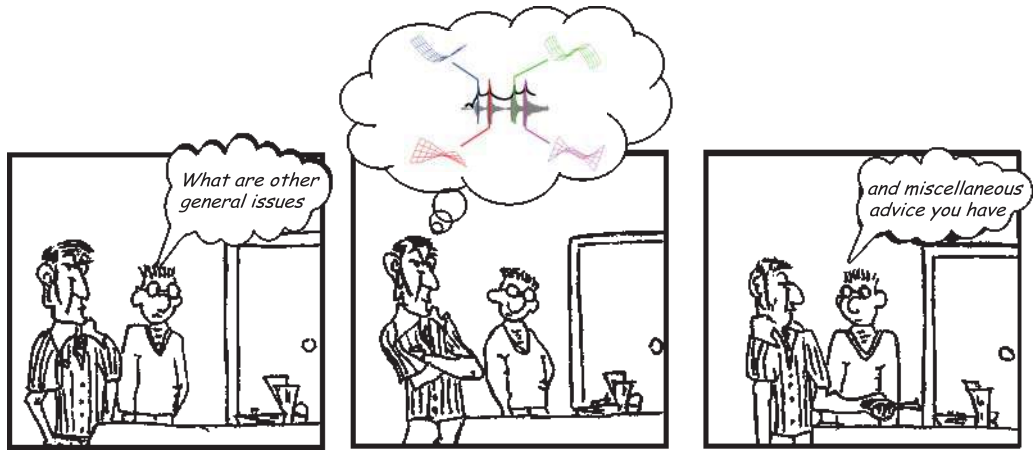

There are many issues with modal analysis that are general in nature and do not necessarily fall into a particular chapter. Some of those items are collected here. Some additional information about the entire test process is described here as well; this is intended to give a more intimate discussion of the test and what steps should be taken during the test. This information has come from decades of running modal tests and some of the things described have become standard parts of modal testing over the years.

But before that is done, let's describe the overall process again. Figure 10.1 shows the entire process and is essentially the big picture of how and why experimental modal testing works and puts everything into proper context. This process was partially discussed at the end of the chapter covering the theory. This will be described again here but from a slightly different perspective; sometimes it is very good to hear the same things twice but with different descriptions to fill in the voids and gaps to give a better overall understanding.

Modal Testing: A Practitioner's Guide, First Edition. Peter Avitabile.

Companion Website: www.wiley.com/go/avitabile/modal-testing

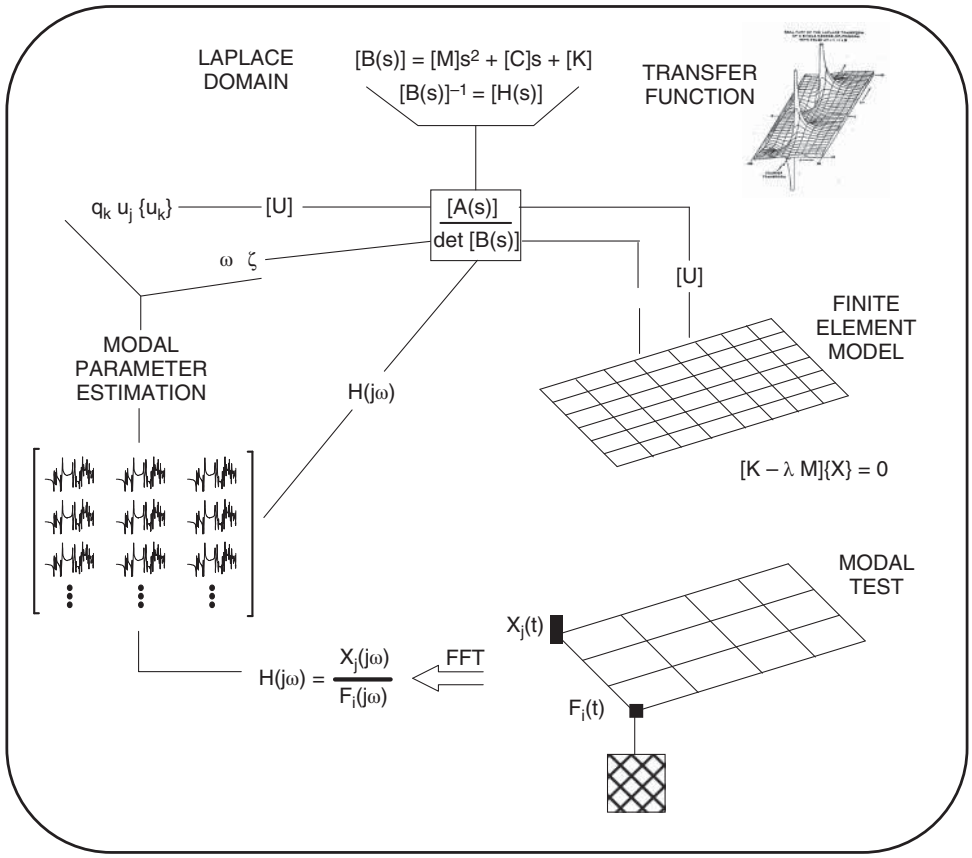

Figure 10.1 Overview of analytical and experimental modal analysis.

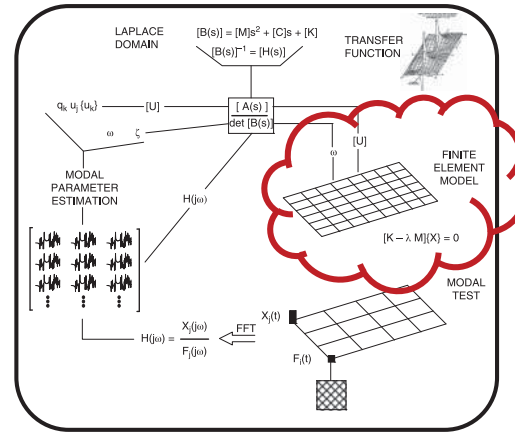

Now finite element models are typically used to generate an analytical approximation of a system for design purposes. From the finite element model, approximations of the system mass and stiffness distributions are made. A very large, complicated set of equations results from this process. A solution sequence called an eigensolution is performed, from which the system frequencies and mode shapes of the system are extracted. The models generated are approximations of the actual system and have assumptions as part of the process. Now these models may be very good overall, but there are assumptions inherent in the model, and the experimental modal test may be performed to help understand the adequacy of the finite element model and its predictions of response.

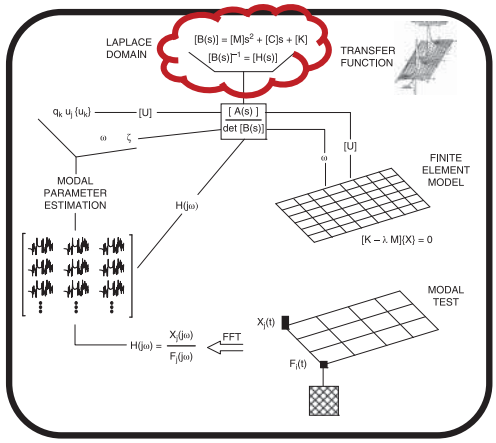

Now this same set of equations can be used, but cast into a new form called the Laplace domain by using a Laplace transform. This is not much different than what was done with the finite element model except that the equations are cast in a different form. Notice that B(s) is the system matrix and that the inverse of B(s) is H(s), which is the system transfer function. Again, some assumptions about the mass, damping, and stiffness matrices are made in developing this model. These equations are cast in the Laplace domain so as to take advantage of some mathematical advantages needed for easy manipulation of some of the equations.

Now the big key here is in the system transfer function matrix, which is equal to the adjoint of B(s) divided by the determinant of B(s). The determinant of B(s) contains the characteristic equation, which gives the poles of the system: the frequency and damping. The adjoint matrix contains the residues, which are directly related to the mode shapes of the system. So the Laplace domain is just another mechanism to get the same information that is obtained from the finite element model.

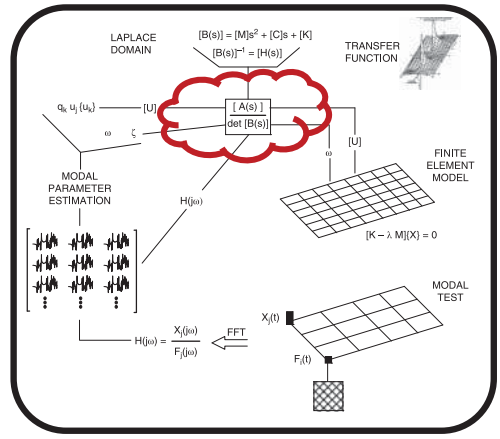

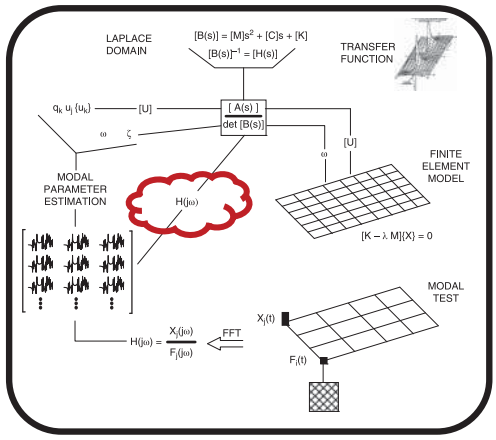

Now the frequency response function can be generated from the system transfer function. The frequency function can be created or synthesized for any particular input–output combination. The frequency response function has extremely important pieces of information from the test data: one is the residue and one is the pole. Remember that the pole is related to the frequency and that the residue is related to the mode shape of the system.

Now in the synthesis process, any input–output combination can be synthesized. All the input–output combinations could be used to generate as many frequency response functions as desired and potentially could fill all the terms of the frequency response function matrix. If at least one row or column of the frequency response matrix is generated, there is a sufficient amount of data to describe the mode shape for the system.

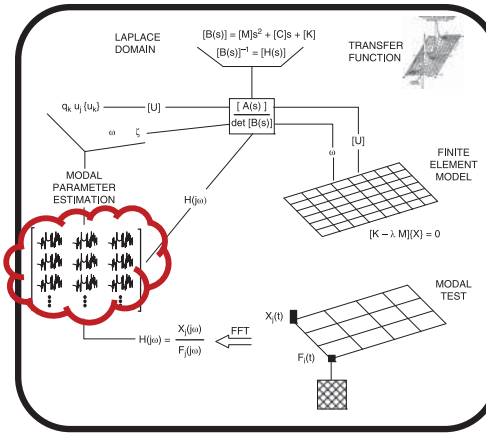

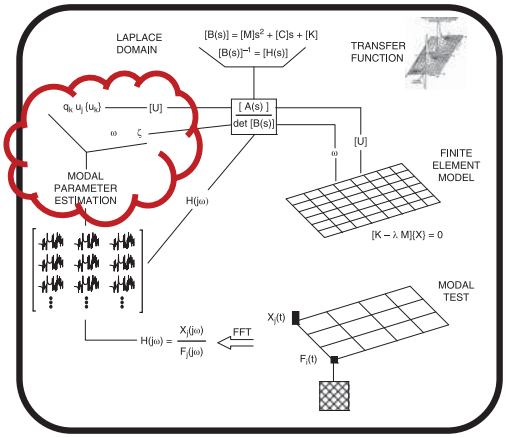

Once all of these frequency response function measurements are generated, buried inside this data are the poles (frequencies) and residues (mode shapes). So it stands to reason that, working backwards from a measurement, the modal parameter estimation process should be able to extract the poles (frequency and damping) and residues (mode shapes). This is the heart of parameter estimation commonly called curvefitting. Mathematical algorithms are used to extract the parameters of interest: the frequency, the damping, and the residue (or mode shape).

Up until this point, assumptions about the mass, damping, and stiffness of the system were needed in order to form the system matrix, the transfer function matrix, and the frequency response function matrix. Now on a real structure, an excitation can be made and the response captured to get the input–output phenomena of the system due to the applied force. The input force and response of the system due to the input force can be measured to obtain the system transfer characteristics. Notice that in this approach there are no assumptions as to what the system mass, damping and stiffness matrices are: the structure knows what its character is. This approach to characterizing the system from measured data is the heart of experimental modal analysis.

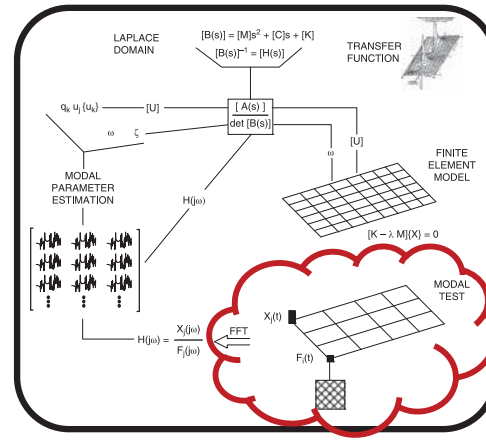

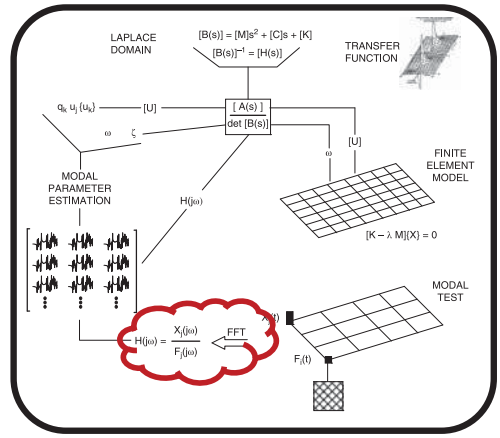

Once time data has been acquired, this will be transformed from the time domain to the frequency domain using the fast Fourier transform. In essence, the ratio of the output response to the input force will be used to compute the frequency response function. This can be done for many points so as to compute the terms in the frequency response matrix. Then the frequency response function will be used to curvefit the measurement to extract the data of interest: the frequency, damping, and residue (or mode shape). Of course, in order to do this, a full understanding of many important concepts of experimental modal analysis pertaining to digital signal processing, excitation techniques, and modal parameter estimation are needed.

And that, modal test folks, is a good description of the entire process of how and why modal testing works.

10.1 An Experimental Modal Test: a Thought Process Divulged

Experimental modal testing is performed for a variety of reasons. Earlier, the process of understanding *why* a test may be needed was described. That information is very important to understand the need for the test and the scope for the test.

In this section, an assumption is made that all of that has been defined. Now there will be some discussion of the thought process required when standing at the test site and starting up the test itself. A larger test is discussed: one that requires testing outside of the normal lab environment, where almost everything is not right at your fingertips. Such a test environment has many aspects that still need to be considered. Of course, a test plan should already have been developed, but once at the test site and looking at the actual structure, additional things come to mind. So let's step through a test and provide some additional guidance and thoughts on conducting the test itself. Much of this is really personal preferences and personal habits that have worked well for years; sharing them may be useful to some.

The trip to the test site involves many steps that may be important regarding special issues that arise during the test. One important item is to make prior arrangements as to who is doing what. Maybe the test site will preinstall all the accelerometers or provide the setup of the structure ahead of the test team's arrival. A clear definition of everyone's role is very important, so that there are personnel assigned to all tasks and people aren't standing looking at each other and saying "I thought you were going to take care of that," which is one phrase heard many times over the years.

Heading to the test site and packing the right equipment is an art in itself. A toolbox (or several toolboxes) can be used for assorted equipment such as tools, miscellaneous screws and nuts and bolts; suffice it to say that duct tape is always useful. The toolbox can have mounting wax, superglue, dental cement and other mounting equipment such as a hot glue gun and glue sticks. Spare cables, BNC connectors, BNC to microdot connectors and so on should also be in the toolbox. Also, a collection of items found in the drawers back in the lab that are always used would seem to be in order. Toolboxes can be used to step on or sit on some cases; stackable cases are also useful, as are roller-toolboxes. A toolbox is an essential part of the equipment used and helps maintain an organized test. Figure 10.2 shows an acquisition system on a cart in the lab along with some good replacements for when testing is to be performed at a remote

Figure 10.2 Possible gear for portable testing.

location. A general equipment checklist is very useful to make sure everything in packed for the test; a typical checklist is shown in Table 10.1.

A foldable desk and chair are useful for the setup of the test equipment. And in some cases, hard hats and harnesses may be required for testing larger structures. When testing large structures, there are many times that the test team may be separated by a distance that makes a walkie-talkie very useful for communications between the team members. And the ability to extend the computer display to remote locations is also useful; setting up a video meeting over the web is one way to share the data acquisition screen to all involved in the test. Figure 10.3 shows a remote table setup for computer work, a cart for the data acquisition system and the testing of a structure that is large enough to make walkie-talkies essential. Another important item is to make sure everyone knows their role:– acquisition setup, impact tester, logbook note taker, and so on. And it is critical that there be a leader to the team to orchestrate the entire test.

Often when a test is critical or the window of opportunity is limited, all the data acquisition administrative data can be set up prior to the test. In some respects, this can be a dress rehearsal, performed prior to leaving for the test site. This approach has always proved to be beneficial and highlight any issues before the actual test is started at the test site. Often, the structure geometry and channel information can all be logged before the team leaves for the test site. For instance, when there is a large number of data acquisition channels, some time is required to enter all the specific information. Table 10.2 shows an excerpt of a spreadsheet of important information in regards to the test of a larger structure.

Of course, there is also a significant amount of detail in regards to the data acquisition system setup; some of this information is included with the previous list but other information – related to test point transducer and sensitivities along with the channel voltage setting – is very important to document. A typical list for a larger modal test is shown in Table 10.3; note that this is all information that can be prepared ahead of the actual test date.

Organization prior to arriving at the test site really helps to address critical items at the test lab. The structure may often already be setup in a particular test configuration (suspended, fixture, etc) as the test team arrives at the test site. The test may require adjusting some of the

Table 10.1 Checklist for necessary equipment for remote testing.

Equipment List for Wind Turbine Testing							
	Check 1			**Check 1**			**Check 1**
Spare Accels			Duct Tape			Accel Level (Structcel Kit)	
BNC Cable (75 Ft)			Tape			Aluminum mounting shims	
Extra BNC cables			Blue books			Cable Ties	
BNC adaptors			Test Sheets			Hot Glue Gun + Sticks	
SCADAS both			Wrenches			Dry Erase Marker	
Laptops (3)			Tape Measure (25 Ft)			Adhesive Labels	
Computer Mouse			Super Glue			Sharpies	
Keyboard			Long Extension Chord			Pliers	
Monitor w/cable			Spare Memory Stick			Screwdrivers	
Big sledge			Handheld Calibrator			Accel Pads	
Small sledge			Sandpaper			ICP Conditioner	
Power Strips			Walkie Talkies			Triax Cables	
Extension Chords			Scissors			Harnesses	
Camera			Wax			Helmets	
Camera Batteries			Lazer Pointer			Safety Glasses	

Figure 10.3 Test lab portable chair/desk, ADC cart and large test situation.

test configurations, especially if the test is to mimic a free–free condition. While the test team starts to lay out all the transducers and cables, a second portable data acquisition system is always useful to make any unscheduled frequency response measurements. The portable system allows for collection of several different drive point measurements over the structure to get a feel for the frequencies and response. These are critical, especially if there is no prior knowledge or information regarding the structure. While it seems very unusual, often customers will not share any information regarding the structure or any of the expected dynamic information; at times, there have been detailed finite element models that customers have refused to share. In these situations, the conduct of the test is more difficult and it is critical that preliminary measurements are reviewed very carefully. With a lack of information, there is always the danger that the reference points for the modal test may not be selected in an optimal fashion. When this is the case, a very abbreviated modal test with only a very few measurements should normally be conducted first to make sure that the anticipated modes can be extracted from a

Table 10.2 Typical equipment list for a sample modal test.

Quantity	Equipment Type	Description	Manufacturer	Model #	Serial #	Sensitivity		Units
1	Computer	Laptop	Dell	Latitude D630	D3L5GG1	–		–
1	Data Acquisition System	48 Channel System	LMS	SC316	41011101	–		–
1	Software	LMS Test.Lab 10A	LMS	–	–	–		–
3	ICP Signal Conditioner	16 Channel, 50-pin input, BNC output	PCB	584 A	600 A	–		–
					601 A	–		–
					805	–		–
4	DB 50 Ribbon Cable	100-ft, 50-pin to 50-pin	PCB	009H100	–	–		–
40	BNC Cable	10-ft, BNC to BNC	TMS	003D10	–	–		–
2	BNC Extension Cable	100-ft, BNC to BNC	TMS	012A100	–	–		–
4	Patch Panel	16 Ch, BNC input, DB50 output	PCB	070C29	1922	–		–
					1630	–		–
					40557	–		–
3	Triaxial extension cable	20-ft, 4-Pin Jack to 4-Pin Plug	PCB	010AY020CA	–	–		–
20	Triaxial accel cable	30-ft, 4-Pin plug to 3-BNC Plug	PCB	078G30	–	–		–
1	Impact Hammer	Modal Sledge	PCB	086D50	23161	1.05		mV/1bf
1	Accelerometer	Triaxial accelerometer	PCB	T356M98	104009	(X)	980.42	mV/g
						(Z)	947.52	
1	Accelerometer	Triaxial accelerometer	PCB	T356M98	104010	(X)	966.55	mV/g
						(Z)	973.43	
1	Accelerometer	Triaxial accelerometer	PCB	T356M98	83168	(X)	995.43	mV/g
						(Z)	1013.52	
NOTE: Entire list not included for brevity								

Table 10.3 Channel/accelerometer information and channel voltage settings for impact test.

Pt.#	Direction	Channel	Serial	Sensitivity	Voltage Ranges at Reference (V)				
				(mV/g)	11:X	13:X	15:X	17:X	2:Z
1	X+	5	104009	980.4171	0.2	0.5	0.2	0.2	0.5
	Z+	6		947.5198	0.2	0.2	0.05	0.1	0.2
2	X+	7	104010	966.5479	0.2	0.5	0.2	0.2	0.5
	Z+	8		973.4251	0.1	0.2	0.2	0.5	0.2
3	X+	9	83168	995.4277	0.1	0.5	0.2	0.5	0.5
	Z+	10		1013.5176	0.1	0.2	0.1	0.2	0.2
4	X+	11	83169	1011.4053	0.1	0.2	0.2	0.5	0.2
	Z+	12		1007.5164	0.2	0.5	0.2	0.5	0.5
5	X+	13	83170	980.596	0.1	0.5	0.2	0.5	0.5
	Z+	14		1002.9363	0.05	0.1	0.1	0.1	0.1
Note: not all channels shown for brevity									
17	X+	37	102929	960.6447	0.5	1.0	0.5	1.0	1.0
	Z+	38		960.953	0.2	0.5	0.5	0.5	0.5
18	X+	39	102930	1049.7962	0.2	1.0	0.5	1.0	1.0
	Z+	40		980.8092	0.2	0.5	0.5	0.5	0.5
19	X+	41	102931	988.3263	0.5	1.0	0.5	1.0	1.0
	Z+	42		1019.6261	0.1	0.5	0.5	0.5	0.5
20	X+	43	102932	1009.0189	0.5	1.0	0.5	1.0	1.0
	Z+	44		1014.2949	0.5	1.0	0.5	2.0	1.0

small set of measurements. Acquiring a large set of measurements may not be a smart idea; a small set allows the test team to make sure that all issues for defining the test are properly done. Performing a very short test has proven to be a wise decision over the years, and is strongly advised, especially when testing a structure that is new or not fully understood.

Using the small portable data acquisition system also represents a benchmark for the expected frequency response measurements for the structure. As work progresses and cabling and transducers are mounted on the structure, additional measurements can be made to see if there is any time variance in the measurements on the system. In addition, the attachment of transducers and cables may have a mass effect on the measurements and can be determined with these measurements from the portable system.

While the test is being setup, photographs should be taken of transducer mounting locations as they are mounted if possible. Capturing the accelerometer model and serial number for instance provides useful information. In one test, a photograph was reviewed overnight and there was concern that two cables may have been swapped at one of the mounting locations; in fact this *was* the case and the error was corrected early the next morning as the team arrived at the test site. Organization of the entire test setup is very important, especially if there are any cabling issues. If there are only a handful of channels to wire, then problems that arise are generally easy to fix. But once the test starts to become very large, organization is a must. Figure 10.4 shows a test in which cable organization became a nightmare when several channels needed to be checked.

Now one general rule followed by this modal tester for many years involves the organization of accelerometers, channels, and point numbers on the structure. This rule has helped to avoid difficulties on large channel systems. Generally, the lower order serial number accelerometers

Figure 10.4 Test setup with a "rats nest" of cabling.

are used in sequentially increasing serial number, starting with the lowest channel numbers on the data acquisition system, which are assigned to the lowest geometric point numbers on the structure. While this may seem burdensome, the benefits have saved countless hours when having to retrace all the accelerometer cables at a test site. And organizing like accelerometer serial numbers in an increasing order in the accelerometer boxes is really not difficult; deploying them in increasing order for the data acquisition channels and following with the lowest geometric point numbers is not very difficult at all. If there is any confusion with the cabling, the tracing of the cables is then much easier. As a general rule, all the accelerometer serial numbers with channel number and geometric point number should be checked twice, and not by the same person who did the initial labeling and layout. This is also the perfect time to take the photos to document the entire test setup. And it is best to do this with two people, one reading out loud all the information to ensure this is all correct. This is also a perfect time to recheck that all connections are tight.

There may often be a full day of test setup: supporting the structure, mounting all the transducers on the structure, running all the cables, and organizing the entire test. If this is the case, there should always be a check that all the channels are live on the structure; a measurement should be made with the full acquisition system or with the portable system. If the testing is to not start at the end of the first day then upon returning in the morning, measurements should be made as soon as possible and compared with all the measurements made over the course of the previous day to see if there is any change in the structure or if the support system has had any appreciable changes overnight.

At the very start of the test, the first measurements should be checked for consistency. The time signals should be reviewed to ensure that there is no overload or saturation of the transducers. The input force spectrum should be assessed to make sure that the proper frequency range is adequately excited. The frequency response and coherence should be reviewed to make sure that a good measurement is made and that comparison to measurements made the previous day does not reveal any shifting in the frequencies for the structure. Often, the drive point measurements are reviewed first; it is not necessary to do them first but it does make the process simpler to do so.

At this point, the test would proceed with the measurements to be acquired for the test for the number of references that will be used to develop the frequency response matrix. As the test progresses, generally it is good practice to look at the time signals and spectra collected. Do not assume because the first measurements were good that there is no reason to look at the measurements as the test progresses.

The experimental modal test may take several hours to complete, depending on the number of measurement points and the type of data that is collected and if the structure is to be evaluated in different configurations. Suffice it to say that the test can become boring; after a while

Table 10.4 Initial spreadsheet showing measurements required.

		References Used			
		23x	23y	41x	41y
Measurement Points	1x				
	1y				
	1z				
	2x				
	2y				
	2z				
	113x				
	113y				
	113z				

the modal testers can become less focused. In order to keep them attentive to the test and to maintain proper documentation a few simple things should always be done during the modal test. Make a spreadsheet for all the points and directions and fill it in manually as each measurement is taken; this sheet should really already be part of the test plan for the test. Table 10.4 shows an example in which all the points (in the x-, y- and z-directions) are listed down the column. The references are all shown across the top row. At times, not all of the three directions may require data to be collected depending on the structure and the modes of the structure. In the table, only certain entries are shaded; these are the points and directions where measurements are to be made. The table is also useful for developing the master and slave degrees of freedom, used to determine the constraint relationships needed for the modal animation to complete the motion of the unmeasured points on the structure.

While the test is proceeding, the table should be updated as each and every measurement is made, to ensure the test group stays focused on the test and knows which is the next measurement to be acquired. This is extremely important when doing a roving hammer test, in which data from many points is to be collected. Boredom during these long tests can easily turn into an error: moving to the wrong point during the test and therefore mislabeling the measured points. Table 10.5 is from a test in progress, showing measurements yet to be made; it is good to reconfirm that certain points are not to be measured.

Of course, when all the testing is complete, the table can be used to check with the computer files saved to reconfirm that all measurements have been taken. Generally, reading out all the points and directions again ensures that the complete set of data has been collected. This is shown in Table 10.6. This is also a good quality control point to make sure that all the data has been obtained. While data should be backed up periodically as the test progresses, this is the time when a complete backup of the test data should be made. This virgin data set should never be modified or edited; only copied and then manipulated.

Before the test site is vacated, there must be a quick assessment of the data to make sure a good model can be derived from the data collected. Certainly, a quick peak pick of the data is one way to see if there are any problems with the data collected. All of the data points should follow a logical motion that appears to make sense. The lower order modes are the easiest to assess, along with the rigid body modes if the measurements are good at low frequencies; at

Table 10.5 Intermediate test spreadsheet showing measurements completed.

		References Used			
		23x	23y	41x	41y
Measurement Points	1x	☑	☑	☑	☑
	1y	☑	☑	☑	☑
	1z	☒	☒	☒	☒
	2x	☑	☑	☑	☑
	2y	☑	☑	☑	☑
	2z	☒	☒	☒	☒
	113x	☑	☑		
	113y	☑	☑		
	113z	☑	☑		

Table 10.6 Final spreadsheet showing all measurements obtained.

		References Used			
		23x	23y	41x	41y
Measurement Points	1x	🗁	🗁	🗁	🗁
	1y	🗁	🗁	🗁	🗁
	1z	☒	☒	☒	☒
	2x	🗁	🗁	🗁	🗁
	2y	🗁	🗁	🗁	🗁
	2z	☒	☒	☒	☒
	113x	🗁	🗁	🗁	🗁
	113y	🗁	🗁	🗁	🗁
	113z	🗁	🗁	🗁	🗁

times the region between the rigid body modes and flexible modes is also a good place to look to see if all the points are moving in a proper pattern. If time permits, a more detailed assessment of the data, with some actual curvefitting, should be performed: not a detailed data reduction but just a quick cut to see if there are any difficulties with the data. The modal participation matrix is another item to look at; this allows an assessment of whether the references selected are all useful for the majority of the modes of the system. Also, looking at the stability diagram and the consistency of the indication of the poles for the measurements is a strong indicator of the quality of the data collected. The data may need to be sifted in order to determine which references and which data are the best to identify the poles of the system. It is necessary to check if the data collected is sufficient for the intended purpose.

Table 10.7 Typical modal test report table of contents.

Table of contents

1.0 Introduction
1.1 Purpose of test
1.2 Scope of the report
1.3 Personnel involved in test and analysis efforts
2.0 Theoretical basis
2.1 Applicable modal theory
2.2 Applicable measurement theory
2.3 Typical impact measurement
2.4 Typical operating measurement
3.0 Data/results/remarks – Important tests/analyses performed
3.1 Modal test results
3.2 Frequency and damping variation study
3.3 Mass loading effects
Appendix A Equipment list
Appendix B Geometry
Appendix C Test photos
Appendix D Test plan
Appendix E Test sheets and logbooks
Appendix F Channel setup
Appendix G Drive point FRFs
Appendix H Stability diagrams
Appendix I Mode shapes
Appendix J Parameter variation assessment
Appendix K Universal file format

At this point, the test site can be vacated. The test data needs to be reduced to obtain the best model possible from the collected data. Generally, a number of different data reduction scenarios need to be performed, depending on the number of individual references obtained. Data can be reduced over narrow bands or wider bands, with different number of references, depending on the data. If all of the data tends to produce similar frequencies and mode shapes, there is good reason to believe that a good model has been developed. Of course, there are many tools to help assess the model overall; the MAC and function synthesis are the tools that help the most with determining the data quality.

Once the data has been reduced, the test report needs to be generated. All the information pertaining to the test needs to be well documented. Photographs, animations, test plan, logbooks, equipment lists, test results, curvefitting results, and data in native or universal format should all be part of the report. A typical table of contents is shown in Table 10.7.

10.2 FFT Analyzer Setup

10.2.1 General FFT Analyzer Setup

There is a wide assortment of FFT analyzers available for making measurements. Each analyzer will have some slight differences but in general there are a series of steps needed to set up almost any FFT analyzer. These steps are included here as a very general set of guidelines for setting up an FFT analyzer for making modal measurements.

Box 10.1 General analyzer setup

1) Pick the frequency range of interest (bandwidth).
2) Pick the number of lines of resolution (N).
3) Select the windows to apply on the data (if necessary).
   - Force/exponential windows are used mainly for impact testing situations especially where the response of the system does not decay to zero by the end of the time record of T seconds.
4) Select the number of averages desired for the measurement. Stable averaging is typically used for most experimental modal tests.
5) Select the analyzer triggering conditions. Channel 1 trigger is typically used for impact testing; the force transducer is connected to channel 1 of the analyzer. For most analyzers, a trigger voltage level is generally set at 15% of the input voltage.
6) The AC/DC coupling should be typically set to AC coupled, unless very low frequency data is to be collected.
7) Select the input voltage range settings
   - Use manual range setting for impact testing. Some analyzers can also be used with autorange feature to set up for impact testing, while with other analyzers this is difficult to accomplish and the manual setting is better. For most impact testing setups, a manual preview or timed preview is useful for viewing the time signals prior to accepting the measurement.
   - Set overload reject to ON for just about any measurement situation for the best possible measurements. Some analyzers also have an underload reject selection, which is useful for ensuring a minimum level.
8) Enter calibration units for all the transducers (transducer model and serial number) and appropriate channel labels where possible (force, acceleration, voltage).

10.2.2 Setup for Impact Testing

Impact testing is a very common testing technique. Each analyzer will have some slight differences but in general there are a series of steps needed to set up almost any FFT analyzer. These steps are included here as a very general set of guidelines for setting up the FFT analyzer for making impact measurements.

Box 10.2 Impact testing

General

1) Set up the input channel range settings for all channels (excitation and response).
2) Set up the bandwidth for initial measurements.

Hammer

3) Pre-trigger parameters.
   - Select pre-trigger delay for all channels to have the same value.
   - Usually a delay of 2–5% of the time record length is sufficient.
4) Select hammer tip.
   - Select a hammer tip to excite all frequencies over the bandwidth selected.
   - There shouldn't be any major force dropout over the frequency range of interest.
5) Window considerations.
   - A force window may be needed if the input signal is noisy.

Response

6) Window considerations.
   - The exponential damping window may need to be used if leakage is of concern.
7) FRF/coherence
   - The coherence should be close to unity at all frequencies, especially at resonances.

10.2.3 Setup for Shaker Testing

Shaker testing can be used for modal testing. Each analyzer will have some slight deviations but in general there are a series of steps needed to set up almost any FFT analyzer. These steps are included here as a very general set of guidelines for setting up the FFT analyzer for making shaker measurements.

Box 10.3 Shaker testing

General

1) Set up the input channel range settings for all channels (excitation and response).
2) Set up the bandwidth for initial measurements and set appropriate voltage ranges for all channels.

Shaker

3) Select excitation.
   - Random excitation is usually set for free run (no trigger).
   - Burst random, pseudo-random, sine chirp excitation are usually triggered from source
   - There shouldn't be any major force dropout over the frequency range of interest.
4) Window considerations.
   - Random excitation requires a Hanning window (or equivalent).
   - Other excitations typically used are intentionally designed to not require windows.

Response

5) Window considerations.
   - The same window used for the excitation should be used for the response.
6) FRF/Coherence
   - The coherence should be close to unity at all frequencies, especially at resonances.

10.3 Log Sheets

When performing any tests, a logbook should always be used. At times, it is helpful to have some standard sheets prepared with the majority of the data identified to ensure that all information is documented properly. Several sample sheets are included at the end of this chapter and are shown here as a snapshot in Figure 10.5.

10.4 Practical Considerations: Checklists

The following pages contain some checklists for some common test setup situations such as:

- Checklist for Analyzer Setup
- Checklist for Impact Testing
- Checklist for Shaker Testing
- Checklist for Measurement Adequacy
- Checklist for Miscellaneous Items

While not every possible scenario could possibly be considered, there are some very basic setup guidelines that are presented that are useful for experimental modal testing. On one hand, pre-defined lists removes the need to think about what needs to be done, but checklists are also useful to focus attention on what's important.

10.4.1 Checklist for Analyzer Setup

- Frequency range (bandwidth)
- Lines of resolution
- Windows
- Number/type of averages
- Trigger conditions
- Input channel settings
- Range settings
- Calibration units

There are a number of basic parameters that need to be set in order to acquire a basic measurement. This list will help with some of these parameters. Use this list as a guideline to set up most tests; it should suffice for most general test setups. If some of the nomenclature is unfamiliar, take a look at some of the information in the digital signal processing section.

Frequency range (bandwidth) Pick the frequency range of interest. Remember that the amount of time needed to acquire the data is inversely proportional to the bandwidth selected. Sometimes the bandwidth is specified as a lower frequency and frequency range or upper frequency; other times it is noted as a center frequency and a bandwidth about the center frequency. It depends on what analyzer is being used.

Lines of resolution Pick the number of lines of resolution (N). Remember that N determines the resolution in the time and frequency domain. The number of lines of resolution comes in powers of 2, for example 512, 1024, 2048, or 4096. Depending on the analyzer, all of the spectral lines may not be available due to aliasing, so the selection may be 400, 800, 1600, or 3200 lines. Remember that N determines the resolution in the time and frequency domains; there are twice as many points in the time domain because the frequency domain has complex valued numbers whereas the time domain is real valued.

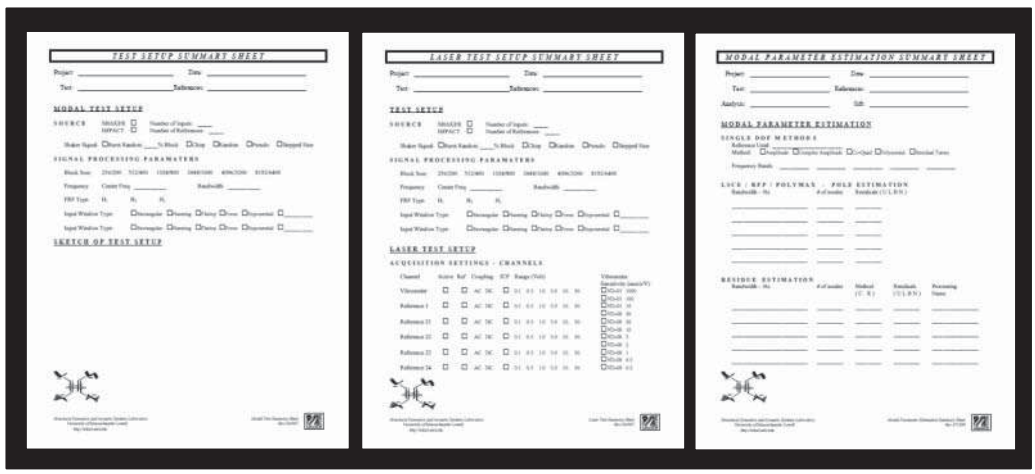

Figure 10.5 Sample of three forms for a logbook (full size samples are shown at the end of the chapter).

Windows While windows should be avoided at all costs, windows may be needed to minimize leakage of the signals. Use a rectangular window for signals that satisfy the periodicity requirement of the FFT. Use a Hanning window for signals that do not satisfy the periodicity requirement of the FFT. Use a flat top window for sinusoidal signals that do not satisfy the periodicity requirement of the FFT. Use the force/exponential windows for impact testing.

Select the windows to apply on the data (if necessary).

- A rectangular window (also called boxcar, uniform, or none) is used for signals that satisfy the periodicity requirement of the FFT process. Typical excitation signals that are used with the rectangular window are sine chirp, burst random, digital stepped sine and periodic discrete sine signals.
- A Hanning window is used for signals that *do not* satisfy the periodicity requirement of the FFT process. Typical excitation signals that are used with the Hanning window are random signals.
- A flat top window is used for discrete sinusoidal signals that *do not* satisfy the periodicity requirement of the FFT process. The flat top window is commonly used for calibration using discrete sine inputs.
- Force/exponential windows are used mainly for impact testing, especially where the response of the system does not decay to zero by the end of the time record of T seconds.

Number/type of averages Select the number of averages desired for the measurement. Stable averaging is typically used for most experimental modal tests; this type of averaging weights each of the measurements equally. The number of averages that are needed will depend on the system being measured. The general rule is that if the measured frequency response does not change appreciably between 10 and 20 averages and the coherence is acceptable, then 10 to 20 averages should suffice for the measurement. However, if the frequency response function shows variation after 20 averages, then more averages are needed.

Trigger conditions The triggering of the analyzer needs to be set. Typically use either free run, channel 1, or source to trigger the analyzer to start a measurement. A free run trigger is typically used for random signals. A channel 1 trigger is usually used for impact testing, where the impact hammer force transducer is hooked up to channel 1 on the analyzer. A source trigger is typically used when performing a shaker test with specialized input excitations where the source signal is fed from the analyzer to start the measurement process. Select the analyzer triggering conditions; either free run, channel 1, or source trigger.

- A free run trigger is typically used for random signals. Once the analyzer measurement is started, measurements will begin.
- A channel 1 trigger is typically used for impact testing where the force transducer is connected to channel 1 of the analyzer. For most analyzers, a trigger voltage level is generally set at approximately 15% of the input voltage.
- A source trigger is usually set when performing shaker excitations using signals that have a special character (such as burst random, sine chirp, and digital stepped sine) and where it is critical that the signal start at a particular time relative to the source signal.

Input channel settings There are several different options that may be selected for the input channels, such as ICP or voltage input mode, grounding or not, antialias filters on or not, and so on. One of the most important of these is the AC/DC coupling. Usually the channels are set to AC coupled unless very low frequency data is to be collected. The purpose of AC coupling is

to filter out any DC offset that exist in the signals. Some of the other settings are specific to the type of instrumentation being used and the measurements that are being made.

Voltage settings The voltage ranges for each channel must be set to appropriate values so that the analog to digital converter is optimized. Often, these ranges need to be manually set for impact testing and can at times be slightly frustrating. When performing shaker tests with the shaker running, it is easy to have the analyzer perform an autoranging operation to find the most appropriate level automatically. For almost any measurement, the overload reject switch should be turned on so that overloaded measurements are not accepted. Select the input voltage range settings:

- Use autorange for shaker excitation tests to set the input levels to appropriate levels. On some analyzers there is an autorange UP selection that is also useful in detecting spurious spikes in the data and setting the level correctly. Remember to change to autorange UP/DOWN if different levels are used.
- Use manual range setting for impact testing. Some analyzers can also be used with the autorange feature to set up for impact testing, while with other analyzers this is difficult to accomplish and manual is better. For most impact testing setups, a manual preview or timed preview is useful for viewing the time signals prior to accepting the measurement.
- Set overload reject to ON for just about any measurement situation for the best possible measurements.
- Some analyzers also have an underload reject selection, which is useful for ensuring a minimum level is obtained.

Calibration units This is fairly straightforward: calibration units for transducers need to be specified. Enter calibration units for all the transducers (transducer model and serial number) and appropriate channel labels where possible (force, acceleration, voltage).

10.4.2 Checklist for Impact Testing

General
- Range settings for channels
- Frequency range (bandwidth)

Hammer
- Pre-trigger settings
- Hammer tip selection
- Windows

Response
- Windows

FRF/coherence
- Measurement considerations

There are a number of basic parameters that need to be set in order to acquire measurements using the impact technique. This list will help with some of these. Use this list as a guideline to set up most impact tests; it should be a good starting point for most general test setups. If some of the nomenclature is unfamiliar to you, take a look at some of the information under the impact excitation section. In particular, take a look at the sequence of impact measurements collected to get an idea of the things to check when making an impact measurement.

General

Range settings for channels When performing impact tests, remember to change the range setting any time the measurement parameters are changed. The most important item is the change in the input–output location but changing the bandwidth and changing the impact

tip are also key points. Set up the input channel range settings for all channels (excitation and response). Remember anytime that the bandwidth is changed, or impact tip changed or input/output location is changed, the input channel range settings may need to be adjusted.

Frequency range (bandwidth) Set up the bandwidth for initial measurements. Anytime the bandwidth is changed, the impact tip may need to be changed and the range may need to be adjusted. When starting preliminary measurements, the bandwidth will often be changed to check for modes of the system. When the bandwidth is changed, the impact tip may need to be changed and the range settings may also need to be adjusted.

Hammer

Pre-trigger settings When impact testing, the pre-trigger delay needs to be set to be the same for all channels, otherwise a phase lag will result in the measurements. A pretrigger delay of 2–5% of the time block is usually sufficient. Some analyzers specify the pre-trigger delay in terms of an absolute time instead of percentage of the time record; make sure that you check the pretrigger delay as different bandwidths are selected and adjust the delay as necessary. Pre-trigger parameters are as follows:

- Select pre-trigger delay for all channels to have the *same* value.
- Usually a delay of 2–5% of the time record length is sufficient.
- If an absolute time is specified (rather than a percentage of the time record), then remember if the bandwidth is changed then the delay may need to be adjusted.

Hammer tip selection The hammer tip should excite all frequencies in the frequency range of interest so that adequate energy is imparted to the system and good coherence results. Double impacts can be seen in the input power spectrum by a non-flat spectrum; there shouldn't be any major force dropout at structural resonances. Select the hammer tip as follows:

- Select a hammer tip to excite all frequencies over the bandwidth selected.
- The hammer tip should produce a reasonably flat input power spectrum over all frequencies, with a force spectrum rolloff of no more than 10 to 20 to 30 dB by the upper frequency range of interest.
- There shouldn't be any major force dropout over the frequency range of interest.
- A non-flat input force spectrum is indicative of double impacts, improper tip selection, or local structure flexibility.

Windows A force window may be necessary if the input signal is noisy.

Response

Windows Use of the exponential damping window may be necessary for impact testing. Before using a window, try to change either the block size or the bandwidth in order to increase the record time length to allow the response to naturally decay to zero. Too much damping window will possibly cause smearing of closely spaced mode peaks and too little damping window will result in leakage. The damping window to be used should be just the right amount in order to minimize leakage. Window considerations are as follows.

- The exponential damping window may need to be used if leakage is of concern. Before a window is used, consider using a narrower bandwidth or consider more time or spectral lines of resolution or do both. The net effect is that the time record of data will be longer, allowing the response of the structure to naturally decay to zero. At worst it will still minimize the need for a heavy damping window to be applied.
- If the response dies out by the end of the sample interval, no window is needed because the signal is totally observed within the sample interval and satisfies the periodicity requirement of the FFT process.
- The damping window may need to be adjusted whenever the impact tip is changed or the bandwidth of the analyzer is changed.

- Too light a damping window (or no damping window) may result in leakage and distortion of the frequency response function.
- Too large a damping window may result in smearing of closely spaced modes such that they are difficult to see.
- The damping window (when necessary) should be selected to minimize the response of the signal by the end of the sample interval to satisfy the periodicity requirement of the FFT process.

FRF/coherence

Measurement considerations The coherence should be close to unity at all frequencies but there are some acceptable drops in the coherence especially at antiresonances.

- The coherence should be close to unity at all frequencies, especially at resonances.
- The coherence can drop at certain frequencies, especially antiresonances, and still be a good measurement.
- Poor coherence at higher frequencies can be the result of force spectrum roll-off due to the selected hammer tip or local structure flexibility.

10.4.3 Checklist for Shaker Testing

General

- Range settings for channels
- Frequency range - bandwidth - BW
- Windows

Excitation

- Triggering
- Shaker considerations

Response

- Signal considerations

FRF/coherence

- Measurement considerations

There are a number of basic parameters that need to be set in order to acquire measurements using the shaker excitation technique. This list will help with some of these. Use this list as a guideline to set up most tests: it should be a good starting point for most general test setups. If some of the nomenclature is unfamiliar to you, take a look at some of the information under the shaker excitation section; in particular, take a look at the sequence of shaker measurements collected to get an idea of the things to check when making shaker measurements.

General

Range settings for channels The ranges need to be set for all the input channels. Almost all analyzers have the ability to autorange the input signals and select appropriate settings for each channel. Usually a measurement should use 10–12 bits on a 12 bit analog to digital converter, 13–16 bits on a 16 bit analog to digital converter and 21–24 bits on a 24 bit analog to digital converter. Set up the input channel range settings for all channels (excitation and response). Autoranging can be used to easily set this up on most analyzers.

Frequency range (bandwidth) Set up the bandwidth for measurements. Pick an appropriate bandwidth for measurements. This depends on the objective of the test.

Windows While most modal tests can be conducted with excitation signals, such as burst random and sine chirp, that don't require windows and which are the preferable mode of testing, at times windows are necessary. Select the appropriate window. Try to use an excitation technique, such as burst random or sine chirp, that does not require the use of a window.

For other excitations, apply windows if necessary (for example, the Hanning window for random signals, the flat top window for calibration, and so on).

Excitation

Triggering Triggering of the analyzer will depend on the type of excitation used. Usually free run triggering is used for random signals and a source trigger is used for burst random, sine chirp, and other special excitation techniques. Select triggering parameters as follows:

- Free run trigger is typically used for random signals.
- Source trigger is usually set when performing shaker excitations using signals that have a special character (such as burst random, sine chirp, and digital stepped sine), where it is critical that the signal start at a particular time relative to the source signal.
- Pre-trigger delay is commonly used for burst random excitation to ensure that the excitation is totally observable within one sample interval of the analyzer. Usually only 1–2% of the time record is needed. At times, there is confusion with the "pre-trigger" and it is not clear if a minus should or should not be applied. This is easy to check, so as to make sure the pre-trigger is applied correctly.

Shaker considerations For most shaker testing, the excitation spectrum should be reasonably flat over the entire frequency range, with no significant force drop out at resonant frequencies. For burst random excitations, the burst is usually selected to be between 50 and 80% of the time record. Shaker considerations are as follows:

- For burst random testing, the excitation signal should only exist over a portion of the time record; typically this burst length is selected to be 50–80% of the time record.
- Check for a flat input power spectrum over the entire bandwidth.
- There should not be any significant force dropout over the frequency range of interest. Force dropout will usually occur at structural resonances due to the impedance mismatch between the shaker and structure; relocating the shaker to another location may minimize this problem.

Response

Signal considerations For burst random excitation, the most important consideration for the response is that the response signal must die to almost zero by the end of the time record or else leakage will exist. If the response does not die out by the end of the sample interval, then consider a shorter burst length. For other excitations, such as sine chirp, digital stepped sine, and pseudo random excitations, it is necessary to continuously play the excitation signal prior to starting the measurement so that the response of the system is at steady state such that no window is needed. For burst random excitation testing, it is very important to ensure that the response decays close to zero by the end of the sample interval or else leakage will occur.

- If the response does not die out by the end of the sample period then the input burst length should be shortened.
- If the response dies out much too quickly, then maybe consider using a longer input burst length.
- For sine chirp, digital stepped sine and pseudo-random, it is necessary to continuously play the signal prior to starting the measurement to ensure that steady state response is achieved or else leakage may exist.

FRF/coherence

Measurement considerations The coherence should be close to unity at all frequencies, but there are some acceptable drops in the coherence, especially at antiresonances.

- The coherence should be close to unity at all frequencies, especially at resonances.
- The coherence can drop at certain frequencies, especially antiresonances and still be a good measurement.

- The coherence will drop at resonant frequencies when using random excitation techniques, due to leakage and impedance mismatch problems; this is not acceptable.
- Poor coherence can be the result of force dropout at certain frequencies, or due to non-linearities in the system, or a number of other problems; this is not desirable.

10.4.4 Checklist for Measurement Adequacy

Poor coherence problems
- ADC optimized
- Rattles
- Noisy background
- Transducer settings
- Transducer sensitivity

Coherence: dropout
- Antiresonances
- Higher frequencies

FRF: considerations
- Clean FRFs
- Don't settle
- Noisy measurements

FRF: other considerations
- High frequency dropoff
- Dropout
- Transducer adequacy

There are a number of basic parameters that need to be set in order to assess your measurement adequacy. This list will help with some of these. Use this list as a guideline to assess measurements; it should be a good starting point for most general test setups. If some of the nomenclature is unfamiliar to you, take a look at some of the information under the digital signal processing and excitation sections.

Poor coherence problems

ADC optimized Check the input channels to ensure that the analog to digital converter is properly set. Possibly the analog to digital converter is not set to proper levels. Try to change the analog to digital converter to a lower setting to see if overload occurs. Try autoranging again to see if a better measurement can be made.

Rattles Check for rattles and other noisy components. At times, there may be some components that cause noise and rattles in the system. This can result in a poor measurement. Try to isolate where the rattles come from and try to minimize or eliminate the problem.

Noisy background Check for noisy signals in the background. If measurements are acquired in a noisy environment, then the coherence of the measurement may not be acceptable. In order to ensure that a good measurement is obtained, more averaging is then needed.

Transducer settings Check to make sure that the proper transducer settings are used (ICP, voltage, charge). Often an inappropriate instrumentation setting is selected for the analyzer. For instance, the input may be from an ICP type accelerometer but the analyzer is set on voltage or charge mode for the input signal. Make sure the proper settings are set.

Transducer sensitivity Check to make sure that the transducer sensitivity is sufficient for the measurement. If the measurement device is not sensitive enough to sense the force or motion of the system, a good measurement may not be possible. Try a more sensitive device to make your measurement.

Coherence: dropout

Antiresonances The coherence can have drop-off at certain frequencies and still be a good measurement; this is especially true at antiresonances, where there is no output response. Remember that an antiresonance is a frequency at which the structure appears to be very stiff and has essentially no output. If the system has no output, all of the measured response is from something other than the input excitation and therefore the coherence should be low.

Higher frequencies The coherence can have drop-off at certain frequencies and still be a good measurement, especially at higher frequencies where the modes may not be of interest. If the coherence drops at higher frequencies and is not of concern with frequencies in this range, then the measurement may still be acceptable; this is especially true with impact testing, where the input force spectrum always rolls off at higher frequencies.

FRF: considerations

Clean FRFs The measurements acquired should be good, clean measurements. Everything possible must be done to obtain the best measurements. These measurements will be used in the curvefitting process; if the measurement doesn't look like the analytical representation used to estimate the parameters, the answers will be corrupt. The frequency response functions measured should be good clean measurements. Remember that these frequency response functions will be used in a mathematical procedure to extract frequency, damping, and residues.

Don't settle Don't settle on just any old measurements; strive to make the best measurements using all the tools at your disposal. Again, remember that these frequency response functions will be used in a mathematical procedure to extract frequency, damping, and residues.

Noisy measurements Noisy, poor frequency response functions may be acceptable for a quick assessment of the problem at hand but are not acceptable when developing a high fidelity dynamic model. If the goal is just to try to get a baseline assessment of a vibration problem, then rough measurements may serve the purpose, especially if additional better data is to be collected.

FRF: other considerations

High frequency dropoff If the frequency response function is poor at higher frequencies only, check the input power spectrum to make sure that adequate energy is imparted to all frequencies; change the shaker input frequency range for shaker testing or the impact tip when impact testing. The frequency response function is often poor only at higher frequencies. This often happens when performing an impact test and the impact tip only excites a portion of the frequency range or when shaker testing and only part of the frequency range is excited. There is nothing wrong with this, provided that the modes of interest in the lower frequency range are adequately excited and are the only modes of interest. However, if the higher frequency range is of interest, the input force spectrum needs to be adjusted by changing the impact tip or adjusting the shaker excitation signal.

Dropout If the frequency response function is poor at the resonant frequencies, check for force dropout due to impedance mismatch or leakage in random testing with shaker excitation or check for double impacts or local structure flexibility problems when impact testing. Double impacts are difficult to avoid at times, and using a different tip or different impact location may possibly correct the problem. Shaker impedance mismatch might be corrected by locating the shaker at a different location, where the mismatch is not as severe. Unfortunately, leakage from random testing is impossible to avoid; the only remedy is to use a different excitation technique.

Transducer adequacy If the frequency response function is poor at low frequencies only, check for the adequacy of the transducer for low frequency application. At times the transducer used is not adequate for low frequency signals. In this case a better low frequency

accelerometer may be needed. At other times, low frequency signals are overpowered by the higher frequency content of the signal; this will result in quantization error. Try a narrower frequency range that just looks at the lower frequency range to see if a better measurement can be obtained.

10.4.5 Checklist for Miscellaneous

Linearity check
- Use deterministic signal
- Double force
- Peripheral equipment
- Rattle & noise
- It is non-linear
- Test at operating level
- Not all modes are non-linear
- Geometric location

Reciprocity check
- Basic requirement
- Roving mass
- SISO vs MIMO
- Non-linear?

Free–free testing
- Separation
- Double bungees

Mass loading effects
- Roving mass
- Lower mass
- Piggy-back

Repeatability checks
- Yesterday - Today
- Take it off - Put it on
- Individuals

Other checks
- Turned on?
- Connections

There are a number of miscellaneous items that may need to be considered. Here is a list of some of the common ones that come to mind.

Linearity check

Use a deterministic signal Always check the linearity of your system. This can be done with a shaker excitation using a deterministic signal, such as sine chirp or digital stepped sine. To check for linearity of the system, use a deterministic excitation technique, such as sine chirp or digital stepped sine.

Double force To check for linearity of the system, double the input force. The frequency response function should be the same for a linear system. Check for the linearity of the system. This can be done with shaker excitation using a deterministic signal, such as sine chirp or digital stepped sine. Check the linearity by making measurements at different input force levels of excitation. The frequency response function should be the same for all the measurements if the system is linear.

Peripheral equipment At times, non-linearities occur in a measurement. If the non-linearity is due to some peripheral equipment that is not critical to the development of the modal model, consider removing the equipment or try to isolate/minimize the non-linear characteristic. If the equipment is not a necessary part of the objective of the test, try removing the equipment causing the problem or minimize the non-linear behavior by modifying the part causing the problem.

Rattle and noise If the non-linearity is due to rattles and noise, consider a non-deterministic excitation signal, such as burst random, to linearize some of the slight non-linearities that may exist in the structure. Non-linearities in measurements are a problem. If they result from rattles and loose components in the system, then try averaging with a non-deterministic signal, such as burst random, which may help to alleviate the problem.

It is non-linear Often the system under test is non-linear or at least some of the modes appear to be non-linear. If the system is non-linear, then some thought needs to be given to the fact that the theory of modal analysis is for linear systems. The results of the modal analysis performed may not be useful. Be very careful using these results.

Test at operating level At times, non-linearities occur in a measurement. If the system is not linear then maybe the modal test could be run at an operating force level. When a system is non-linear then one option would be to run the modal test at a force level that is somewhat similar to the actual operating force levels. Then the data extracted is somewhat representative of the structure, but only for that condition of excitation.

Not all modes are non-linear Just because one mode is non-linear, doesn't necessarily mean that all of the modes are non-linear. There are many cases where not all of the modes are extremely non-linear. If the modes of interest appear linear and one mode that is not of interest is non-linear, then maybe the results of the modal survey may still be useful.

Geometric location Non-linearities are very sensitive to geometric location and level of the input force. Non-linearities are very tricky. The effects of non-linearities are extremely sensitive to geometric location of the input force. Depending on where the force is applied on the structure will have an important impact on the non-linearity of the system. Be very careful using the data if the system is non-linear.

Reciprocity check

Basic requirement Always check the reciprocity of your system. There should be reciprocity in your system. If there isn't, check why. Reciprocity in the measurements is a basic requirement from the theory of modal analysis being invoked.

Roving mass There can be a problem with reciprocity when using a roving mass on the structure. The use of low mass accelerometers or dummy masses may help alleviate the problem. Check for reciprocity. If there is a problem with roving accelerometer mass on the structure, consider using low mass accelerometers or use dummy masses for all measurement points to obtain consistent data.

SISO vs MIMO If there is a problem with shaker stinger stiffnesses when performing single input excitation testing procedures to acquire multiple reference data, consider using multiple input–output testing procedures to obtain consistent data. Often data is collected using multiple reference shaker test data using many single input excitation tests. Due to shaker mass loading, stinger stiffness, and other considerations, reciprocity of the different tests cannot be guaranteed. This can pose a problem when extracting modal data using multiple reference algorithms. MIMO testing helps alleviate this problem.

Non-linearities Check for the system linearity. If the system is non-linear, then there will be difficulty in showing the reciprocity. Address the non-linearity first, because time may be wasted checking reciprocity if the system is non-linear.

Free–free testing

Separation When performing free–free testing, the structure should be supported such that the rigid body modes and flexible modes are far spaced relative to each other. In other words the effects of the rigid body mode frequencies should not be dynamically coupled to the flexible modes.

Double Bungees When performing free–free testing, if the structure test support stiffness is changed, there should not be an appreciable change in the flexible modes of the system. Try doubling the support stiffness (use twice as many bungees for instance) and check to see if the frequency response function of the flexible modes changes significantly. To check how dynamically coupled the rigid body modes and flexible are, try doubling or halving the suspension support stiffness and see if the flexible mode frequencies are affected by the change. If they are, the rigid body modes are not adequately decoupled from the flexible modes and the free–free conditions need to be re-evaluated. It may not be a problem, but it should be checked and documented.

Mass loading effects

Roving mass When making a measurement, the frequency response function should not change significantly due to the mass of the response accelerometer. There should not be a significant change in the measurement of the frequency response function when the mass of the accelerometer is moved from one location to the next. If the measurement changes then some care needs to be exercised when extracting modal parameters and more sophisticated extraction techniques, such as global or polyreference curvefitting, may produce confusing results.

Lower mass If the frequency response function changes as the mass of the accelerometer moves from one location to another, a low mass accelerometer may be needed. Alternatively, mount dummy masses throughout the structure at all measurement locations so that a consistent set of measurements can be obtained.

Piggy-back The simplest way to check for mass loading is to piggy-back two accelerometers at one location and check the difference in the frequency response function with and without the two accelerometers; the frequency response function should be basically the same.

Repeatability checks

Yesterday to today The measurements should be repeatable. The frequency response function should not change over time. Make a measurement today and check it against one made yesterday. They should be the same. Measurements made yesterday should look the same as ones collected today for the system to be time invariant. If they are not the same, then which modal model is the correct one to describe the system? The one made yesterday or the one made today?

Take it off, put it on The measurements should be repeatable. Mount an accelerometer on a structure and take a measurement; remove the accelerometer and re-mount it, take another measurement and compare to check to see how repeatable the mounting process is.

Individuals The measurements should be repeatable. Have several people in the lab make the same measurement to see how repeatable the procedure is for making measurements depending on who makes the measurement. Now while the tester may prove that the tester can repeat a measurement, how about when different people are involved in the same modal test. How repeatable is everyone who is involved in making measurement? Check it out.

Other checks

Turned on? Make sure the amplifiers and instrumentation are turned on. It sounds funny, but it happens all the time. People get involved in the details of making the measurement and forget to check the instrumentation.

Connections Check to make sure that all screw connections are tight for all cabling. The screw connections for microdot cabling can produce some very strange results when the cabling is not tightened correctly. It's more sensitive than you think.

10.5 Summary

This chapter provided some basic thoughts regarding the set up and manner of conducting a typical modal test. In addition, there were a variety of different checklists to help when performing a modal test. Many different measurement issues with the data acquisition system were also addressed.

Appendix: Logbook Forms

TEST SETUP SUMMARY SHEET

Structural Dynamics and Acoustic Systems Laboratory
University of Massachusetts Lowell

Modal Test Summary Sheet
Rev 010507

Project: _____ Date: _____

Test: _____ References: _____

MODAL TEST SETUP

SOURCE SHAKER ☐ Number of inputs: _____

IMPACT ☐ Number of references: _____

Shaker signal: ☐Burst random _____% Block ☐Chirp ☐Random ☐Pseudo ☐Stepped sine

SIGNAL PROCESSING PARAMATERS

Block size: 256/200 512/400 1024/800 2048/1 600 4096/3200 8192/6400

Frequency Center freq _____ Bandwidth _____

FRF Type H_1 H_2 H_v

Input window type: ☐Rectangular ☐Hanning ☐Flattop ☐Force ☐Exponential ☐_____

Output window type: ☐Rectangular ☐Hanning ☐Flattop ☐Force ☐Exponential ☐_____

SKETCH OF TEST SETUP

LASER TEST SETUP SUMMARY SHEET

Structural Dynamics and Acoustic Systems Laboratory
University of Massachusetts Lowell

Modal Test Summary Sheet
Rev 010507

Project: _____ Date: _____

Test: _____ References: _____

TEST SETUP

SOURCE Shaker ☐ Number of inputs: _____

impact ☐ Number of references: _____

Shaker signal: ☐Burst random _____% Block ☐ Chirp ☐ Random ☐ Pseudo ☐ Stepped sine

SIGNAL PROCESSING PARAMATERS

Block size: 256/200 512/400 1024/800 2048/1600 4096/3200 8192/6400

Frequency Center freq _____ Bandwidth _____

FRF Type H_1 H_2 H_v

Input window type: ☐ Rectangular ☐ Hanning ☐ Flattop ☐ Force ☐ Exponential ☐_____

Output window type: ☐ Rectangular ☐ Hanning ☐ Flattop ☐ Force ☐ Exponential ☐_____

LASER TEST SETUP ACQUISITION SETTINGS - CHANNELS

Channel	Active	Ref	Coupling	ICP	Range (Volt)	Vibrometer Sensitivity (mm/s/V)
Vibrometer	☐	☐	AC DC	☐	0.1 0.3 1.0 3.0 10. 30.	☐VD-03 1000 ☐VD-03 100
Reference 1	☐	☐	AC DC	☐	0.1 0.3 1.0 3.0 10. 30.	☐VD-03 10 ☐VD-08 50
Reference 21	☐	☐	AC DC	☐	0.1 0.3 1.0 3.0 10. 30.	☐VD-08 20 ☐VD-08 10
Reference 22	☐	☐	AC DC	☐	0.1 0.3 1.0 3.0 10. 30.	☐VD-08 5 ☐VD-08 2
Reference 23	☐	☐	AC DC	☐	0.1 0.3 1.0 3.0 10. 30.	☐VD-08 1 ☐VD-08 0.5
Reference 24	☐	☐	AC DC	☐	0.1 0.3 1.0 3.0 10. 30.	☐VD-08 0.2

MODAL PARAMETER ESTIMATION SUMMARY SHEET

Structural Dynamics and Acoustic Systems Laboratory
University of Massachusetts Lowell

Modal Test Summary Sheet
Rev 010507

Project: _____ Date: _____

Test: _____ References: _____

Analysis: _____ Sift: _____

MODAL PARAMETER ESTIMATION

SINGLE DOF METHODS

Reference used: _____

Method: ☐ Amplitude ☐ Complex Amplitude ☐ Co-Quad ☐ Polynomial ☐ Residual terms

Frequency bands _____ _____ _____ _____ _____

LSCE / RFP / POLYMAX - POLE ESTIMATION

Bandwidth – Hz	# of modes	Residuals (U L B N)
_____	_____	_____
_____	_____	_____
_____	_____	_____

RESIDUE ESTIMATION

Bandwidth – Hz	# of modes	Method (C R)	Residuals (U L B N)	Processing name
_____	_____	_____	_____	_____
_____	_____	_____	_____	_____
_____	_____	_____	_____	_____

11

Tips, Tricks, and Other Stuff

Over the years, there have been many different scenarios in which some special test was performed, or some gimmick was introduced to make a test easier, or some unique test was performed. Knowledge of these novelties may be useful when a certain test has some complications. The majority of this chapter has a wide assortment of tips, tricks, and other stuff that has been assembled here. Unfortunately, organization of all this material is very difficult. Some of the sections have similar material and are grouped together, but there is also a very wide assortment of miscellaneous topics that are difficult to organize and are presented in a scattered fashion. Hopefully all the material is useful in one way or another.

But before starting, a simple primer is used here to walk through a set of measurements for the simple 3DOF system that was discussed in an earlier chapter. Both impact measurements and shaker measurements are discussed to demonstrate all the information that is part of the frequency response matrix.

Modal Testing: A Practitioner's Guide, First Edition. Peter Avitabile.

Companion Website: www.wiley.com/go/avitabile/modal-testing

11.1 Modal Testing Primer

Let's step through a simple example to see how to acquire data and some things that may be of concern for modal testing. Measurements will be described from an impact test and then from a shaker test to show the differences in these two test techniques.

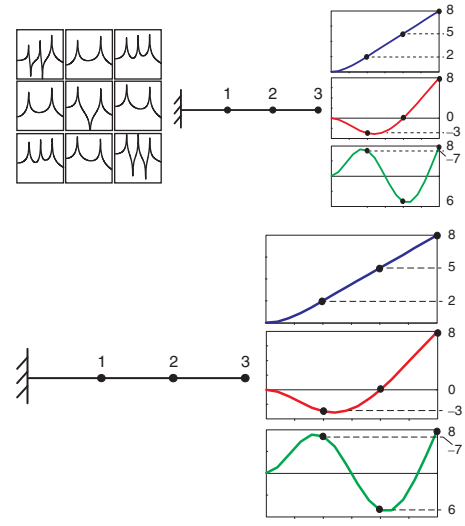

Let's take a look at a cantilever beam with three measurement locations. And let's just say for argument purposes that the points are numbered 1, 2, 3 from left to right so that point 3 is at the tip of the beam. Considering all the possible combinations of input locations and output locations, then there are nine possible measurements that could be made: three inputs times three outputs. Let's look at the measurements that could be made by first considering an impact testing situation and then by considering a shaker testing situation.

11.1.1 Impact Setup

The first measurement is made by impacting the beam at point 3 and measuring the response of the beam at point 3. This is called the H_{33} frequency response function; it's the output at 3 due to an input at 3. This is also a special measurement referred to as a drive point measurement: it's where the input and response are measured at the same location. Notice that there are three resonant peaks separated by anti-resonances, which is characteristic of a drive point measurement.

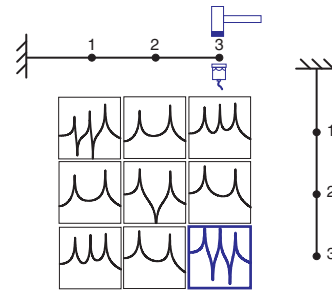

Now let's impact the beam at point 2 and measure the response of the beam at point 3. This is the H_{32} frequency response function; it is the output at 3 due to an input at 2. The accelerometer remains at point 3, which is called the reference location. Notice that there are only 2 resonant peaks. This is because the second measurement location is located at the node of the second mode, which has no response at this particular measurement location.

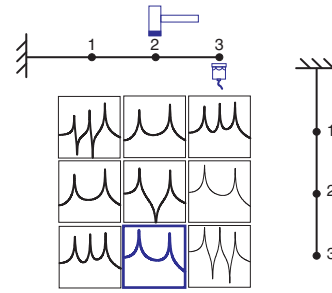

Now let's impact the beam at point 1 and measure the response of the beam at point 3. This is the H_{31} frequency response function; it's the output at 3 due to an input at 1. The accelerometer again remains at point 3, which is the reference location. Notice that there are three resonant peaks again, because all three modes are activated at this input–output location.

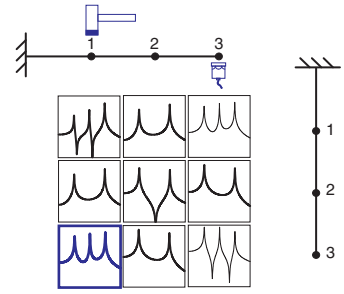

When an impact test is conducted, usually the hammer "roves" around the structure to all the measurement locations, with one fixed response location, which is the reference for all the measurements. So the measurements made are H_{31}, H_{32}, and H_{33}, which corresponds to a row of the frequency response function matrix. In this case, it is row 3.

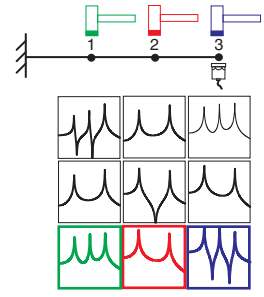

11.1.2 Shaker Setup

The first measurement is made by shaking the beam at point 3 and measuring the response of the beam at point 3. This is called the H_{33} frequency response function; it's the output at 3 due to an input at 3. We also recognize this as a special measurement, referred to as a drive point measurement; it's where the input and response are measured at the same location. Notice that there are three resonant peaks separated by anti-resonances; which is characteristic of a drive point measurement.

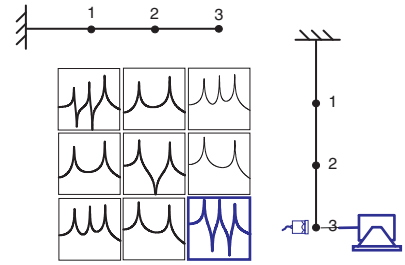

Now let's shake the beam at point 3 and measure the response of the beam at point 2. This is the H_{23} frequency response function; it is the output at 2 due to an input at 3. The shaker remains at point 3, which is called the reference location. Notice that there are only two resonant peaks; this is because the second measurement location is located at the node of the second mode, which has no response at this particular measurement location.

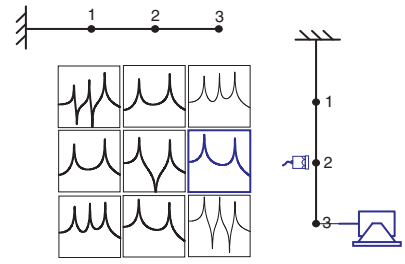

Now let's shake the beam at point 3 and measure the response of the beam at point 1. This is the H_{13} frequency response function; it is the output at 1 due to an input at 3. The shaker again remains at point 3, which is the reference location. Notice that there are three resonant peaks again because all three modes are activated at this input–output location.

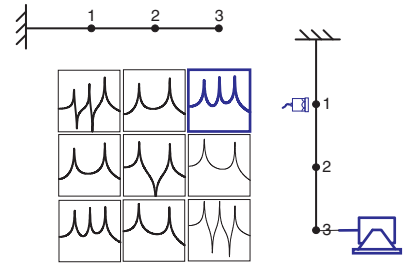

When a shaker test is run, usually the response transducer "roves" around the structure to all the measurement locations, with one fixed input location, which is the reference for all the measurements. So the measurements are H_{13}, H_{23}, and H_{33}, which is a column of the frequency response function matrix. Now the response transducer may actually be moved from one measurement location to the next location. Or if a multiple channel acquisition system is available, then all of the response transducers could be measured simultaneously.

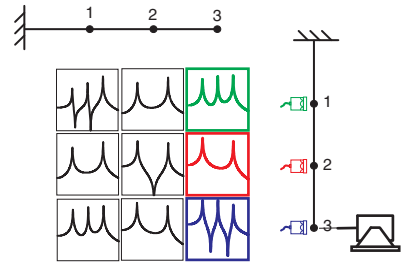

11.1.3 Drive Point Measurements

Notice that for this cantilever beam there are three possible drive point locations at which to take measurements. The H_{11} drive point measurement is shown in green, the H_{22} drive point measurement in red, and the H_{33} drive point measurement in blue. Notice that all the drive point measurements have the same characteristic, namely that the resonances are separated by antiresonances.

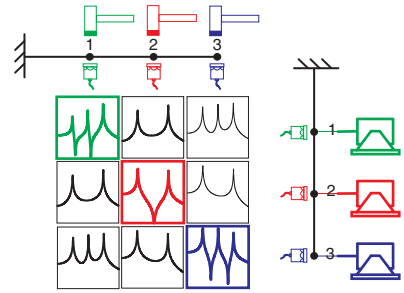

11.1.4 Reciprocity

Another very important characteristic of the frequency response function matrix is that reciprocity must be true; that is $H_{ij} = H_{ji}$. Consider H_{23}, which is an impact at point 3 and the response at point 2, shown in blue. Also consider H_{32}, which is an impact at point 2 and the response at point 3, shown in red. Notice that these two measurements are exactly the same. They should be because of reciprocity.

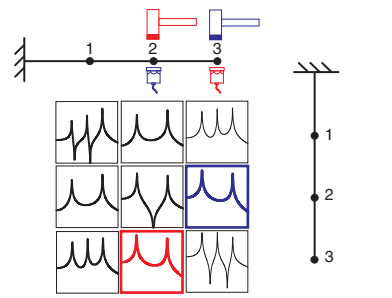

This is also true for a shaker measurement. Consider H_{23}, which is an excitation at point 3 and the response at point 2, shown in blue. Also consider H_{32}, which is an excitation at point 2 and the response at point 3, shown in red. Notice that these two measurements are also the same, as expected, due to reciprocity.

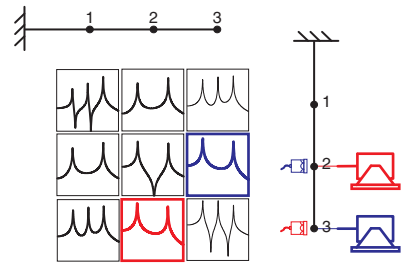

So all the off-diagonal terms satisfy reciprocity for the corresponding "ij" locations. Modal theory tells us that this must be true and should be seen in the measurements collected on an actual structure. Of course, there may be some practical situations where reciprocity may not hold true in a test situation.

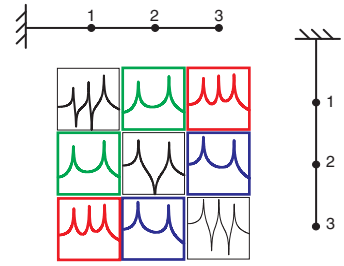

11.1.5 Inappropriate Reference Location

Now if a reference point is selected to be the node of the second mode, point 2 for this cantilever example, then whether an impact test with the stationary accelerometer at point 2 or a shaker test with the excitation at point 2 was conducted, the row or column of the frequency response function matrix will not contain any information pertaining to mode 2 because the reference is located at the node of the mode. The measurement would never have any of the characteristics of the second mode of the system and the frequency response measurement would miss this mode in the modal model. It is very important to select this reference location appropriately. Sometimes it is impossible to adequately see all of the modes of the system from one reference location. Even though theory indicates that only one row or column of the frequency response function matrix is necessary to extract all of the modes of the system, there are some exceptions to this rule, as seen here. This is why multiple reference testing is often performed.

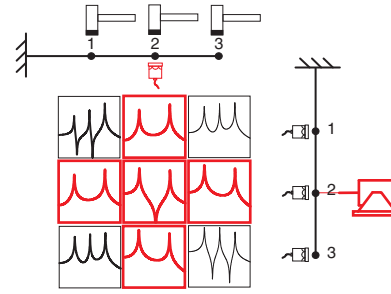

11.1.6 Multiple-input, Multiple-output Testing

There are many times when it is advantageous to perform a modal test with multiple inputs applied to the structure. These tests are often conducted on larger structures to help better distribute energy throughout the structure. This should give better measurements but also may be done to provide redundant data in the frequency response function matrix. Notice that two input locations are shown here, and for three response locations, a total of six frequency response functions are measured, which corresponds to two columns of the frequency response function matrix. Notice that while the second mode from the reference at point 2 cannot be observed, the second mode from the reference at point 3 *can* be observed, so the possibility of missing a mode is minimized.

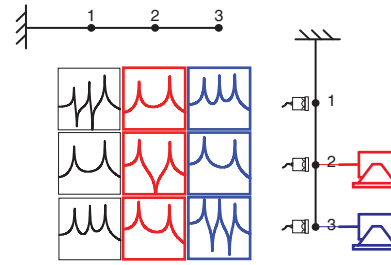

11.1.7 Multiple Reference Testing

While not truly the same as a multiple input test, multiple reference data can also be collected using an impact testing strategy. Several reference transducers can be placed on the structure (in this case two), and measurements can be collected by impacting all the points on the structure. For this scenario, two rows of the frequency response function matrix are measured.

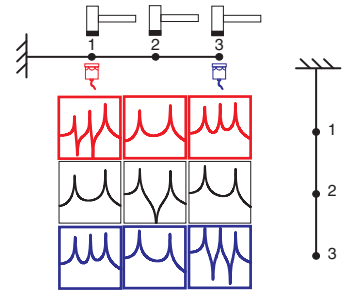

11.2 Impact Hammer and Impulsive Excitation

Impact test excitation is by far the most common and most popular for all the modal tests performed. This is a very useful technique for acquiring frequency response measurements. Probably more than 75–80% of all modal testing performed is done using the impact technique. Some thoughts, tips, and tricks related to impact testing are provided in this section.

11.2.1 The Right Hammer for the Test

There are many different sized hammers to accommodate the wide range of structures that may need to be tested. From very small impact hammers to larger sledgehammer designs, selecting the right hammer for the test is important. Using too small a hammer for a larger structure results in an inappropriate situation. But there have been countless times where hammers tips in test labs have been battered almost to destruction; clearly a larger hammer is needed if excessive force having to be applied to obtain a measurable response. A larger hammer is definitely needed. Similarly, there can be situations where too large a hammer is used to test a small structure and these result in poor measurements. A few different sized hammers are necessary depending on the range of structures typically tested. A selection of hammers is shown in Figure 11.1.

Figure 11.1 Assortment of commercially available impact hammers. Image courtesy of PCB Piezotronics, Inc.

11.2.2 Hammer – Get the Swing of it

There is actually an art to swinging an impact hammer. It certainly is not like driving nails in a construction project. The hammer should not be gripped too tightly in your hand. And the swinging action is really more a wrist action than arm swinging. The idea is to let the hammer do the work; the modal tester should not be aggressively hammering the structure. If the test engineer is using a large amount of effort and energy in swinging the hammer then for sure the wrong hammer is possibly being used and a larger hammer may be needed. Another concern is that often the structure is impacted and then the modal testers will be still moving the hammer about after the impact. The hammer should remain still after the impact so that any additional force from swinging the hammer is not captured by the force transducer. Try to get in the habit of not having the hammer moving after the impact is made.

11.2.3 Hammer Tripod

Often, when testing smaller structures, the ability to excite the same point consistently can be challenging. A simple tripod arrangement can be used to help with this common problem. The hammer can be inserted into a straw and then attached to a small swivel camera tripod. Figure 11.2 shows this arrangement. This very simple setup has proven to be very useful over the years and has allowed testers to make more consistent impacts as well as to hit the same point repeatedly. Figure 11.3 shows another configuration, in which a pendulum is used to provide impact force into the structure. This is useful for medium sized structures and can also be used on larger structures. Of course, a larger pendulum can be used for larger structures to impart more energy.

11.2.4 Hammer tip selection

Selecting the proper hammer tip can sometimes be confusing to the novice. Basically, what is needed is to make sure that a hammer tip is selected that will excite a frequency range similar to the range of frequencies that will be excited when the structure is in service. Of course, that

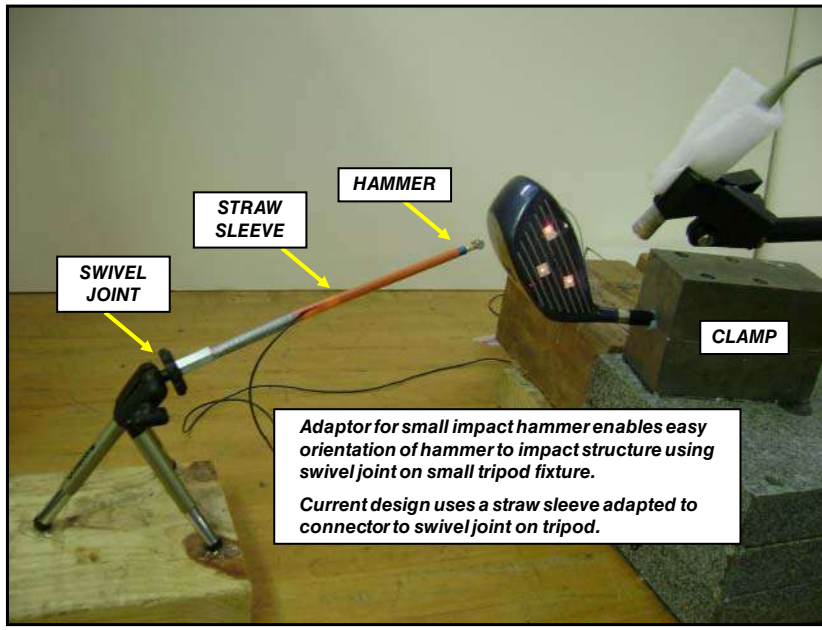

Figure 11.2 Small hammer configured with camera tripod.

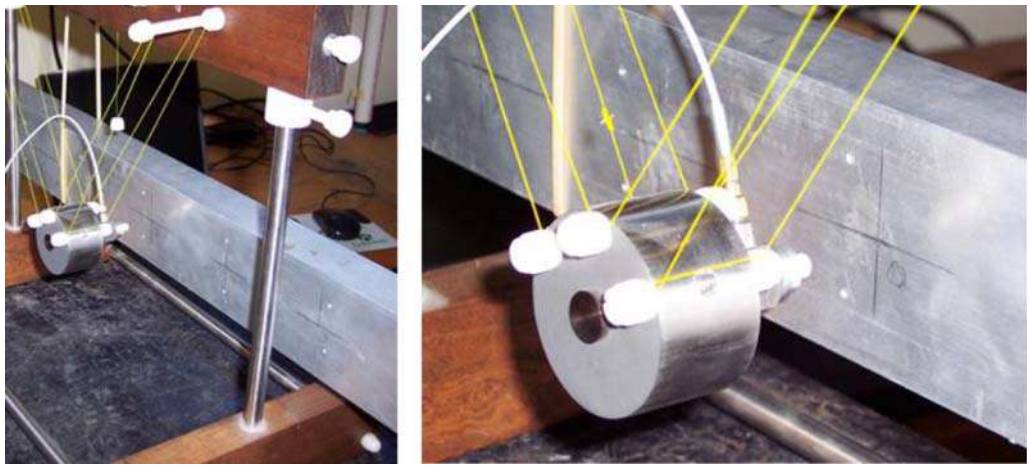

Figure 11.3 Pendulous mass configuration.

means that some idea of that frequency range is really important. Many years ago, there were some modal tests on baseball bats and there was a very long discussion as to what would be the best tip to use. Of course, a hammer tip that would excite a similar range of frequencies as those excited by the actual ball hitting the bat is needed. The next day in the lab the testers took a baseball and put a 10-32 tapped stud into the baseball and then screwed that onto the hammer. Of course, this was a brilliant idea because it is as close to the actual impact scenario for the ball hitting the bat as can be performed.

Often, the hammer tips provided may not provide the specific input force spectrum desired. It turns out that duct tape fixes everything, so it is often used with hammer tips. There are many different compositions of duct tape. A single piece on a hammer tip (or a few) will help to customize the input force spectrum to some degree. Several different types of duct tape should be in the lab with the hammer kits at all times.

But remember that the hammer tip is not the only thing that controls the input force spectrum. The local flexibility of the structure can also play a critical role in the actual force spectrum imparted into the structure for the modal test. This needs to be looked at closely. Note that the published curves received from the hammer manufacturer can be put aside because those are all generated by impacting a massive, stiff steel block, which is never what exists when performing a modal test.

11.2.5 No Hammer: Improvise

At times, there may not be access to a small hammer when testing smaller structures. In the early days of modal testing, a small ball bearing would be used with a straw to create a controlled input to the structure. The ball was dropped through the straw to create an impact that was consistent and repeatable. Variations of this approach are still useful today.

11.2.6 Pete's Hammer Test Impact Ritual

Every time I set up to perform an impact test, there is a ritual that I go through to make sure that I can make the best possible frequency response function measurements. There isn't a specific set of steps that I take every time I do this but there are certainly key things that I do every time I make a measurement. Of course, I am talking about taking a measurement on something that I have never tested before or something that is completely new to me; if it is a structure that I test

every day then maybe some of these steps will not be needed because I have apriori information that gives me a good understanding of what is expected.

So when I start a measurement I never take anything for granted. I start with a measurement with a frequency bandwidth that is higher than the frequency range that everyone "believes" is the frequency range of interest. I then use a hammer tip to excite the structure over this range of interest and I always check the input power force spectrum applied to the structure under test. Of course, while I make this first measurement, I may need to adjust the voltage level for the hammer input as well as the accelerometer responses. This may need to be done manually unless if the acquisition system has provision to "autorange" all of the response levels. Of course, at this point I may need to change the hammer tip to excite the appropriate frequency range of interest and then check to make sure that all the proper response ranges are still appropriate as the different hammer tips are studied.

Once I have a good input excitation then I will start to look at the response and frequency response function and coherence. But the first thing to do is to look at the response decay to see if the entire response can be captured within one time sample of the measurement. If this condition is satisfied, then we do not need to apply a window. If it is not satisfied, we may want to consider a longer time window. If this is not possible then we may need to apply a window, which in this case would be an exponentially decaying window.

Once this has been done, we would want to take several averages to look at the frequency response function and coherence. If this is an acceptable measurement then the next step would be to change the hammer tip to excite a slightly lower frequency range; remember that when I started this process, I selected a higher frequency range than what was prescribed for the test. This is a good opportunity to make sure that the hammer tip is actually exciting the frequency range of interest (because the frequency range is still set for the higher frequency range). But now that less input force is being applied to the structure, it is important to make sure that all the voltage ranges are still set properly, that the damping window, if originally used, is still necessary, along with other parameters set for the initial set of tests. Once this has all been checked then a measurement would be made to assess the frequency response function and coherence.

Then the frequency range of the FFT analyzer could be changed to the lower frequency range associated with the actual softer hammer tip excitation range of the last measurement. And again, all the same parameters would need to be checked to make sure that an appropriate level was set and that a good measurement was obtained. So, for the measurement process I have just described, you can see that all of the parameters need to be checked each time I change each and every one of the individual items that can change. Remember that I have the ability to change the bandwidth of the measurement, the number of spectral lines, the hammer tip, and the use of windows, if needed. All of these need to be considered when making the measurement. And I keep changing all these parameters until I am happy with the measurement that has been made. At this point I would start to collect sets of measurements for the experimental modal test.

11.3 Accelerometer Issues

There are several additional items of concern related to accelerometers and their use.

11.3.1 Mass Loading

Accelerometers come in many sizes and sensitivities. Often even a small accelerometer may mass load the structure and cause a downwards shift of the frequencies of the structure.

While the accelerometer weight may be very small in relation to the weight of the structure, the weight must be considered relative to the effective weight of the structure at the attachment point. One way to check this is to measure the structure with and without the accelerometer attached. But if the accelerometer is removed, the measurement cannot be made. One way to overcome this is to add another accelerometer right on top of the mounted accelerometer or on the opposite side of the structure to where the accelerometer is mounted. However, it does make a difference where the accelerometer is mounted and a check of this will be revealing.

If there is no appreciable shift in the peaks in the frequency response function then the mass loading effect is insignificant. If not, then the mass loading needs to be considered. If the modal test is for a correlation to a finite element model effort then it is a very easy task to add a lumped mass to the model at the nodal location of the accelerometer on the structure. At times, this mass inclusion can give marked improvements in the correlation and MAC values for the analysis.

11.3.2 Mass Loading Effects from Tri-axial Accelerometers

From time to time, there will be mass loading effects, especially when a very large channel count is used. If single axis accelerometers are available but a full 3D modal test needs to be performed, then one trick is to have mounting cubes mounted on the structure at all measurement locations. For instance, for the first test, all the accelerometers could be attached in the x direction only. Then all of the accelerometers could be switched to the y direction for the next test and then to the z direction for the third test. In this way, the mass of the accelerometer is relatively fixed in each of the three tests. This is a much better option than mounting tri-axial accelerometers to the structure at one-third of the locations and then roving them around the structure. The measurements are much better overall when this is done.

Mass loading can have a significant effect, especially when trying to reduce data. All too often when the curvefitting results are confusing or appear distorted, the effects will be blamed on noise or nonlinearities. This is often a "blanket statement" that people use when they don't understand or can't explain something easily. Let's look at why data consistency is important and what effects mass loading will have.

The first thing to recall is that the model used to fit data comes from a linear, symmetric set of equations where the poles (frequency and damping) are defined in terms of global quantities, and reciprocity is assumed to be inherent in the formulation of the equations. So long as the data fits that model then everything is OK. But how does the testing and data acquisition have an effect? Let's consider a simple plate test setup that is driven by two shakers for a MIMO test with an 8 channel data acquisition system. Frequency response measurements are acquired using good measurement techniques to ensure the best possible measurements. These are obtained for the six accelerometers mounted on the plate, as shown in Figure 11.4. The solid fill points are for the first test and the other points are associated with the second test and are obtained by roving the accelerometers on the structure.

The mode indicator function for the measurements acquired is shown in Figure 11.5, and the stability diagram is shown in Figure 11.6. The poles are extracted for the first two modes only, for illustration purposes. The stability diagram shows these two poles very clearly. Notice that as the order of the model increases, the poles are clearly identified (overlaid on the summation function). Once the poles are extracted, then the residues or mode shapes are obtained to provide modal data associated with these six measurement points; a typical curvefit is shown in Figure 11.7. However, this first set of data only consists of six measurement points. In order to better define the mode shapes, more measurement points are needed.

For the additional points, the accelerometers are relocated to the measurement points shown (the non-filled points) and a second set of MIMO measurements is collected. The poles are

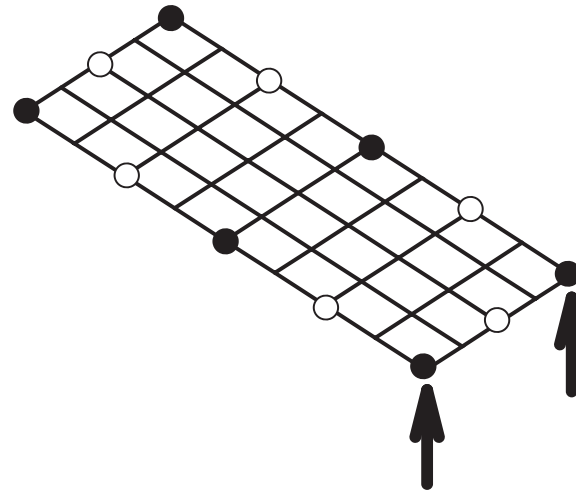

Figure 11.4 MIMO test setup with two sets of measurement points.

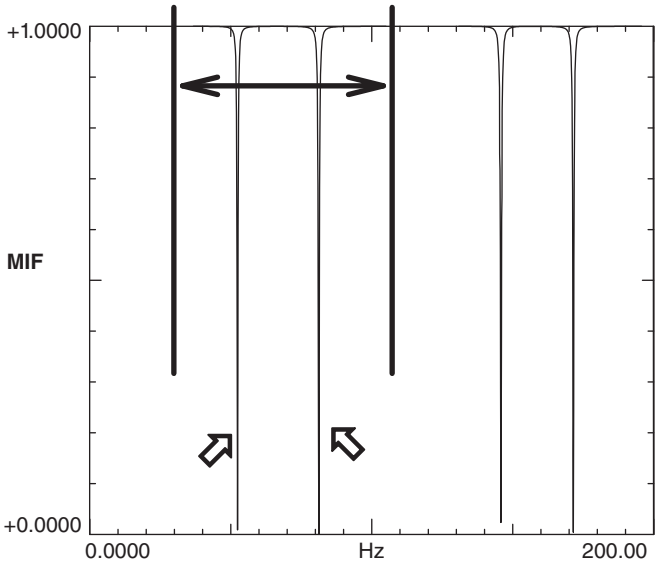

Figure 11.5 MIF for data from first test.

again extracted using just this second set of measurement points and a stability diagram is obtained. The poles are clearly identified and the mode shapes associated with these six points are identified. These results are not shown here but are similar to the first case. However, the two sets of data are evaluated separately to estimate the poles and residues.

Now let's combine the two datasets together and evaluate the data. The mode indicator function and stability diagram are computed again. Instead of two distinct peaks, as seen earlier in the MIF, there are now four distinct peaks over the same band (Figure 11.8). The estimation of the poles for the same frequency band (Figure 11.9) as used earlier now shows four modes instead of two modes. How could this possibly be? The plate didn't change, but the test setup did! The roving accelerometers have a mass effect that caused the modes to shift slightly. So when all the data is processed simultaneously, some of the measurements indicate the poles at a certain frequency and the other measurements indicate the poles at a different frequency.

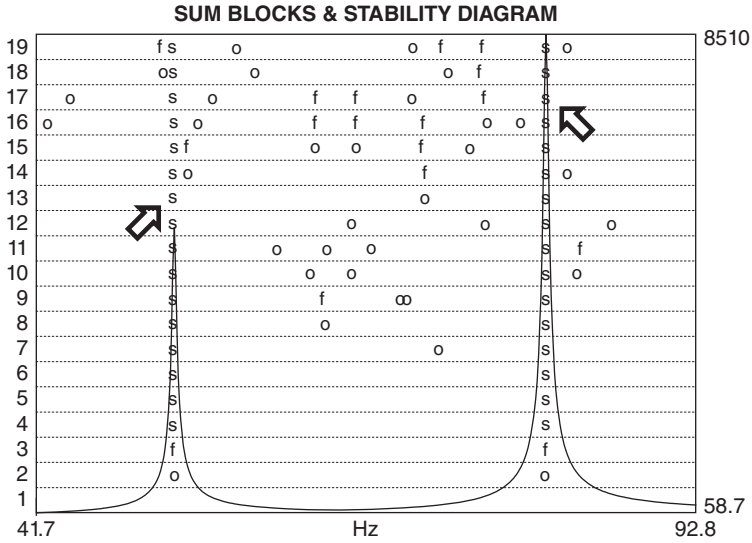

Figure 11.6 Stability diagram for data from first test.

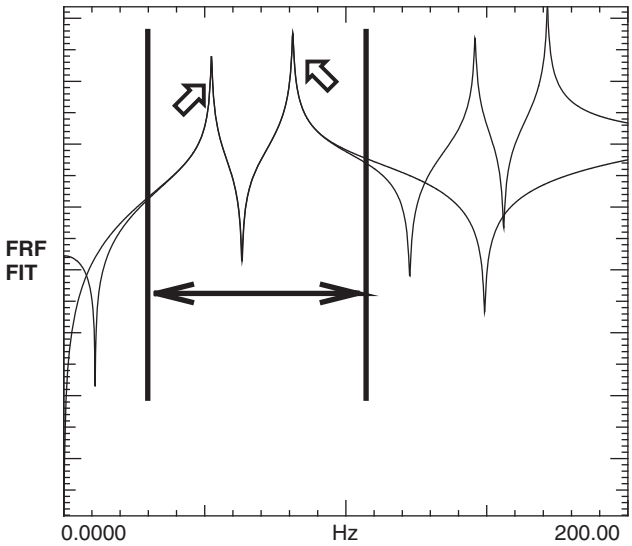

Figure 11.7 Typical curvefit from first test.

So which is correct? It is likely that neither is correct. That's because the test setup had an effect on the measured modes of the system. But which poles are the correct ones to be used for the modal parameter estimation process? You really can't identify a global set of poles for all the measurements because they are not "global" for all the measurements. The correct way to extract parameters in this case is to collect a "consistent" set of data by eliminating the mass loading effect by mounting all the instrumentation on the structure (or adding dummy masses) for the duration of the test. This will provide more "consistent" data that conforms to the model being used to fit the data. Of course, it is very important to point out that the structure is modified due to the addition of the masses. But at least all the data will be consistent and the modal parameter estimation process will not be distorted by mass loading effects.

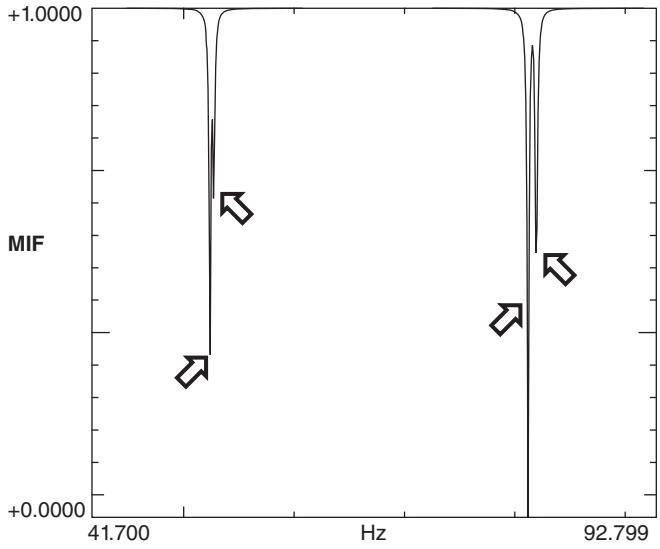

Figure 11.8 MIF for tests 1 and 2 combined.

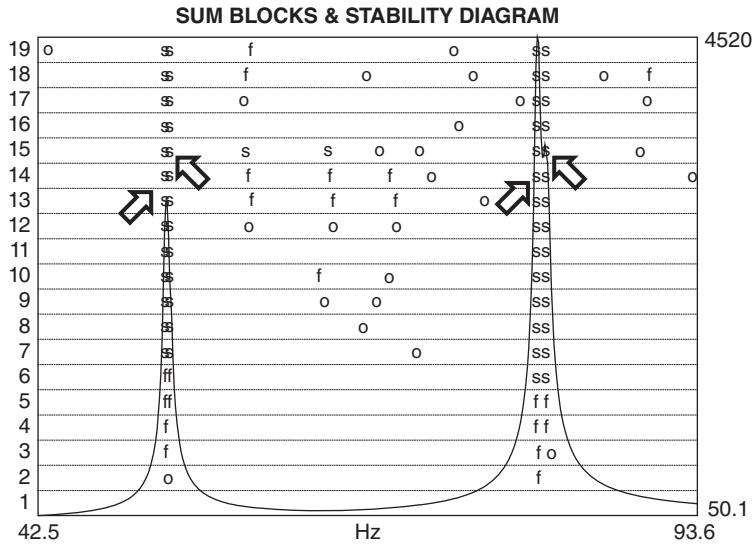

Figure 11.9 Stability diagram for tests 1 and 2 combined.

Of course, real world structures have all kinds of measurement problems with respect to noise, linearity, time variability, and so on. The modal parameter estimation process is complicated enough. Don't complicate the process further by letting simple items such as mass loading distort the data.

11.3.3 Accelerometer Sensitivity Selection

Often, the correct sensitivity of accelerometers to use is not known. The structure's response is often unknown because the damping is critical to identifying the response and is not easily known without a measurement. Often, people have purchased expensive, more sensitive

accelerometers to use for a test because the perception is that they are "better". But the reality is that if the structure is very responsive then either the front end of the data acquisition system may overload or the transducer may become saturated. Neither of these scenarios is good. There have been several times over the years where the original 100 mV/g accelerometers were very well suited for the test at hand and the newer, so called "better", 1000 mV/g accelerometers were not useful because the response of the structure only needed the 100 mV/g accelerometer.

The best way to circumvent this problem is to mount three accelerometers with different sensitivities on the structure and then take a preliminary measurement. Use 10 mV/g, 100 mV/g, and 1000 mV/g accelerometers mounted at the same location and make a measurement. One accelerometer may overload and one may underload and the third one may be "just right". There really is no way to determine which ahead of time. Of course, experience goes a long way and after running many, many tests, testers may develop an instinct as to which accelerometers may be best for the job. And in fact, if a test has been previously run on similar hardware, the data acquisition hardware settings showing the voltage settings for each channel are extremely useful for deciding on what accelerometer sensitivities are likely to be needed.

11.3.4 Tri-axial Accelerometers

Tri-axial accelerometers are good to have in a collection of transducers, but having only tri-axial accelerometers is not a good idea. While many structures have 3D motion, there are many instances where only a single direction or two directions will suffice. This needs to be discussed in a little more depth.

First, triaxial accelerometers are very useful in many, many applications. They allow for a very compact package to be used to monitor all three directions from one physical mounted transducer on a structure. Yes, they are used often, but as it turns out they are not used constantly and there are many cases where tri-axial accelerometers should not be used. The reasons for this are discussed here.

First of all, a tri-axial accelerometer can be made by mounting three separate accelerometers onto one mounting block. Now of course this is not as elegant as a tri-axial accelerometer, but it is one simple and economical way to accomplish the same thing. And, of course, it also means that three separate accelerometers can be purchased, at just about the same price as the tri-axial accelerometer. But remember that there is one different distinction. When the tri-axial accelerometer is mounted on the structure under test and it is only necessary to analyze one direction, then two accelerometers have been wasted for all practical purposes. And if someone else needs to make some measurements, three accelerometers are tied up in that one package for each measurement location, whether or not all three are necessary. Now if you had three separate accelerometers then you wouldn't be tying up all the accelerometer inventory! Now this may sound silly, but when you don't have a lot of accelerometers and all of them are tri-axial, then you may have tied up a lot of instrumentation when you really only needed a single axis accelerometer. Some laboratories that have bought only tri-axial accelerometers have found that when there are multiple tests to be run, all the instrumentation is tied up on one test.

So now let's discuss a few more things. Let's first start with a simple free–free beam test. To test a simple beam and find the modes in transverse bending in only one direction, we would have a test setup something like that shown in Figure 11.10, where there are 15 measurement locations along the length of the beam.

Now if all that was available was tri-axial accelerometers, then 45 measurement transducers would be tied up, while only 15 were actually needed for the measurement at hand. Now of

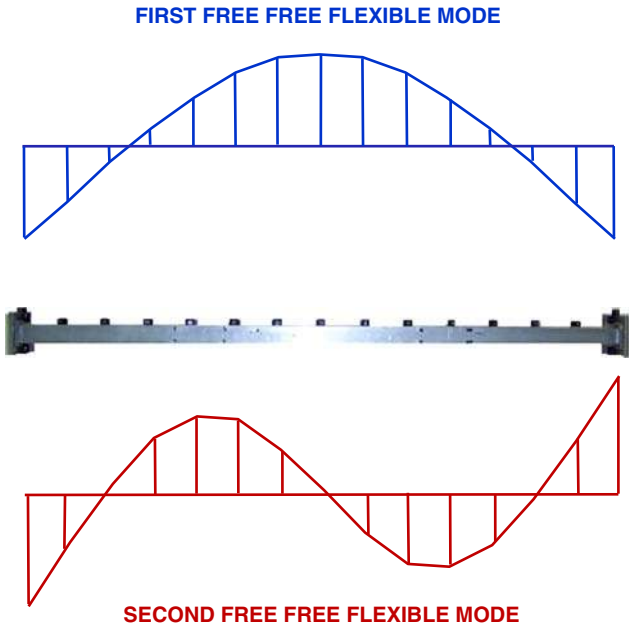

Figure 11.10 Schematic planar beam modal test.

course an argument can be made that there might be a need to also test the other planar beam bending direction too, which would need another 15 accelerometers. But there still would be 15 measurement transducers that were not utilized if the axial direction was not needed. But, of course, a simple beam is an academic situation, and those tri-axial accelerometers may truly be needed for a real-world application. But here are a few cases that might make you rethink this idea.

Big wind turbine blade testing is a perfect example, with bending in two directions (referred to as the "flapwise" and "edgewise" modes of the anchored wind turbine blade). This is nothing more than a really big beam, for all practical purposes. Figure 11.11 shows the schematic for a 9 m wind turbine blade test with some accelerometer configurations. Notice that there are only measurements in two directions (x and y) because the axial direction is really not of interest. This test was run with a very portable eight channel system with seven accelerometers and one hammer. When the test was run, the first set of measurements was made with seven accelerometers at seven points, but all in the x-direction. Then the accelerometers were all reoriented to the y-direction for the second set of measurements. Eventually the accelerometers were all roved to all the points of interest. One advantage of using single axis accelerometers here was that all the cables remained attached to the accelerometer and DAQ as they were reoriented and then roved to all points. In this way, there was never a concern about cable swaps resulting in a mismatch between accelerometer location or direction. Had only tri-axial accelerometers been used, there would have been a much greater possibility of getting cabling problems, and also the axial orientation of every tri-axial accelerometer would have been wasted because there was no motion of interest in that direction.

Another modal test was performed for a wind turbine blade that was in the 50 m length range. This test was really only concerned about modes in the flapwise and edgewise directions of the blade, but several people involved argued that it might be necessary to also measure the axial

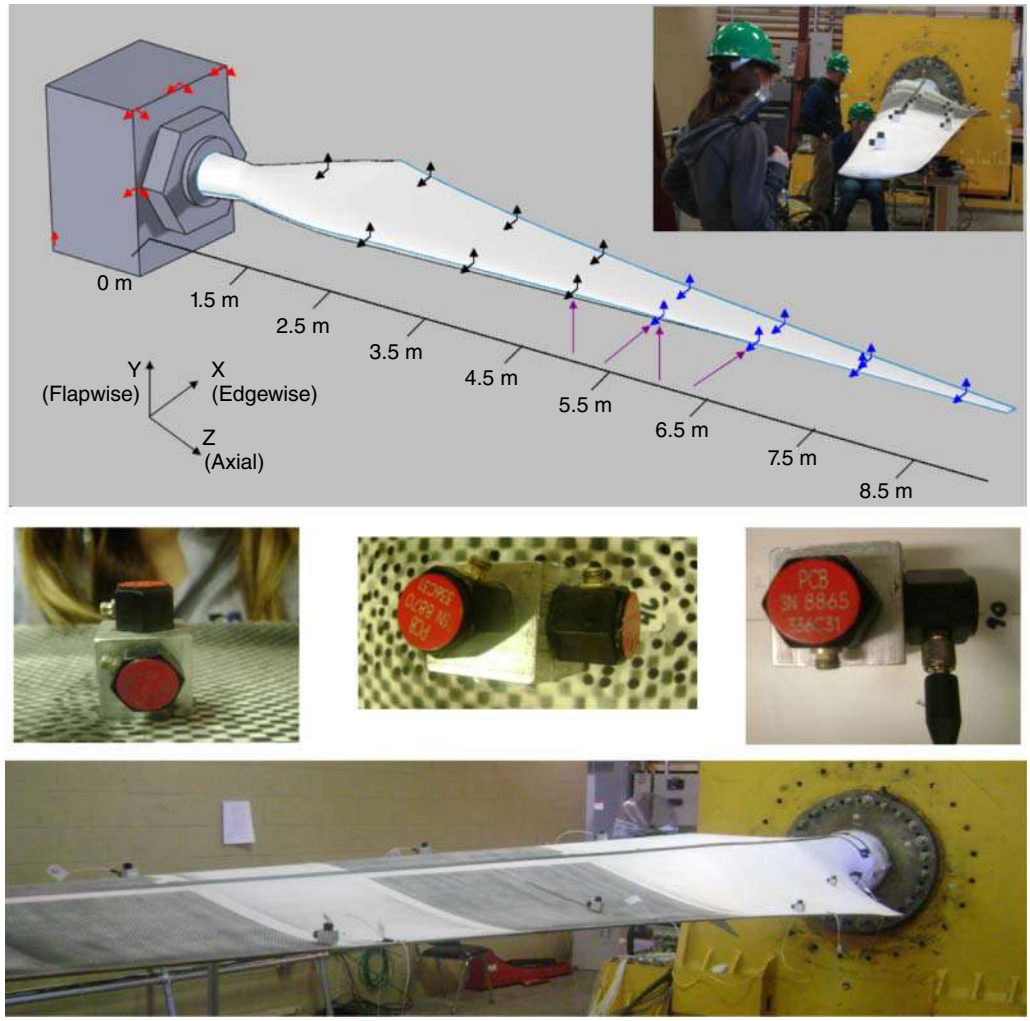

Figure 11.11 Schematic for 9 m wind turbine blade test.

direction. Figure 11.12 shows the blade test, with the cabling configuration and expected mode shapes for the test, along with a related measurement.

The axial direction is very stiff compared to the two flap and edge motions, and the displacement is very small. Now for this test, tri-axial accelerometers were mounted just in case all three directions turned out to require measurement, but fortunately many realized that there was very little to measure in the axial direction. However, there was another very important concern that many never really considered.

The flap and edge motions are large and an accelerometer sensitivity of 100 mV/g is very suitable for motion in these two flexible directions. However, the motion is very small in the axial direction and a sensitivity of 1 V/g or higher is necessary in order to make a good measurement. The problem with a tri-axial accelerometer is that the sensitivity in all three directions is nominally the same, so the measurement in the axial direction with a tri-axial accelerometer at 100 mV/g would be plagued by noise and poor signal strength and for all practical purposes would not provide a suitable measurement at all.

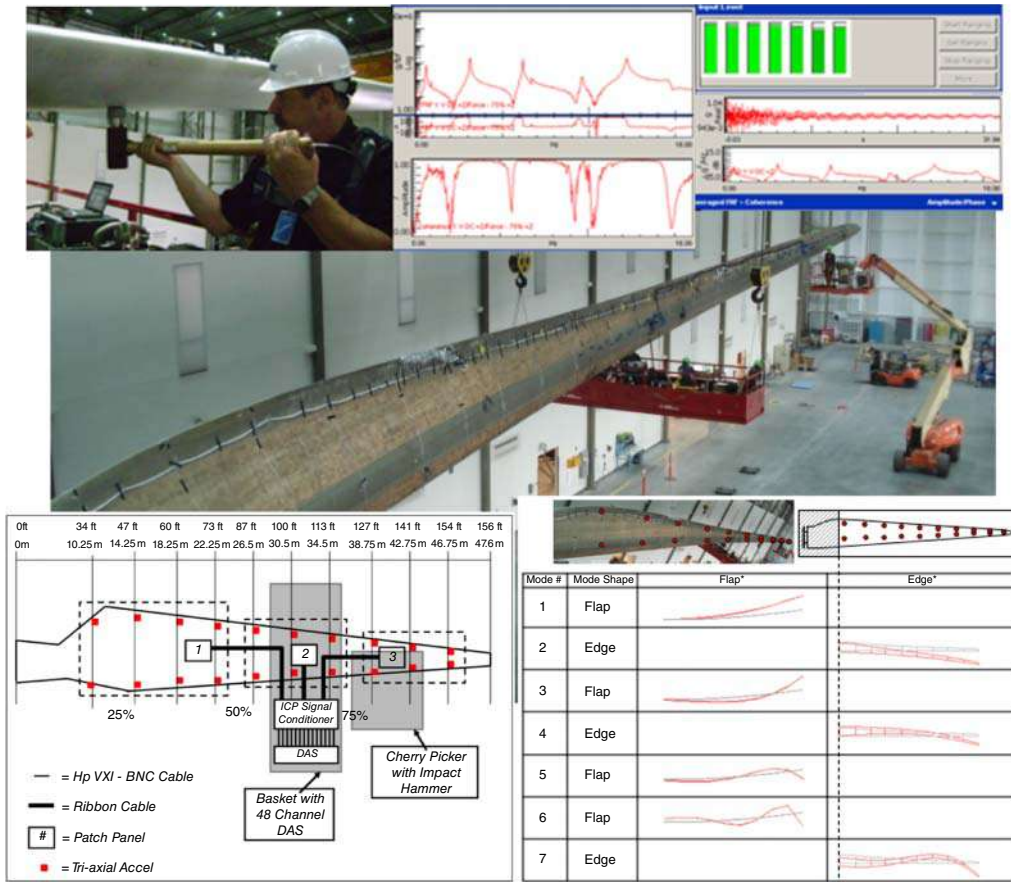

Figure 11.12 Schematic for large wind turbine blade test.

11.4 Curvefitting Considerations

Modal parameter estimation, commonly called curvefitting, can be a very difficult process, especially when the data is not collected with the utmost care and attention to all the details that have been presented in this book. Of course, it is critical to state that not all modal tests need to be conducted with high precision and accuracy – it depends on the application. If the goal is just to find out which is the first bending mode, what the shape looks like, and at approximately what frequency it is found, then the level of sophistication and care in collecting the data can have that same level of care and attention. But if the model is going to be used for some very detailed model simulations or correlation/updating of a finite element model, then the level of care and attention needs to be high.

Once the data has been collected, the mode indicator tools can be used to interrogate the data to identify what poles exist in the data. All tools available should be used, because each gives a slightly different view of the data. However, in general, the trends of all the tools are usually the same. The stability diagram is probably the best and most used tool for selecting the poles of the system.

11.4.1 Should all Measurements be used when Curvefitting

This is a very good question. There is no reason to not include all the data collected, providing that the data is well measured and consistently related. Providing that there is good dynamic range, with accurate sensitive transducers, and provided that all modes are well excited from all reference points and at all the response locations, all the data can be used for estimating modal parameters. However, it is highly unlikely that all the measurements meet these requirements. What was just described is a measurement situation that will likely only occur with an analytical model with infinite dynamic range and infinite frequency resolution. From a practical standpoint, this will probably never happen. So let's discuss the reality of the situation and some practical approaches to minimizing some of the measurement shortcomings.

An example of a common measurement problem is found in a test that was run many years ago on an aerospace structure: a satellite. This structure had very directional modes as well as numerous local modes. The structure is shown in Figure 11.13 along with some typical frequency response functions. Notice that the lower frequency response function only shows a few modes, but the upper frequency response function shows all of the modes of the structure.

However, this problem isn't just an aerospace problem; it is a general problem that can be seen in many structures tested. In fact, the measurements shown are typical of those currently being measured for a consumer product, which is housed in a very flimsy cabinet. This situation is common in almost any structure subject to modal testing. This particular structure shown had several bending and torsional lower order modes, as well as many local modes with bending, torsion, in-phase, and out-of-phase types of modes for the panels and peripheral equipment on the structure. The actual structure was tested using five independent shaker excitations (three vertical and two separate horizontal directions).

The first mode of the structure consisted of bending in the x-direction, with almost no response in the y-direction. Obviously the shaker in the x-direction can do a very good job of exciting the x-direction modes, but the shaker in the y-direction does not excite the structure in the x-direction. So the measurements obtained from the y shaker are obviously going to be very poor due to the lack of participation of the first mode in the y-direction. This is a physical

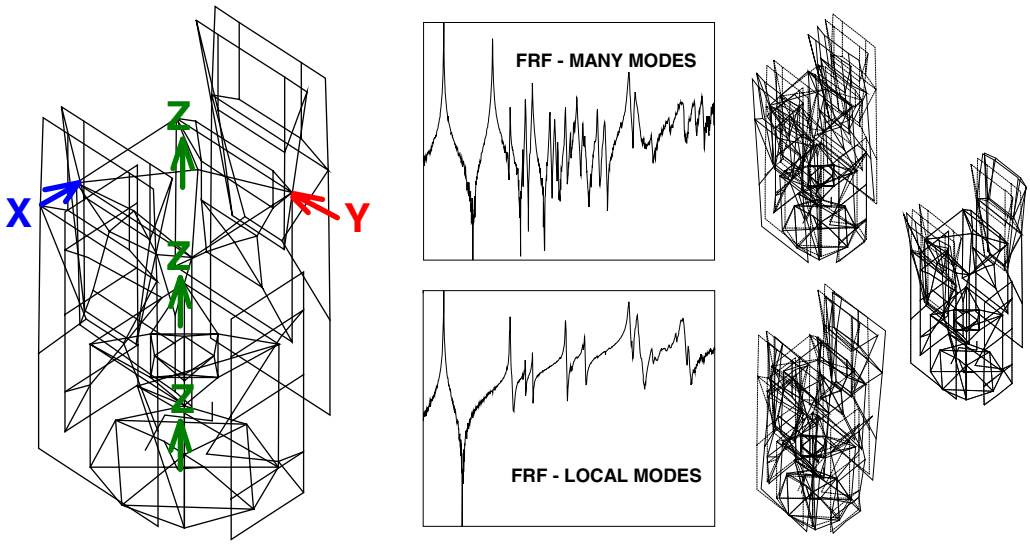

Figure 11.13 Aerospace structure with FRFs and several modes.

reality of most test structures that is typically impossible to overcome. On the other hand, the second mode of the structure consisted of bending in the y-direction, with almost no response in the x-direction. Here the situation is the opposite of that just discussed: the y shaker can do a very good job of exciting the structure in the y-direction but the shaker in the x-direction cannot excite the structure in the y-direction. However, both shakers can do a very good job of exciting the torsional mode. This directly implies that all of the measurements will not be measured with the same degree of accuracy for each mode. During the MIMO excitation with five shakers, all of the frequency response functions are collected simultaneously, but clearly not all of the modes are excited equally from each of the shaker locations. So how can all of this data be efficiently and accurately processed?

Most modal parameter estimation performed today utilizes a two step process. First, the poles are estimated and then the residues or mode shapes are computed (once the global poles have been extracted). With this in mind, the poles of the system do not need to be estimated using all the measurements collected. The poles can be estimated using only the subset of measured functions that best describes the poles of interest. Once the global poles have been estimated, the residues or mode shapes can be extracted using all the measurement DOFs; it is not necessary to estimate residues for all references, especially if the references do not sufficiently excite all the modes. The selection of particular frequency response functions for the extraction of poles is schematically shown in Figure 11.14.

In the satellite example, the first x-bending mode was estimated using only the x-response from the x-excitation location. Only the y-response locations were used for the y-excitation

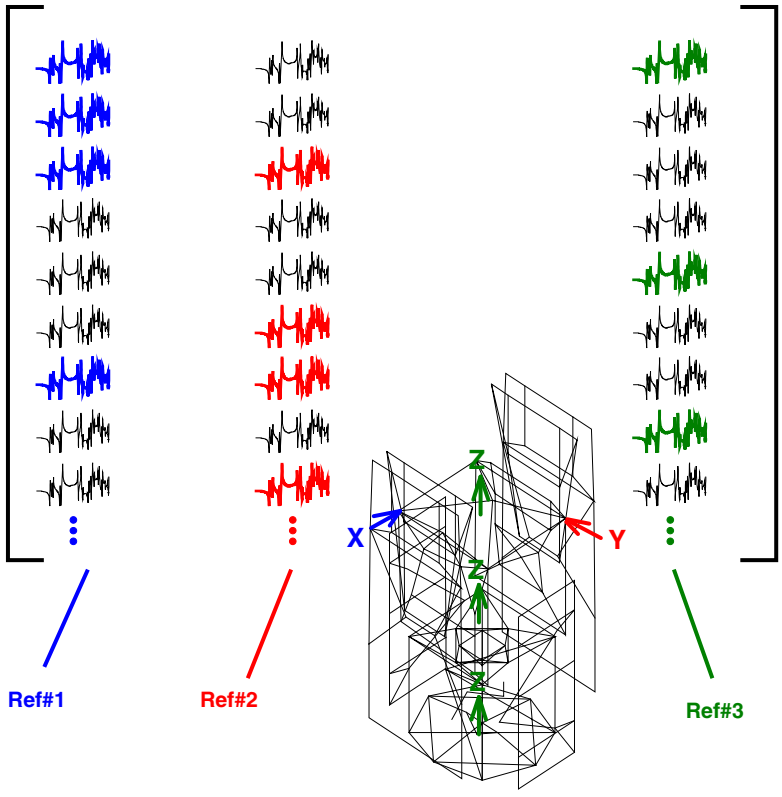

Figure 11.14 Schematic depiction of measurement selection.

location for the y-bending modes. But both x- and y-excitations with the x- and y-responses were used for the torsional mode. Notice that the z-direction excitation and response were not used for the estimation of any of these poles. This is because the z-excitation locations have a very hard time exciting either the x- or y-direction modes efficiently. While these references/excitations are necessary for the excitation of some of the higher frequency modes, the vertical excitations are not very good for the excitation of the lower order x- and y-direction modes. But, of course, once the poles are estimated, the residues or mode shapes are estimated using all the measurements in the x-, y- and z-directions but only using the x and y shaker excitations.

During the modal parameter estimation process, extreme care needs to be exercised to extract the best possible poles to describe the system characteristics. However, many of the measurements and often all of the references are not optimum for all the modes of the system. As an example, a large telescope structure was tested with four reference excitation locations. Clearly, the references were not all optimum for all the lower order directional modes of the structure. As a first pass on evaluating the data, all the frequency response functions from all the reference locations were used to extract poles and residues for the structure. Once parameters had been selected, a synthesized frequency response function was generated and compared to the actual acquired measurement as part of the validation process. The synthesized and measured frequency response function are shown in Figure 11.15a. *Please carefully note that this is not a good comparison*. However, after a very careful evaluation of the data and careful selection of measurements to extract the poles of the system (followed by residue extraction), a far better model was obtained. This is confirmed by the comparison of the synthesized and measured frequency response functions, as shown in Figure 11.15b. Of course, this approach requires significant effort, but the modal parameters are generally greatly improved.

11.5 Blue Frame with Three Plate Subsystem

Now let's use a slightly more complicated structure and step through the thought process of selecting references and measurement points for a structure with several components. This structure is referred to as the "blue frame". This frame was originally used because the first bending and first torsion modes were very close in frequency (about 1 Hz apart) and these closely spaced modes could create some difficulties if care wasn't exercised in extracting the modes. The structure was further complicated by adding three modally active plates, which were mounted with an elastomeric mount. This mount would make it more difficult to excite from just one location of the structure and is a very good example of a structure with very localized modes as well as global modes of the system; this was useful to show how reference selection was very important for these types of structures.

The test evolved from a test performed on a warship propulsion system, in which the main frame of the propulsion system was attached to three separate subframes via an isolation system. The propulsion system was 50 feet long by 20 feet high by 12 feet wide and weighed 150 tons. The modal test of the propulsion system consisted of 150 measurement locations with 18 references. All of these references were needed because it was very difficult to excite one subframe from another subframe. The data for this actual propulsion system cannot be shared, but the system was mimicked using the blue frame and the three separate plate subsystems, which were mounted with an isolator mounting arrangement. The blue frame with the three attached plates is shown in Figure 11.16, along with the test geometry. All three plates are different from each other. Figure 11.17 shows a typical set of mode shapes for this system; note that only out of plane motion is considered for this example.

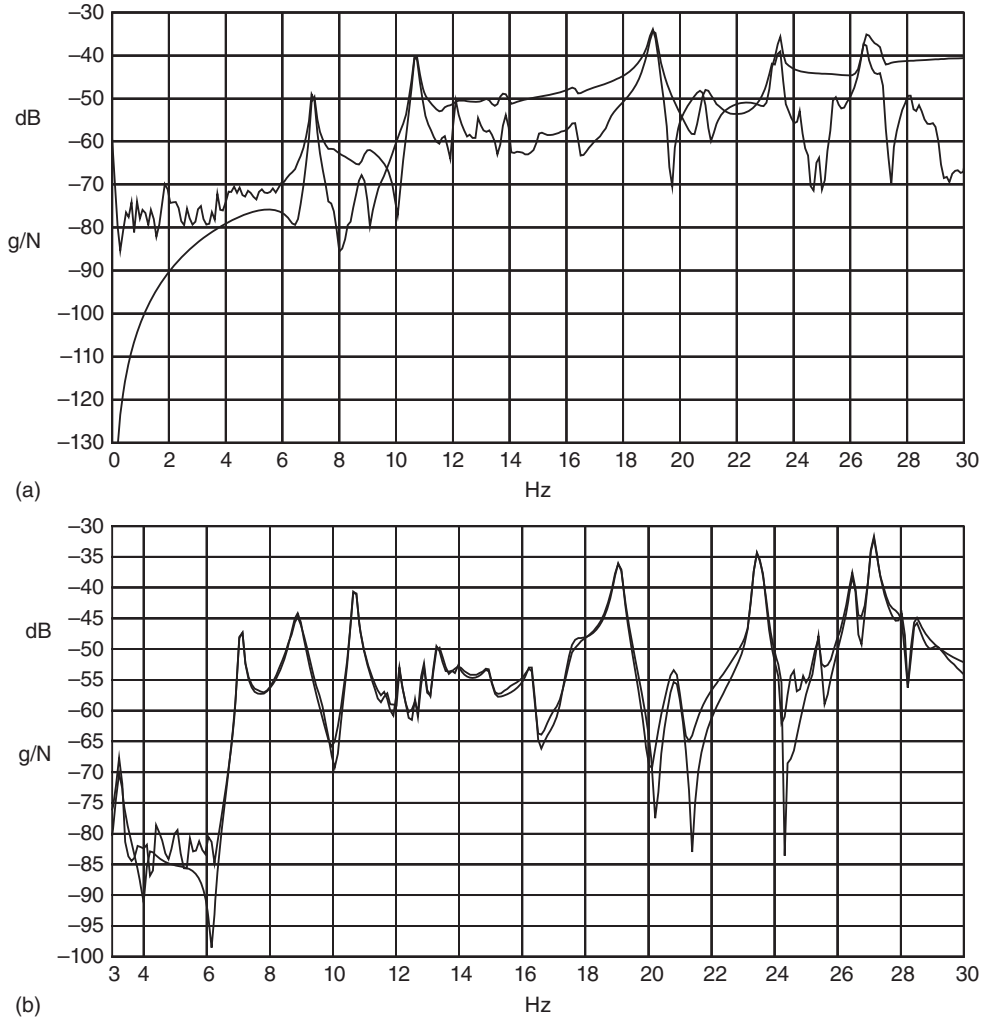

Figure 11.15 Extraction and synthesis of FRFs: (a) poor; (b) good.

Reviewing each of the mode shapes for this plate, there are many items to note. First, there are some modes that are global modes and the motion of the mode shape is seen in the frame as well as in each of the three plates. Then there are some mode shapes where the frame appears to have little motion but all three plates have significant motion in each of the three plates. There are modes where the frame has significant motion but the plates have essentially no motion. Then there are modes where only one plate has significant motion or two plates have significant motion. Another important item to note is that there are modes where all three plates have similar in phase motion and some modes where the plates are out of phase with similar motion. So, in general, there is very complicated motion for all of the modes of this structure.

Now if a modal test were to be performed, where should the reference accelerometer be located? In order to see all the modes, the reference must be at a location from which all of the modes can be equally observed. Immediately, it becomes clear that identifying a single reference location to observe all of the modes will be very difficult. This is exactly why multiple reference data is typically required for any real modal test to be undertaken. But looking at the

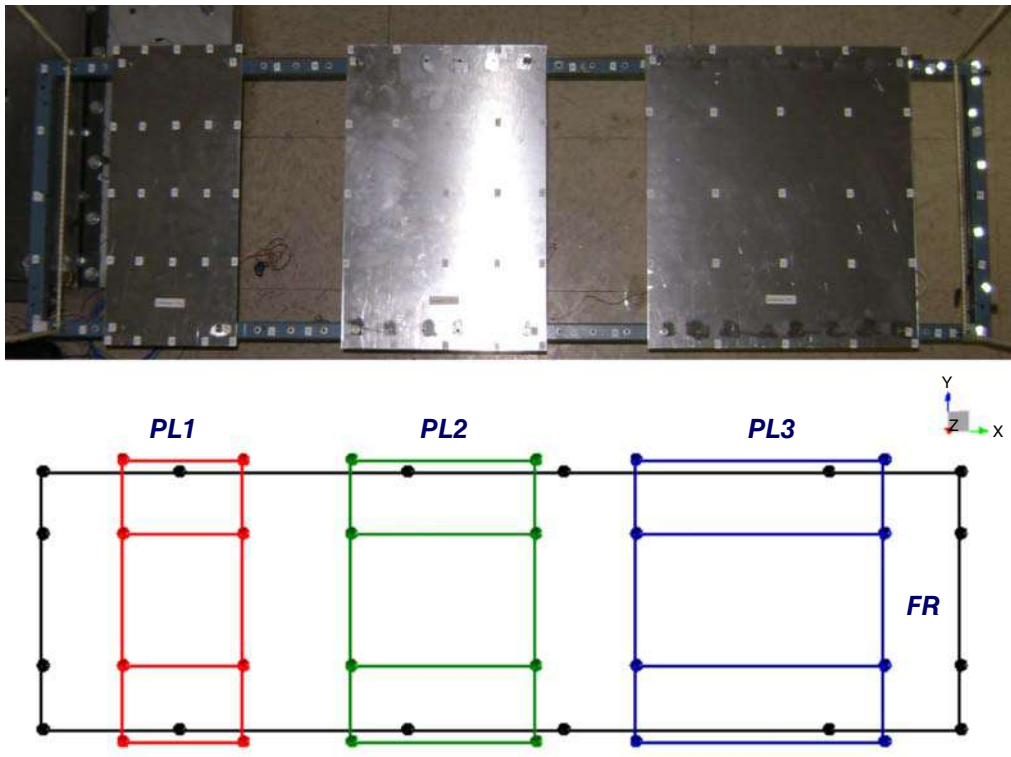

Figure 11.16 Blue frame with three plates (top) with the test geometry (bottom).

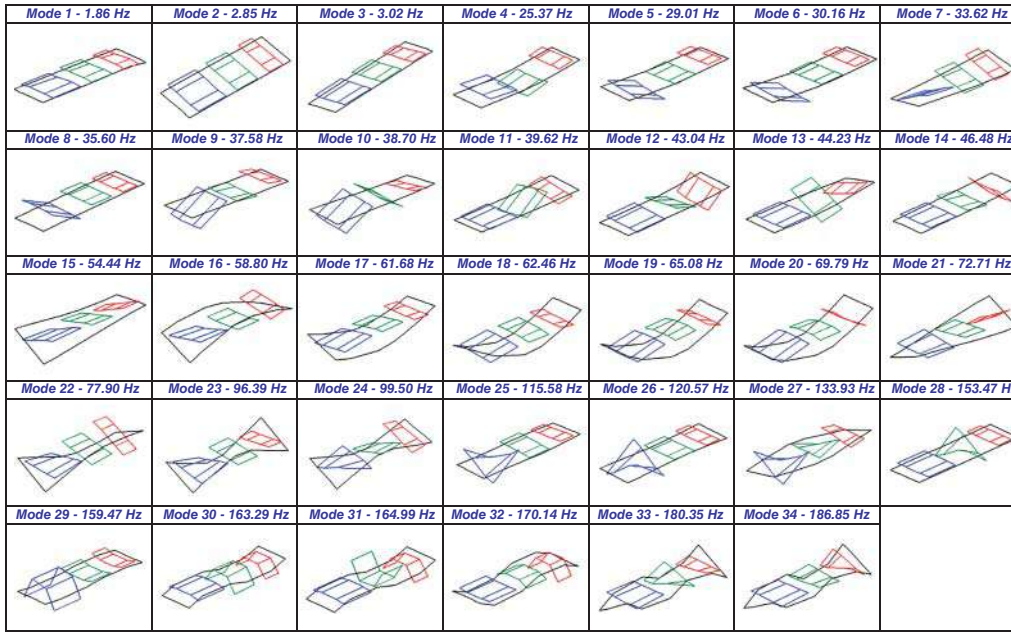

Figure 11.17 The typical flexible modes for the blue frame with three plate subsystems.

mode shapes, the references seem to be required on each of the individual components of the structure. For the example here, the goal is not necessarily to define all the mode shapes. The goal is to step through some of the measurement scenarios envisioned and to acquire some data to show some of the inconsistencies that might result. So looking at the frame, any one of the four corners could be a good reference; and looking at the plates, any point at the edge but not in the middle could be a good reference. These possible reference locations are shown in Figure 11.18.

So now let's take a variety of different measurements with impact or shaker and point out some of the issues and difficulties with measurements for this particular structure; note that there are some nonlinearities associated with the frame structure, which will make the measurements a little more interesting. A few different preliminary test configurations with a shaker excitation and an impact excitation, along with the data acquisition system, are shown in Figure 11.19 (for reference only to illustrate a typical setup).

So an impact measurement is the easiest to make. The impact hammer was used to make reciprocal measurements

- between the red plate and the green plate (Figure 11.20a)
- between the red plate and the blue plate (Figure 11.20b)
- across the frame (Figure 11.20c).

These measurements have noticeable differences in several regions of the frequency range. This is likely due to the effects of the nonlinearities in the structure. Nonlinearities are very sensitive to the input location of the impact locations and will be excited differently depending on where the impact excitation is located.

So these measurements can now be used in conjunction with the stability diagram as a tool to identify the consistency of the data collected. The stability diagram for the data collected from all seven references was used to create the stability diagram: four references on the frame and one reference on each of the individual plates. Clearly the stability diagram shows a significant amount of inconsistency between the sets of data collected. This is best illustrated with the stability diagram for one reference, which is typical of all the separate references. Note that there are some other modes that are indicated but only out of plane measurements are used in this evaluation and some of the modes in plane have a minor contribution. The stability diagram is shown in Figure 11.21, with all the references evaluated together in the upper plot and just one

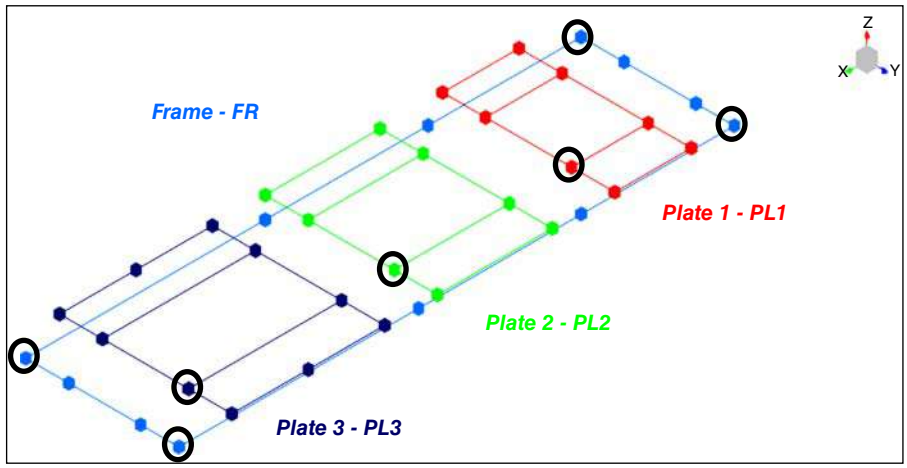

Figure 11.18 Some possible reference points for the blue frame with three plates.

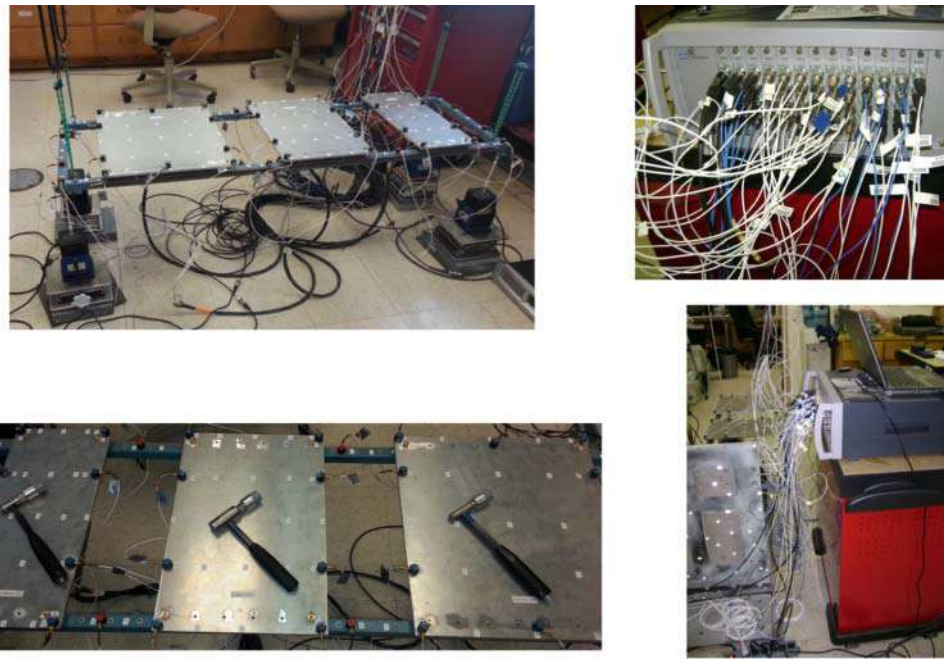

Figure 11.19 Typical test setups for shaker test and impact test with data acquisition system.

of the seven references in the lower plot. The lower plot indicates that the data relative to one reference produces very acceptable results when reviewing the stable poles that are achieved. However, when all the data from all the references are combined, the stability diagram does not produce acceptable results. This is likely because the system is nonlinear and each of the references tends to excite the nonlinearities differently. There is then an inconsistency between the datasets. The upper plot of the stability diagram clearly shows that it is difficult to obtain a stable pole.

So the next case to consider is collecting all the data at the same time. Of course, this cannot be done with an impact approach. Using four small modal shakers located at the four corners of the frame structure, a multiple-input, multiple-output set of measurements was collected. One important aspect of this arrangement is that all the data is collected at the same time and with the same set of transducers mounted on the structure. This arrangement maintains consistency in the measurement set. The other important aspect of this arrangement is that the excitations used for the test are generally at a slightly lower level because there are four shakers all providing an input that is more uniformly distributed over the entire structure. They generally do not excite all the nonlinearities to the same degree as a single input impact excitation. In this way, a much better set of consistently measured data is obtained. This data is less sensitive to any nonlinearities in the system. Figure 11.22 shows the structure and three of the reciprocal measurements that were made. In all cases, the measurements are very good and all provide very good reciprocal measurements.

Now using this set of measurements, the data was assessed using the stability diagram as a quality assessment tool. Figure 11.23 shows the stability diagram obtained. Now remember that only the response in the out of plane direction is considered; there will be some in plane motion that will appear in the stability diagram. Overall, the stability diagram gives a clear indication of stable poles in the measurements and the data overall is considered very good. So

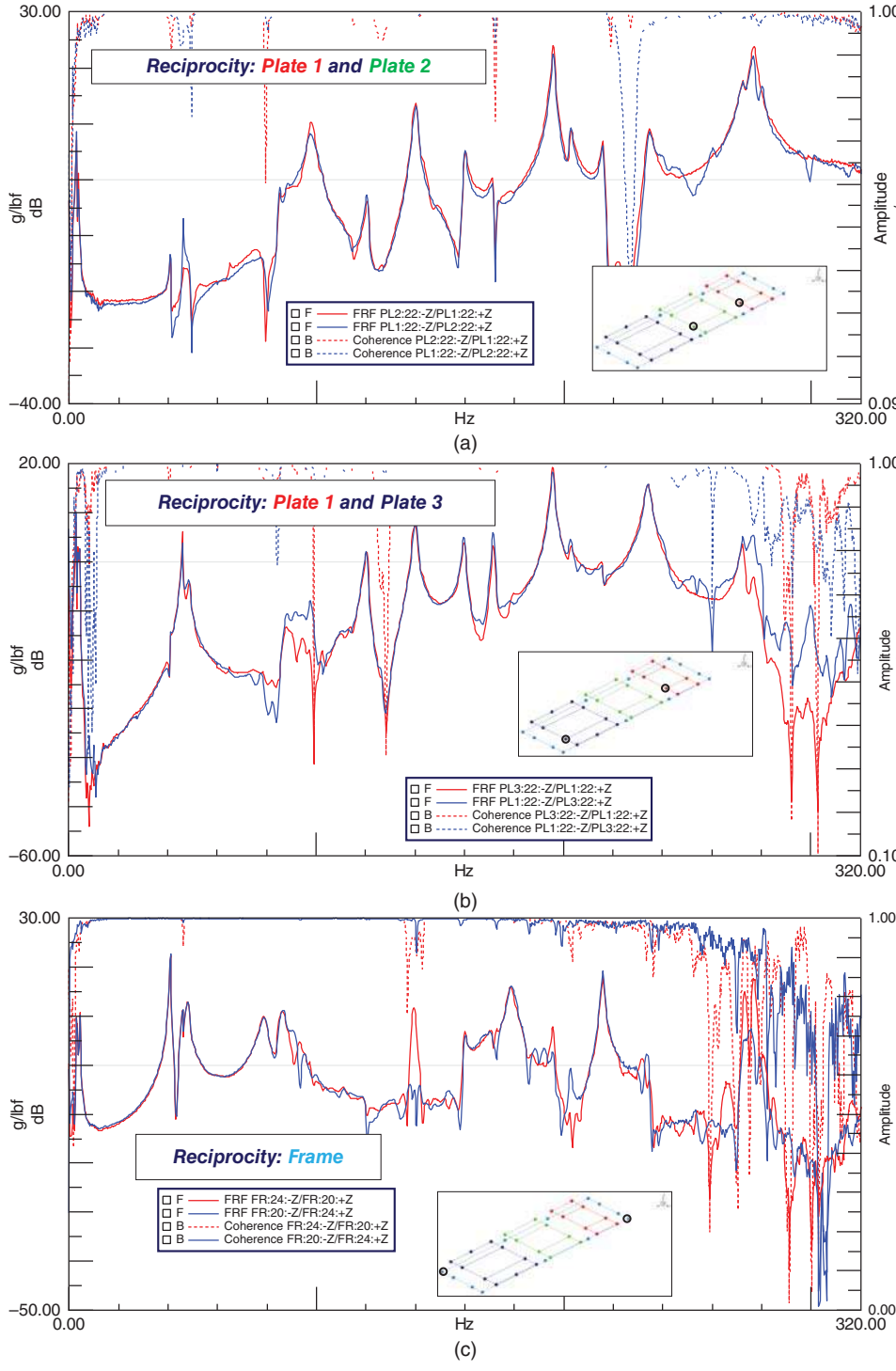

Figure 11.20 Reciprocity measurements: (a) between the red plate and the green plate; (b) between the red plate and the blue plate; (c) across the frame.

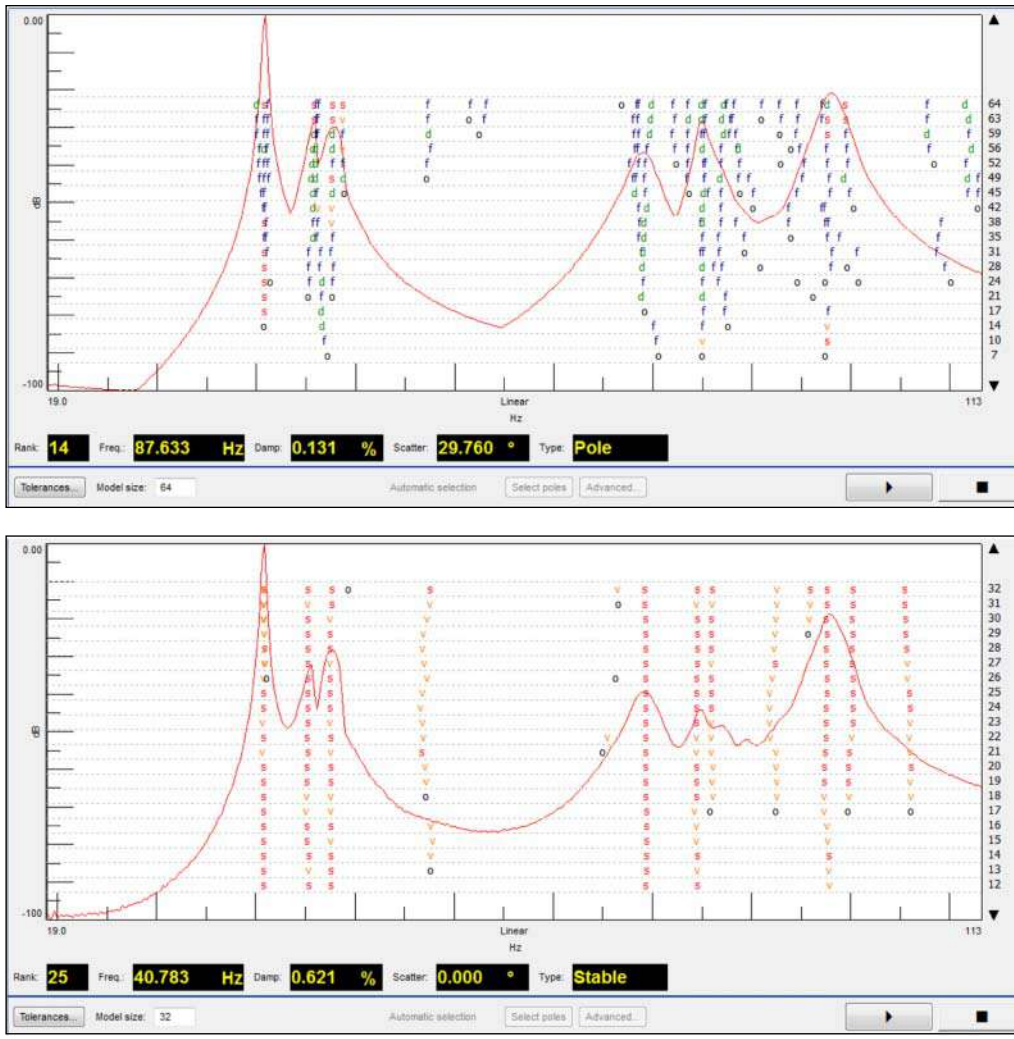

Figure 11.21 Stability diagram for blue frame with all references (top) and one reference (bottom).

the multiple-input, multiple-output excitation provides a much better dataset than the earlier impact test. This is a good reason to utilize a multiple-input, multiple-output testing strategy: the overall measurements are greatly improved, as seen in the stability diagram.

This test was performed with the shakers at the four corners of the frame structure. An additional multiple input, multiple out test was performed with four shakers: one on each of the three plates and one on the frame. Figure 11.24 shows the structure and three reciprocal measurements. Again, all the measurements are very good overall because all the data is collected simultaneously and the excitation energy is distributed more evenly throughout the structure, which avoids any significant nonlinearities being excited. While not shown, the stability diagram was just as good as that shown in Figure 11.23.

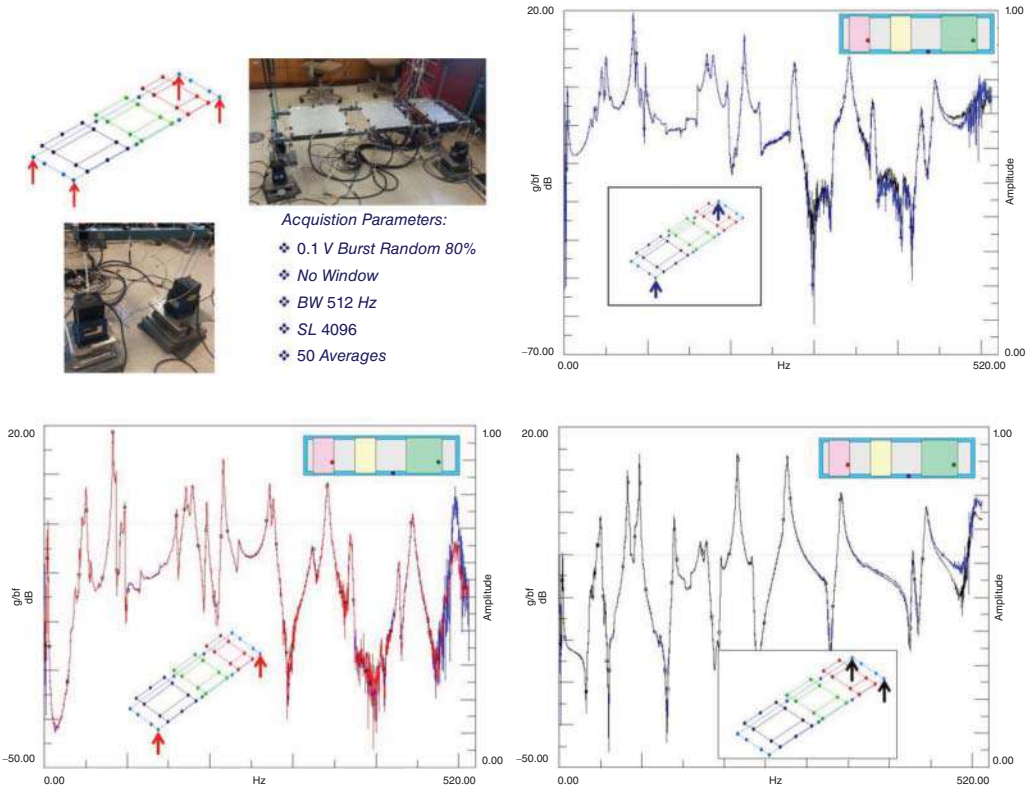

Figure 11.22 MIMO test setup and results for MIMO configuration for shakers on frame.

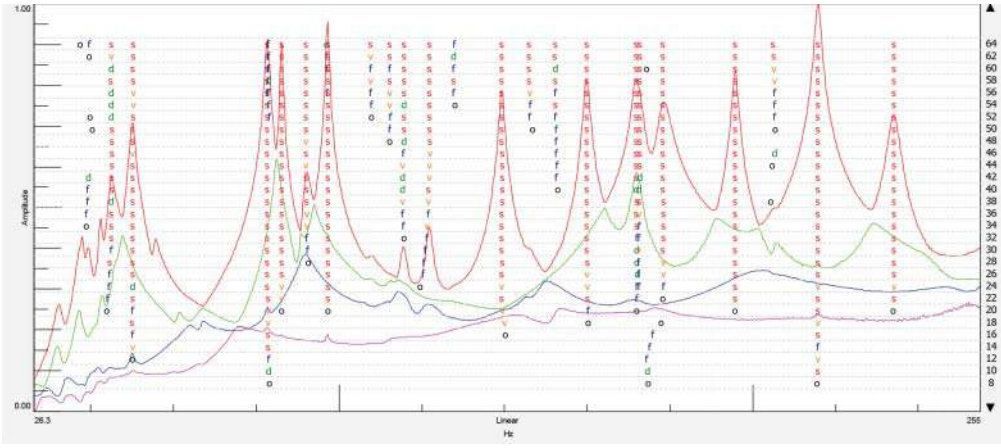

Figure 11.23 Stability diagram from multiple-input, multiple-output test for blue frame structure.

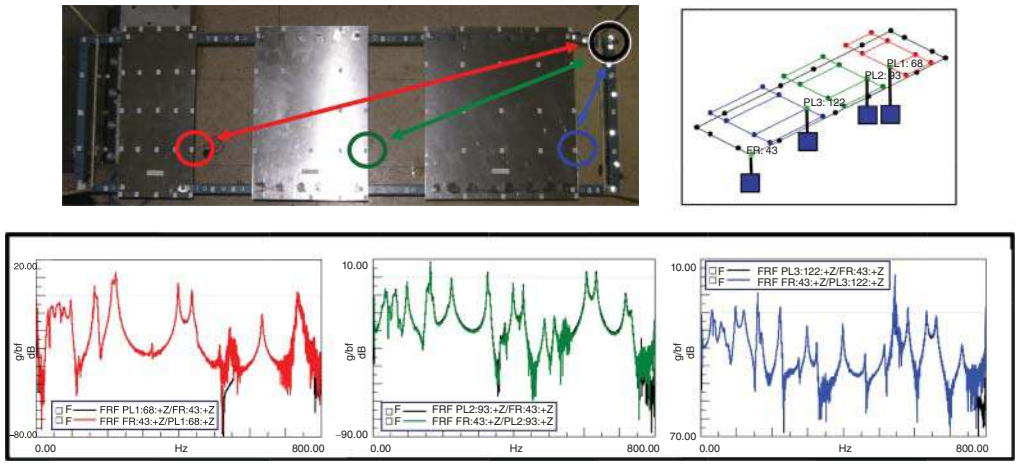

Figure 11.24 MIMO test setup and results for MIMO configuration for shakers distributed on structure.

11.6 Miscellaneous Issues

There are some miscellaneous items that are covered in this section.

11.6.1 Modal Test Axis Labels

While this may seem trivial, labeling the axes clearly at the test site has been extremely important, especially when larger structures or long days of testing are involved. Having the labels drawn out on the floor near the test article helps to reaffirm directions when labeling points. As an impact test proceeds, there is good reason to call out each and every point and direction that is measured at the start of the measurement. This ensures that everyone knows the current point and direction and the software entry can easily be checked as the test progresses. Figure 11.25 shows a typical test lab axis label.

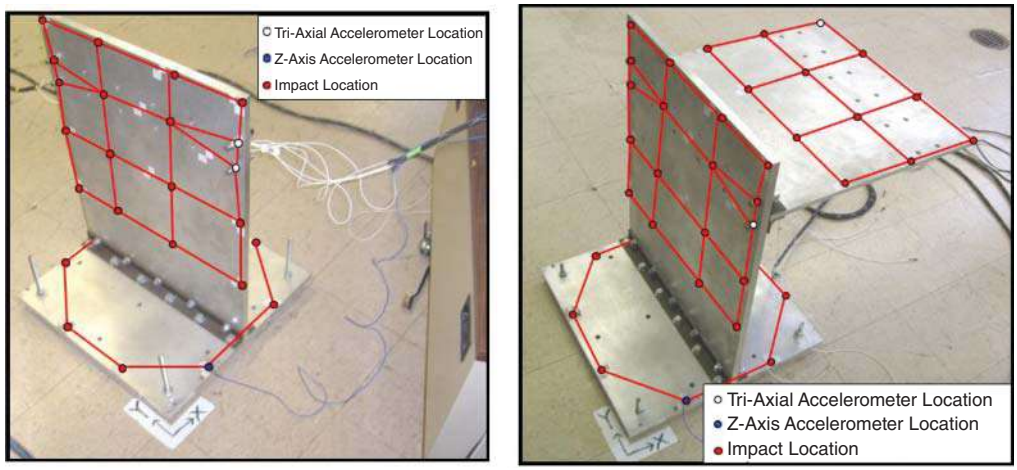

Figure 11.25 Test structure axis labels.

11.6.2 Testing Does Not Need to Start at point 1

Once a test is started, there really is no need to start at point 1 and proceed in ascending order. Actually, point 1 may not be the best measurement and may possibly be the worst measurement, especially if it is close to the constrained boundary. A measurement point somewhere on the structure may produce better results overall; less desirable points may give poor frequency response measurements and poor coherence; this may well be expected at that point and a poor measurement may distract the team, who may waste time trying to improve a measurement that is as good as it is going to get.

Also, there is no need to measure points sequentially. In fact, using points scattered around the structure may actually be better. There may be many points to be collected but most are there to augment or provide additional definition. Obtaining a "straw man" of points (an abbreviated set of points and not the entire set of points ultimately needed) on the structure first allows a quick assessment of the data and a reasonably good idea of the lower order modes. Another reason is that if all the initial points are selected so that they are all congregated in one area of the structure and something catastrophic occurred preventing the completion of the test, you would only have a set of points that did not describe the structure overall. But if a "straw man" of points is obtained and something goes wrong, at least there is sufficient data to make a preliminary assessment.

11.6.3 Test to a Wider Frequency Range

Always test to a wider frequency range than that requested to make sure that the measured data makes sense. One test required that all the modes up to 100 Hz be identified; this was clearly specified in the contract paperwork. The test team did everything expected, but the frequency response measurements did not look very good at all. Many attempts were made to improve the measurement, with many of the tips and suggestions outlined in this chapter, but the measurements did not look very good at all. Finally, a suggestion was made to test to a higher bandwidth. Very reluctantly the test engineers complied, but identified that the contract clearly specified that testing to only 100 Hz was to be done. Once measurements to 200 Hz had been made, the reason for the poor measurements became clear. The first mode of the structure was at above 150 Hz. So all the attention to making a good measurement below 100 Hz was focused on the stiffness line of the first mode of the system and the difficulty with the measurement was then clear. Requirements and specifications and guidelines are very useful but they never replace common sense: thinking is required!

11.6.4 U_i times U_j; the key to many questions

Now this is probably the biggest item to consider. So what does this mean. Well let's write an equation down to explain what this means.

The frequency response function can be written in terms of residues or in terms of mode shapes (and has been used in many different chapters), as shown in Figure 11.26. The lower equation in the figure is the way that it is normally written in the literature. This is useful, but only if you really understand what a residue is. The upper equation is actually the same equation but with the residues expressed in terms of mode shape information. Specifically, the residue (which is directly related to the amplitude of the frequency response measurement) is related to the value of the mode shape at the input excitation location multiplied by the value of the mode shape at the output response location for a particular mode of interest. The residue will determine the amplitude of the frequency response function for that particular mode, and, of course, the overall effect of the modes is the linear summation of all the modes of the system.

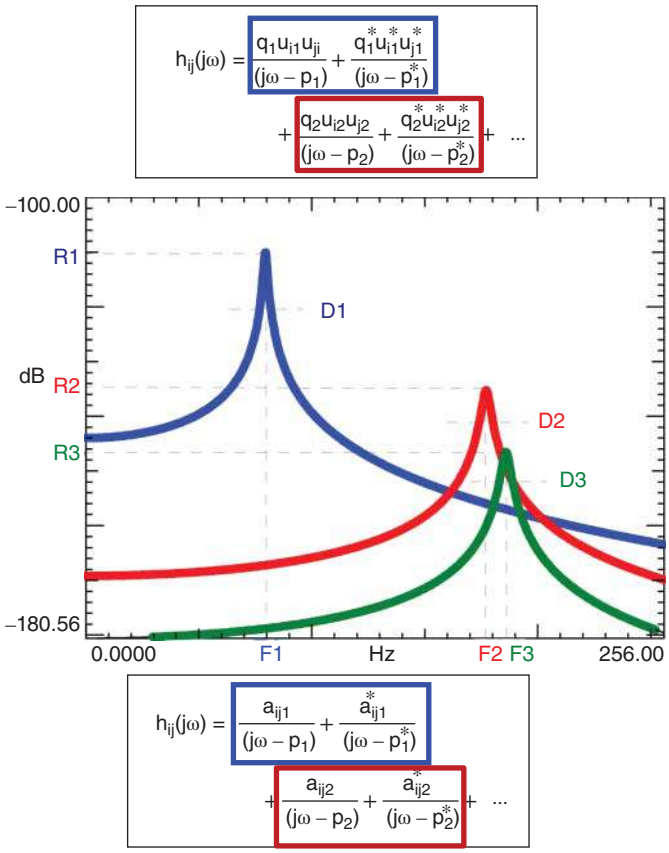

Figure 11.26 Frequency response function written on a mode by mode basis using the residue formulation and the mode shape formulation.

So what does this tell us? Basically, it gives a very clear definition of the peak amplitude of the frequency response function: it is related to the values of the mode shape for a particular mode at the input–output location.

Often, people will ask why the amplitude of a particular mode is very low for a particular measurement. This equation identifies that, for that particular mode, either the input excitation or output response (or both) is a very small value and probably close to the node of a mode. If you want to see that mode with a more pronounced peak in the frequency response function, you really need to change the input and/or output location so that is at a place where the mode shape values are much larger and away from the node points.

If you want to conduct a test and select good locations for measurements, you really need to look to see where the mode shapes are large for each of the modes of the system. The finite element model is a very good tool to use to help decide where to place all of your transducers. While the model may not be perfect, certainly it is a reasonable representation of your structure.

And if you look at a good number of the modal space series articles, the theme for many of the articles is exactly that. Firmly understanding this principle will be a great asset to your understanding of many questions that arise in the conduct of an experimental modal test.

11.7 Summary

This chapter provided some basic material regarding some modal testing issues. There were several tips and tricks that can help in making better measurements or that have helped decide on approaches for extracting modal parameters. A few examples were presented to illustrate some common difficulties and approaches to improving the data overall. Examples of data reduction difficulties that are directly related to common measurement approaches that can easily be improved were presented. Many of the measurement situations are frequently seen in industry and are very easily corrected to improve the collected data overall. One section has a fairly complete impact test discussion to guide analysts through the things to consider when starting to setup an impact measurement sequence; these are the typical steps that are needed for any impact test. There are also many different discussions on the reduction of data and the importance of the data collected to extract useful results. Overall there are many good items that help run a better modal test.

A

Linear Algebra: Basic Operations Needed for Modal Analysis Operations

Let's just review some basic linear algebra material that is needed for modal analysis.

A.1 Define a Matrix

We can define a general matrix [A] to be of size n by m, meaning that it has n rows by m columns.

$$[A] = \begin{bmatrix} a_{11} & a_{12} & \cdots & a_{1m} \\ a_{21} & a_{22} & \cdots & a_{1m} \\ & & \cdots & \\ \vdots & \vdots & a_{ij} & \vdots \\ a_{n1} & a_{n1} & \cdots & a_{nm} \end{bmatrix}$$

The indices of the matrix indicate the specific row column: a_{ij} indicates the ith row and jth column of the matrix [A]. Typically, we will use a capital letter to denote a matrix and a lower case letter to indicate a particular term of the matrix. It is called a rectangular matrix when n is not equal to m; it is called a square matrix when n is equal to m, meaning that you have as many rows as columns defining the matrix.

A.2 Define a Column Vector

We can define a general column vector {B} to be of size n by 1, meaning that it has n rows by one column.

$$\{B\} = \begin{Bmatrix} b_1 \\ b_2 \\ \vdots \\ b_i \\ \vdots \\ b_n \end{Bmatrix}$$

The indices of the vector indicate a specific row of the vector: b_i indicates the ith row of the vector. Typically we use a capital letter to denote a vector and a lower case letter to indicate a particular term of the vector.

Modal Testing: A Practitioner's Guide, First Edition. Peter Avitabile.

Companion Website: www.wiley.com/go/avitabile/modal-testing

A.3 Define a Row Vector

We can define a general row vector $\lfloor C \rfloor$ to be of size 1 by m, meaning that it has one row by m columns.

$$\lfloor C \rfloor = \lfloor c_1 \; c_2 \; \cdots \; c_j \; \cdots \; c_m \rfloor$$

The indices of the vector indicate a specific column of the vector: c_j indicates the jth column of the vector. Typically we use a capital letter to denote a vector and a lower case letter to indicate a particular term of the vector.

A.4 Define a Diagonal Matrix

We can define a diagonal matrix [D], where non-zero terms exist only on the diagonal of the matrix.

$$[D] = \begin{bmatrix} d_{11} & & & & & \\ & d_{22} & & & & \\ & & \ddots & & & \\ & & & d_{ii} & & \\ & & & & \ddots & \\ & & & & & d_{nn} \end{bmatrix} \quad \text{where} \quad d_{ij} = 0 \quad \text{for} \quad i \neq j$$

A diagonal matrix is square. A special form of this matrix is the identity matrix, which has all diagonal terms equal to 1.

A.5 Define Matrix Addition

We can add two matrices together, but they must be the same size

$$[C] = [A] + [B] \quad \Rightarrow \quad c_{ij} = a_{ij} + b_{ij}$$

Each of the corresponding terms of the matrix [A] and [B] are added together to form the terms of matric [C]. For example:

$$[A] = \begin{bmatrix} 2 & 3 \\ 1 & 4 \\ 3 & 2 \end{bmatrix}; \quad [B] = \begin{bmatrix} 1 & 0 \\ 0 & 1 \\ 1 & 1 \end{bmatrix}; \quad [C] = [A] + [B] = \begin{bmatrix} 2 & 3 \\ 1 & 4 \\ 3 & 2 \end{bmatrix} + \begin{bmatrix} 1 & 0 \\ 0 & 1 \\ 1 & 1 \end{bmatrix} = \begin{bmatrix} 3 & 3 \\ 1 & 5 \\ 4 & 3 \end{bmatrix}$$

A.6 Define Matrix Scalar Multiply

We can scale the terms of a matrix by a scalar

$$[B] = s^*[A] \quad \Rightarrow \quad b_{ij} = s^* a_{ij}$$

Each term of the matrix [A] is multiplied by the scalar s to form matrix [B]. For example:

$$s = 2; \quad [A] = \begin{bmatrix} 2 & 3 \\ 1 & 4 \\ 3 & 2 \end{bmatrix}; \quad [B] = 2^*[A] = \begin{bmatrix} 4 & 6 \\ 2 & 8 \\ 6 & 2 \end{bmatrix}$$

A.7 Define Matrix Multiply

We can multiply two matrices together. However, the number of columns of the matrix [A] must be the same as the number of rows of the matrix [B] in order to do this multiplication.

$$[C] = [A][B] \;\Rightarrow\; c_{ij} = \lfloor a_i \rfloor \{b_j\}$$

$$c_{ij} = \begin{bmatrix} & & & \\ a_{il} & a_{i2} & \cdots & a_{ik} \\ & & & \end{bmatrix} \begin{bmatrix} b_{1j} \\ b_{2j} \\ \vdots \\ b_{kj} \end{bmatrix} \Rightarrow \; c_{ij} = \sum_k a_{ik} b_{kj}$$

Each term of the matrix [C] is made up of a row of the matrix [A] multiplied by a column of the matrix [B], which in essence is a dot product; an individual ij term of the matrix [C] is formed from the summation of the product of each sequential term of the row vector of the matrix [A] and the corresponding sequential term of the column vector of matrix [B]. For example:

$$[A] = \begin{bmatrix} 1 & 2 & 3 \\ 0 & 1 & 0 \\ 1 & 0 & 1 \end{bmatrix}; \quad [B] = \begin{bmatrix} 1 & 0 & 0 & 0 & 1 \\ 0 & 1 & 0 & 1 & 0 \\ 0 & 0 & 1 & 0 & 0 \end{bmatrix}$$

$$[C] = [A][B] = \begin{bmatrix} 1 & 2 & 3 & 2 & 1 \\ 0 & 1 & 0 & 1 & 0 \\ 1 & 0 & 1 & 0 & 1 \end{bmatrix}$$

A.8 Matrix Multiplication Rules

The following rules of matrix multiplication apply:

- $[A][B] = [C] \neq [B][A]$
- $[A]([B] + [C]) = [A][B] + [A][C]$
- $([A][B])[C] = [A]([B][C])$
- $[A][B] = [0]$ does not imply that $[A] = [0]$ or $[B] = [0]$!!!

Premultiplication of a matrix [A] by a diagonal matrix [D] multiplies the rows of matrix [A] by corresponding diagonal terms of the matrix [D]:

$$\begin{bmatrix} \ddots & & \\ & D & \\ & & \ddots \end{bmatrix} [A] = \begin{bmatrix} d_{11} & \lfloor a_{11} & a_{12} & \cdots & a_{1m} \rfloor \\ d_{22} & \lfloor a_{21} & a_{22} & \cdots & a_{2m} \rfloor \\ d_{ii} & \lfloor a_{i1} & a_{i2} & \cdots & a_{im} \rfloor \\ d_{nn} & \lfloor a_{n1} & a_{n2} & \cdots & a_{nm} \rfloor \end{bmatrix}$$

Postmultiplication of a matrix [A] by a diagonal matrix [D] multiplies the columns of matrix [A] by the corresponding diagonal terms of the matrix [D]:

$$[A] \begin{bmatrix} \ddots & & \\ & D & \\ & & \ddots \end{bmatrix} = \begin{bmatrix} d_{11} \begin{Bmatrix} a_{11} \\ a_{21} \\ \vdots \\ a_{n1} \end{Bmatrix} & d_{22} \begin{Bmatrix} a_{12} \\ a_{22} \\ \vdots \\ a_{n2} \end{Bmatrix} & \cdots & d_{ii} \begin{Bmatrix} a_{1i} \\ a_{2i} \\ \vdots \\ a_{ni} \end{Bmatrix} \end{bmatrix}$$

For example:

$$[A] = \begin{bmatrix} 1 & 2 & 3 \\ 2 & 4 & 6 \\ 3 & 6 & 9 \end{bmatrix}; \quad [D] = \begin{bmatrix} 3 & & \\ & 1.5 & \\ & & 1 \end{bmatrix}$$

$$[C] = [A][D] = \begin{bmatrix} 3 & 3 & 3 \\ 6 & 6 & 6 \\ 9 & 9 & 9 \end{bmatrix}$$

A.9 Transpose of a Matrix

We can define the tranpose of a matrix, where the rows and columns are interchanged as follows:

$$[A] = \begin{bmatrix} a_{11} & a_{12} & & \\ a_{21} & a_{22} & & \\ & & & \\ & & a_{ij} & \\ & & & \end{bmatrix} \Rightarrow [B] = [A]^T = \begin{bmatrix} a_{11} & a_{21} & & \\ a_{12} & a_{22} & & \\ & & & \\ & & a_{ji} & \\ & & & \end{bmatrix}$$

For example:

$$[A] = \begin{bmatrix} 1 & 2 \\ 3 & 4 \\ 5 & 6 \end{bmatrix}; \quad [A]^T = \begin{bmatrix} 1 & 3 & 5 \\ 2 & 4 & 6 \end{bmatrix}$$

A.10 Transposition Rules

The following rules of matrix transposition apply:

- $([A] + [B])^T = [A]^T + [B]^T$
- $[[A]^T]^T = [A]$
- $([A][B])^T = [B]^T[A]^T$
- $([A][B][C])^T = [C]^T[B]^T[A]^T$

A.11 Symmetric Matrix Rules

The following rules apply for symmetric matrices; symmetric matrices are square and corresponding ij terms are equal to ji terms due to symmetry:

- $[A] = [A]^T; \quad [B] = [B]^T; \quad [A][B] \neq ([A][B])^T$
- $[A] = [A]^T; \quad [C] = [B]^T[A][B]; \quad [C] = [C]^T$

A.12 Define a Matrix Inverse

We can define a matrix inverse as:

$$[A]^{-1} = \frac{\text{Adj}[A]}{\det[A]}; \quad \text{Adj}[A] = [C]^T \text{ where } c_{ij} = (-1)^{(i+j)}|[M_{ij}]|$$

For example:

$$[A] = \begin{bmatrix} 2 & -1 \\ -1 & 1 \end{bmatrix} \quad \Rightarrow \quad [A]^{-1} = \begin{bmatrix} 1 & 1 \\ 1 & 2 \end{bmatrix}$$

A.13 Matrix Inverse Properties

The following properties of matrix inverse apply:

- If the inverse of [A] exists, then the matrix [A] is not singular.
- If the inverse of [A] does not exist, the the matrix [A] is singular.

$$[[A]^{-1}]^{-1} = [A]$$
$$([A][B])^{-1} = [B]^{-1}[A]^{-1}$$

A.14 Define an Eigenvalue Problem

We can decompose two square non-singular, symmetric matrices into their associated eigenvalues and eigenvectors using:

$$[[A] - \lambda[B]]\{X\} = \{0\} \quad \Rightarrow \quad \omega_i^2; \{x_i\}$$

There will exist a pair of eigenvalue/eigenvectors for as many equations as there are for the system. For example:

$$[A] = \begin{bmatrix} 2 & -1 \\ -1 & 1 \end{bmatrix}; \quad [B] = \begin{bmatrix} 1 & 0 \\ 0 & 1 \end{bmatrix} \quad \Rightarrow \quad \left[\begin{bmatrix} 2 & -1 \\ -1 & 1 \end{bmatrix} - \lambda \begin{bmatrix} 1 & 0 \\ 0 & 1 \end{bmatrix}\right] \begin{Bmatrix} x_1 \\ x_2 \end{Bmatrix} = \begin{Bmatrix} 0 \\ 0 \end{Bmatrix}$$
$$\omega_1^2 = 0.382; \quad \{x_1\} = \begin{Bmatrix} 0.5257 \\ 0.8507 \end{Bmatrix}; \quad \omega_2^2 = 2.618; \quad \{x_1\} = \begin{Bmatrix} 0.8507 \\ -0.5257 \end{Bmatrix}$$

A.15 Generalized Inverse

Any general rectangular matrix can be inverted, but when the number of rows or columns are not equal then the inverse is referred to as a generalized inverse:

$$\{x\} = [U]\{p\} \quad \Rightarrow \quad \{p\} = [U]^g\{x\}$$
$$[U]^g = ([U]^T[U])^{-1}[U]^T$$

The Moore–Penrose conditions of the generalized inverse are:

(i) $[U][U]^g[U] = [U]$
(ii) $[U]^g[U][U]^g = [U]^g$

(iii) $([U]^g[U])^T = [U]^g[U]$
(iv) $([U][U]^g)^T = [U][U]^g$

If all four of the Moore-Penrose conditions are met then this is a pseudo-inverse. For example:

$$[x] = \begin{bmatrix} 1 & 2 \\ 3 & 4 \\ 5 & 6 \end{bmatrix} \Rightarrow [x]^g = \begin{bmatrix} -1.333 & -0.333 & 0.667 \\ 1.083 & 0.333 & -0.417 \end{bmatrix}$$

A.16 Singular Value Decomposition

Any matrix can be decomposed into its spectral parts (eigenvalues and eigenvectors):

$$[A] = [U][S][V]^T$$

$$[A] = [\{u_1\} \quad \{u_2\} \quad \cdots] \begin{bmatrix} s_1 & & \\ & s_2 & \\ & & \ddots \end{bmatrix} [\{v_1\} \quad \{v_2\} \quad \cdots]^T$$

$$[A] = \{u_1\}s_1\{v_1\}^T + \{u_2\}s_2\{v_2\}^T + \cdots = \sum_{k=1}^{n} \{u_k\}s_k\{v_k\}^T$$

For example:

$$\begin{bmatrix} 1 & 2 & 3 \\ 2 & 4 & 6 \\ 3 & 6 & 9 \end{bmatrix} = [A] = \{u_1\}s_1\{u_1\}^T = \begin{Bmatrix} 1 \\ 2 \\ 3 \end{Bmatrix} 1 \lfloor 1 \quad 2 \quad 3 \rfloor^T$$

For example:

$$\begin{bmatrix} 2 & 3 & 5 \\ 3 & 5 & 8 \\ 5 & 8 & 13 \end{bmatrix} = \{u_1\}s_1\{v_1\}^T + \{u_2\}s_2\{v_2\}^T = \begin{Bmatrix} 1 \\ 2 \\ 3 \end{Bmatrix} 1 \lfloor 1 \quad 2 \quad 3 \rfloor^T + \begin{Bmatrix} 1 \\ 1 \\ 2 \end{Bmatrix} 1 \lfloor 1 \quad 1 \quad 2 \rfloor^T$$

$$\begin{bmatrix} 1 & 2 & 3 \\ 2 & 4 & 6 \\ 3 & 6 & 9 \end{bmatrix} + \begin{bmatrix} 1 & 1 & 2 \\ 1 & 1 & 2 \\ 2 & 2 & 4 \end{bmatrix}$$

B

Example Using Two Degree of Freedom System: Eigenproblem

Using the two degree of freedom system shown in Figure B.1, let's step through all the equations we have developed and compute the following items:

- Formulate the characteristic polynomial.
- Find the eigenvalues.
- Find the mode shape for mode 1 using both equation 1 and 2 of the system.
- Show that the modes are orthogonal with respect to the system matrices.
- Compute the modal mass and modal stiffness.
- Normalize the mode shapes for unit modal mass.

Performing a force balance for each mass in the system results in two equations:

$$m_1\ddot{x}_1 + k_1x_1 - k_2(x_2 - x_1) = f_1(t)$$
$$m_2\ddot{x}_2 + k_3x_2 + k_2(x_2 - x_1) = f_2(t)$$

Substituting in the values gives

$$\ddot{x}_1 + 428400x_1 - 132900x_2 = f_1(t)$$
$$\ddot{x}_2 - 132900x_1 + 532800x_2 = f_2(t)$$

This can be conveniently written in matrix form as

$$[M]\{\ddot{x}\} + [K]\{x\} = \begin{bmatrix}1 & 0\\ 0 & 1\end{bmatrix}\begin{Bmatrix}\ddot{x}_1\\ \ddot{x}_2\end{Bmatrix} + \begin{bmatrix}428400 & -132900\\ -132900 & 532800\end{bmatrix}\begin{Bmatrix}x_1\\ x_2\end{Bmatrix}$$

Now we recall that the eigen solution can be written as

$$[[K] - \lambda[M]]\{X\} = \{0\} \text{ where } \lambda \text{ is the eigenvalue } \omega^2$$

If we substitute in the values for the mass and stiffness matrices for this equation we get

$$\left[\begin{bmatrix}428400 & -132900\\ -132900 & 532800\end{bmatrix} - \omega^2\begin{bmatrix}1 & 0\\ 0 & 1\end{bmatrix}\right]\begin{Bmatrix}x_1\\ x_2\end{Bmatrix} = \begin{Bmatrix}0\\ 0\end{Bmatrix}$$

Regrouping terms we get

$$\begin{bmatrix}(-\omega^2 + 428400) & -132900\\ -132900 & (-\omega^2 + 532800)\end{bmatrix}\begin{Bmatrix}x_1\\ x_2\end{Bmatrix} = \begin{Bmatrix}0\\ 0\end{Bmatrix}$$

Now the characteristic equation comes from

$$\det\begin{bmatrix}(-\omega^2 + 428400) & -132900\\ -132900 & (-\omega^2 + 532800)\end{bmatrix} = 0$$

Modal Testing: A Practitioner's Guide, First Edition. Peter Avitabile.

Companion Website: www.wiley.com/go/avitabile/modal-testing

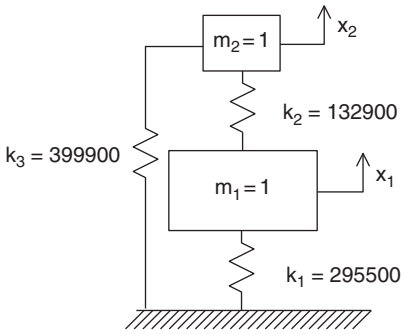

Figure B.1 2-DOF system.

which is $\omega^4 - 961200\omega^2 + 2.10588 \times 10^{11} = 0$. Using the quadratic equation to solve this gives

$$\omega_1^2, \omega_2^2 = \frac{961200 \pm \sqrt{(961200)^2 - 4(1)(2.10588 \times 10^{11}}}{2}$$

which results in the eigenvalues of

$$\omega_1^2 = 337816 \quad \Rightarrow \quad \omega_1 = 581 \text{ rad/sec} \quad \Rightarrow \quad f_1 = 92 \text{ Hz}$$
$$\omega_2^2 = 623384 \quad \Rightarrow \quad \omega_2 = 790 \text{ rad/sec} \quad \Rightarrow \quad f_2 = 125 \text{ Hz}$$

Now in order to find the mode shapes, let's write out Eqs B.1 and B.2 from the system equation

$$(-\omega^2 + 428400)x_1 - 132900x_2 = 0 \tag{B.1}$$
$$-132900x_1 + (-\omega^2 + 532800)x_2 = 0 \tag{B.2}$$

Now in order to find the mode shape for mode 1, we can use either Eq (B.1) or Eq. (B.2). From Eq. (B.1), substitute in ω_1

$$(-337816 + 428400)x_1 - 132900x_2 = 0 \quad \Rightarrow \quad x_1 = 1.467x_2$$

From Eq. (B.2), substitute in ω_1

$$-132900x_1 + (-337816 + 532800)x_2 = 0 \quad \Rightarrow \quad x_1 = 1.467x_2$$

Now in order to find the mode shape for mode 2, we can use either Eq. (B.1) or Eq. (B.2). In Eq. (B.1), substitute in ω_1

$$(-623384 + 428400)x_1 - 132900x_2 = 0 \quad \Rightarrow \quad x_1 = -0.682x_2$$

In Eq. (B.2), substitute in ω_1

$$-132900x_1 + (-623384 + 532800)x_2 = 0 \quad \Rightarrow \quad x_1 = -0.682x_2$$

so that the eigenvalues/vectors are

$$\begin{bmatrix} \omega_1^2 & \\ & \omega_2^2 \end{bmatrix} = \begin{bmatrix} 337816 & 0 \\ 0 & 623384 \end{bmatrix}$$

$$\begin{bmatrix} u_1^{(1)} & u_1^{(2)} \\ u_2^{(1)} & u_2^{(2)} \end{bmatrix} = \begin{bmatrix} 1 & 1 \\ 0.682 & -1.467 \end{bmatrix}$$

$$[\{u_1\} \quad \{u_2\}] = \left[\begin{Bmatrix} u_1^{(1)} \\ u_2^{(1)} \end{Bmatrix} \quad \begin{Bmatrix} u_1^{(2)} \\ u_2^{(2)} \end{Bmatrix} \right] = \left[\begin{Bmatrix} 1 \\ 0.682 \end{Bmatrix} \quad \begin{Bmatrix} 1 \\ -1.467 \end{Bmatrix} \right]$$

Now we recall that the ith modal vector is orthogonal with respect to the jth modal vector using the system matrices. Let's check this with the mass matrix.

$$\{u_j\}^T[M]\{u_i\} \stackrel{?}{\equiv} 0 \quad \Rightarrow \quad \{1 \quad -1.467\}\begin{bmatrix}1 & 0\\ 0 & 1\end{bmatrix}\begin{Bmatrix}1\\ 0.682\end{Bmatrix} \equiv 0$$

Now from the system equations we can write the modal mass and modal stiffness matrices:

$$[U]^T[M][U] = \begin{bmatrix}1 & 0.682\\ 1 & -1.467\end{bmatrix}\begin{bmatrix}1 & 0\\ 0 & 1\end{bmatrix}\begin{bmatrix}1 & 1\\ 0.682 & -1.467\end{bmatrix} = \begin{bmatrix}1.465 & \\ & 3.152\end{bmatrix}$$

$$[U]^T[K][U] = \begin{bmatrix}1 & 0.682\\ 1 & -1.467\end{bmatrix}\begin{bmatrix}428400 & -132900\\ -132900 & 532800\end{bmatrix}\begin{bmatrix}1 & 1\\ 0.682 & -1.467\end{bmatrix}$$

$$= \begin{bmatrix}494900 & \\ & 1965000\end{bmatrix}$$

Now if we normalize the mode shapes to unit modal mass (recall that the normalized mode shapes are the original mode shapes post multiplied by one over the square root of the modal mass), then the mode shape matrix becomes:

$$[U^n] = [U][N] = \begin{bmatrix}1 & 1\\ 0.682 & -1.467\end{bmatrix}\begin{bmatrix}\sqrt{\frac{1}{1.465}} & \\ & \sqrt{\frac{1}{3.152}}\end{bmatrix} = \begin{bmatrix}0.826 & 0.563\\ 0.563 & -0.826\end{bmatrix}$$

and the modal mass and modal stiffness matrices become

$$[U^n]^T[M][U^n] = \begin{bmatrix}0.826 & 0.563\\ 0.563 & -0.826\end{bmatrix}\begin{bmatrix}1 & 0\\ 0 & 1\end{bmatrix}\begin{bmatrix}0.826 & 0.563\\ 0.563 & -0.826\end{bmatrix} = \begin{bmatrix}1 & \\ & 1\end{bmatrix}$$

$$[U^n]^T[K][U^n] = \begin{bmatrix}0.826 & 0.563\\ 0.563 & -0.826\end{bmatrix}\begin{bmatrix}428400 & -132900\\ -132900 & 532800\end{bmatrix}\begin{bmatrix}0.826 & 0.563\\ 0.563 & -0.826\end{bmatrix}$$

$$= \begin{bmatrix}337816 & \\ & 623384\end{bmatrix}$$

C

Pole, Residue, and FRF Problem for 2-DOF System

Using the 2-DOF system in Figure C.1, which is the same as the one used in Appendix B but now with damping, let's step through rest of the equations we have developed and compute the following items:

- Formulate the characteristic polynomial and the resulting poles of the system.
- Formulate the system transfer matrix, the residue matri,x and the frequency response matrix.
- Compute the residues for the first column of the system matrix for modes 1 and 2.
- Compute the modal mass, modal damping, and modal stiffness matrices using the normalized mode shapes from the eigenvalue problem, as done in Appendix B.

Performing a force balance for each mass in the system results in two equations, which are shown below in matrix form:

$$[M]\{\ddot{x}\} + [C]\{\dot{x}\} + [K]\{x\} = \begin{bmatrix} 1 & 0 \\ 0 & 1 \end{bmatrix} \begin{Bmatrix} \ddot{x}_1 \\ \ddot{x}_2 \end{Bmatrix} + \begin{bmatrix} 100 & 0 \\ 0 & 100 \end{bmatrix} \begin{Bmatrix} \dot{x}_1 \\ \dot{x}^2 \end{Bmatrix} + \begin{bmatrix} 428400 & -132900 \\ -132900 & 532800 \end{bmatrix} \begin{Bmatrix} x_1 \\ x_2 \end{Bmatrix}$$

Now we can write the system matrix as:

$$[B(s)] = \left[[M]s^2 + [C]s + [K]\right] = \left[\begin{bmatrix} 1 & 0 \\ 0 & 1 \end{bmatrix} s^2 + \begin{bmatrix} 100 & 0 \\ 0 & 100 \end{bmatrix} s + \begin{bmatrix} 428400 & -132900 \\ -132900 & 532800 \end{bmatrix}\right]$$

The characteristic equation comes from

$$\det[B(s)] = 0 \quad \Rightarrow \quad \det \begin{bmatrix} (s^2 + 100s + 428400) & -132900 \\ -132900 & (s^2 + 100s + 532800) \end{bmatrix} = 0$$

$$(s^2 + 100s + 428400)(s^2 + 100s + 53280000) - (132900)^2 = 0$$

$$s^4 + 200s^3 + 971200s^2 + 96120000s + 21058911000 = 0$$

Solving this gives the roots or poles of the system as:

$$p_1 = -50 + j579,\ p_1{}^* = -50 - j579,\ p_2 = -50 + j788,\ p_2{}^* = -50 - j788$$

The system transfer matrix is:

$$[H(s)] = [B(s)]^{-1} = \frac{\text{Adj}[B(s)]}{\det[B(s)]} = \frac{\begin{bmatrix} (s^2 + 100s + 532800) & 132900 \\ 132900 & (s^2 + 100s + 428400) \end{bmatrix}}{\det[B(s)]}$$

Modal Testing: A Practitioner's Guide, First Edition. Peter Avitabile.

Companion Website: www.wiley.com/go/avitabile/modal-testing

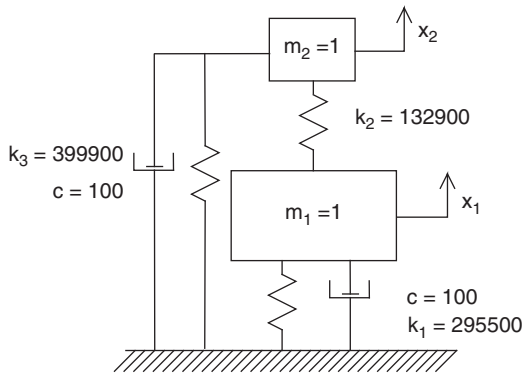

Figure C.1 2-DOF system.

or

$$[H(s)] = [B(s)]^{-1} = \frac{\text{Adj}[B(s)]}{\det[B(s)]} = \frac{\begin{bmatrix}(s^2 + 100s + 532800) & 132900 \\ 132900 & (s^2 + 100s + 428400)\end{bmatrix}}{(s - p_1)(s - p_1{}^*)(s - p_2)(s - p_2{}^*)}$$

We can write out each term of the system transfer matrix as:

$$h_{11}(s) = \frac{(s^2 + 100s + 532800)}{\det[B(s)]} \qquad h_{12}(s) = \frac{132900}{\det[B(s)]}$$
$$h_{21}(s) = \frac{132900}{\det[B(s)]} \qquad h_{22}(s) = \frac{(s^2 + 100s + 428400)}{\det[B(s)]}$$

or as:

$$h_{11}(s) = \frac{(s^2 + 100s + 532800)}{(s - p_1)(s - p_1{}^*)(s - p_2)(s - p_2{}^*)} \qquad h_{12}(s) = \frac{132900}{(s - p_1)(s - p_1{}^*)(s - p_2)(s - p_2{}^*)}$$
$$h_{21}(s) = \frac{132900}{(s - p_1)(s - p_1{}^*)(s - p_2)(s - p_2{}^*)} \qquad h_{22}(s) = \frac{s^2 + 100s + 428400}{(s - p_1)(s - p_1{}^*)(s - p_2)(s - p_2{}^*)}$$

Let's compute the residues for each mode of the system for the 1-1 term of the matrix:

$$a_{11k}(s) = h_{11}(s)(s - p_k)\big|_{s \to p_k} = \frac{(s^2 + 100s + 532800)}{(s - p_1)(s - p_1{}^*)(s - p_2)(s - p_2{}^*)}(s - p_k)$$

Now for pole 1, $p_1 = -50 + j579$, (and its conjugate $p_1{}^* = -50 - j579$), the residue for the 1-1 term becomes

$$a_{111}(p_1) = \frac{(p_1{}^2 + 100p_1 + 532800)}{(p_1 - p_1{}^*)(p_1 - p_2)(p_1 - p_2{}^*)} = 0.11791 \times 10^{-2}/2j$$
$$a_{11k}{}^*(p_1{}^*) = -0.11791 \times 10^{-2}/2j$$

and for pole 2, $p_2 = -50 + j788$ (and its conjugate $p_2{}^* = -50 - j788$), the residue for the 1-1 term becomes

$$a_{112}(p_2) = \frac{(p_2{}^2 + 100p_2 + 532800)}{(p_2 - p_1)(p_2 - p_1{}^*)(p_2 - p_2{}^*)} = 0.4025 \times 10^{-3}/2j$$
$$a_{112}{}^*(p_2{}^*) = -0.4025 \times 10^{-3}/2j$$

Since we have the residues, we can write the system transfer function for the 1-1 term as

$$h_{11}(s) = \sum_{k=1}^{2}\left[\frac{a_{11k}}{(s-p_k)} + \frac{a_{11k}{}^*}{(s-p_k{}^*)}\right] = \frac{a_{111}}{(s-p_1)} + \frac{a_{111}{}^*}{(s-p_1{}^*)} + \frac{a_{112}}{(s-p_2)} + \frac{a_{112}{}^*}{(s-p_2{}^*)}$$

$$h_{11}(s) = \frac{0.11791\times10^{-2}/2j}{(s-(-50+j579))} + \frac{-0.11791\times10^{-2}/2j}{(s-(-50-j579))} + \frac{0.4025\times10^{-3}/2j}{(s-(-50+j788))} + \frac{-0.4025\times10^{-3}/2j}{(s-(-50-j788))}$$

Let's compute the residues for each mode of the system for the 2-1 term of the matrix:

$$a_{21k}(s) = h_{21}(s)(s-p_k)\big|_{s\to p_k} = \frac{132900}{(s-p_1)(s-p_1{}^*)(s-p_2)(s-p_2{}^*)}(s-p_k)$$

Now for pole 1, $p_1 = -50 + j579$, (and its conjugate $p_1{}^* = -50 - j579$), the residue for the 2-1 term becomes

$$a_{211}(p_1) = \frac{(p_1{}^2 + 100p_1 + 532800)}{(p_1-p_1{}^*)(p_1-p_2)(p_1-p_2{}^*)} = 0.8037\times10^{-3}/2j$$

$$a_{211}{}^*(p_1{}^*) = -0.8037\times10^{-3}/2j$$

and for pole 2, $p_2 = -50 + j788$ (and its conjugate $p_2{}^* = -50 - j788$), the residue for the 2-1 term becomes

$$a_{212}(p_2) = \frac{(p_2{}^2 + 100p_2 + 532800)}{(p_2-p_1)(p_2-p_1{}^*)(p_2-p_2{}^*)} = 0.5906\times10^{-3}/2j$$

$$a_{212}{}^*(p_2{}^*) = -0.5906\times10^{-3}/2j$$

Since we have the residues, we can write the system transfer function for the 2-1 term as

$$h_{21}(s) = \sum_{k=1}^{2}\left[\frac{a_{21k}}{(s-p_k)} + \frac{a_{21k}{}^*}{(s-p_k{}^*)}\right] = \frac{a_{211}}{(s-p_1)} + \frac{a_{211}{}^*}{(s-p_1{}^*)} + \frac{a_{212}}{(s-p_2)} + \frac{a_{212}{}^*}{(s-p_2{}^*)}$$

$$h_{21}(s) = \frac{0.8037\times10^{-3}/2j}{(s-(-50+j579))} + \frac{-0.8037\times10^{-3}/2j}{(s-(-50-j579))} + \frac{0.5906\times10^{-3}/2j}{(s-(-50+j788))} + \frac{-0.5906\times10^{-3}/2j}{(s-(-50-j788))}$$

Recall that the eigenvalues/vectors from the undamped solution were

$$\begin{bmatrix}\omega_1^2 & \\ & \omega_2^2\end{bmatrix} = \begin{bmatrix}337816 & 0\\ 0 & 623384\end{bmatrix}$$

$$\begin{bmatrix}u_1^{(1)} & u_1^{(2)}\\ u_2^{(1)} & u_2^{(2)}\end{bmatrix} = \begin{bmatrix}1 & 1\\ 0.682 & -1.467\end{bmatrix}$$

$$[\{u_1\}\ \{u_2\}] = \left[\begin{Bmatrix}u_1^{(1)}\\ u_2^{(1)}\end{Bmatrix}\begin{Bmatrix}u_1^{(2)}\\ u_2^{(2)}\end{Bmatrix}\right] = \left[\begin{Bmatrix}1\\ 0.682\end{Bmatrix}\begin{Bmatrix}1\\ -1.467\end{Bmatrix}\right]$$

and the normalized mode shapes were

$$[U^n] = [U][N] = \begin{bmatrix}1 & 1\\ 0.682 & -1.467\end{bmatrix}\begin{bmatrix}\sqrt{\frac{1}{1.465}} & \\ & \sqrt{\frac{1}{3.152}}\end{bmatrix} = \begin{bmatrix}0.826 & 0.563\\ 0.563 & -0.826\end{bmatrix}$$

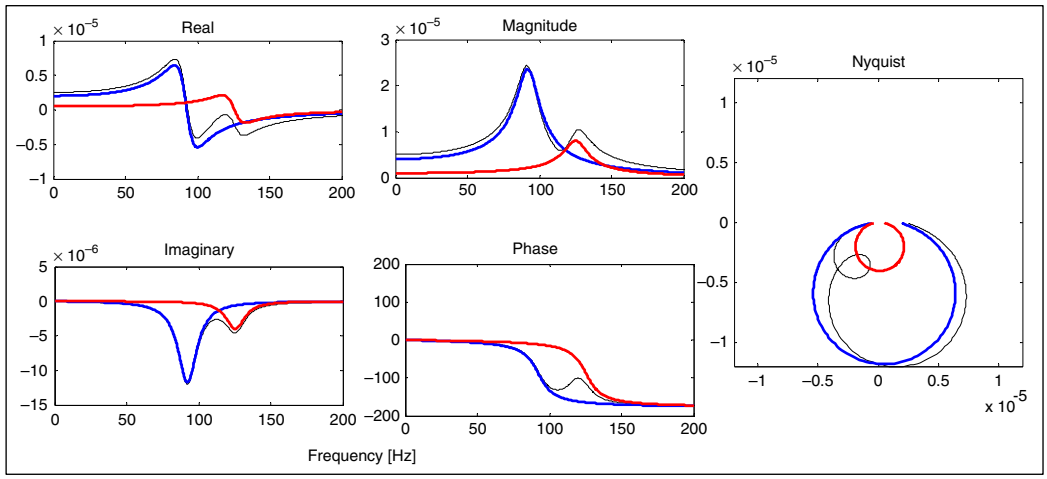

(a)

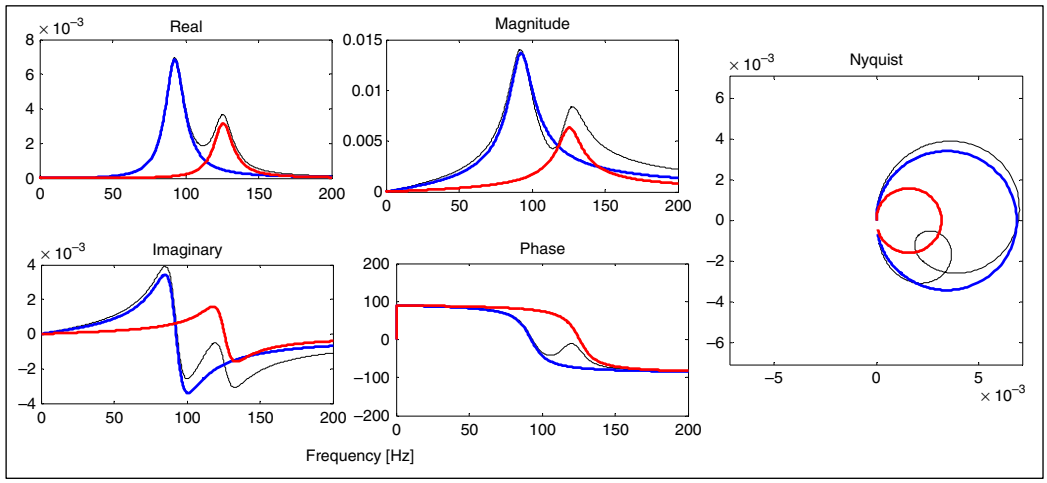

(b)

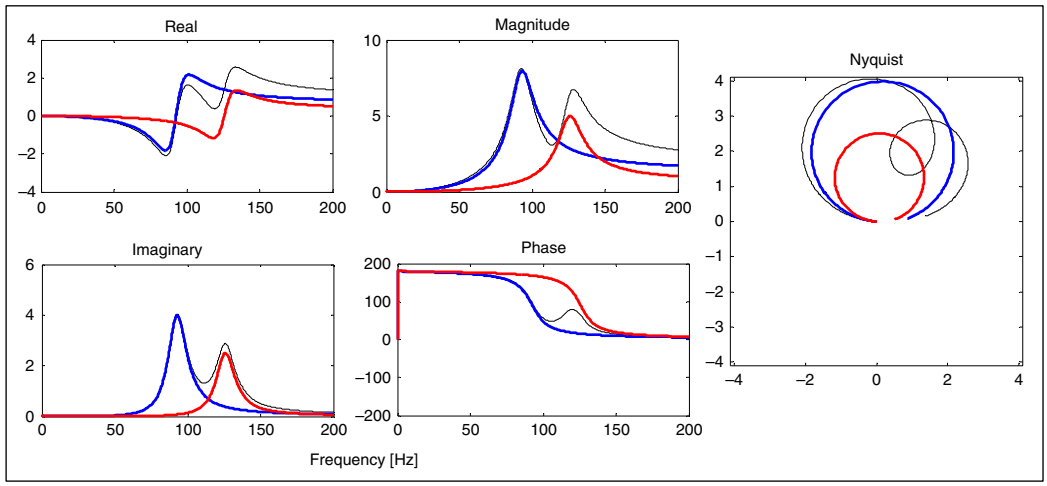

(c)

Figure C.2 D/F FRF (a), V/F (b), A/F (c) FRF for drive point H_{11} FRF with real, imaginary, magnitude, phase, and Nyquist forms of the FRF.

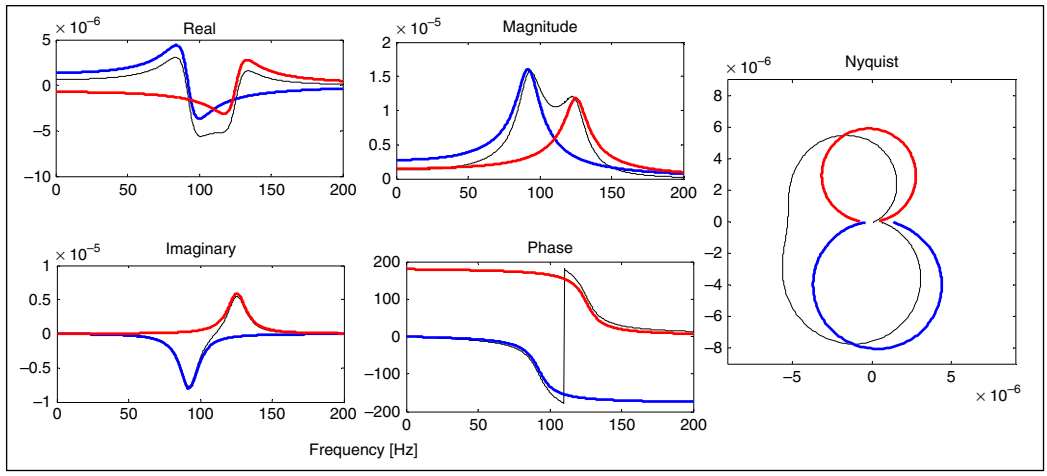

(a)

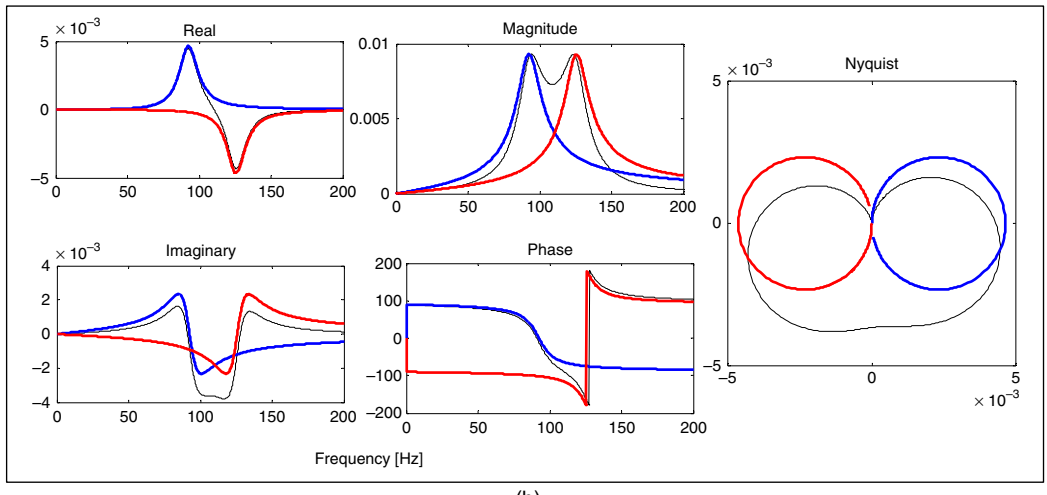

(b)

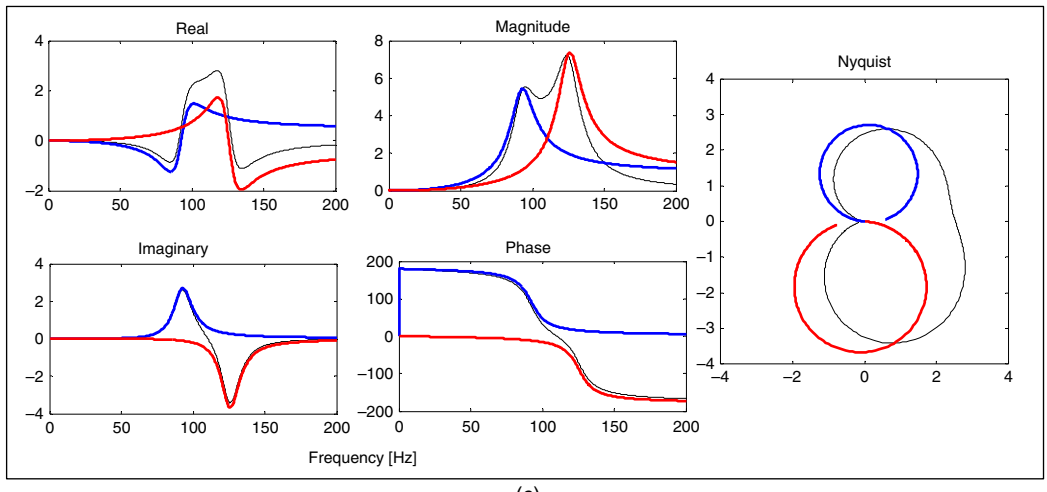

(c)

Figure C.3 D/F FRF (a), V/F (b), A/F (c) FRF for H_{21} cross FRF with real, imaginary, magnitude, phase, and Nyquist forms of the FRF.

The modal mass and modal stiffness matrices written earlier are

$$[U^n]^T[M][U^n] = \begin{bmatrix} 0.826 & 0.563 \\ 0.563 & -0.826 \end{bmatrix} \begin{bmatrix} 1 & 0 \\ 0 & 1 \end{bmatrix} \begin{bmatrix} 0.826 & 0.563 \\ 0.563 & -0.826 \end{bmatrix} = \begin{bmatrix} 1 & \\ & 1 \end{bmatrix}$$

$$[U^n]^T[K][U^n] = \begin{bmatrix} 0.826 & 0.563 \\ 0.563 & -0.826 \end{bmatrix} \begin{bmatrix} 428400 & -132900 \\ -132900 & 532800 \end{bmatrix} \begin{bmatrix} 0.826 & 0.563 \\ 0.563 & -0.826 \end{bmatrix}$$

$$= \begin{bmatrix} 337816 & \\ & 623384 \end{bmatrix}$$

We can now write the modal damping matrix as

$$[U^n]^T[C][U^n] = \begin{bmatrix} 0.826 & 0.563 \\ 0.563 & -0.826 \end{bmatrix} \begin{bmatrix} 100 & 0 \\ 0 & 100 \end{bmatrix} \begin{bmatrix} 0.826 & 0.563 \\ 0.563 & -0.826 \end{bmatrix} = \begin{bmatrix} 100 & \\ & 100 \end{bmatrix}$$

For completeness, the FRFs are plotted as displacement, velocity, and acceleration for the 2-DOF system, for H_{11} and H_{21} in Figures C.2 and C.3, respectively.

D

Example using Three Degree of Freedom System

Using the 3-DOF system shown in Figure D.1 some additional equations will be written to illustrate some additional key points:

- Formulate the equations of motion of the system.
- Formulate the eigensolution and find the eigenvalues/eigenvectors.
- Formulate the equations of motion in modal space.
- Compute the residue matrix and show the frequency response functions.
- Compute the scaling factors using real normal modes.
- Compute the scaling factors using complex modes.

The equations of motion are:

$$[M]\{\ddot{x}\} + [C]\{\dot{x}\} + [K]\{x\} = [F(t)]$$

$$\begin{bmatrix} 1 & & \\ & 1 & \\ & & 1 \end{bmatrix} \begin{Bmatrix} \ddot{x}_1 \\ \ddot{x}_2 \\ \ddot{x}_3 \end{Bmatrix} + \begin{bmatrix} 0.2 & -0.1 & \\ -0.1 & 0.2 & -0.1 \\ & -0.1 & 0.2 \end{bmatrix} \begin{Bmatrix} \dot{x}_1 \\ \dot{x}_2 \\ \dot{x}_3 \end{Bmatrix} + \begin{bmatrix} 20000 & -10000 & \\ -10000 & 20000 & -10000 \\ & -10000 & 20000 \end{bmatrix} \begin{Bmatrix} x_1 \\ x_2 \\ x_3 \end{Bmatrix} = \begin{Bmatrix} f_1 \\ f_2 \\ f_3 \end{Bmatrix}$$

The eigensolution is:

$$[[K] - \lambda[M]]\{X\} = \{0\}$$

$$[\Omega^2] = \begin{bmatrix} 5858 & & \\ & 20000 & \\ & & 34142 \end{bmatrix};$$

$$[U] = [\{u_1\}\ \{u_2\}\ \{u_3\}] = \left[\begin{Bmatrix} 0.500 \\ 0.707 \\ 0.500 \end{Bmatrix} \begin{Bmatrix} 0.707 \\ 0 \\ -0.707 \end{Bmatrix} \begin{Bmatrix} -0.500 \\ 0.707 \\ -0.500 \end{Bmatrix} \right]$$

The equations of motion in modal space are:

$$\begin{bmatrix} \ddots & & \\ & \overline{M} & \\ & & \ddots \end{bmatrix} \begin{Bmatrix} \ddot{p}_1 \\ \ddot{p}_2 \\ \ddot{p}_3 \end{Bmatrix} + \begin{bmatrix} \ddots & & \\ & \overline{C} & \\ & & \ddots \end{bmatrix} \begin{Bmatrix} \dot{p}_1 \\ \dot{p}_2 \\ \dot{p}_3 \end{Bmatrix} + \begin{bmatrix} \ddots & & \\ & \overline{K} & \\ & & \ddots \end{bmatrix} \begin{Bmatrix} p_1 \\ p_2 \\ p_3 \end{Bmatrix} = \begin{Bmatrix} \bar{f}_1 \\ \bar{f}_2 \\ \bar{f}_2 \end{Bmatrix}$$

$$\begin{bmatrix} 1 & & \\ & 1 & \\ & & 1 \end{bmatrix} \begin{Bmatrix} \ddot{p}_1 \\ \ddot{p}_2 \\ \ddot{p}_3 \end{Bmatrix} + \begin{bmatrix} 0.058 & & \\ & 0.200 & \\ & & 0.341 \end{bmatrix} \begin{Bmatrix} \dot{p}_1 \\ \dot{p}_2 \\ \dot{p}_3 \end{Bmatrix} + \begin{bmatrix} 5858 & & \\ & 20000 & \\ & & = 34142 \end{bmatrix} \begin{Bmatrix} p_1 \\ p_2 \\ p_3 \end{Bmatrix} = \begin{Bmatrix} \bar{f}_1 \\ \bar{f}_2 \\ \bar{f}_2 \end{Bmatrix}$$

Modal Testing: A Practitioner's Guide, First Edition. Peter Avitabile.

Companion Website: www.wiley.com/go/avitabile/modal-testing

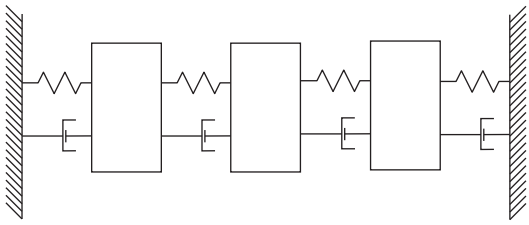

Figure D.1 3-DOF system.

Now the complex pole solution gives the pole information shown in Table D.1:

Table D.1 Frequency and damping for 3-DOF system.

Mode	f_d	f	ζ	Complex pole
	(Hz)	(Hz)	% critical	(rad/sec)
1	12.18	12.18	0.038%	−0.029 ± j 76.537
2	22.51	22.51	0.071%	−0.100 ± j 141.42
3	29.41	29.41	0.092%	−0.171 ± j 184.78

Now the residues (note that these are R and not A) for the first column of the frequency response matrix are as shown in Table B.2.

Table D.2 Residues for the 3-DOF system.

	Mode 1	Mode 2	Mode 3
h_{11}	0.003266 ± j 0.0	0.003536 ± j 0.0	0.001353 ± j 0.0
h_{21}	0.004619 ± j 0.0	0.0 ± j 0.0	0.001913 ± j 0.0
h_{31}	0.003266 ± j 0.0	−0.003536 ± j 0.0	0.001353 ± j 0.0

Now the residues for the first column of the frequency response matrix are:

$$
\begin{aligned}
h_{11} = {} & \frac{0.003266 + j0}{j\omega - (-0.029 + 76.537)} + \frac{0.003266 - j0}{j\omega - (-0.029 - 76.537)} \\
& + \frac{0.003536 + j0}{j\omega - (-0.100 + 141.42)} + \frac{0.003536 - j0}{j\omega - (-0.100 - 141.42)} \\
& + \frac{0.001353 + j0}{j\omega - (-0.171 + 184.78)} + \frac{0.001353 - j0}{j\omega - (-0.171 - 184.78)} \\
h_{21} = {} & \frac{0.004619 + j0}{j\omega - (-0.029 + 76.537)} + \frac{0.004619 - j0}{j\omega - (-0.029 - 76.537)} \\
& + \frac{0.0 + j0}{j\omega - (-0.100 + 141.42)} + \frac{0.0 - j0}{j\omega - (-0.100 - 141.42)} \\
& + \frac{0.001913 + j0}{j\omega - (-0.171 + 184.78)} + \frac{0.001913 - j0}{j\omega - (-0.171 - 184.78)} \\
h_{31} = {} & \frac{0.003266 + j0}{j\omega - (-0.029 + 76.537)} + \frac{0.003266 - j0}{j\omega - (-0.029 - 76.537)} \\
& + \frac{-0.003536 + j0}{j\omega - (-0.100 + 141.42)} + \frac{-0.003536 - j0}{j\omega - (-0.100 - 141.42)} \\
& + \frac{0.001353 + j0}{j\omega - (-0.171 + 184.78)} + \frac{0.001353 - j0}{j\omega - (-0.171 - 184.78)}
\end{aligned}
$$

The residues can be computed using real normal modes as follows. Recall that the residue matrix is:

$$\begin{bmatrix} r_{11} & r_{12} & r_{13} \\ r_{21} & r_{22} & r_{23} \\ r_{31} & r_{32} & r_{33} \end{bmatrix}^{(k)} = \frac{1}{\overline{m}_k \overline{\omega}_k} \begin{bmatrix} u_1u_1 & u_1u_2 & u_1u_3 \\ u_2u_1 & u_2u_2 & u_2u_3 \\ u_3u_1 & u_3u_2 & u_3u_3 \end{bmatrix}^{(k)}$$

Recall for a drive point measurement, we can compute

- modal mass $\overline{m}_k - \frac{1}{q_k \overline{\omega}_k}$
- modal damping $\overline{c}_k = 2\sigma_k \overline{m}_k$
- modal stiffness $\overline{k}_k = (\sigma_k^2 + \overline{\omega}_k^2)\overline{m}_k$

Now using unit modal mass scaling, the first column of the frequency response matrix can be written as

$$\begin{Bmatrix} r_{11} \\ r_{21} \\ r_{31} \end{Bmatrix}^{(k)} = q_k \begin{Bmatrix} u_1u_1 \\ u_2u_1 \\ u_3u_1 \end{Bmatrix}^{(k)} = q_k u_1 \begin{Bmatrix} u_1 \\ u_2 \\ u_3 \end{Bmatrix}^{(k)}$$

For Mode 1,

$$\begin{Bmatrix} 0.32664E-2 \\ 0.46194E-2 \\ 0.32664E-2 \end{Bmatrix} = \begin{Bmatrix} r_{11} \\ r_{21} \\ r_{31} \end{Bmatrix}^{(1)} == q_1 u_1 \begin{Bmatrix} u_1 \\ u_2 \\ u_3 \end{Bmatrix}^{(1)} = \frac{1}{76.537}(0.500) \begin{Bmatrix} 0.500 \\ 0.707 \\ 0.500 \end{Bmatrix}$$

For Mode 2,

$$\begin{Bmatrix} 0.3536E-2 \\ 0.0 \\ -0.3536E-2 \end{Bmatrix} = \begin{Bmatrix} r_{11} \\ r_{21} \\ r_{31} \end{Bmatrix}^{(2)} == q_2 u_1 \begin{Bmatrix} u_1 \\ u_2 \\ u_3 \end{Bmatrix}^{(2)} = \frac{1}{141.42}(0.707) \begin{Bmatrix} 0.707 \\ 0.0 \\ 0.707 \end{Bmatrix}$$

For Mode 3,

$$\begin{Bmatrix} 0.13530E-2 \\ -0.19134E-2 \\ 0.13530E-2 \end{Bmatrix} = \begin{Bmatrix} r_{11} \\ r_{21} \\ r_{31} \end{Bmatrix}^{(3)} == q_3 u_1 \begin{Bmatrix} u_1 \\ u_2 \\ u_3 \end{Bmatrix}^{(3)} = \frac{1}{184.78}(-0.500) \begin{Bmatrix} -0.500 \\ 0.707 \\ -0.500 \end{Bmatrix}$$

This 3-DOF system was actually first used by the Dynamic Systems Laboratory at the Michigan Technological University and had a companion analog circuit derived for simulation studies. This analog circuit was also assembled at the University of Massachusetts Lowell in the former Modal Analysis and Controls Laboratory. This model was developed in MATLAB for simulation; the analog circuit was also used to acquire measurements. The circuit allowed for input forces at each of the three DOFs and allowed for response measurement of displacement, velocity and acceleration ar each of the three DOFs of the system. The remaining figures show the FRFs (in various forms) related to this analog circuit. Note that these FRFs are actual measurements taken from an equivalent analog circuit of the system.

MTU ANALOG – FREQUENCY RESPONSE FUNCTION – H11

$$h_{11} = \frac{0.003266 + j0}{j\omega - (-0.029 + 76.537)} + \frac{0.003266 - j0}{j\omega - (-0.029 - 76.537)}$$
$$+ \frac{0.003536 + j0}{j\omega - (-0.100 + 141.42)} + \frac{0.003536 - j0}{j\omega - (-0.100 - 141.42)}$$
$$+ \frac{0.001353 + j0}{j\omega - (-0.171 + 184.78)} + \frac{0.001353 - j0}{j\omega - (-0.171 - 184.78)}$$

PLOT: 7 Magnitude of H11 FRF - synthesized

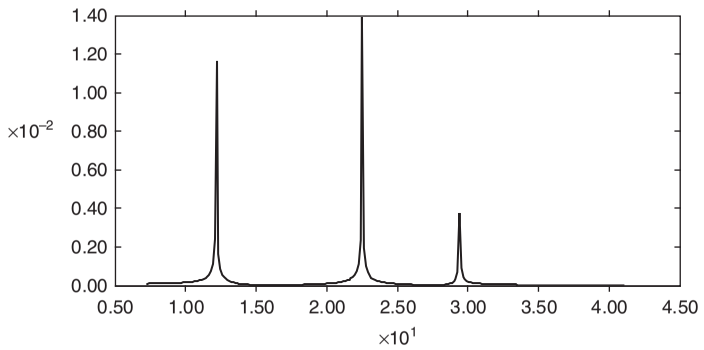

3 DOF ANALOG MODEL

PLOT: 1 Real part of H11 FRF - synthesized

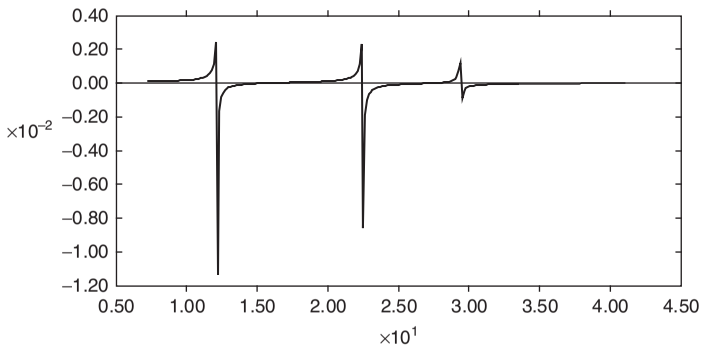

3 DOF ANALOG MODEL

PLOT: 8 Phase of H11 FRF - synthesized

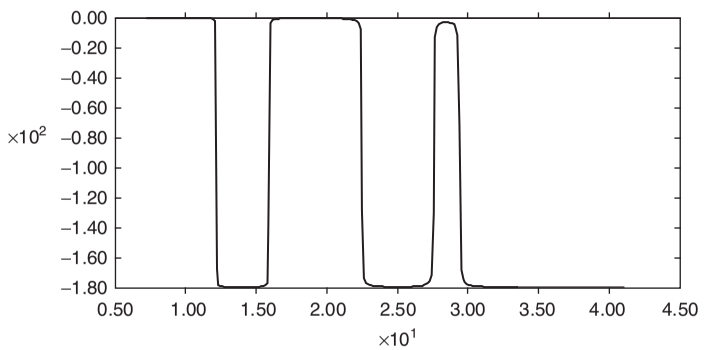

3 DOF ANALOG MODEL

PLOT: 2 Imaginary part of H11 FRF - synthesized

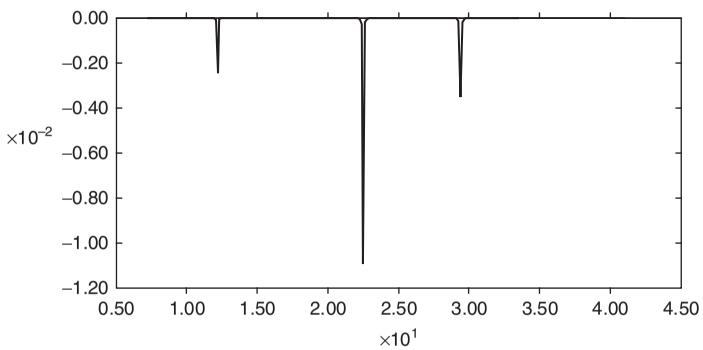

3 DOF ANALOG MODEL

MTU ANALOG – FREQUENCY RESPONSE FUNCTION – H21

$$h_{21} = \frac{0.004619 + j0}{j\omega - (-0.029 + 76.537)} + \frac{0.004619 - j0}{j\omega - (-0.029 - 76.537)}$$
$$+ \frac{0.0 + j0}{j\omega - (-0.100 + 141.42)} + \frac{0.0 - j0}{j\omega - (-0.100 - 141.42)}$$
$$+ \frac{0.001913 + j0}{j\omega - (-0.171 + 184.78)} + \frac{0.001913 - j0}{j\omega - (-0.171 - 184.78)}$$

PLOT: 9 Magnitude of H21 FRF - synthesized

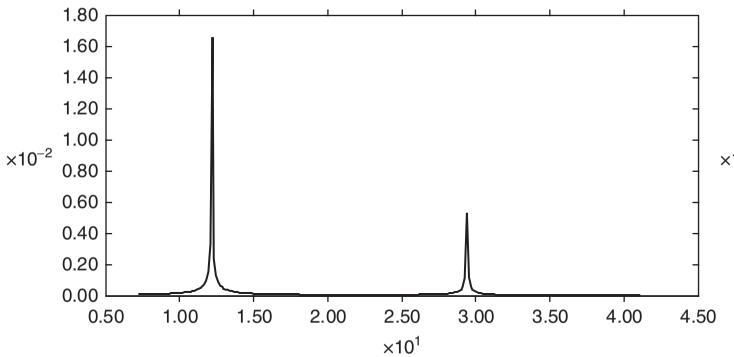

3 DOF ANALOG MODEL

PLOT: 3 Real part of H21 FRF - synthesized

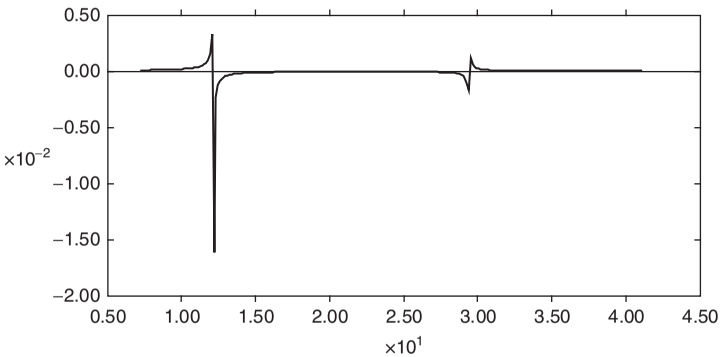

3 DOF ANALOG MODEL

PLOT: 10 Phase of H21 FRF - synthesized

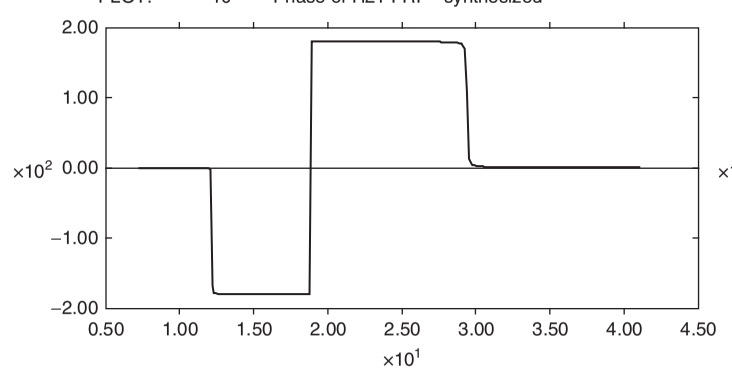

3 DOF ANALOG MODEL

PLOT: 4 Imaginary part of H21 FRF - synthesized

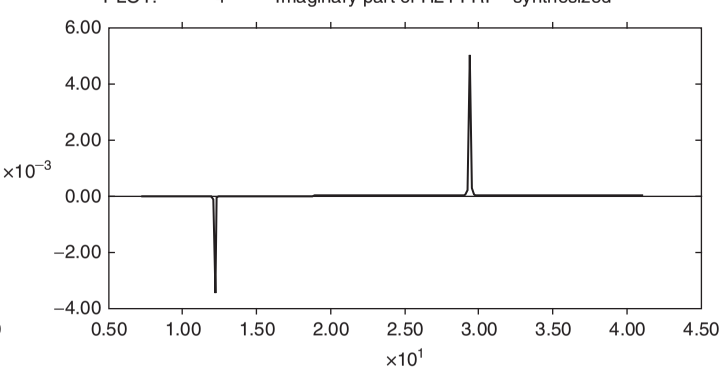

3 DOF ANALOG MODEL

MTU ANALOG – FREQUENCY RESPONSE FUNCTION – H31

$$h_{31} = \frac{0.003266 + j0}{j\omega - (-0.029 + 76.537)} + \frac{0.003266 - j0}{j\omega - (-0.029 - 76.537)}$$
$$+ \frac{-0.003536 + j0}{j\omega - (-0.100 + 141.42)} + \frac{-0.003536 - j0}{j\omega - (-0.100 - 141.42)}$$
$$+ \frac{0.001353 + j0}{j\omega - (-0.171 + 184.78)} + \frac{0.001353 - j0}{j\omega - (-0.171 - 184.78)}$$

PLOT: 11 Magnitude of H31 FRF - synthesized

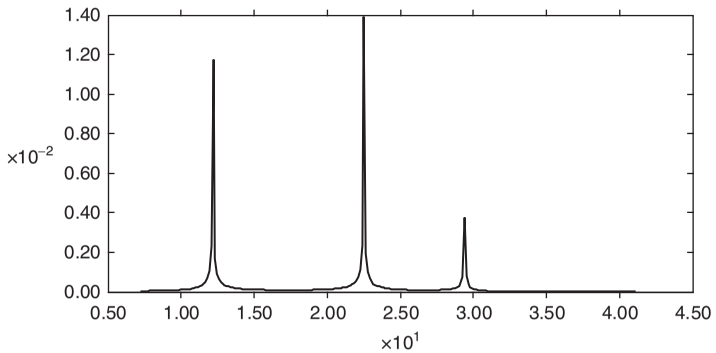

3 DOF ANALOG MODEL

PLOT: 5 Real part of H31 FRF - synthesized

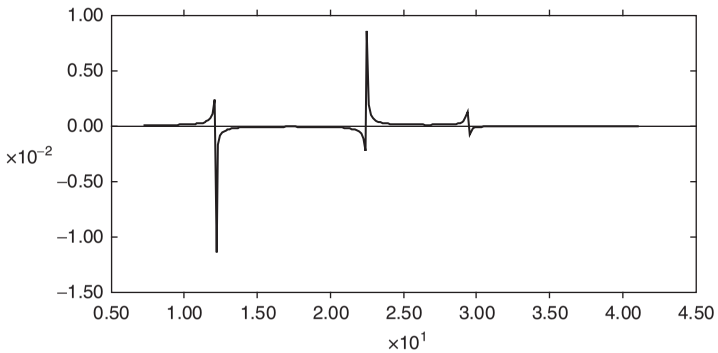

3 DOF ANALOG MODEL

PLOT: 12 Phase of H31 FRF - synthesized

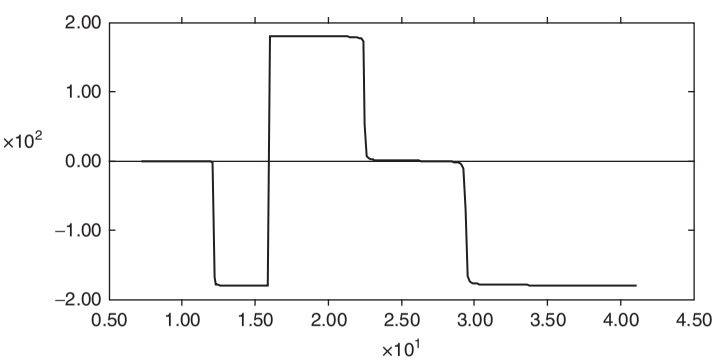

3 DOF ANALOG MODEL

PLOT: 6 Imaginary part of H31 FRF - synthesized

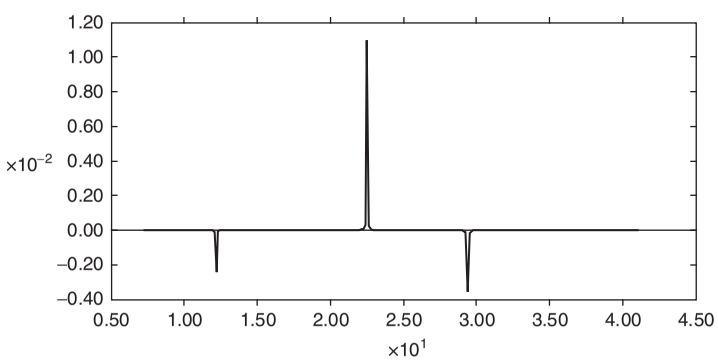

3 DOF ANALOG MODEL

MTU ANALOG – FREQUENCY RESPONSE FUNCTION MATRIX

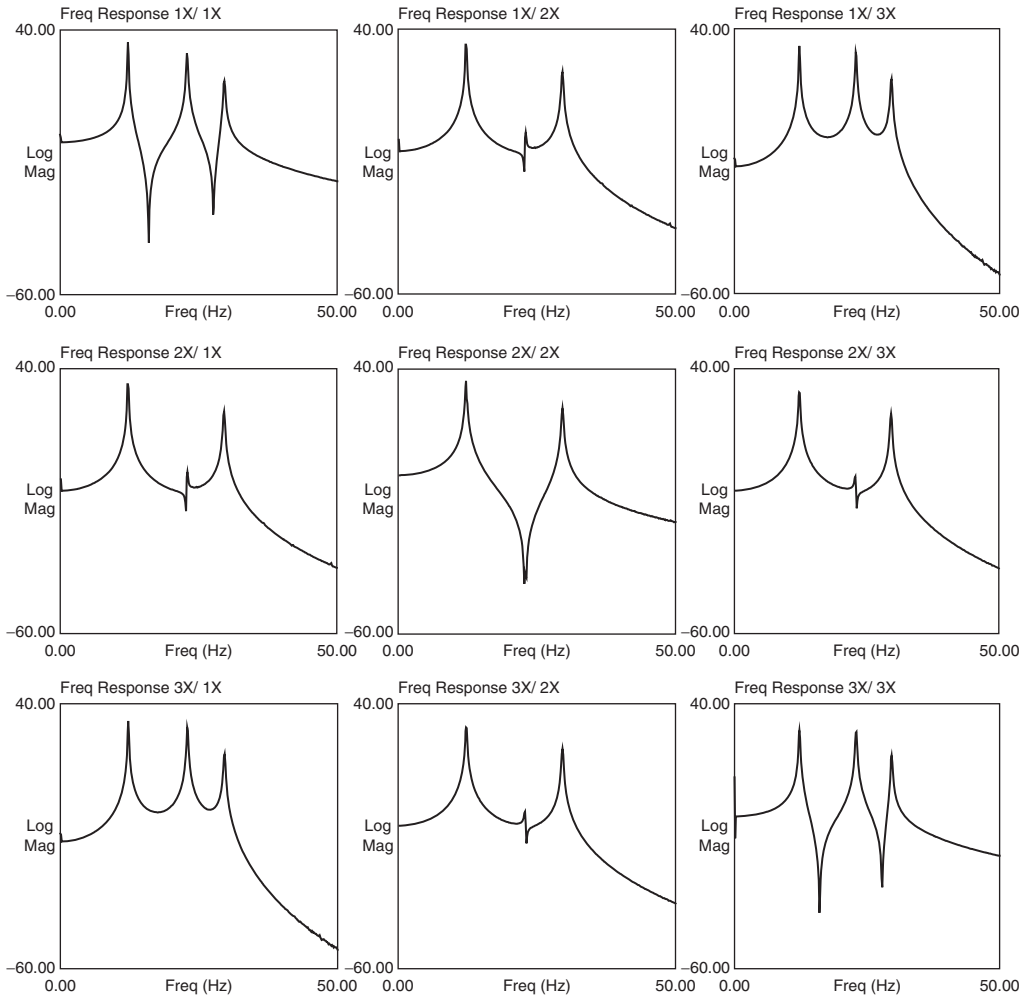

(NOTE: these FRFs are actual measurement taken from an equivalent analog circuit of the system.)

MTU ANALOG – FREQUENCY RESPONSE FUNCTION ACCELERATION/VELOCITY/DISPLACEMENT PLOTS

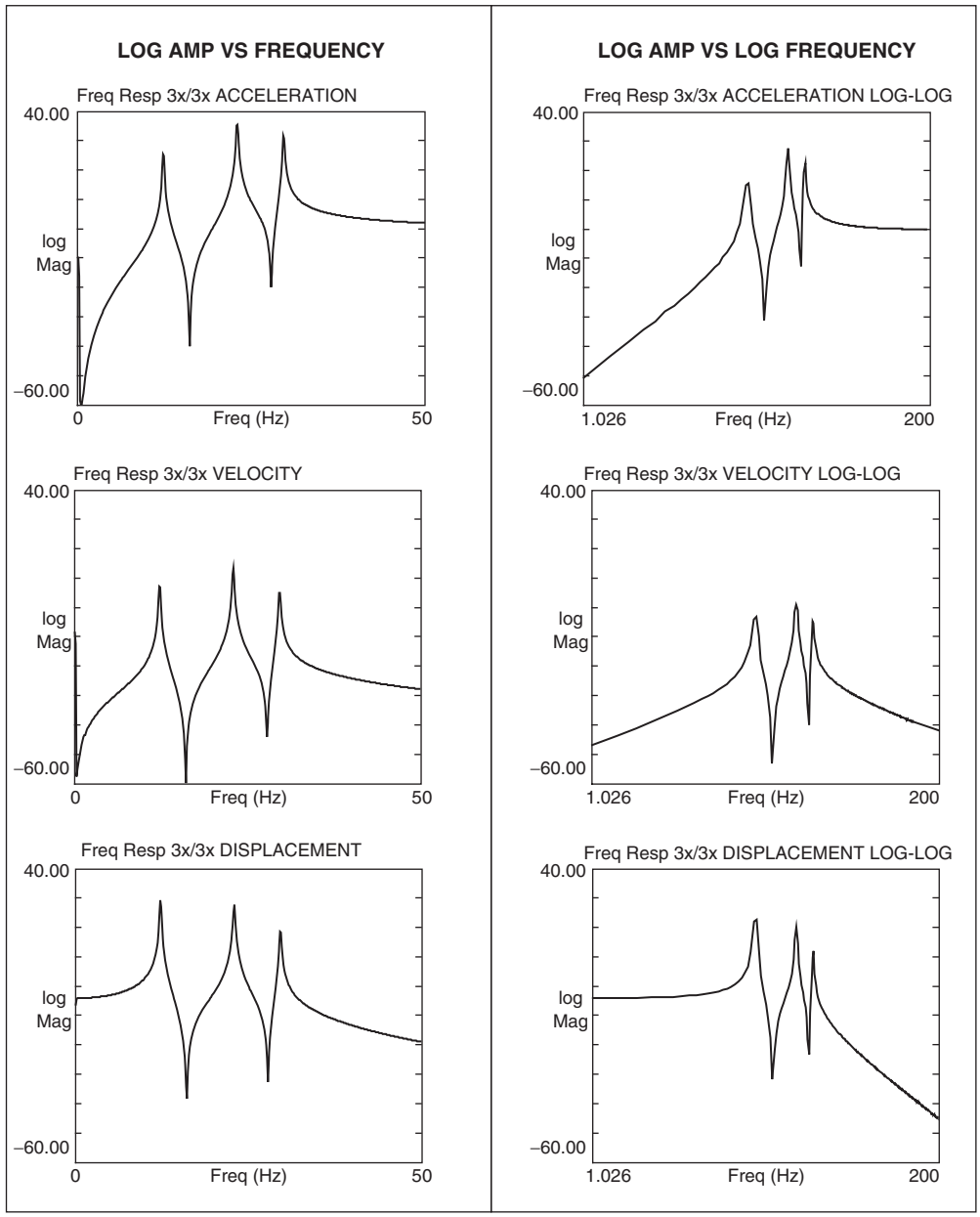

(NOTE: these FRFs are actual measurement taken from an equivalent analog circuit of the system.)

E

DYNSYS Website Materials

An NSF engineering education grant (EEC-0314875) entitled "Multi-semester interwoven project for teaching basic core STEM material critical for solving dynamic systems problems" was funded from July 2003 to June 2006. This project was intended to address the disconnect between teaching and understanding this material because generally students do not understand how basic math and science material fits into all of their engineering courses.

The efforts of this work were directed towards the integration of materials important to solving dynamic systems problems, in a multi-semester integrated approach. To meet this goal, a variety of materials were developed, along with an online acquisition system that embodied all of the typical problems that must be addressed to solve the response of a second order mechanical system due to impulsive and initial conditions loadings.

Analytical tools were developed with a simple graphical user interface (GUI) that allowed students to easily explore characteristic responses of a variety of different systems; both LabVIEW and MATLAB were employed, being commonly used educational tools. GUIs were developed for first and second order system characteristics and responses, along with pertinent processing tools for integration, differentiation, and regression analyses. In addition, Fourier series and signal processing techniques were also included, along with complex frequency response and s-plane representations. Several other GUIs and tutorials were also developed as part of the project. These materials are described here and available at the book website.

E.1 Technical Materials Developed

A series of tutorial modules was developed to address first and second order systems. These tutorials are intended to address mechanical systems from an analytical standpoint as well as the measurement of those analytical systems that introduce electrical signal conditioning/measurement issues that also involve first and second order systems. These tutorials can be roughly broken down as:

- theoretical aspects of first and second order systems
- first order systems: modeling step with ODE and block diagram
- second order systems: modeling step, impulse, IC with ODE and block diagram
- mathematical modeling considerations
- Simulink and MATLAB primer materials
- miscellaneous materials.

These tutorials are briefly described below. The website contains all of the tutorials and exercises that accompany each tutorial. In addition, all of the tutorial GUIs and exercises are voice annotated using Flash on the project website.

Modal Testing: A Practitioner's Guide, First Edition. Peter Avitabile.

Companion Website: www.wiley.com/go/avitabile/modal-testing

E.1.1 Theoretical Aspects of First and Second Order Systems

This tutorial is a basic overview of the underlying information regarding the classical treatment of this material.

E.1.2 First Order Systems: Modeling Step with ODE and Block Diagram

Response of first order systems: step response, impulse response and free response covers basic development of a model for a first order system. A MATLAB script with variable parameter selection via a GUI as well as a LabVIEW VI allows the user to explore parameters other than the specific values used in the tutorial.

Block diagram modeling of first order systems covers basic development of a model. A block diagram using Simulink is the end result of this tutorial. The user can vary parameters in Simulink to explore the effects of parameter variation.

Filtering using RC circuits covers basic development of a first order system but using the frequency domain rather than the time domain response approach. Concepts of time response, cutoff frequency, and roll-off are described and the filter effect on simple sine wave is introduced. A MATLAB script with variable parameter selection via a GUI and a LabVIEW VI allows the user to explore parameters other than the specific values used in the tutorial.

E.1.3 Second Order Systems: Modeling Step, Impulse, IC with ODE and Block Diagram

Response of second order systems: step, impulse and initial conditions covers basic development of a model. A MATLAB script with variable parameter selection via a GUI as well as a LabVIEW VI allows the user to explore parameters other than the specific values used in the tutorial.

Block diagram modeling of second order systems covers basic development of a model. A block diagram using Simulink is the end result of this tutorial. A MATLAB script with variable parameter selection via a GUI allows the user to explore parameters other than the specific values used in the tutorial.

E.1.4 Mathematical Modeling Considerations

Fourier series tutorial covers basic concepts of generating a set of Fourier series terms to approximate general waveforms. A Simulink script (as well as a LabVIEW VI) with variable Fourier series terms selection via a GUI allows the user to explore the generation of arbitrary waveforms other than the specific values used in the tutorial.

Numerical integration/differentiation tutorial covers basic concepts of general integration and differentiation of second order system response of displacement, velocity, and acceleration. A MATLAB/Simulink GUI allows the user to easily modify noise contaminants on the signal and view the effects upon integrating or differentiating the data.

Regression analysis tutorial covers basic concepts of generation of least squares error fit of a set of data that consists of higher order effects but can be evaluated as piecewise linear over regimes of the data provided. A MATLAB GUI allows the user to easily select different data sets, order model, and other parameters to view the effect on the computed analytical model that best describes the data.

Convolution analysis tutorial covers basic concepts of the convolution integral and application to pure mathematical representations of some common waveforms as well as a specific

application to a second order mechanical system subjected to an impulse excitation. A LabVIEW GUI allows the user to easily select different mathematical functions to understand convolution concepts by interacting with the integration process to move forward or backward in the numerical process and see the complete development of the resulting computation as well as the individual function relationship during the process.

E.1.5 Simulink and MATLAB Primer Materials

1) Basic tutorial on the use of Simulink.
2) Importing and exporting data from MATLAB and Simulink to Excel.
3) Using state space and transfer function blocks in Simulink.
4) Modeling an impulse in Simulink.
5) Use of the LTI viewer and MUX blocks in Simulink.

E.1.6 Miscellaneous Materials

S-plane 3D uses a MATLAB GUI that allows the user to explore the S-Plane through a GUI interface to see the effects of parameters on the system characteristics

Frequency response function has a MATLAB GUI that allows the user to explore the complex frequency response function (real, imag, mag, phase) for effects of parameters on the system characteristics.

E.2 DYNSYS.UML.EDU Website

The DYNSYS.UML.EDU website was developed to house all the materials developed (Figure E.1).

One important page of the website is the "filemap" page, which has an image map to jump to any of the tutorials, GUIs, or online materials available. Figure E.2 provides an excellent overview of the entire set of materials available.

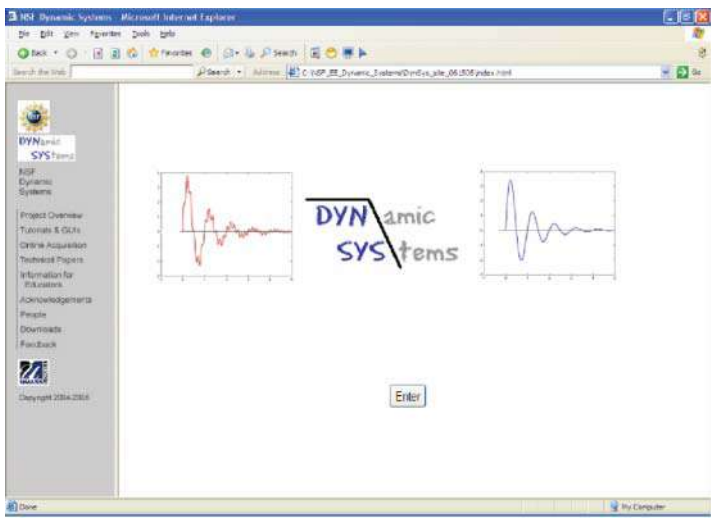

Figure E.1 Website front page.

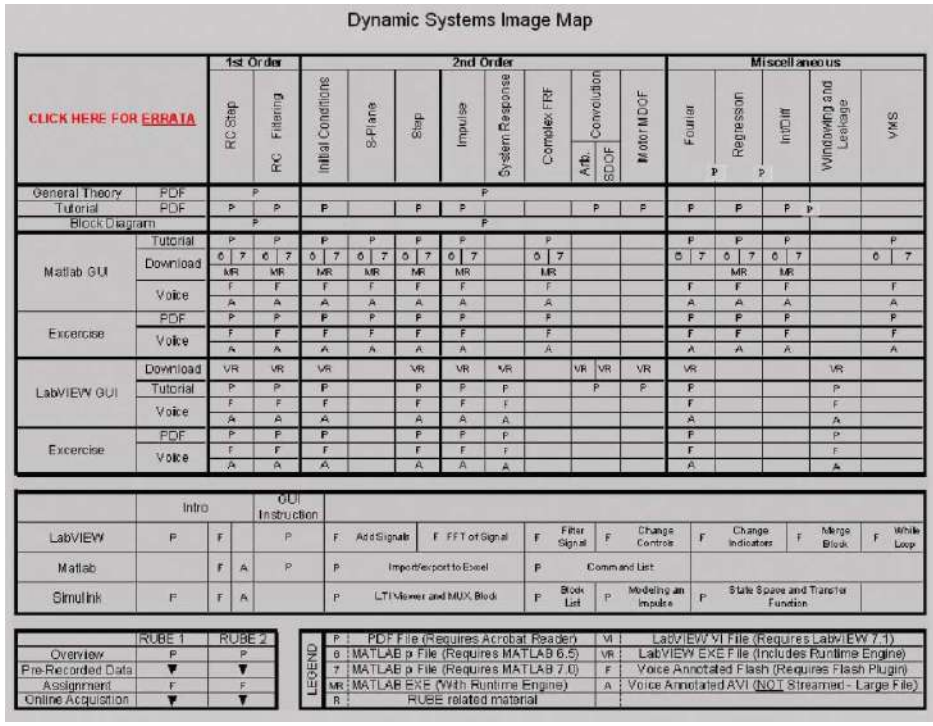

Figure E.2 The filemap page.

The work on this project was funded by the NSF Engineering Education Division Grant EEC-0314875 entitled "Multi-semester interwoven project for teaching basic core STEM material critical for solving dynamic systems problems". Any opinions, findings, and conclusions or recommendations expressed in this material are those of the authors and do not necessarily reflect the views of the National Science Foundation The authors are grateful for the support obtained from NSF to further engineering education.

The efforts of the co-PIs on this project need to be recognized; they have provided unique perspectives, ideas, and support throughout this effort. But the real acknowledgement should go to the students that essentially created all the materials. There were many students that participated in this project starting mainly as undergraduates and then progressing on to graduate work. These students have been the driving force of this effort. This could not have been done without their dedication and devotion to developing these materials and RUBE online acquisition system. It has been a privilege and pleasure working with them and having them contribute to this effort.

Contributing Professors

Peter Avitabile, Associate Professor, Mechanical Engineering
John White, Professor, Chemical & Nuclear Engineering
Stephen Pennell, Professor, Department of Mathematical Sciences
Chuck Van Karsen, Associate Professor, Michigan Technological University

Participating Students

Tracy Van Zandt, Undergraduate & Graduate Student, Mechanical Engineering
Nels Wirkkala, Undergraduate & Graduate Student, Mechanical Engineering
Jeffrey Hodgkins, Undergraduate & Graduate Student, Mechanical Engineering
Narine Malkhasyan, Graduate Student, Chemical Engineering
Charles Wes Goodman, Undergraduate & Graduate Student, Mechanical Engineering
Dana Nicgorski, Undergraduate Student, Mechanical Engineering
Adam Butland, Undergraduate Student, Mechanical Engineering
Christopher Chipman, Undergraduate Student, Mechanical Engineering
Aaron Williams, Undergraduate Student, Mechanical Engineering
Tiffini Johnson, Undergraduate Student, Mechanical Engineering

Undergraduate Capstone Projects

RUBE 0 (Initial Conceptualization of Second Order Mechanical System)
Charles Wes Goodman, Undergraduate Student, Mechanical Engineering
Jeffrey Hodgkins, Undergraduate Student, Mechanical Engineering
RUBE 1 (Second Order Mechanical System with Initial Displacement)
Nels Wirkkala, Undergraduate Student, Mechanical Engineering
Tiffini Johnson, Undergraduate Student, Mechanical Engineering
Dereck Ouellet, Undergraduate Student, Mechanical Engineering
RUBE 2 (Second Order Mechanical System with Impact and Initial Displacement)
Adam Butland, Undergraduate Student, Mechanical Engineering
Dana Nicgorski, Undergraduate Student, Mechanical Engineering

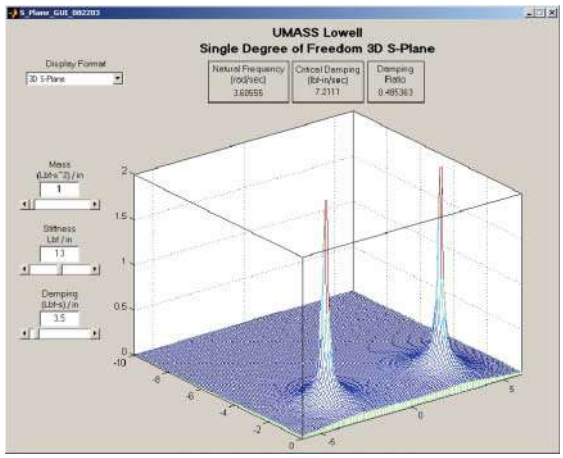

MATLAB: Single DOF 3D S-plane GUI

User enters M, C, K and natural frequency, critical damping and damping are reported.

User can vary the physical parameters with slide bars. The user can select various 3D transfer function display options of real, imaginary, magnitude, phase, and root locus plots.

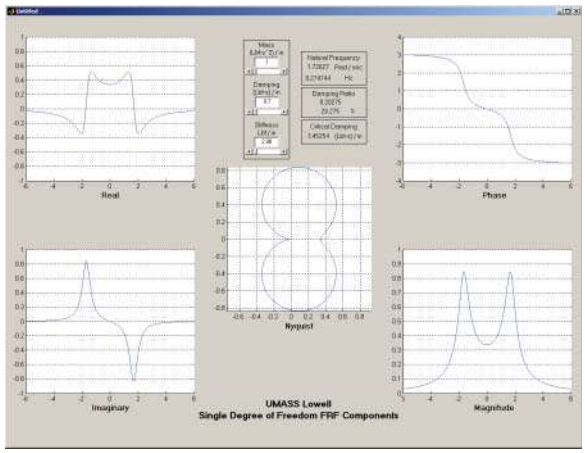

MATLAB: Single DOF complex FRF plot GUI

User enters M, C, K and natural frequency, critical damping, and damping are reported.

User can vary the physical parameters with slide bars. The complex frequency response function is displayed simultaneously as real, imaginary, magnitude, phase, and Nyquist plots.

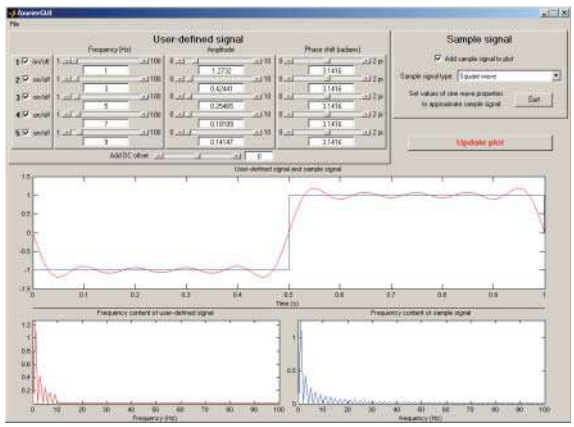

MATLAB: Fourier series signal generation GUI

User enters frequency, amplitude and phase components of a user-defined signal to display the resulting signal. The user can also select sample signals such as square, triangle, and so on, and the pre-determined Fourier coefficients are applied to the user-defined signal. The time signal and the corresponding frequency component are displayed.

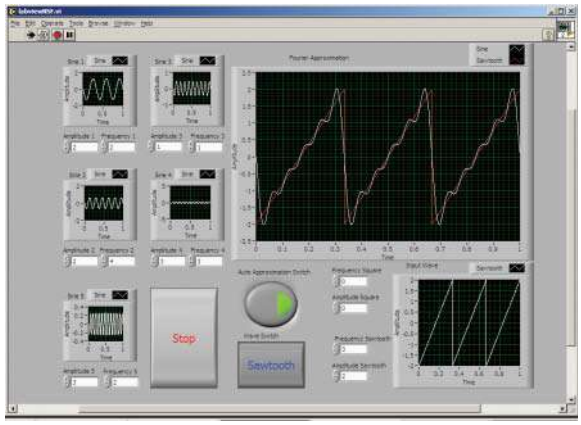

Labview: Fourier series signal generation GUI

User enters frequency, amplitude, and phase components of a user-defined signal to display the resulting signal. The user can also select sample signals such as square, triangle, and so on. The pre-determined Fourier coefficients are applied to the user-defined signal. The time signal and the corresponding frequency component are displayed.

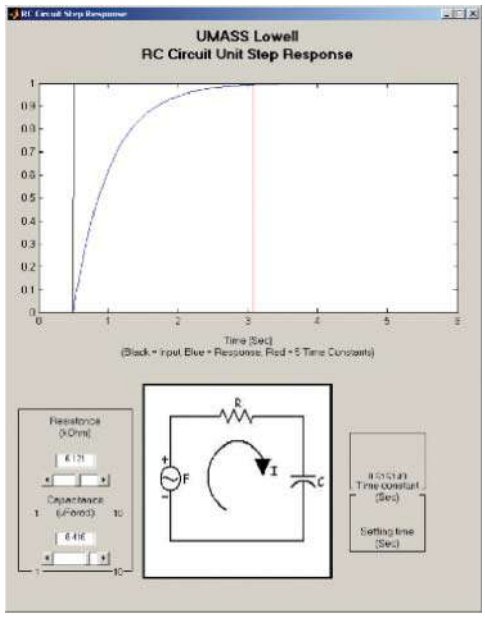

MATLAB: First order step function GUI

User enters resistance and capacitance values to observe the time response due to a step function. The time response is displayed, showing the rise to the step value.

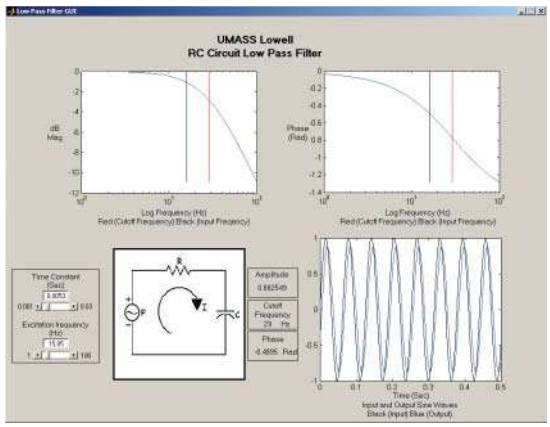

MATLAB: First order low pass filter GUI

User enters time constant and sinusoidal frequency. The Bode plot is displayed with the cutoff frequency and the sinusoidal frequency applied. The initial sinusoidal signal and "filtered" time signal are also displayed.

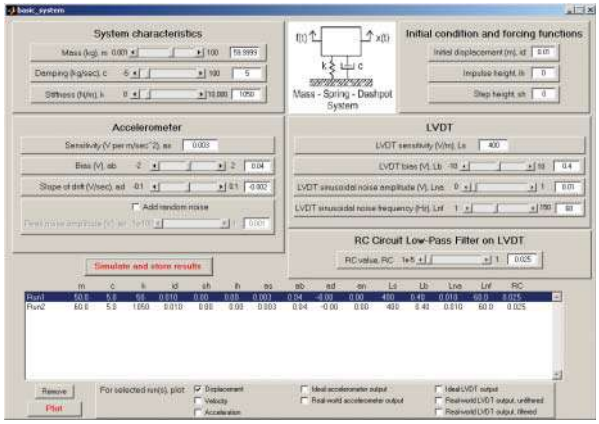

MATLAB/Simulink: Virtual representation of an actual measurement system GUI

User enters M, C, K system. User enters the amount of experimental distortion on the accelerometer (sensitivity, bias, drift) and displacement LVDT (sensitivity, bias, noise) and the low pass filter characteristics to "simulate" the measurement environment. Data can be exported, with ability to select which outputs and what effects are included on the measurement.

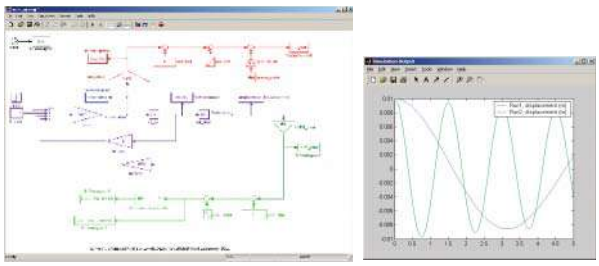

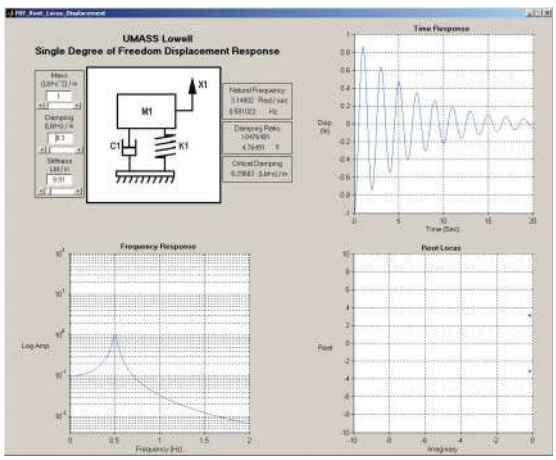

MATLAB: Second order system initial condition response GUI

User enters M, C, K and natural frequency, critical damping and damping are reported. User can vary the physical parameters with slide bars. The frequency response function magnitude is displayed root locus and time response.

MATLAB: Second order system impulse response GUI (not shown)

This is similar to the GUI above.

MATLAB: Second order system step response GUI (not shown)

This is similar to the GUI above.

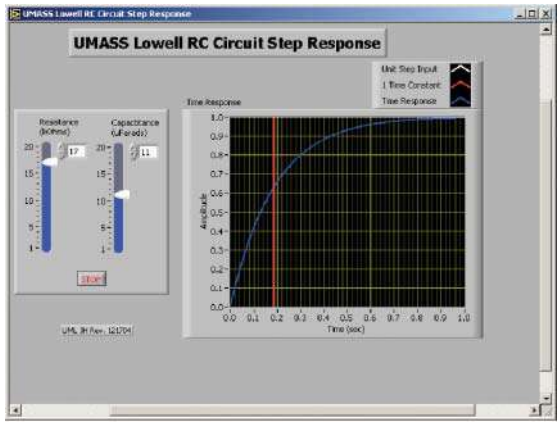

LabVIEW: First order step response GUI

User enters resistance and capacitance values to observe the time response due to a step function. The time response is displayed, showing the rise to the step value.

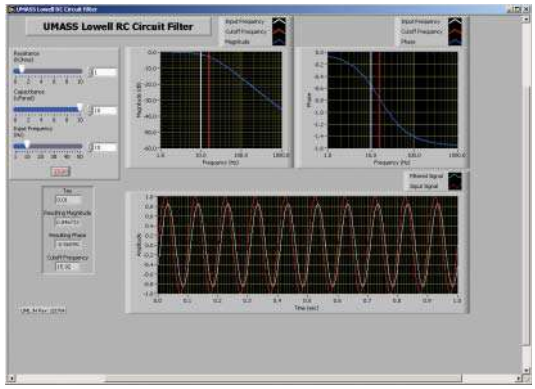

LabVIEW: First order low pass filter GUI

User enters the resistance and capacitance to identify a time constant, along with an input sinusoidal frequency. The Bode plot is displayed with the cutoff frequency and the sinusoidal frequency applied. The initial sinusoidal signal and "filtered" time signal are also displayed. The GUI reports the time constant and related magnitude and phase of the signal. The GUI allows for adjustment of the parameters, with updating of all plotted and reported data to give the user quick visual information regarding the system characteristics.

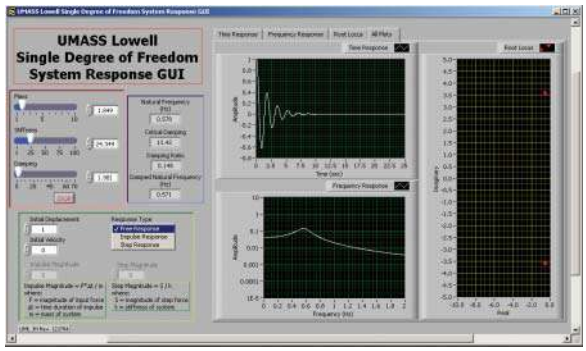

LabVIEW: Second order system response GUI

User enters M, C, K and natural frequency, critical damping, and damping are reported. User can vary the physical parameters with slide bars. User can also specify response type for free response, impulse, or step, along with initial conditions. The frequency response function magnitude is displayed, along with the root locus and time response, either as individual plots or all three plots displayed simultaneously (as shown).

LabVIEW: Second order system response GUI – step, impulse, free

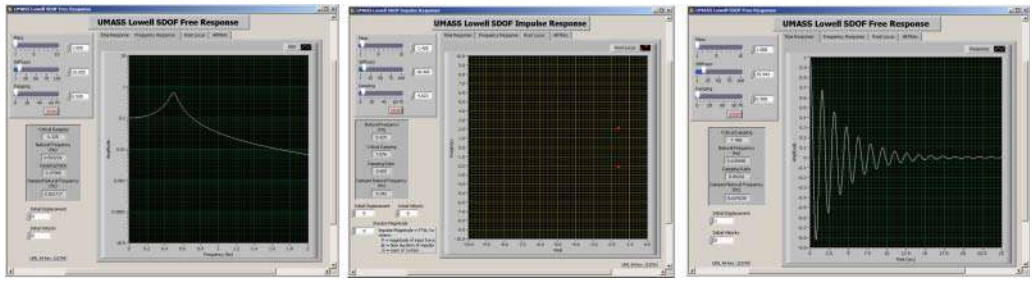

Similar to the GUI above but each response is in its own GUI

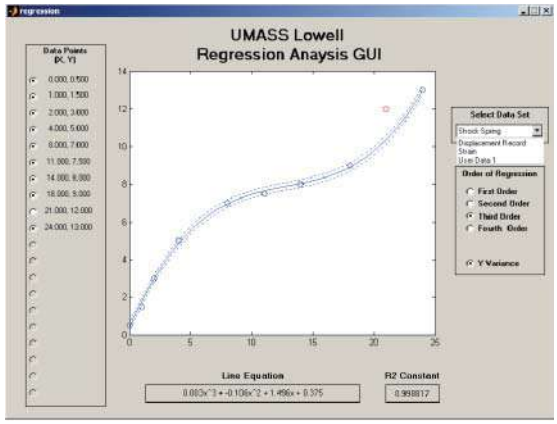

MATLAB: Regression analysis GUI

User can take existing data, representing several typical types of data found, and select the order of the regression and inclusion of y variance, and manually select and deselect individual data points to be used for the regression analysis. The GUI reports the equation of the best fit line based on the parameter selection, along with the regression coefficient. The user is also allowed to create personal data sets for inclusion in the GUI.

MATLAB: Integration/differentiation GUI

User enters a variety of different noise contaminants (bias, drift, random noise, sinusoidal noise) onto a damped exponential sine wave. The signal can then be processed using either differentiation or integration of the signal (once or twice applied) and the results observed.

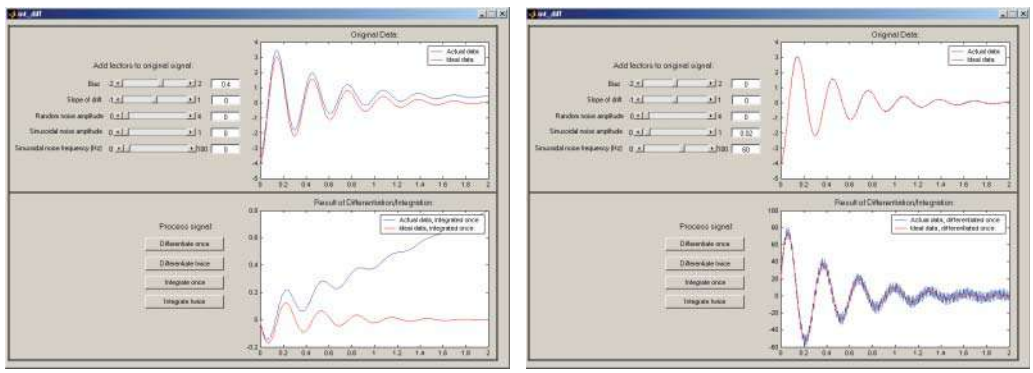

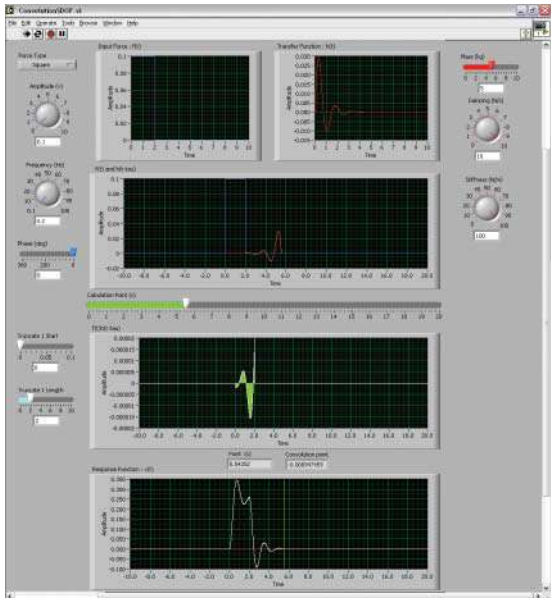

Labview: Convolution integral simulation GUI

Two variations of this GUI exist. Considering the convolution for a second order mechanical system, the user enters system characteristics such as mass, damping, and stiffness for the characteristic function and then can observe the response due to an impulse function. The GUI allows the user to take complete control of the development of the entire convolution function computation with a scroll bar to parade forward or backward to any particular time of the numerical process. An alternate variation of the GUI is set up for pure mathematical representation of arbitrary signals to show the convolution integral from a mathematical prospective.

F

Basic Modal Analysis Information

F.1 SDOF Definitions

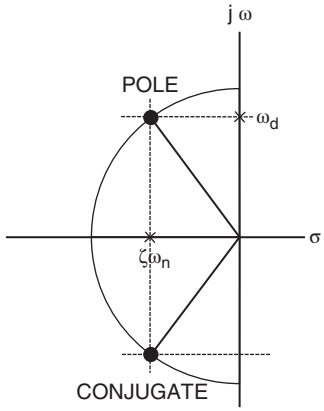

Characteristic equation $m s^2 + c s + k = 0$

Poles $s_{1,2} = -\zeta\omega_n \pm \sqrt{(\zeta\omega_n)^2 - \omega_n{}^2} = -\sigma \pm j\omega_d$

where

$\sigma = \zeta\omega_n$	damping factor
$\omega_n = \sqrt{\frac{k}{m}}$	natural frequency
$\zeta = \frac{c}{c_c}$	percent of critical damping
$c_c = 2m\omega_n$	critical damping
$\omega_d = \omega_n \sqrt{1-\zeta^2}$	damped natural frequency

F.1.1 Damping Estimates

$$Q = \frac{1}{2\zeta} = \frac{\omega_n}{\omega_2 - \omega_1} \qquad \delta = \ln\frac{x_1}{x_2} \approx 2\pi\zeta$$

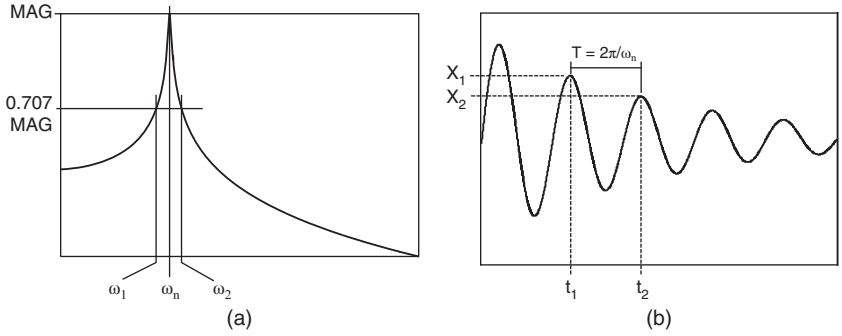

Figure F.1 Damping estimates: (a) half power method; (b) log decrement method.

Modal Testing: A Practitioner's Guide, First Edition. Peter Avitabile.

Companion Website: www.wiley.com/go/avitabile/modal-testing

F.1.2 System Transfer Function

$$h(s) = \frac{1}{ms^2 + cs + k}$$

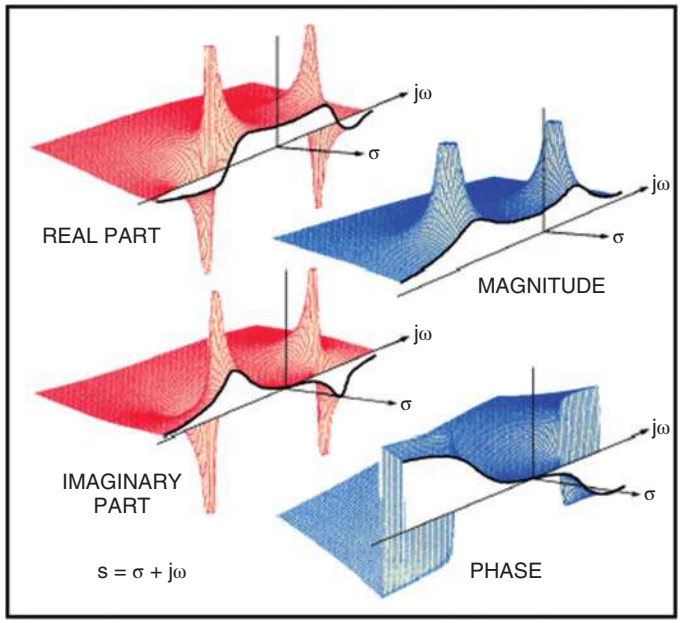

Figure F.2 System transfer function.

F.1.3 Different Forms of the System Transfer Function

Polynomial form $$h(s) = \frac{1}{ms^2 + cs + k}$$

Pole-zero form $$h(s) = \frac{1/m}{(s - p_1)(s - p_1^*)}$$

Partial fraction form $$h(s) = \frac{a_1}{(s - p_1)} + \frac{a_1^*}{(s - p_1^*)}$$

Complex exponential form $$h(t) = \frac{1}{m\omega_d} e^{-\zeta\omega t} \sin \omega_d t$$

F.1.4 Frequency Response Function

$$h(j\omega) = h(s)\big|_{s=j\omega} = \frac{a_1}{(j\omega - p_1)} + \frac{a_1^*}{(j\omega - p_1^*)}$$

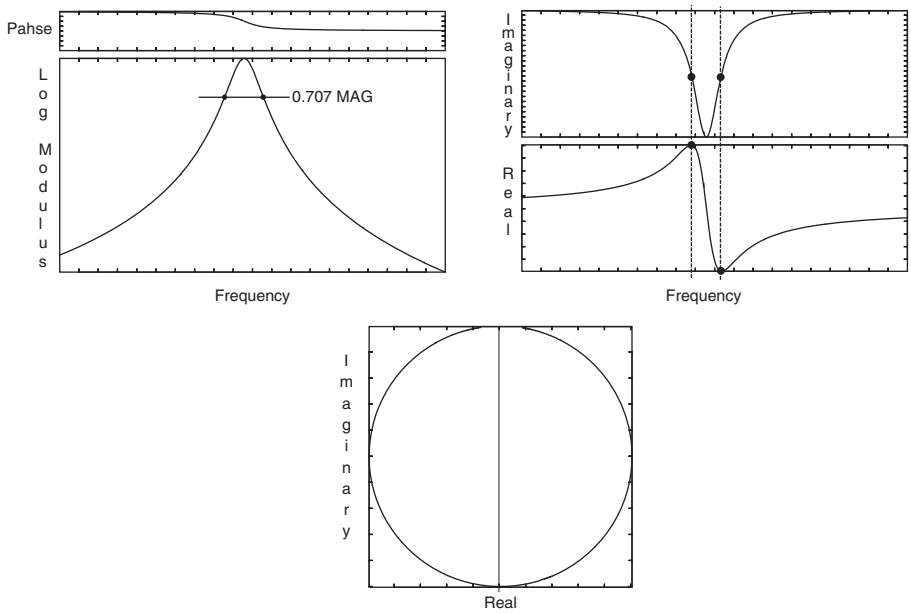

Figure F.3 Frequency response function.

F.1.5 System Transfer Function/Frequency Response Function/S-Plane

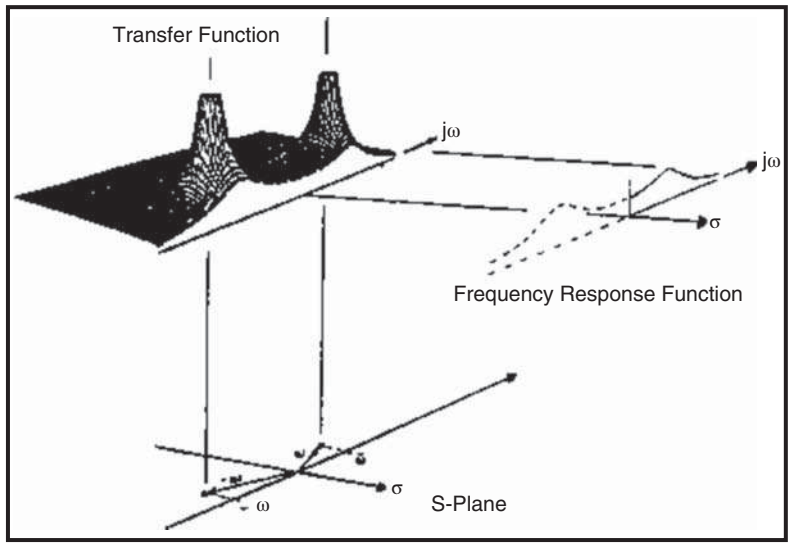

Figure F.4 System transfer function/frequency response function/S-plane.

F.2 MDOF Definitions

Characteristic equation

$$\left[[M]\,s^2 + [C]\,s + [K]\right] = 0 \quad \Rightarrow \quad p_k = -\sigma_k \pm j\omega_{dk}$$

System transfer function

$$[B(s)]^{-1} = [H(s)] = \frac{\text{Adj}[B(s)]}{\det[B(s)]} = \frac{[A(s)]}{\det[B(s)]}$$

Frequency response function

$$[H(s)]_{s=j\omega} = [H(j\omega)] = \sum_{k=1}^{m} \frac{[A_k]}{(j\omega - p_k)} + \frac{[A_k^*]}{(j\omega - p_k^*)}$$

$$[H(s)] = \sum_{k=1}^{m} \frac{q_k\{u_k\}\{u_k\}^T}{(s - p_k)} + \frac{q_k\{u_k^*\}\{u_k^*\}^T}{(s - p_k^*)}$$

Residues and mode shapes

$$\begin{bmatrix} a_{11k} & a_{12k} & a_{13k} & \cdots \\ a_{21k} & a_{22k} & a_{23k} & \cdots \\ a_{31k} & a_{32k} & a_{33k} & \cdots \\ \vdots & \vdots & \vdots & \ddots \end{bmatrix} = q_k \begin{bmatrix} u_{1k}u_{1k} & u_{1k}u_{2k} & u_{1k}u_{3k} & \cdots \\ u_{2k}u_{1k} & u_{2k}u_{2k} & u_{2k}u_{3k} & \cdots \\ u_{3k}u_{1k} & u_{3k}u_{2k} & u_{3k}u_{3k} & \cdots \\ \vdots & \vdots & \vdots & \ddots \end{bmatrix}$$

$$h_{ij}(j\omega) = \frac{a_{ij1}}{(j\omega - p_1)} + \frac{a_{ij1}^*}{(j\omega - p_1^*)} + \frac{a_{ij2}}{(j\omega - p_2)} + \frac{a_{ij2}^*}{(j\omega - p_2^*)} + \frac{a_{ij3}}{(j\omega - p_3)} + \frac{a_{ij3}^*}{(j\omega - p_3^*)}$$

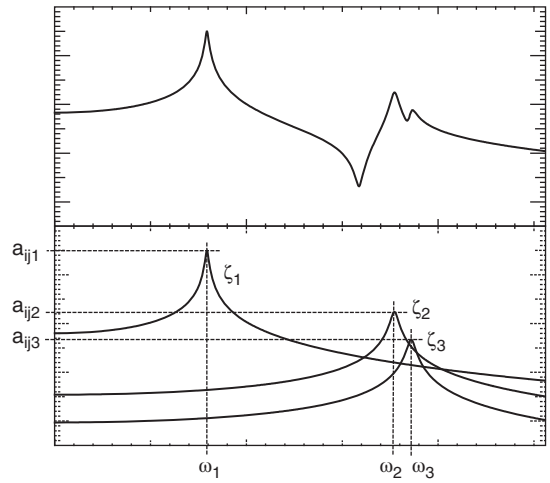

Figure F.5 FRF written in partial fraction form.

Part III

Collection of Sets of Modal Data Collected for Processing

G

Repeated Root Frame: Boundary Condition Effects

A small frame, called the RR (repeated root) frame, was designed such that the first two modes of the frame, which are bending and torsion modes, are extremely close to each other and have pseudo-repeated roots. The RR frame was tested with two slightly different arrangements of a very soft boundary condition (from large marshmallows). These were located at the corners in one test and at the midplane in the other test, as shown in Figure G.1; the nominal dimensions are also shown, with a simple finite element model of the structure.

This test employed an impact excitation technique. There were 16 impact locations used; excitation was only applied in the z-direction normal to the face of the frame (in the out of plane direction). This test employed a roving hammer excitation to avoid any mass loading effects; the reference accelerometers were located at one end of the structure at point 1 and point 7 in the

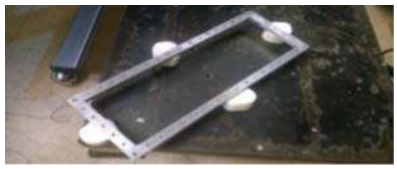

Geometric Properties
- Length = 17" (neutral axis)
- Width = 6" (neutral axis)
- Thickness = 0.75" (uniform)

Material Properties
- Elastic Modulus = 10E6 psi
- Density = 0.1 lb/in**3
- Poisson ratio = 0.33

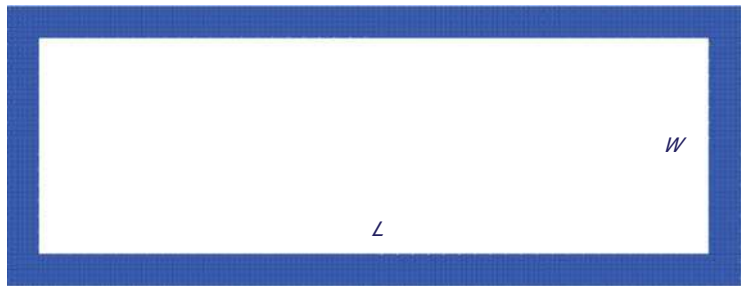

Figure G.1 Rectangular frame with closely spaced (or pseudo-repeated) modes.

Modal Testing: A Practitioner's Guide, First Edition. Peter Avitabile.

Companion Website: www.wiley.com/go/avitabile/modal-testing

z-direction. FRFs were measured to 2000 Hz. Testing was performed as part of a student class project in Spring 2016. FRFs are provided with this dataset over a 2000 Hz bandwidth.

G.1 Corner Supports Set #1

A frequency band from 140–1240 Hz was selected with two references. The data was evaluated to obtain the summation function, MMIF, and CMIF shown in Figures G.2–G.4. There are several peaks. Using a model order of 32, the stability diagram was generated for the band considered and five roots were selected as shown in Figures G.5 and G.6. The first figure shows a zoom in on the first peak, where there are two very closely spaced modes. The modes are then calculated as shown in Figure G.7, which shows the frequencies obtained and a schematic showing the measurement locations. In addition, a drive point synthesized FRF is shown in Figure G.8. This demonstrates the goodness of the fit of the data. The mode participation factors are shown in Table G.1, demonstrating that both shakers have significant input for all modes. An AutoMAC is shown in Table G.2, illustrating the goodness of the fit of the data.

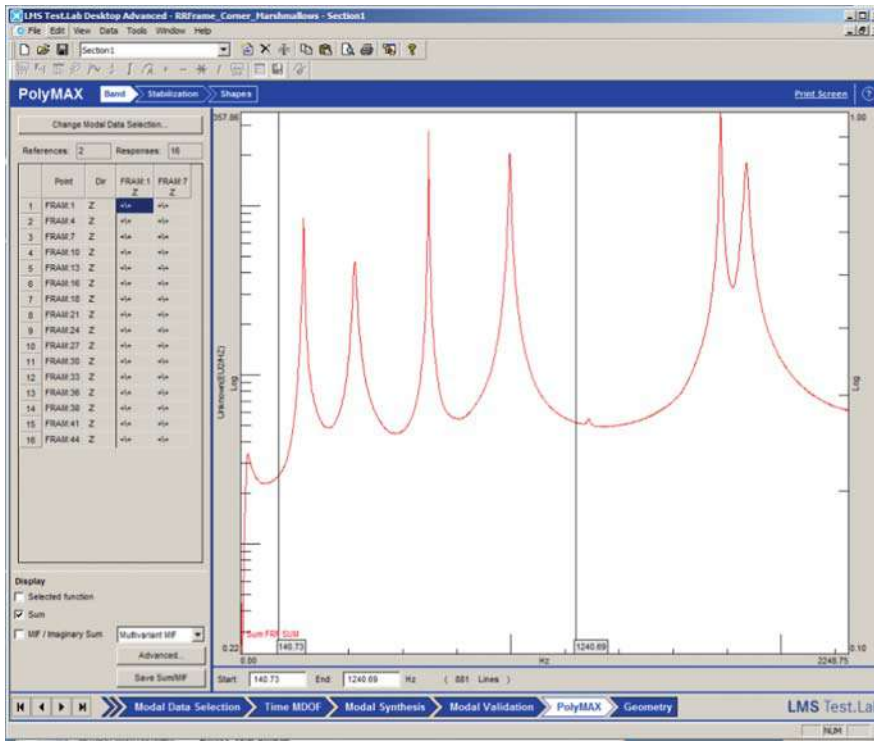

Figure G.2 Summation function for corner support modal test.

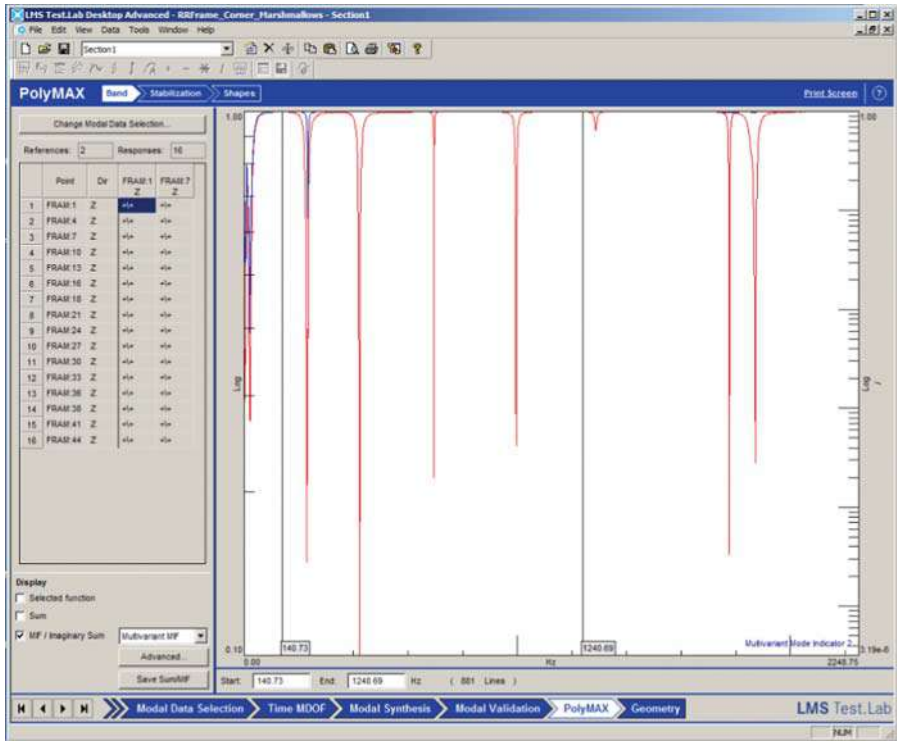

Figure G.3 MMIF function for corner support modal test.

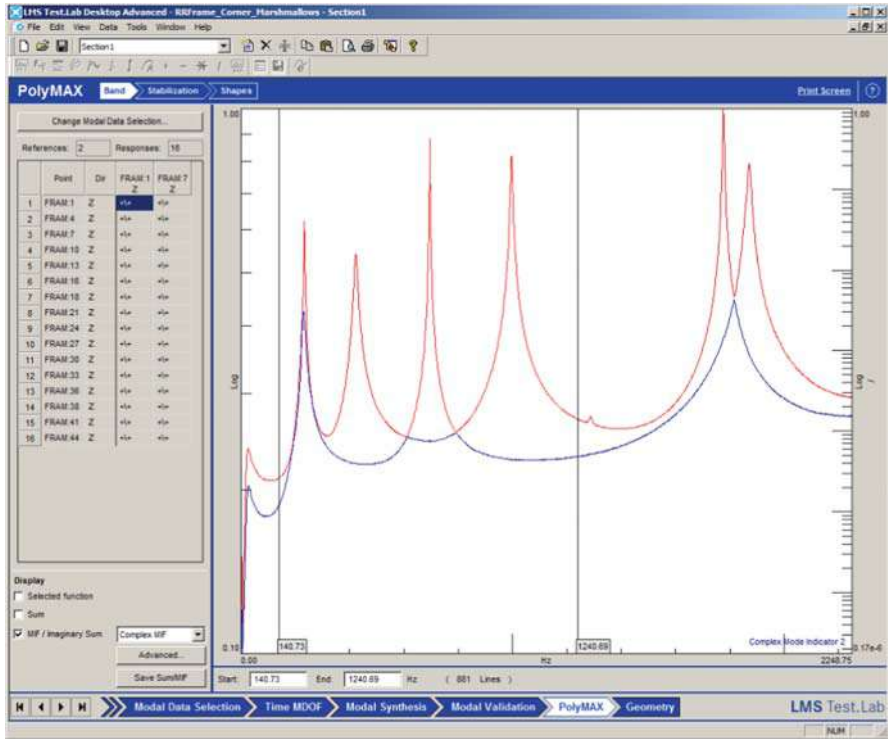

Figure G.4 CMIF function for corner support modal test.

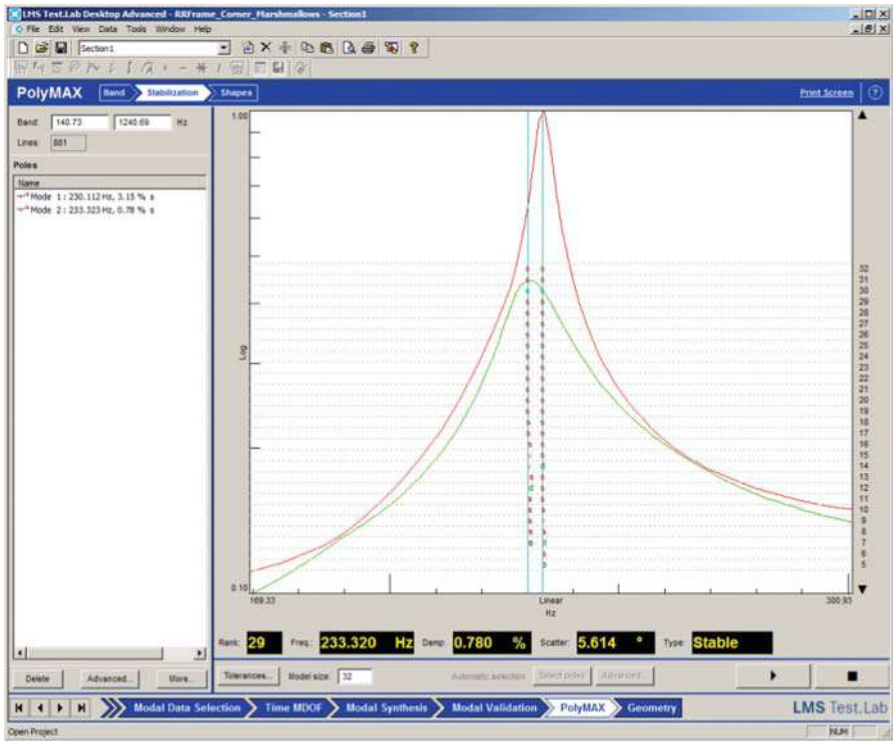

Figure G.5 Zoom for stability diagram for corner support modal test.

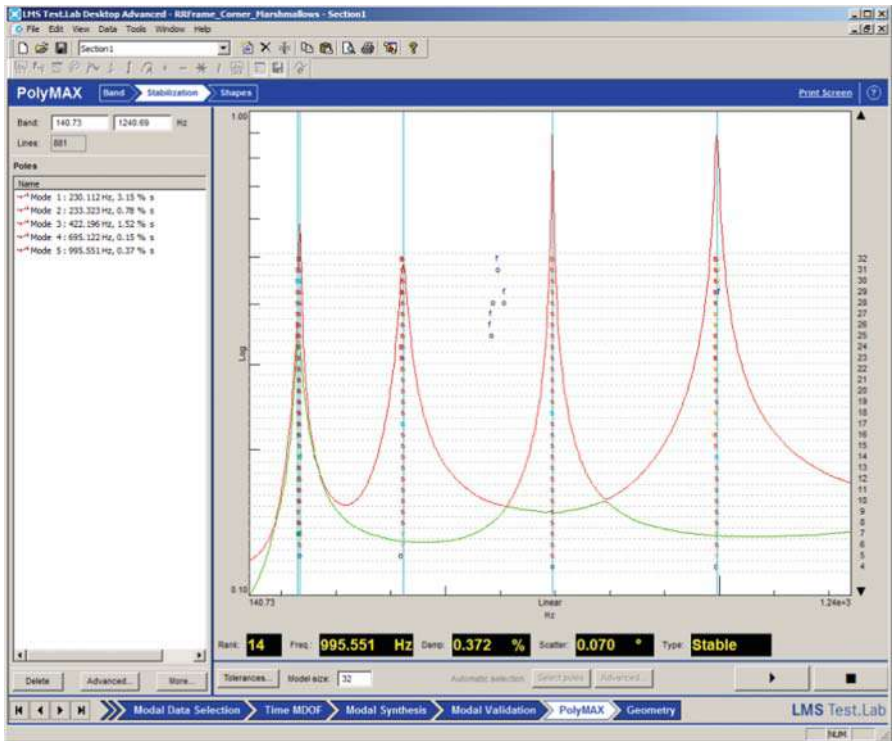

Figure G.6 Stability diagram for corner support modal test.

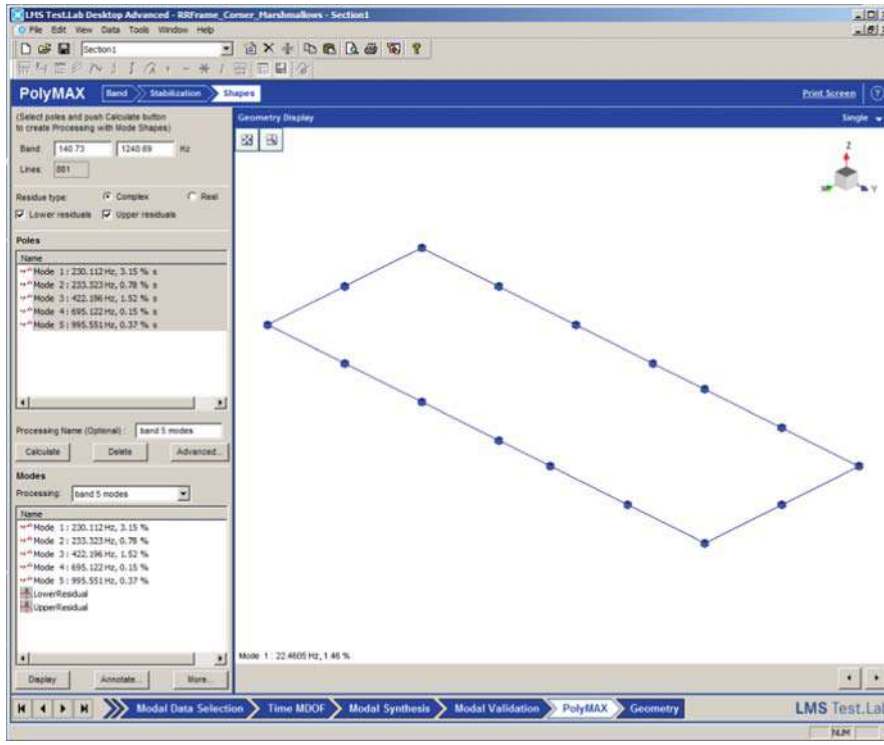

Figure G.7 Test locations with extracted frequencies for corner support modal test.

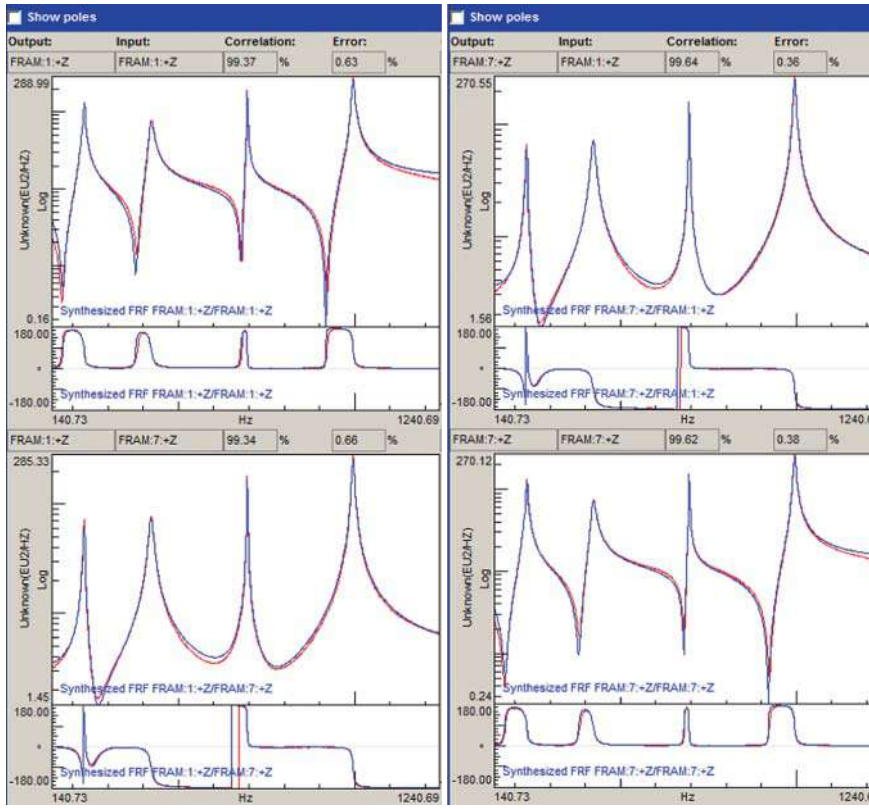

Figure G.8 Synthesized drive point FRF for corner support modal test.

Table G.1 Mode participation factors for corner support modal test.

Reference DOF	FRAM:1:+Z	FRAM:7:+Z
Mode 1	1.00	0.98
Mode 2	0.95	1.00
Mode 3	0.99	1.00
Mode 4	1.00	0.96
Mode 5	1.00	0.99

Table G.2 AutoMAC for corner support modal test.

Mode No.		1	2	3	4	5
	Frequency	230.11	233.32	422.20	695.12	995.55
1	230.11	100.00	3.13	0.27	0.05	0.21
2	233.32	3.13	100.00	0.06	0.37	0.00
3	422.20	0.27	0.06	100.00	0.01	0.30
4	695.12	0.05	0.37	0.01	100.00	0.08
5	995.55	0.21	0.00	0.30	0.08	100.00

G.2 Midlength Supports Set #2

The same frequency band from 140 Hz to 1240 Hz was selected with two references. The data was evaluated to obtain the summation function and CMIF shown in Figures G.9 and G.10. There are several peaks noted. Using a model order of 32, the stability diagram was generated for the band considered and five roots were selected, as shown in Figures G.11 and G.12; the first figure shows a zoom in on the first peak, where there are two very closely spaced modes. The modes are then calculated as shown in Figure G.13, which shows the frequencies obtained and a schematic showing the measurement locations. In addition, a drive point synthesized FRF is shown in Figure G.14, demonstrating the goodness of the fit of the data. The mode participation factors are shown in Table G.3, which shows both shakers have significant input for all modes. An AutoMAC is also shown in Table G.4, demonstating the goodness of the fit of the data.

G.3 Modal Correlation between Set #1 and Set #2

The two sets of modal data collected were then compared with a CrossMAC. Notice that the first two modes have swapped order between the two tests, as shown in Table G.5, which shows the results of the correlation; the MAC is shown in Figure G.15. Clearly, the boundary condition had a significant effect on the order of the modes for this case.

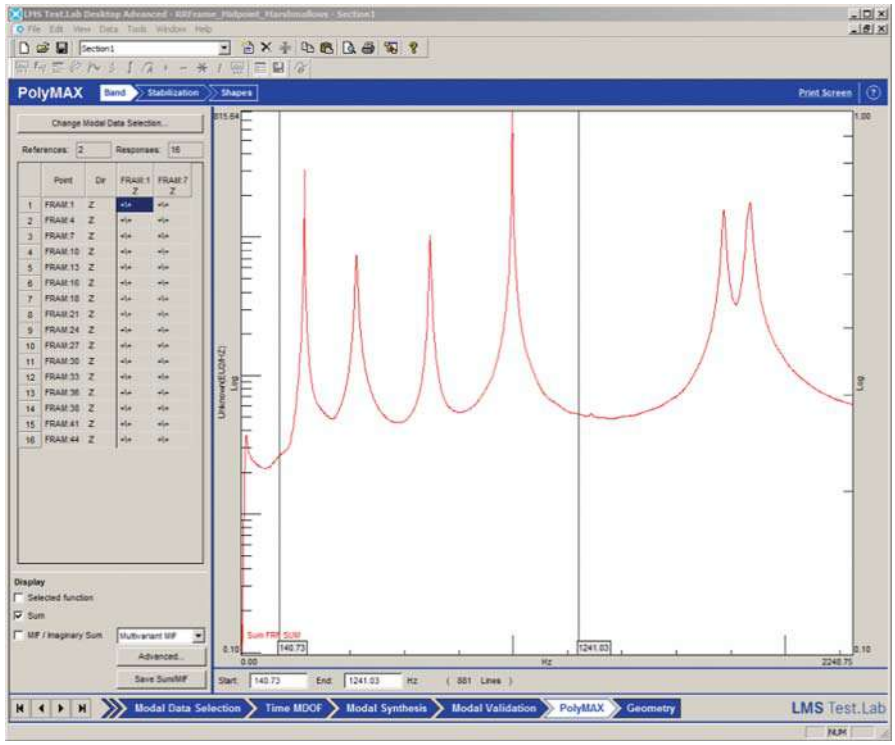

Figure G.9 Summation function for midlength support modal test.

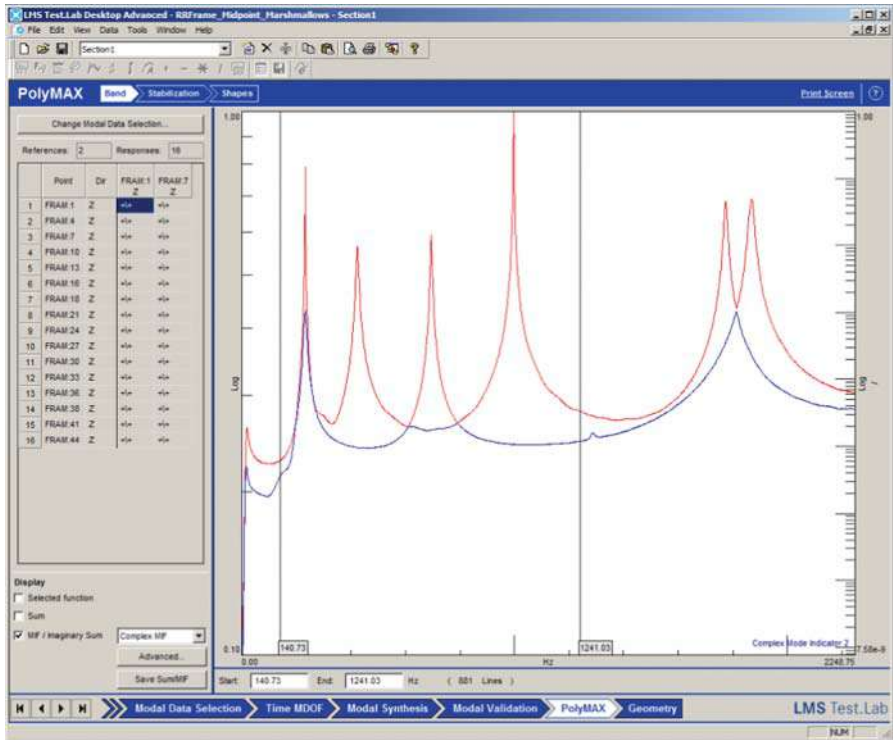

Figure G.10 CMIF function for midlength support modal test.

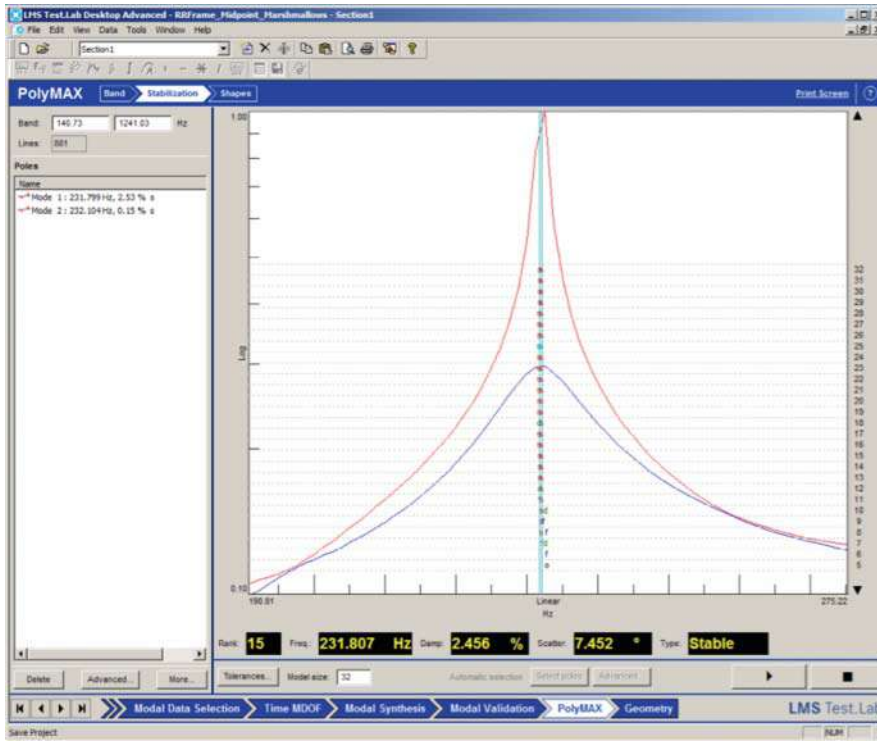

Figure G.11 Zoom for stability diagram for midlength support modal test.

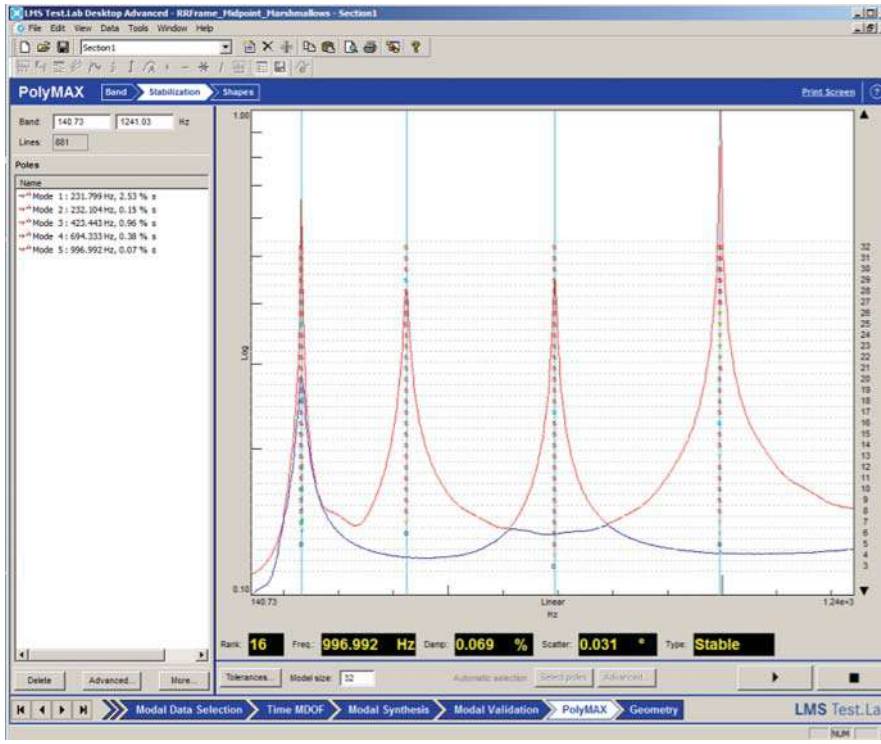

Figure G.12 Stability diagram for midlength support modal test.

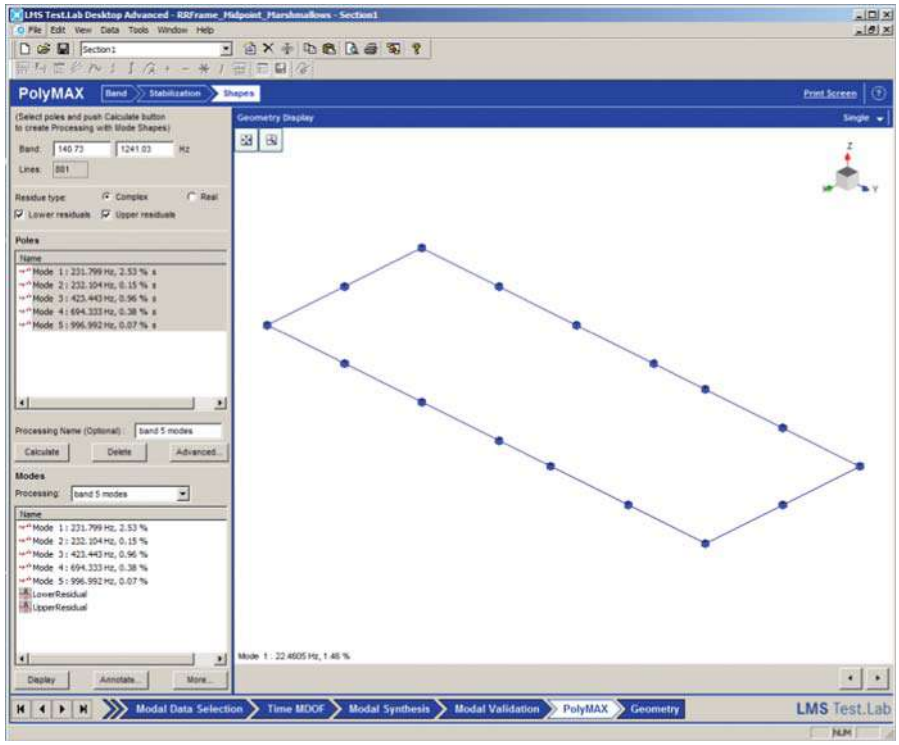

Figure G.13 Test locations with extracted frequencies for midlength support modal test.

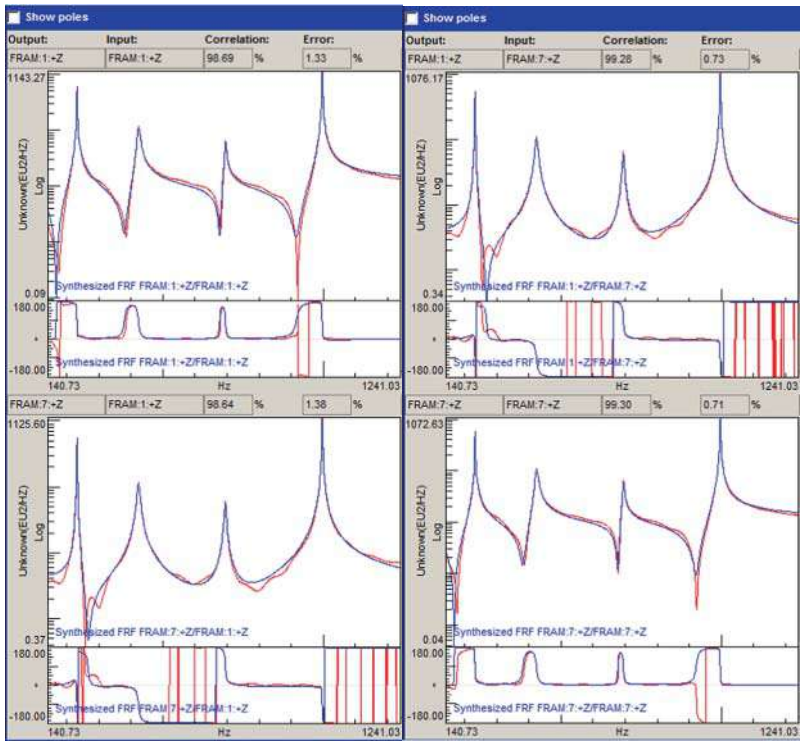

Figure G.14 Synthesized drive point FRF for midlength support modal test.

Table G.3 Mode participation factors for midlength support modal test.

MPF	FRAM:1:+Z	FRAM:7:+Z
Mode 1	1.00	0.97
Mode 2	1.00	1.00
Mode 3	1.00	1.00
Mode 4	1.00	0.97
Mode 5	1.00	0.99

Table G.4 AutoMAC for midlength support modal test.

Mode No.		1	2	3	4	5
	Frequency	231.8	232.1	423.4	694.3	997.0
1	231.8	100.00	3.07	0.01	0.32	0.02
2	232.1	3.07	100.00	0.21	0.02	0.35
3	423.4	0.01	0.21	100.00	0.00	0.37
4	694.3	0.32	0.02	0.00	100.00	0.13
5	997.0	0.02	0.35	0.37	0.13	100.00

Table G.5 MAC comparing the modal data from the two different boundary conditions.

			Corner				
	Mode No.		1	2	3	4	5
		Frequency	231.82 Hz	232.11 Hz	423.44 Hz	694.33 Hz	996.99 Hz
Midpoint	1	230.11 Hz	0.47	**96.18**	0.19	0.04	0.43
	2	233.32 Hz	**97.12**	0.01	0.02	0.37	0.03
	3	422.16 HZ	0.02	0.30	**99.73**	0.00	0.31
	4	695.12 Hz	0.33	0.04	0.00	**99.83**	0.11
	5	995.69 Hz	0.01	0.23	0.37	0.09	**98.93**

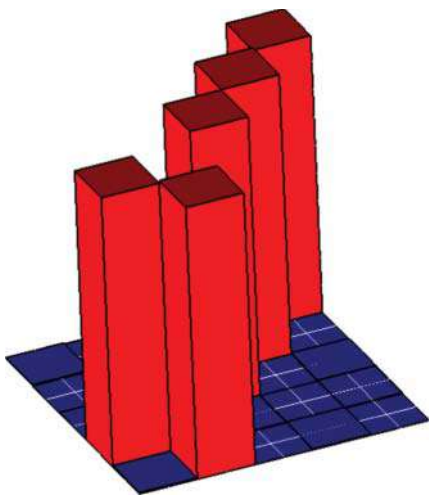

Figure G.15 MAC Comparing the modal data from the two different boundary conditions.

H

Radarsat Satellite Testing

A MIMO modal test was conducted on the RADARSAT satellite mock up in March 1993. The base of the structure was rigidly mounted to a 260 ton anchor. All accelerometers were mounted and remained in place throughout the test. Burst random excitation with 80% burst was used. The dataset contains FRFs from five uncorrelated references and 240 response DOFs. Only FRFs are provided with this dataset. Figure H.1 shows the structure.

For the evaluation presented here, only data reductions for four MIMO shakers and two MIMO shakers are presented, and each of these separate analyses are performed over different bandwidths. The intent is to show that there is no one exact way to reduce data to obtain modal parameters and that different approaches can produce very similar results.

H.1 Data Reduction Set 1: Reference BUS:109:Z, BUS:118:Z, PMS:217:X and PMS:1211:Y

A frequency band from 13 Hz to 43 Hz was selected, with the four references identified: two references in horizontal directions x and y and two references in the vertical direction z. The data was evaluated to obtain the summation function shown in Figure H.2. There are several peaks in the summation function. Using a model order of 64, the stability diagram was generated for the band considered, and nine roots were selected, as shown in Figure H.3. The modes are than calculated as shown in Figure H.4. In addition, a drive point synthesized FRF is shown in Figure H.5, demonstrating the goodness of the fit of the data.

The modal participation factors for the four references are shown for the nine modes evaluated as shown in Table H.1. The interesting point to note is that the two vertical shakers in the z- direction have essentially no influence on the modes extracted. In fact, the first 40 or so modes are primarily modes in the horizontal x -and y-directions. So the inclusion of the two vertical shakers really has no impact on the lower modes and they do not need to be included in this dataset. However, these vertical input excitations are important for some of the higher modes beyond the band evaluated here. The next analysis will use only the two horizontal shakers and evaluate a wider band for modal parameter estimation.

H.2 Data Reduction Set 2: Reference PMS:217:X and PMS:1211:Y

A frequency band from 13 Hz to 63 Hz was selected, with the two references in horizontal directions x and y; no references in the vertical direction z were included. The data was evaluated to obtain the summation, MIF, and CMIF functions, which are shown in Figures H.6–H.8.

Modal Testing: A Practitioner's Guide, First Edition. Peter Avitabile.

Companion Website: www.wiley.com/go/avitabile/modal-testing

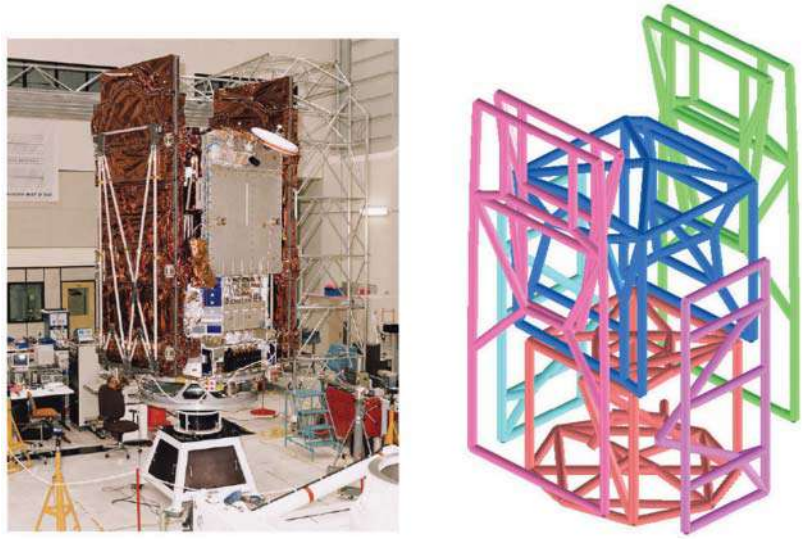

(a) (b)

Figure H.1 Canadian Space Agency RADARSAT satellite mock up test: (a) photo; (b) test geometry.

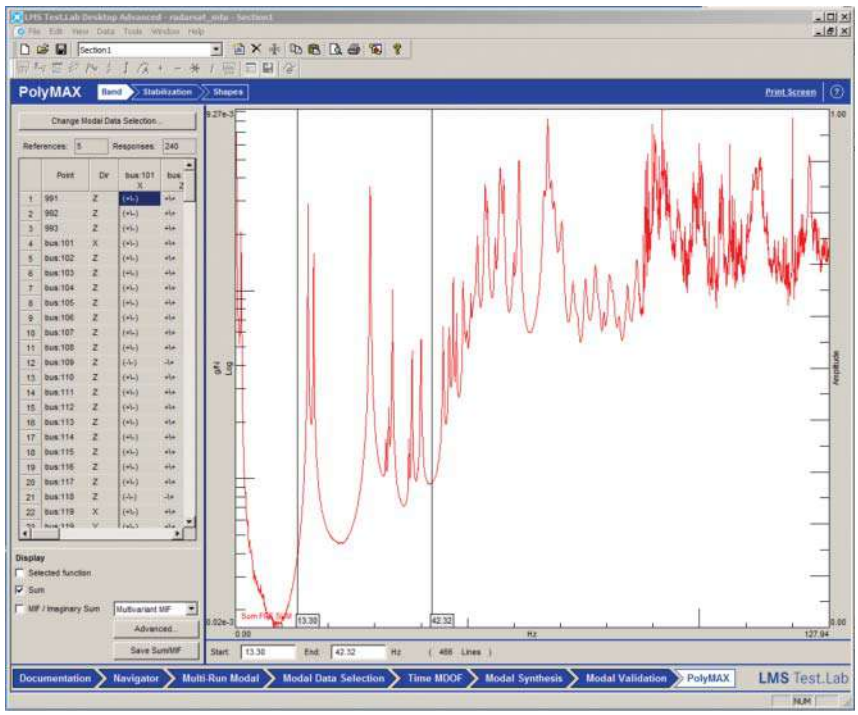

Figure H.2 Summation function using all four references.

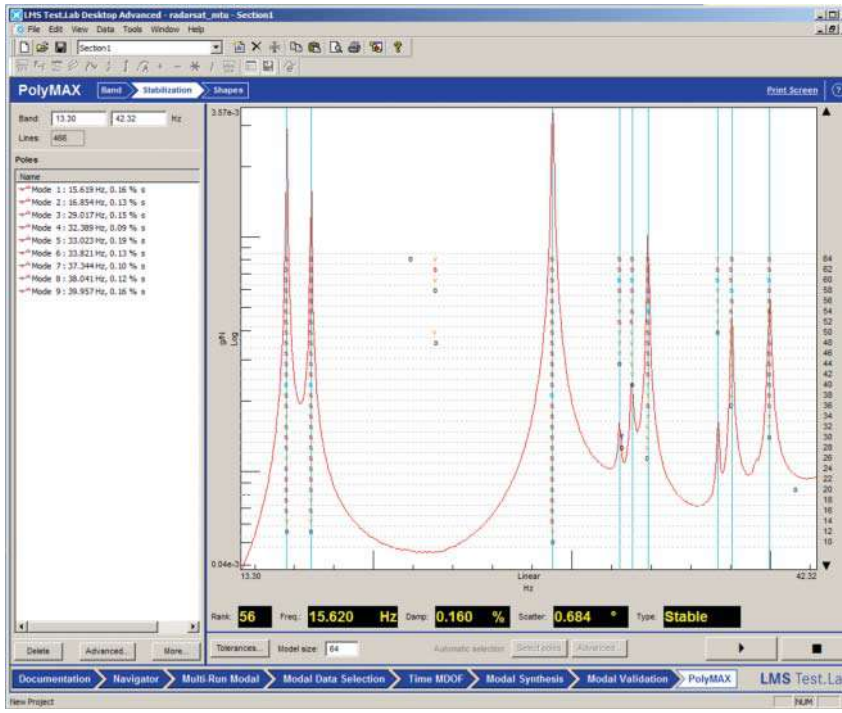

Figure H.3 Stability diagram using all four references.

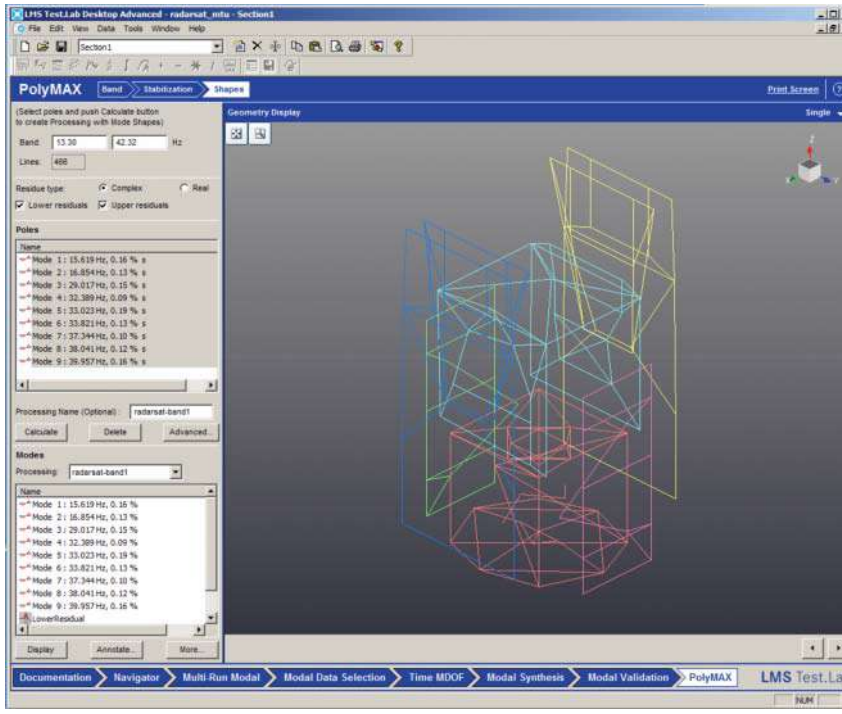

Figure H.4 Modal data extracted using all four references.

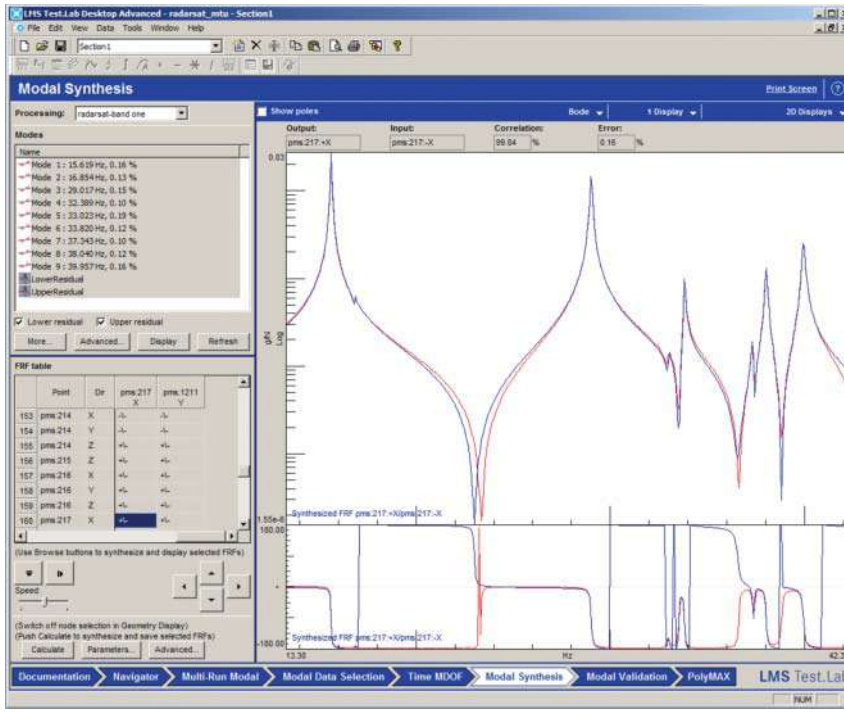

Figure H.5 Synthesized drive point FRF using using all four references.

Table H.1 Modal participation factors using all four references.

M.P.F.	bus:109:+Z	bus:118:+Z	pms:217:+X	pms:1211:+Y
Mode 1	0.05	0.01	1.00	0.02
Mode 2	0.02	0.01	0.04	1.00
Mode 3	0.00	0.02	0.98	1.00
Mode 4	0.09	0.09	0.73	1.00
Mode 5	0.09	0.03	1.00	0.36
Mode 6	0.15	0.05	1.00	0.24
Mode 7	0.11	0.13	1.00	0.03
Mode 8	0.09	0.01	1.00	0.13
Mode 9	0.08	0.03	1.00	0.11

There are many more peaks in the summation function. Using a model order of 64, the stability diagram was generated for the band considered and 24 roots were selected, as shown in Figure H.9. In addition, the drive point and cross FRF for the two references were synthesized and are shown in Figure H.10, demonstrating the goodness of the fit of the data.

The MAC was calculated to compare these two different approaches to obtaining modal parameters. The MAC matrix is shown in Table H.2. The most important thing to note is that the diagonal terms all show extremely well correlated modal vectors from the two different datasets evaluated: one dataset fit 9 modes with 4 references whereas the other dataset used only 2 references and extracted 24 modes. The 9 modes show few differences, with two significantly different data reductions. This type of analysis is always recommended in order to provide credibility to the modes extracted from the data collected.

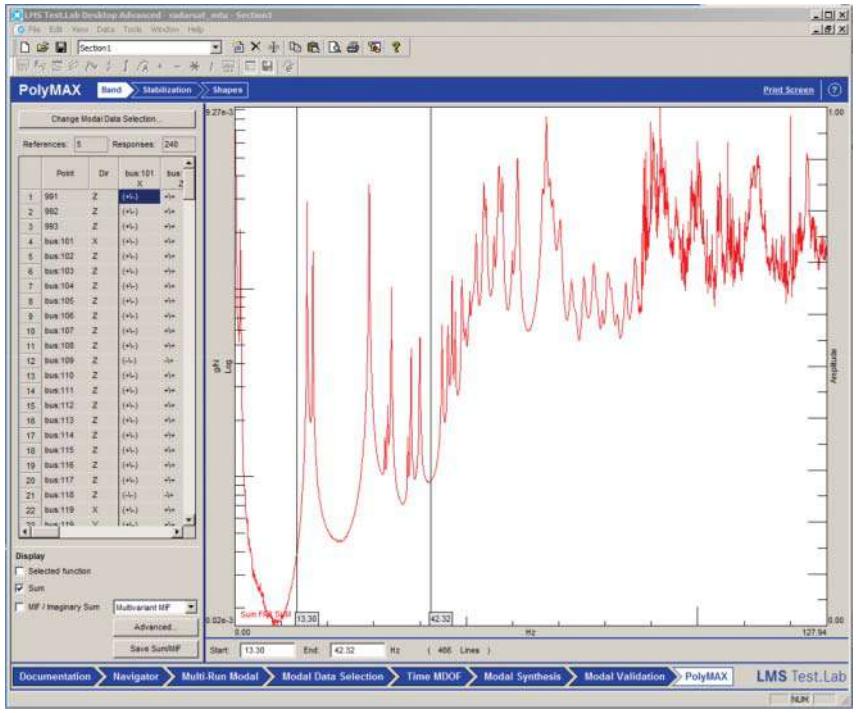

Figure H.6 Summation function using only two z and y references.

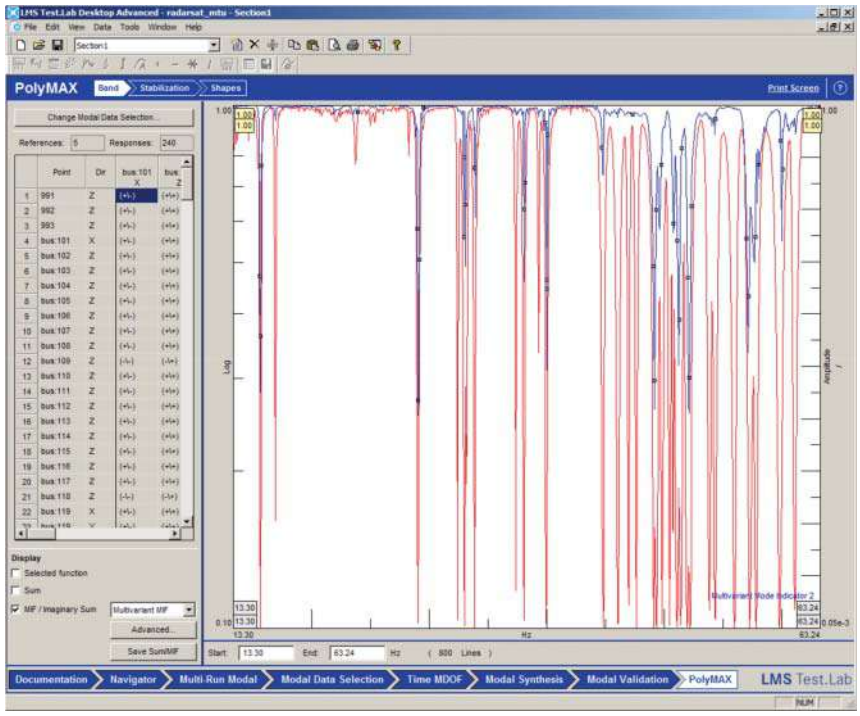

Figure H.7 MMIF function using only two z and y references.

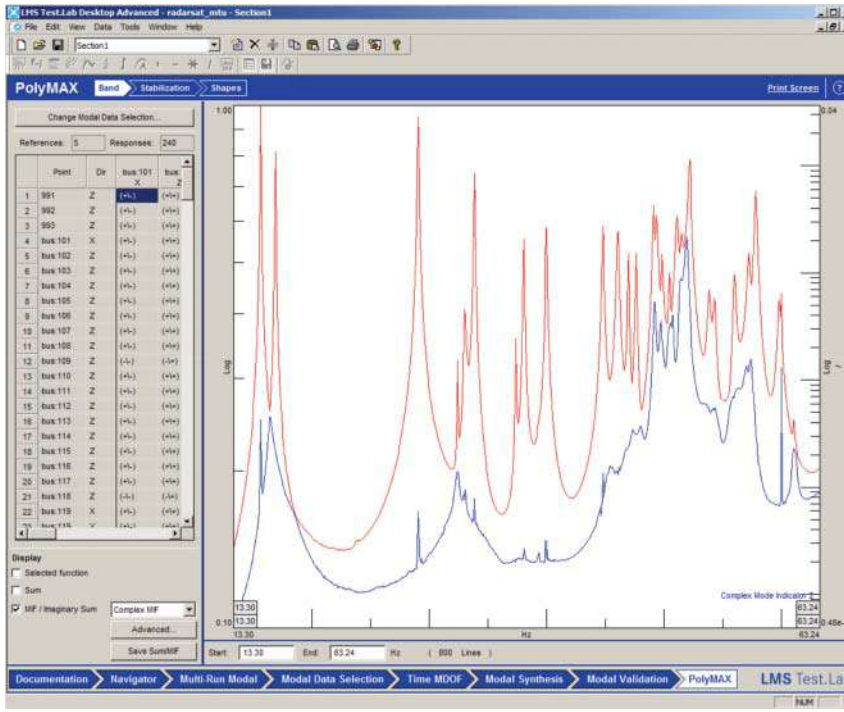

Figure H.8 CMIF function using only two z and y references.

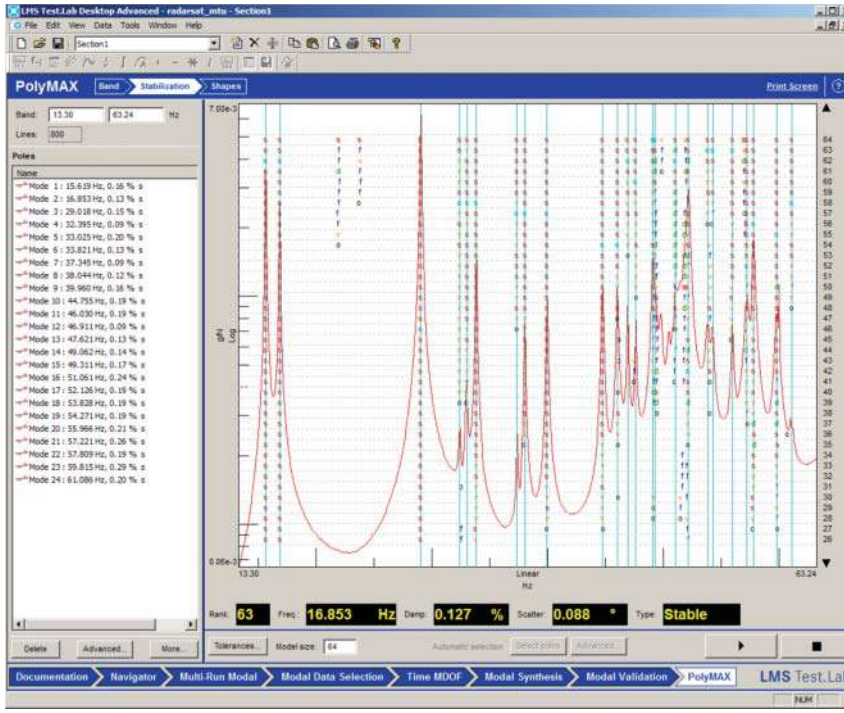

Figure H.9 Stability diagram using only two z and y references.

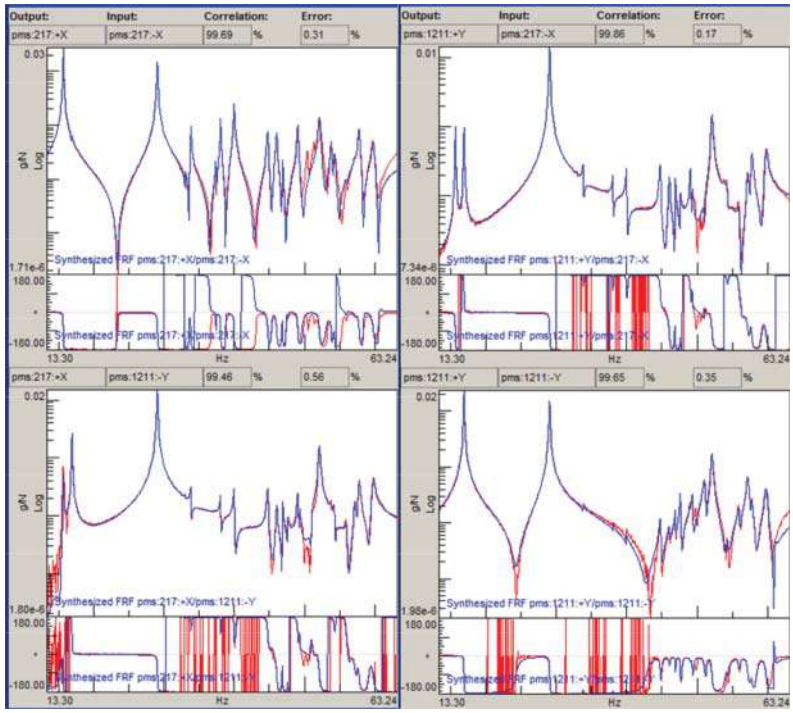

Figure H.10 Synthesis of drive point FRFs using only two z and y references.

Table H.2 MAC comparing modes extracted from two different sets of references.

Mode No.	Frequency	15.619 Hz	16.853 Hz	29.018 Hz	32.395 Hz	33.025 Hz	33.821 Hz	37.345 Hz	38.044 Hz	39.960 Hz
1	15.619 Hz	**99.986**	0.005	0.689	0.44	0.246	47.275	0.574	0.965	5.121
2	16.854 Hz	0.004	**99.987**	0.094	0.012	0.008	0.007	0.002	0.002	0.003
3	29.017 Hz	0.686	0.096	**99.996**	0.018	0.013	0.787	0.015	0.022	0.01
4	32.389 Hz	0.459	0.006	0.014	**99.548**	0.183	0.075	28.829	2.112	0.083
5	33.023 Hz	0.244	0.008	0.022	0.149	**99.614**	3.196	1.013	25.944	3.039
6	33.821 Hz	47.292	0.009	0.796	0.067	3.226	**99.981**	1.619	3.908	1.681
7	37.344 Hz	0.542	0.001	0.005	28.89	0.85	1.58	**99.34**	0.098	0.285
8	38.041 Hz	0.968	0.001	0.015	2.135	25.492	3.923	0.048	**99.899**	4.843
9	39.957 Hz	5.061	0.004	0.007	0.117	3.051	1.615	0.338	5.078	**99.901**

I

Demo Airplane Testing

A demo airplane has been used by several vendors for shows and demonstrations of measurements. This structure was used for several tests. Several different excitations techniques were utilized.

I.1 Impact Testing

This test employed an impact excitation technique. There were 15 PCB Y356A32 triaxial accelerometers that were permanently mounted on the structure for all testing performed. The structure was supported by four plungers at the root of the wings at the fuselage on the left and right side and fore and aft on the wings. The 15 measurement locations are shown in Figure I.1, along with the points shown on a finite element model that was available. Testing was performed as part of a student class project in Spring 2016. Only FRFs over a 256 Hz bandwidth are provided with this dataset.

A frequency band from 17 Hz to 190 Hz was selected to obtain the summation function, MIF and CMIF shown in Figures I.2–I.4. There are several peaks in the summation function. Using a model order of 24, the stability diagram was generated for the band considered and 10 roots were selected as seen in Figure I.5. The modes are then calculated, as shown in Figure I.6, with a drive point synthesized FRF to show the goodness of the fit of the data.

I.2 SIMO Testing with Skewed Shaker

This test employed a SIMO test with a shaker skewed to the x, y, z coordinate system for the airplane, to attempt to excite most of the major modes of the structure with a single reference shaker; the shaker was located at the front wing attachment on the fuselage with 45° orientation to the x, y, z axis system for the airplane. Fifteen PCB Y356A32 triaxial accelerometers were permanently mounted on the structure for all testing performed. The structure was supported by four plungers at the root of the wings at the fuselage on the left and right side and fore and aft on the wings. The 15 measurement locations are shown in Figure I.7, and also on a finite element model that was available. Testing was performed as part of a student class project in Spring 2016. Only FRFs over a 256 Hz bandwidth are provided with this dataset. A 80% burst random excitation was used for the test.

A frequency band from 17 Hz to 190 Hz was selected to obtain the summation function, MIF, and CMIF, as shown in Figures I.8–I.10. There are several peaks in the summation function. Using a model order of 32, the stability diagram was generated for the band considered and 11 roots were selected, as shown in Figure I.11. The skewed shaker was able to identify an

Modal Testing: A Practitioner's Guide, First Edition. Peter Avitabile.

Companion Website: www.wiley.com/go/avitabile/modal-testing

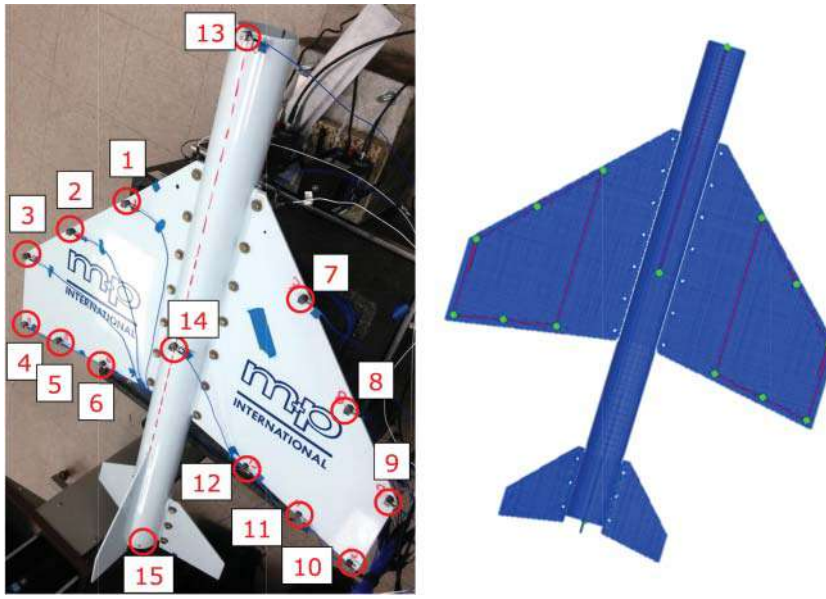

Figure I.1 Demo airplane modal test measurement points.

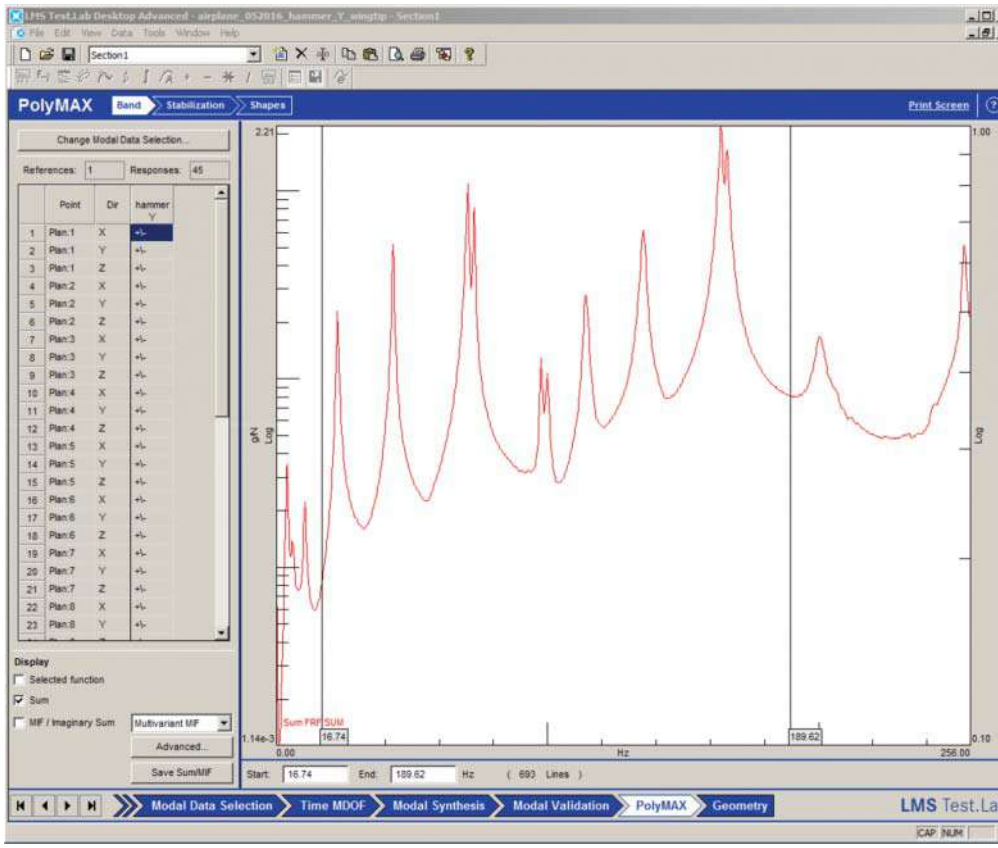

Figure I.2 Summation function for demo airplane impact data.

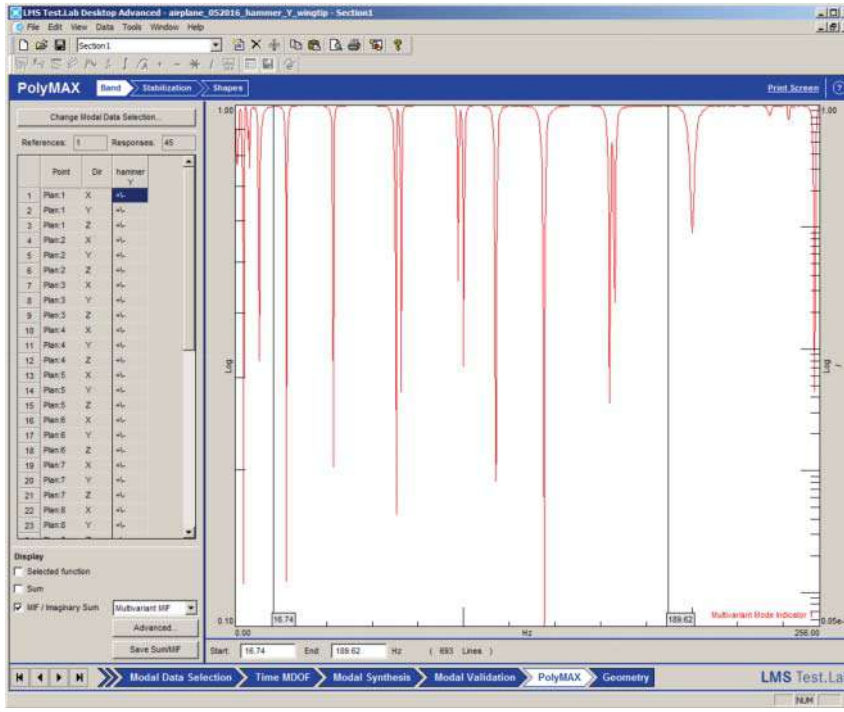

Figure I.3 MMIF function for demo airplane impact data.

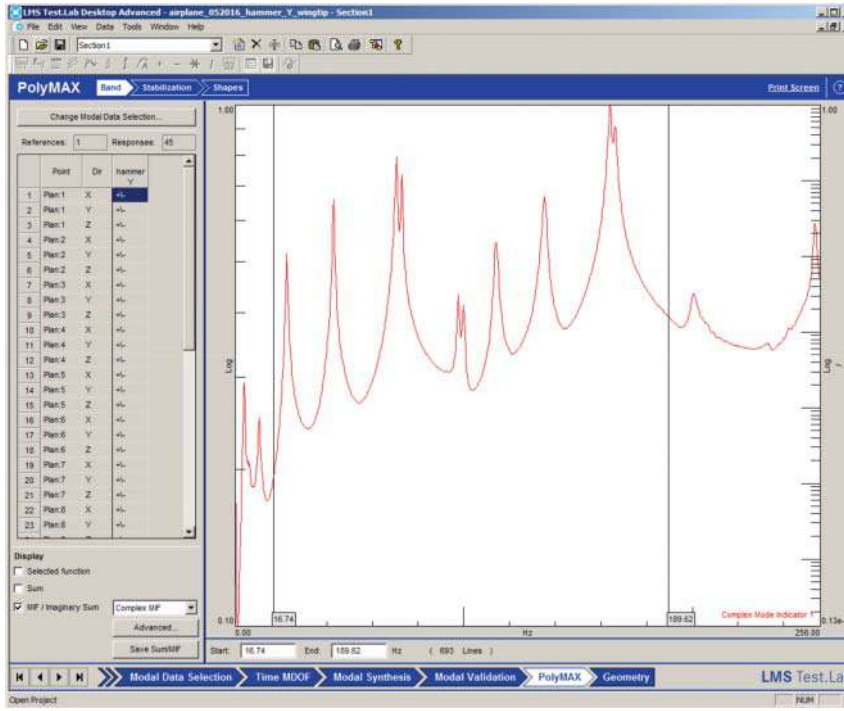

Figure I.4 CMIF function for demo airplane impact data.

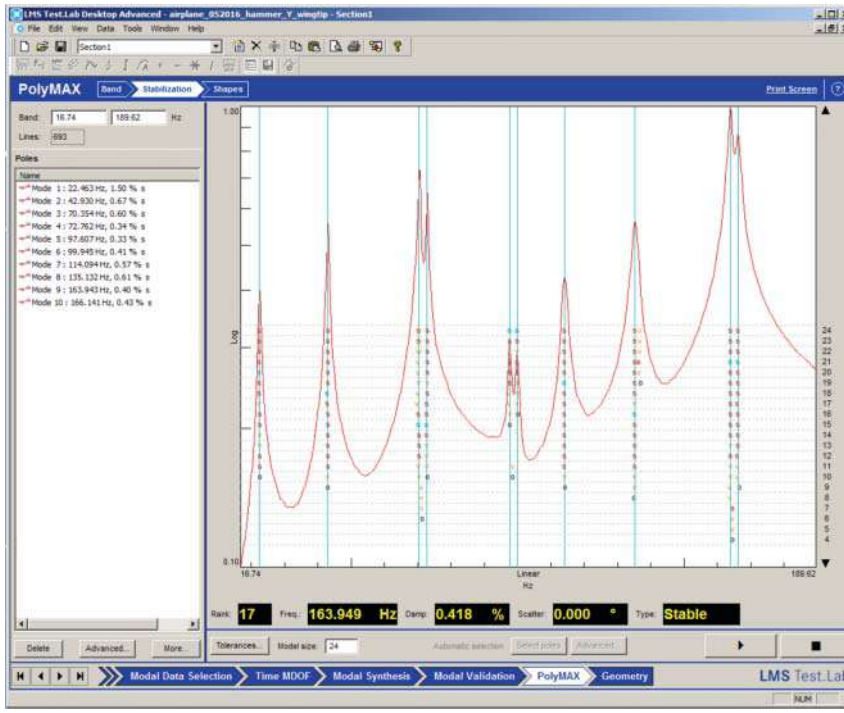

Figure I.5 Summation function for demo airplane impact data.

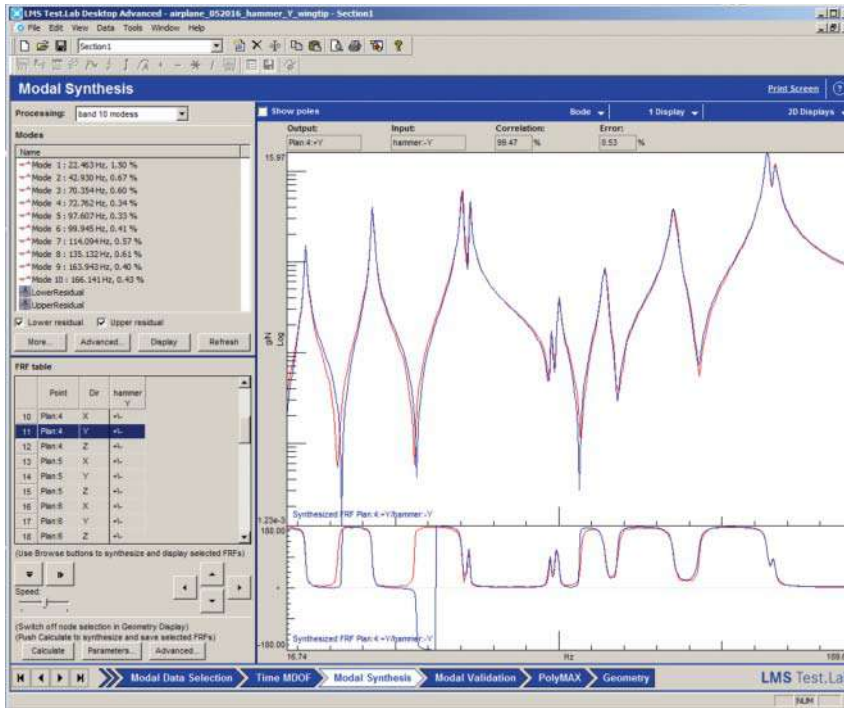

Figure I.6 Synthesis of drive point FRF for demo airplane impact data.

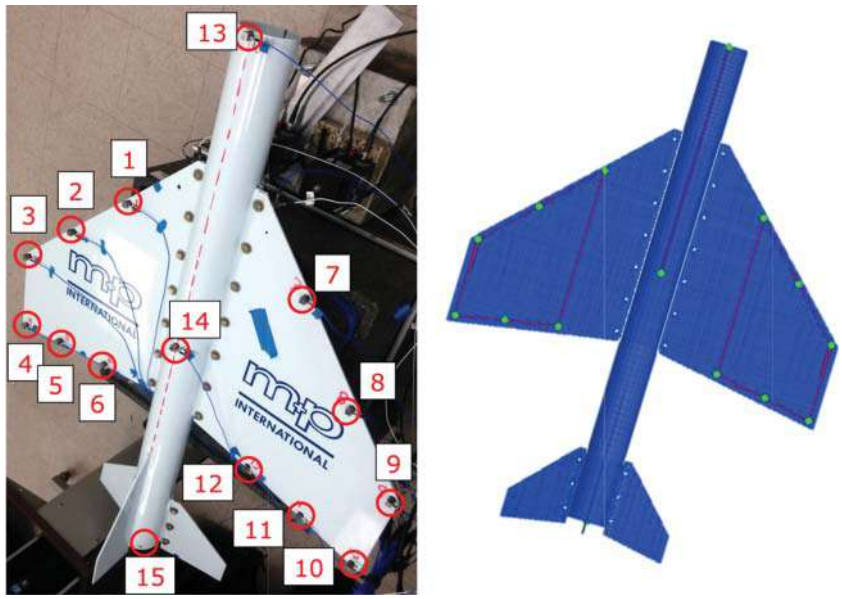

Figure I.7 Demo airplane modal test measurement points.

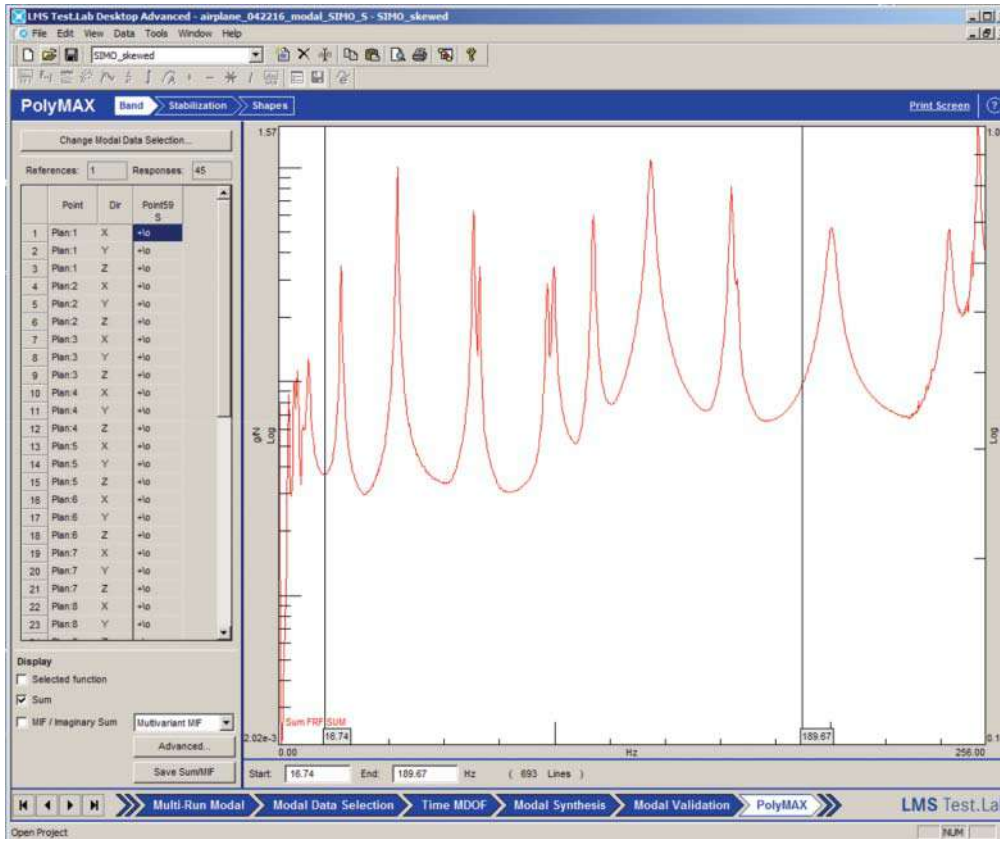

Figure I.8 Summation function for demo airplane skewed shaker data.

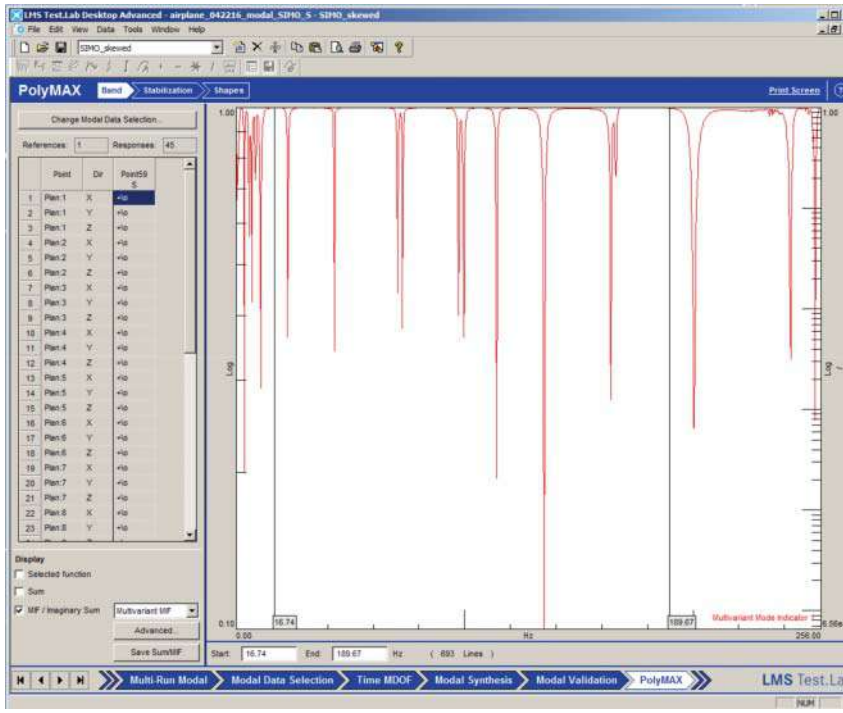

Figure I.9 MMIF function for demo airplane skewed shaker data.

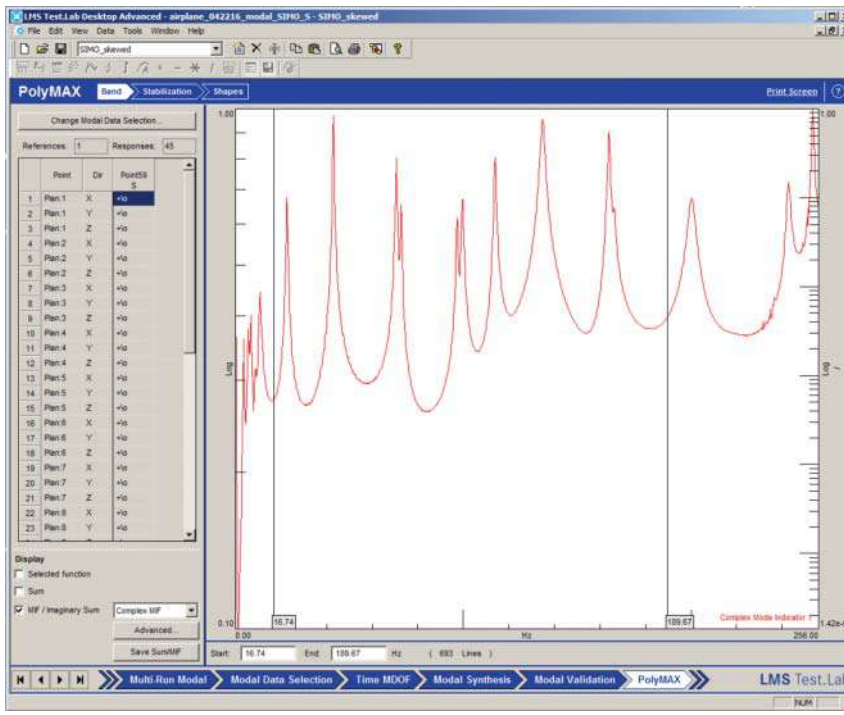

Figure I.10 CMIF function for demo airplane skewed shaker data.

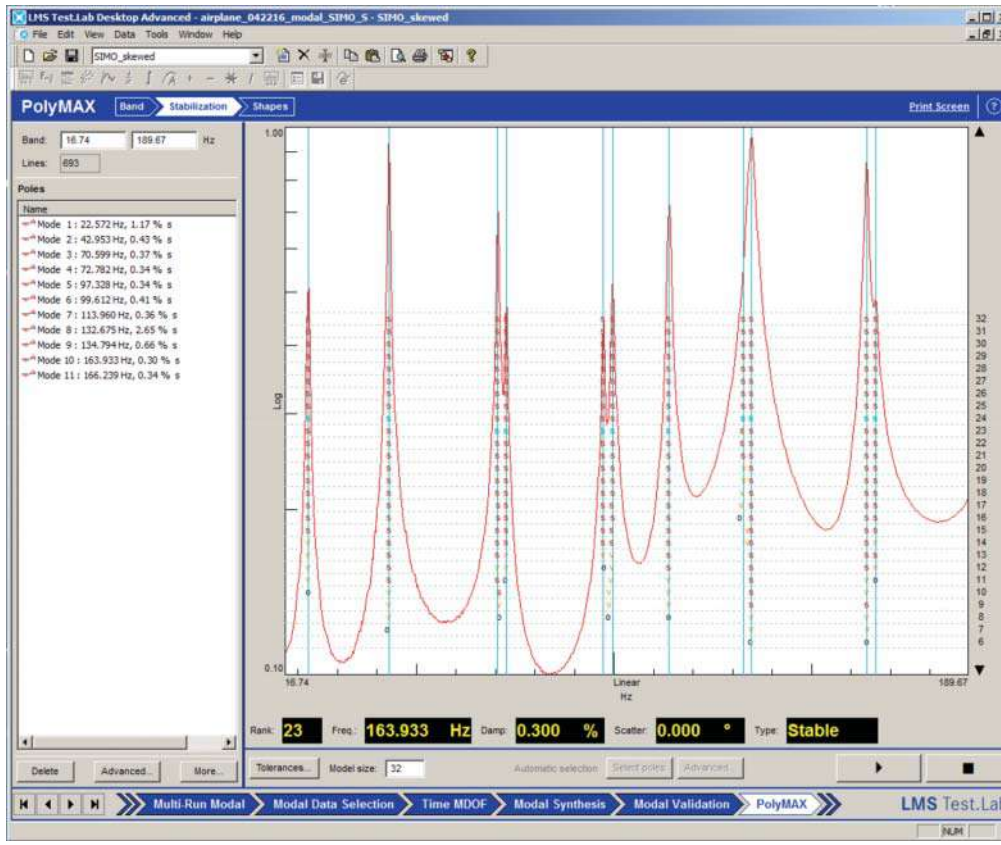

Figure I.11 Summation function for demo airplane skewed shaker data.

additional mode not easily seen in the impact test. There is no synthesis due to lack of a drive point measurement.

I.3 MIMO Testing with Two Vertical Modal Shakers

This test employed a MIMO test with two vertical shakers; the shakers were located at the front wing attachment on the fuselage on the left and right side of the airplane. Fifteen PCB Y356A32 triaxial accelerometers were permanently mounted on the structure for all testing performed. The structure was supported by four plungers at the root of the wings at the fuselage on the left and right side and fore and aft on the wings. The 15 measurement locations are shown in Figure I.12, along with the points shown on a finite element model that was available. Testing was performed as part of a student class project in Spring 2016. Only FRFs are provided with this dataset over a 256 Hz bandwidth. A 80 % burst random excitation was used for the test.

A frequency band from 17 Hz to 190 Hz was selected to obtain the summation function, MIF, and CMIF, as shown in Figures I.13–I.15. There are several peaks in the summation function. Using a model order of 32, the stability diagram was generated for the band considered and 10 roots were selected, as shown in Figure I.16. There is no synthesis due to a labeling error in the measurements. A modal participation factor is shown in Table I.1 for the two shakers for all modes; most of the modes are excited well by both shakers.

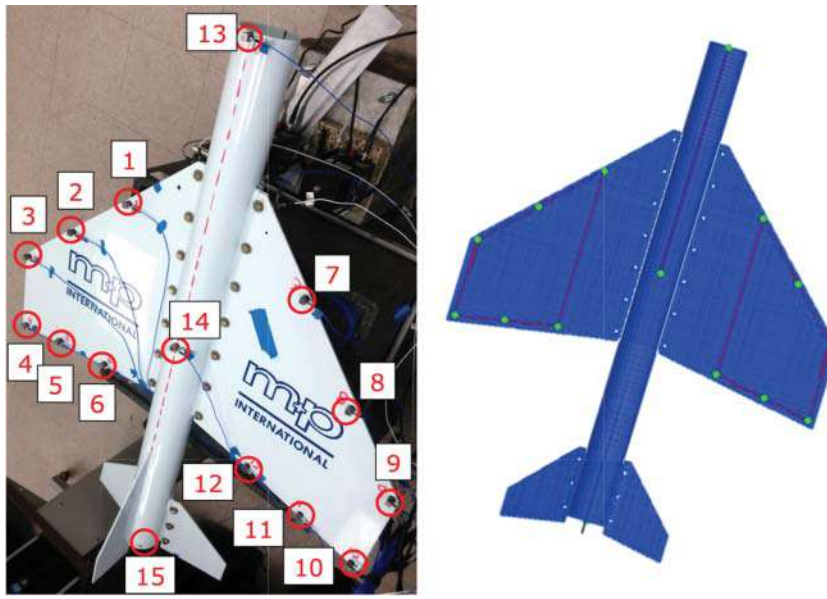

Figure I.12 Demo Airplane modal test measurement points.

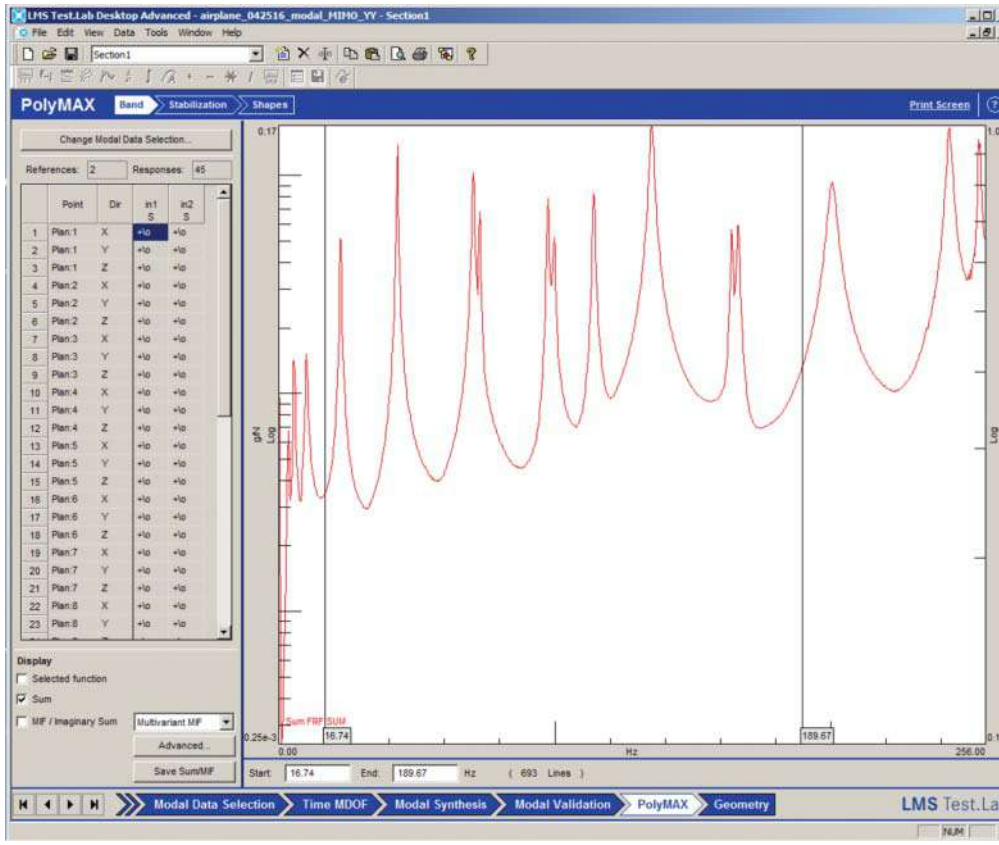

Figure I.13 Summation function for demo airplane MIMO data.

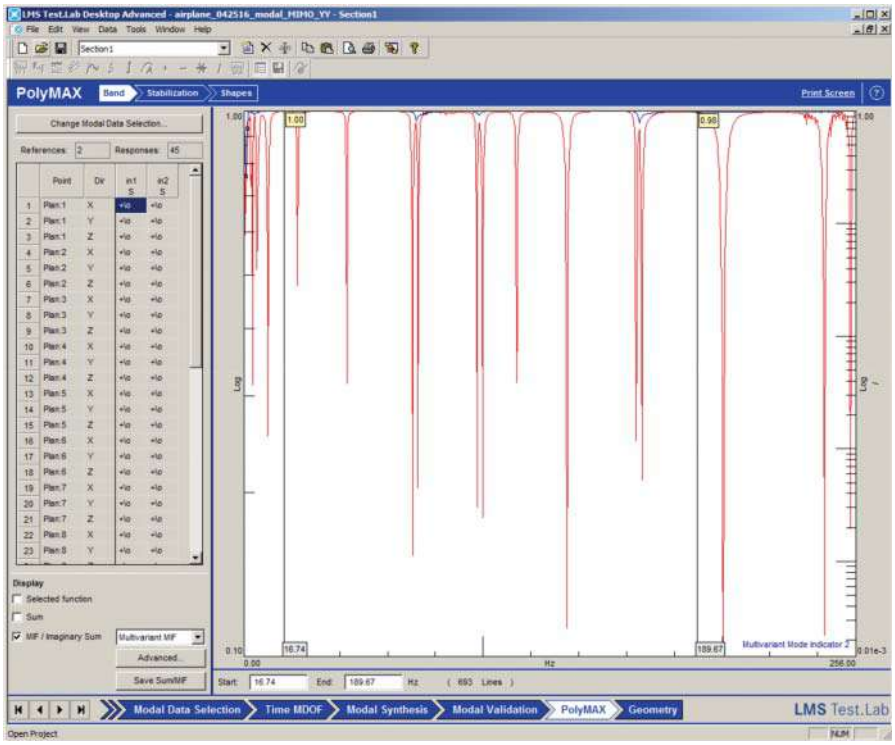

Figure I.14 MMIF function for demo airplane MIMO data.

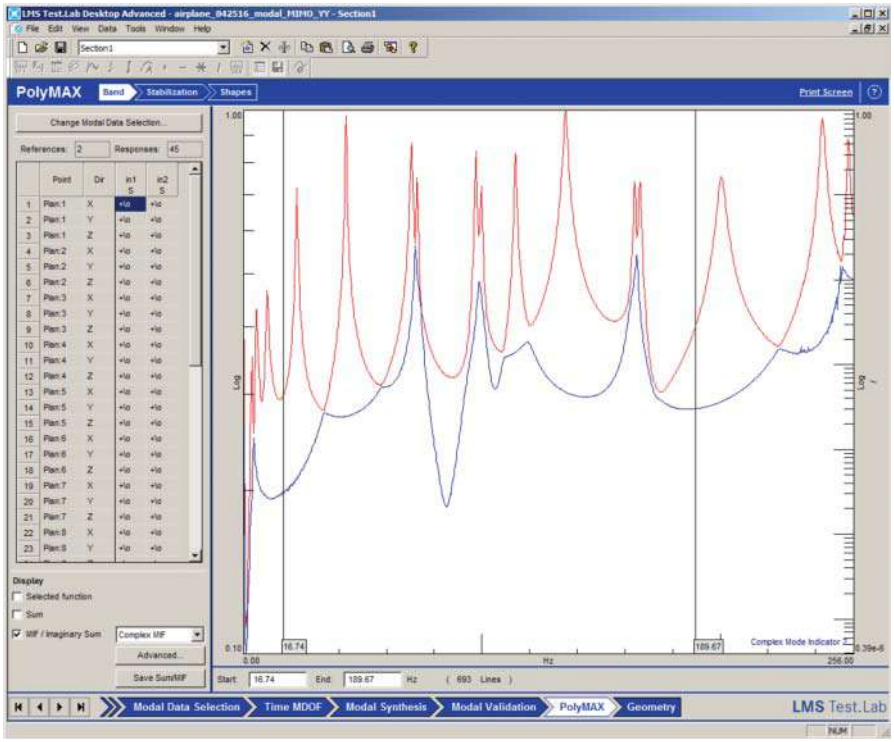

Figure I.15 CMIF function for demo airplane MIMO data.

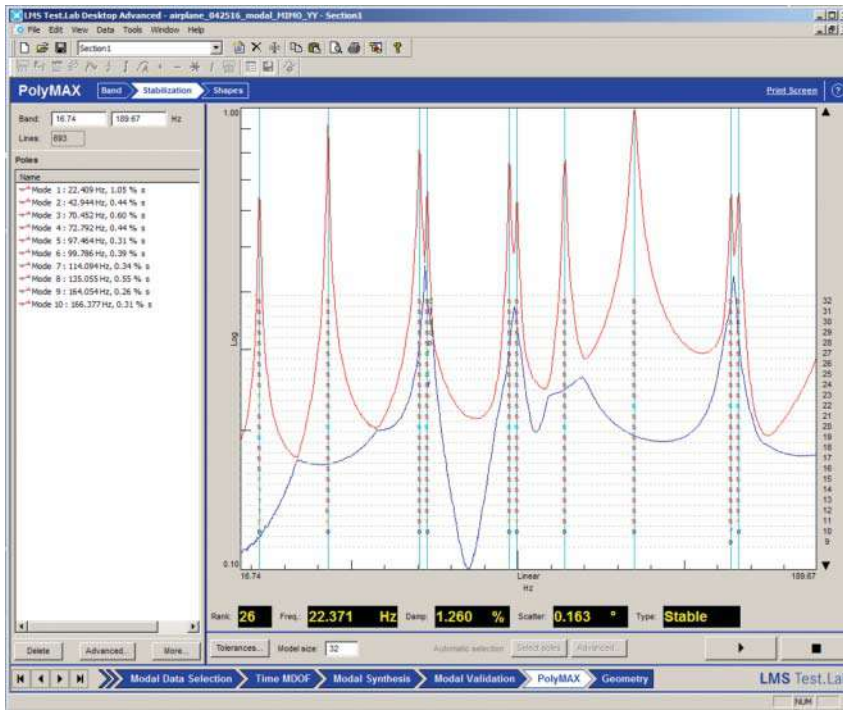

Figure I.16 Summation function for demo airplane MIMO data.

Table I.1 Mode participation for demo airplane MIMO data.

Reference	Shaker 1	Shaker 2
Mode 1	0.99	1.00
Mode 2	1.00	0.97
Mode 3	0.97	1.00
Mode 4	1.00	0.93
Mode 5	1.00	0.21
Mode 6	0.52	1.00
Mode 7	0.61	1.00
Mode 8	1.00	1.00
Mode 9	0.66	1.00
Mode 10	0.97	1.00

J

Whirlpool Dryer Cabinet Modal Testing

A MIMO modal test was conducted on a Whirlpool Dryer Cabinet in the late 1990s by the Dynamic Systems Laboratory at Michigan Technological University. The cabinet was supported on the mounting feet and four shakers were used to collect frequency response measurements. There were 29 lightweight accelerometers permanently mounted on the base of the cabinet and the balance of the measurements was obtained with a scanning laser vibrometer (with 100 points on each face: left, right, and back). Figures J.1 and J.2 show the structure.

A frequency band from 13 Hz to 63 Hz was selected with the four references. The data was evaluated to obtain the summation function shown in Figure J.3. There are many peaks in the summation function. Using a model order of 128, the stability diagram was generated for the band considered and 21 roots were selected, as shown in Figure J.4. The modes are calculated as shown in Figure J.5. The modal participation factors for the four references are shown for the 21 modes evaluated as shown in Table J.1. Reviewing the table, the need for all four shakers is confirmed; there are many modes where different combinations of shakers are needed to adequately excite all the modes in the structure.

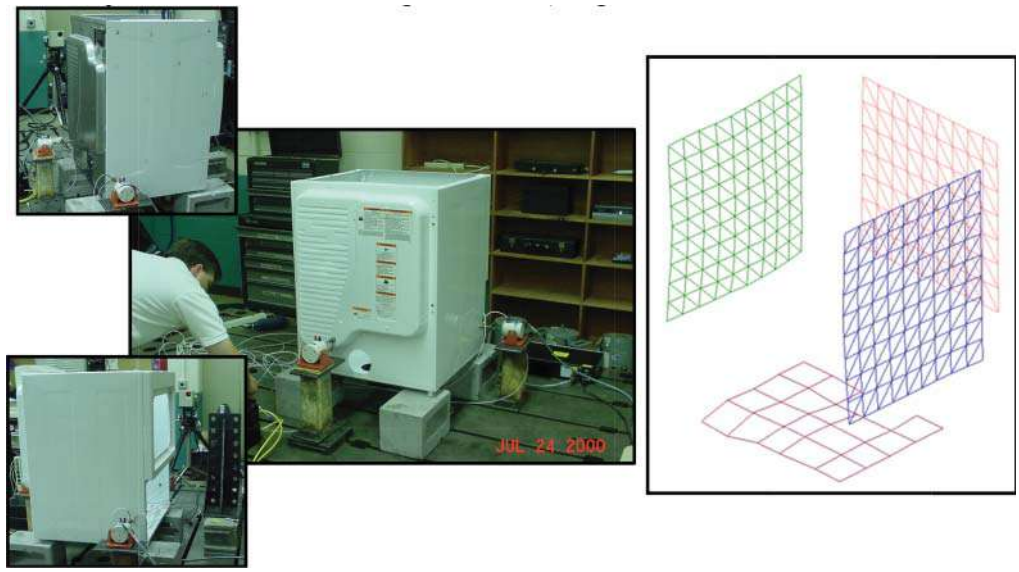

(a) (b)

Figure J.1 Whirlpool dryer cabinet: (a) photos; (b) test geometry.

Modal Testing: A Practitioner's Guide, First Edition. Peter Avitabile.

Companion Website: www.wiley.com/go/avitabile/modal-testing

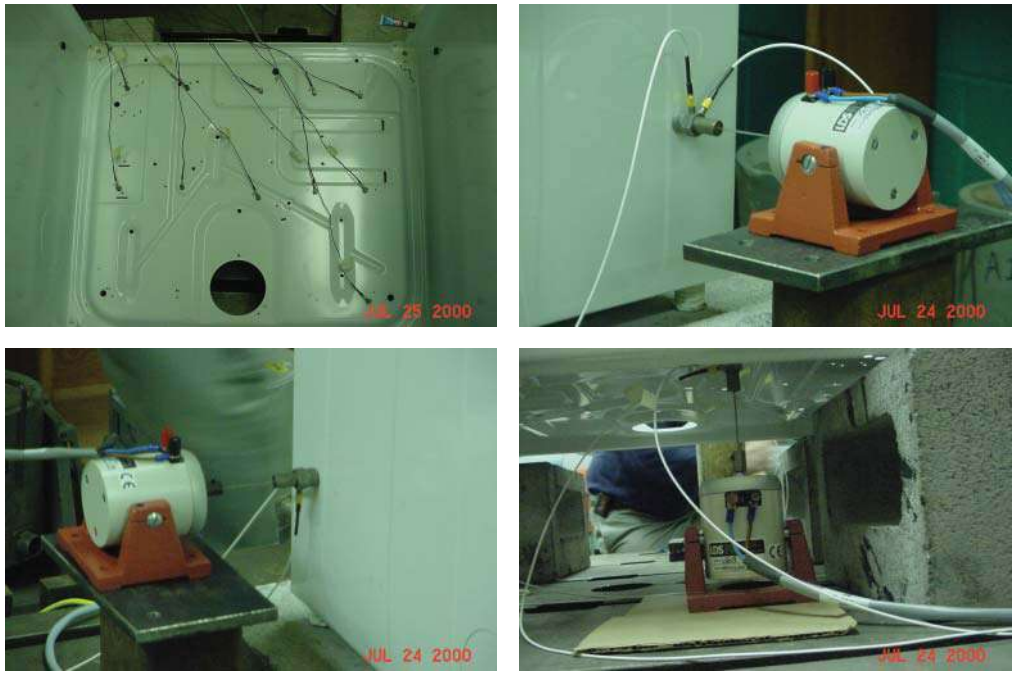

Figure J.2 Whirlpool dryer cabinet test set up.

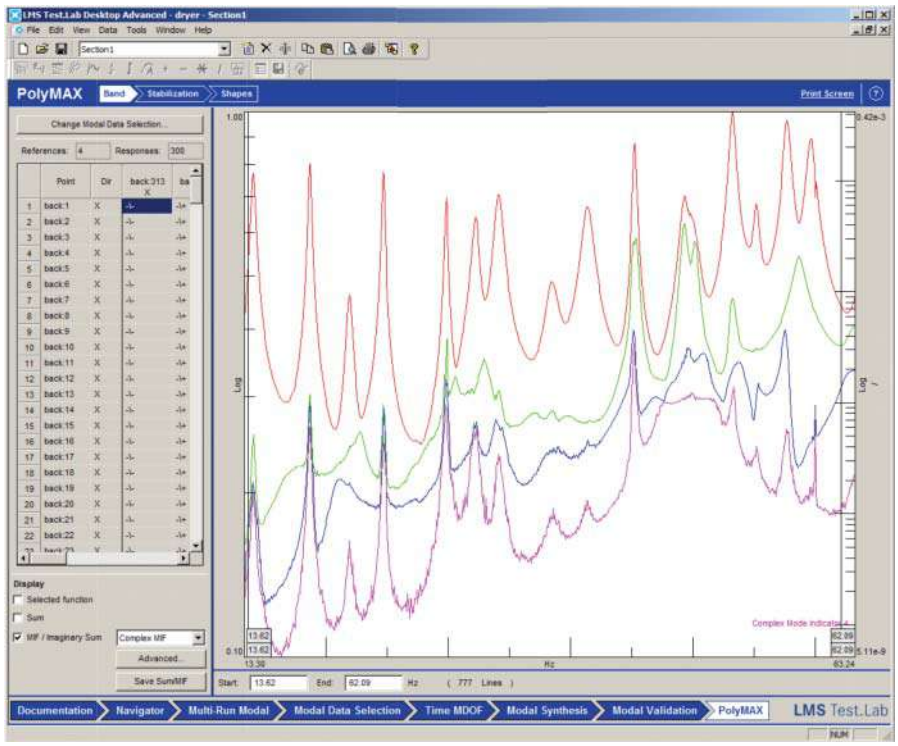

Figure J.3 Summation function using all four references.

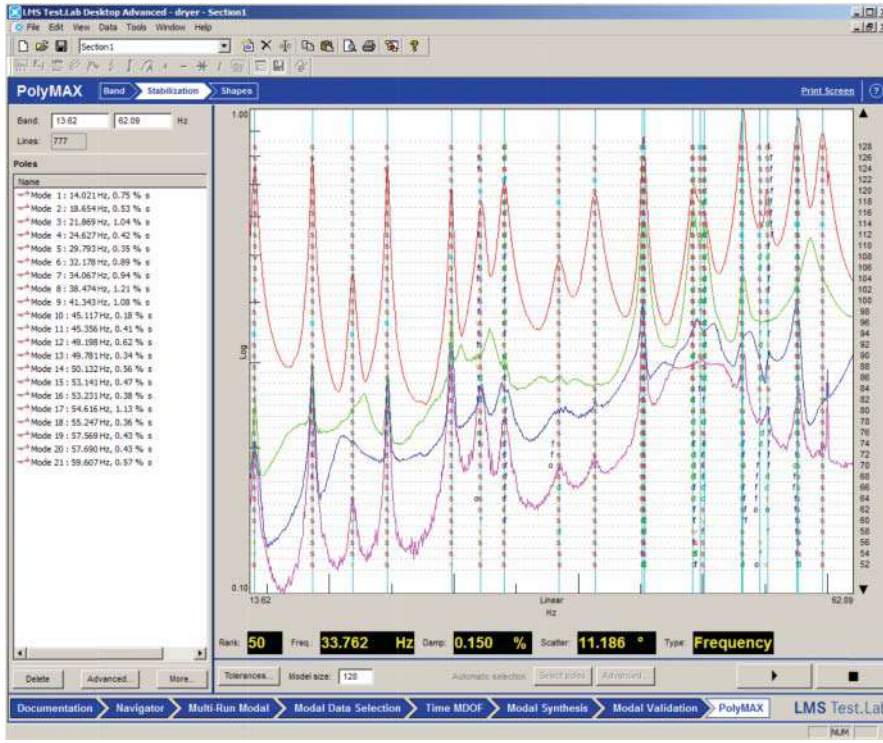

Figure J.4 Stability diagram using all four references.

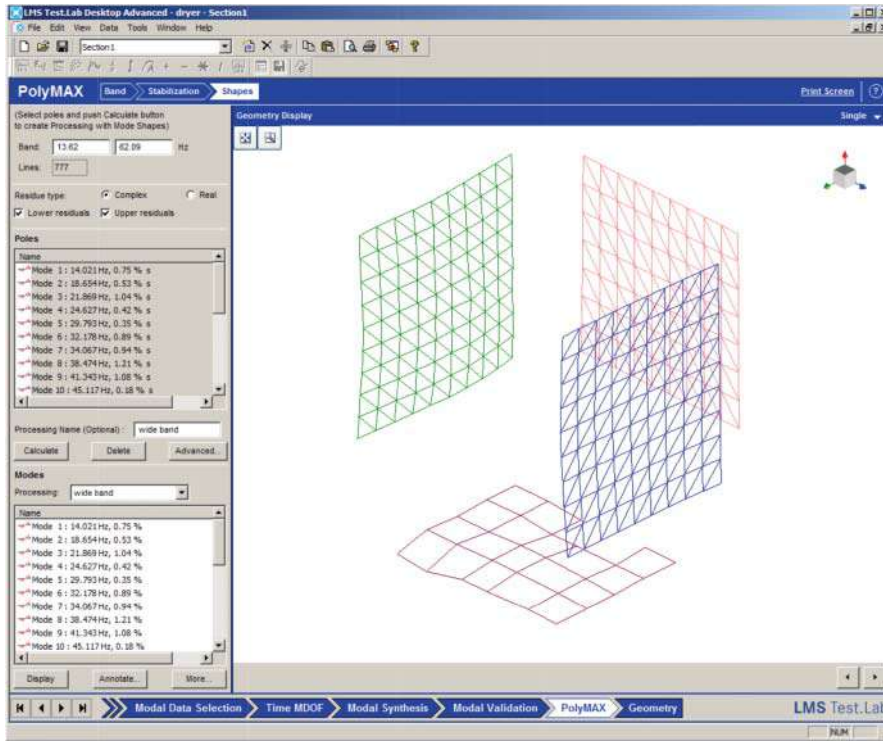

Figure J.5 Modal data extracted using all four references.

Table J.1 Modal participation factors using all four references.

M.P.F.	back:313: + X	base:312: + Z	left:311: + Y	rght:310: + Y
Mode 1	0.07	0.04	1.00	0.63
Mode 2	0.31	0.06	0.08	1.00
Mode 3	1.00	0.01	0.08	0.15
Mode 4	0.06	0.04	1.00	0.23
Mode 5	1.00	0.07	0.24	0.42
Mode 6	0.04	0.05	1.00	0.28
Mode 7	0.66	0.07	1.00	0.57
Mode 8	0.16	0.19	0.65	1.00
Mode 9	0.03	0.08	0.06	1.00
Mode 10	0.68	0.06	1.00	0.31
Mode 11	0.11	0.05	0.45	1.00
Mode 12	1.00	0.74	0.13	0.14
Mode 13	0.71	1.00	0.20	0.18
Mode 14	0.83	1.00	0.10	0.18
Mode 15	0.11	0.03	1.00	0.08
Mode 16	0.23	0.02	1.00	0.05
Mode 17	0.10	0.06	0.94	1.00
Mode 18	0.11	0.01	1.00	0.53
Mode 19	0.32	0.05	1.00	0.26
Mode 20	0.18	0.03	1.00	0.36
Mode 21	0.02	0.01	0.15	1.00

K

GM MTU Automobile Round Robin Modal Testing

A MIMO modal test was conducted on a GM automotive structure and the data was used as part of a round robin exercise by Michigan Technological University at IMAC 28. The car was supported in a normal testing configuration at the GM modal test lab. Four shakers were used, and several hundred measurements were collected. Figure K.1 shows the structure.

A frequency band from DC to 128 Hz was tested. The analysis band selected here was 10–70 Hz with the four references; the frequencies below 10 Hz were rigid body modes. The data was evaluated to obtain the summation function shown in Figure K.2. There are many peaks in the summation function. Using a model order of 128, the stability diagram was generated for the band considered and over 20 roots were selected, as shown in Figure K.3. The modes were calculated, as shown in Figure K.4. No further assessment was performed. This dataset is available.

Figure K.1 Typical automotive modal test setup.

Modal Testing: A Practitioner's Guide, First Edition. Peter Avitabile.

Companion Website: www.wiley.com/go/avitabile/modal-testing

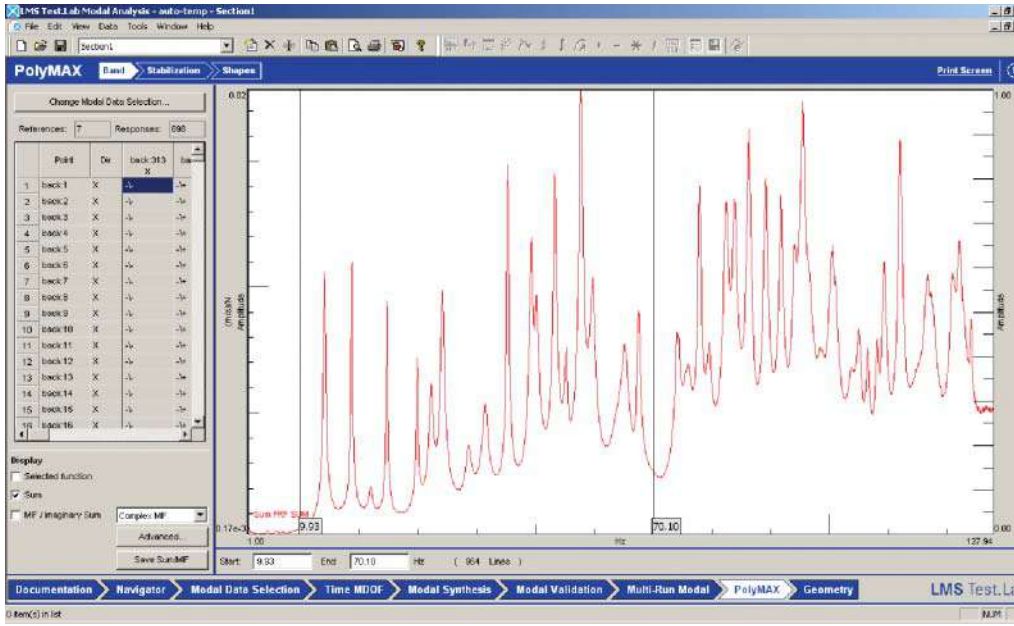

Figure K.2 Summation function using all four references.

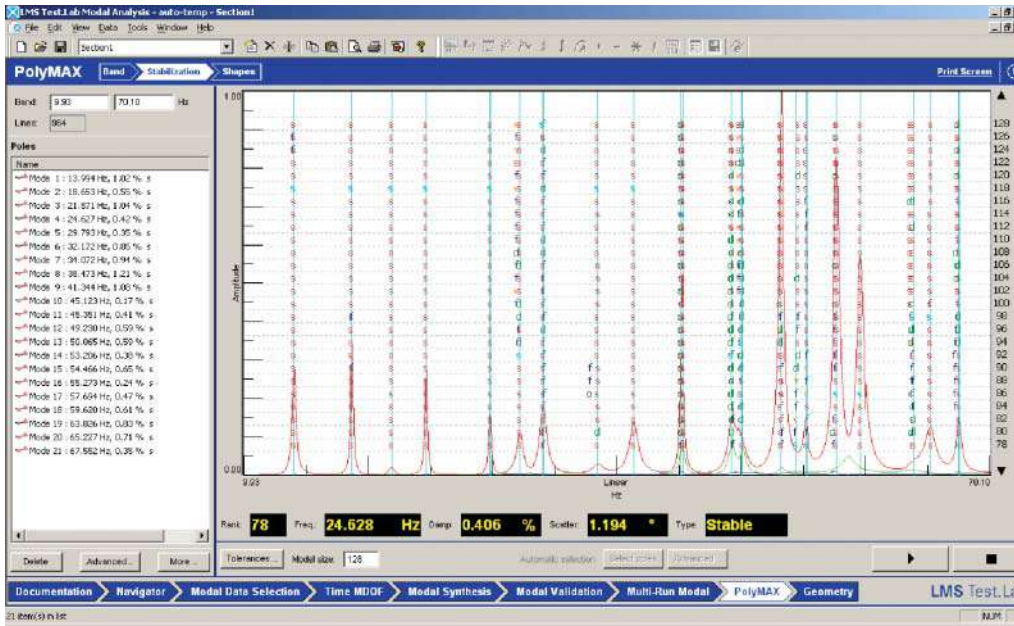

Figure K.3 Stability diagram using all four references.

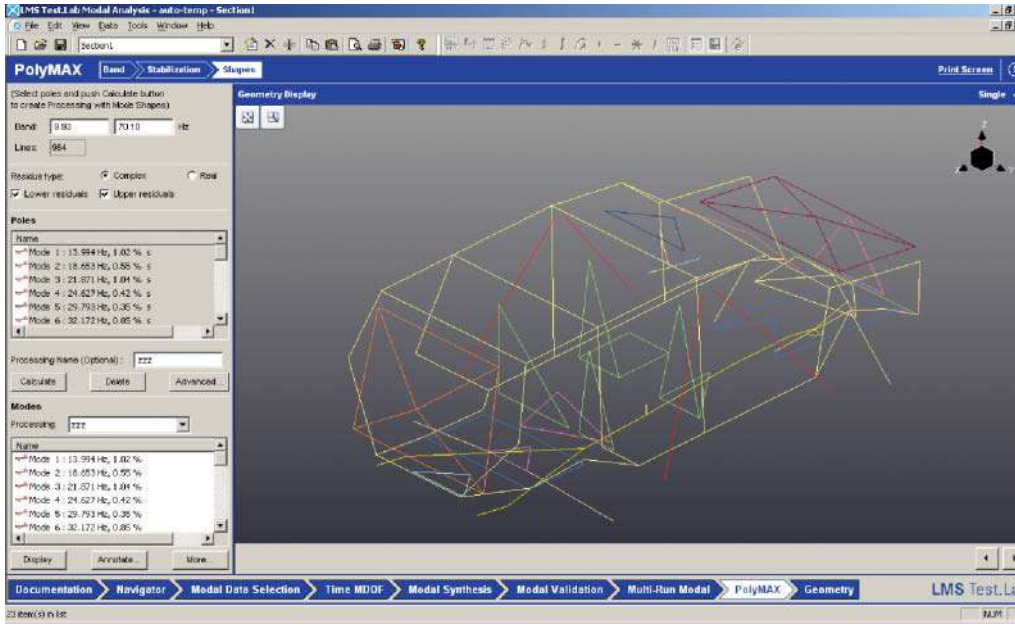

Figure K.4 Modal data extracted using all four references.

L

UML Composite Spar Modal Testing

A composite spar (of unknown origin) has been used at the University of Massachusetts Lowell in the Structural Dynamics and Acoustic Systems Laboratory since 2000. This is a general structure that has a I beam style geometry, with a T shape on the top and an L shape on the bottom that tapers along the length of the structure; essentially there is no symmetry in this structure. There is no known design information on the spar and no model of the spar. The structure has been used for academic purposes and has been used many times. The data presented here is from the first test that was performed using an impact technique. Only one reference accelerometer was used and approximately 100 frequency response measurements were made. Figure L.1 shows the structure.

Measurements were made over a 800 Hz bandwidth. The first curvefit was performed over the 91–681 Hz range. The summation function indicates that there are six modes in the band, as shown in Figure L.2. Using six modes in this band, a global rational fraction polynomial curvefitter was used to extract the modes. The results of the curvefit are shown in Figure L.3. In general, all of the modes appear to be well described, with very reasonable mode shapes. All the synthesized frequency response functions all compared reasonably well to most of the acquired measurements.

However, there was some concern regarding the second peak and if there were one or two modes in that band. Over 90% of the measurements appeared to have only a single peak but there were some cross measurements that seem to indicate two modes. That band was refit with two different approaches, using one mode and using two modes, for that second peak. The results are shown in Figures L.4 and L.5. Upon reviewing the mode shapes there definitely appear to be two modes in that band. Figure L.6 shows the single mode approximation and the two mode approximation. The single mode approximation shows bending in both the long axis and short axis simultaneously; the two mode approximation shows one mode with bending along the long axis and one mode with bending along the short axis. The single mode is seen to be the linear combination of the two modes. This model shows the need to carefully assess all the measured data and be careful in the modal extraction process.

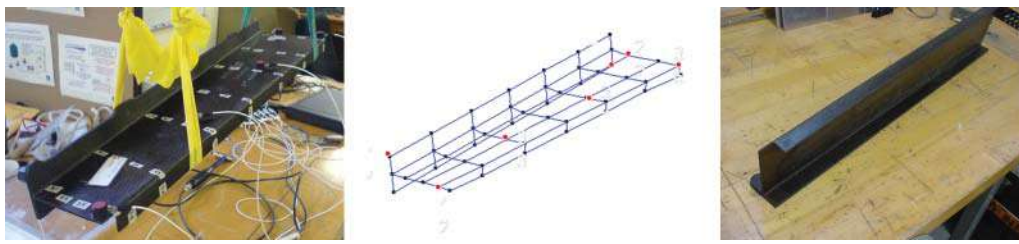

Figure L.1 Typical modal test set up.

Modal Testing: A Practitioner's Guide, First Edition. Peter Avitabile.

Companion Website: www.wiley.com/go/avitabile/modal-testing

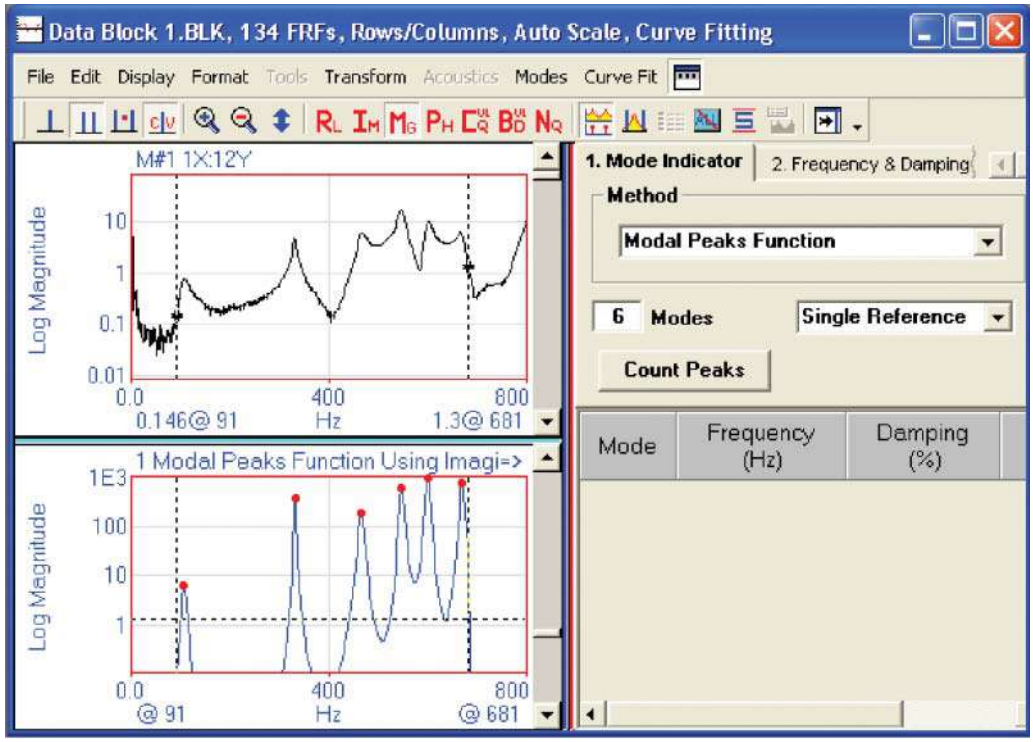

Figure L.2 Summation function.

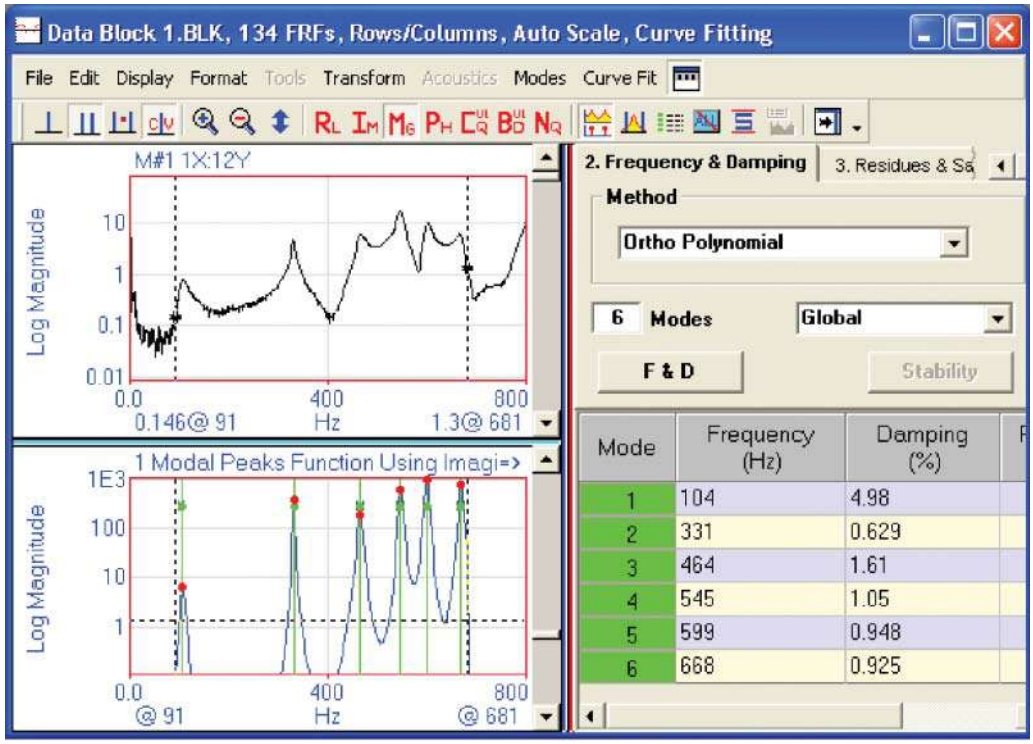

Figure L.3 Orthogonal polynomial fit for six modes.

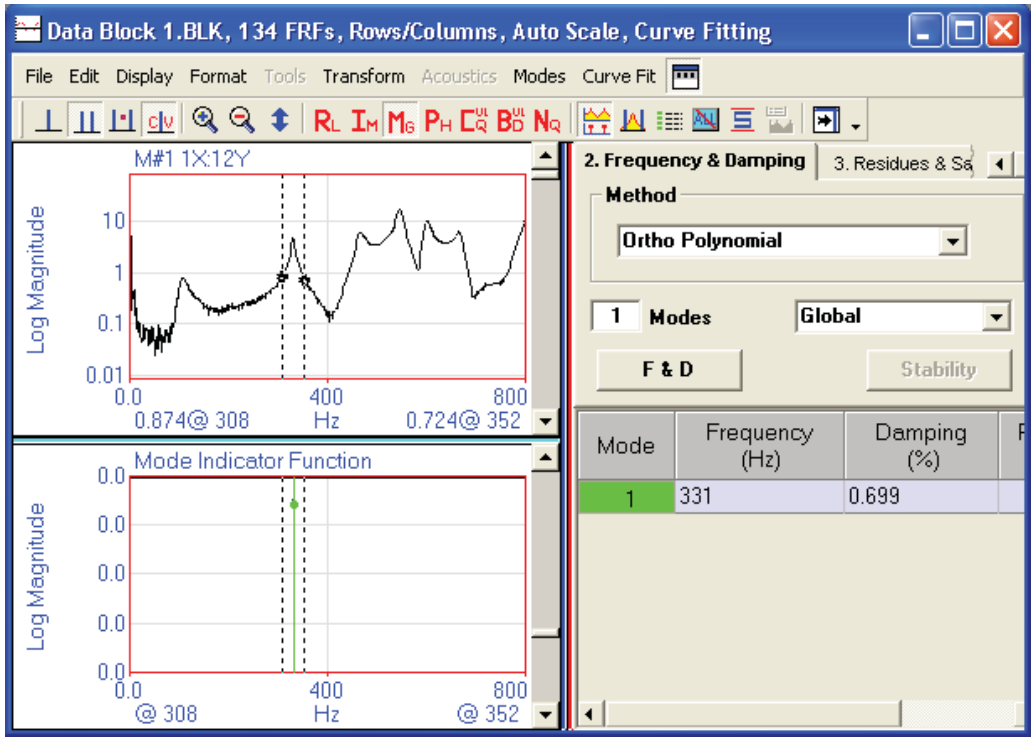

Figure L.4 Orthogonal polynomial fit for 1 mode over 308 Hz to 352 Hz band.

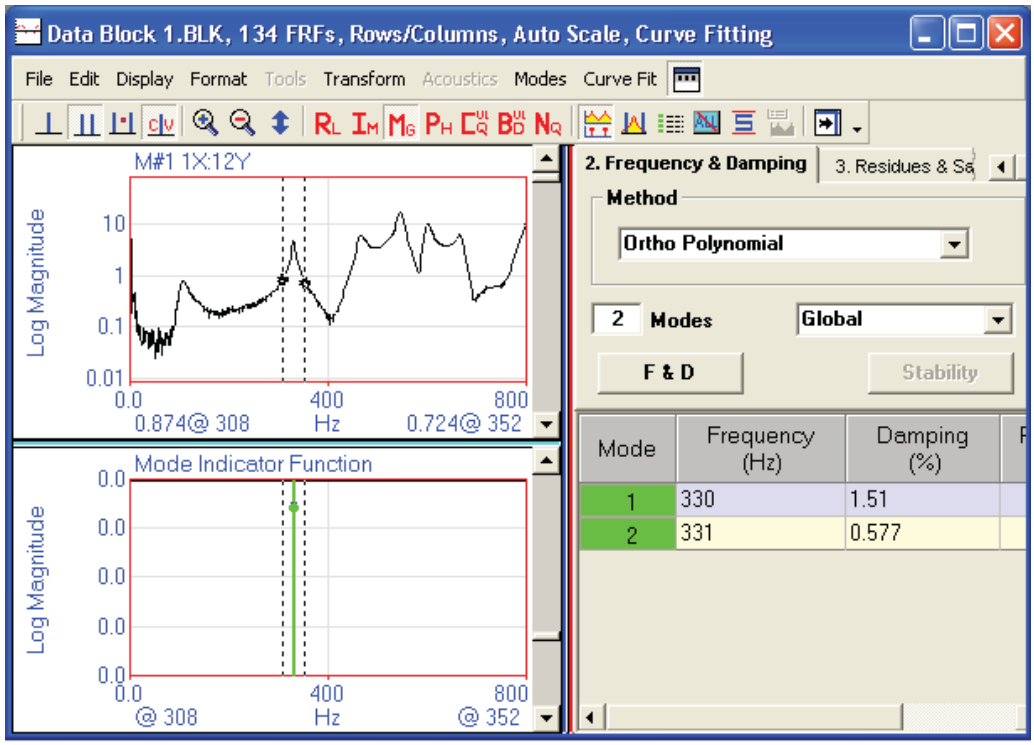

Figure L.5 Orthogonal polynomial fit for 2 modes over 308–352 Hz band.

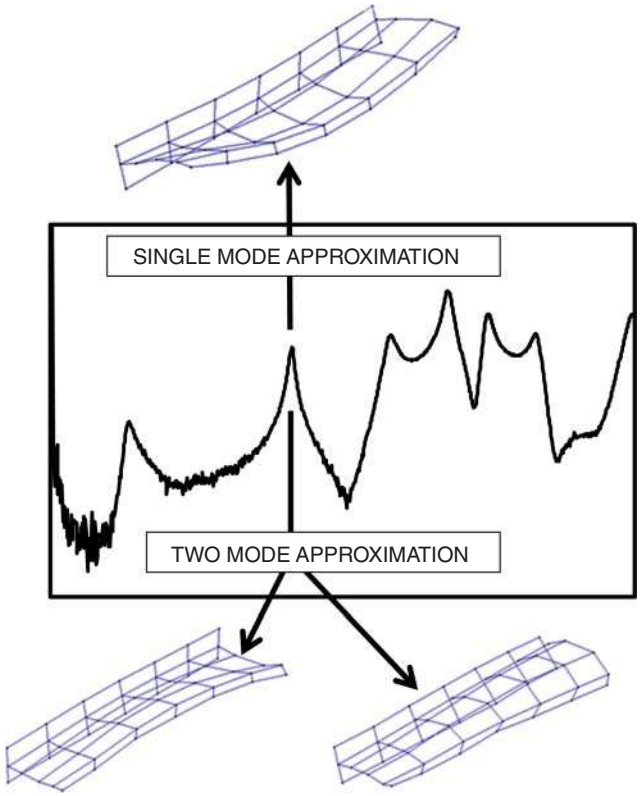

Figure L.6 Single mode and two mode extracted mode shapes.

M

UML BUH Modal Testing

A generic academic structure has been used since 2000 at the University of Massachusetts Lowell in the Structural Dynamics and Acoustic Systems Laboratory. It is referred to as BUH (base-upright-horizontal). This structure has been tested in pieces and as an assembled structure; this structure has been used for many substructuring studies and various types of modal tests over the years. Correlations to finite element models have also been performed.

A multiple reference impact test was performed with seven reference accelerometers mounted on the structure; 72 excitation points were used for impact. Figure M.1 shows the structure, with the components identified and measurement locations shown.

Data was collected to 2000 Hz but only modes up to 325 Hz are evaluated here. The sum function in Figure M.2 shows many modes of this structure and the CMIF in Figure M.3 shows the same peaks with no apparent repeated roots. Figure M.4 shows the stability diagram, with 15 modes selected for modal extraction; the modes are shown in Figure M.5. Table M.1 shows the results of a correlation study with a finite element model.

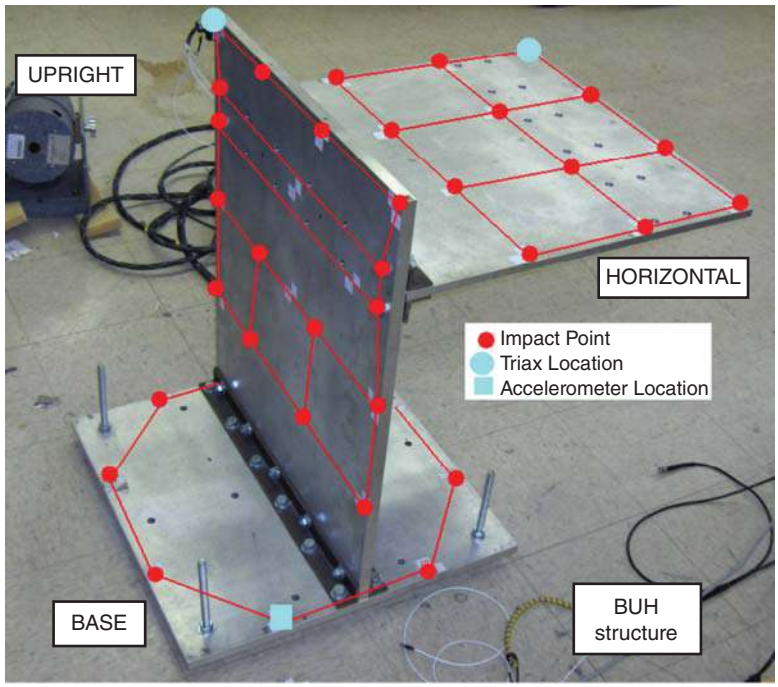

Figure M.1 Typical BU modal test set up.

Modal Testing: A Practitioner's Guide, First Edition. Peter Avitabile.

Companion Website: www.wiley.com/go/avitabile/modal-testing

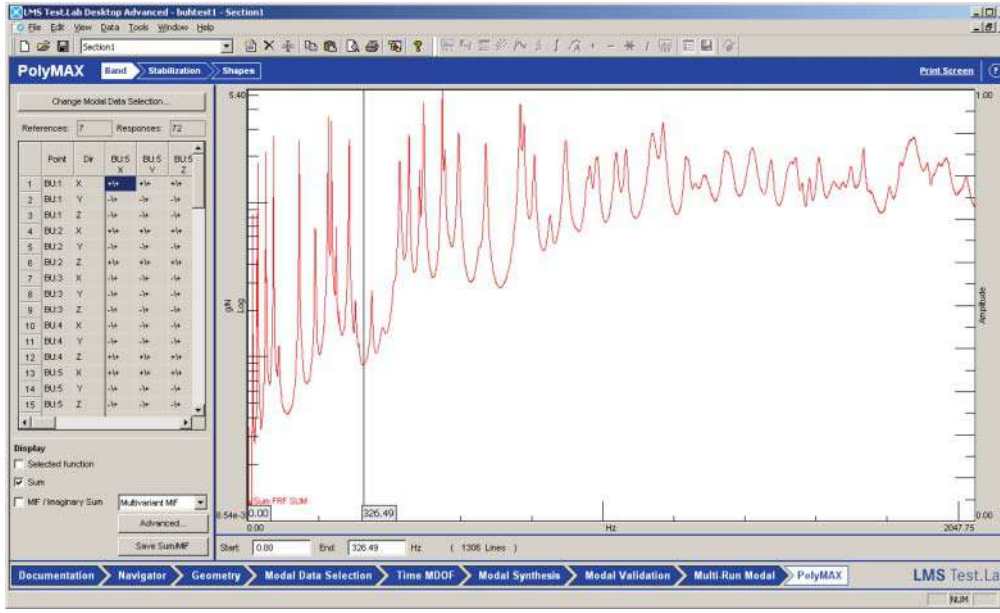

Figure M.2 Summation function using all seven references.

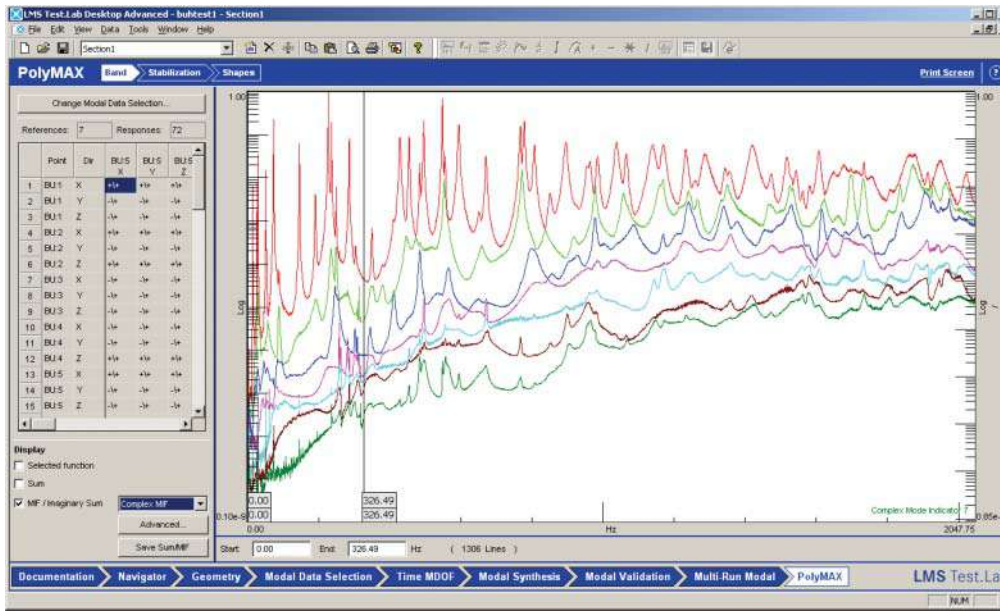

Figure M.3 CMIF using all seven references.

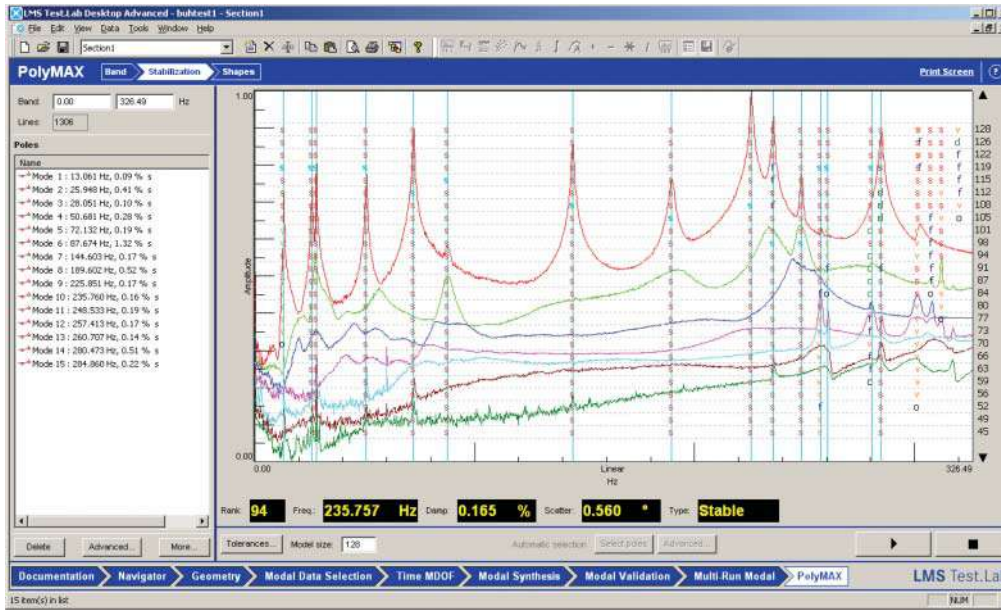

Figure M.4 Stability diagram using all seven references.

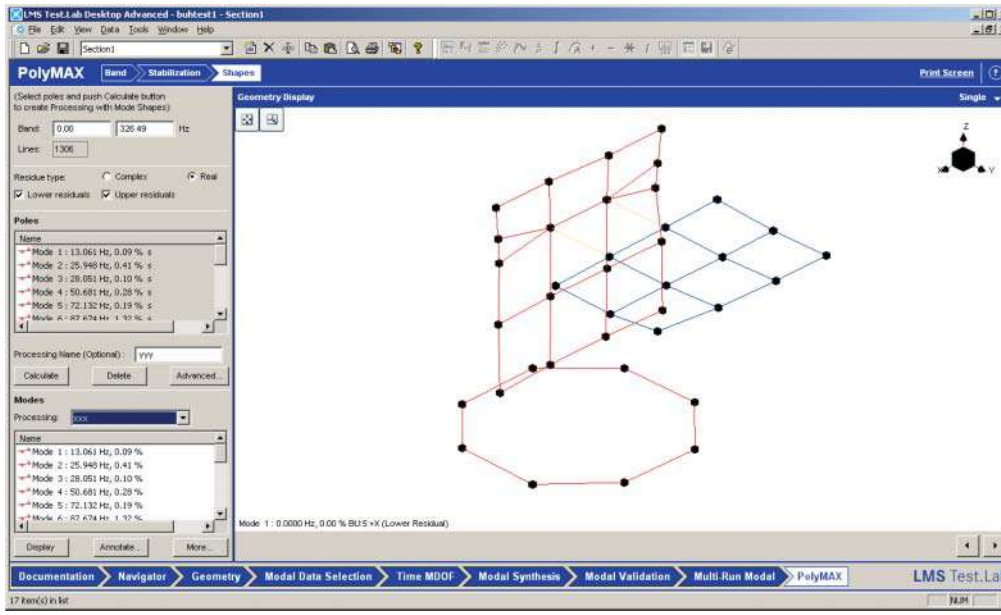

Figure M.5 Modal data extracted using all seven references.

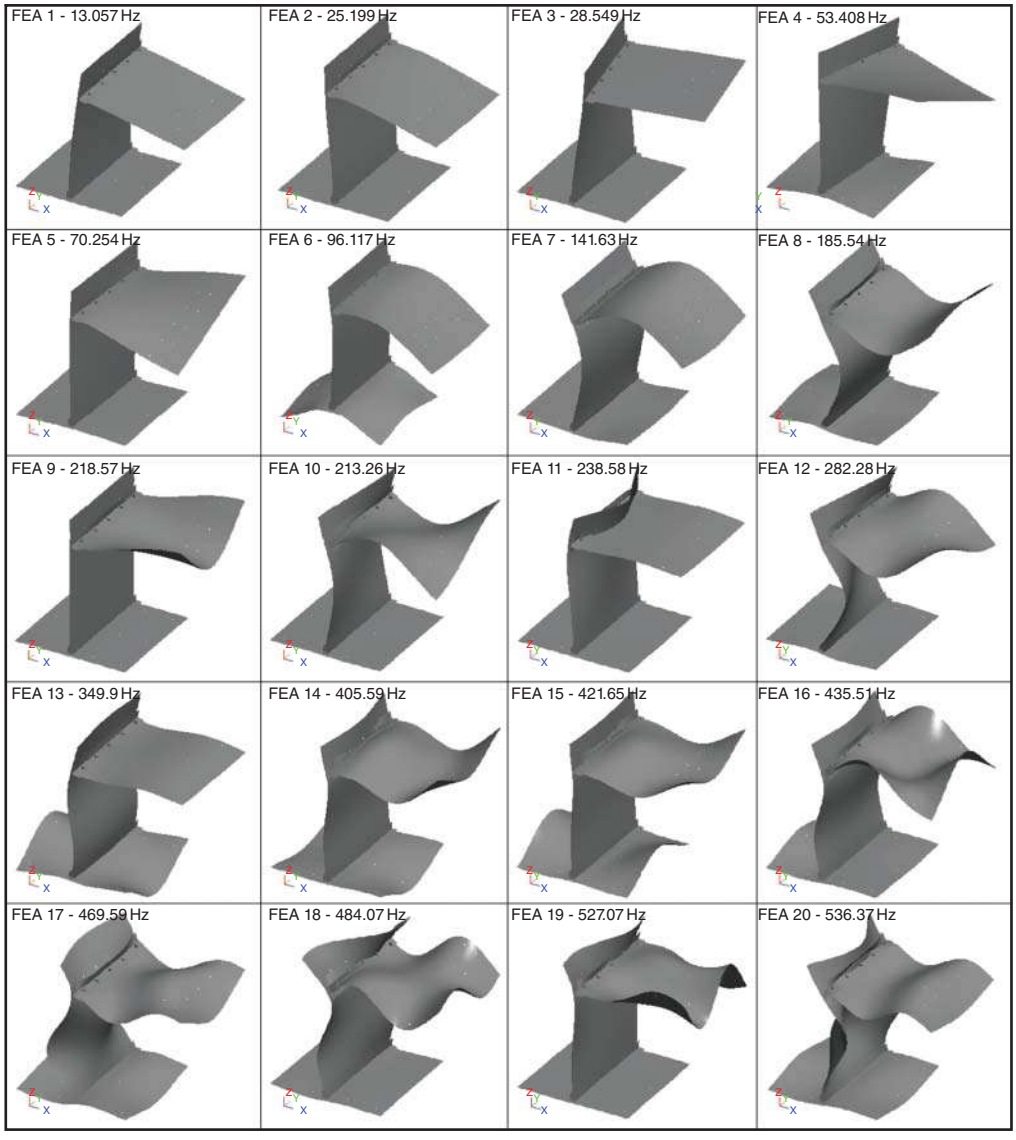

Figure M.6 First twenty finite element mode shapes (for reference only).

Table M.1 Correlation of assembly test-data and FEA model along with MAC matrix.

Mode Number	(Fig. A4) FEA Freq. (Hz)	Experimental Frequencies (Hz)	Frequency % Difference	MAC Value	20 Mode POC Value
1	13.06	13.29	−1.76	98.8	0.993
2	25.2	26.03	−3.29	99.1	1.055
3	28.55	28.57	−0.07	99.1	1.075
4	53.41	52.36	1.97	98.6	1.019
5	70.25	72.28	−2.89	99.4	0.983
6	96.12	93.5	2.73	99.1	1.033
7	141.63	145.81	−2.95	99.1	1.052
8	185.54	191.72	−3.33	98.6	1.010
9	218.57	226.33	−3.55	97.3	0.998
10	231.27	237.02	−2.49	93.4	1.015

FEA, finite element analysis; POC, pseudo orthogonality check.

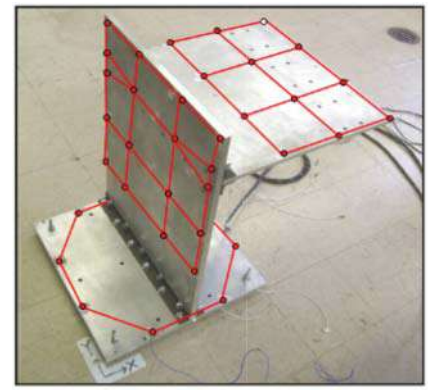

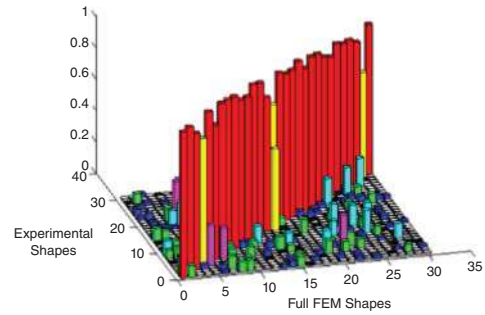

N

Nomenclature

Upper case	Lower case	description
General terms		
ADC		Analog to digital converter
DOF	dof	Degrees of freedom
FFT		Fast Fourier transform
IFT		Inverse Fourier transform
FRF	frf	Frequency response function
MAC		Modal assurance criterion
MPE		Modal parameter estimation
DSP		Digital signal processing
MRIT		Multiple reference impact test
LTI		Linear time invariant
SVD		Singular value decomposition
RBM		Rigid body mode
FEA		Finite element analysis
FEM		Finite element model
AC		Alternating current
DC		Direct current
ICP		Integrated circuit piezotronic
BW		Bandwidth
SDOF	sdof	Single degree of freedom
MDOF	mdof	Multiple degree of freedom

Modal Testing: A Practitioner's Guide, First Edition. Peter Avitabile.

Companion Website: www.wiley.com/go/avitabile/modal-testing

Upper case	Lower case	description
Measurements		
H	h	Transfer function or frequency response function
H(s)	h(s)	Transfer function
H(jω)	h(jω)	Frequency response function
D/F		Displacement to force frequency response function
V/F		Velocity to force frequency response function
A/F		Acceleration to force frequency response function
MG		Magnitude
PH		Phase
RE		Real
IM		Imaginary
S		Linear spectrum
G		Power spectrum
COH		Coherence
Q		Quality factor, amplification factor
SUM		Summation function
MIF		Mode indicator function
MMIF		Multivariate mode indicator function
CMIF		Complex mode indicator function
SD		Stability diagram
Matrices/vectors		
[M]		Mass matrix
[C]		Damping matrix
[K]		Stiffness matrix
	m	Mass: scalar element of a matrix
	c	Damping: scalar element of a matrix
	k	Stiffness: scalar element of a matrix
{x}		Displacement vector
{F}		Force vector
	x	Displacement: scalar element of a vector
	f	Force: scalar element of a vector
[U]		Modal matrix: mode shapes in column format
{u}		Modal vector
	u	Mode shape: scalar element of vector or matrix
{p}		Modal displacement vector

Upper case	Lower case	description
[B(s)]		System matrix
[H(s)]		Transfer function matrix
[H(jω)]		Frequency response matrix
[A(s)]		Residue matrix
Bar overscore		Modal space quantity
Subscripts		
i		Input or output designation
j		Input or output designation
Superscripts		
T		Transpose: generally of a matrix

Index

a

AC coupling 100–101, 382
Actuator 161 *see also* Shaker
Aliasing
  frequency 18–19, 95–97, 103, 105–106, 110, 129, 274, 291, 380
  spatial 236, 352
Amplification factor 42, 516
Analog to digital converter (ADC) 19, 96–101, 133, 155, 168–169, 262–263, 274, 282–283, 386, 515
  overload 100
  underload 98
Analyzer (FFT) 18–19, 23, 53, 95–97, 105, 107, 111–112, 122–123, 132, 137, 140, 147, 150, 157, 167, 169–171, 259, 262, 274, 283, 294, 377–385, 403
Anti-aliasing filter 19, 95–97, 105, 274
Anti-resonance 10, 124, 262, 396–397
Argand plot 49
Auto correlation 126
Autopower spectrum 126
Autorange 378, 382–384, 403
Averaging 19, 126, 164–165, 168–169, 173–174, 218, 280, 378–380, 386, 389
  noise 20, 119, 121–123, 126, 127–128, 137, 163, 191, 196, 386, 389, 404

b

Backup 244–245, 375
Band
  curvefitting 192, 196, 213, 343–346, 412
  frequency 9, 115, 147, 172, 187, 192, 256, 259, 262, 291, 308, 329–330, 394, 403, 405
Bode diagram 49
Bode plots 49
Boundary conditions 228
Burst random 23–25, 132, 168–170, 172–180, 184–185, 269, 293–294, 379, 381, 384–385, 389, 392

c

Characteristic equation 39, 47, 66–67, 202, 367
Chirp 23, 25, 132, 170–172, 174–175, 293, 379, 381, 384–385, 389, 392
Circle, fitting 199
  form of SDOF plots 49
Coherence
  mode indicator function 206–208, 328, 330, 516
  multiple 182
  ordinary 19, 21, 96, 123–124, 136–138, 155–157, 164–165, 170–177, 182, 213, 249, 251, 256, 259, 261–262, 269–272, 277, 280, 282–288, 292, 295, 318, 378–379, 381–387, 423, 516
  partial 182
Coincident-quadrature diagram 49
Compensation 28, 191, 192
  residual 28
Correlation functions
  cross-correlation 126
Critical damping 39, 43, 66
Cross spectrum 19, 124, 218
Curvefitting
  CMIF 207–210, 321, 328–330, 340
  considerations 441
  data included 192, 213, 343–344, 347, 412
  examples 331–333, 346–357, 412–414, 433, 437, 469, 479, 487, 497, 501, 505, 509
  frequency domain 189, 192, 194, 196–197, 200, 203–205, 208, 219

Modal Testing: A Practitioner's Guide, First Edition. Peter Avitabile.

Companion Website: www.wiley.com/go/avitabile/modal-testing

Curvefitting (*contd.*)
global 197, 328, 332
local 197, 328, 331–332
MDOF models 201–204, 330
MMIF 207, 209–210, 328–330, 340
polyreference 197, 203
SDOF models 199–200, 330
stability 206, 208–212, 321, 323–325, 328, 330–331, 337, 339–340, 346–348, 351, 356–358, 376, 404, 411, 417–418, 420
summation 206, 208–210, 328–330, 334–335
time domain 197, 201–204, 209, 347

d

Damped systems
critically damped 40
MDOF proportionally damped 58, 62–63
MDOF viscously damped 38
SDOF 38, 43
undamped 40, 66
underdamped 39–40, 47
Damping
critical damping coefficient 39–40, 43, 47, 66
factor 39
modal 62–63, 88
proportional 38, 57–58, 62–63
viscous 38
Digital stepped sine 25, 132, 170, 293
Discrete, Fourier transform 107–108
Drive point FRF 11, 76, 81, 183, 235, 281, 287, 296, 302–303, 315–317, 319, 328, 371, 374, 396–398
Dummy mass 234, 390, 406

e

Eigensolution 58–61, 87
Eigenvalues 59, 61, 71 *see also* Poles
Eigenvectors 59, 61, 71 *see also* Residue
Elastic forces 43, 46, 51, 60
Equation of motion
linear time invariant (LTI) 204–205, 515
MDOF systems 56–91
SDOF systems 37–56
Excitation
burst random 23, 132, 168–170, 172–180, 184–185, 269, 294, 392
chirp 23–25, 132, 170, 172, 174–175, 392
digital stepped sine 25, 132, 170
harmonic 41, 73
impulse 25, 40, 111, 136, 140, 400
location 72, 160, 239, 346, 350, 413–414, 423
periodic random 167–169
pseudorandom 25, 132, 167–168
random 4, 5, 23, 25, 29–30, 106, 111, 132, 162–166, 172–177, 179–180, 185, 392
sine 163, 170
sine chirp 23, 25, 132, 170, 172, 174–175, 178
swept sine 132, 163, 170–171
Exciter *see* Shaker
Exponential window 22, 25, 111, 119, 140, 143, 157, 159, 247, 279, 282

f

Fast Fourier transform (FFT) 7, 10, 18–20, 22–23, 25, 30, 53, 94–96, 105–108, 121, 123, 126, 139–140, 147, 157, 163, 165, 167–171, 256, 259, 270, 274, 279, 283, 294, 355, 379, 515
non-periodic signal 108
periodic signal 108
Filter
high pass 101, 137, 264
ICP effect 264–265, 515
low pass 95–96, 103, 105, 277
ring 274–275
Force
drop out 295
excitation 5, 218, 316, 319
gage 135, 190, 238, 249, 293–294, 297–304
impedance head 160, 238, 294, 297–298, 300–303
shaker 80, 131, 161–162, 181
Forced vibration
excitation methods 24, 131, 238
excitation techniques 23, 107, 131–132, 161–164, 168, 172–173, 181, 185, 238, 293–294, 369
harmonic excitation 40, 72
Fourier series 93, 106–108
Fourier transform
discrete (DFT) 107–108
fast (FFT) 7, 10, 18–20, 22–23, 25, 30, 53, 94–96, 105–108, 121, 123, 126, 139–140, 147, 157, 163, 165, 167–171, 256, 259, 270, 274, 279, 283, 294, 355, 379, 515
forward/inverse 202–203, 515

Free–free 226, 228, 371
Frequency
  high 5, 6, 19, 105, 135, 230–232
  low 96, 135, 163, 226, 230–232, 239, 264
  measurement range 19, 21, 28, 68, 95, 105, 135–140, 147, 155, 170, 200, 212, 218, 225, 228–232, 239, 248–249, 256, 259–262, 274–278, 283, 286, 295, 375, 401–403, 423
  measurement resolution 102–103, 109
Frequency response function (FRF)
  dynamic stiffness 52
  inertance 52
  mobility 52
  plots of 50, 54–55, 69–70, 72, 73–75, 79–86
  regions (mass, damping, stiffness) 52
  residual terms 193, 202–203, 212, 394
Function
  complex mode indicator 206–208, 328, 330, 516
  mode indicator 206–208, 215, 321, 327–330, 335, 404–405, 411, 516
  summation 206, 208–210, 328–330, 334–335

g

Global
  poles 197–198, 413
  rational fraction polynomial 201, 331, 335
  residues 49, 69, 75, 77, 90, 189, 196–198, 204–205, 213, 327, 330–332, 337, 343–346, 367–368, 413–414, 423
Global curvefitting 197, 328, 332
Guidelines 378–391

h

Half-power
  bandwidth 42, 49–51, 198
  points 42, 49–51, 198
Hammer
  force spectrum 136, 286
  impact 18, 80, 131–132, 135, 140, 143, 147, 150, 238, 248–249, 255–256, 259, 267, 400–401, 417
  tips 135, 247–248, 274, 402–403
Hanning window 23, 25, 111, 116, 165–166, 173–175, 180

i

Impact *see also* Hammer
  double impact 133, 140–141, 247, 268–269, 274, 289–292
  example measurement sequence 147–159, 402–403
  excitation 19, 22, 25, 119, 133, 137, 140, 238, 249, 272, 281, 283–286, 290, 418
  exponential window (response) 22, 25–26, 111, 119, 141–143, 157, 160, 247, 279, 282
  force window 25, 119, 132, 137, 140
  hammer 18, 80, 131–132, 135, 140, 143, 147, 150, 238, 248–249, 255–256, 259, 267, 400–401, 417
  multiple impact 140, 268–274
  rolloff 136, 248–249, 259–263
  skew/offset 162, 256–258
  spectrum 5, 136–140, 147–156, 249, 259, 261–262, 268, 286, 290, 402–403
  tip 135, 247–248, 274, 402–403
Impact test, multiple reference 144, 209, 268, 515
Impedance 52, 160, 238, 294, 297–298, 300–303, 306, 316
Inertance 52

k

Kennedy and Pancu 199

l

Laplace
  domain 38, 46, 66, 90, 367
  s-plane 39–41, 47, 51
  transform 47–48, 51, 66, 68, 205, 281, 367
  variable 66
Leakage 19, 22–25, 96–97, 107, 109, 111–112, 116, 132, 140, 147, 157, 163–170, 173–175, 203, 279, 282, 327
Least squares complex exponential 201–203
Local curvefitting 197, 331–332
Location
  exciter 182, 185, 316, 356, 413
  impact 145, 237, 247, 251, 255, 267, 387, 417
  shaker 182, 185, 316, 356, 413
Log decrement 42–43

m

Mass loading 159, 231, 234, 239, 242–243, 267, 305, 403–404, 406–407
Matrix
  damping 58, 516
  frequency response function 13, 79–86

Matrix (*contd.*)
mass 58, 516
modal 61, 516
stiffness 58, 516
Measurement
baseband 180
broadband 264
frequency range 19, 21, 28, 68, 95, 105, 135–140, 147, 155, 170, 200, 212, 218, 225, 228–232, 239, 248–249, 256, 259–262, 274–278, 283, 286, 295, 375, 401–403, 423
frequency resolution 102–103, 109
frequency response functions 16, 28, 75, 137, 288, 302, 304–305, 307, 316–321, 325, 368
point 14–17, 61, 75, 144, 232, 234–236, 292, 332, 346, 374, 404–405, 414, 423
reciprocity 159, 181, 264, 307, 419
Modal
damping 62–63, 88
mass 61–63, 71, 88
matrix 61, 516
model 131, 176, 193, 212, 235, 389, 399
overlap 193, 195, 331
participation factor 204, 251, 347
participation matrix 353, 376
stiffness 61–63, 88
testing 19, 23, 25, 33, 38–39, 96, 131–132, 159–160, 162–164, 168, 197, 203, 208, 238, 240, 264, 286, 294, 297–298, 302, 316, 332, 365, 369, 396, 400, 402, 412
Modal assurance criteria (MAC) 213, 215, 226–227, 289, 291–292, 335, 347, 352, 358–363, 377, 404, 515
Mode indicator
CMIF 207–210, 321, 328–330, 340
MMIF 207, 209–210, 328–330, 340
stability 206, 208–212, 321, 323–325, 328, 330–331, 337, 339–340, 346–348, 351, 356–358, 376, 404, 411, 417–418, 420
sum 206, 208–210, 328–330, 334–335
Mode
overlap 193, 195, 331
residual 193, 212
Multiple Degree of Freedom (MDOF)
FRF plots 69–70, 72, 73–75, 79–86
modal model 131, 176, 193, 212, 235, 389, 399
Multiple-input, multiple-output (MIMO) 175–176, 179, 181–186, 314, 316–325, 328, 334, 357, 405, 413
Multiplexed 96
Multivariate mode indicator function 207, 209–210, 328–330, 340

n

Natural frequency
damped SDOF system 39
undamped SDOF system 39
Noise 122–129, 137

o

Operating data 24, 29–34
Operating deflection shape 31, 33
Operating modal analysis 38, 216–219, 358, 362
Output only 216, 219, 238
Overlap processing 165–166, 173
Overload 100, 262, 277, 282–283, 374

p

Parameters
modal 28–29, 31, 34, 187, 189, 192–193, 198, 201, 205, 210, 212, 216, 238, 240, 264, 288, 292, 297, 319–321, 327–328, 334, 341, 343, 347, 350, 353, 356, 412, 414
Partial fraction form 48–49, 53, 68, 192, 197, 201, 203–204, 330, 341, 464
Peak pick 26–27, 198–199, 376
Periodic random 167–168
Pole 39–41, 47–49, 51–53, 66–68, 90, 180, 189, 196–200, 203–212, 321, 323–325, 327, 330–332, 337, 340–347, 351–352, 356, 367–368, 404–406, 412–414, 418
PolyMAX 210–212, 346, 352, 356, 358
Polyreference 197, 203
Pretrigger delay 169
Properties, dynamic 6
Proportional damping 38, 57–58, 62–63
Pseudo-repeated roots 207, 209, 328, 330, 334–335
Purpose of test 223–224

q

Quantization 19, 97–98, 156, 264
Quill *see* Stinger

r

Random signals 111, 132
Rational fraction polynomial 201, 331, 335
Reciprocity 13, 18, 67, 143, 159, 178–179, 181, 264, 306–307, 319, 321, 398–399, 404
Record keeping 375
Rectangular window 25, 111–112, 116, 119, 137
Reference location 16, 77, 80, 143, 178, 185, 237, 248, 251, 268, 295, 297, 319–320, 347, 351, 396–399, 414–417
Repeated roots
  mathematical 206–207, 329, 334
  pseudo 207, 209, 328, 330, 334–335
Residual, compensation 28
Residual mode 193, 212
Residuals 193, 202–203, 212, 394
Residue 49, 69, 75, 77, 90, 189, 196–198, 204–205, 213, 327, 330–332, 337, 343–346, 367–368, 413–414, 423
Residue matrix 66–69, 81, 517
Resonance 10–11, 42–44, 46, 50–51, 207, 262, 294, 329–330
Rigid body modes 226–230, 239, 375–376
Roving accelerometer 267, 405
Roving hammer 143, 146, 237, 248, 267, 375

s

Sampling
  frequency 103
  rate 19, 102
Shaker
  alignment 296–300
  collet 298
  current amplifier 294
  force gage mounting 300–301
  setup 161, 241, 297, 319, 397
  trunnion 295–296
  voltage amplifier 294
Single
  SISO 178–180, 185, 239, 307, 316–325
Single degree of freedom (SDOF)
  frequency response function (FRF) 51–53
  plots 50, 54–55
Singular value decomposition 181, 207, 515
Spectrum rolloff 136, 248–249, 259–263
Stability diagram 159, 180, 185, 208–210, 321, 323–325, 328, 330, 337, 339–340, 346–347, 352, 404–405, 411, 417–418, 420
  demystified 337
Stationary hammer 143, 267
Stiffness
  matrix 58, 516
  modal 61–63, 88
Stinger 18, 159–162, 238, 293, 296–325
SUM function 206, 208–210, 328–330, 334–335
Superposition 88
Synthesis 193, 212–214, 228, 368, 377
Synthesized FRF 212–214, 344–346
System
  damping 58
  mass 58, 65, 366, 368
  stiffness 58
System transfer function 47–53, 66–68, 71, 341, 367–368

t

Techniques
  curvefitting 27, 189, 203
  measurement 132, 404
  testing 132
Test
  boundary conditions 226–229
  inconsistencies 146, 178, 180, 297, 417
  plan 224–225, 234, 253, 369, 375, 377
  procedure 252
  purpose 223
  set up 80, 144, 160–161, 184–185, 223–228, 241, 243–244, 252, 267, 293, 298, 304–308, 318, 321, 373–374, 379, 404–408, 418
Testing
  impact 16, 21–22, 25, 80, 111, 132, 137, 140, 147, 150, 238, 247, 249, 274, 283, 396, 400
  vibration 159, 163
Time invariant 57, 204–205, 321, 515
Transducer, saturated 82
Transfer function 47–53, 66–68, 71, 341, 367–368

u

Underdamped systems 39–40, 47
Underload 98
Universal files 245

v

Viscous damping 38

w

Weighting functions (windows) 19, 96, 108, 165
Windows
  box car 112
  exponential 22, 25, 111, 119, 140–143, 157, 159, 247, 279, 283
  flat top 25, 111–112, 116, 119
  force 25, 119, 132, 137, 140
  Hanning 23, 25, 111, 116, 165–166, 175, 180
  rectangular 25, 111–112, 116, 119
  uniform 25, 111